SYNTHETIC BIOLOGY FOR THE SUSTAINABLE PRODUCTION OF BIOCHEMICALS IN ENGINEERED MICROBES

EDITED BY: Shuobo Shi, Jingyu Wang and Hua Ling

PUBLISHED IN: Frontiers in Bioengineering and Biotechnology

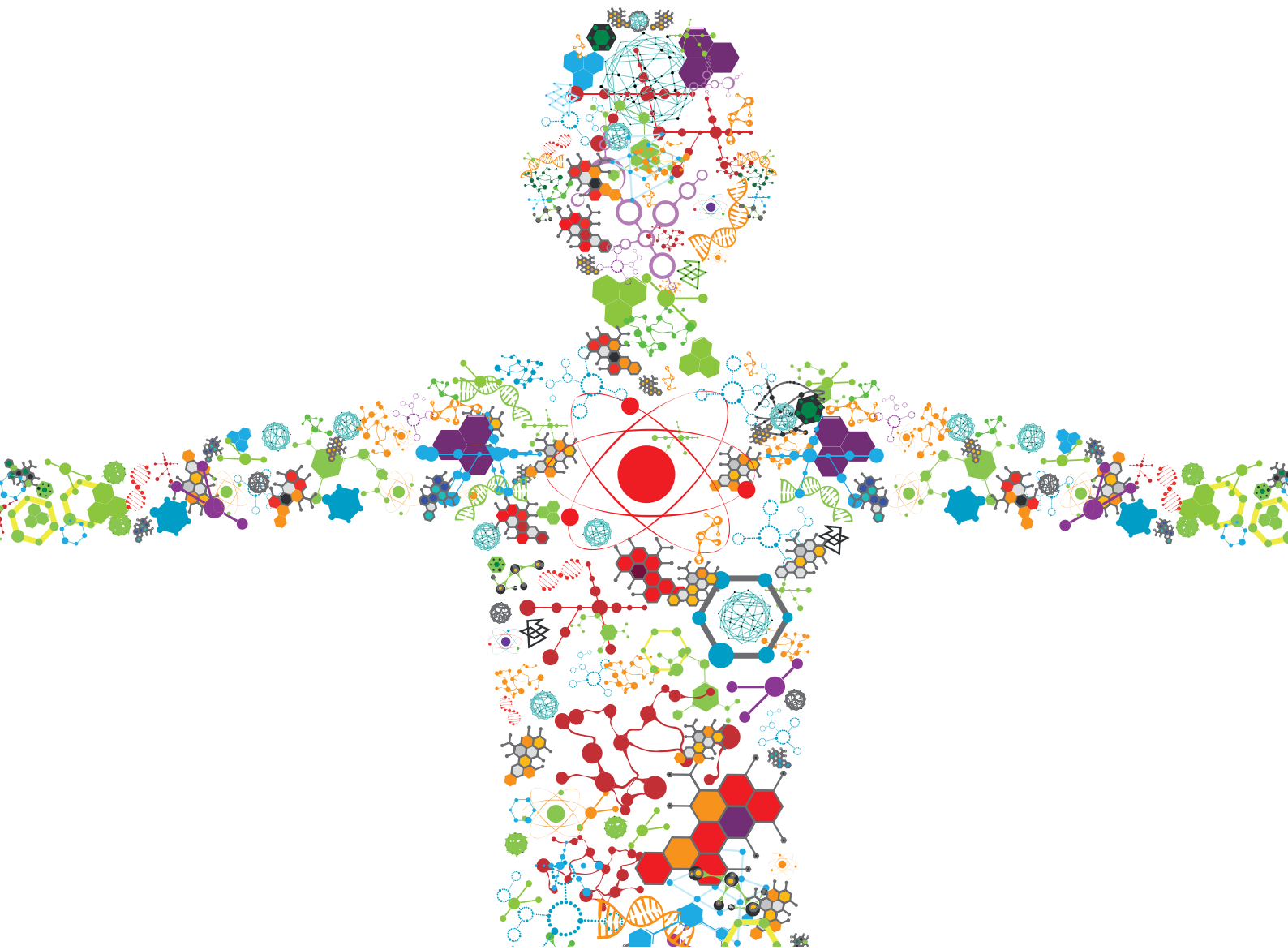

frontiers Research Topics

frontiers

ISSN 1664-8714
ISBN 978-2-83250-063-7
DOI 10.3389/978-2-83250-063-7

About Frontiers

Frontiers is more than just an open-access publisher of scholarly articles: it is a pioneering approach to the world of academia, radically improving the way scholarly research is managed. The grand vision of Frontiers is a world where all people have an equal opportunity to seek, share and generate knowledge. Frontiers provides immediate and permanent online open access to all its publications, but this alone is not enough to realize our grand goals.

Frontiers Journal Series

The Frontiers Journal Series is a multi-tier and interdisciplinary set of open-access, online journals, promising a paradigm shift from the current review, selection and dissemination processes in academic publishing. All Frontiers journals are driven by researchers for researchers; therefore, they constitute a service to the scholarly community. At the same time, the Frontiers Journal Series operates on a revolutionary invention, the tiered publishing system, initially addressing specific communities of scholars, and gradually climbing up to broader public understanding, thus serving the interests of the lay society, too.

Dedication to Quality

Each Frontiers article is a landmark of the highest quality, thanks to genuinely collaborative interactions between authors and review editors, who include some of the world's best academicians. Research must be certified by peers before entering a stream of knowledge that may eventually reach the public - and shape society; therefore, Frontiers only applies the most rigorous and unbiased reviews.
Frontiers revolutionizes research publishing by freely delivering the most outstanding research, evaluated with no bias from both the academic and social point of view. By applying the most advanced information technologies, Frontiers is catapulting scholarly publishing into a new generation.

What are Frontiers Research Topics?

Frontiers Research Topics are very popular trademarks of the Frontiers Journals Series: they are collections of at least ten articles, all centered on a particular subject. With their unique mix of varied contributions from Original Research to Review Articles, Frontiers Research Topics unify the most influential researchers, the latest key findings and historical advances in a hot research area! Find out more on how to host your own Frontiers Research Topic or contribute to one as an author by contacting the Frontiers Editorial Office: frontiersin.org/about/contact

SYNTHETIC BIOLOGY FOR THE SUSTAINABLE PRODUCTION OF BIOCHEMICALS IN ENGINEERED MICROBES

Topic Editors:
Shuobo Shi, Beijing University of Chemical Technology, China
Jingyu Wang, Westlake Institute for Advanced Study (WIAS), China
Hua Ling, Wilmar International, Singapore

Citation: Shi, S., Wang, J., Ling, H., eds. (2022). Synthetic Biology for the Sustainable Production of Biochemicals in Engineered Microbes. Lausanne: Frontiers Media SA. doi: 10.3389/978-2-83250-063-7

Table of Contents

frontiers | Frontiers in Bioengineering and Biotechnology

TYPE Editorial
PUBLISHED 15 August 2022
DOI 10.3389/fbioe.2022.984875

OPEN ACCESS

EDITED AND REVIEWED BY
Jean Marie François,
Institut Biotechnologique de Toulouse (INSA), France

*CORRESPONDENCE
Shuobo Shi,
shishuobo@mail.buct.edu.cn
Jingyu Wang,
wangjingyu@westlake.edu.cn
Hua Ling,
linghua.cqcn@gmail.com

†PRESENT ADDRESS
Wilmar Innovation Centre,
Wilmar International Limited, Singapore, Singapore

SPECIALTY SECTION
This article was submitted to Synthetic Biology, a section of the journal Frontiers in Bioengineering and Biotechnology

RECEIVED 02 July 2022
ACCEPTED 12 July 2022
PUBLISHED 15 August 2022

CITATION
Shi S, Wang J and Ling H (2022), Editorial: Synthetic biology for the sustainable production of biochemicals in engineered microbes.
Front. Bioeng. Biotechnol. 10:984875.
doi: 10.3389/fbioe.2022.984875

Editorial: Synthetic biology for the sustainable production of biochemicals in engineered microbes

Shuobo Shi[1]*, Jingyu Wang[2]* and Hua Ling[3,4,5,6]*†

[1]Beijing Advanced Innovation Center for Soft Matter Science and Engineering, College of Life Science and Technology, Beijing University of Chemical Technology, Beijing, China, [2]School of Engineering, Westlake University, Hangzhou, China, [3]NUS Synthetic Biology for Clinical and Technological Innovation (SynCTI), National University of Singapore, Singapore, Singapore, [4]Synthetic Biology Translational Research Programme, Yong Loo Lin School of Medicine, National University of Singapore, Singapore, Singapore, [5]Department of Biochemistry, Yong Loo Lin School of Medicine, National University of Singapore, Singapore, Singapore, [6]Wilmar-NUS Corporate Laboratory (WIL@NUS), National University of Singapore, Singapore, Singapore

KEYWORDS

synthetic biology, cell factory, biochemical, metabolic engineering, CRISPR-Cas, biosensor, carbon fixation

Editorial on the Research Topic
Synthetic biology for the sustainable production of biochemicals in engineered microbes

The rapid increase in greenhouse gas (GHG) emission due to the extensive use of fossil resources has necessitated the production of renewable energies and chemicals to sustain the current economic activities while realigning the carbon balance. In particular, the microbial production of biochemicals has provided an attractive route to alleviate the current energy crisis and global climate change. In the past, engineering strategies such as random mutagenesis and conventional selection have long been used for strain development, which is time consuming and at low efficiency. In a fast and efficient manner, synthetic biology approaches are poised to revolutionize strain development for biochemical production in several aspects, including design of non-natural biosynthetic pathways, modular pathway assembly, dynamic sensing and regulation, compartmentalization, pathway balancing and rewiring, cofactor engineering as well as high-throughput screening of biological analytes. This Research Topic brings a collection of recent advances in the development of microbial cell factories for biochemical production using various synthetic biology approaches. Briefly, a general description and summary of the articles in this topic can be found below.

Escherichia coli and *Saccharomyces cerevisiae* are now considered the two most attractive microbial cell factories. Masuo et al. engineered *E. coli* for the *de novo* production of raspberry ketone from a simple carbon source with the strategy of increasing the metabolic precursors tyrosine and *p*-coumaric acid. Qin et al. enabled the production of D-penyllactic acid in engineered *E. coli* via fusion protein engineering for an artificial redox self-equilibrium system.

In *S. cerevisiae*, Jiang et al. reported that three new target genes *AtGRP7*, *AtMSBP1*, and *AtCOL4* could improve the functional expression of two cytochrome P450 enzymes, CYP76AD1 and CYP736A167. This finding was used to enhance the production of betaxanthin by 1.36-fold and Z-α-santalol by 1.97-fold. Zou et al. reported the effects of the unfolded protein response (UPR) and the metabolic burden in two host strains of yeast. Their results showed that the host strain *S. cerevisiae* W303-1A had better capacity to produce secretory protein, β-glucosidase, which will greatly facilitate the fermentation process from cheap cellobiose feedstock. Raajaraam and Raman proposed an algorithm to optimize co-production of multiple metabolites. This tool was combined with the use of genome-scale metabolic models of *E. coli* and *S. cerevisiae* and aided the design of metabolic engineering strategies.

Non-conventional microbes show many unique physiological and biochemical characteristics and have been developed as new microbial chassis in the synthetic biology era. Yang et al. expressed *Abies grandis* pinene synthase in the cyanobacterium *Synechococcus* sp. PCC 7002 and the engineered cyanobacteria achieved the production of pinene directly from CO_2. Chang et al. explored *Corynebacterium glutamicum* as a host for efficient 3-hydroxypropionic acid production from acetate by regulating the malonyl-CoA pathway. Rong et al. constructed an engineered *Yarrowia lipolytica* for itaconic acid production from waste cooking oil by expressing cis-aconitic acid decarboxylase. They then investigated the impact of the acetyl-CoA biosynthesis pathway on itaconic acid production.

In some cases, completion of complex tasks within a single organism is extremely challenging. Zhu et al. built an artificial microbial consortium composed of engineered *E. coli* and *Pseudomonas putida* using a strategy named 'nutrition supply-detoxification'. This co-culture system maximized the advantages of both strains, enabling efficient accumulation of medium-chain-length polyhydroxyalkanoate from glucose–xylose mixtures.

A complex synthetic cell factory is usually composed of many functional components. Now, identification and characterization of basic or improved genetic elements plays a key role in biotechnological and synthetic biology applications. Tong et al. found a variant of amine dehydrogenase via combinatorial active-site saturation test/iterative saturation mutagenesis, and the variant showed a significant improved activity in *E. coli*, which facilitated the biosynthesis of enantiopure amino alcohols. Zou et al. characterized the activity of a putative UDP-glucose 4-epimerase (UGE) in both *E. coli* and *S. cerevisiae*. This work identified its multiple functions in the production of polysaccharides as well as in the formation of structures and activity of polysaccharides, which provided a guide for future biomanufacturing of polysaccharides. Miyake et al. first constructed and optimized a biosensor for short branched-chain fatty acids (SBCFAs) in *S. cerevisiae*, providing the possibility for high-throughput screening of improved producers of SBCFAs. In parallel, a rapid assembly of genetic elements forms the cornerstone in the implementation of synthetic biology designs. Li et al. developed an effective DNA assembly approach that can be applied for NHEJ-based integration in *Y. lipolytica*. This method was subsequently used to optimize the mevalonate pathway for (-)-α-bisabolol production.

Of equal importance, several experts discussed current challenges and future trends in harnessing synthetic biology for the sustainable production of biochemicals in engineered microbes. Feng et al. reviewed how synthetic biology significantly accelerated the development of microbial cell factories for resveratrol, and systematically summarized recent achievements in resveratrol production. Jiang et al. gave a detailed summary of the 5-aminolevulinic acid synthesis in microbial cells, and proposed perspectives for further improvement. Meanwhile, they reviewed the applications and detection methods of 5-aminolevulinic acid. Yu et al. provided an overview of advances in the development and application of CRISPR-Cas systems in C1 metabolizing microorganisms and envisioned various Cas9 variant proteins or effectors, which can be implemented for more powerful genome engineering to promote carbon-negative microbial manufacturing.

This Research Topic presents fabulous examples for the sustainable and cost-effective production of biochemicals in microbial cell factories. As a revolutionary technology, advancing synthetic biology strategies has greatly assisted the strain creation process, maximizing the metabolic pathway of certain microorganisms. However, more advanced tools, especially for non-conventional microbes are in urgent need and insufficient for the relative applications. Furthermore, the discovery or engineering of more functional elements is expected to play significant roles in design and development of complex natural or non-natural biosystems for chemical production.

Author contributions

SS wrote the manuscript. JW and HL revised the manuscript. All authors approved the manuscript.

Funding

This work was supported by the Tianjin Synthetic Biotechnology Innovation Capacity Improvement Project (TSBICIP-KJGG-009).

Acknowledgments

The editors appreciate the contribution of all authors to this Research Topic, the constructive comment of all the reviewers,

and the editorial support from Frontiers throughout the publication process.

Conflict of interest

The authors declare that the research was conducted in the absence of any commercial or financial relationships that could be construed as a potential conflict of interest.

Publisher's note

frontiers in Bioengineering and Biotechnology

ORIGINAL RESEARCH
published: 25 November 2021
doi: 10.3389/fbioe.2021.796278

Characterization and Heterologous Expression of UDP-Glucose 4-Epimerase From a *Hericium erinaceus* Mutant with High Polysaccharide Production

Gen Zou[1†], *Juanbao Ren*[1,2†], *Di Wu*[1], *Henan Zhang*[1], *Ming Gong*[1], *Wen Li*[1], *Jingsong Zhang*[1] *and Yan Yang*[1*]

[1]National Engineering Research Center of Edible Fungi, Institute of Edible Fungi, Shanghai Academy of Agricultural Sciences, Shanghai, China, [2]College of Food Sciences and Technology, Shanghai Ocean University, Shanghai, China

OPEN ACCESS

Edited by:
Shuobo Shi,
Beijing University of Chemical Technology, China

Reviewed by:
Fengjie Cui,
Jiangsu University, China
Limin Cao,
Capital Normal University, China
Wenjing Sun,
Jiangsu University, China

***Correspondence:**
Yan Yang
yangyan@saas.sh.cn

[†]These authors have contributed equally to this work

Specialty section:
This article was submitted to Synthetic Biology, a section of the journal Frontiers in Bioengineering and Biotechnology

Received: 16 October 2021
Accepted: 03 November 2021
Published: 25 November 2021

Citation:
Zou G, Ren J, Wu D, Zhang H, Gong M, Li W, Zhang J and Yang Y (2021) Characterization and Heterologous Expression of UDP-Glucose 4-Epimerase From a Hericium erinaceus Mutant with High Polysaccharide Production. Front. Bioeng. Biotechnol. 9:796278. doi: 10.3389/fbioe.2021.796278

Hericium erinaceus is an important medicinal fungus in traditional Chinese medicine because of its polysaccharides and other natural products. Compared terpenoids and polyketides, the analysis of synthetic pathway of polysaccharides is more difficult because of the many genes involved in central metabolism. In previous studies, *A6180*, encoding a putative UDP-glucose 4-epimerase (UGE) in an *H. erinaceus* mutant with high production of active polysaccharides, was significantly upregulated. Since there is no reliable genetic manipulation technology for *H. erinaceus*, we employed *Escherichia coli* and *Saccharomyces cerevisiae* to study the function and activity of A6180. The recombinant overexpression vector pET22b-A6180 was constructed for heterologous expression in *E. coli*. The enzymatic properties of the recombinant protein were investigated. It showed that the recombinant A6180 could strongly convert UDP-α-D-glucose into UDP-α-D-galactose under optimal conditions (pH 6.0, 30°C). In addition, when *A6180* was introduced into *S. cerevisiae* BY4742, xylose was detected in the polysaccharide composition of the yeast transformant. This suggested that the protein coded by *A6180* might be a multifunctional enzyme. The generated polysaccharides with a new composition of sugars showed enhanced macrophage activity *in vitro*. These results indicate that A6180 plays an important role in the structure and activity of polysaccharides. It is a promising strategy for producing polysaccharides with higher activity by introducing *A6180* into polysaccharide-producing mushrooms.

Keywords: polysaccharide synthesis, heterologous expression, immune activity, enzymatic properties, polysaccharide, *Hericium erinaceus*

INTRODUCTION

Hericium erinaceus, which grows widely in the mountains of eastern Asia, is a valuable fungus for both medicinal and food use and has a long history in the field of medicine in China. Polysaccharides, the main active substance of *H. erinaceus*, have high biological activity, such as immunomodulation (Wu et al., 2019; Nowak et al., 2020), regulation of glucolipid metabolism (Du et al., 2015; Cai et al., 2020), hypolipidemia (Liang et al., 2013), anti -tumor properties (Zeng and Zhu, 2018; Zhang et al.,

2021), anti-fatigue properties (Liu et al., 2015), liver protection, and stomach protection (Chen et al., 2020). They have also been widely used in medicine (Li et al., 2018; Jithendra et al., 2020), materials (Low et al., 2015), cosmetics, and other fields. Due to the large number of key enzymes involved in the synthesis of polysaccharides and their unknown characteristics, the synthesis pathway of *H. erinaceus* polysaccharides has not been clearly clarified. In our previous study, two mutant strains with high polysaccharide production of *H. erinaceus* were bred by atmospheric pressure room temperature plasma (ARTP) mutagenesis, and polysaccharide production was significantly enhanced, compared with the original strain (Zhu et al., 2019). Through multi-omics analysis, the increased carbohydrate metabolism and the production of glucose-6-phosphate constituted the basis of high polysaccharide yield. The differentially expressed proteins A6180 involved in the mushroom polysaccharide biosynthetic pathways occurred in the mutant strain compared with the original strain, which belonged to GAL10 (UDP-glucose-4-epimerase) involved in the synthesis of polysaccharide repeat units, and upregulated mRNA and protein expression based on transcriptome and proteomics data (Gong et al., 2021). Upregulation of the A6180 gene is known to be involved in the biosynthesis of polysaccharide repeat units, which is associated with the higher yield of polysaccharides in the mutated strains. However, the function of this gene still needs to be verified through genetic engineering technology.

Using the method of gene overexpression is an important approach to analyze gene function. For example, Jesus et al. constructed recombinant overexpressed strains and homologous overexpressed BL23 gene (encoding UGP) in *Lactobacillus casei*. In the subsequent enzyme activity detection, it was found that the enzyme activity of *L. casei* increased by approximately 70 times, and the concentration of UDP-Glu increased by 8.5 times. Therefore, it is inferred that the BL23 gene is a key gene in the UDP-glucose synthesis pathway (Rodriguez-Diaz and Yebra, 2011).

Since genetic manipulation techniques in most macro fungi are not sophisticated, it is difficult to investigate the function of a gene by knockout or overexpression of a nativegene. Therefore, genetic verification in heterologous or model microorganisms can more effectively detect the functions of target genes (Bachmann et al., 2014). *Escherichia coli* and *Saccharomyces cerevisiae*, as typical eukaryotic model organisms and microbial cell factories, have been widely used in metabolic engineering, system biology, and synthetic biology. For example, *S. cerevisiae* cannot directly use xylan as a carbon source, and strains with high expression can be obtained by integrating xylanase with high enzyme activity into the *S. cerevisiae* genome by means of molecular biology (Lu et al., 2017; Wang et al., 2017). Researchers (Biely et al., 2000) expressed the Xyn2 gene of *Trichoderma reesei* in *S. cerevisiae* using different promoters, *ADH2* and *PGK1*, and the enzyme activity was 200 and 160 nkat/ml. Besides, the *de novo* synthesis pathway of m-cresol was constructed from *S. cerevisiae* glucose by introducing the heterologous pathway of 6-MSA (Hitschler and Boles, 2019). The high yield of emodin reached 528.4 mg/L in *S. cerevisiae* BJ5464-NPGA by heterologous reconstruction of the biosynthesis pathway of endorphin and emodin (Sun et al., 2019).

In this study, *E. coli* and *S. cerevisiae* were used as heterologously expressing chassis organisms to further verify the biological function of the gene *A6180*, which is closely related to high polysaccharide production in *H. erinaceus*. The *A6180* gene clone and different recombinant overexpression vector constructs for heterologous expression will be further studied to find out the functional role of this gene in polysaccharide synthesis. The enzyme properties of the protein expressed by the *A6180* gene were studied to provide a theoretical reference for later development and utilization.

MATERIALS AND METHODS

Strain and Plasmids

The experimental strain used in this study was *H. erinaceus* 321, preserved at the Institute of Edible Mushrooms, Shanghai Academy of Agricultural Sciences. Plasmid pET-22b (+) cells were preserved in our laboratory. *E. coli* strains TOP10 and BL21 (DE3) competent cells were purchased from Weidi Biotechnology (Shanghai, China). *S. cerevisiae* BY4742 was purchased from Zoman Biotechnology (Beijing, China). The pESC-Leu plasmid was purchased from TIANDZ Gene Technology (Beijing, China). To construct the heterologous expression vector, the mycelium of *H. erinaceus* was scraped and total RNA was extracted using TRIzol RNA Isolation Reagents (TAKARA) kit, followed by Hifair TM II 1st Strand cDNA Synthesis Kit (YEASEN, Shanghai, China). The obtained cDNA was used as a template for amplification of the *A6180* coding sequence. Yeast genomic DNA was extracted from cultured *Saccharomyces cerevisiae* BY4742 using the Plant Genomic DNA Extraction Kit (TIANGEN, Beijing, China). The extracted gDNA was used as a template for amplification of the *TDH3* promoter. Primers A6180EC-F and A6180EC-R were designed to amplify the *A6180* gene fragment using Primer Premier 5.0 based on the results of whole genome sequencing of *H. erinaceus* 321, and all the primer sequences used in this study are shown in **Table 1**. The PCR amplification procedure for the *A6180* target gene was as follows: 3 min at 98°C; 30 cycles of 98°C for 10 s, 58°C for 20 s, 72°C for 80 s; and a final extension at 72°C for 5 min. The pET-22b (+) vector was amplified with restriction endonucleases (QuickCut Nde I and Xho I; TAKARA, Dalian, China). Double digestion was performed, followed by the construction of the recombinant vector (pET22b-A6180) using the Hieff Clone® Plus Multi One Step Cloning Kit (YEASEN) kit.

Expressing *A6180* in *E. coli* BL21

The constructed vector harboring *A6180* (pET22b-A6180) was propagated in TOP10. For heterologous expression of recombinant proteins in *E. coli*, pET22b-A6180 was transformed into *E. coli* BL21 (DE3) competent cells. Positive colonies were screened using ampicillin and designated as BL21-A6180. To obtain sufficient recombinant protein, the optimal induction conditions were tested at different temperatures (15°C

TABLE 1 | Primer design of the *Hericium erinaceus A6180* gene and related functional fragment.

Primer	Sequence (5′-3′)	Descriptions
A6180EC-F	AACTTTAAGAAGGAGATATACATATGGCTGTTGCCGATACCTC	For full-length *A6180*
A6180EC-R	TCAGTGGTGGTGGTGGTGGTGCTCGAGCTTGGACTCGGTATCGTAGCCG	
A6180SC-F	CACACATAAACAAACAAAGCGGCCGCATGGCTGTCGCTGATACCTCTCT	For full-length *A6180*
A6180SC-R	CCTTGTAATCCATCGATACTAGTTCAATGATGATGATGATGCTTCGACTCGGTATCGTATCCATTC	
TDH3-F	AACCCTCACTAAAGGCATATGATACTAGCGTTGAATGTTAGCGTC	For full-length *TDH3* promoter
TDH3-R	ATCAGCGACAGCCATGCGGCCGCTTTGTTTGTTTATGTGTGTTTATTC	

and 37°C) with various doses of isopropyl-β-D-thiogalactopyranoside (IPTG) (1.0 and 0.2 mmol/L). The recombinant protein was purified using a His-tagged protein purification kit (Beyotime, Shanghai, China) for assays of enzymatic properties.

Determination of Enzymatic Properties of Recombinant Protein

High performance liquid chromatography (HPLC) was employed to evaluate the recombinant putative UGE by detecting the conversion rate of UDP-α-D-glucose (UDP-Glu) into UDP-α-D-galactose (UDP-Gal) (Goulard et al., 2001). Thereafter, to study the enzymatic properties of recombinant UGE proteins, such as optimum pH and temperature. In optimal pH assay, different buffers including 10 mM citric acid-sodium citrate buffer (pH 3.0, 4.0, 5.0, and 6.0), 10 mM Tris-HCl buffer (pH 7.0, 8.0 and 9.0), 10 mM sodium carbonate-sodium hydroxide buffer (pH 10.0, and 11.0) were prepared for reaction at 35°C for 1 h. In optimal temperature assay, the enzyme reaction mixture was incubated at different temperatures (15°C, 20°C, 25°C, 30°C, 35°C, 40°C, 45°C, 50°C, and 55°C) for 1 h at optimal pH. In order to determine the effect of different ions on UGE activity, 1.0 mM ions were respectively added into the reaction system, including K^+, Ni^{2+}, Mg^{2+}, Ba^{2+}, Ca^{2+}, Cu^{2+}, Co^{2+}, and Fe^{3+}. The optimal separation conditions were: Athena NH_2 (250 mm × 4.6 mm, 5 μm); mobile phase: KH_2PO_4 buffer (0.125 mol/L, pH 3.6): ethanol = 40:60 (v:v); column temperature: 30°C; flow rate: 1.0 ml/min; detector: UV absorption detector; detection wavelength: 254 nm; injection volume: 20 μL. One unit of enzyme activity is defined as the amount of enzyme required to convert 1 μmol of substrate UDP-Glu in 1 min.

Transforming *A6180* Into *S. cerevisiae*

Saccharomyces cerevisiae competent cells were prepared using the Super Yeast Transformation Kit (Coolaber). The recombinant vector pESC-Leu-A6180 was transformed into *S. cerevisiae* according to the manufacturer's instructions. Positive transformants were screened by PCR and designated as BY4742-A6180. Western blotting was used to further verify the correct expression of the protein encoded by *A6180* (**Supplementary Data S1**). Yeast cells were harvested after 24 h incubation in yeast extract peptone dextrose medium (YPD) (1% yeast extract, 2% peptone, and 2% dextrose) at 28°C and 160 r/min. The collected cells were frozen in liquid nitrogen and ground in a mortar with a pestle. The intracellular protein was extracted using RIPA lysis buffer (Yeasen) for western blotting. In the fermentation assay, all the *S. cerevisiae* strains were inoculated in 4 ml YPD for 18 h at 28°C and 160 r/min. One milliliter of culture suspension was used as a seed to transfer into 100 ml YPD for scale-up fermentation on different culture days (28°C 160 r/min).

Yeast Polysaccharide Extraction and *in vitro* Immune Activity Evaluation

Yeast cells were collected by centrifuging day 1–9 of fermentation. The precipitates were washed with distilled water and freeze-dried to obtain dried cell debris. The polysaccharides of yeast cells were extracted and determined according to a previously reported method (Zhang et al., 2021). The β-glucan content of polysaccharides was determined using β-glucan assay kits provided by Megazyme International Ireland Limited (yeast and mushroom). The polysaccharide samples were hydrolyzed and analyzed by HPAEC system (Dionex ICS-2500, Dionex, Sunnyvale, CA, United States) equipped with a CarboPac™ PA20 column (Dionex, Sunnyvale, CA, United States) for monosaccharide composition testing according to the reference (Jiang et al., 2016). The generated polysaccharide solution was dialyzed (with a molecular weight of 3.0 kDa intercepted) by distilled water for 48 h and then freeze-dried. The freeze-dried sample was prepared into a 5 mg/ml original liquor with PBS (phosphate-buffered saline, pH 7.4) solution and centrifuged at 12,000 × *g* for 30 min. The supernatant was diluted to 0.5, 2.0, and 5.0 mg/ml for cell testing (final concentrations in cell culture medium were 50, 200, and 500 μg/ml, respectively). The *in vitro* immune activity of the dialyzed polysaccharide samples was studied by measuring the NO production of RAW264.7, according to the previous report (Wu et al., 2019), and the *in vitro* immunoactivity was assessed based on the amount of NO released.

Statistical Analysis

Statistical analysis was carried out using SPSS 26.0 software (SPSS Inc., Chicago, United States). A probability level of $p < 0.05$ was set as statistical significance. Data of the NO production of RAW264.7were presented as mean ± standard deviation (SD) of at least three independent experiments.

RESULTS

A6180 Contains a Typical UGE Domain

To understand the functions of the protein encoded by *A6180*, a neighbor-joining phylogenetic tree was established to analyze the evolutionary relationships of fungi, including Ascomycetes and

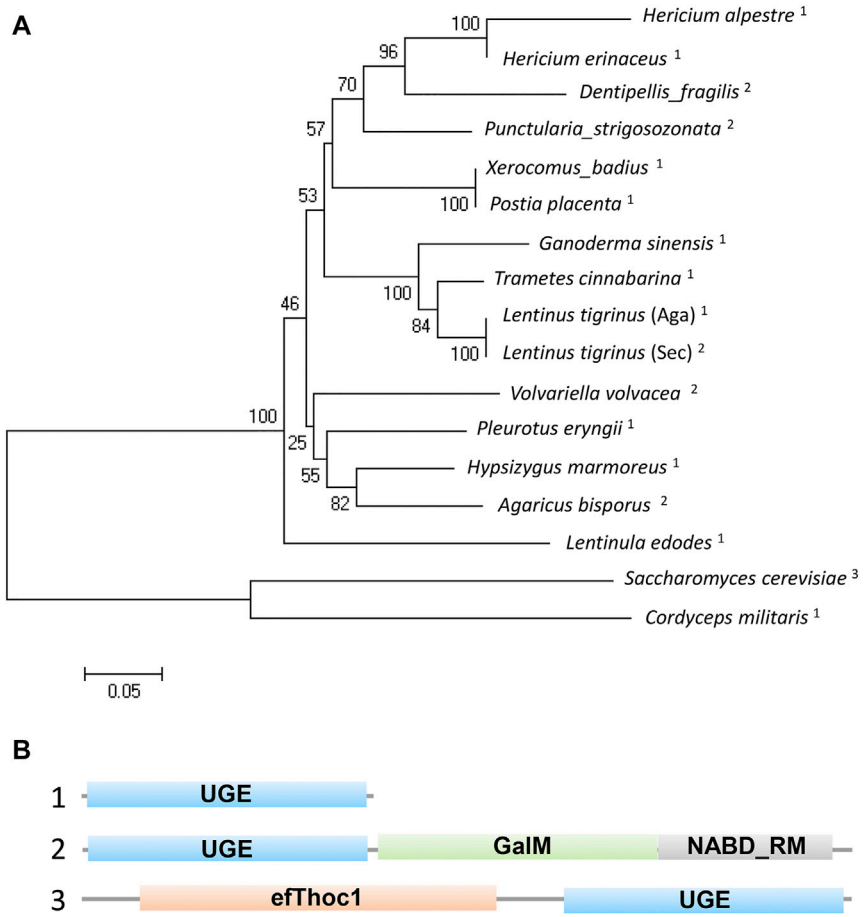

FIGURE 1 | Phylogenetic and structural analysis of UDP-glucose-4-epimerases in fungi. **(A)** Phylogenetic analysis of UDP-glucose-4-epimerases of fungi including: *Hericium erinaceus* (DATA S1), *H. alpestre* (accession no. TFY78463.1), *Dentipellis_fragilis* (accession no. TFY62748.1), *Punctularia_strigosozonata* (accession no. XP_009540529.1), *Xerocomus_badius* (accession no. KAF8559888.1), *Postia_placenta* (accession no. KAF8559888.1), *Ganoderma_sinensis_ZZ*0214-1 (accession no. PIL31081.1), *Trametes_cinnabarina* (accession no. CDO77294.1), *Lentinus_tigrinus_*(Aga) (accession no. RPD64555.1), *Lentinus_tigrinus_*(Sec) (accession no. RPD82942.1), *Volvariella_volvacea_*(accession no. KAF8665304.1) *Pleurotus_eryngii_*(accession no. KDQ31371.1), *Hypsizygus_marmoreus* (accession no. RDB19506.1), *Agaricus_bisporus* (accession no. XP_006454268.1), *Lentinula_edodes* (accession no. GAW00910.1), *Saccharomyces_cerevisiae* (accession no. AJQ11874.1:), and *Cordyceps_militaris* (accession no. XP_006672787.1). A neighbor-joining tree was built using MEGA5.0 and the bootstrap method with 1000 replicates. The superscript numbers represent three types of orthologs shown in B. **(B)** The structural functional domain analysis of UDP-glucose-4-epimerases. 1) Typical UGE with unique functional domain. 2) A yeast UGE containing N-terminal epimerase domain and a C-terminal mutarotase domain. 3) An exclusive UGE to basidiomycetes containing N-terminal THO complex subunit 1 transcription elongation factor domain and C-terminal epimerase domain.

Basidiomycetes. The results showed that *H. erinaceus* was close to the fungus *H. alpestre* (**Figure 1A**). Intriguingly, the ortholog in *Dentipellis fragilis* was also closely related to *A6180*, although it was incorporated with an N-terminal THO complex subunit 1 transcription elongation factor domain and a C-terminal epimrase domain (**Figure 1B**). In *S. cerevisiae*, the ortholog protein Gal10P contains a galactose mutarotase domain (**Figure 1B**). Thus, the orthologs of UDP-glucose-4-epimerases in fungi are classified into three forms with distinct protein structures (**Figure 1B**). Based on sequence alignment in the SWISS-MODLE server (https://swissmodel.expasy.org/), the crystal structure of UDP-glucose-4-epimerases of *Burkholderia pseudomallei* (PDB ID: 3enk.1) was chosen as the template, and the tertiary structure of *A6180* was modeled using the SWISS-MODLE server (**Figure 2**). Combined with the prediction of conserved domains on NCBI, *A6180* was predicted to be a homodimeric UDP-glucose-4-epimerases catalyzing the NAD-dependent interconversion of UDP-galactose and UDP-glucose (**Figure 2A**). It has an N-form catalytic tetrad composed of residues N126, S150, Y174, and K178 (**Figure 2B**). Twenty-one residues (G16, A18, G19, Y20, I21, C80, D81, L82, V106, A107, A108, K110, N125, S148, S149, S150, Y174, K178, Y203, F204, and P206) were predicted as NAD binding sites (**Figure 2C**) and eighteen residues were substrate binding sites (S150, A151, T152, Y174, Y203, F204, N205, G222, N225, L226, L243, K244, V245, F246, C257, R259, Y260, and V307) (**Figure 2D**). These regions were so close that some of the residues overlapped, such as S150, Y174, and Y178. In the

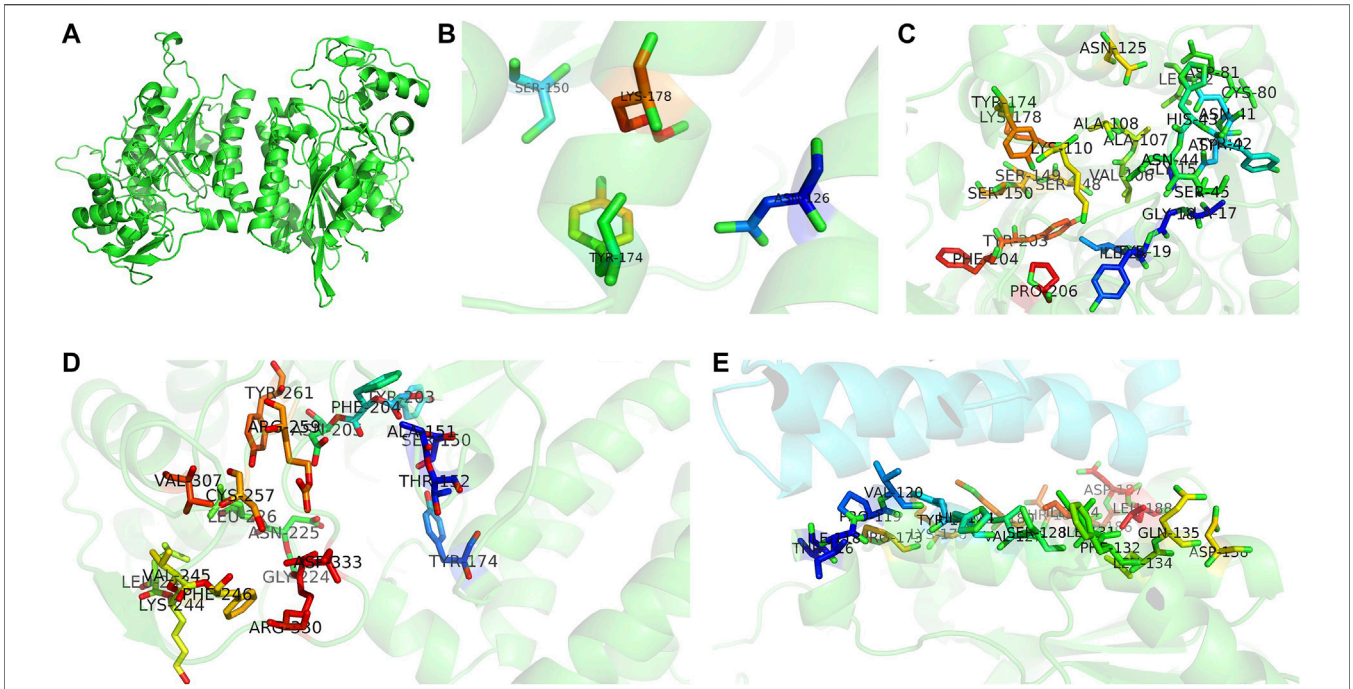

FIGURE 2 | Three-dimensional structures of UDP-glucose-4-epimerases in *H. erinaceus*. **(A)** Homodimer was developed by homology modeling. **(B)** Active sites (N126, S150, Y174, K178) were illustrated in colored sticks. **(C)** NAD binding sites of *H. erinaceus* UGE were shown in colored sticks (G16, A18, G19, Y20, I21, C80, D81, L82, V106, A107, A108, K110, N125, S148, S149, S150, Y174, K178, Y203, F204, and P206). **(D)** Homology modeling of substrate binding sites (S150, A151,T152, Y174, Y203, F204, N205, G222, N225, L226, L243, K244, V245, F246, C257, R259, Y260, and V307). **(E)** Monomer interactions caused by peptide binding sites in homodimer interface (T116, I118, P119, V120, Y123, H124, V127, S128, I131, F132, L134, Q135, D138, P173, K176, M180, T183. I184, D186. D187, and L188). All models were generated by PyMOL.

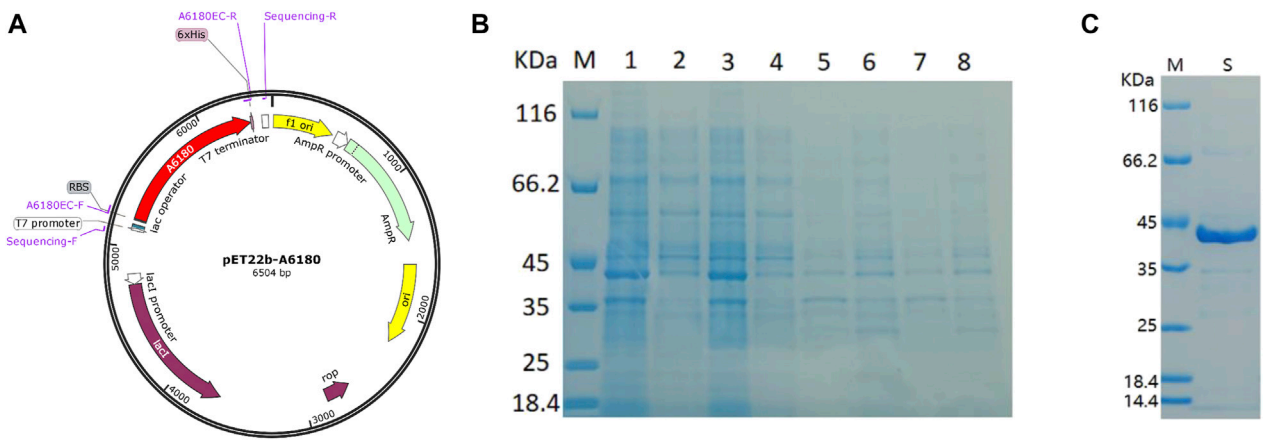

FIGURE 3 | Heterologous expression of A6180 in *E. coli*. **(A)** Schematic diagram of the construction of recombinant overexpression vector. **(B)** SDS-PAGE analysis of the protein expression of positive transformants under the four inductive expression conditions. M: protein marker; 1: 37°C 1.0 mmol/L IPTG induced precipitation; 2: 37°C 1.0 mmol/L IPTG induced supernatant sample; 3: 37°C 0.2 mmol/L IPTG induced precipitation sample; 4: 37°C 0.2 mmol/L IPTG induced supernatant sample; 5: 15°C 1.0 mmol/L IPTG induced precipitation sample; 6: 15°C 1.0 supernatant sample after induction of mmol/L IPTG; 7: precipitation sample after induction of 0.2 mmol/L IPTG at 15°C; 8: sample of supernatant after induction of 0.2 mmol/L IPTG at 15°C. **(C)** Purified recombinant protein expressed in *E. coli*. M: marker; S: Purified protein.

intermediate region of the homodimer, polypeptide binding motif (constituted by T116, I118, P119, V120, Y123, H124, V127, S128, I131, F132, L134, Q135, D138, P173, K176, M180, and T183. I184, D186. D187, and L188) were located in the α-helix (**Figure 2E**). This indicated that the monomers interacted to form homodimers.

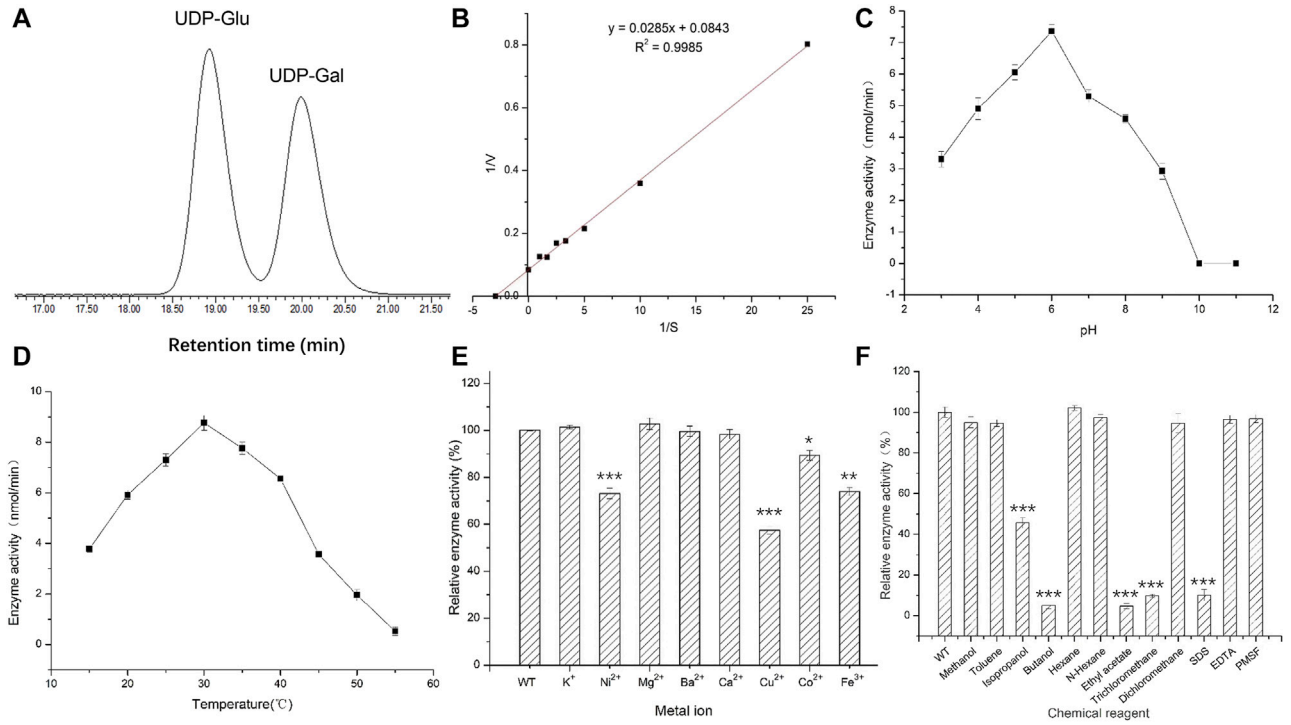

FIGURE 4 | Activities of recombinant protein expressed in *E. coli*. **(A)** High performance liquid chromatography detection separation UDP-Glu and UDP-Gal. Peak 1: UDP-Glu; Peak 2: UDP-Gal. **(B)** Double reciprocal graph. **(C)** Optimal pH for activity. **(D)** Optimal temperature for activity. **(E)** The effect of metal ions on enzyme activity. **(F)** The effect of chemical reagents on enzyme activity.

A6180 Is Highly Expressed in *E. coli*

The *E. coli* heterologous expression system is a reliable tool for characterizing protein function. Thus, *A6180* fragments were ligated into the pET22b (+) vector for protein expression. A schematic of the recombinant overexpression vector construction is shown in **Figure 3A**. The selected positive clones were cultured under various culture conditions. Crude extracts of cultured cell debris were verified by SDS-PAGE. The full-length recombinant putative UGE had a predicted molecular weight of 41.7 kD with 379 amino acids. SDS–PAGE analysis indicated that recombinant UGE was expressed under all the test conditions. Among these, the highest yield of recombinant protein was observed in precipitates and supernatants when the clones were induced by 1.0 mmol/L IPTG at 37°C (**Figure 3B**). Although most of the recombinant proteins existed as inclusion bodies in the precipitate under these conditions, the recombinant proteins in the supernatant were also the highest of all the tested conditions. Thus, *E. coli* cells were harvested from 2 L of culture suspension after 4 h of induction with 1.0 mmol/L IPTG at 37°C. Finally, the SDS-PAGE purified samples of recombinant UGE protein were analyzed using Quantity One gel analysis software, which showed that the target protein reached 95% purity (**Figure 3C**).

Enzyme Activity Characteristics Show *A6180* Is a Real UGE

The optimum chromatographic conditions were selected for the detection and separation of UDP-Glu and UDP-Gal by screening the mobile phase ratio and flow rate conditions of HPLC. As shown in **Figure 4A**, the absorption peaks of UDP-Glu and UDP-Gal standards appeared at 18.90 min (UDP-Glu) and 20.10 min (UDP-Gal). This indicated that the two standards could be effectively separated under the tested conditions (**Supplementary Figure S1**). The enzymatic reaction rate of UGE was measured for different concentrations of UDP-Glu substrate. The double inverse equation (**Figure 4B**) showed that the V_m of the target protein to UDP-Glu is 11.86 mmol/min and K_m is 0.34 mM. This suggests that *A6180* encodes a real UGE with the activity of converting UDP-Glu into UDP-Gal.

Under the reaction conditions of T = 35°C, the enzymatic activity of UGE protein showed an initial increasing trend and then a decreasing trend with the increase in pH, and had the highest enzymatic activity at pH 6, while the enzymatic activity was basically lost when the pH was 10.0 and 11.0, respectively (**Figure 4C**) (**Supplementary Figure S2**). This indicates that the change in pH affects the rate of enzymatic reaction by affecting the dissociation of the enzyme active center and the substrate of UGE protein, while at pH 10.0 and 11.0, the hyperalkaline state denatures the enzyme protein and thus loses its enzymatic activity.

Under the optimum pH condition for enzymatic hydrolysis, the enzyme activity first increased and then decreased with increasing temperature, and the UGE protein had the highest enzyme activity at a temperature of 30°C, but the enzyme activity decreased rapidly in the range of 35–50°C, and reached 0 at 50°C.

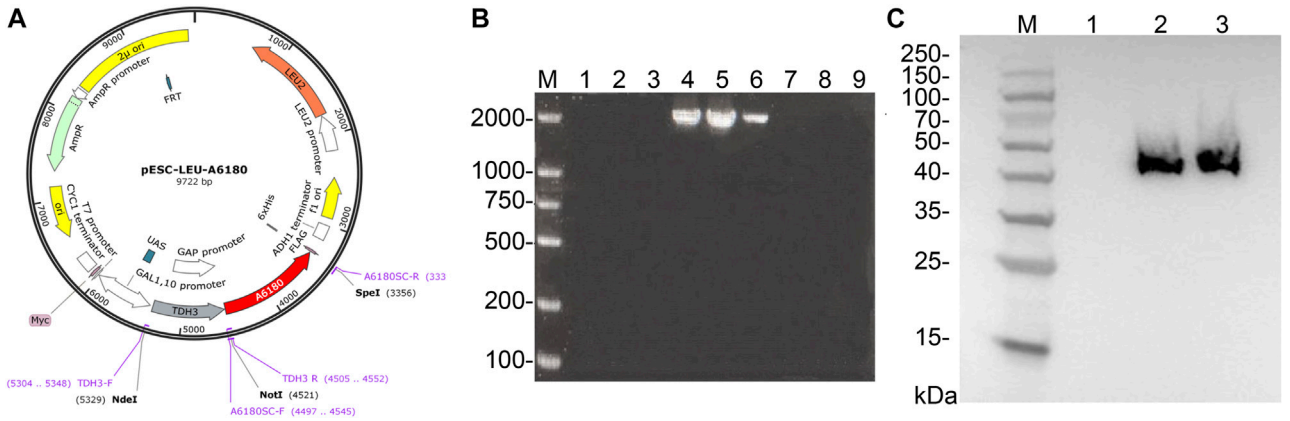

FIGURE 5 | Expression of A6180 in yeast. **(A)** Schematic diagram of the construction of recombinant overexpression vector pESC-Leu-A6180. **(B)** Verification for positive transformants of yeast. M: D2000 Marker; 1–3: blank controls; 4–9: transformants 1–6. **(C)** Western blot results of positive transformants. M: Prestained protein Marker 10–180 kDa; 1: Parent strain. 2–3: Positive transformants.

However, when the temperature was higher than the optimum temperature, the protein gradually denatured and inactivated the enzyme, resulting in a significant decrease in enzyme activity (**Figure 4D**) (**Supplementary Figure S3**).

The general culture conditions for the mycelium of *H. erinaceus* were 26°C and natural pH medium (pH 5.8), and the results of the study also showed that the optimum pH and optimum temperature of UGE were closer to the culture conditions.

Effects of Metal Ions and Organic Reagents on UGE Enzyme Activity

The addition of the same concentration of several metal ions at pH 6 and 30°C produced different effects on enzyme activity. Among them, K^+ and Mg^{2+} had 2.8 and 4% enhancement effects on enzyme activity, while Ni^{2+}, Cu^{2+}, Co^{2+}, and Fe^{3+} showed different degrees of inhibition of enzyme activity, with Cu^{2+} having the most inhibitory effect, reducing the enzyme activity to 58% of the original activity. In contrast, Ba^{2+} and Ca^{2+} had no effect on enzyme activity. This could be attributed to the metal ions combining with the sparse group, sulfur group, or amino group in the target enzyme protein molecule, thus affecting the structure of the active center of the enzyme protein molecule and leading to a reduction in enzyme activity (**Figure 4E**) (**Supplementary Figure S4**).

The different chemical reagents added to the enzyme reaction system at pH 6 and 30°C produced different degrees of inhibition of enzyme activity, with isopropanol, *n*-butanol, ethyl acetate, and trichloromethane, which showed the strongest inhibition of enzyme activity. The reaction enhanced the contact between organic solvents and water molecules through oscillation, resulting in the removal of the hydrophilic residues surrounding the surface of the enzyme protein molecules, causing changes in the spatial configuration of the protein thus reducing the enzyme activity to different degrees. The strong electrostatic interaction between SDS as an anionic surfactant and the enzyme molecule caused a change in enzyme conformation, which led to a significant decrease in enzyme activity (Guo et al., 2006) (**Figure 4F**).

A6180 Expressed in *S. cerevisiae* Constitutively

A schematic diagram of the recombinant overexpression vector is shown in **Figure 5A**. Since the GAL1, GAL10 promoter of the pESC-Leu overexpression vector was repressed in the presence of glucose in the culture medium, the *TDH3* strong promoter of *S. cerevisiae* BY4742, which is not repressed by glucose, was added between the GAL1 and GAL10 promoters and the A6180 target gene, thus enabling stable and efficient expression of the *A6180* target gene in *S. cerevisiae* BY4742. Moreover, a 6×His protein tag coding sequence was fused to the 3′ terminal of *A6180* for Western blot analysis using the responding monoclonal antibody.

PCR was performed on nine randomly selected single colonies, and the results are shown in **Figure 5B**. According to the previous primer design, it can be seen that the results of lanes 4, 5, and 6 are consistent with the expected size and brightness, so the single colonies corresponding to lanes 4, 5, and 6 can be identified as positive transformant single colonies BY4742-A6180.

The total protein of the positive transformant BY4742-A6180 was verified by western blotting, and the results are shown in **Figure 5C**. A clear band at the size of 42 kDa consisted with the size of the target protein expressed by the *A6180* gene predicted by Expasy (https://web.expasy.org/protparam/), which can be determined that the target protein, was normally induced to be expressed in the positive transformant BY4742-A6180 induction group.

Effect of Gene *A6180* Transformation on Physicochemical Properties of *S. cerevisiae* Polysaccharides

The total dextran of yeast polysaccharides in the original and transformed strains is shown in **Figure 6A**, with the blue line for

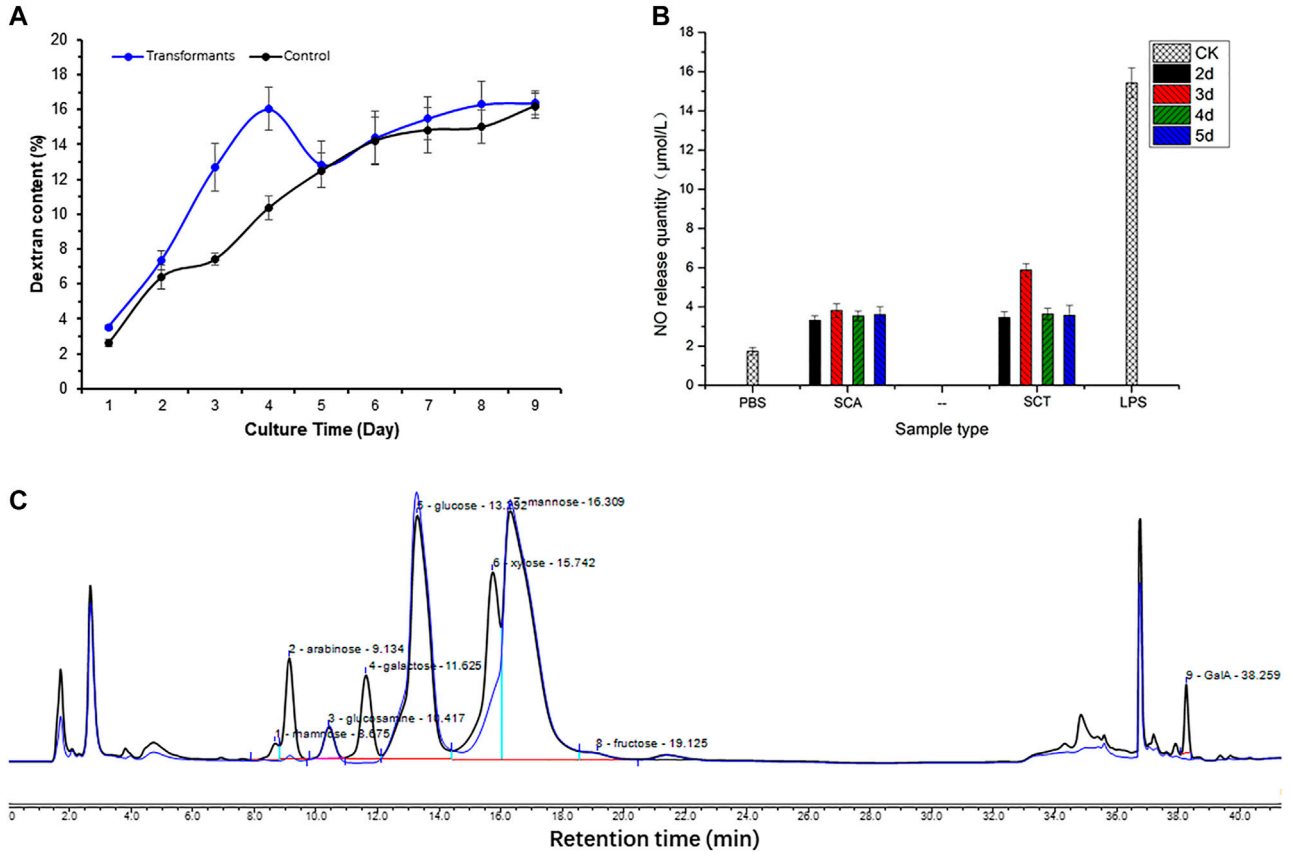

FIGURE 6 | Effect on polysaccharide after expressing A6180 in yeast. **(A)** The trend of glucan in *S. cerevisiae* control group and transformation group. The result of the control group is a blue curve and the result of the transformation group is a black curve. **(B)** Monosaccharide composition results of *S. cerevisiae* control group and transformation group on day 3. The result of the control group can be seen in the blue curve, and the result of the transformation group is present in the black curve. **(C)** Immune activity of polysaccharides from *S. cerevisiae* control group and transformation group. PBS (phosphate-buffered saline): blank control; SCT: polysaccharides from *S. cerevisiae* control group; SCA: polysaccharides from *S. cerevisiae* transformation group; LPS (Lipopolysaccharides): positive control.

the original strain (control group) and the black line for the transformed strain. The dextran content of the control group showed an increasing trend in the first 4 days, while there was a decreasing trend on the fifth day, but it slowly increased and stabilized during the sixth to ninth days. The total dextran content in the transformed and control groups was similar after cultivation for 5 days, but there was an obvious decrease in the transformed strain on the third and fourth days. This indicated that the *A6180* gene became functional on the third and fourth days, and was consistent with the bioinformatics analysis of its function as a UDP-glucose-4-epimerase (EC:5.1.3.2). *The A6180* gene was transformed into yeast by converting UDP-Glu to UDP-Gal, which in turn led to the reduction in the amount of glucan synthesis precursor substance (UDP-Glu) and consequently to a reduction in the total amount of glucan on days three and four in the transformed group compared to the control group.

Cells were collected to determine the monosaccharide composition of polysaccharide after 1–9 days of culture. After comparing the monosaccharide composition of yeast polysaccharide produced on each day, only the monosaccharide composition of the third day changed to a larger extent, and the monosaccharide composition of yeast polysaccharide on the other days remained the same (**Figure 6B**). The results of the monosaccharide composition data of the third day are shown in **Table 2**, which shows that a variety of new monosaccharides appeared in the transformation group compared with the control group. Yeast polysaccharides, usually, contain only glucose and mannose and a small amount of fructose, as shown in **Table 2**, and the monosaccharide composition of the polysaccharides produced by the yeast transformed with the A6180 gene contained four new monosaccharides (rhamnose, galactose, xylose, and galacturonic acid) which accounted for 0.55, 9.24, 11.83, and 1.54% of the total sugars, respectively. The percentage of arabinose increased by 3.1% and the percentage of glucosamine, glucose, mannose, and fructose decreased by 0.29, 7.88, 16.87, and 1.23%, respectively.

Due to the overexpression of the *A6180* gene in the transformed group of *S. cerevisiae* BY4742-A6180, a new target protein was produced to participate in the polysaccharide synthesis pathway in *S. cerevisiae* cells. In turn,

TABLE 2 | The proportion of monosaccharide composition in *S. cerevisiae* and its transformant on day 3.

Monosaccharide type	Monosaccharide in control group	Monosaccharide in transformed group (%)	Increased monosaccharides in transformed group	Reduced monosaccharides in transformed group
Rhamnose	N.D[a]	0.55	0.55%	N.A[b]
Arabinose	0.15%	3.25	3.10%	N.A.
Glucosamine	0.82%	0.53	N.A.	0.29%
Galactose	N.D	9.24	9.24%	N.A.
Glucose	33.50%	25.62	N.A.	7.88%
Xylose	N.D.	11.83	11.83%	N.A.
Mannose	61.81%	44.94	N.A.	16.87%
Fructose	3.72%	2.49	N.A.	1.23%
GalA	N.D.	1.54	1.54%	N.A.

[a]*N.D: not detected.*
[b]*N.A: not application.*

a new conversion pathway from glucose to galactose emerged, resulting in the production of galactose products that did not exist in the transformant strain and accounted for 9.24% of the total sugars. The increase in galactose content in the transformed group led to the production of galacturonic acid which also appeared in the transformed group. However, the target protein did not have an efficient catalytic function in the galactose-to-galacturonic acid pathway, resulting in an increase of galacturonic acid by 1.54%. Protein function prediction of the *A6180* gene by the Protein Family Data Bank (http://pfam.xfam.org/) Pfam showed that it also functions as a GDP-mannose 4,6 dehydratase (PF16363) (EC: 4.2.1.47), which converts GDP-α-D-mannose to GDP-4-dehydro-α-D-rhamnose, corroborating the appearance of rhamnose in the monosaccharide composition of the transformed yeast polysaccharide. The results also showed a small amount of rhamnose produced in polysaccharides of the Brewer's yeast BY4742-A6180 transformation group, which did not appear in the Brewer's yeast BY4742 control group, although not as significant as the elevation of galactose. Moreover, PF16363 domain is also contained in UDP-xylose synthase which converts UDP-glucuronic acid into UDP-xylose (Borg et al., 2021).

Compared with the control group, the composition of glucose, mannose, fructose, and glucosamine was reduced to different degrees in the transformed group. This could be attributed to the protein expressed by the *A6180* gene promoting the conversion of glucose to galactose and galacturonic acid, leading to a significant decrease in the conversion of glucose to mannose, fructose, and glucosamine. Overexpression of the *A6180* gene promoted the simultaneous conversion of glucose as a reaction substrate to multiple monosaccharide conversions, leading to an increase in the consumption of glucose, which in turn led to a 7.88% decrease in the total sugar percentage of glucose.

In vitro Bioactivity of Polysaccharides From the *S. cerevisiae* BY4742-A6180

Enhancing macrophage activity *in vitro* is one way to evaluate the immune activity of polysaccharide fractions (Hitschler and Boles, 2019). After the pre-experiment of the *in vitro* immunoreactivity by determining the NO production of RAW264.7 cells treated with the *S. cerevisiae* polysaccharide on the third day at different concentrations, the highest activity of the sample was found at 500 μg/ml concentration. The 500 μg/ml concentration, therefore, was chosen to continue the immunoreactivity assay of the polysaccharide obtained from *S. cerevisiae* BY4742-A6180 transformation strain and control strain cultivated on days 2–5. The results showed that the polysaccharide activity in the transformed group increased by 71.8% on the third day compared to the control group, and there was no significant change after 4 days incubation (**Figure 6C**). This is also consistent with the previous results for monosaccharide composition, in which only the third day of the transformation group showed a significant change in monosaccharide composition. This indicates that the activity of yeast polysaccharides is closely related to their structure, and is especially related to the composition of its monosaccharide. The transformation of A6180 into yeast changed the structure of the yeast polysaccharides and further changed the activity of its polysaccharide.

In this study, heterologous expression of *A6180* in *E. coli* and yeast confirmed that UGE encoded by *A6180* is involved in polysaccharide production by *H. erinaceus* (**Figure 7**). In particular, the expression results in yeast indicated that UGE derived from *H. erinaceus* could change the composition of fungal polysaccharides and increase their activity. In the future, it is promising to use it to engineer strains for producing polysaccharides with high activity.

DISCUSSION

Most of the current research on UDP-glucose-4-epimerases is limited to model species, including *E. coli* (Zhu et al., 2019), *Aspergillus* (Lee et al., 2014; Park et al., 2014), and *Arabidopsis thaliana* (Barber et al., 2006), rather than macrofungi. In our previous study, a predicted UDP-glucose-4-epimerases could be involved in the high yield of high-bioactivity polysaccharides in an *H. erinaceus* mutant. To date, there have been limited reports on the function of UDP-glucose-4-epimerases in macrofungi. In the present study, the enzymatic characteristics of the purified UGE (heterologously expressed in *E. coli*) showed that the optimum conditions were consistent with the cultivation conditions of *H. erinaceus*. Moreover, the heterologous expression of UGE in *S. cerevisiae* also indicates that UGE participates in the synthesis of polysaccharides.

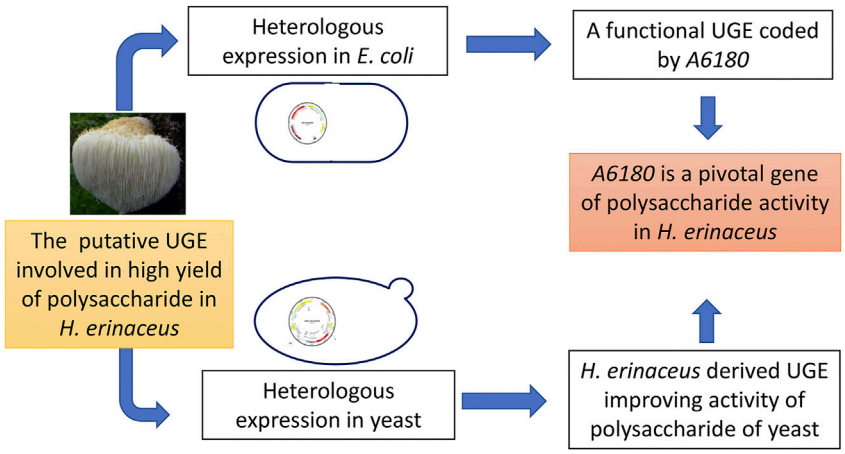

FIGURE 7 | Schematic diagram of this study.

The general culture conditions for the mycelium of *H. erinaceus* were 26°C and natural pH medium (approximately 5.8), and the results of the study showed that the optimum pH and optimum temperature of UGE were closer to the culture conditions. The optimum pH and temperature of UGE from oyster (Song et al., 2018), *E. coli* (Guo et al., 2006) were 8.5 and 8, 16°C and 37°C, respectively. This indicates that the reaction conditions of UGE from *H. erinaceus* are close to the optimum conditions for fungal growth, which is more suitable for practical production applications of UDP-Gal. This suggests that this UGE encoding gene could be used to engineer other fungi to produce highly active polysaccharides under optimal conditions with the highest activity.

The heterologous expression and polysaccharide properties of the *A6180* gene in *S. cerevisiae* yielded three results. First, the overall trend of glucan content in the experimental group was similar to that of the control group, with a significant decrease in glucan content on days 3 and 4, which tentatively demonstrated that the *A6180* gene functions on days 3 and 4; and was found to have the ability to convert glucose into other monosaccharides. UDP-glucose-4-epimerase (EC:5.1.3.2) converts UDP-α-D-glucose to UDP-α-D-galactose, corroborating the appearance of galactose in the monosaccharide composition results. It also functions as GDP-mannose 4,6 dehydratase (EC: 4.2.1.47), which converts GDP-α-D-mannose to GDP-4-dehydro-α-D-rhamnose, corroborating the appearance of rhamnose in the monosaccharide composition results. As shown by the monosaccharide composition results, it can also promote the production of xylose, and it accounts for a larger proportion of monosaccharide conversion (11.83%). The polysaccharide composition of *S. cerevisiae* is generally considered to be mainly composed of glucan and mannan. The analysis of the results of our control group is consistent with the previous report (Free, 2013). The *A6180* gene is the only difference between the transformed group and the control group. Therefore, we speculate that *A6180* coded a protein with multi-function besides the isomerization between different hexoses. This speculation is similar to that of a previously reported bifunctional UGE. It catalyzes the isomerization between a variety of UDP-sugars, including UDP-hexose and UDP-pentose (Schäper et al., 2019). In addition, the possible activities of the conserved functional domains contained in A6180 include GDP-mannose 4,6-dehydratase (Li et al., 2021), UDP-glucuronate 4-epimerase (Gauttam et al., 2021), and UDP-glucuronate decarboxylase (Woo et al., 2019), and so on. This versatile A6180 that may cause the dramatic change in the composition and proportions of yeast polysaccharides.

In the budding yeast *S. cerevisiae*, Gal10p contains both galactose mutarotase (mutarotase) and UDP-galactose-4-epimerase (referred to as epimerase) (Majumdar et al., 2004). This dual activity appears to be unique to *S. cerevisiae* and other yeasts such as *Kluyveromyces fragilis*, *K. lactis*, and *Pachysolen tannophilus* (Brahma and Bhattacharyya, 2004). It is not usual to see two non-sequential enzymatic activities encoded in the same protein, and it is not clear why the two activities are linked this way in yeasts. Previous reports have indicated that this biofunctional protein would have the advantage of sequestering galactose 1-phosphate, which is toxic to both yeasts and mammals (Tsakiris et al., 2002; Scott and Timson, 2007). However, this study showed that the expression of UGE with a single function did not cause toxicity in yeast (Scott and Timson, 2007). Moreover, large amounts of galactose were detected in the polysaccharides. Therefore, we hypothesize that the bifunctional GAL10P in yeast is responsible for the absence of galactose in wild-type yeast polysaccharides (Lozančić et al., 2021). However, it is difficult to explain the special structure of basidiomycetes. Research is yet to be carried out on the N-terminal THO complex subunit 1 transcription elongation factor domain in fungi. In humans, it functions in the cotranscriptional recruitment of mRNA to export proteins to the nascent transcript (Luo et al., 2012).

In our previous study, *A6180* was speculated to be related to polysaccharide production. However, we found that heterologous expression in yeast was not significantly related to polysaccharide yield. This may be related to the fact that we are only heterologously expressed instead of replacing the endogenous

UGE gene in yeast. However, in some plant UGE functional studies, it is related to the production of polysaccharides. In *Brassica rapa*, BrUGE1 was cloned and introduced into the genome of wild type rice (Gopum) using the *Agrobacterium*-mediated transformation method. Agronomic trait evaluation of the transgenic plants under optimal field conditions revealed enriched biomass production, particularly in panicle length, number of productive tillers, number of spikelets per panicle, filled spikelets, and polysaccharide content (Guevara et al., 2014; Abdula et al., 2016). In addition, our results reveal that UGE is not only related to polysaccharide production, but also to the structure and activity of polysaccharides. It is important to conduct in-depth research on the functions of UGE.

DATA AVAILABILITY STATEMENT

The original contributions presented in the study are included in the article/**Supplementary Material**, further inquiries can be directed to the corresponding author.

AUTHOR CONTRIBUTIONS

YY and GZ designed the experiments. All experiment data were acquired by JR, GZ, DW, MG, HZ, WL, and JZ, YY, JR, and GZ wrote the paper. JR and GZ analyzed the data. YY and GZ edited the article. All authors read and approved the article.

FUNDING

This work was supported financially by Shanghai Agriculture Applied Technology Development Program, China (Grant No. Z 20180101), Shanghai leading Talent Project (2018).

SUPPLEMENTARY MATERIAL

The Supplementary Material for this article can be found online at: https://www.frontiersin.org/articles/10.3389/fbioe.2021.796278/full#supplementary-material

REFERENCES

Abdula, S. E., Lee, H. J., Kim, J., Niño, M. C., Jung, Y.-J., Cho, Y.-C., et al. (2016). *Br*UGE1 Transgenic rice Showed Improved Growth Performance with Enhanced Drought Tolerance. *Breed. Sci.* 66 (2), 226–233. doi:10.1270/jsbbs.66.226

Bachmann, B. O., Van Lanen, S. G., and Baltz, R. H. (2014). Microbial Genome Mining for Accelerated Natural Products Discovery: Is a Renaissance in the Making? *J. Ind. Microbiol. Biotechnol.* 41 (2), 175–184. doi:10.1007/s10295-013-1389-9

Barber, C., Rösti, J., Rawat, A., Findlay, K., Roberts, K., and Seifert, G. J. (2006). Distinct Properties of the Five UDP-D-Glucose/UDP-D-Galactose 4-epimerase Isoforms of *Arabidopsis thaliana*. *J. Biol. Chem.* 281 (25), 17276–17285. doi:10.1074/jbc.M512727200

Biely, P., Hirsch, J., La Grange, D. C., Van Zyl, W. H., and Prior, B. A. (2000). A Chromogenic Substrate for a β-Xylosidase-Coupled Assay of α-Glucuronidase. *Anal. Biochem.* 286 (2), 289–294. doi:10.1006/abio.2000.4810

Borg, A. J. E., Beerens, K., Pfeiffer, M., Desmet, T., and Nidetzky, B. (2021). Stereo-Electronic Control of Reaction Selectivity in Short-Chain Dehydrogenases: Decarboxylation, Epimerization, and Dehydration. *Curr. Opin. Chem. Biol.* 61, 43–52. doi:10.1016/j.cbpa.2020.09.010

Brahma, A., and Bhattacharyya, D. (2004). UDP-Galactose 4-Epimerase from Kluyveromyces Fragilis. *Eur. J. Biochem.* 271 (1), 58–68. doi:10.1046/j.1432-1033.2003.03902.x

Cai, W.-D., Ding, Z.-C., Wang, Y.-Y., Yang, Y., Zhang, H.-N., and Yan, J.-K. (2020). Hypoglycemic Benefit and Potential Mechanism of a Polysaccharide from *Hericium erinaceus* in Streptozotoxin-Induced Diabetic Rats. *Process Biochem.* 88, 180–188. doi:10.1016/j.procbio.2019.09.035

Chen, W., Wu, D., Jin, Y., Li, Q., Liu, Y., Qiao, X., et al. (2020). Pre-protective Effect of Polysaccharides Purified from *Hericium erinaceus* against Ethanol-Induced Gastric Mucosal Injury in Rats. *Int. J. Biol. Macromol.* 159, 948–956. doi:10.1016/j.ijbiomac.2020.05.163

Du, X., Zhang, Y., Mu, H., Lv, Z., Yang, Y., and Zhang, J. (2015). Structural Elucidation and Antioxidant Activity of a Novel Polysaccharide (TAPB1) from *Tremella Aurantialba*. *Food Hydrocolloids* 43, 459–464. doi:10.1016/j.foodhyd.2014.07.004

Free, S. J. (2013). Fungal Cell Wall Organization and Biosynthesis. *Adv. Genet.* 81, 33–82. doi:10.1016/B978-0-12-407677-8.00002-6

Gauttam, R., Desiderato, C. K., Radoš, D., Link, H., Seibold, G. M., and Eikmanns, B. J. (2021). Metabolic Engineering of *Corynebacterium Glutamicum* for Production of UDP-N-Acetylglucosamine. *Front. Bioeng. Biotechnol.* 9, 748510. doi:10.3389/fbioe.2021.748510

Gong, M., Zhang, H., Wu, D., Zhang, Z., Zhang, J., Bao, D., et al. (2021). Key Metabolism Pathways and Regulatory Mechanisms of High Polysaccharide Yielding in *Hericium erinaceus*. *BMC Genomics* 22 (1), 160. doi:10.1186/s12864-021-07480-x

Goulard, F., Diouris, M., Deslandes, E., and Floc'h, J. Y. (2001). An HPLC Method for the Assay of UDP-Glucose Pyrophosphorylase and UDP-Glucose-4-Epimerase in *Solieria Chordalis* (Rhodophyceae). *Phytochem. Anal.* 12 (6), 363–365. doi:10.1002/pca.604

Guevara, D. R., El-Kereamy, A., Yaish, M. W., Mei-Bi, Y., and Rothstein, S. J. (2014). Functional Characterization of the rice UDP-Glucose 4-epimerase 1, *Os*UGE1: a Potential Role in Cell wall Carbohydrate Partitioning during Limiting Nitrogen Conditions. *PLoS One* 9 (5), e96158. doi:10.1371/journal.pone.0096158

Guo, H., Li, L., and Wang, P. G. (2006). Biochemical Characterization of UDP-GlcNAc/Glc 4-Epimerase from *Escherichia coli* O86:B7. *Biochemistry* 45 (46), 13760–13768. doi:10.1021/bi0612770

Hitschler, J., and Boles, E. (2019). De Novo production of Aromatic M-Cresol in *Saccharomyces cerevisiae* Mediated by Heterologous Polyketide Synthases Combined with a 6-methylsalicylic Acid Decarboxylase. *Metab. Eng. Commun.* 9, e00093. doi:10.1016/j.mec.2019.e00093

Jiang, Y., Qi, X., Gao, K., Liu, W., Li, N., Cheng, N., et al. (2016). Relationship between Molecular Weight, Monosaccharide Composition and Immunobiologic Activity of *Astragalus* Polysaccharides. *Glycoconj J.* 33 (5), 755–761. doi:10.1007/s10719-016-9669-z

Jithendra, T., Reddy, O. S., Subha, M., Madhavi, C., and Rao, K. C. (2020). Xanthan Gum Graft Copolymer/sodium Alginate Micro Beads Coated with Chitosan for Controlled Release of Chlorthalidone Drug. *Int. J. Pharm. Sci. Res.* 11, 1132–1145. doi:10.13040/IJPSR.0975-8232

Lee, M. J., Gravelat, F. N., Cerone, R. P., Baptista, S. D., Campoli, P. V., Choe, S.-I., et al. (2014). Overlapping and Distinct Roles of *Aspergillus fumigatus* UDP-Glucose 4-Epimerases in Galactose Metabolism and the Synthesis of Galactose-Containing Cell Wall Polysaccharides. *J. Biol. Chem.* 289 (3), 1243–1256. doi:10.1074/jbc.M113.522516

Li, T., Li, C., Wu, D., Yang, Y., and Jin, Y. (2018). "Studies on the Acid Degradation Process and *In Vitro* Immune Activity of the Polysaccharide H6PC20 in Hericium Erinaceus," in IOP Conference Series: Materials Science and Engineering, Zhuhai, June 22–24, 2018 (IOP Publishing), 052014.

Li, W., Zhu, Y., Wan, L., Guang, C., and Mu, W. (2021). Pathway Optimization of 2′-Fucosyllactose Production in Engineered *Escherichia coli*. *J. Agric. Food Chem.* 69 (5), 1567–1577. doi:10.1021/acs.jafc.0c07224

Liang, B., Guo, Z., Xie, F., and Zhao, A. (2013). Antihyperglycemic and Antihyperlipidemic Activities of Aqueous Extract of *Hericium erinaceus* in Experimental Diabetic Rats. *BMC Complement. Altern. Med.* 13 (1), 253–257. doi:10.1186/1472-6882-13-253

Liu, J., Du, C., Wang, Y., and Yu, Z. (2015). Anti-Fatigue Activities of Polysaccharides Extracted from *Hericium erinaceus*. *Exp. Ther. Med.* 9 (2), 483–487. doi:10.3892/etm.2014.2139

Low, A., Mohd Yusof, H., Reza, F., Abdullah Nurul, A., Sritharan, S., Haania Zain Ali, N., et al. (2015). Gypsum-based Biomaterials: Evaluation of Physical and Mechanical Properties, Cellular Effects and its Potential as a Pulp Liner. *Dent. Mater. J.* 34 (4), 522–528. doi:10.4012/dmj.2015-029

Lozančić, M., Žunar, B., Hrestak, D., Lopandić, K., Teparić, R., and Mrša, V. (2021). Systematic Comparison of Cell wall-related Proteins of Different Yeasts. *J. Fungi (Basel)* 7 (2), 128. doi:10.3390/jof7020128

Lu, Y., Zhong, H., Tang, Q., Huang, Z., Jing, N., Smith, J., et al. (2017). Construction and Verification of CYP3A5 Gene Polymorphisms Using a *Saccharomyces cerevisiae* Expression System to Predict Drug Metabolism. *Mol. Med. Rep.* 15 (4), 1593–1600. doi:10.3892/mmr.2017.6214

Luo, Z., Lin, C., and Shilatifard, A. (2012). The Super Elongation Complex (SEC) Family in Transcriptional Control. *Nat. Rev. Mol. Cel Biol.* 13 (9), 543–547. doi:10.1038/nrm3417

Majumdar, S., Ghatak, J., Mukherji, S., Bhattacharjee, H., and Bhaduri, A. (2004). UDPgalactose 4-epimerase from *Saccharomyces cerevisiae*. *Eur. J. Biochem.* 271 (4), 753–759. doi:10.1111/j.1432-1033.2003.03974.x

Nowak, B., Śróttek, M., Ciszek-Lenda, M., Skałkowska, A., Gamian, A., Górska, S., et al. (2020). Exopolysaccharide from *Lactobacillus Rhamnosus* KL37 Inhibits T Cell-dependent Immune Response in Mice. *Arch. Immunol. Ther. Exp.* 68 (3), 17. doi:10.1007/s00005-020-00581-7

Park, J., Tefsen, B., Arentshorst, M., Lagendijk, E., van den Hondel, C. A., van Die, I., et al. (2014). Identification of the UDP-Glucose-4-Epimerase Required for Galactofuranose Biosynthesis and Galactose Metabolism in *A. niger*. *Fungal Biol. Biotechnol.* 1, 6. doi:10.1186/s40694-014-0006-7

Rodríguez-Díaz, J., and Yebra, M. J. (2011). Enhanced UDP-Glucose and UDP-Galactose by Homologous Overexpression of UDP-Glucose Pyrophosphorylase in *Lactobacillus Casei*. *J. Biotechnol.* 154 (4), 212–215. doi:10.1016/j.jbiotec.2011.05.015

Schäper, S., Wendt, H., Bamberger, J., Sieber, V., Schmid, J., and Becker, A. (2019). A Bifunctional UDP-Sugar 4-epimerase Supports Biosynthesis of Multiple Cell Surface Polysaccharides in *Sinorhizobium Meliloti*. *J. Bacteriol.* 201 (10), e00801–00818. doi:10.1128/JB.00801-18

Scott, A., and Timson, D. J. (2007). Characterization of the Saccharomyces Cerevisiaegalactose mutarotase/UDP-Galactose 4-epimerase Protein, Gal10p. *FEMS Yeast Res.* 7 (3), 366–371. doi:10.1111/j.1567-1364.2006.00204.x

Song, H.-B., He, M., Cai, Z.-P., Huang, K., Flitsch, S., Liu, L., et al. (2018). UDP-Glucose 4-Epimerase and β-1,4-Galactosyltransferase from the Oyster Magallana Gigas as Valuable Biocatalysts for the Production of Galactosylated Products. *Int. J.Mol.Sci.* 19 (6), 1600. doi:10.3390/ijms19061600

Sun, L., Liu, G., Li, Y., Jiang, D., Guo, W., Xu, H., et al. (2019). Metabolic Engineering of *Saccharomyces cerevisiae* for Efficient Production of Endocrocin and Emodin. *Metab. Eng.* 54, 212–221. doi:10.1016/j.ymben.2019.04.008

Tsakiris, S., Marinou, K., and Schulpis, K. H. (2002). Thein vitroEffects of Galactose and its Derivatives on Rat Brain Mg2+-ATPase Activity. *Pharmacol. Toxicol.* 91 (5), 254–257. doi:10.1034/j.1600-0773.2002.910506.x

Wang, H.-Y., Xiao, D.-F., Zhou, C., Wang, L.-L., Wu, L., Lu, Y.-T., et al. (2017). YLL056C from *Saccharomyces cerevisiae* Encodes a Novel Protein with Aldehyde Reductase Activity. *Appl. Microbiol. Biotechnol.* 101 (11), 4507–4520. doi:10.1007/s00253-017-8209-5

Woo, J. E., Seong, H. J., Lee, S. Y., and Jang, Y.-S. (2019). Metabolic Engineering of *Escherichia coli* for the Production of Hyaluronic Acid from Glucose and Galactose. *Front. Bioeng. Biotechnol.* 7, 351. doi:10.3389/fbioe.2019.00351

Wu, D., Tang, C., Liu, Y., Li, Q., Wang, W., Zhou, S., et al. (2019). Structural Elucidation and Immunomodulatory Activity of a β-D-glucan Prepared by Freeze-Thawing from Hericium erinaceus. *Carbohydr. Polym.* 222, 114996. doi:10.1016/j.carbpol.2019.114996

Zeng, D., and Zhu, S. (2018). Purification, Characterization, Antioxidant and Anticancer Activities of Novel Polysaccharides Extracted from Bachu Mushroom. *Int. J. Biol. Macromol.* 107 (Pt A), 1086–1092. doi:10.1016/j.ijbiomac.2017.09.088

Zhang, T., Shi, L., Li, Y., Mu, W., Zhang, H., Li, Y., et al. (2021). Polysaccharides Extracted from *Rheum Tanguticum* Ameliorate Radiation-Induced Enteritis via Activation of Nrf2/HO-1. *J. Radiat. Res.* 62 (1), 46–57. doi:10.1093/jrr/rraa093

Zhu, L., Wu, D., Zhang, H., Li, Q., Zhang, Z., Liu, Y., et al. (2019). Effects of Atmospheric and Room Temperature Plasma (ARTP) Mutagenesis on Physicochemical Characteristics and Immune Activity *In Vitro* of *Hericium erinaceus* Polysaccharides. *Molecules* 24 (2), 262. doi:10.3390/molecules24020262

Conflict of Interest: The authors declare that the research was conducted in the absence of any commercial or financial relationships that could be construed as a potential conflict of interest.

Publisher's Note: All claims expressed in this article are solely those of the authors and do not necessarily represent those of their affiliated organizations, or those of the publisher, the editors and the reviewers. Any product that may be evaluated in this article, or claim that may be made by its manufacturer, is not guaranteed or endorsed by the publisher.

frontiers in Bioengineering and Biotechnology

BRIEF RESEARCH REPORT
published: 09 December 2021
doi: 10.3389/fbioe.2021.764851

Improved Functional Expression of Cytochrome P450s in *Saccharomyces cerevisiae* Through Screening a cDNA Library From *Arabidopsis thaliana*

Lihong Jiang[1], *Chang Dong*[1,2], *Tengfei Liu*[1], *Yi Shi*[1], *Handing Wang*[1,2], *Zeng Tao*[3], *Yan Liang*[3] *and Jiazhang Lian*[1,2]*

[1]Key Laboratory of Biomass Chemical Engineering of Ministry of Education, College of Chemical and Biological Engineering, Zhejiang University, Hangzhou, China, [2]Hangzhou Global Scientific and Technological Innovation Center, Zhejiang University, Hangzhou, China, [3]Ministry of Agriculture Key Laboratory of Molecular Biology of Crop Pathogens and Insects, Institute of Biotechnology, Zhejiang University, Hangzhou, China

OPEN ACCESS

Edited by:
Shuobo Shi,
Beijing University of Chemical Technology, China

Reviewed by:
Jingwen Zhou,
Jiangnan University, China
Soo Rin Kim,
Kyungpook National University, South Korea
Farshad Darvishi,
Alzahra University, Iran

***Correspondence:**
Jiazhang Lian
jzlian@zju.edu.cn

Specialty section:
This article was submitted to Synthetic Biology, a section of the journal Frontiers in Bioengineering and Biotechnology

Received: *26 August 2021*
Accepted: *24 November 2021*
Published: *09 December 2021*

Citation:
Jiang L, Dong C, Liu T, Shi Y, Wang H, Tao Z, Liang Y and Lian J (2021) Improved Functional Expression of Cytochrome P450s in Saccharomyces cerevisiae *Through Screening a cDNA Library From* Arabidopsis thaliana. *Front. Bioeng. Biotechnol. 9:764851. doi: 10.3389/fbioe.2021.764851*

Cytochrome P450 enzymes (P450s) are a superfamily of heme-thiolate proteins widely existing in various organisms and play a key role in the metabolic network and secondary metabolism. However, the low expression levels and activities have become the biggest challenge for P450s studies. To improve the functional expression of P450s in *Saccharomyces cerevisiae*, an *Arabidopsis thaliana* cDNA library was expressed in the betaxanthin-producing yeast strain, which functioned as a biosensor for high throughput screening. Three new target genes *AtGRP7*, *AtMSBP1*, and *AtCOL4* were identified to improve the functional expression of *CYP76AD1* in yeast, with accordingly the accumulation of betaxanthin increased for 1.32-, 1.86-, and 1.10-fold, respectively. In addition, these three targets worked synergistically/additively to improve the production of betaxanthin, representing a total of 2.36-fold improvement when compared with the parent strain. More importantly, these genes were also determined to effectively increase the activity of another P450 enzyme (CYP736A167), catalyzing the hydroxylation of α-santalene to produce Z-α-santalol. Simultaneous overexpression of *AtGRP7*, *AtMSBP1*, and *AtCOL4* increased α-santalene to Z-α-santalol conversion rate for more than 2.97-fold. The present study reported a novel strategy to improve the functional expression of P450s in *S. cerevisiae* and promises the construction of platform yeast strains for the production of natural products.

Keywords: cytochrome P450 enzymes, *Arabidopsis thaliana* cDNA overexpression library, biosensor, betaxanthin, Z-α-santalol, *Saccharomyces cerevisiae*

INTRODUCTION

Cytochrome P450 enzymes (P450s), first discovered in the early 1960s, are a superfamily of heme-thiolate proteins widely existing in animals, plants, and microorganisms (Elfaki et al., 2018; Guengerich et al., 2016). P450s play important roles in the metabolic networks, due to various biocatalytic activities such as oxidation, epoxidation, hydroxylation, and demethylation (Stavropoulou et al., 2018). More importantly, P450s are involved in the biosynthesis of many natural products, such as opioids (Galanie et al., 2015), artemisinic acid (Paddon et al., 2013), and glycyrrhetinic acid (Zhu et al., 2018). As a thoroughly studied model organism, *Saccharomyces cerevisiae* has advantages of clear genetic background, easy cultivation, and post-translational processing capability (Schuler and Werck-Reichhart 2003). Most importantly, the

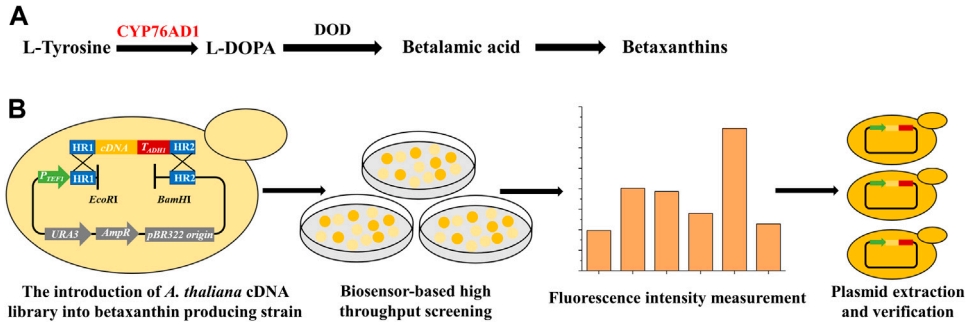

FIGURE 1 | Establishment of a high throughput screening method for identifying new target genes of the *A. thaliana* cDNA library to improve the functional expression of P450s. **(A)** The betaxanthin biosynthetic pathway starting from L-tyrosine, including a P450 enzyme (CYP76AD1, shown in red) and an L-DOPA dioxygenase (DOD). CYP76AD1 has been determined to be rate-limiting for betaxanthin production, indicating that the production of betaxanthin (yellow color or fluorescence) can function as a biosensor for the expression level of *CYP76AD1*. **(B)** Workflow of the genome-scale engineering experiments. The *A. thaliana* cDNA overexpression library was introduced into the betaxanthin-producing yeast (yJS1256, biosensor strain) *via in vivo* homologous recombination. Clones with obvious color changes were selected and inoculated into SCD-URA medium in 96 deep-well plates and the fluorescence intensities were measured using a microplate reader. Then the isolated plasmids were re-transformed into the biosensor strain and the corresponding genes were identified by DNA sequencing.

inner membrane systems of *S. cerevisiae* allow the functional anchoring of P450s and cytochrome P450 reductases (CPRs) (Hausjell et al., 2018). Therefore, *S. cerevisiae* is often selected as a preferred host for functional expression of P450s and accordingly biosynthesis of natural products.

Although a variety of P450s have been successfully expressed in *S. cerevisiae*, low expression level and activity have become the biggest challenge for fundamental and biotechnological application studies of P450s (Jiang et al., 2021). Accordingly, different strategies have been implemented to increase the expression level and/or activity of P450s in *S. cerevisiae*, including N-terminal truncation, protein molecular modification of P450s through protein engineering, and co-expression with CPRs (Jiang et al., 2021). Unfortunately, the effects of these engineering strategies are often varied case by case. In other words, it is of great demand to develop a generally applicable strategy to improve the functional expression of a wide range of P450s in *S. cerevisiae*.

In plants, there are many kinds of P450s, interacting with a variety of substrates to participate in the synthesis and degradation of alkaloids, terpenes, flavonoids, fatty acids, plant hormones, and signal molecules (Bolwell et al., 1994). Thus, plants have evolved a complex gene regulation system to control the expression and folding of P450s (Yang et al., 2016). It is speculated that the introduction of key genes involved in the plant regulatory network may have positive effects on the functional expression of a series of P450s in yeast.

The present study aims to identify key genes that can improve the functional expression of P450s in *S. cerevisiae* through screening a genome-scale cDNA library from *Arabidopsis thaliana*, a model plant widely used in plant genetic, cellular, developmental, and molecular biology researches (Hayashi and Nishimura 2006). Firstly, an *A. thaliana* cDNA library was overexpressed in *S. cerevisiae*, which was combined with biosensor-based high-throughput screening (**Figure 1A**) to identify target genes that can improve the functional expression of a P450 (*CYP76AD1*) in yeast. Then, the synergistic interactions and molecular mechanisms of these newly identified targets were further explored. Finally, these plant genes were overexpressed to increase the activity of another P450 protein (encoded by *CYP736A167*) involved in the hydroxylation of α-santalene to Z-α-santalol. The present study promises the establishment of a platform yeast strain for functional expression of a wide variety of P450s.

MATERIALS AND METHODS

Strains and Plasmids

The yeast biosensor strain yJS1256 for high throughput screening was kindly provided by Prof. Dueber from the University of California at Berkeley (DeLoache et al., 2015). The *A. thaliana* cDNA library under the control of *ADH1* promoter and *ADH1* terminator in plasmid pGADT7-AD was kindly provided by Prof. Zeng Tao from Zhejiang University. To facilitate the construction of the *A. thaliana* cDNA overexpression library in *S. cerevisiae*, a helper plasmid pRS416-TEF1p was constructed by cloning *TEF1* promoter, upstream and downstream homology arms of the cDNA library, as well as *EcoR*I and *BamH*I restriction sites into pRS416. Then pRS416-TEF1p was digested by *EcoR*I and *BamH*I and co-transformed with the PCR amplified cDNA library fragments with homology arms into yJS1256 for *in vivo* assembly (**Figure 1B**). The identified plasmids from the *A. thaliana* cDNA library were isolated using a ZymoPrep Yeast Plasmid Miniprep Kit (Zymo Research, Irvine, CA) and transformed into *Escherichia coli* DH5α for plasmid amplification. The Z-α-santalol producing *S. cerevisiae* strain was constructed by integrating four copies of the α-santalene synthase (SAS) gene (Dong et al., 2020) and one copy of *CYP736A167* and *CPR2* from *Santalum album* (XII5 locus) into the genome of BY4741 (*MATa his△1 leu2△0 met15△0 ura3△0*), *via* CRISPR-Cas9-mediated genome editing technology (Lian et al., 2017; Lian et al., 2019). In addition, the mevalonate (MVA) pathway genes were overexpressed to enhance the precursor supply for Z-α-santalol biosynthesis, with *tHMG1-ERG8-ERG13-ERG20-ERG12* overexpression cassettes and *EGR10-MVD1-IDI1-tHMG1* overexpression cassettes integrated into X4 and XI3 loci,

respectively. Q5 polymerase, T4 DNA ligase, and all restriction enzymes used were purchased from New England Biolabs (Ipswich, MA). All chemicals were bought from Sigma (Sigma Aldrich, St. Louis, MO) unless otherwise stated.

Growth Conditions

E. coli strain DH5α for cloning and plasmid propagation was cultured at 37°C in Luria-broth (LB) medium containing 100 μg/ml ampicillin. Yeast strains were cultivated in standard yeast peptone dextrose (YPD) medium consisting of 2% glucose, 2% peptone, and 1% yeast extract. Recombinant yeast strains were grown on complete synthetic (SCD-URA) medium consisting of 0.17% yeast nitrogen base (YNB, Difco, Boom, Netherlands), 0.5% ammonium sulfate, and the appropriate amino acid drop-out mix (CSM-URA, MP Biomedicals, Solon, Ohio) supplemented with 2% glucose at 30°C.

High-Throughput Screening and Fluorescence Intensity Measurement

The *A. thaliana* cDNA overexpression library was constructed by the *in vivo* DNA assembly method in *S. cerevisiae*. After transformation, 10^6 independent clones were observed on SCD-URA agar plates, indicating at least a 50-fold coverage of the *A. thaliana* cDNA library. For biosensor-based high-throughput screening, 76 clones with the highest yellow color intensities were selected from SCD-URA agar plates and inoculated into 1 ml SCD-URA medium in a 96 deep-well plate. The yeast strains were pre-cultured for 2 days and then inoculated into fresh SCD-URA medium with an initial OD_{600} of 0.1. Mid-log phase yeast cells were collected and diluted 2-fold in ddH_2O for measuring betaxanthin fluorescence intensity at 498–533 nm using a Tecan microplate reader. The fluorescence intensity (relative fluorescence units; RFU) was normalized to cell density that was determined by the same microplate reader.

Z-α-Santalol Production and Quantification

Z-α-Santalol producing strains were pre-cultured in SCD-URA medium for 2 days, inoculated into 50 ml fresh medium in 250 ml shaker flasks with an initial OD_{600} of 0.1, and cultured at 30°C and 250 rpm for 5 days. Then 2 ml yeast cells were collected by centrifuge at 12,000×*g* for 2 min and resuspended in 700 μL ethyl acetate to be disrupted by bead milling. The cell lysate was centrifuged for 10 min and the supernatant was filtered for GCMS (SHIMADZU, Japan) analysis on a DB-5MS column. 2 μL of each sample was injected with a 20:1 split mode at 280°C. The initial column temperature was 40°C and kept for 3 min. Subsequently, the temperature was increased to 130°C at a rate of 10°C/min, followed by to 180°C at a rate of 2°C/min and to 300°C at a rate of 50°C/min, and finally kept at 300°C for 10 min. The production of *α*-santalene and Z-α-santalol was quantified using the standard curve method. The *α*-santalene to Z-α-santalol conversion rate was calculated as [Z-α-santalol]/([α-santalene]+[Z-α-santalol]).

Transcriptomic Analysis

Yeast cells in biological triplicates were grown at 30°C overnight in 5 ml of SCD medium for 2 days and inoculated into 50 ml SCD medium in 250 ml shaker flasks with an initial OD_{600} of 0.1. Then cells were harvested in the early stationary phase by centrifugation at 4,000 g for 15 min at 4°C, with the total RNA extracted and sequenced (RNA-Seq) by Shanghai Majorbio Bio-pharm Technology Co., Ltd. RNA-Seq data manipulation and differential gene expression profiling were performed on the free online Majorbio Cloud Platform (www.majorbio.com) with default settings. The RNA-Seq data are available from the NCBI Sequence Read Archive, with an accession number PRJNA760804.

RESULTS

Biosensor-Based High Throughput Screening of *A. thaliana* cDNA Overexpression Library in *S. cerevisiae*

A major challenge for P450 engineering is the lack of a high throughput screening method. The betaxanthin-producing yeast strain yJS1256 developed by the Dueber group (DeLoache et al., 2015) was employed as a biosensor for high-throughput screening of yeast strains with improved functional expression of P450s. The biosensor is composed of a P450 enzyme mutant ($CYP76AD1^{W13L–F309L}$) from *Beta vulgaris* and an L-DOPA (dihydroxyphenylalanine) dioxygenase (DOD) from *Mirabilis jalapa*, which can catalyze the conversion of L-tyrosine to produce betaxanthin (**Figure 1A**). In addition, two transporter genes, encoding Qdr2p and Yor1p, were deleted to accumulate betaxanthin intracellularly (Savitskaya et al., 2019). With the introduction of an additional copy of $CYP76AD1^{W13L–F309L}$, the production of betaxanthin was significantly improved, indicating that betaxanthin biosynthesis in yeast was limited by CYP76AD1 (**Supplementary Figure S1**), which was consistent with the previous report (DeLoache et al., 2015). Considering the color and fluorescence characteristics of betaxanthin and rate-limiting of CYP76AD1 in betaxanthin biosynthesis, a biosensor-based high throughput screening method was established to isolate yeast mutants with improved production of betaxanthin (**Figure 1B**). Then the *A. thaliana* cDNA library was cloned into the single-copy plasmid pRS416 and overexpressed in *S. cerevisiae*. After yeast transformation, 20 clones were randomly selected for diagnostic PCR verification to investigate the diversity of the *A. thaliana* cDNA library in *S. cerevisiae* (**Supplementary Figure S2A**). Clones with obvious color changes were selected and inoculated into SCD-URA medium to measure the change in fluorescence intensities (**Supplementary Figure S2B**). Compared with the control strain containing empty plasmid, the fluorescence intensities of 25 clones were increased to varying degrees. The plasmids from these clones were extracted and sequenced to identify the candidate genes which could improve the production of betaxanthin in yeast.

Verification of the Candidate Genes for Improved Functional Expression of *CYP76AD1*

After the extraction of plasmids from the isolated clones, they were re-transformed into the biosensor strain yJS1256 to verify the ability of these genes to improve the functional expression of

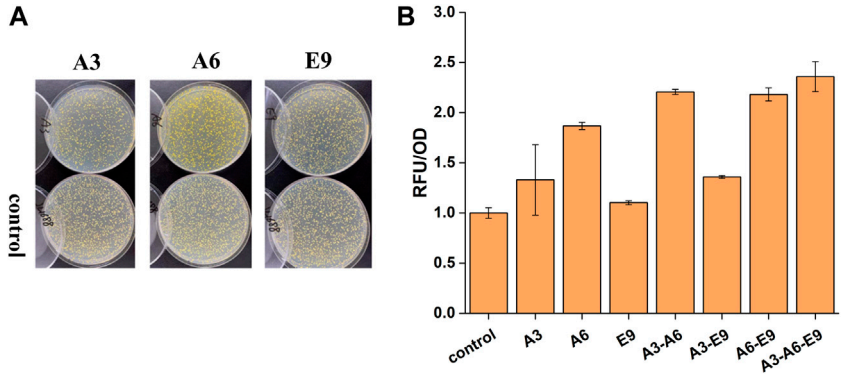

FIGURE 2 | The effects of *AtGRP7* (A3), *AtMSBP1* (A6), and *AtCOL4* (E9) on the functional expression of *CYP76AD1* and accordingly the production of betaxanthin. **(A)** The change of clone color on agar plates after transformation of the target genes. **(B)** The change of fluorescence intensity after transformation of the target genes, as well as synergistic/additive interactions between *AtGRP7* (A3), *AtMSBP1* (A6), and *AtCOL4* (E9). Error bars represented the mean ± s.d. of biological triplicates. RFU/OD refers to the fluorescence intensity normalized to cell density.

CYP76AD1 and accordingly the production of betaxanthin in yeast. Three plasmids, A3, A6, and E9 harboring the genes of *A. thaliana* glycine-rich RNA-binding protein (*AtGRP7*), membrane steroid binding protein 1 (*AtMSBP1*), and *A. thaliana* CO-like four protein (*AtCOL4*), showed 1.32-, 1.86-, and 1.10-fold improvement in betaxanthin production, respectively (**Figures 2A**,**B**). AtGRP7 (A3) participates in the negative feedback loop of circadian rhythm regulation and pre-mRNA splicing and plays an important role in a complex network of transcripts in *A. thaliana* (Koster et al., 2014; Streitner et al., 2010). AtMSBP1 (A6), an ER-located protein, demonstrates steroid-binding activity *in vitro* and is involved in the inhibition of elongation and brassinosteroid signaling (Shi et al., 2011). More importantly, MSBP1 and its homologue MSBP2 can form homomers and heteromers on the ER membrane, which interact with three monolignin P450 enzymes to form MSBP-P450 protein complexes, thereby improving the stability and activity of P450s as well as the production of lignin (Gou et al., 2018). AtCOL4 (E9), a putative novel transcription factor, has transcriptional activation activity and is an important regulator of plant tolerance to abiotic stress (Min et al., 2015).

Afterwards, the synergistic or additive interactions among *AtGRP7*, *AtMSBP1*, and *AtCOL4* were further investigated. Considering the stability of heterologous genes, these gene expression cassettes were integrated into XII5, X4, and XI3 loci of the yeast genome for combinatorial optimization (**Figure 2B**). When *AtGPR7* (A3) or *AtCOL4* (E9) was expressed together with *MSBP1* (A6), synergistic and/or additive effects on the production of betaxanthin were observed, representing 2.21- and 2.18-fold higher than the control strain, respectively. In contrast, the effect of simultaneous expression of *AtGPR7* (A3) and *AtCOL4* (E9) was not obvious. The highest production of betaxanthin was achieved in the strain with these three genes (A3-A6-E9) being expressed simultaneously, representing a 2.36-fold improvement over the control strain. These results indicated that there might be synergistic interactions between *AtMSBP1* and *AtGRP7*, as well as *AtMSBP1* and *AtCOL4*, but not *AtGRP7* and *AtCOL4*.

Effects of the *A. thaliana* Target Gene Overexpression on the Synthesis of Z-α-Santalol in *S. cerevisiae*

To further demonstrate the general applicability of *AtGRP7*, *AtMSBP1*, and *AtCOL4* from *A. thaliana* in improving the functional expression of P450s, these genes were overexpressed in a Z-α-santalol producing yeast strain and their effects on the functional expression of *CYP736A167*, whose gene product catalyzes the hydroxylation of α-santalene to produce Z-α-santalol, was investigated (**Figure 3A**). Based on the previously constructed α-santalene producing strain (Dong et al., 2020), *CYP736A167* and *CPR2* were further integrated into the yeast genome to produce Z-α-santalol. To increase the accumulation of α-santalene, the substrate of CYP736A167 and the precursor of Z-α-santalol biosynthesis, genes involved in MVA pathway were overexpressed, including *tHMG1*, *ERG8*, *ERG10*, *ERG12*, *ERG13*, *ERG20*, *IDI1*, and *MVD1*. As shown in **Supplementary Figures S3, S4**, α-santalene was accumulated to a relatively high level, indicating that the production of Z-α-santalol was limited by the low activity of CYP736A167. The introduction of *AtGRP7* (A3), *AtMSBP1* (A6), and *AtCOL4* (E9) all demonstrated positive effects on the hydroxylation of α-santalene to Z-α-santalol, with the conversion rate increased for 1.89-, 1.71-, and 1.73-fold, respectively. What's more, when these three genes (A3-A6-E9) were overexpressed simultaneously (integrated into XI2, XII2, and XI3 loci of the yeast genome), the conversion rate was the highest, representing a 2.97-fold improvement when compared with the control strain (**Figure 3B**). Surprisingly, the titer of Z-α-santalol was not increased as significantly as the α-santalene to Z-α-santalol conversion rate (**Supplementary Figure S5**). To figure out the possible reasons, the expression level of MVA pathway genes were profiled. As shown in **Supplementary Figure S6**, all the MVA pathway genes except for *ERG10* were down-regulated to different degrees. In other words, the advantage of overexpressing *AtGRP7* (A3), *AtMSBP1* (A6), and *AtCOL4* (E9) in improving the functional expression of

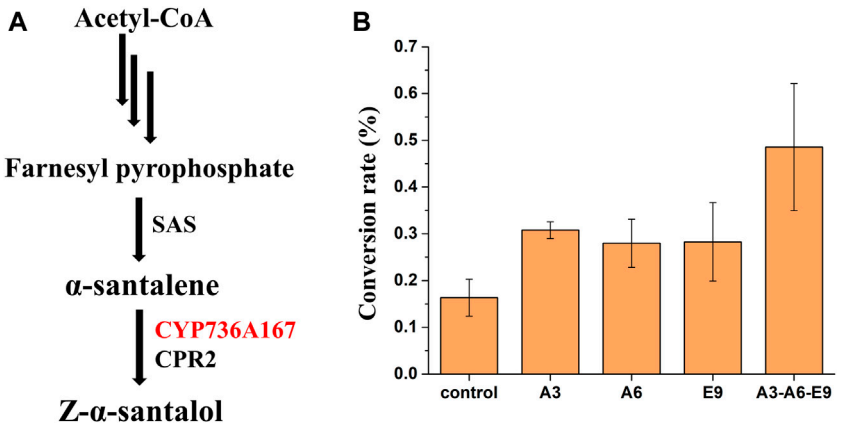

FIGURE 3 | The effects of *AtGRP7* (A3), *AtMSBP1* (A6), and *AtCOL4* (E9) on the functional expression of *CYP736A167* (shown in red) and accordingly the hydroxylation of α-santalene to produce Z-α-santalol. **(A)** The Z-α-santalol biosynthetic pathway from acetyl-CoA. **(B)** The effects of *AtGRP7* (A3), *AtMSBP1* (A6), and *AtCOL4* (E9) on the α-santalene to Z-α-santalol conversion rate, either overexpressed alone (A3, A6, and E9) or in combination (A3-A6-E9). Error bars represented the mean ± s.d. of biological triplicates. SAS: α-santalene synthase.

CYP736A167 should be combined with other metabolic engineering strategies to enhance the MVA pathway fluxes, which has been well established in yeast.

Exploration of the Molecular Mechanisms of Improved P450 Expression in Yeast

Finally, the molecular mechanisms of *AtGRP7*, *AtMSBP1*, and *AtCOL4* in improving P450 expression were explored using transcriptomic analysis. mRNAs were extracted from yJS1256-*AtMSBP1* (A6), yJS1256-*AtGRP7-AtMSBP1* (A3-A6), and yJS1256-*AtGRP7-AtMSBP1-AtCOL4* (A3-A6-E9) and sent for next-generation sequencing (RNA-Seq). Compared with the control strain yJS1256, 163 (105 up-regulated and 58 down-regulated), 405 (317 up-regulated and 88 down-regulated), and 76 (56 up-regulated and 20 down-regulated) genes had expression level changes by more than 2-fold with a threshold of <0.05 in yJS1256-*AtMSBP1* (A6), yJS1256-*AtGRP7-AtMSBP1* (A3-A6), and yJS1256-*AtGRP7-AtMSBP1-AtCOL4* (A3-A6-E9) (**Figure 4A** and **Supplementary Figure S7**). Gene ontology enrichment analysis revealed that the expression level of genes associated with cytoplasmic translation, ribosomal small subunit assembly, peptide biosynthetic process, amide biosynthetic process, and peptide metabolic process were significantly changed (**Figure 4B** and **Supplementary Figure S8**). Specifically, some genes involved in integral component of membrane, such as *COX3*, *COS12*, *COB*, and *NCW1* were up-regulated. Genes related to response to stress conditions, including *GPX2* and *GRX5*, were also up-regulated. *HAC1*, a transcription factor, which was reported to induce the expression of genes related to the folding capacity of endoplasmic reticulum (ER) (Schuck et al., 2009), was apparently up-regulated. Furthermore, *MUP3* was found to be significantly up-regulated in all strains, yJS1256-*AtMSBP1* (A6), yJS1256-*AtGRP7-AtMSBP1* (A3-A6), and yJS1256-*AtGRP7-AtMSBP1-AtCOL4* (A3-A6-E9). *MUP3* encodes a methionine permease, whose overexpression increases methionine availability and is important to maintain the stability and abundance of membrane proteins (Lee et al., 2019). *HMX1*, an ER-localized heme oxygenase, was down-regulated in all three strains. The deletion of *HMX1* has been proved to increase heme concentration and improve the activity of CYP76AD1 and CYP102A1 in yeast (Savitskaya et al., 2019). In short, a variety of genes, including some genes with unknown functions, demonstrated significant changes at the transcriptional level, indicating complex regulatory mechanisms of the expression and folding of P450s.

DISCUSSION

In recent years, there is a growing interest in establishing yeast as cell factories for the production of plant natural products. Considering the significance in natural product biosynthesis as well as the low activity of P450s, various strategies have been attempted to address the challenges in functional expression of P450s in yeast. In contrast to previous strategies, such as N-terminal truncation and protein molecular engineering, the establishment of platform strains, especially those with ER expansion, has attracted more attention (Jiang et al., 2021). As most eukaryotic P450s and CPRs are membrane-bound proteins and anchored to the ER outer membranes, ER expansion has been determined to be a generally applicable strategy to improve the functional expression of P450s Emmerstorfer et al. found that the overexpression of *ICE2* could increase the stability and activity of P450/CPR (Emmerstorfer et al., 2015). DNA repair and recombination gene *RAD52* was also reported to improve the functional expression level of P450s (Wriessnegger et al., 2016). The overexpression of *IN O 2* and the deletion of *PAH1* and *OPI1*, which had been found to enlarge the ER, could also improve the functional expression of P450s (Schuck et al., 2009; Arendt et al., 2017; Kim et al., 2019). Therefore, the identification of novel genetic engineering targets is a promising

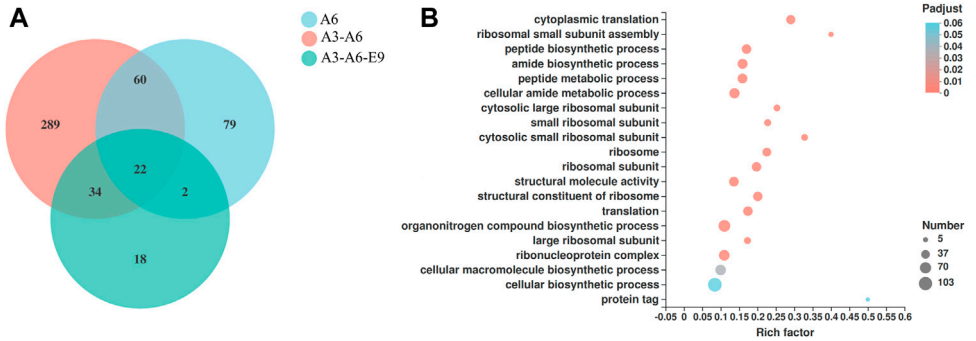

FIGURE 4 | RNA-Seq analysis of the engineered strains with improved functional expression of P450s. **(A)** Venn diagram showing the number of genes with significantly different expression levels (fold change ≥2 and *p*-value < 0.05) of the engineered strains (A6, A6-A3, and A6-A3-E9) when compared with the control strain (yJS1256). **(B)** GO function enrichment bubble plot of genes that show different expression levels in yJS1256-*AtGRP7-AtMSBP1* (A3-A6).

strategy for the construction of platform strains for functional expression of s wide variety of P450s.

Considering the complex regulatory machinery in P450 expression and folding, genome-scale engineering has been proved as an effective strategy to overcome our limited knowledge and identify new engineering targets (Lian et al., 2018; Lian et al., 2019). Among various genome-scale engineering strategies, cDNA overexpression library is the simplest and most commonly employed, with the advantages of high-level expression and the introduction of heterologous genes to enable improved and even novel phenotypes of interests. Baumann et al. successfully screened two new targets that could increase the titer of octanoic acid by overexpressing the yeast cDNA library in the octanoic acid-producing *S. cerevisiae* (Baumann et al., 2021). Similarly, Shi et al. overexpressed the *Yarrowia lipolytica* cDNA library and identified key targets that could improve the production of fatty acids in *S. cerevisiae* (Shi et al., 2016). Encouraged by these successful examples, the present study screened the *A. thaliana* cDNA library to identify the key genes that were closely related to functional expression of P450s. Using the biosensor-based high throughput screening method, three target genes from *A. thaliana* (*AtGRP7*, *AtMSBP1*, and *AtCOL4*) were identified and proved to be effective in improving the functional expression of *CYP76AD1* and *CYP736A167*, whose gene products had been determined to be rate-limiting for the production of betaxanthin and Z-α-santalol, respectively. The positive role of these genes in improving the functional expression of P450s with different origins (*CYP76AD1* from *B. vulgaris* and *CYP736A167* from *S. album*) indicated the potential of general applicability in functional expression of a wide variety of P450s.

In conclusion, an *A. thaliana* cDNA library was successfully expressed in yeast, and three target genes *AtGRP7*, *AtMSBP1*, and *AtCOL4* from *A. thaliana* were identified to be effective in improving the functional expression of CYP76AD1 and accordingly the production of betaxanthin. More importantly, these target genes could also effectively increase the activity of CYP736A167, catalyzing the hydroxylation of α-santalene to produce Z-α-santalol, whose conversion rate was increased for 2.97-fold when these three genes were overexpressed simultaneously. The target genes identified in the present study promise the construction of a platform yeast strain for functional expression of P450s and accordingly production of natural products.

DATA AVAILABILITY STATEMENT

The raw reads of the NGS data were deposited into the NCBI Sequence Read Archive (SRA) database (accession number: PRJNA760804).

AUTHOR CONTRIBUTIONS

LJ and JL designed the study, analyzed the data, and wrote the paper. LJ, CD, and TL conducted the experiments. All authors revised and approved the manuscript.

FUNDING

This work was supported by the National Key Research and Development Program of China (2018YFA0901800), the Natural Science Foundation of China (21808199), and the Natural Science Foundation of Zhejiang Province (LR20B060003).

ACKNOWLEDGMENTS

We would like to express our gratitude to Prof. John Dueber from the University of California at Berkeley for kindly sharing the biosensor yeast strain yJS1256.

SUPPLEMENTARY MATERIAL

The Supplementary Material for this article can be found online at: https://www.frontiersin.org/articles/10.3389/fbioe.2021.764851/full#supplementary-material

Supplementary Table S1 | List of plasmids used in the study.

Supplementary Table S2 | Primers used in this study.

REFERENCES

Arendt, P., Miettinen, K., Pollier, J., De Rycke, R., Callewaert, N., and Goossens, A. (2017). An Endoplasmic Reticulum-Engineered Yeast Platform for Overproduction of Triterpenoids. *Metab. Eng.* 40, 165–175. doi:10.1016/j.ymben.2017.02.007

Baumann, L., Bruder, S., Kabisch, J., Boles, E., and Oreb, M. (2021). High-throughput Screening of an Octanoic Acid Producer Strain Library Enables Detection of New Targets for Increasing Titers in *Saccharomyces cerevisiae*. *ACS Synth. Biol.* 10, 1077–1086. doi:10.1021/acssynbio.0c00600

Bolwell, G. P., Bozak, K., and Zimmerlin, A. (1994). Plant Cytochrome P450. *Phytochemistry* 37, 1491–1506. doi:10.1016/s0031-9422(00)89567-9

DeLoache, W. C., Russ, Z. N., Narcross, L., Gonzales, A. M., Martin, V. J. J., and Dueber, J. E. (2015). An Enzyme-Coupled Biosensor Enables (*S*)-reticuline Production in Yeast from Glucose. *Nat. Chem. Biol.* 11, 465–471. doi:10.1038/nchembio.1816

Dong, C., Jiang, L., Xu, S., Huang, L., Cai, J., Lian, J., et al. (2020). A Single Cas9-VPR Nuclease for Simultaneous Gene Activation, Repression, and Editing in *Saccharomyces cerevisiae*. *ACS Synth. Biol.* 9, 2252–2257. doi:10.1021/acssynbio.0c00218

Elfaki, I., Mir, R., Almutairi, F. M., and Duhier, F. M. A. (2018). Cytochrome P450: Polymorphisms and Roles in Cancer, Diabetes and Atherosclerosis. *Asian Pac. J. Cancer Prev.* 19, 2057–2070. doi:10.22034/APJCP.2018.19.8.2057

Emmerstorfer, A., Wimmer-Teubenbacher, M., Wriessnegger, T., Leitner, E., Müller, M., Kaluzna, I., et al. (2015). Over-expression ofICE2stabilizes Cytochrome P450 Reductase inSaccharomyces cerevisiaeandPichia Pastoris. *Biotechnol. J.* 10, 623–635. doi:10.1002/biot.201400780

Galanie, S., Thodey, K., Trenchard, I. J., Filsinger Interrante, M., and Smolke, C. D. (2015). Complete Biosynthesis of Opioids in Yeast. *Science* 349, 1095–1100. doi:10.1126/science.aac9373

Gou, M., Ran, X., Martin, D. W., and Liu, C.-J. (2018). The Scaffold Proteins of Lignin Biosynthetic Cytochrome P450 Enzymes. *Nat. Plants* 4, 299–310. doi:10.1038/s41477-018-0142-9

Guengerich, F. P., Waterman, M. R., and Egli, M. (2016). Recent Structural Insights into Cytochrome P450 Function. *Trends Pharmacol. Sci.* 37, 625–640. doi:10.1016/j.tips.2016.05.006

Hausjell, J., Halbwirth, H., and Spadiut, O. (2018). Recombinant Production of Eukaryotic Cytochrome P450s in Microbial Cell Factories. *Biosci. Rep.* 38. doi:10.1042/BSR20171290

Hayashi, M., and Nishimura, M. (2006). Arabidopsis Thaliana-A Model Organism to Study Plant Peroxisomes. *Biochim. Biophys. Acta (Bba) - Mol. Cel Res.* 1763, 1382–1391. doi:10.1016/j.bbamcr.2006.08.014

Jiang, L., Huang, L., Cai, J., Xu, Z., and Lian, J. (2021). Functional Expression of Eukaryotic Cytochrome P450s in Yeast. *Biotechnol. Bioeng.* 118, 1050–1065. doi:10.1002/bit.27630

Kim, J.-E., Jang, I.-S., Son, S.-H., Ko, Y.-J., Cho, B.-K., Kim, S. C., et al. (2019). Tailoring the *Saccharomyces cerevisiae* Endoplasmic Reticulum for Functional Assembly of Terpene Synthesis Pathway. *Metab. Eng.* 56, 50–59. doi:10.1016/j.ymben.2019.08.013

Köster, T., Meyer, K., Weinholdt, C., Smith, L. M., Lummer, M., Speth, C., et al. (2014). Regulation of Pri-miRNA Processing by the hnRNP-like Protein AtGRP7 in *Arabidopsis*. *Nucleic Acids Res.* 42, 9925–9936. doi:10.1093/nar/gku716

Lee, S., Ho, H.-C., Tumolo, J. M., Hsu, P.-C., and MacGurn, J. A. (2019). Methionine Triggers Ppz-Mediated Dephosphorylation of Art1 to Promote Cargo-specific Endocytosis. *J. Cel Biol.* 218, 977–992. doi:10.1083/jcb.201712144

Lian, J., HamediRad, M., Hu, S., and Zhao, H. (2017). Combinatorial Metabolic Engineering Using an Orthogonal Tri-functional CRISPR System. *Nat. Commun.* 8, 1688. doi:10.1038/s41467-017-01695-x

Lian, J., Mishra, S., and Zhao, H. (2018). Recent Advances in Metabolic Engineering of *Saccharomyces cerevisiae*: New Tools and Their Applications. *Metab. Eng.* 50, 85–108. doi:10.1016/j.ymben.2018.04.011

Lian, J., Schultz, C., Cao, M., HamediRad, M., and Zhao, H. (2019). Multi-functional Genome-wide CRISPR System for High Throughput Genotype-Phenotype Mapping. *Nat. Commun.* 10, 5794. doi:10.1038/s41467-019-13621-4

Min, J.-H., Chung, J.-S., Lee, K.-H., and Kim, C. S. (2015). The CONSTANS-like 4 Transcription Factor, AtCOL4, Positively Regulates Abiotic Stress Tolerance through an Abscisic Acid-dependent Manner in *Arabidopsis*. *J. Integr. Plant Biol.* 57, 313–324. doi:10.1111/jipb.12246

Paddon, C. J., Westfall, P. J., Pitera, D. J., Benjamin, K., Fisher, K., McPhee, D., et al. (2013). High-level Semi-synthetic Production of the Potent Antimalarial Artemisinin. *Nature* 496, 528–532. doi:10.1038/nature12051

Savitskaya, J., Protzko, R. J., Li, F.-Z., Arkin, A. P., and Dueber, J. E. (2019). Iterative Screening Methodology Enables Isolation of Strains with Improved Properties for a FACS-Based Screen and Increased L-DOPA Production. *Sci. Rep.* 9, 5815. doi:10.1038/s41598-019-41759-0

Schuck, S., Prinz, W. A., Thorn, K. S., Voss, C., and Walter, P. (2009). Membrane Expansion Alleviates Endoplasmic Reticulum Stress Independently of the Unfolded Protein Response. *J. Cel Biol.* 187, 525–536. doi:10.1083/jcb.200907074

Schuler, M. A., and Werck-Reichhart, D. (2003). Functional Genomics of P450s. *Annu. Rev. Plant Biol.* 54, 629–667. doi:10.1146/annurev.arplant.54.031902.134840

Shi, Q.-M., Yang, X., Song, L., and Xue, H.-W. (2011). *Arabidopsis* MSBP1 Is Activated by HY5 and HYH and Is Involved in Photomorphogenesis and Brassinosteroid Sensitivity Regulation. *Mol. Plant* 4, 1092–1104. doi:10.1093/mp/ssr049

Shi, S., Ji, H., Siewers, V., and Nielsen, J. (2016). Improved Production of Fatty Acids bySaccharomyces Cerevisiaethrough Screening a cDNA Library from the Oleaginous yeastYarrowia Lipolytica. *FEMS Yeast Res.* 16, fov108. doi:10.1093/femsyr/fov108

Stavropoulou, E., Pircalabioru, G. G., and Bezirtzoglou, E. (2018). The Role of Cytochromes P450 in Infection. *Front. Immunol.* 9, 89. doi:10.3389/fimmu.2018.00089

Streitner, C., Hennig, L., Korneli, C., and Staiger, D. (2010). Global Transcript Profiling of Transgenic Plants Constitutively Overexpressing the RNA-Binding Protein AtGRP7. *BMC Plant Biol.* 10, 221. doi:10.1186/1471-2229-10-221

Wriessnegger, T., Moser, S., Emmerstorfer-Augustin, A., Leitner, E., Müller, M., Kaluzna, I., et al. (2016). Enhancing Cytochrome P450-Mediated Conversions in *P. Pastoris* through *RAD52* Over-expression and Optimizing the Cultivation Conditions. *Fungal Genet. Biol.* 89, 114–125. doi:10.1016/j.fgb.2016.02.004

Yang, F., Ouma, W. Z., Li, W., Doseff, A. I., and Grotewold, E. (2016). Establishing the Architecture of Plant Gene Regulatory Networks. *Methods Enzymol.* 576, 251–304. doi:10.1016/bs.mie.2016.03.003

Zhu, M., Wang, C., Sun, W., Zhou, A., Wang, Y., Zhang, G., et al. (2018). Boosting 11-Oxo-β-Amyrin and Glycyrrhetinic Acid Synthesis in *Saccharomyces cerevisiae* via Pairing Novel Oxidation and Reduction System from Legume Plants. *Metab. Eng.* 45, 43–50. doi:10.1016/j.ymben.2017.11.009

Conflict of Interest: The authors declare that the research was conducted in the absence of any commercial or financial relationships that could be construed as a potential conflict of interest.

frontiers in Bioengineering and Biotechnology

ORIGINAL RESEARCH
published: 17 December 2021
doi: 10.3389/fbioe.2021.795885

Using Unnatural Protein Fusions to Engineer a Coenzyme Self-Sufficiency System for D-Phenyllactic Acid Biosynthesis in *Escherichia coli*

Zhao Qin[1], *Dan Wang*[1]*, *Ruoshi Luo*[1], *Tinglan Li*[1], *Xiaochao Xiong*[2] *and Peng Chen*[1]

[1]School of Chemistry and Chemical Engineering, Chongqing University, Chongqing, China, [2]Department of Biological Systems Engineering, Washington State University, Pullman, WA, United States

The biosynthetic production of D-penyllactic acid (D-PLA) is often affected by insufficient supply and regeneration of cofactors, leading to high production cost, and difficulty in industrialization. In this study, a D-lactate dehydrogenase (D-LDH) and glycerol dehydrogenase (GlyDH) co-expression system was constructed to achieve coenzyme NADH self-sufficiency and sustainable production of D-PLA. Using glycerol and sodium phenylpyruvate (PPA) as co-substrate, the *E. coli* BL21 (DE3) harboring a plasmid to co-express LfD-LDH and BmGlyDH produced 3.95 g/L D-PLA with a yield of 0.78 g/g PPA, similar to previous studies. Then, flexible linkers were used to construct fusion proteins composing of D-LDH and GlyDH. Under the optimal conditions, 5.87 g/L D-PLA was produced by expressing LfD-LDH-l_3-BmGlyDH with a yield of 0.97 g/g PPA, which was 59.3% increased compared to expression of LfD-LDH. In a scaled-up reaction, a productivity of 5.83 g/L/h was reached. In this study, improving the bio-catalytic efficiency by artificial redox self-equilibrium system with a bifunctional fusion protein could reduce the bio-production cost of D-PLA, making this bio-production of D-PLA a more promising industrial technology.

Keywords: coenzyme self-sufficiency, d-Lactate dehydrogenase, phenyllactic acid, D-PLA, glycerol dehydrogenase, fusion protein

OPEN ACCESS

Edited by:
Jingyu Wang,
Westlake Institute for Advanced Study (WIAS), China

Reviewed by:
Min Jiang,
Nanjing Tech University, China
Friso Aalbers,
University of Groningen, Netherlands

***Correspondence:**
Dan Wang
dwang@cqu.edu.cn

Specialty section:
This article was submitted to Synthetic Biology, a section of the journal Frontiers in Bioengineering and Biotechnology

Received: *15 October 2021*
Accepted: *01 December 2021*
Published: *17 December 2021*

Citation:
Qin Z, Wang D, Luo R, Li T, Xiong X and Chen P (2021) Using Unnatural Protein Fusions to Engineer a Coenzyme Self-Sufficiency System for D-Phenyllactic Acid Biosynthesis in Escherichia coli. *Front. Bioeng. Biotechnol. 9:795885. doi: 10.3389/fbioe.2021.795885*

INTRODUCTION

Phenyllactic acid (PLA) widely exists in honey and fermented food and includes two enantiomers as D-phenyllactic acid (D-PLA) and L-phenyllactic acid (L-PLA) (Sorrentino et al., 2018; Luo et al., 2020a). Due to its safety, antimicrobial activity, low odor and good hydrophilicity, PLA has potential applications in the food, animal feed, pharmaceutical, and cosmetic industries (Valerio et al., 2016; Sun et al., 2019). Previous researchers found that the bactericidal effect of D-PLA was stronger than that of L-PLA (Dieuleveux et al., 1998) and D-PLA can be used as biological preservatives, antiviral compounds, hypoglycemic drugs, and protein inhibitors (Xu et al., 2015; Zhu et al., 2017; Liu et al., 2021). Moreover, because PLA can be polymerized into the aromatic polymers poly-PLA, it is a promising bio-based

Abbreviations: DCW, cell catalyst; D-LDH, d-lactate dehydrogenase; D-PLA, d-phenyllactic acid; FDH, formate dehydrogenase; GDH, glucose dehydrogenase; GlyDH, glycerol dehydrogenase; HPLC-MS, high performance liquid chromatography-mass spectrometry; IPTG, isopropyl-β-d-thiogalactoside; l1, (GGGGS)1; l2, (GGGGS)2; l3, (GGGGS)3; l6, (GGGGS)6; PCR, polymerase chain reaction; PLA, phenyllactic acid; PPA, sodium phenylpyruvate.

material (Wu et al., 2020). Although chemical methods of PLA production have been well studied, some limitations such as complex technology routes, harsh reaction conditions, excessive by-products and environmental pollution have hampered the chemical synthesis of PLA. (Wang et al., 2018a; Costa et al., 2020; Xu et al., 2020). Compared with chemical methods, biological methods have advantages of mild action conditions, energy savings, and environmental compatibility (Zhao et al., 2018). Therefore, the development of a eco-friendly biosynthesis method for PLA production is highly desirable.

PLA could be generally produced by a wide range of lactic acid bacteria or *Escherichia coli* with PPA, phenylalanine or glucose as starting materials in previous studies (Sorrentino et al., 2018; Wu et al., 2020). *L. plantarum* IMAU10124, *P. pentosaceus*, *E. coli* GK1, and *L. crustorum* NWAFU1078 produced 0.229 g/L (Zhang et al., 2014), 0.136 g/L (Yu et al., 2015a), 1.429 g/L (Kawaguchi et al., 2015), and 2.526 g/L (Xu et al., 2020) of PLA grown in MRS broth. Overall, since these methods produce various by-products and have relatively low yields, enzymatic/whole-cell cascade onecatalyst emerged as a green alternative for PLA production (Hou et al., 2019). Whole-cell catalytic conversion of PPA to PLA by strain overexpressing of NADH-dependent lactate dehydrogenase (LDH) is regarded as a more cost-efficient technology (Li et al., 2008; Mu et al., 2012; Luo et al., 2020b). D-LDH was overexpressed to produce D-PLA from PPA in *Leuconostoc mesenteroides* ATCC 8293, and the results showed that growing cells produced 35 mM D-PLA with a yield of 75.2–83.3% (Li et al., 2014). A novel NADH-dependent LDH gene, named *lrldh*, was cloned from *Lactobacillus rossiae* and heterologously expressed in recombinant *E. coli*/pET28a-*lrldh*. 20.5 g/L D-PLA was produced with a productivity of 49.2 g/L/d in a fed-batch biotransformation process (Luo et al., 2020a). Glucose and Phe need to undergo intermediate metabolism to produce PLA, which results in the increased fermentation time and decreased productivity. PPA is considered as a feasible precursor for the large-scale production of PLA, because it can biosynthesize PLA in one-step method and improve the catalytic efficiency (Li et al., 2014; Wang et al., 2018b).

However, the conversion from PPA to PLA by LDH requires the consumption of expensive coenzyme NADH. So the pathway involved in NADH regeneration is considered as an auxiliary pathway for PLA biosynthesis (Wu et al., 2020). Therefore, the whole-cell cascade catalysis using recombinant *E. coli* co-expression of glucose dehydrogenase (GDH)/formate dehydrogenase (FDH) and LDH has been widely used in the synthesis of PLA (Zhao et al., 2018; Rajanikar et al., 2021). Recombinant *E. coli* co-expressing LDH and GDH produced 17.25 g/L PLA from PPA with a productivity of 0.86 g/L/h (Zhu et al., 2017). Recombinant *E. coli* co-expressing D-LDH and FDH produced 10.02 g/L D-PLA from phenylalanine with a productivity of 1.67 g/L/h (Zheng et al., 2018). Unlike FDH or GDH, glycerol dehydrogenase (GlyDH) catalyzes the reduction of glycerol to dihydroxyacetone without the formation of toxic formic acid or gluconic acid (Xu et al., 2016), therefore, among these whole-cell reaction systems, co-expression of GlyDH and LDH might be a novel strategy for PLA synthesis. Furthermore, the co-substrate glucose was replaced with cost-effective glycerol to decrease the cost and improve the intracellular cofactor concentration.

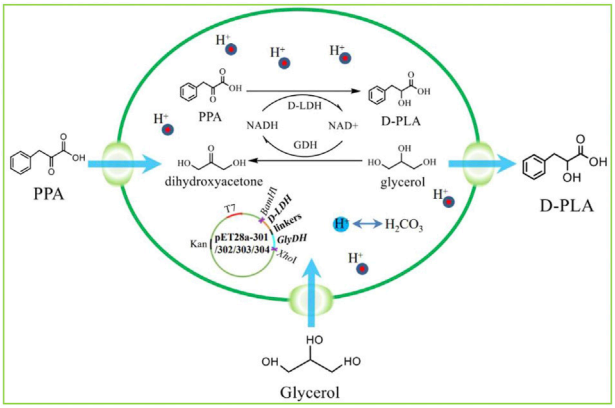

FIGURE 1 | The program of redox self-balanced coenzyme regeneration and whole-cell synthesis of D-PLA.

Fusion proteins have been emerged recently as a new technology in biocatalysts, protein switches and therapeutics, aiming to channel substrates in sequential reactions, reduce effective reaction volume, facilitate cofactor regeneration and improve electron transfer (Yu et al., 2015b; Aalbers and Fraaije, 2019; Wu et al., 2021). Linkers have a critical role in the functionality and bioactivity of the destined fusion proteins, which can increase the stability/folding, expression, improve the biological activity, target to specific sites (Anami et al., 2018; He et al., 2019). Fan *et al.* constructed bifunctional and trifunctional fusions Mdh-Hps, Hps-Phi, and Mdh-Hps-Phi with flexible linkers $(GGGGS)_3$ and $(GGGGS)_6$, and the results showed that fusing Mdh with Hps or Hps-Phi enhanced methanol conversion to fructose-6-phosphate by 30% (Fan et al., 2018). Patgiri *et al.* engineered a fusion protein composed of lactate oxidase and catalase, which normalized the intracellular NADH:NAD + ratio by converting lactate and oxygen to pyruvate and water (Patgiri et al., 2020).

In this study, fusion protein engineering of D-LDH and GlyDH is conducted to aim for effective regeneration of coenzyme NADH for D-PLA biosynthesis. Firstly, a NADH-dependent D-LDH was overexpressed in recombinant *E. coli* CP101 to produce D-PLA from PPA. Then, plasmids for co-expression of *D-LDH* (two different genes) and *GlyDH* (two different genes) were transformed in *E. coli* (CP201, CP202, CP203, CP204) to achieve coenzyme self-sufficiency. To further improve the regeneration efficiency of coenzyme and to increase the yield of D-PLA, artificial fusion protein technology was used to construct D-LDH and GlyDH bifunctional fusion proteins as shown in **Figure 1**.

MATERIALS AND METHODS

Strains, Plasmids, and Chemicals

Enzymes (DNA polymerases, T4 DNA ligase, *BamH*I, and *Xho*I) and kits (DNA purification kit, plasmid isolation, DNA ligation kit, and competent cell preparation kit) were supplied by Takara

(Dalian, China). With the exception of PPA, PLA, and NADH (Tsingke Biotechnology Co. Ltd., Beiing, China), all chemical reagents were purchased from China National Medicines Co. Ltd. (Beijing, China).

The Construction Process of the Plasmids

All bacterial strains and plasmids used in this study are listed in **Supplementary Table S1**. The *D-LDH* genes *of Lactobacillus fermentum*, *Lactobacillus sp*.SK007, and *GlyDH* genes of *Bacillus megaterium*, *Exiguobacterium sibiricum* were amplified via polymerase chain reaction (PCR) by using the relevant primer pairs listed in **Supplementary Table S3**. The PCR products were digested with *BamH*I and *Xho*I and ligated to pET28a to construct pET28a-*LfD-LDH*, pET28a-*LsD-LDH*, pET28a-*BmGlyDH* and pET28a-*EsGlyDH*, and then introduced into BL21 (DE3) individually to form the novel corresponding recombinant strains CP101, CP102, CP103, and CP104. The *LfD-LDH* and Bm*GlyDH* were ligated by fusion PCR, and then the PCR product was digested with *BamHI* and *XhoI* and ligated to pET28a to construct pET28a-*LfD-LDH-BmGlyDH*. Using the same method as above, plasmids pET28a-*LfD-LDH-EsGlyDH*, pET28a-*LsD-LDH-BmGlyDH*, and pET28a-*LsD-LDH-EsGlyDH* could be constructed. Subsequently, plasmids above were introduced into BL21 (DE3) individually to form the novel corresponding recombinant strains CP201, CP202, CP203, and CP204. To construct fused *D-LDH-GlyDH* genes, fragments encoding flexible linkers were added to the C-terminal of *D-LDH* and N-terminal of *GlyDH* by overlap extension PCR using the primer pairs listed in **Supplementary Table S3**. Flexible linkers $(GGGGS)_1$ $(GGGGS)_2$, $(GGGGS)_3$, and $(GGGGS)_6$ listed in **Supplementary Table S2** were added to the C-terminal of *LfD-LDH* and N-terminal of *BmGlyDH* and then ligated to pET28a to construct pET28a-*LfD-LDH-*l_1*-BmGlyDH*, pET28a-*LfD-LDH-*l_2*-BmGlyDH*, pET28a-*LfD-LDH-*l_3*-BmGlyDH*, and pET28a-*LfD-LDH-*l_6*-BmGlyDH*, and then introduced into BL21 (DE3) individually to construct recombinant strains CP301, CP302, CP303, and CP304. Successfully constructed recombinant plasmids were verified by DNA sequencing (Tsingke Biotechnology Co., Ltd., Beijing, China). CP100 carrying the backbone plasmid pET28a was constructed as the control strain.

Preparation of Whole-Cell Biocatalyst

Recombinant *E. coli* were inoculated into 40 ml LB medium (10 g/L tryptone, 5 g/L yeast extract, 10 g/L NaCl) containing kanamycin (50 μg/ml) and grown in a rotary shaker (200 RPM) at 37°C overnight. 400 μL seed culture was inoculated into 40 ml LB medium containing 50 μg/ml kanamycin, and incubated at 37°C and 200 RPM to OD_{600} = 0.8. The recombinant *E. coli* was induced with 0.2 mM isopropyl-β-D-thiogalactoside (IPTG) at 25°C for 10 h. The cells were obtained via centrifugation at 4°C and 6,000 r/min for 10 min and washed three times with pH 7.0 PBS buffer. Cell catalyst (DCW) concentration was checked spectrophotometrically (722s, Shanghai Precision Scientific Instrument Co., Ltd., Shanghai, China) at an optical density of 600 (Yang et al., 2013). The concentrations of NADH, PPA, and PLA were measured as reported previously (Hou et al., 2017).

Optimization of D-LDH Induction and Enzymatic Catalysis Conditions

The recombinant *E. coli* was inoculated into 40 ml LB medium containing kanamycin (50 μg/ml) and grown overnight in a rotary shaker (200 RPM) at 37°C. 400 μL seed culture was inoculated into 50 ml LB medium for expression. The induction conditions, including temperature (20°C, 25°C, 30°C, 35°C, and 40°C), pH (6.0, 6.5, 7.0, 7.5, and 8.0), and concentration of IPTG (0.1, 0.2, 0.3, 0.4 and 0.5 mM), were investigated.

The enzymatic catalysis conditions of PPA to D-PLA were optimized. For D-PLA bioconversion, the catalytic system had 5 ml, which included 5 g/L PPA, 5.61 g/L glycerol, 9 g/L DCW, and 2% glucose. The bioconversion reactions were performed at 35°C on a 200 RPM shaker for 10 min for D-PLA production. The effects of temperature (25°C, 30°C, 35°C, 37°C, and 40°C), pH (6.0, 6.5, 7.0, 7.5, and 8.0), and PPA concentration (5, 6, 7, 8, and 9 g/L) on D-PLA production were determined.

Scale-Up of Bioconversions

Scale-up biotransformation is usually achieved by fed-batch cultures in a bioreactor (Abadli et al., 2021; Parizotto et al., 2021). The cell culture was concentrated and suspended (OD_{600} = 1.6) in 1-L PBS buffer (pH 7.0) with 60 g/L PPA and 66.5 g/L glycerol. Additional 40 g/L PPA and 16.78 g/L glycerol were added after 8 h bioconversion. The total concentration of PPA used in the system was 100 g/L. The scaled-up bioconversion was performed in a 5-L fermenter at 200 RPM, pH 7.0, 35°C.

Analytical Methods

The successful synthesis of PLA was confirmed by HPLC-MS (Agilent1260 series, Hewlett-Packard) with a C-18 5 μm column (4.6*25 mm) and the analysis was performed at 40°C with a mobile phase comprising 20% acetonitrile in water at a flow rate of 1 ml/min, wavelength 210 nm, 10 μL injection volume (Cheng et al., 2020) (**Supplementary Figures S1, S2**).

RESULTS AND DISCUSSION

Construction of the D-PLA Biosynthetic Pathway in *E. coli*

Firstly, the synthesis pathway of D-PLA was constructed in single-enzyme expressing strains by overexpressing the D-LDH or GlyDH, so as to select suitable genes for the construction of co-expressing strains as shown in **Figure 2A**. CP101 with *Lf*D-LDH and CP103 with *Bm*GlyDH showed better productivity than CP102 with *Ls*D-LDH and CP104 with *Es*GlyDH, with maximum conversion rates of 60.7 and 70.4% for PPA and glycerol, respectively, within 12 h. At the same time, their production capacity to the D-PLA was measured as shown in **Figure 2B**. CP101 could achieve the highest yield of D-PLA (5 g/L PPA to 3.07 g/L D-PLA) without co-expression of a cofactor regeneration system, while CP100, CP103 and CP104 lacking *D-LDH* gene could hardly produce PLA as reported (Jung et al., 2019). No D-PLA was detected in the control system, indicating that no enzyme could catalyze PPA to D-PLA in CP100.

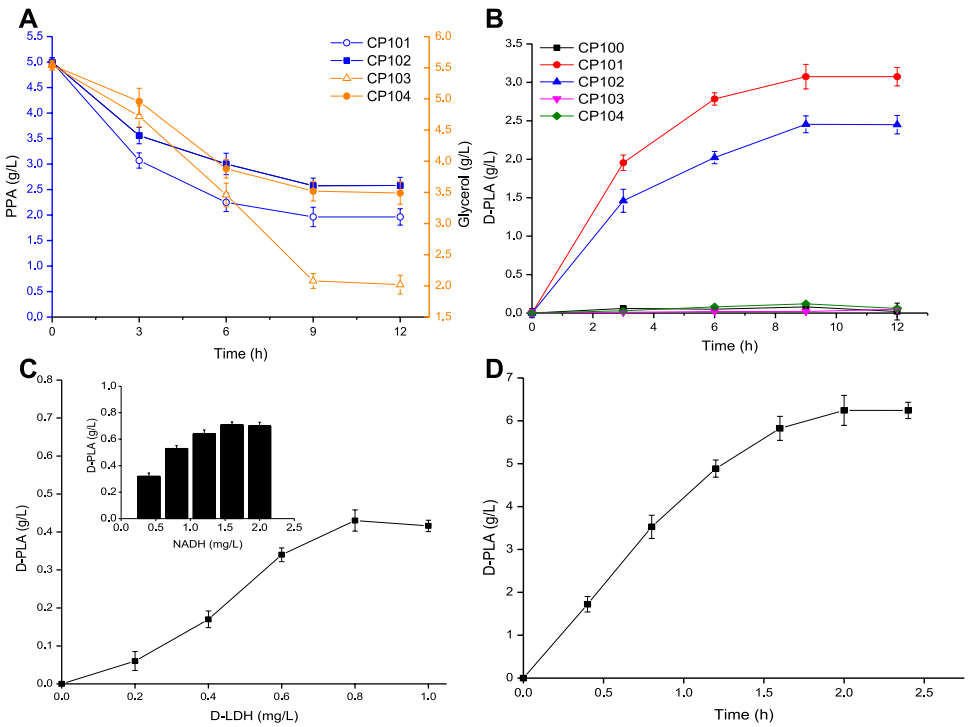

FIGURE 2 | (A) Time course of the consumption of PPA (by CP101, CP102), and glycerol (by CP103, CP104); **(B)** Time course of the production of PLA by CP100, CP101, CP102, CP103, and CP104; **(C)** The effect of D-LDH and NADH concentration on D-PLA titer; **(D)** Time course of the production of D-PLA by enzyme catalysis. Data are means ± SD (n = 3).

Therefore, one-step biosynthesis of D-PLA using PPA as raw material has been successfully realized.

D-LDH is a NADH-dependent enzyme, which has commonly used in the biosynthesis of D-PLA (Li et al., 2008; Mu et al., 2012). The effects of D-LDH and NADH concentration on D-PLA titer were determined. As it could be seen from **Figure 2C**, with the increase of enzyme dosage, D-PLA increased up to a maximum of 0.43 g/L at 0.8 mg/L D-LDH and 0.71 g/L at 1.6 mg/L NADH within 10 min, respectively. D-PLA cannot be produced without NADH addition indicating that NADH-dependent D-LDH must rely on NADH to catalyze the conversion of PPA to D-PLA. Similar studies have reported that the enzymatic production of PLA by *P. pentosaceus* improved by 30-folds on supplementation with NADH and NADH-regeneration catalyst (Yu et al., 2014). As it could be seen from **Figure 2D**, under the optimal conditions at pH 7 and 35°C, with PPA 7 g/L, 0.8 mg/L D-LDH, and NADH 1.6 mg/L in the fermentation broth, the D-PLA titer reached 6.24 g/L with a yield of 0.881 g/g PPA, respectively, within 2 h. Although it has been proved that the production of D-PLA by D-LDH enzyme catalysis can be achieved by adding coenzyme NADH, the high cost of NADH limits its industrial application.

The Self-Sufficient System of NADH With Coordinated Enzyme

In order to make up for the shortage of NADH in single-enzyme expressing strains and further increase yield of D-PLA in recombinant *E. coli*, a co-expression system was constructed for PLA biosynthesis. As it could be seen from **Figure 3A**, the co-expressing strains CP201, CP202, CP203, and CP204 catalyzed the synthesis of D-PLA, and obtained 3.95, 3.62, 3.73, and 3.50 g/L D-PLA from 5 g/L PPA in the biotransformation process for 12 h, respectively, while the control CP101 only obtained 3.07g/L. Therefore, for the single-enzyme expression of D-LDH, the co-expression of D-LDH and GlyDH can increase the yield of D-PLA by about 29.7%.

The above enzymatic catalysis results (**Figure 2C**) show that the concentration of NADH is an important limiting factor affecting the production of PLA by D-LDH catalysis. The cost of using NADH was expensive, so the intracellular NADH concentration was increased by using co-substrates (Hou et al., 2019). Therefore, the NADH concentration can be increased by using co-substrates (PPA and glycerol) in the co-expression system. The concentration of NADH in whole-cell *E. coli* was measured during the biosynthesis of D-PLA as shown in **Figure 3B**. In the control strain CP101 with PPA as the substrate of D-LDH single-enzyme expression, NADH decreased by 47.8% at 9 h. However, the intracellular NADH concentration of co-expressing strains (CP201, CP202, CP203, and CP204) with PPA and glycerol as co-substrates showed an increasing trend. This is because GlyDH in co-expressing strains oxidizes glycerol to dihydroxyacetone and produces coenzyme NADH, so more abundant NADH can be provided. A similar

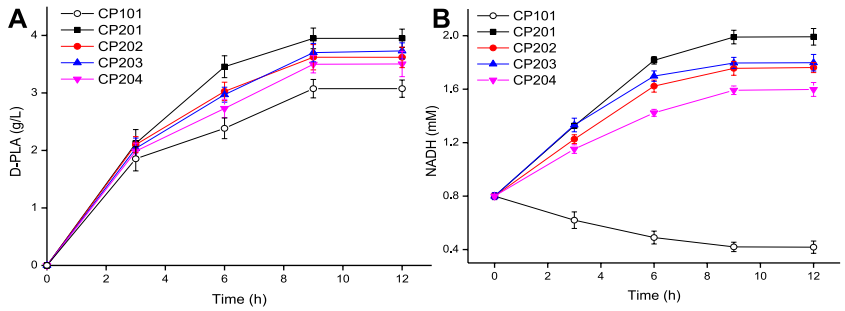

FIGURE 3 | (A) Time course of the production of D-PLA by D-LDH and GlyDH co-expressed strains CP201, CP202, CP203, and CP204; **(B)** Time course of intracellular NADH concentration. Data are means ± SD (n = 3).

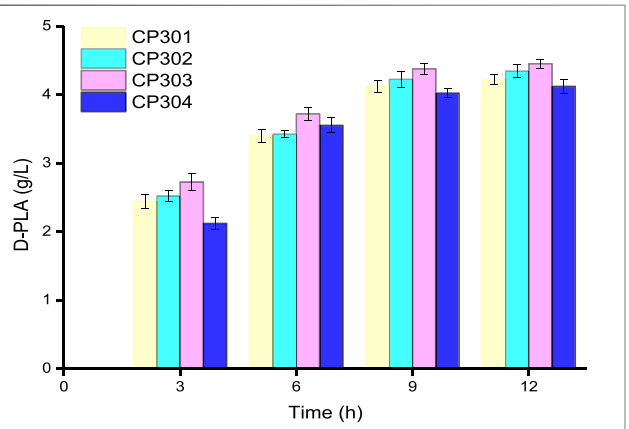

FIGURE 4 | Time course of the production of D-PLA by fusion protein strains CP301, CP302, CP303, and CP304. Data are means ± SD (n = 3).

study reported whole-cell biocatalyst of co-expressing GDH and D-LDH was constructed to produce 262.8 g/L/d D-PLA without supplement of NADH (Luo et al., 2020b). Therefore, the co-substrate and co-expression system successfully constructed in this study can realize the regeneration of NADH to better produce D-PLA.

Improve the Efficiency of the Self-Sufficient System by Fusion Enzyme Engineering

In the area of enzyme engineering, early attempts were made to create two-protein fusions either to increase consecutive enzyme reaction rates or to generate bifunctional enzymes (Lindbladh et al., 1992; Beguin, 1999; Xiong et al., 2021). For example, a 77-fold improvement in the final product titer using a synthetic scaffold protein by recruiting three heterologous pathway enzymes in a designable manner (Dueber et al., 2009). For another example, a bifunctional enzyme coupling dihydroxyacetone kinase and fructose-1,6-bisphosphate aldolase was constructed to promote a 20-fold increase in the initial rate of the overall aldol reaction (Iturrate et al., 2010). According to previous studies, fusion enzyme engineering is a promising method for *in situ* recovery of co-enzyme NADH (Prachayasittikul et al., 2006).

Based on the results of the above researchers in the area of fusion enzyme engineering, flexible Linkers $(GGGGS)_1$, $(GGGGS)_2$, $(GGGGS)_3$, and $(GGGGS)_6$ were used to construct D-LDH and GlyDH bifunctional fusion proteins by over-lap PCR technique. As it could be seen from **Figure 4**, the four fusion protein strains CP301 (*LfD-LDH-l_1-BmGlyDH*), CP302 (*LfD-LDH-l_2-BmGlyDH*), CP303 (*LfD-LDH-l_3-BmGlyDH*), and CP304 (*LfD-LDH-l_6-BmGlyDH*) were used to catalyze the transformation of 5 g/L PPA into D-PLA, and 4.23, 4.35, 4.45, and 4.12 g/L PLA were obtained, respectively, within 12 h. The strain CP303 achieved 4.45 g/L titer D-PLA with a yield of 0.879 g/g PPA, which is 1.13 times that of the strain CP201. This benefits from the flexible peptide linker which was likely to bring enzyme moieties in close proximity for superior cofactor channeling, making D-LDH and GlyDH catalysis more efficient (Dueber et al., 2009). A similar study reported the application of peptide linker in the construction of bifunctional FDH and leucine dehydrogenase enzymatic complex for efficient cofactor regeneration, showing the production rate of fusion enzymatic complex with suitable flexible peptide linker was increased by 1.2 times compared with free enzyme mixture (Zhang et al., 2017). In addition, this linker might provide the proper space and flexibility to accommodate the different subunits of the LDH and GlyDH, as dehydrogenases are typically multimeric, and the fusion of dehydrogenases has been found to perturb proper oligomerization (Lerchner et al., 2016; Aalbers and Fraajie, 2017; Peters et al., 2017). Therefore, we successfully constructed D-LDH and GlyDH bifunctional fusion proteins to accelerate the cyclic regeneration of NADH and improve the efficiency of enzyme catalysis.

Optimization of Induction Conditions and Co-Substrates

In order to improve the ability and efficiency of the fusion proteins to catalyze the synthesis of D-PLA, the induction conditions of *E. coli* CP303 expressing D-LDH/GlyDH were optimized. Single factor experiments were used to optimize the induction conditions of recombinant *E. coli* in shake flasks, namely the influence of IPTG concentration, induction

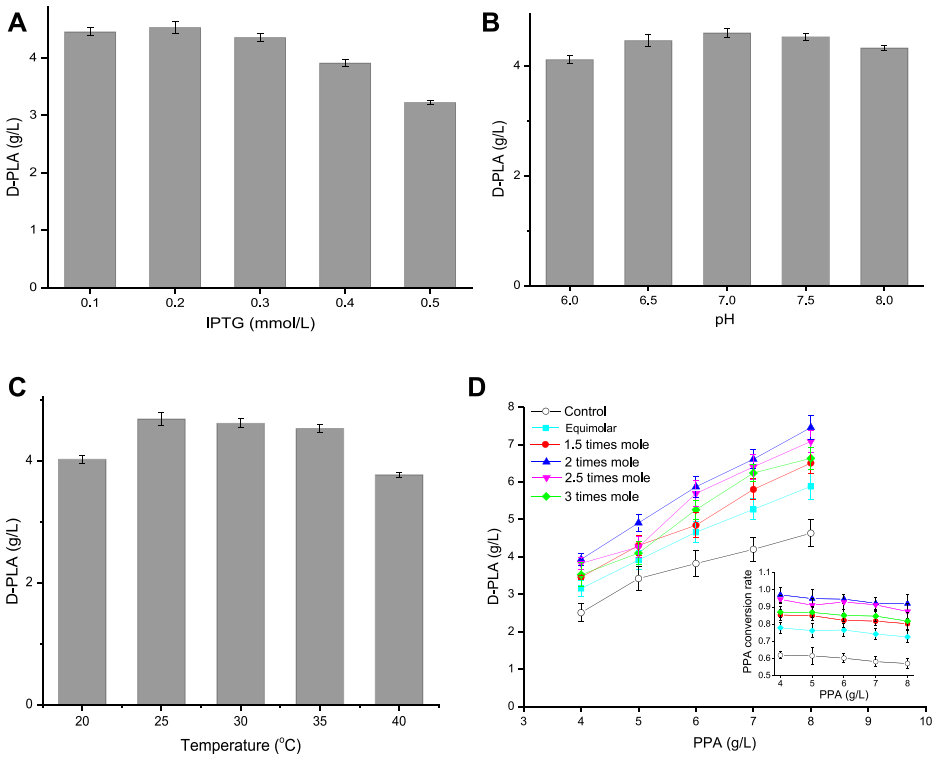

FIGURE 5 | (A) Effect of IPTG concentration on D-PLA titer; **(B)** Effect of pH on D-PLA titer; **(C)** Effect of temperature on D-PLA titer; **(D)** Effect of substrate (glycerol, relative to PPA) on D-PLA titer. Data are means ± SD (n = 3).

temperature, and pH on the catalytic synthesis of D-PLA by recombinant *E. coli* CP303. In addition, the ratio of substrate PPA, glycerol and cell catalyst were also optimized. Recombinant *E. coli* basic induction and co-substrate conditions: OD_{600} = 0.8, 0.1 mM IPTG, 5 g/L PPA, 5.61 g/L glycerol and induce expression at 25°C for 12 h.

As it could be seen from **Figure 5A**, when the IPTG concentration increased from 0.1 to 0.5 mM, the D-PLA titer increased first and then decreased. Compared with 0.1 mM IPTG, the expression of D-LDH/GlyDH fusion increased by induction with 0.2 mM IPTG and achieved a highest titer (4.53 g/L) D-PLA. However, when the IPTG concentration increased to 0.3 mM, it began to inhibit the growth of *E. coli* CP303, especially when the IPTG concentration was 0.5 mM. Therefore, the optimal IPTG concentration was 0.2 mM, the cell growth was better and D-LDH/GlyDH enzyme activity was the highest at this concentration. pH can affect the spatial structure and activity of enzymes, so an optimal pH needs to be explored. The effect of pH on D-PLA production as shown in **Figure 5B**. When the reaction system pH was 7.0, the D-PLA titer catalyzed by *E. coli* CP303 was higher than other pH, indicating that the neutral environment can maintain the good catalytic activity of D-LDH and GlyDH at the same time, so the high yield of D-PLA can be achieved by maintaining the pH at 7.0. Temperature affects the growth rate, cell metabolic activity and protein production rate of *E. coli* CP303, so induction temperature has also been studied as shown in **Figure 5C**. When the induction temperature was 20°C, the slow metabolism of recombinant *E. coli* led to the slow expression rate of D-LDH/GlyDH fusion protein and the low yield of D-PLA. When the induction temperature was higher than 30°C, the yield of D-PLA began to decrease, mainly because the fusion proteins at high temperature began to exist in the inclusion form. Therefore, the optimal induction temperature is 25°C, the highest titer 4.68 g/L of D-PLA can be obtained, with a yield of 0.925 g/g PPA.

The strategy of increasing intracellular NADH concentration by co-substrate has been demonstrated (Hou et al., 2019), and glycerol is also commonly used for dehydrogenation to produce lactic acid (Bharath et al., 2020). Therefore, in this study, intracellular NADH concentration was increased by using glycerol as the co-substrate of PPA. The influence of co-substrate on the yield of D-PLA was explored by adjusting the concentration and proportion of PPA and glycerol as shown in **Figure 5D**. D-PLA titer increased with the increase of PPA concentration, but the yield showed a trend of continuous decline, because the increase of PPA concentration enhanced the toxic effect on *E. coli* CP303. When the concentration of PPA increased to 7–8 g/L, the strong inhibitory effect made the conversion rate of PPA decreased greatly. Therefore, the optimal PPA concentration was 6 g/L. Furthermore, the addition amount of glycerol was optimized. When the glycerol concentration increased from equal molar concentration to 3 times molar concentration (relative to PPA), both the yield of D-PLA and PPA conversion showed a trend of first increasing

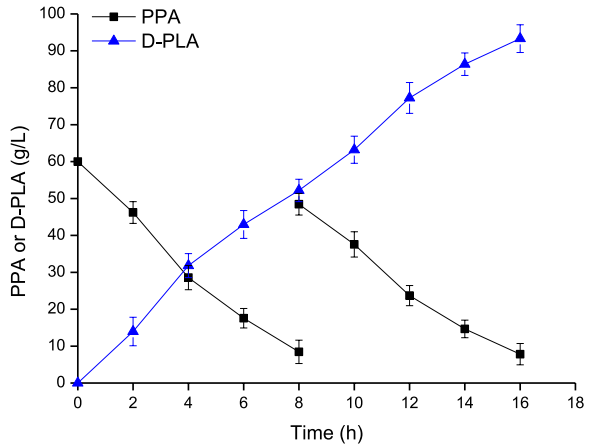

FIGURE 6 | D-PLA production by whole-cell bioconversion using the CP303 strain in a 5 L bioreactor. Data are means ± SD (n = 3).

and then decreasing at the same PPA concentration. This is because the low concentration of glycerol oxidizes itself to dihydroxyacetone through GlyDH and cannot provide sufficient coenzyme NADH, while the high concentration of glycerol has a certain inhibitory effect on the growth of *E. coli* and enzyme activity. Furthermore, without glycerol as the control, the maximum yield of D-PLA was only 4.63 g/L. Therefore, the optimal glycerol dosage was 2 times of the molar concentration of PPA. Under optimal conditions (6 g/L PPA, 6.73 g/L glycerol, 0.2 mM IPTG, pH 7, 25°C) of whole-cell catalytic production for 12 h, the maximum titer 5.87 g/L of D-PLA can be obtained with a yield of 0.967 g/g PPA.

Scale-Up of D-PLA Production

The whole-cell bioconversion was performed in a 5-L reactor using *E. coli* CP303 as biocatalyst as shown in **Figure 6**. When the fermentation executed for 8 h, and the concentration of substrate PPA and glycerol reduced from 60 g/L to 8.45 g/L and form 66.5 g/L to 37.6 g/L, respectively. Another PPA and glycerol addition into the bioreactor were conducted to reach a level of 48.45 g/L and 54.36 g/L, respectively. The whole-cell catalysis lasted for 16 h, and the final concentration of D-PLA was 93.3 g/L (561.53 mM), with a productivity of 5.83 g/L/h, and yield of 0.922 g/g PPA.

CONCLUSION

In this study, we reported for the first time the one-step synthesis of D-PLA using PPA as substrate by co-expression of D-LDH and GlyDH, achieving the regeneration of coenzyme NADH. At the same time, in order to further improve the regeneration efficiency of NADH and the yield of D-PLA, the D-LDH/GlyDH fusion protein strains were constructed with flexible glycine-rich linkers. The results showed that the fusion protein strain CP303 achieved a yield of 0.967 g/g PPA. In our study, cheap glycerol was used as co-substrate and coenzyme NADH was not needed to be added. A high-efficiency and low-cost pathway was constructed to sustainably produce high value-added product D-PLA, which is a technology with industrial potential.

DATA AVAILABILITY STATEMENT

The original contributions presented in the study are included in the article/**Supplementary Material**, further inquiries can be directed to the corresponding author.

ETHICS STATEMENT

Ethical review and approval was not required for the study on human participants in accordance with the local legislation and institutional requirements. The patients/participants provided their written informed consent to participate in this study.

AUTHOR CONTRIBUTIONS

ZQ and RL performed the experiments, analyzed the data, and drafted the article. TL and PC analyzed the data. DW and XX conceived and coordinated the study. ZQ and DW finalized the article. All authors contributed to the article and approved the submitted version.

FUNDING

This research was financially supported by the National Natural Science Foundation of China (21978027), the Fundamental Research Funds for the Central Universities (2020CDCGJ020, 2020CDCGHG068), Scientific Research Foundation of State Key Lab of Coal Mine Disaster Dynamics and Control (2011DA105287-ZR202002).

SUPPLEMENTARY MATERIAL

The Supplementary Material for this article can be found online at: https://www.frontiersin.org/articles/10.3389/fbioe.2021.795885/full#supplementary-material

REFERENCES

Aalbers, F. S., and Fraaije, M. W. (2017). Coupled Reactions by Coupled Enzymes: Alcohol to Lactone cascade with Alcohol Dehydrogenase-Cyclohexanone Monooxygenase Fusions. *Appl. Microbiol. Biotechnol.* 101 (20), 7557–7565. doi:10.1007/s00253-017-8501-4

Aalbers, F. S., and Fraaije, M. W. (2019). Enzyme Fusions in Biocatalysis: Coupling Reactions by Pairing Enzymes. *Chembiochem* 20 (1), 20–28. doi:10.1002/cbic.201800394

Abadli, M., Dewasme, L., Tebbani, S., Dumur, D., and Vande Wouwer, A. (2021). An Experimental Assessment of Robust Control and Estimation of Acetate Concentration in *Escherichia coli* BL21(DE3) Fed-Batch Cultures. *Biochem. Eng. J.* 174, 108103. doi:10.1016/j.bej.2021.108103

Anami, Y., Yamazaki, C. M., Xiong, W., Gui, X., Zhang, N., An, Z., et al. (2018). Glutamic Acid-Valine-Citrulline Linkers Ensure Stability and Efficacy of Antibody-Drug Conjugates in Mice. *Nat. Commun.* 9 (1), 2512. doi:10.1038/s41467-018-04982-3

Béguin, P. (1999). Hybrid Enzymes. *Curr. Opin. Biotechnol.* 10 (4), 336–340. doi:10.1016/s0958-1669(99)80061-5

Bharath, G., Rambabu, K., Hai, A., Taher, H., and Banat, F. (2020). Development of Au and 1D Hydroxyapatite Nanohybrids Supported on 2D Boron Nitride Sheets as Highly Efficient Catalysts for Dehydrogenating Glycerol to Lactic Acid. *ACS Sust. Chem. Eng.* 8 (19), 7278–7289. doi:10.1021/acssuschemeng.9b06997

Cheng, Z., Ran, Q., Liu, J., Deng, X., Qiu, H., Jia, Z., et al. (2020). Rapid Determination for Benzoic Acid, Sorbic Acid, Phenyllactic Acid, Phenylalanine, and Saccharin Sodium in Vinegar by High-Performance Liquid Chromatography-UV. *Food Anal. Methods* 13 (8), 1673–1680. doi:10.1007/s12161-020-01784-6

Costa, J. R., Tonon, R. V., Cabral, L., Gottschalk, L., Pastrana, L., and Pintado, M. E. (2020). Valorization of Agricultural Lignocellulosic Plant Byproducts through Enzymatic and Enzyme-Assisted Extraction of High-Value-Added Compounds: A Review. *ACS Sust. Chem. Eng.* 8 (35), 13112–13125. doi:10.1021/acssuschemeng.0c02087

de Almeida Parizotto, L., Krebs Kleingesinds, E., Manfrinato Pedrotti da Rosa, L., Effer, B., Meira Lima, G., Herkenhoff, M. E., et al. (2021). Increased Glycosylated L-Asparaginase Production through Selection of Pichia pastoris Platform and Oxygen-Methanol Control in Fed-Batches. *Biochem. Eng. J.* 173, 108083. doi:10.1016/j.bej.2021.108083

Dieuleveux, V., Lemarinier, S., and Guéguen, M. (1998). Antimicrobial Spectrum and Target Site of D-3-Phenyllactic Acid. *Int. J. Food Microbiol.* 40 (3), 177–183. doi:10.1016/s0168-1605(98)00031-2

Dueber, J. E., Wu, G. C., Malmirchegini, G. R., Moon, T. S., Petzold, C. J., Ullal, A. V., et al. (2009). Synthetic Protein Scaffolds Provide Modular Control over Metabolic Flux. *Nat. Biotechnol.* 27 (8), 753–759. doi:10.1038/nbt.1557

Fan, L., Wang, Y., Tuyishime, P., Gao, N., Li, Q., Zheng, P., et al. (2018). Engineering Artificial Fusion Proteins for Enhanced Methanol Bioconversion. *Chembiochem* 19 (23), 2465–2471. doi:10.1002/cbic.201800424

He, R., Finan, B., Mayer, J. P., and DiMarchi, R. D. (2019). Peptide Conjugates with Small Molecules Designed to Enhance Efficacy and Safety. *Molecules* 24 (10), 1855. doi:10.3390/molecules24101855

Hou, Y., Gao, B., Cui, J., Tan, Z., Qiao, C., and Jia, S. (2019). Combination of Multi-Enzyme Expression fine-tuning and Co-substrates Addition Improves Phenyllactic Acid Production with an *Escherichia coli* Whole-Cell Biocatalyst. *Bioresour. Tech.* 287, 121423. doi:10.1016/j.biortech.2019.121423

Hou, Y., Hossain, G. S., Li, J., Shin, H.-D., Du, G., Chen, J., et al. (2017). Metabolic Engineering of Cofactor Flavin Adenine Dinucleotide (FAD) Synthesis and Regeneration inEscherichia Colifor Production of α-keto Acids. *Biotechnol. Bioeng.* 114 (9), 1928–1936. doi:10.1002/bit.26336

Iturrate, L., Sánchez-Moreno, I., Oroz-Guinea, I., Pérez-Gil, J., and García-Junceda, E. (2010). Preparation and Characterization of a Bifunctional Aldolase/Kinase Enzyme: A More Efficient Biocatalyst for C-C Bond Formation. *Chem. Eur. J.* 16 (13), 4018–4030. doi:10.1002/chem.200903096

Jung, S., Hwang, H., and Lee, J.-H. (2019). Effect of Lactic Acid Bacteria on Phenyllactic Acid Production in Kimchi. *Food Control* 106, 106701. doi:10.1016/j.foodcont.2019.06.027

Kawaguchi, H., Teramura, H., Uematsu, K., Hara, K. Y., Hasunuma, T., Hirano, K., et al. (2015). Phenyllactic Acid Production by Simultaneous Saccharification and Fermentation of Pretreated Sorghum Bagasse. *Bioresour. Tech.* 182, 169–178. doi:10.1016/j.biortech.2015.01.097

Lerchner, A., Daake, M., Jarasch, A., and Skerra, A. (2016). Fusion of an Alcohol Dehydrogenase with an Aminotransferase Using a PAS Linker to Improve Coupled Enzymatic Alcohol-To-Amine Conversion. *Protein Eng. Des. Selection* 29 (12), 557–562. doi:10.1093/protein/gzw039

Li, L., Shin, S.-Y., Lee, K. W., and Han, N. S. (2014). Production of Natural Antimicrobial Compound D -phenyllactic Acid Using Leuconostoc Mesenteroides ATCC 8293 Whole Cells Involving Highly Active D -lactate Dehydrogenase. *Lett. Appl. Microbiol.* 59 (4), 404–411. doi:10.1111/lam.12293

Li, X., Jiang, B., Pan, B., Mu, W., and Zhang, T. (2008). Purification and Partial Characterization of Lactobacillus Species SK007 Lactate Dehydrogenase (LDH) Catalyzing Phenylpyruvic Acid (PPA) Conversion into Phenyllactic Acid (PLA). *J. Agric. Food Chem.* 56 (7), 2392–2399. doi:10.1021/jf0731503

Lindbladh, C., Persson, M., Bulow, L., and Mosbach, K. (1992). Characterization of a Recombinant Bifunctional Enzyme, Galactose Dehydrogenase/bacterial Luciferase, Displaying an Improved Bioluminescence in a Three-Enzyme System. *Eur. J. Biochem.* 204 (1), 241–247. doi:10.1111/j.1432-1033.1992.tb16630.x

Liu, J., Huang, R., Song, Q., Xiong, H., Ma, J., Xia, R., et al. (2021). Combinational Antibacterial Activity of Nisin and 3-Phenyllactic Acid and Their Co-production by Engineered Lactococcus Lactis. *Front. Bioeng. Biotechnol.* 9, 612105. doi:10.3389/fbioe.2021.612105

Luo, X., Zhang, Y., Yin, F., Hu, G., Jia, Q., Yao, C., et al. (2020a). Enzymological Characterization of a Novel D-Lactate Dehydrogenase from Lactobacillus Rossiae and its Application in D-Phenyllactic Acid Synthesis. *3 Biotech.* 10 (3), 101. doi:10.1007/s13205-020-2098-5

Luo, X., Zhang, Y., Yin, L., Zheng, W., and Fu, Y. (2020b). Efficient Synthesis of D-Phenyllactic Acid by a Whole-Cell Biocatalyst Co-expressing Glucose Dehydrogenase and a Novel D-Lactate Dehydrogenase from Lactobacillus Rossiae. *3 Biotech.* 10 (1), 14. doi:10.1007/s13205-019-2003-2

Mu, W., Yu, S., Jiang, B., and Li, X. (2012). Characterization of D-Lactate Dehydrogenase from Pediococcus Acidilactici that Converts Phenylpyruvic Acid into Phenyllactic Acid. *Biotechnol. Lett.* 34 (5), 907–911. doi:10.1007/s10529-012-0847-1

Patgiri, A., Skinner, O. S., Miyazaki, Y., Schleifer, G., Marutani, E., Shah, H., et al. (2020). An Engineered Enzyme that Targets Circulating Lactate to Alleviate Intracellular NADH:NAD+ Imbalance. *Nat. Biotechnol.* 38 (3), 309–313. doi:10.1038/s41587-019-0377-7

Peters, C., Rudroff, F., Mihovilovic, M. D., and T. Bornscheuer, U. (2017). Fusion Proteins of an Enoate Reductase and a Baeyer-Villiger Monooxygenase Facilitate the Synthesis of Chiral Lactones. *Biol. Chem.* 398 (1), 31–37. doi:10.1515/hsz-2016-0150

Prachayasittikul, V., Ljung, S., Isarankura-Na-Ayudhya, C., and Bülow, L. (2006). NAD(H) Recycling Activity of an Engineered Bifunctional Enzyme Galactose Dehydrogenase/lactate Dehydrogenase. *Int. J. Biol. Sci.* 2 (1), 10–16. doi:10.7150/ijbs.2.10

Rajanikar, R. V., Nataraj, B. H., Naithani, H., Ali, S. A., Panjagari, N. R., and Behare, P. V. (2021). Phenyllactic Acid: A green Compound for Food Biopreservation. *Food Control* 128, 108184. doi:10.1016/j.foodcont.2021.108184

Sorrentino, E., Tremonte, P., Succi, M., Iorizzo, M., Pannella, G., Lombardi, S. J., et al. (2018). Detection of Antilisterial Activity of 3-Phenyllactic Acid Using Listeria Innocua as a Model. *Front. Microbiol.* 9, 1373. doi:10.3389/fmicb.2018.01373

Sun, H.-L., Chuai, J., Wei, H., Zhang, X., and Yu, H. (2019). Multi-functional Organic Gelator Derived from Phenyllactic Acid for Phenol Removal and Oil Recovery. *J. Hazard. Mater.* 366, 46–53. doi:10.1016/j.jhazmat.2018.11.095

Valerio, F., Di Biase, M., Lattanzio, V. M. T., and Lavermicocca, P. (2016). Improvement of the Antifungal Activity of Lactic Acid Bacteria by Addition to the Growth Medium of Phenylpyruvic Acid, a Precursor of Phenyllactic Acid. *Int. J. Food Microbiol.* 222, 1–7. doi:10.1016/j.ijfoodmicro.2016.01.011

Wang, X., Hou, Y., Liu, L., Li, J., Du, G., Chen, J., et al. (2018a). A New Approach for Efficient Synthesis of Phenyllactic Acid from L-Phenylalanine: Pathway Design and Cofactor Engineering. *J. Food Biochem.* 42 (5), e12584. doi:10.1111/jfbc.12584

Wang, Y., Ren, H., and Zhao, H. (2018b). Expanding the Boundary of Biocatalysis: Design and Optimization of *In Vitro* Tandem Catalytic Reactions for Biochemical Production. *Crit. Rev. Biochem. Mol. Biol.* 53 (2), 115–129. doi:10.1080/10409238.2018.1431201

Wu, W., Deng, G., Liu, C., Gong, X., Ma, G., Yuan, Q., et al. (2020). Optimization and Multiomic Basis of Phenyllactic Acid Overproduction by Lactobacillus Plantarum. *J. Agric. Food Chem.* 68 (6), 1741–1749. doi:10.1021/acs.jafc.9b07136

Wu, X., Zhang, C., Xing, X. H., Yun, Z., Zhao, L., and Wu, Q. (2021). Construction and Characterization of Novel Bifunctional Fusion Proteins Composed of

Alcohol Dehydrogenase and NADH Oxidase with Efficient Oxidized Cofactor Regeneration. *Biotechnol. Appl. Biochem* doi:10.1002/bab.2225

Xiong, W., Liu, B., Shen, Y., Jing, K., and Savage, T. R. (2021). Protein Engineering Design from Directed Evolution to De Novo Synthesis. *Biochem. Eng. J.* 174, 108096. doi:10.1016/j.bej.2021.108096

Xu, G.-C., Zhang, L.-L., and Ni, Y. (2016). Enzymatic Preparation of D-Phenyllactic Acid at High Space-Time Yield with a Novel Phenylpyruvate Reductase Identified from Lactobacillus Sp. CGMCC 9967. *J. Biotechnol.* 222, 29–37. doi:10.1016/j.jbiotec.2015.12.011

Xu, J. J., Fu, L. J., Si, K. L., Yue, T. L., and Guo, C. F. (2020). 3-phenyllactic Acid Production by Free-whole-cells of Lactobacillus Crustorum in Batch and Continuous Fermentation Systems. *J. Appl. Microbiol.* 129 (2), 335–344. doi:10.1111/jam.14599

Xu, J., Xu, X., Wang, Q., and Fan, X. (2015). Chiral Separation of Phenyllactic Acid by Helical Structure from spring Dextrin. *J. Incl Phenom Macrocycl Chem.* 82 (3-4), 515–521. doi:10.1007/s10847-015-0487-x

Yang, H., Liu, L., Shin, H.-d., Chen, R. R., Li, J., Du, G., et al. (2013). Comparative Analysis of Heterologous Expression, Biochemical Characterization Optimal Production of an Alkaline α-amylase from alkaliphilicAlkalimonas amylolyticainEscherichia coliandPichia Pastoris. *Biotechnol. Prog.* 29 (1), 39–47. doi:10.1002/btpr.1657

Yu, K., Liu, C., Kim, B.-G., and Lee, D.-Y. (2015a). Synthetic Fusion Protein Design and Applications. *Biotechnol. Adv.* 33 (1), 155–164. doi:10.1016/j.biotechadv.2014.11.005

Yu, S., Zhou, C., Zhang, T., Jiang, B., and Mu, W. (2015b). 3-Phenyllactic Acid Production in Milk by SK25 during Laboratory Fermentation Process. *J. Dairy Sci.* 98 (2), 813–817. doi:10.3168/jds.2014-8645

Yu, S., Zhu, L., Zhou, C., An, T., Jiang, B., and Mu, W. (2014). Enzymatic Production of D-3-Phenyllactic Acid by Pediococcus Pentosaceus D-Lactate Dehydrogenase with NADH Regeneration by Ogataea Parapolymorpha Formate Dehydrogenase. *Biotechnol. Lett.* 36 (3), 627–631. doi:10.1007/s10529-013-1404-2

Zhang, X. X., Abd Elazim, A. M., Ruiz, G., and Yu, R. C. (2014). Fracture Behaviour of Steel Fibre-Reinforced concrete at a Wide Range of Loading Rates. *Int. J. Impact Eng.* 71, 89–96. doi:10.1016/j.ijimpeng.2014.04.009

Zhang, Y., Wang, Y., Wang, S., and Fang, B. (2017). Engineering Bi-functional Enzyme Complex of Formate Dehydrogenase and Leucine Dehydrogenase by Peptide Linker Mediated Fusion for Accelerating Cofactor Regeneration. *Eng. Life Sci.* 17 (9), 989–996. doi:10.1002/elsc.201600232

Zhao, W., Ding, H., Lv, C., Hu, S., Huang, J., Zheng, X., et al. (2018). Two-step Biocatalytic Reaction Using Recombinant *Escherichia coli* Cells for Efficient Production of Phenyllactic Acid from L-Phenylalanine. *Process Biochem.* 64, 31–37. doi:10.1016/j.procbio.2017.09.019

Zheng, Z., Xia, M., Fang, X., Jiang, T., and Ouyang, J. (2018). Enhanced Biosynthesis of Chiral Phenyllactic Acid from L-Phenylalanine through a New Whole-Cell Biocatalyst. *Bioproc. Biosyst Eng* 41 (8), 1205–1212. doi:10.1007/s00449-018-1949-5

Zhu, Y., Wang, Y., Xu, J., Chen, J., Wang, L., and Qi, B. (2017). Enantioselective Biosynthesis of L-Phenyllactic Acid by Whole Cells of Recombinant *Escherichia coli*. *Molecules* 22 (11), 1966. doi:10.3390/molecules22111966

Conflict of Interest: The authors declare that the research was conducted in the absence of any commercial or financial relationships that could be construed as a potential conflict of interest.

Publisher's Note: All claims expressed in this article are solely those of the authors and do not necessarily represent those of their affiliated organizations, or those of the publisher, the editors and the reviewers. Any product that may be evaluated in this article, or claim that may be made by its manufacturer, is not guaranteed or endorsed by the publisher.

frontiers in Bioengineering and Biotechnology

ORIGINAL RESEARCH
published: 17 December 2021
doi: 10.3389/fbioe.2021.779437

Photosynthetic Conversion of CO_2 Into Pinene Using Engineered *Synechococcus* sp. PCC 7002

Ruigang Yang[1†], Lingyun Zhu[1†], Tao Li[2], Lv-yun Zhu[1], Zi Ye[2] and Dongyi Zhang[3]**

[1]Department of Biology and Chemistry, College of Liberal Arts and Sciences, National University of Defense Technology, Changsha, China, [2]State Key Laboratory of Freshwater Ecology and Biotechnology, Institute of Hydrobiology, Chinese Academy of Sciences, Wuhan, China, [3]Hunan Key Laboratory of Economic Crops, Genetic Improvement, and Integrated Utilization, School of Life Sciences, Hunan University of Science and Technology, Xiangtan, China

Metabolic engineering of cyanobacteria has received much attention as a sustainable strategy to convert CO_2 to various longer carbon chain fuels. Pinene has become increasingly attractive since pinene dimers contain high volumetric energy and have been proposed to act as potential aircraft fuels. However, cyanobacteria cannot directly convert geranyl pyrophosphate into pinene due to the lack of endogenous pinene synthase. Herein, we integrated the gene encoding *Abies grandis* pinene synthase into the model cyanobacterium *Synechococcus* sp. PCC 7002 through homologous recombination. The genetically modified cyanobacteria achieved a pinene titer of 1.525 ± 0.145 mg L^{-1} in the lab-scale tube photobioreactor with CO_2 aeration. Specifically, the results showed a mixture of α- and β-pinene (~33:67 ratio). The ratio of β-pinene in the product was significantly increased compared with that previously reported in the engineered *Escherichia coli*. Furthermore, we investigated the photoautotrophic growth performances of *Synechococcus* overlaid with different concentrations of dodecane. The work demonstrates that the engineered *Synechococcus* is a suitable potential platform for β-pinene production.

Keywords: terpenoids, pinene, cyanobacteria, pinene synthase, dodecane

OPEN ACCESS

Edited by:
Shuobo Shi,
Beijing University of Chemical Technology, China

Reviewed by:
Michael Jahn,
Royal Institute of Technology, Sweden
Rajib Saha,
University of Nebraska-Lincoln, United States

****Correspondence:***
Zi Ye
yezi@ihb.ac.cn
Dongyi Zhang
dongyizhang@nudt.edu.cn

[†]These authors have contributed equally to this work and share first authorship

Specialty section:
This article was submitted to Synthetic Biology, a section of the journal Frontiers in Bioengineering and Biotechnology

Received: *18 September 2021*
Accepted: *22 November 2021*
Published: *17 December 2021*

Citation:
Yang R, Zhu L, Li T, Zhu L-y ,Ye Z and Zhang D (2021) Photosynthetic Conversion of CO_2 Into Pinene Using Engineered Synechococcus *sp. PCC 7002. Front. Bioeng. Biotechnol. 9:779437. doi: 10.3389/fbioe.2021.779437*

INTRODUCTION

Growing concerns about environmental pollution issues and demands for alternative energy have stimulated photosynthetic organisms emerging as powerful platforms converting CO_2 to various bio-based products. As one of the oldest living phyla (Schopf and Packer, 1987), cyanobacteria are oxygenic photosynthetic autotrophic bacteria widely distributed in aquatic and terrestrial habitats (Díez and Ininbergs, 2014). They play a crucial role in the biogeochemical cycles of carbon and nitrogen with the capacity of fixing carbon dioxide and atmospheric nitrogen (Parmar et al., 2011). Moreover, cyanobacteria possess the dramatic property of photosynthetically converting CO_2 to various beneficial organic compounds, including drugs (Simmons et al., 2005; Teruya et al., 2009), cosmetics (Conde et al., 2000; Rajneesh et al., 2017), food additives (Ma et al., 2019), and biofuels (Sarma et al., 2016; Singh et al., 2016; Choi et al., 2020), benefiting from high growth rates, ease of genetic engineering, and large-scale cultivation (Rajneesh et al., 2017). In addition, the increasingly abounding toolboxes for genetic manipulation impel cyanobacteria to become attractive platforms for bio-based production (Markley et al., 2015; Carroll et al., 2018; Sun et al., 2018; Xia et al., 2019).

Terpenoids are a large group of high-value compounds and have been successfully produced by multiple microbial cell factories (Davies et al., 2015; Wang et al., 2018; Moser and Pichler, 2019).

Cyanobacteria synthesize terpenoid precursors isopentenyl diphosphate (IPP) and dimethylallyl diphosphate (DMAPP) with the endogenous methylerythritol phosphate (MEP) pathway (Lin and Pakrasi, 2019), which has been engineered to produce various terpenoids (Pattanaik and Lindberg, 2015; Betterle and Melis, 2019). Pinene is a plant natural monoterpene (C10) and has shown a wide range of commercial applications in flavorings (Gomes-Carneiro et al., 2005), fragrances (Kirby and Keasling, 2009), and pharmaceuticals (Zhao et al., 2018). Furthermore, pinene dimers' high energy density is comparable to tactical fuels JP-10, and this has made pinene emerge as a potential bio-jet fuel used in aircraft and aircraft-launched missiles (Harvey et al., 2010).

Microbial factories have been employed to produce pinene with various genetic tools. Currently, the highest pinene production efficiency was achieved in the engineered *Escherichia coli* (*E. coli*) and yeast, reaching respective titers of 166.5 mg L^{-1} (Niu et al., 2018) and 36.1 mg L^{-1} (Wei et al., 2021). In order to build a photosynthetic microbial platform for pinene production, several efforts have been successfully carried in the photosynthetic microorganisms, including *Rhodobacter sphaeroides* and *Synechocystis* sp. PCC 6803 (Tashiro et al., 2016; Wu et al., 2021). The highest pinene production titer was achieved at 0.540 mg L^{-1} in the engineered *R. sphaeroides* by optimizing the expression of the critical enzymes in the MEP pathway (Wu et al., 2021). In contrast, only 0.08 mg L^{-1} pinene was harvested with the cold trap in the transgenic *Synechocystis* sp. PCC 6803 integrated with the mutant pinene synthase (PS) gene (Tashiro et al., 2016). Developing a superior cyanobacterial chassis for synthetic biology and metabolic engineering applications is supposed to be an effective effort to further improve the productivities of terpenoids for commercial production.

In cyanobacteria, the condensation reaction of IPP and DMAPP catalyzed by geranyl diphosphate synthase (GPPS) produces geranyl diphosphate (GPP), the substrate of PS. In the present study, we engineered *Synechococcus* sp. PCC 7002 (*Synechococcus*) to produce pinene by introducing a recombinant plasmid containing the *Abies grandis* PS (AgPS) gene. The AgPS gene was integrated into the cyanobacteria genome by homologous recombination and was overexpressed under the control of the *cpcBA* (phycocyanin) operon promoter (*PcpcBA*) from *Synechocystis* sp. PCC 6803 (Xu et al., 2011). The successful pinene production of transgenic *Synechococcus* was achieved at the highest rate of 1.525 ± 0.145 mg L^{-1} under the condition of CO_2 aeration and continuous light. Furthermore, the ratio of two pinene isomers, α- and β-pinene, was also determined in the final product.

MATERIALS AND METHODS

Strains and Construction of Plasmids

Strains and plasmids used in this study are listed in **Table 1**. The AgPS gene was amplified from pAgGPPS-$(GSG)_2$-AgPS by PCR with specific primers AgPS_F: 5′-CAGCATATGCGTCGTG-GTAAATCTATCAC-3′ and AgPS_R: 5′-GCGGGATCCTTA-CAGCGGAACAGATTCCAG-3′. The PCR product was purified and ligated into the cloning vector pBZ (TransGen Biotech, China) to perform sequencing. The AgPS gene with the correct sequence was inserted into pAQ1EX-PcpcBA to generate pAQ1EX-AgPS plasmid *via Nde*I and *Bam*HI (Thermo Scientific) digestion. The plasmid pAQ1EX-AgPS was aiming at integrating the functional genes into the endogenous high-copy plasmid pAQ1 through homologous recombination. A modified protocol following that described previously (Stevens and Porter, 1980; Frigaard et al., 2004) was used to transform pAQ1EX-AgPS into *Synechococcus*. To select the transformant strain, 100 μg ml^{-1} streptomycin was applied, and the successful transgene incorporation was confirmed by colony PCR and sequencing using the primers PAQIN_F: 5′-GGAATTGTGCGTGTGGTTTC-3′ and PAQIN_R: 5′-CTAACG ATCAGCGCGAAAAG-3′.

Growth Experiments

Synechococcus wild-type (WT) and AgPS transformant (7002-PS) strains were grown in liquid medium A+ containing the following: 18 g L^{-1} NaCl, 5 g L^{-1} $MgSO_4$ $7H_2O$, 1 g L^{-1} $NaNO_3$, 0.6 g L^{-1} KCl, 0.050 g L^{-1} KH_2PO_4, 0.270 g L^{-1} $CaCl_2$, 0.020 g L^{-1} Na_2CO_3, 0.030 g L^{-1} $Na_2EDTA{\cdot}2H_2O$, 3.890 mg L^{-1} $FeCl_3{\cdot}6H_2O$, 1 g L^{-1} Tris HCl (pH 8.2), 2.860 mg L^{-1} H_3BO_3, 1.810 mg L^{-1} $MnCl_2{\cdot}4H_2O$, 0.220 mg L^{-1} $ZnSO_4{\cdot}7H_2O$, 0.390 mg L^{-1} $Na_2MoO_4{\cdot}2H_2O$, 0.100 mg L^{-1} $CuSO_4{\cdot}5H_2O$, 0.050 mg L^{-1} $Co(NO_3)_2{\cdot}6H_2O$, and 4 μg L^{-1} vitamin B12 (Stevens and Porter, 1980; Ludwig and Bryant, 2011). The 7002-PS strain containing Sm^R cassette was selected on solid A+ medium, adding 1.2% (*w*/*v*) Bacto Agar (BD) and streptomycin with the required concentration. Seed cultures were performed in 50-ml Erlenmeyer flasks using an orbital shaker at 100 r min^{-1}. The flasks contained 30 ml of liquid A+ medium in the presence of antibiotic. All *Synechococcus* strains were grown at 30°C under continuous illumination of 100 μmol photons m^{-2} s^{-1}, and optical density (OD) was measured to monitor cell growth using a spectrophotometer (Varian) at 730 nm.

Western Blotting

Synechococcus cultures used for western blotting were inoculated into 50 ml fresh A+ medium with an initial $OD_{730} = 0.1$ and grown for 24 h under continuous aeration supplement with 1% (*v*/*v*) CO_2. Cells were harvested by centrifugation and disrupted with a motor-driven tissue grinder (Sangon Biotech). Equal amounts of total proteins in crude cell lysates were subjected to western blotting analysis. AgPS was identified with anti-His mouse monoclonal antibody (TransGen Biotech, China) followed by goat anti-mouse IgG (H + L) (TransGen Biotech, China) and visualized using a DAB horseradish peroxidase color development kit (Beyotime, China).

Pulse Amplitude Modulation Fluorometry

The Water-PAM (Walz) was used to measure the variable chlorophyll fluorescence with a Water-S stirring device capable of keeping the samples homogenous and preventing sedimentation of the cells. Light-emitting diodes supplied red

TABLE 1 | Strains and plasmids used in this study.

Name	Description	Source
Strains		
Escherichia coli Trelief™ 5α	*E. coli* strain used for cloning and plasmid construction	Tsingke, China
WT	Model marine cyanobacterium *Synechococcus* sp. PCC 7002 used as the host for transgene integration	Yang et al. (2013)
7002-PS	*Synechococcus* with streptomycin resistance (Sm^R) cassette and AgPS gene	This work
Plasmids		
pBZ	pEASY®-Blunt Zero Cloning Vector containing a suicide gene mutated by ligation of PCR fragment	TransGen Biotech, China
pAQ1EX	*Synechococcus* expression vector containing flanking regions of endogenous plasmid pAQ1 in *Synechococcus* for homologous recombination of Sm^R cassette and the integrated gene driven by *PcpcBA*	Xu et al. (2011)
pAgGPPS-$(GSG)_2$-AgPS	Plasmid harboring codon-optimized fusion genes of *A. grandis* GPPS and AgPS with a $(GSG)_2$ linker	Sarria et al. (2014)
pBS-AgPS	pBZ harboring AgPS gene for cloning and sequencing	This work
pAQ1EX-AgPS	pAQ1EX harboring AgPS gene and Sm^R cassette	This work

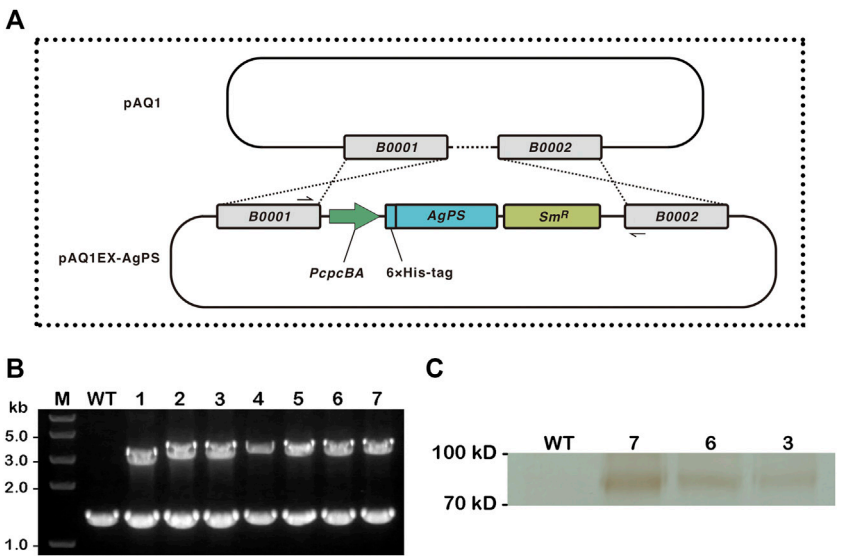

FIGURE 1 | Construction of *Synechococcus* sp. PCC 7002 overexpressing *Abies grandis* pinene synthase. **(A)** Illustrations of the integration of endogenous plasmid pAQ1 in wild-type *Synechococcus* with the inserted *A. grandis* pinene synthase (AgPS) cassette in the recombinant plasmid pAQ1EX-AgPS. The AgPS cassette contained *PcpcBA* to drive transgene expression, and a spectinomycin resistance (Sm^R) selectable marker. The specific primers PAQIN_F and PAQIN_R shown in black solid half arrows are used for demonstrating the successful integration of AgPS cassette into pAQ1 (between open-reading frames *B0001* and *B0002*) *via* double homologous recombination. **(B)** Confirmation of transgene integration by colony PCR using the above-mentioned primers. The wild-type (WT) strain and seven independent transformants of the 7002-PS strain (1–7) were verified. Lane M: *Trans2*K® Plus II DNA Marker (TransGen Biotech, China). Each number above the image of the agarose gel correlated with PCR product. **(C)** Western blotting analysis of the total protein extract isolated from WT and three independent transformants of the 7002-PS strain (3, 6, and 7). Sample from the WT strain was used as a control. Proteins were detected using anti-His mouse monoclonal antibody (TransGen Biotech, China) followed by the incubation with anti-mouse secondary antibody conjugated with HRP. Reactions were visualized using a DAB horseradish peroxidase color development kit (Beyotime, China).

measuring light (spectral peak at 650 nm), actinic light, and saturation pulses (spectral peak at 660 nm). After 20 min of dark adaption, a 2-ml sample was used to analyze fluorescence parameters Fv/Fm by measuring Fo and Fm. Light treatment strategy and stirrer operation in this study were according to the previous reports (Campbell et al., 1998; Cosgrove and Borowitzka, 2006).

Pinene Production and Analysis

Synechococcus cultures used for pinene production were inoculated into 60 ml fresh A+ medium without antibiotic with an initial $OD_{730} = 1.0$. The cultures were grown for 72 h under continuous aeration supplement with 1% (*v*/*v*) CO_2, and a 6-ml dodecane (Aladdin) overlay was applied at the beginning to trap the pinene excreted from the cells. Samples of 500 μl dodecane overlay were harvested at the end of the production period. The procedure of sample pretreatment was following a modified method as described previously (Sarria et al., 2014), adding (R)-(+)-limonene (Aladdin) as an internal standard. These samples were analyzed on a gas chromatography–mass spectrometer (GC-MS) (Agilent 7890A with Agilent 5975C MS detector) by a standard curve of (−)-α- and β-pinene (Aladdin).

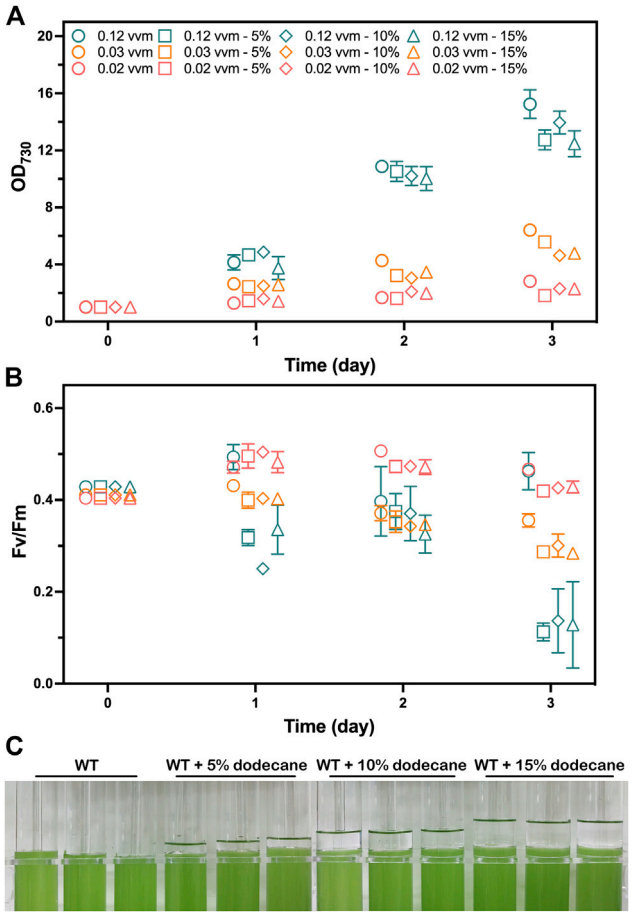

FIGURE 2 | Photoautotrophic performance analysis of the WT strain grown with 1% (*v/v*) CO_2 aeration at 0.12, 0.03, and 0.02 vvm for 3 days. The mediums were overlaid with 0%, 5%, 10%, and 15% (*v/v*) of dodecane, respectively. Samples were collected for the analysis at 1-day intervals. **(A)** The photoautotrophic growth parameters monitored by OD_{730}. **(B)** Photosynthetic efficiency evaluated by chlorophyll fluorescence parameter Fv/Fm. The works on the WT strain grown with 0%, 5%, 10%, and 15% (*v/v*) of dodecane overlay are shown as circles, squares, diamonds, and triangles, respectively. The works on the WT strain grown with 1% (*v/v*) CO_2 aeration at 0.12, 0.03, and 0.02 vvm are shown as teal, tangerine, and salmon colors, respectively. **(C)** Image of the WT strain cultivated in A+ medium with 0%, 5%, 10%, and 15% (*v/v*) of dedocane overlay, respectively. The error bars represent standard deviations of means (mean ± SD, $n = 3$).

The GC-MS was equipped with a DB-5MS column (30 m × 0.25 mm × 0.25 μm) to separate hydrophobic molecules. The analysis conditions were as follows: He (1 ml min^{-1}) as a carrier gas, split ratio of 5:1; an injector temperature of 300°C; and an oven program of 50°C for 5 min, ramp at 10°C min^{-1} to 150°C, ramp at 30°C min^{-1} to 280°C and held for 5 min.

RESULTS AND DISCUSSION

Determination of Candidate PS Genes

Synechococcus is capable of utilizing the endogenous MEP pathway to synthesize GPP. In order to build *Synechococcus* a platform for pinene production, we need to integrate an exogenous pinene synthase into the genome of *Synechococcus* to convert GPP into α- or β-pinene with high fidelity. Although both pinene isomers can be found in turpentine (Behr and Johnen, 2009), the β-pinene isomer is considered preferable for higher economic value (Sarria et al., 2014) and dimerization efficiency (Walls and Rios-Solis, 2020). Thus, the AgPS gene was selected to produce pinene with more proportion of β-pinene (Bohlmann et al., 1997) and had shown the highest activity for pinene synthesis in *E. coli* among the high-fidelity pinene synthases (Sarria et al., 2014).

Construction of Synechococcus Strain Integrated With AgPS Transgene

The nucleotide sequence of the AgPS gene from Sarria et al. (2014) had been modified and expressed according to the codon usage preference of *E. coli*. A comparison of the modified AgPS gene sequence with the codon usage of *Synechococcus* was predicted with the Graphical Codon Usage Analyser (Fuhrmann et al., 2004), and the results showed that the relative adaptiveness values are all higher than 30% (**Supplementary Material S1**). We therefore directly amplified the modified AgPS gene from plasmid pAgGPPS-$(GSG)_2$-AgPS and therewith integrated it into the pAQ1EX vector between the *Nde*I and *Bam*HI sites. The insertion of AgPS gene into the neutral region of pAQ1 between two open-reading frames encoding hypothetical proteins (**Figure 1A**) was confirmed by colony PCR and sequencing in numerous transformants of the 7002-PS strain (**Figure 1B**). Interestingly, although the 7002-PS strain was isolated using the streak plate method three times, as the colony PCR results showed, the neutral region of pAQ1 between two open-reading frames had still not been entirely replaced by the integrated sequence. We supposed that the region replaced by the transgenes in pAQ1EX-PS was essential for the growth of *Synechococcus* (Xu et al., 2011), and the complete integration of the exogenous genes in pAQ1EX was hard to realize. The potential different amount of the transgenic pAQ1 might eventually lead to the differences in pinene production performance among the independent transformants of the 7002-PS strain. The expression of AgPS was confirmed by western blotting (**Figure 1C**).

The Effect of Dodecane on the Photoautotrophic Growth of *Synechococcus*

Dodecane overlay has been turned out as an effective method for terpenes harvesting (Davies et al., 2014; Sarria et al., 2014; Niu et al., 2018; Dienst et al., 2020). This article utilized 1% (*v/v*) CO_2 bubbles to supply inorganic carbon for pinene production in the 7002-PS strain. Photoautotrophic cultivation of cyanobacteria with sodium bicarbonate as an inorganic carbon source and using orbital shakers or magnetic stirrers seem adequate for terpenes production (Silva et al., 2016). However, CO_2 used as the inorganic carbon source has environmentally friendly advantages in integrating atmospheric CO_2 into biomass. Although filling the upper space of the medium with CO_2 could maintain continuous production of terpene (Davies et al., 2014), we

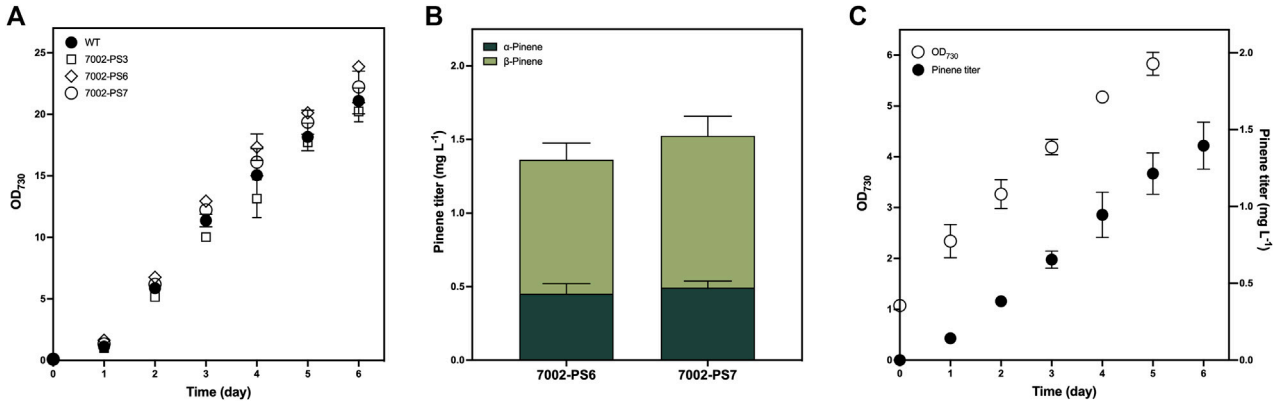

FIGURE 3 | Growth and pinene production of the 7002-PS strain. **(A)** Photoautotrophic growth of the WT strain and three independent transformants of the 7002-PS strain grown with 1% (*v/v*) CO_2 aeration at 0.12 vvm for 6 days. Samples were collected for the analysis at 1-day intervals. **(B)** Pinene production of 7002-PS6 and 7002-PS7 after a 72-h cultivation with 10% (*v/v*) dodecane overlay and 1% (*v/v*) CO_2 aeration at 0.12 vvm. **(C)** Photoautotrophic growth and pinene production of 7002-PS7 grown with 10% (*v/v*) dodecane overlay and 1% (*v/v*) CO_2 aeration at 0.03 vvm for 6 days. Samples were collected for the analysis at 1-day intervals. The growth parameters were monitored by OD_{730}, and the pinene titers were analyzed on a gas chromatography–mass spectrometer (GC-MS). The error bars represent standard deviations of means (mean ± SD, $n = 3$).

need to develop deeper insight into the production performance of engineered strains grown with CO_2 bubble aeration.

To investigate whether dodecane overlay limits the photoautotrophic growth of cyanobacteria ventilated with CO_2, we inspected the photoautotrophic growth of the WT strain overlaid with different dodecane concentrations over a 72-h time course at various aeration rates. Cell growth rates were measured by OD_{730}, and the photosynthetic performance was evaluated by the chlorophyll fluorescence parameter Fv/Fm. The chlorophyll fluorescence parameter Fv/Fm and OD_{730} of the WT cells were compared when growing with 0%, 5%, 10%, and 15% (*v/v*) dodecane overlay. As the organic phase could not maintain stability with an aeration rate higher than 0.12 vvm (volume of gas per volume of liquid per minute) in this work, the aeration rates were initially set to 0.02, 0.03, and 0.12 vvm. Apparently, the limited CO_2 provision caused by the lower aeration rates (0.02 and 0.03 vvm) had an adverse effect on the photoautotrophic growth of *Synechococcus*. Meanwhile, the OD_{730} of the WT cells cultivated with aeration rate at 0.12 vvm exhibited obvious variation (**Figure 2A**). The chlorophyll fluorescence parameter Fv/Fm of the cells without dodecane overlay was higher than the that of the cells overlaid with dodecane after 2 days, and the cells aerating at 0.12 vvm presented the greatest gap, which was supposed to aggravate the difference of OD_{730} (**Figure 2B**). However, neither the Fv/Fm nor OD_{730} of the WT cells showed apparent difference whenever the aeration rate was 0.02 or 0.03 vvm. The results indicated that the dodecane overlay led to a slight restriction to the photosynthetic growth of *Synechococcus* cultivated with CO_2 bubble aeration at a high rate (0.12 vvm), and the three concentrations (5%, 10%, and 15%) of the dodecane overlay had no significant difference in the limitation effect. However, the dramatic variance of Fv/Fm between the WT cells overlaid with and without dodecane demonstrated that cultivation with dodecane overlay at a high aeration rate enables to impair the photosystem II efficiency of *Synechococcus*, which suggests that dodecane overlay is not the best choice for long-term product harvest in the condition of high gas aeration rate for *Synechococcus*.

The different concentrations of dodecane overlay resulted in the liquid level differences of the organic phase in the tube photobioreactor (**Figure 2C**). Considering the disturbance of the interface between two phases caused by bubble breakage, the moderate thickness of the organic phase is supposed to be of great significance for reducing pinene loss and the inhibition effect of dodecane overlay on cell growth. Besides, a slight loss of dodecane volume caused by gas aeration was observed on the tube wall (data not shown), which demanded an appropriate volume to reduce the calculation error caused by the volume change. Thus, we determined that a 10% (*v/v*) dodecane overlay was suitable for pinene harvesting from the culture medium in our tube photobioreactor.

Growth and Pinene Production of the 7002-PS Strain

To investigate the influence of genetic modification on the photoautotrophic growth of *Synechococcus*, we compared the photoautotrophic growth rates measured by daily OD_{730} between the WT strain and three transformants of the 7002-PS strain grown in tube photobioreactor for 6 days (**Figure 3A**). No significant variation was observed among the examined strains under culture conditions of 30°C, 100 μmol photons m^{-2} s^{-1}, and 1% (*v/v*) CO_2 aeration. Obviously, metabolic stress caused by the overexpression of transgene and the engineered flux of GPP towards pinene production has no adverse effect on the growth of cyanobacteria grown under the conditions described above.

As the colony PCR results confirmed that the integrated sequence had not entirely replaced the neutral region of pAQ1 between two open-reading frames (**Figure 1B**), numerous transformants of the 7002-PS strain were supposed to exhibit discrepant production performance. In this work, aeration rates at 0.12 and 0.03 vvm were applied to realize a 72-h and a 6-day period of pinene production, respectively. Two independent

transformants of the 7002-PS strain were selected for 72-h pinene production with 10% (*v*/*v*) dodecane and 1% (*v*/*v*) CO_2 aeration at 0.12 vvm, resulting in the pinene titer at 1.362 ± 0.148 mg L^{-1} and $1.525 \pm 0.l45$ mg L^{-1} (pinene productivity at 0.110 ± 0.018 mg L^{-1} $OD_{730}{}^{-1}$ and 0.114 ± 0.013 mg L^{-1} $OD_{730}{}^{-1}$), respectively (**Figure 3B**). The transformant with higher pinene-producing performance, named 7002-PS7, showed relatively stable pinene productivity of 0.246 ± 0.05 mg L^{-1} day^{-1} for a 6-day period of pinene production with 10% (*v*/*v*) dodecane and 1% (*v*/*v*) CO_2 aeration at 0.03 vvm (**Figure 3C**). Besides, the α/β isomer ratios exhibited by the 7002-PS strain were also investigated (**Figure 3B**). Interestingly, AgPS expressed in *Synechococcus* resulted in a ~33:67 mixture of α- to β-pinene, in which a significant increase in β-pinene production was realized compared to that produced in *E. coli* (Sarria et al., 2014). We hypothesized that the cellular metabolic environment of *Synechococcus* is suitable for forming the β-pinene isomer.

CONCLUSION

Pinene is of particular interest due to the excellent potential for its dimer to be aircraft fuel. This study described the construction of pinene-producing strain harboring AgPS-overexpressing cassette in *Synechococcus* and investigated its performance of photoautotrophic growth and pinene production using CO_2 bubble aeration. Moreover, we determined the concentration of dodecane overlay suitable for collecting volatile pinene under aeration conditions. As a result, we successfully realized the photosynthetic production of pinene directly from CO_2 with a productivity of up to $1.525 \pm 0.l45$ mg l^{-1} (α/β isomer ratios at ~33: 67) after 72 h of cultivation. However, the cultivation condition and the pinene-producing pathway could be further optimized, and the gas-trapping system (Kiyota et al., 2014) is more likely suitable for long-term production. Therefore, there still exists a significant opportunity for higher productivity of pinene in *Synechococcus*.

DATA AVAILABILITY STATEMENT

The original contributions presented in the study are included in the article/**Supplementary Material**, further inquiries can be directed to the corresponding authors.

AUTHOR CONTRIBUTIONS

RY and LZ designed the experiments. RY and ZY performed the experiments. LZ, TL, and DZ directed the research. L-YZ participated in the research. RY and LZ wrote and revised the manuscript. All authors contributed to the article and approved the submitted version.

FUNDING

This work was financially supported by grants from the National Key Research and Development Program of China (2021YFA0910700), the "Huxiang Young Talents Plan" Project of Hunan Province (2019RS2030), the National Natural Science Foundation of China (31870855 and 32171429), and the Fund for NUDT Young Innovator Awards (20190104).

ACKNOWLEDGMENTS

The authors acknowledge Ding He, Hui Wang, and Tianzhong Liu for the support of experimental conditions.

SUPPLEMENTARY MATERIAL

The Supplementary Material for this article can be found online at: https://www.frontiersin.org/articles/10.3389/fbioe.2021.779437/full#supplementary-material

REFERENCES

Behr, A., and Johnen, L. (2009). Myrcene as a Natural Base Chemical in Sustainable Chemistry: A Critical Review. *Chemsuschem* 2 (12), 1072–1095. doi:10.1002/cssc.200900186

Betterle, N., and Melis, A. (2019). Photosynthetic Generation of Heterologous Terpenoids in Cyanobacteria. *Biotechnol. Bioeng.* 116 (8), 2041–2051. doi:10.1002/bit.26988

Bohlmann, J., Steele, C. L., and Croteau, R. (1997). Monoterpene Synthases from Grand Fir (Abies Grandis). *J. Biol. Chem.* 272 (35), 21784–21792. doi:10.1074/jbc.272.35.21784

Campbell, D., Hurry, V., Clarke, A. K., Gustafsson, P., and Öquist, G. (1998). Chlorophyll Fluorescence Analysis of Cyanobacterial Photosynthesis and Acclimation. *Microbiol. Mol. Biol. Rev.* 62(3), 667–683. doi:10.1128/mmbr.62.3.667-683.1998

Carroll, A. L., Case, A. E., Zhang, A., and Atsumi, S. (2018). Metabolic Engineering Tools in Model Cyanobacteria. *Metab. Eng.* 50, 47–56. doi:10.1016/j.ymben.2018.03.014

Choi, Y.-N., Lee, J. W., Kim, J. W., and Park, J. M. (2020). Acetyl-CoA-derived Biofuel and Biochemical Production in Cyanobacteria: a Mini Review. *J. Appl. Phycol* 32 (3), 1643–1653. doi:10.1007/s10811-020-02128-x

Conde, F. R., Churio, M. S., and Previtali, C. M. (2000). The Photoprotector Mechanism of Mycosporine-like Amino Acids. Excited-State Properties and Photostability of Porphyra-334 in Aqueous Solution. *J. Photochem. Photobiol. B* 56 (2-3), 139–144. doi:10.1016/s1011-1344(00)00066-x

Cosgrove, J., and Borowitzka, M. (2006). Applying Pulse Amplitude Modulation (PAM) Fluorometry to Microalgae Suspensions: Stirring Potentially Impacts Fluorescence. *Photosynth Res.* 88 (3), 343–350. doi:10.1007/s11120-006-9063-y

Davies, F. K., Jinkerson, R. E., and Posewitz, M. C. (2015). Toward a Photosynthetic Microbial Platform for Terpenoid Engineering. *Photosynth Res.* 123 (3), 265–284. doi:10.1007/s11120-014-9979-6

Davies, F. K., Work, V. H., Beliaev, A. S., and Posewitz, M. C. (2014). Engineering Limonene and Bisabolene Production in Wild Type and a Glycogen-Deficient Mutant of Synechococcus Sp. PCC 7002. *Front. Bioeng. Biotechnol.* 2, 21. doi:10.3389/fbioe.2014.00021

Dienst, D., Wichmann, J., Mantovani, O., Rodrigues, J. S., and Lindberg, P. (2020). High Density Cultivation for Efficient Sesquiterpenoid Biosynthesis in Synechocystis Sp. PCC 6803. *Sci. Rep.* 10 (1), 5932. doi:10.1038/s41598-020-62681-w

Díez, B., and Ininbergs, K. (2014). "Ecological Importance of Cyanobacteria," in *Cyanobacteria* (Hoboken, NJ: John Wiley & Sons, Ltd), 41–63. doi:10.1002/9781118402238.ch3

Frigaard, N.-U., Sakuragi, Y., and Bryant, D. A. (2004). "Using In Vitro-Made DNA Constructs and Natural Transformation," in *Gene Inactivation in the Cyanobacterium Synechococcus Sp. PCC 7002 and the Green Sulfur Bacterium Chlorobium tepidum Photosynthesis Research Protocols*. Editor R. Carpentier (Totowa, NJ: Humana Press), 325–340.

Fuhrmann, M., Hausherr, A., Ferbitz, L., Schödl, T., Heitzer, M., and Hegemann, P. (2004). Monitoring Dynamic Expression of Nuclear Genes in

Chlamydomonas Reinhardtii by Using a Synthetic Luciferase Reporter Gene. *Plant Mol. Biol.* 55 (6), 869–881. doi:10.1007/s11103-004-2150-610.1007/s11103-005-2150-1

Gomes-Carneiro, M. R., Viana, M. E. S., Felzenszwalb, I., and Paumgartten, F. J. R. (2005). Evaluation of β-myrcene, α-terpinene and (+)- and (−)-α-Pinene in the Salmonella/microsome Assay. *Food Chem. Toxicol.* 43 (2), 247–252. doi:10.1016/j.fct.2004.09.011

Harvey, B. G., Wright, M. E., and Quintana, R. L. (2010). High-Density Renewable Fuels Based on the Selective Dimerization of Pinenes. *Energy Fuels* 24 (1), 267–273. doi:10.1021/ef900799c

Kirby, J., and Keasling, J. D. (2009). Biosynthesis of Plant Isoprenoids: Perspectives for Microbial Engineering. *Annu. Rev. Plant Biol.* 60, 335–355. doi:10.1146/annurev.arplant.043008.091955

Kiyota, H., Okuda, Y., Ito, M., Hirai, M. Y., and Ikeuchi, M. (2014). Engineering of Cyanobacteria for the Photosynthetic Production of Limonene from CO2. *J. Biotechnol.* 185, 1–7. doi:10.1016/j.jbiotec.2014.05.025

Lin, P.-C., and Pakrasi, H. B. (2019). Engineering Cyanobacteria for Production of Terpenoids. *Planta* 249 (1), 145–154. doi:10.1007/s00425-018-3047-y

Ludwig, M., and Bryant, D. A. (2011). Transcription Profiling of the Model Cyanobacterium Synechococcus Sp. Strain PCC 7002 by Next-Gen (SOLiD) Sequencing of cDNA. *Front. Microbio.* 2, 41. doi:10.3389/fmicb.2011.00041

Ma, Z., Ahmed, F., Yuan, B., and Zhang, W. (2019). Fresh Living Arthrospira as Dietary Supplements: Current Status and Challenges. *Trends Food Sci. Tech.* 88, 439–444. doi:10.1016/j.tifs.2019.04.010

Markley, A. L., Begemann, M. B., Clarke, R. E., Gordon, G. C., and Pfleger, B. F. (2015). Synthetic Biology Toolbox for Controlling Gene Expression in the Cyanobacterium Synechococcus Sp. Strain PCC 7002. *ACS Synth. Biol.* 4 (5), 595–603. doi:10.1021/sb500260k

Moser, S., and Pichler, H. (2019). Identifying and Engineering the Ideal Microbial Terpenoid Production Host. *Appl. Microbiol. Biotechnol.* 103 (14), 5501–5516. doi:10.1007/s00253-019-09892-y

Niu, F.-X., He, X., Wu, Y.-Q., and Liu, J.-Z. (2018). Enhancing Production of Pinene in *Escherichia coli* by Using a Combination of Tolerance, Evolution, and Modular Co-culture Engineering. *Front. Microbiol.* 9, 1623. doi:10.3389/fmicb.2018.01623

Parmar, A., Singh, N. K., Pandey, A., Gnansounou, E., and Madamwar, D. (2011). Cyanobacteria and Microalgae: a Positive prospect for Biofuels. *Bioresour. Tech.* 102 (22), 10163–10172. doi:10.1016/j.biortech.2011.08.030

Pattanaik, B., and Lindberg, P. (2015). Terpenoids and Their Biosynthesis in Cyanobacteria. *Life* 5 (1), 269–293. doi:10.3390/life5010269

Rajneesh, Singh, S. P., Pathak, J., and Sinha, R. P. (2017). Cyanobacterial Factories for the Production of green Energy and Value-Added Products: An Integrated Approach for Economic Viability. *Renew. Sust. Energ. Rev.* 69, 578–595. doi:10.1016/j.rser.2016.11.110

Sarma, M. K., Kaushik, S., and Goswami, P. (2016). Cyanobacteria: A Metabolic Power House for Harvesting Solar Energy to Produce Bio-Electricity and Biofuels. *Biomass and Bioenergy* 90, 187–201. doi:10.1016/j.biombioe.2016.03.043

Sarria, S., Wong, B., Martín, H. G., Keasling, J. D., and Peralta-Yahya, P. (2014). Microbial Synthesis of Pinene. *ACS Synth. Biol.* 3 (7), 466–475. doi:10.1021/sb4001382

Schopf, J. W., and Packer, B. M. (1987). Early Archean (3.3-billion to 3.5-Billion-Year-Old) Microfossils from Warrawoona Group, Australia. *Science* 237, 70–73. doi:10.1126/science.11539686

Silva, C. E. D., Gris, B., Sforza, E., La Rocca, N., and Bertucco, A. (2016). "Effects of Sodium Bicarbonate on Biomass and Carbohydrate Production in Synechococcus PCC 7002," in 5th International Symposium on Industrial Biotechnology (Ibic 2016), Bologna, Italy, April 10–11, 2016, 49, 241–246. doi:10.3303/Cet1649041

Simmons, T. L., Andrianasolo, E., McPhail, K., Flatt, P., and Gerwick, W. H. (2005). Marine Natural Products as Anticancer Drugs. *Mol. Cancer Ther.* 4 (2), 333–342.

Singh, V., Chaudhary, D. K., Mani, I., and Dhar, P. K. (2016). Recent Advances and Challenges of the Use of Cyanobacteria towards the Production of Biofuels. *Renew. Sust. Energ. Rev.* 60, 1–10. doi:10.1016/j.rser.2016.01.099

Stevens, S. E., and Porter, R. D. (1980). Transformation in Agmenellum Quadruplicatum. *Proc. Natl. Acad. Sci.* 77 (10), 6052–6056. doi:10.1073/pnas.77.10.6052

Sun, T., Li, S., Song, X., Diao, J., Chen, L., and Zhang, W. (2018). Toolboxes for Cyanobacteria: Recent Advances and Future Direction. *Biotechnol. Adv.* 36, 1293–1307. doi:10.1016/j.biotechadv.2018.04.007

Tashiro, M., Kiyota, H., Kawai-Noma, S., Saito, K., Ikeuchi, M., Iijima, Y., et al. (2016). Bacterial Production of Pinene by a Laboratory-Evolved Pinene-Synthase. *ACS Synth. Biol.* 5 (9), 1011–1020. doi:10.1021/acssynbio.6b00140

Teruya, T., Sasaki, H., Fukazawa, H., and Suenaga, K. (2009). Bisebromoamide, a Potent Cytotoxic Peptide from the marine Cyanobacterium Lyngbya sp.: Isolation, Stereostructure, and Biological Activity. *Org. Lett.* 11 (21), 5062–5065. doi:10.1021/ol9020546

Walls, L. E., and Rios-Solis, L. (2020). Sustainable Production of Microbial Isoprenoid Derived Advanced Biojet Fuels Using Different Generation Feedstocks: A Review. *Front. Bioeng. Biotechnol.* 8, 599560. doi:10.3389/fbioe.2020.599560

Wang, C., Liwei, M., Park, J.-B., Jeong, S.-H., Wei, G., Wang, Y., et al. (2018). Microbial Platform for Terpenoid Production: *Escherichia coli* and Yeast. *Front. Microbiol.* 9, 2460. doi:10.3389/fmicb.2018.02460

Wei, L.-J., Zhong, Y.-T., Nie, M.-Y., Liu, S.-C., and Hua, Q. (2021). Biosynthesis of α-Pinene by Genetically Engineered Yarrowia Lipolytica from Low-Cost Renewable Feedstocks. *J. Agric. Food Chem.* 69 (1), 275–285. doi:10.1021/acs.jafc.0c06504

Wu, X., Ma, G., Liu, C., Qiu, X.-y., Min, L., Kuang, J., et al. (2021). Biosynthesis of Pinene in Purple Non-sulfur Photosynthetic Bacteria. *Microb. Cel Fact* 20 (1), 101. doi:10.1186/s12934-021-01591-6

Xia, P. F., Ling, H., Foo, J. L., and Chang, M. W. (2019). Synthetic Biology Toolkits for Metabolic Engineering of Cyanobacteria. *Biotechnol. J.* 14 (6), 1800496. doi:10.1002/biot.201800496

Xu, Y., Alvey, R. M., Byrne, P. O., Graham, J. E., Shen, G., and Bryant, D. A. (2011). Expression of Genes in Cyanobacteria: Adaptation of Endogenous Plasmids as Platforms for High-Level Gene Expression in Synechococcus Sp. PCC 7002. *Methods Mol. Biol. (Clifton, N.J.)* 684, 273–293. doi:10.1007/978-1-60761-925-3_21

Yang, M.-k., Qiao, Z.-x., Zhang, W.-y., Xiong, Q., Zhang, J., Li, T., et al. (2013). Global Phosphoproteomic Analysis Reveals Diverse Functions of Serine/Threonine/Tyrosine Phosphorylation in the Model Cyanobacterium Synechococcus Sp. Strain PCC 7002. *J. Proteome Res.* 12 (4), 1909–1923. doi:10.1021/pr4000043

Zhao, Y., Chen, R., Wang, Y., and Yang, Y. (2018). α-Pinene Inhibits Human Prostate Cancer Growth in a Mouse Xenograft Model. *Chemotherapy* 63 (1), 1–7. doi:10.1159/000479863

Conflict of Interest: The authors declare that the research was conducted in the absence of any commercial or financial relationships that could be construed as a potential conflict of interest.

Publisher's Note: All claims expressed in this article are solely those of the authors and do not necessarily represent those of their affiliated organizations, or those of the publisher, the editors, and the reviewers. Any product that may be evaluated in this article, or claim that may be made by its manufacturer, is not guaranteed or endorsed by the publisher.

frontiers in Bioengineering and Biotechnology

ORIGINAL RESEARCH
published: 05 January 2022
doi: 10.3389/fbioe.2021.778584

Biosynthesis of Chiral Amino Alcohols via an Engineered Amine Dehydrogenase in *E. coli*

Feifei Tong[1,2†], Zongmin Qin[2†], Hongyue Wang[2†], Yingying Jiang[2], Junkuan Li[2,3], Hui Ming[2,4], Ge Qu[2,5], Yazhong Xiao[1] and Zhoutong Sun[2,5]**

[1]School of Life Sciences, Anhui University, Hefei, China, [2]Tianjin Institute of Industrial Biotechnology, Chinese Academy of Sciences, Tianjin, China, [3]Department of Chemistry, School of Science, Tianjin University, Tianjin, China, [4]Department of Life Sciences and Medicine, University of Science and Technology of China, Hefei, China, [5]National Technology Innovation Center of Synthetic Biology, Tianjin, China

OPEN ACCESS

Edited by:
Hua Ling,
National University of Singapore, Singapore

Reviewed by:
Wen Shan Yew,
National University of Singapore, Singapore
Lei Shao,
Shanghai University of Medicine and Health Sciences, China
Shuke Wu,
Huazhong Agricultural University, China

***Correspondence:**
Yazhong Xiao
yzxiao@ahu.edu.cn
Zhoutong Sun
sunzht@tib.cas.cn

†These authors have contributed equally to this work

Specialty section:
This article was submitted to Synthetic Biology, a section of the journal Frontiers in Bioengineering and Biotechnology

Received: 17 September 2021
Accepted: 15 November 2021
Published: 05 January 2022

Citation:
Tong F, Qin Z, Wang H, Jiang Y, Li J, Ming H, Qu G, Xiao Y and Sun Z (2022) Biosynthesis of Chiral Amino Alcohols via an Engineered Amine Dehydrogenase in E. coli. Front. Bioeng. Biotechnol. 9:778584. doi: 10.3389/fbioe.2021.778584

Chiral amino alcohols are prevalent synthons in pharmaceuticals and synthetic bioactive compounds. The efficient synthesis of chiral amino alcohols using ammonia as the sole amino donor under mild conditions is highly desired and challenging in organic chemistry and biotechnology. Our previous work explored a panel of engineered amine dehydrogenases (AmDHs) derived from amino acid dehydrogenase (AADH), enabling the one-step synthesis of chiral amino alcohols via the asymmetric reductive amination of α-hydroxy ketones. Although the AmDH-directed asymmetric reduction is in a high stereoselective manner, the activity is yet fully excavated. Herein, an engineered AmDH derived from a leucine dehydrogenase from *Sporosarcina psychrophila* (*Sp*AmDH) was recruited as the starting enzyme, and the combinatorial active-site saturation test/iterative saturation mutagenesis (CAST/ISM) strategy was applied to improve the activity. After three rounds of mutagenesis in an iterative fashion, the best variant wh84 was obtained and proved to be effective in the asymmetric reductive amination of 1-hydroxy-2-butanone with 4-fold improvements in k_{cat}/K_m and total turnover number (TTN) values compared to those of the starting enzyme, while maintaining high enantioselectivity (*ee* >99%) and thermostability (T_{50}^{15} >53°C). In preparative-scale reaction, the conversion of 100 and 200 mM 1-hydroxy-2-butanone catalyzed by wh84 was up to 91–99%. Insights into the source of an enhanced activity were gained by the computational analysis. Our work expands the catalytic repertoire and toolbox of AmDHs.

Keywords: biosynthesis, protein engineering, directed evolution, amine dehydrogenase, chiral amino alcohol

INTRODUCTION

As essential structural moieties, chiral α-amino alcohols are widely applied to produce synthetic and natural bioactive molecules (Ager et al., 1996; Erlanson et al., 2011). For instance, many pharmaceuticals consist of α-amino alcohols that serve as chiral building blocks (**Supplementary Scheme S1**). Direct asymmetric reductive amination of ketones with free ammonia to produce chiral amino alcohols is a highly aspirational transformation (Abrahamson et al., 2013; Pushpanath et al., 2017). In the traditional chemical synthesis, it mainly relies on stoichiometric amounts of chemical reducing agents or organometallic catalysts, which are limited by low stereoselectivities, the formation of the alcohol as side product, and the requirement of extreme reaction conditions

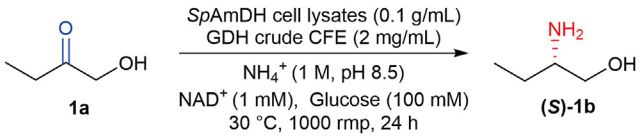

SCHEME 1 | *Sp*AmDH-catalyzed asymmetric reductive amination of 1a to (*S*)-1b by using ammonia as the sole amino donor, and glucose dehydrogenase (GDH) cell-free extract (CFE) for NADH cofactor regeneration.

(Larrow et al., 1996; Breuer et al., 2004; Ma et al., 2010; Nugent and El-Shazly, 2010; Karjalainen and Koskinen, 2012; Xie et al., 2020; Hollmann et al., 2021). Alternatively, enzymes as catalysts are increasingly explored as essential tools in asymmetric reductive aminations (Reetz, 2011; Abrahamson et al., 2013; Schrittwieser et al., 2015; Chen and Arnold, 2020; Winkler et al., 2021). In recent years, a number of enzymes have been identified that are capable of catalyzing the asymmetric reductive amination of ketones (Wu et al., 2021), including lipases (Francalanci et al., 1987), acylases (Wang et al., 2016), transaminases (Wu et al., 2017), and imine reductases (Matzel et al., 2017). Moreover, native amine dehydrogenases (AmDHs) have been identified that they can directly utilize ammonia as a sole amino source in reductive amination but with insufficient enantioselectivity (Itoh et al., 2000; Mayol et al., 2019).

Apart from the native AmDHs, the Bommarius group at Georgia Tech has engineered two natural amino acid dehydrogenases (AADHs), including a leucine dehydrogenase from *Bacillus stearothermophilus* (Abrahamson et al., 2012) and a phenylalanine dehydrogenase from *Bacillus badius* (Abrahamson et al., 2013). After altering two determinant residues of carboxylate recognition, the natural AADHs were transformed to AmDHs, thereby eliminating the activity toward ketone acids while affording new activity toward ketones. Taking this advantage, more natural AADHs from diverse organisms have been explored and engineered to AmDHs based on the introduction of two-point mutations, which were then harnessed in the asymmetric production of chiral amines (Au et al., 2014; Chen et al., 2015; Ye et al., 2015; Franklin et al., 2020; Liu et al., 2020). In addition, the engineered AmDHs derived from AADHs were also utilized in the preparation of chiral amino alcohols, which are usually with very high enantioselectivity (>99% *ee*), making these enzymes of potential value in biocatalysis (Chen et al., 2019). Our previous work has characterized and engineered five novel AmDHs from natural AADHs by genome mining, these newly identified AmDHs provided reductive amination of a broad range of prochiral α- and β-hydroxy ketones in a high stereoselective manner (Wang et al., 2020). As an example, the engineered AmDH derived from the leucine dehydrogenase from *Sporosarcina psychrophila* (*Sp*AmDH), enabled the reduction of 1-hydroxybutan-2-one (1a) to (*S*)-2-aminobutan-1-ol ((*S*)-1b, **Scheme 1**) with >99% selectivity, while the conversion is modest (~60%) at a substrate concentration of 50 mM (Wang et al., 2020).

In this work, we sought to optimize the activity of *Sp*AmDH in the biosynthesis of (*S*)-1b, which is an important intermediate desired in the preparation of antitubercular drugs ethambutol (Pablos-Méndez et al., 1998; **Supplementary Scheme S1**). When aiming at the improvement of activity and/or selectivity, the combinatorial active-site saturation test (CAST) combined with iterative saturation mutagenesis (ISM) has been emerged as a powerful means in protein engineering (Reetz et al., 2005; Yanai et al., 2013; Qu et al., 2020; Li D. et al., 2021; Li J. et al., 2021; Qu et al., 2021; Zheng et al., 2021). Taking the advantage of CAST/ISM, three robust variants of *Sp*AmDH with improved activity and high stereoselectivity were obtained, and their potential as biocatalysts in the preparative scale reactions was explored. Computational docking simulations were also performed to rationalize the elevated activity of *Sp*AmDH variants.

MATERIALS AND METHODS

Chemicals and Reagents

Hydroxy ketones, chiral amino alcohols, and other chemical reagents were purchased from Bidepharm (Shanghai, China), Energy Chemical (Shanghai, China), Kaiwei Chemical (Shanghai, China), Acmec (Shanghai, China), Arkpharm (Chicago, United States), Accela (Shanghai, China), Aladdin (Shanghai, China), Macklin (Shanghai, China), Heowns (Tianjin, China), and CINC (Shanghai, China). PrimeSTAR DNA polymerase and restriction enzyme Dpn I were ordered from TAKARA and NEB, respectively. The primer synthesis and sequencing were carried out by GENEWIZ. A plasmid preparation kit was purchased from TIANGEN Biotech. All other chemical reagents can be obtained through commercialization, unless otherwise noted.

Site-Directed Mutagenesis

Mutagenesis was constructed by using the overlap PCR and megaprimer approach (Tyagi et al., 2004) with high-fidelity master mix polymerase. Reaction mixtures (50 μl) typically contained ddH_2O (22 μl), 2× high-fidelity master mix polymerase (25 μl), template DNA (1 μl, 50 ng), forward primer (1 μl, 0.2 μM), and reverse primer (1 μl, 0.2 μM). The PCR conditions for short fragment were as follows: 98°C, 2 min (98°C, 10 s; 55°C, 15 s; 72°C, 30 s) 30 cycles; 72°C, 3 min. For mega-PCR (Tyagi et al., 2004), 1st PCR product (2 μl, 800 ng) was used as primer, and the PCR conditions as below: 98°C, 2 min (98°C, 10 s; 60°C, 15 s; 72°C, 3.5 min) 30 cycles, 72°C, 5 min. The PCR products were treated with restriction endonuclease Dpn I for 3 h and then electroporated into *E. coli* BL21 (DE3). After culturing for 12 h, the colonies on the plate were washed with ddH_2O, and the plasmids were extracted and sequenced.

The primers used for constructing single-site saturation mutagenesis and combinatory saturation libraries were listed in **Supplementary Tables S1, S2**, respectively.

Screening of Saturation Mutagenesis Libraries

Clones from the plate were transferred to 96-well deep-well culture plates containing 300 μl of LB medium (50 μg/ml kanamycin), shaking at 37°C and 800 rpm for 10 h. Then 120 μl of the aforementioned culture broth was transferred to a 96-well glycerol plate, 60 μl of glycerol (60%, v/v) was added, and stored at −80°C. At the same time, 800 μl of the TB medium was added to the 96-well deep-well culture plates, IPTG (0.2 mM) and kanamycin (50 μg/ml) were added, and the culture was shaken at 30°C, 800 rpm for 12 h for protein expression. The cells were collected by centrifugation at 4,000 rpm, 4°C for 10 min. The cells were washed and resuspended with 400 μl of potassium phosphate buffer (PBK, 50 mM, pH 7.4). DNase I (6 U/ml) and lysozyme (1 mg/ml) were added to the culture and were shaken at 30°C for 1 h to lysis cells. After low-temperature centrifugation (4°C, 4,000 rpm, for 30 min), the supernatant was used for enzyme activity determination. The reductive amination reaction was performed in $NH_4Cl/NH_3{\cdot}H_2O$ buffer (1 M, pH 8.5) containing 200 μl supernatant, 10 mM substrate 1a, 1 mM NAD^+, 100 mM glucose, and 2 mg/ml GDH at 30°C, 800 rpm for 24 h. After that, 1 μl of 1M para-methoxy-2-amino benzamidoxime (PMA) was added to 99 μl of the reaction solution, and fluorescence was measured using an excitation wavelength of 380 nm and emission wavelength of 520 nm for substrate consumption (Mei et al., 2020).

Active Assay

For single point saturation mutation library rescreening, the best clones from 96-well glycerol plates were cultivated, expressed in a shake flask and used for biotransformation. Reductive amination reactions were performed in a reaction mixture (0.5 ml) containing 1 M $NH_4Cl/NH_3{\cdot}H_2O$ buffer (pH 8.5), 1 mM NAD^+, 100 mM glucose, 2 mg/ml GDH cell-free extract (CFE), 6 U/ml DNase I, 20 mM 1a, and 20 mg/ml mutant CFE in 2 ml Eppendorf tubes at 30°C, 1,000 rpm for 24 h in a thermostatic metal bath. For the combinatorial saturation mutation library screening, using the same procedure as before, except for that, the concentration of 1a and the wet cell of mutant were 40 mM and 0.1 g/ml, respectively. After the reaction was over, the aforementioned reaction solution was boiled for 5 min and then centrifuged at 12,000 rpm for 10 min to remove the precipitate. The supernatant was measured by HPLC to detect the conversion of 1a. The conversions of hydroxy ketones substrates (1a–8a) to chiral amino alcohol products (1b-8b) were measured with Marfey's reagent (1-fluoro-2, 4-dinitrophenyl-5-L-alanine amide) for pre-column derivatization. The reaction mixture was mixed with 100 μl sample, 30 μl of Marfey's reagent (14 mM), 80 μl $NaHCO_3$ (1 M), and 200 μl DMSO at 80°C, 1,000 rpm for 10 min. Finally, 10 μl HCl (4 M) was added to stop the reaction. Detection conditions were given as follows: Zorbax SB-C18 column (4.6 × 150 mm, 5 μm), detection wavelength: 340 nm, temperature: 25°C, flow rate: 1 ml/min, loading volume: 10 μl, mobile phase buffer A: ddH_2O (0.1% trifluoroacetic acid), buffer B: methanol (0.1% trifluoroacetic acid), gradient program: 40% B, hold for 6 min, increase B to 60% in 9 min, hold for 3 min, decrease B to 40% in 2 min, and hold for 5 min. More details are listed in **Supplementary Table S3**.

Protein Expression and Purification

E. coli BL21(DE3) glycerol bacteria containing *Sp*AmDH gene were cultivated in 5 ml LB liquid medium (50 μg/ml kanamycin) for 10 h. The previous culture was transferred to the TB medium (100 ml) (50 μg/ml kanamycin) and was cultured at 37°C, 220 rpm. The culture was induced by the addition of IPTG (0.1 mM) when OD_{600} reached 0.8 and was then allowed to grow for an additional 12 h at 20°C. The cells expressing AmDHs were harvested, sonicated, and centrifuged (4°C, 12,000 rpm) for 60 min to remove the precipitate. The supernatant with soluble His-tagged protein was filtered using a 0.45-μm filter membrane and was verified by SDS-PAGE analysis (**Supplementary Figure S1**). The column (HisTrap FF, 5 ml) was washed with A buffer (50 mM PBK containing 300 mM NaCl and 20 mM imidazole, pH 8.0) before and after the supernatant was loaded. The proteins were eluted with B buffer containing a high concentration of salt (50 mM PBK containing 300 mM NaCl and 500 mM imidazole, pH 8.0). The eluates were ultrafiltered (4°C, 3,500 rpm) with an ultrafiltration tube (10,000 Da) to concentrate and replace the buffer (25 mM PBK, 100 mM NaCl, 5% glycerol, pH 8.0). The protein concentration was confirmed by measuring the absorbance at 280 nm using a Nano-300 micro-spectrophotometer.

Total Turnover Numbers Assay for Conversion of Substrate 1a to 1b Using *Sp*AmDH Variants

The asymmetric reductive amination reactions were performed with 0.32–0.64 mg/ml purified enzyme, 1 M $NH_4Cl/NH_3{\cdot}H_2O$ buffer (pH 8.5), 1 mM NAD^+, 100 mM glucose, 2 mg/ml GDH CFE, and 40 mM 1a. The reaction mixture was proceeded at 30°C, 1,000 rpm for 24 h. The product was then detected by HPLC. TTN was defined as the molar number of the product yield divided by the catalyst concentration (Qu et al., 2019).

Determination of Kinetic Parameters and Thermostability

The kinetic parameters were obtained by measuring the initial velocities of NADH consumption (the initial rate of change in absorbance at 340 nm) in the enzymatic reaction and fitting the curve according to the Michaelis–Menten equation (**Supplementary Figure S2**). The activity assay was performed in a mixture containing 0.2 mM NADH, 1–30 mM 1-hydroxy-2-butanone, 1 M $NH_4Cl/NH_3{\cdot}H_2O$ (pH 8.5), and the purified enzyme (1 mg/ml). The reaction was initiated by the addition of the enzyme and was monitored for 5 min at 30°C. The activity was determined by measuring NADH oxidation from a decrease

TABLE 1 | Key residues selected for engineering *Sp*AmDH based on published data.

Entry	*Sp*AmDH site	Data collection			References
		Beneficial position	Enzyme	Comment	
1	L40	L40	*Bs*LeuDH	Lining the binding pocket	Abrahamson et al. (2012)
2	G41	G41	*Bs*LeuDH	Lining the binding pocket	Abrahamson et al. (2012)
3	G42	G42	*Bs*LeuDH	Lining the binding pocket	Abrahamson et al. (2012)
4	T43	T41	*Rs*PheDH	Within 6Å from the substrate	Ye et al. (2015)
5	M65	M65	*Bs*LeuDH	Lining the binding pocket	Abrahamson et al. (2012)
6	K68	K66	*Rs*PheDH	Carboxylate recognition	Ye et al. (2015)
7	K68	K68	*Lf*LeuDH	Altering the substrate specificity	Chen et al. (2019)
8	N69	M67	*Rs*PheDH	Within 6Å from substrate	Ye et al. (2015)
9	I111	W114	*Rs*PheDH	Within 6Å from substrate	Ye et al. (2015)
10	T112	T115	*Rs*PheDH	Within 6Å from substrate	Ye et al. (2015)
11	A113	A113	*Bs*LeuDH	Altering the substrate specificity	Abrahamson et al. (2012)
12	A113	A113	*Lf*LeuDH	Enlarging the active-site	Chen et al. (2019)
13	E114	E114	*Bs*LeuDH	Altering the substrate specificity	Abrahamson et al. (2012)
14	D115	D115	*Bs*LeuDH	Essential to the catalytic mechanism	Abrahamson et al. (2012)
15	V116	V116	*Bs*LeuDH	Altering the substrate specificity	Abrahamson et al. (2012)
16	T134	T134	*Lf*LeuDH	Enlarging the active-site	Chen et al. (2019)
17	P146	S149	*Rs*PheDH	Within 6Å from substrate	Ye et al. (2015)
18	T150	T153	*Rs*PheDH	Within 6Å from substrate	Ye et al. (2015)
19	A187	A187	*Bs*LeuDH	Altering the substrate specificity	Abrahamson et al. (2012)
20	N261	N261	*Lf*LeuDH	Responsible for altering the substrate specificity	Chen et al. (2019)
21	N262	N262	*Rs*PheDH	Interact with the carboxyl group of the natural substrate	Ye et al. (2015)
22	N287	N288	*Rs*PheDH	Within 6Å from substrate	Ye et al. (2015)
23	S288	A289	*Rs*PheDH	Within 6Å from substrate	Ye et al. (2015)
24	G290	G291	*Rs*PheDH	Within 6Å from substrate	Ye et al. (2015)
25	V291	V291	*Bs*LeuDH	Lining the binding pocket	Abrahamson et al. (2012)
26	I292	I292	*Bs*LeuDH	Altering the substrate specificity	Abrahamson et al. (2012)
27	V294	V294	*Bs*LeuDH	Lining the binding pocket	Abrahamson et al. (2012)
28	E297	E297	*Bs*LeuDH	Changing the substrate specificity	Abrahamson et al. (2012)
29	L61	—	—	Lining the binding pocket	This study
30	L239	—	—	Lining the binding pocket	This study
31	A295	—	—	Lining the binding pocket	This study

in the absorbance at 340 nm (ε = 6,220 M^{-1} cm^{-1}) and then Origin was used to perform the nonlinear fitting of the Michaelis–Menten equation. One unit (1 U) of activity is defined as the amount of enzyme required to consume 1 μM NADH in 1 minute. For thermostability, 1 mg/ml pure enzyme solution was incubated at different temperatures (30–70°C) for 15 min, followed by measuring the residual activity in 1 M $NH_4Cl/NH_3{\cdot}H_2O$ (pH 8.5) containing 0.2 mM NADH, 10 mM substrate 1a at 50°C for 2 min. All experiments were conducted in triplicate.

Preparative-Scale Reactions Using *Sp*AmDH Mutants

The *Sp*AmDH mutants wh18 and wh84 were inoculated in the 5 ml LB medium (50 μg/ml kanamycin) for 10 h (37°C, 220 rpm). The aforementioned culture was inoculated into the 1,000 ml TB medium (50 μg/ml kanamycin) and cultured at 37°C, 220 rpm until the OD_{600} reached 0.8–0.9. IPTG was then added to a final concentration of 0.1 mM, and the culture was allowed to grow for additional 16 h at 20°C, 220 rpm. The cells were pelleted by centrifugation for 20 min (4°C, 4,000 rpm) and washed once with phosphate buffer (50 mM, pH 7.4). Subsequently, 0.1 g/ml wet cells, 1 M $NH_4Cl/NH_3{\cdot}H_2O$ buffer (pH 8.5), 1 mM NAD^+, 100 mM glucose, 2 mg/ml GDH CFE, 6 U/ml DNase I, 1 mg/ml lysozyme, and 1a (100, 200 mM) were mixed for 10 ml in a Erlenmeyer flask. The reaction was performed at 30°C, 220 rpm for 24 h in a shaker with triple replica. Then 200 μl samples were taken at 0, 1, 2, 3, 4, 8, 12, 18, and 24 h and then prepared and analyzed by HPLC. The 100 mM scaled-up reaction of 1a catalyzed by wh84 was terminated by adding 5% H_2SO_4 to pH <2 and then centrifuged at an rpm of 4,000 for 20 min at 4°C, to collect the supernatant. The product ((*S*)-2a) was purified via an ion exchange method with Dowex® 50WX8 ion exchange resin (Chen et al., 2015). The column was prepared by washing with 100 ml ddH_2O and 50 ml 5% w/v H_2SO_4. Then, the acidified reaction supernatant was loaded into the column at a low flow rate, washed with ddH_2O until pH ~7.0, eluted with 9% w/v NH_4OH (100 ml), and dried via rotary evaporation to harvest the final product (*S*)-2a. ^1H NMR (400 MHz, D_2O) δ 3.61 (dd, J = 11.8, 4.1 Hz, 1H), 3.51–3.33 (m 1H), 3.06–2.82 (m, 1H), 1.57–1.33 (m, 2H), and 0.98–0.81 (m, 3H).

Model Generation and Substrate Docking

The structure of the mutant wh84 (K68S/N261L/I111F/V294C/E114V) was generated by PyMol program (http://www.pymol.org) using the crystallographic structure of *Sp*LeuDH (PDB ID: 3VPX, Zhao et al., 2012) as a template. The initial structure of wh84 was relaxed/repacked before docking using Rosetta relax program (Conway et al., 2014). The generated pose with the

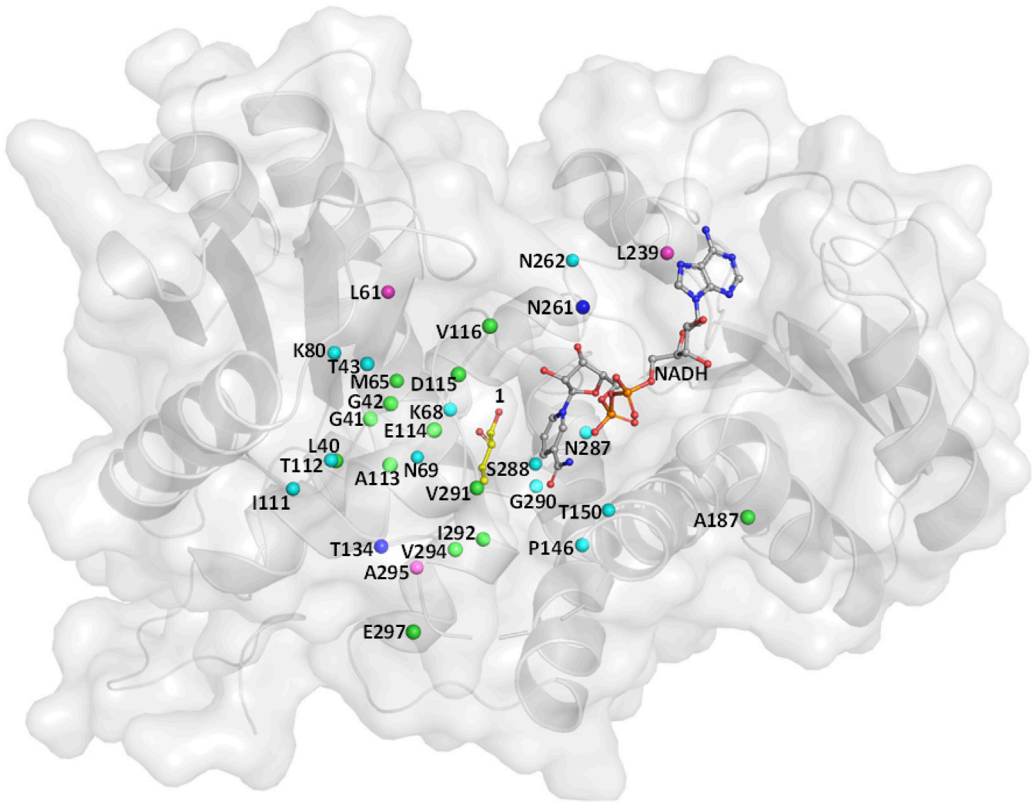

FIGURE 1 | Residues lining the substrate-binding pocket of *Sp*LeuDH (PDB ID: 3VPX). The sites marked in green, cyan, and blue are obtained from the three studies Abrahamson et al. (2012); Ye et al. (2015); Chen et al. (2019), respectively. The sites marked in magenta are found in this study.

lowest Rosetta_total_score was selected as input file for docking. The cofactor NADH, substrate 1a, and NH_4^+ were prepared in Schrödinger Maestro software (Schrödinger, 2015). Thereafter, NADH and 1a were stepwise docked into the active site of wh84 by using Rosetta docking program (Combs et al., 2013). Thereafter, 1a was docked to the protein–NADH complex using the same procedure as NADH, only by replacing the input files. After that, NH_4^+ was docked to the protein–NADH-1a complex by using AutoDock Vina (Trott and Olson, 2010). For docking NH_4^+, a total of 16 poses were generated by Vina, and only the pose with proper interactions with D115 and 1a was kept.

RESULTS AND DISCUSSION

Knowledge-Based and Structural Guided Engineering of SpLeuDH

Wild-type (WT) leucine dehydrogenase from *Sporosarcina psychrophila* (*Sp*LeuDH, Accession No.: WP_067209859) has been successfully engineered to an amine dehydrogenase (*Sp*AmDH) by implanting the double mutations K68S/N261L in our recent work (Wang et al., 2020). Based on the crystallographic structure of *Sp*LeuDH (PDB ID: 3VPX, Zhao et al., 2012), this *Sp*AmDH variant (K68S/N261L, dubbed wh18) showed excellent stereoselectivity (>99% ee) in the transformation of 1a to 1b, while the catalytic efficiency was modest when it was applied in large-scale production (Wang et al., 2020). Thus, the CAST/ISM strategy was employed with the aim of enhancing the activity of *Sp*AmDH. To identify the hot spot positions that may manipulate the activity, the beneficial mutations reported in other engineering studies toward AmDHs were collected (**Table 1**). We anticipated that targeting these residues at the equivalent positions in *Sp*AmDH may give rise to more proficient variants. Moreover, three additional positions L61, L239, and A295 were also selected as they are situated at the substrate binding pocket (**Table 1**; **Figure 1**).

The 27 positions were then performed site-directed saturation mutagenesis using wh18 as the template, each site was substituted by the other 19 amino acids with NNK codon degeneracy (32 codons). To satisfy the 95% library coverage, 96 clones were screened for each position by using *para*-methoxy-2-amino benzamidoxime (PMA) as colorimetric probe (Mei et al., 2020). After the initial assaying, the improved variants (hits) were then picked up for further evaluation using the reaction conditions shown in **Scheme 1**. As a result, several active variants showing pronounced degrees of conversion for substrate 1a were

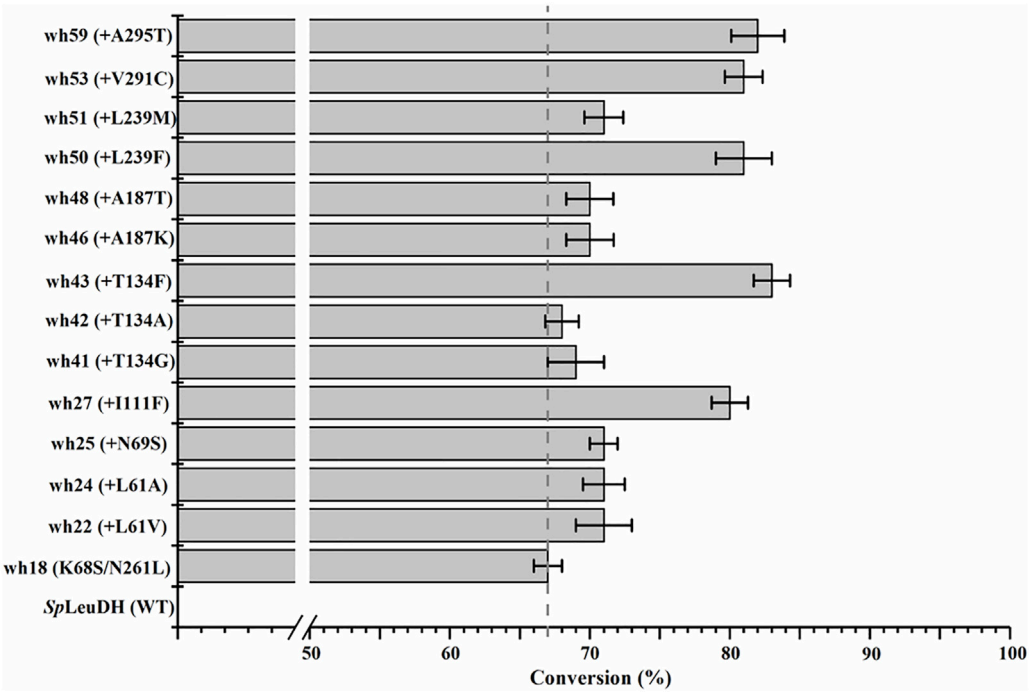

FIGURE 2 | Improved variants obtained by screening the single point saturation mutagenesis libraries on the 27 positions. Reductive amination reactions were performed in a reaction mixture (0.5 ml) containing 1 M $NH_4Cl/NH_3{\cdot}H_2O$ buffer (pH 8.5), 1 mM NAD^+, 100 mM glucose, 2 mg/ml GDH cell-free extract (CFE), 6 U/ml DNase I, 20 mM 1a, and 20 mg/ml mutant CFE at 30°C, 1,000 rpm for 24 h. The conversion was detected by HPLC at least three times.

TABLE 2 | Specific activity of *Sp*AmDH mutants toward substrate 1a.

Code	Mutants	Specific activity (U/mg)[a]
wh18	K68S/N261L	0.118 ± 0.005
wh27	K68S/N261L/I111F	0.177 ± 0.03
wh43	K68S/N261L/T134F	0.07 ± 0.005
wh50	K68S/N261L/L239F	0.15 ± 0.017
wh53	K68S/N261L/V291C	0.167 ± 0.005
wh59	K68S/N261L/A295T	0.054 ± 0.007

[a]*Reaction was performed in 1 M $NH_4Cl/NH_3{\cdot}H_2O$ buffer (pH 8.5) containing 0.2 mM NADH, 1 mg/ml purified enzyme and 10 mM substrate 1a, at 30°C for 5 min.*

obtained (**Figure 2**). Five of them including wh27, wh43, wh50, wh53, and wh59 showed more than 10% increment on the formation of (*S*)-1b compared to the starting enzyme wh18 (**Figure 2**).

Combinatorial Engineering of SpAmDH Using Reduced Amino Acid Alphabets

After purification, the five variants were then assayed for the specific activity, three of which including wh27, wh50, and wh53 displayed a higher specific activity than that of wh18 (**Table 2**). In order to investigate the potential epistatic interactions operating between the individual point mutations shown in **Table 2**, ten additional double mutants (wh61–wh70, **Supplementary Table S4**) were constructed and tested using the whole-cell lysate system. As a result, the variant wh43 showed the highest conversion of 85%, while none of the ten combinatorial mutants can exceed the conversion of 80%. It suggests that no additive effects among the five single mutations I111F, T134F, L239F, V291C, and A295T were in pairs, and the triple to quintuple mutants were therefore not constructed further.

In parallel, we noted that the three mutants with improved activity, shown in **Table 2**, are all composed of the substitutions of phenylalanine and cysteine (e.g., I111F, L239F, and V291C), indicating that hydrophobic interaction and steric hindrance may play key roles in tailoring the activity. Therefore, phenylalanine and cysteine were chosen as building blocks for the further saturation mutagenesis to determine the interactions among the positions in adjacent to residues 111, 239, and 291. As such, two focused libraries A and B were constructed using F and C as reduced amino acid alphabets based on the double-code saturation mutagenesis (DCSM) concept (Sun et al., 2016): library A using wh53 as template with residues M65, S68, N69, and S288 involved, while library B applying wh27 as template with residues L40, A113, T134, and V294 arrested. As a result, two improved mutants wh76 (K68S/N261L/V291C/S68C/N69C) and wh81 (K68S/N261L/I111F/V294C) were obtained from libraries A and B, respectively. The variants wh76 and wh81 gave a conversion of 87 and 90% in the transformation of 1a, respectively, with >99% ee.

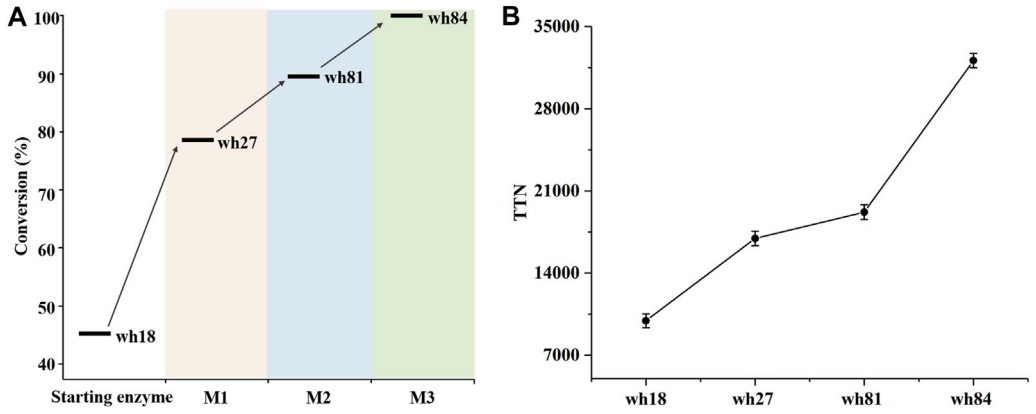

FIGURE 3 | Conversion **(A)** and TTN **(B)** analysis of the key variants using 40 mM substrate 1a. M1~M3 depicted the three rounds of mutagenesis.

TABLE 3 | Thermostability and kinetic parameters of purified *Sp*AmDH mutants for substrate 1a.

Code	Thermostabiliy T_{50}^{15} (°C)[a]	Mutations	K_m (mM)[b]	k_{cat} (s^{-1})[b]	k_{cat}/K_m ($s^{-1}mM_)^{-1}$[b]	Specific activity (U/mg)[b]
wh18	51	K68S/N261L	9.45 ± 1.44	0.83 ± 0.05	0.088	0.118 ± 0.005
wh27	50	K68S/N261L/I111F	18.52 ± 1.42	1.74 ± 0.07	0.094	0.177 ± 0.030
wh81	51	K68S/N261L/I111F/V294C	21.5 ± 3.37	3.14 ± 0.27	0.146	0.362 ± 0.019
wh84	53	K68S/N261L/I111F/E114V/V294C	17.53 ± 1.11	6.07 ± 0.19	0.346	0.884 ± 0.044

[a]*For determining thermostability, purified* SpAmDH *enzymes (1 mg/ml) were incubated at different temperatures (30–70°C) for 15 min, followed by measuring the residual activity toward substrate 1a.*

[b]*For assaying kinetic parameters, the reaction was performed in 1 M $NH_4Cl/NH_3{\cdot}H_2O$ buffer (pH 8.5) containing 0.2 mM NADH and 0.5–30 mM substrate 1a, at optimum temperatures (50°C) for 2 min. Michaelis–Menten plots are shown in* ***Supplementary Figure S2****.*

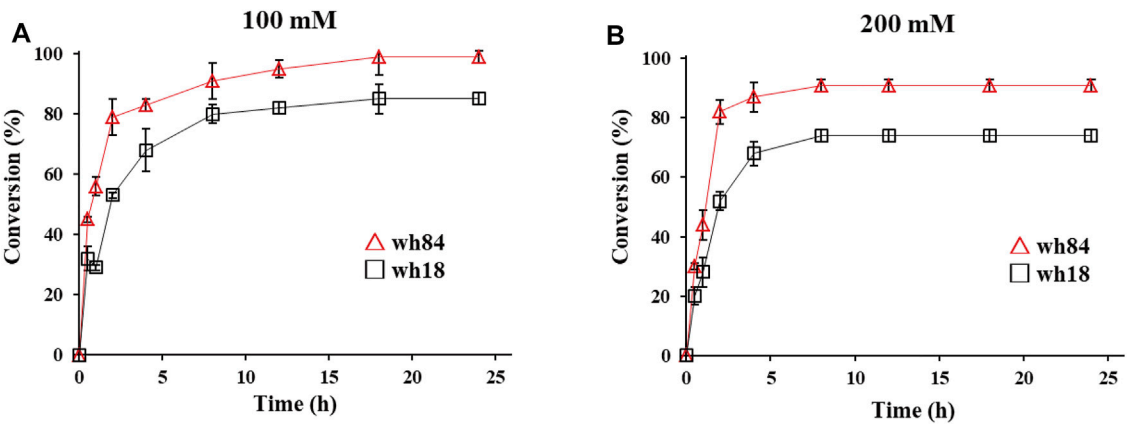

FIGURE 4 | Preparative-scale of the asymmetric amination reactions of substrate 1a 100 mM **(A)** and 200 mM **(B)** catalyzed by wh18 and wh84 (□: wh18, △: wh84). Reaction system: 0.1 g/ml wet cell, 1 M $NH_4Cl/NH_3{\cdot}H_2O$ buffer (pH 8.5), 1 mM NAD^+, 100 mM glucose, 2 mg/ml GDH CFE, 6 U/mL DNase I, 1 mg/ml lysozyme, and 1a (100 and 200 mM) were mixed in Erlenmeyer flask. The reaction was performed at 30°C, 220 rpm for 24 h. The samples taken at 0, 1, 2, 3, 4, 8, 12, 18, and 24 h were prepared and analyzed by HPLC.

Third Round of Mutagenesis Toward SpAmDH, Characterization, and Preparative-Scale Reduction

The variant wh81 was further used as template for the third round of mutagenesis. In this scenario, an important single mutation E114V was considered because it has been reported that this residue can function on the ammonia activation, and thereby affecting the enzyme activity (Abrahamson et al., 2012; Chen et al., 2018; Patil et al., 2018; Lee et al., 2021). To our delight, the resultant quintuple variant wh84 (K68S/N261L/I111F/V294C/

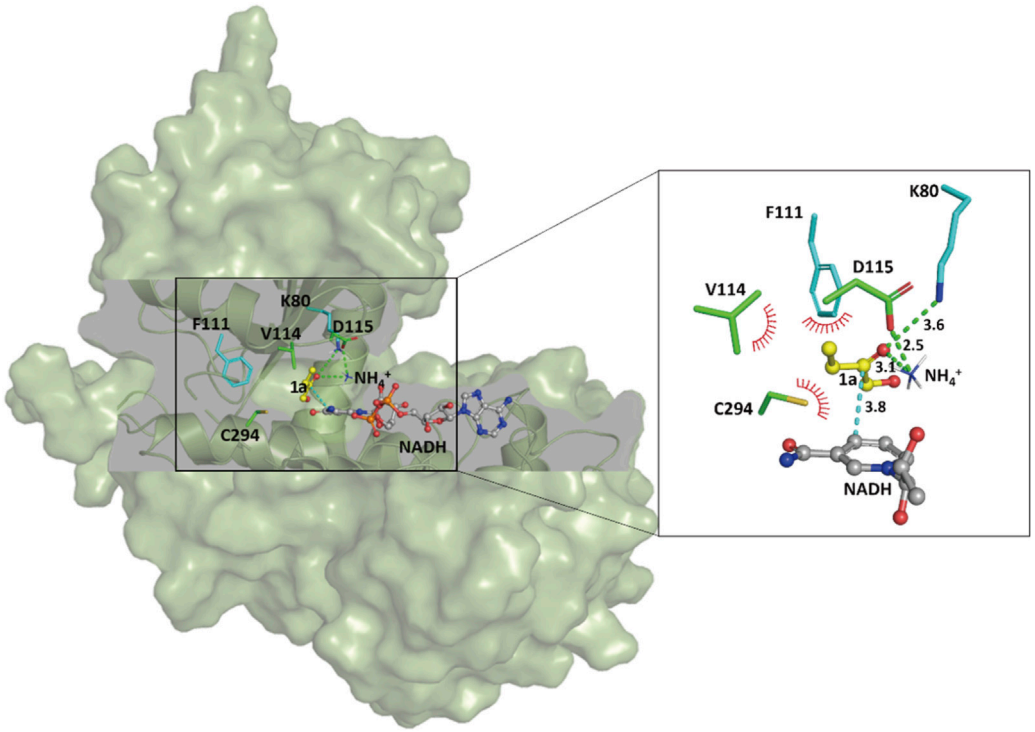

FIGURE 5 | Docking analysis of substrate 1a in the catalytic pocket of the *Sp*AmDH variant wh84. Green lines and red spikes represent the hydrogen bonds and the penitential hydrophobic interactions, respectively. The cyan line indicates the nucleophilic attack. Distances are shown in angstroms.

E114V) showed 99% conversion and >99% ee toward 1a. Taken together, after three rounds of mutagenesis, the conversion of 1a directed by the *Sp*AmDH mutants was successfully elevated from 46 to 99% (**Supplementary Figure S3**; **Figure 3A**). Thereafter, the best mutants in each round of mutagenesis were then purified and characterized by total turnover numbers (TTN), thermostability, and enzyme kinetics. Likewise, wh27, wh81, and wh84 increased the TTN stepwise for substrate 1a (**Figure 3B**). In particular, wh84 increased the TTN up to 32108, which is 3.2-fold in contrast to that of wh18.

To evaluate the enzyme robustness of the engineered variants, thermostability was assessed by measuring T_{50}^{15}, the temperature at which 50% of the enzyme activity is lost following a heat treatment for 15 min. Intriguingly, all of the three variants constructed based on wh18 showed comparable T_{50}^{15} values, reflecting no trade-off between the thermostability and the improved activity (**Table 3**). Kinetic studies showed that wh84 has the highest catalytic efficiency (k_{cat}/K_m) (0.346 $s^{-1}mM^{-1}$) among all the mutants, a more than 3.9-fold increase to the starting template wh18.

Preparative-scale amination reactions were performed using whole-cell lysates as catalysts for the selected variants in 10 ml of reaction volume, with 100 mM substrate 1a. The mutant wh84 achieved an excellent conversion (>99%), with the high enantioselectivity of >99% ee within 18 h, while wh18 used as a control only showed ca. 80% conversion (**Figure 4A**). (*S*)-2b was subsequently isolated as pure form (164 mg, 62% yield) in the reaction system catalyzed by wh84. To further examine the catalytic potential of wh84, the concentration of 1a was raised up to 200 mM. Interestingly, wh84 enabled 91% conversion (**Figure 4B**).

Gaining Insight on the Improved Activity of SpAmDH

In order to shed light on the improved activity of the *Sp*AmDH variant wh84, computational docking analyses were performed to gain insights into the relationship between reshaping of the active site and the effect on activity. The homology structure of wh84 was directly constructed based on the X-ray structure of *Sp*LeuDH (PDB ID: 3VPX, Zhao et al., 2012) by introducing the corresponding mutations in PyMol program (http://www.pymol.org). After relaxing the initial structure of wh84, cofactor NADH, substrate 1a, and ammonium ion (NH_4^+) were docked into the active site one after another to generate the protein–NADH-1a–NH_4^+ quaternary complex. It is of interest to note that the catalytic sites K80 and D115 form hydrogen bond interactions with the substrate carbonyl group and the ammonium ion, while the substitutions I111F, E114V, and V294C contribute to hydrophobic interactions with the substrate carbon chain (**Figure 5**). These strengthened interactions may benefit the substrate recognition and orientation, thereby promoting the activity and maintaining the stereoselectivity. Moreover, on the basis of the proposed mechanism of the engineered AmDHs and their parent AADHs (Sharma et al., 2017), this preferred binding orientation of 1a

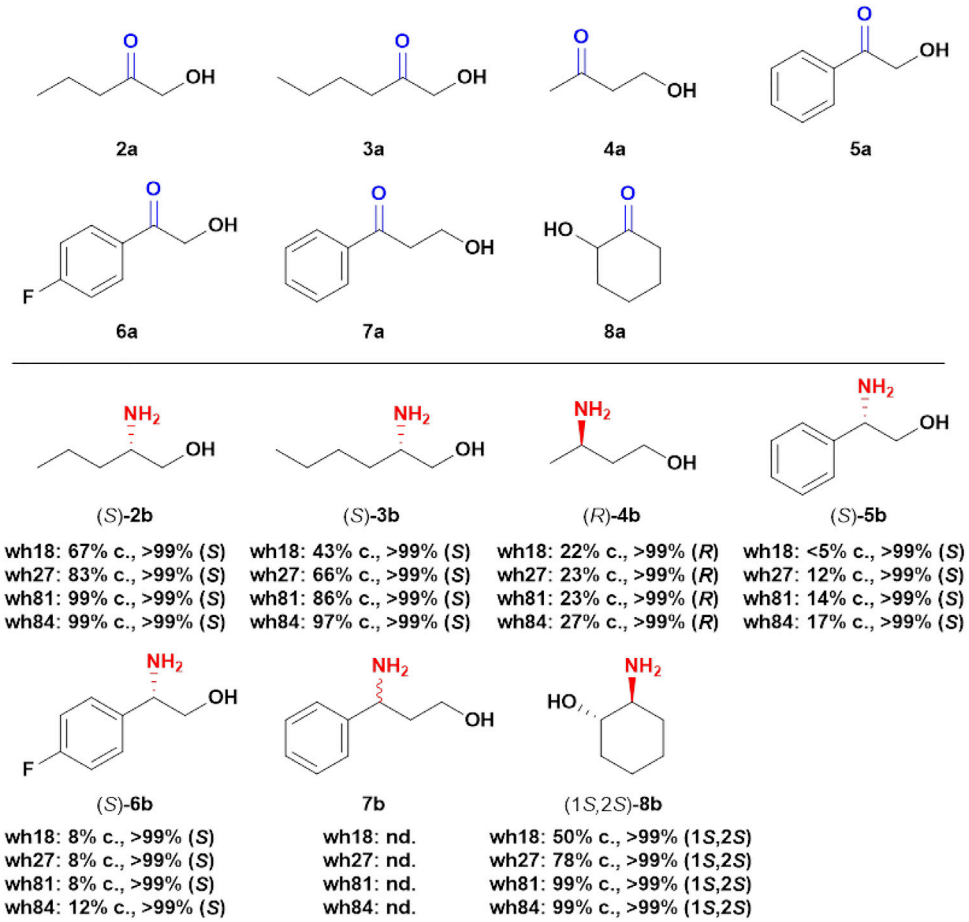

FIGURE 6 | Asymmetric transformations of hydroxy ketones. Reaction system: 0.1 g/ml wet cell, 1 M $NH_4Cl/NH_3{\cdot}H_2O$ buffer (pH 8.5), 1 mM NAD^+, 100 mM glucose, 2 mg/ml GDH CFE, 6 U/ml DNase I, 1 mg/ml lysozyme, and 2a-8a (5 mM) were mixed in 2 ml Eppendorf tubes. The reaction was performed at 30°C, 1,000 rpm for 24 h in a thermostatic metal bath. c, conversion; nd, not detectable.

with respect to NADH determines the *Re* face of the C=O bond undergoes nucleophilic attack and profits the (*S*)-configure product, which is consistent with the experimental results.

Substrate Scope Analysis Toward Other Prochiral Hydroxy ketones

With the aim to explore the catalytic potential of the engineered variants toward other prochiral hydroxy ketones, seven structurally different substrates were assayed using wh18, wh27, wh81, and wh84 as catalysts (**Figure 6**). For the four aliphatic compounds 2a–4a and cyclic ketone 8a, the variants showed high stereoselectivity (>99%), and interestingly, the conversions were elevated from wh18 to wh84 in all the four cases (**Supplementary Figures S4–S6, S10**). For example, the conversion of 3a was improved from 43% (wh18) to 97% (wh84). However, in the scenario of the aromatic substrates, the four variants displayed relatively lower activity in the asymmetric reduction of 5a–7a (**Figure 6**), while the stereoselectivities were still inherently maintained (>99%, **Supplementary Figures S7–S9**).

CONCLUSION

Reductive amination of carbonyl compounds employing AmDHs is an attractive route for the biosynthesis of chiral amino alcohols. It provides several advantages, including lower costs (the amino donor (NH_4^+) is inexpensive, and water is the main byproduct), elimination of heavy metals, and high stereoselectivity. As such, AmDHs have been reported in the selective synthesis of chiral compounds used as pharmaceutical intermediates. However, the limited catalytic efficiency can be a major obstacle to its industrial application. This work reports the engineering of *Sp*AmDH with the aim to improve the activity. After three rounds of CAST/ISM-guided mutagenesis, mutant wh84 was obtained with the best performance toward substrate 1a, resulting in an excellent TTN (32108) and a k_{cat}/K_m value of 0.346 s^{-1} mM^{-1}, amounting to 3.2-fold and 3.9-fold improvements relative to the starting enzyme, respectively, while maintaining the high enantioselectivity (>99% *ee*). In the 100 mM preparative reaction, the conversion of 1a catalyzed by wh84 was up to 99% with a 62% yield, which is comparable with the recent work that

employed an engineered AmDH from *Lysinibacillus fusiformis* as catalyst (Chen et al., 2019).

Overall, this work paves the way toward engineering AmDHs with increased activity and also expands the biocatalytic toolbox for asymmetric reductive aminations, and should prove useful insights for further development of other AmDHs as catalysts in the biosynthesis of enantiopure amino alcohols.

DATA AVAILABILITY STATEMENT

The original contributions presented in the study are included in the article/**Supplementary Material**, and further inquiries can be directed to the corresponding authors.

AUTHOR CONTRIBUTIONS

YX, ZS, and GQ designed and planned the study. FT, ZQ, HW, YJ, HM, and JL performed the experiments. GQ wrote the manuscript. All authors were involved in the discussions, planning the experiments, and editing manuscript.

FUNDING

This work was financially supported by the National Key Research and Development Program of China (No. 2019YFA0906400), the National Natural Science Foundation of China (No. 31870779), and the Tianjin Synthetic Biotechnology Innovation Capacity Improvement Project (TSBICIP-CXRC-009, TSBICIP-KJGG-003). GQ also thanks financial supports from the Youth Innovation Promotion Association (2021175), CAS.

SUPPLEMENTARY MATERIAL

The Supplementary Material for this article can be found online at: https://www.frontiersin.org/articles/10.3389/fbioe.2021.778584/full#supplementary-material

REFERENCES

Abrahamson, M. J., Vázquez-Figueroa, E., Woodall, N. B., Moore, J. C., and Bommarius, A. S. (2012). Development of an Amine Dehydrogenase for Synthesis of Chiral Amines. *Angew. Chem. Int. Ed.* 51, 3969–3972. doi:10.1002/anie.201107813

Abrahamson, M. J., Wong, J. W., and Bommarius, A. S. (2013). The Evolution of an Amine Dehydrogenase Biocatalyst for the Asymmetric Production of Chiral Amines. *Adv. Synth. Catal.* 355, 1780–1786. doi:10.1002/adsc.201201030

Ager, D. J., Prakash, I., and Schaad, D. R. (1996). 1,2-Amino Alcohols and Their Heterocyclic Derivatives as Chiral Auxiliaries in Asymmetric Synthesis. *Chem. Rev.* 96, 835–876. doi:10.1021/cr9500038

Au, S. K., Bommarius, B. R., and Bommarius, A. S. (2014). Biphasic Reaction System Allows for Conversion of Hydrophobic Substrates by Amine Dehydrogenases. *ACS Catal.* 4, 4021–4026. doi:10.1021/cs4012167

Breuer, M., Ditrich, K., Habicher, T., Hauer, B., Kesseler, M., Stürmer, R., et al. (2004). Industrial Methods for the Production of Optically Active Intermediates. *Angew. Chem. Int. Ed.* 43, 788–824. doi:10.1002/anie.200300599

Chen, F.-F., Cosgrove, S. C., Birmingham, W. R., Mangas-Sanchez, J., Citoler, J., Thompson, M. P., et al. (2019). Enantioselective Synthesis of Chiral Vicinal Amino Alcohols Using Amine Dehydrogenases. *ACS Catal.* 9, 11813–11818. doi:10.1021/acscatal.9b03889

Chen, F.-F., Liu, Y.-Y., Zheng, G.-W., and Xu, J.-H. (2015). Asymmetric Amination of Secondary Alcohols by Using a Redox-Neutral Two-Enzyme Cascade. *ChemCatChem* 7, 3838–3841. doi:10.1002/cctc.201500785

Chen, F.-F., Zheng, G.-W., Liu, L., Li, H., Chen, Q., Li, F.-L., et al. (2018). Reshaping the Active Pocket of Amine Dehydrogenases for Asymmetric Synthesis of Bulky Aliphatic Amines. *ACS Catal.* 8, 2622–2628. doi:10.1021/acscatal.7b04135

Chen, K., and Arnold, F. H. (2020). Engineering New Catalytic Activities in Enzymes. *Nat. Catal.* 3, 203–213. doi:10.1038/s41929-019-0385-5

Combs, S. A., Deluca, S. L., Deluca, S. H., Lemmon, G. H., Nannemann, D. P., Nguyen, E. D., et al. (2013). Small-molecule Ligand Docking into Comparative Models with Rosetta. *Nat. Protoc.* 8, 1277–1298. doi:10.1038/nprot.2013.074

Conway, P., Tyka, M. D., DiMaio, F., Konerding, D. E., and Baker, D. (2014). Relaxation of Backbone Bond Geometry Improves Protein Energy Landscape Modeling. *Protein Sci.* 23, 47–55. doi:10.1002/pro.2389

Erlanson, D. A., Arndt, J. W., Cancilla, M. T., Cao, K., Elling, R. A., English, N., et al. (2011). Discovery of a Potent and Highly Selective PDK1 Inhibitor via Fragment-Based Drug Discovery. *Bioorg. Med. Chem. Lett.* 21, 3078–3083. doi:10.1016/j.bmcl.2011.03.032

Francalanci, F., Cesti, P., Cabri, W., Bianchi, D., Martinengo, T., and Foa, M. (1987). Lipase-Catalyzed Resolution of Chiral 2-amino 1-alcohols. *J. Org. Chem.* 52, 5079–5082. doi:10.1021/jo00232a002

Franklin, R. D., Mount, C. J., Bommarius, B. R., and Bommarius, A. S. (2020). Separate Sets of Mutations Enhance Activity and Substrate Scope of Amine Dehydrogenase. *ChemCatChem* 12, 2436–2439. doi:10.1002/cctc.201902364

Hollmann, F., Opperman, D. J., and Paul, C. E. (2021). Biocatalytic Reduction Reactions From a Chemist's Perspective. *Angew. Chem. Int. Ed.* 60, 5644–5665. doi:10.1002/anie.20180034310.1002/anie.202001876

Itoh, N., Yachi, C., and Kudome, T. (2000). Determining a Novel NAD+-dependent Amine Dehydrogenase with a Broad Substrate Range from Streptomyces Virginiae IFO 12827: Purification and Characterization. *J. Mol. Catal. B: Enzymatic* 10, 281–290. doi:10.1016/S1381-1177(00)00111-9

Karjalainen, O. K., and Koskinen, A. M. P. (2012). Diastereoselective Synthesis of Vicinal Amino Alcohols. *Org. Biomol. Chem.* 10, 4311–4326. doi:10.1039/C2OB25357G

Larrow, J. F., Schaus, S. E., and Jacobsen, E. N. (1996). Kinetic Resolution of Terminal Epoxides via Highly Regioselective and Enantioselective Ring Opening with TMSN3. An Efficient, Catalytic Route to 1,2-Amino Alcohols. *J. Am. Chem. Soc.* 118, 7420–7421. doi:10.1021/ja961708+

Lee, S., Jeon, H., Giri, P., Lee, U.-J., Jung, H., Lim, S., et al. (2021). The Reductive Amination of Carbonyl Compounds Using Native Amine Dehydrogenase from *Laribacter hongkongensis*. *Biotechnol. Bioproc. E.* 26, 384–391. doi:10.1007/s12257-021-0113-2

Li, D., Chen, X., Chen, Z., Lin, X., Xu, J., and Wu, Q. (2021). Directed Evolution of Lipase A from *Bacillus Subtilis* for the Preparation of Enantiocomplementary *Sec*-Alcohols. *Green. Synth. Catal.* 2, 290–294. doi:10.1016/j.gresc.2021.07.003

Li, J., Qu, G., Shang, N., Chen, P., Men, Y., Liu, W., et al. (2021). Near-Perfect Control of the Regioselective Glucosylation Enabled by Rational Design of Glycosyltransferases. *Green. Synth. Catal.* 2, 45–53. doi:10.1016/j.gresc.2021.01.005

Liu, L., Wang, D.-H., Chen, F.-F., Zhang, Z.-J., Chen, Q., Xu, J.-H., et al. (2020). Development of an Engineered Thermostable Amine Dehydrogenase for the Synthesis of Structurally Diverse Chiral Amines. *Catal. Sci. Technol.* 10, 2353–2358. doi:10.1039/D0CY00071J

Ma, S. K., Gruber, J., Davis, C., Newman, L., Gray, D., Wang, A., et al. (2010). A Green-by-Design Biocatalytic Process for Atorvastatin Intermediate. *Green. Chem.* 12, 81–86. doi:10.1039/B919115C

Matzel, P., Gand, M., and Höhne, M. (2017). One-step Asymmetric Synthesis of (*R*)- and (*S*)-rasagiline by Reductive Amination Applying Imine Reductases. *Green. Chem.* 19, 385–389. doi:10.1039/c6gc03023h

Mayol, O., Bastard, K., Beloti, L., Frese, A., Turkenburg, J. P., Petit, J.-L., et al. (2019). A Family of Native Amine Dehydrogenases for the Asymmetric Reductive Amination of Ketones. *Nat. Catal.* 2, 324–333. doi:10.1038/s41929-019-0249-z

Mei, Z., Zhang, K., Qu, G., Li, J.-K., Liu, B., Ma, J.-A., et al. (2020). High-throughput Fluorescence Assay for Ketone Detection and its Applications in Enzyme Mining and Protein Engineering. *ACS Omega* 5, 13588–13594. doi:10.1021/acsomega.0c00245

Nugent, T. C., and El-Shazly, M. (2010). Chiral Amine Synthesis - Recent Developments and Trends for Enamide Reduction, Reductive Amination, and Imine Reduction. *Adv. Synth. Catal.* 352, 753–819. doi:10.1002/adsc.200900719

Pablos-Méndez, A., Raviglione, M. C., Laszlo, A., Binkin, N., Rieder, H. L., Bustreo, F., et al. (1998). Global Surveillance for Antituberculosis-Drug Resistance, 1994-1997. *N. Engl. J. Med.* 338, 1641–1649. doi:10.1056/nejm199806043382301

Patil, M. D., Grogan, G., Bommarius, A., and Yun, H. (2018). Oxidoreductase-Catalyzed Synthesis of Chiral Amines. *ACS Catal.* 8, 10985–11015. doi:10.1021/acscatal.8b02924

Pushpanath, A., Siirola, E., Bornadel, A., Woodlock, D., and Schell, U. (2017). Understanding and Overcoming the Limitations of *Bacillus badius* and *Caldalkalibacillus thermarum* Amine Dehydrogenases for Biocatalytic Reductive Amination. *ACS Catal.* 7, 3204–3209. doi:10.1021/acscatal.7b00516

Qu, G., Li, A., Acevedo-Rocha, C. G., Sun, Z., and Reetz, M. T. (2020). The Crucial Role of Methodology Development in Directed Evolution of Selective Enzymes. *Angew. Chem. Int. Ed.* 59, 13204–13231. doi:10.1002/anie.201901491

Qu, G., Liu, B., Jiang, Y., Nie, Y., Yu, H., and Sun, Z. (2019). Laboratory Evolution of an Alcohol Dehydrogenase Towards Enantioselective Reduction of Difficult-to-Reduce Ketones. *Bioresour. Bioproc.* 6, 18. doi:10.1186/s40643-019-0253-9

Qu, G., Sun, Z., and Reetz, M. T. (2021). "Iterative Saturation Mutagenesis for Semi-rational Enzyme Design," in *Protein Engineering: Tools and Applications*. Editor H. Zhao (Weinheim: Wiley-VCH Press), 105–132. doi:10.1002/9783527815128.ch5

Reetz, M. T., Bocola, M., Carballeira, J. D., Zha, D., and Vogel, A. (2005). Expanding the Range of Substrate Acceptance of Enzymes: Combinatorial Active-Site Saturation Test. *Angew. Chem. Int. Ed.* 44, 4192–4196. doi:10.1002/anie.200500767

Reetz, M. T. (2011). Laboratory Evolution of Stereoselective Enzymes: a Prolific Source of Catalysts for Asymmetric Reactions. *Angew. Chem. Int. Ed.* 50, 138–174. doi:10.1002/anie.201000826

Schrittwieser, J. H., Velikogne, S., and Kroutil, W. (2015). Biocatalytic Imine Reduction and Reductive Amination of Ketones. *Adv. Synth. Catal.* 357, 1655–1685. doi:10.1002/adsc.201500213

Schrödinger (2015). *Schrödinger Suite 2015-1*. New York: LLC.

Sharma, M., Mangas-Sanchez, J., Turner, N. J., and Grogan, G. (2017). NAD(P)H-dependent Dehydrogenases for the Asymmetric Reductive Amination of Ketones: Structure, Mechanism, Evolution and Application. *Adv. Synth. Catal.* 359, 2011–2025. doi:10.1002/adsc.201700356

Sun, Z., Lonsdale, R., Li, G., and Reetz, M. T. (2016). Comparing Different Strategies in Directed Evolution of Enzyme Stereoselectivity: Single- Versus Double-Code Saturation Mutagenesis. *ChemBioChem* 17, 1865–1872. doi:10.1002/cbic.201600296

Trott, O., and Olson, A. J. (2009). AutoDock Vina: Improving the Speed and Accuracy of Docking with a New Scoring Function, Efficient Optimization, and Multithreading. *J. Comput. Chem.* 31, 455–461. doi:10.1002/jcc.21334

Tyagi, R., Lai, R., and Duggleby, R. G. (2004). A New Approach to 'megaprimer' Polymerase Chain Reaction Mutagenesis Without an Intermediate Gel Purification Step. *BMC Biotechnol.* 4, 2. doi:10.1186/1472-6750-4-2

Wang, H., Qu, G., Li, J.-K., Ma, J.-A., Guo, J., Miao, Y., et al. (2020). Data Mining of Amine Dehydrogenases for the Synthesis of Enantiopure Amino Alcohols. *Catal. Sci. Technol.* 10, 5945–5952. doi:10.1039/D0CY01373K

Wang, J., Liu, N., Cheng, X., and Chen, L. (2016). Efficient Continuous Kinetic Resolution of Racemic 2-Aminobutanol Over Immobilized Penicillin G Acylase. *Synth. Commun.* 46, 956–962. doi:10.1080/00397911.2016.1181763

Winkler, C. K., Schrittwieser, J. H., and Kroutil, W. (2021). Power of Biocatalysis for Organic Synthesis. *ACS Cent. Sci.* 7, 55–71. doi:10.1021/acscentsci.0c01496

Wu, H.-L., Zhang, J.-D., Zhang, C.-F., Fan, X.-J., Chang, H.-H., and Wei, W.-L. (2017). Characterization of Four New Distinct ω-Transaminases from Pseudomonas Putida NBRC 14164 for Kinetic Resolution of Racemic Amines and Amino Alcohols. *Appl. Biochem. Biotechnol.* 181, 972–985. doi:10.1007/s12010-016-2263-9

Wu, S., Snajdrova, R., Moore, J. C., Baldenius, K., and Bornscheuer, U. T. (2021). Biocatalysis: Enzymatic Synthesis for Industrial Applications. *Angew. Chem. Int. Ed.* 60, 88–119. doi:10.1002/anie.202006648

Xie, C., Song, J., Hua, M., Hu, Y., Huang, X., Wu, H., et al. (2020). Ambient-temperature Synthesis of Primary Amines via Reductive Amination of Carbonyl Compounds. *ACS Catal.* 10, 7763–7772. doi:10.1021/acscatal.0c01872

Yanai, N., Sindoro, M., Yan, J., and Granick, S. (2013). Electric Field-Induced Assembly of Monodisperse Polyhedral Metal-Organic Framework Crystals. *J. Am. Chem. Soc.* 135, 34–37. doi:10.1021/ja309361d

Ye, L. J., Toh, H. H., Yang, Y., Adams, J. P., Snajdrova, R., and Li, Z. (2015). Engineering of Amine Dehydrogenase for Asymmetric Reductive Amination of Ketone by Evolving *Rhodococcus* Phenylalanine Dehydrogenase. *ACS Catal.* 5, 1119–1122. doi:10.1021/cs501906r

Zhao, Y., Wakamatsu, T., Doi, K., Sakuraba, H., and Ohshima, T. (2012). A Psychrophilic Leucine Dehydrogenase from *Sporosarcina psychrophila*: Purification, Characterization, Gene Sequencing and Crystal Structure Analysis. *J. Mol. Catal. B Enzym.* 83, 65–72. doi:10.1016/j.molcatb.2012.06.018

Zheng, W., Yu, H., Fang, S., Chen, K., Wang, Z., Cheng, X., et al. (2021). Directed Evolution of L-Threonine Aldolase for the Diastereoselective Synthesis of β-Hydroxy-α-Amino Acids. *ACS Catal.* 11, 3198–3205. doi:10.1021/acscatal.0c04949

Conflict of Interest: This work has been included in patent applications by the Tianjin Institute of Industrial Biotechnology.

Publisher's Note: All claims expressed in this article are solely those of the authors and do not necessarily represent those of their affiliated organizations, or those of the publisher, the editors, and the reviewers. Any product that may be evaluated in this article, or claim that may be made by its manufacturer, is not guaranteed or endorsed by the publisher.

frontiers in Bioengineering and Biotechnology

ORIGINAL RESEARCH
published: 07 January 2022
doi: 10.3389/fbioe.2021.779405

A Computational Framework to Identify Metabolic Engineering Strategies for the Co-Production of Metabolites

Lavanya Raajaraam[1,2,3] *and Karthik Raman*[1,2,3]*

[1]Department of Biotechnology, Bhupat and Jyoti Mehta School of Biosciences, Indian Institute of Technology (IIT) Madras, Chennai, India, [2]Centre for Integrative Biology and Systems mEdicine (IBSE), IIT Madras, Chennai, India, [3]Robert Bosch Centre for Data Science and Artificial Intelligence (RBCDSAI), IIT Madras, Chennai, India

Microbial production of chemicals is a more sustainable alternative to traditional chemical processes. However, the shift to bioprocess is usually accompanied by a drop in economic feasibility. Co-production of more than one chemical can improve the economy of bioprocesses, enhance carbon utilization and also ensure better exploitation of resources. While a number of tools exist for *in silico* metabolic engineering, there is a dearth of computational tools that can co-optimize the production of multiple metabolites. In this work, we propose co-FSEOF (co-production using Flux Scanning based on Enforced Objective Flux), an algorithm designed to identify intervention strategies to co-optimize the production of a set of metabolites. Co-FSEOF can be used to identify all pairs of products that can be co-optimized with ease using a single intervention. Beyond this, it can also identify higher-order intervention strategies for a given set of metabolites. We have employed this tool on the genome-scale metabolic models of *Escherichia coli* and *Saccharomyces cerevisiae*, and identified intervention targets that can co-optimize the production of pairs of metabolites under both aerobic and anaerobic conditions. Anaerobic conditions were found to support the co-production of a higher number of metabolites when compared to aerobic conditions in both organisms. The proposed computational framework will enhance the ease of study of metabolite co-production and thereby aid the design of better bioprocesses.

Keywords: metabolic modelling, genome-scale models, bioproduction, concomitant production, co-synthesis, constraint-based modelling

OPEN ACCESS

Edited by:
Hua Ling,
National University of Singapore, Singapore

Reviewed by:
*Meiyappan Lakshmanan, Bioprocessing Technology Institute (A*STAR), Singapore*
Guoqiang Xu, Jiangnan University, China

***Correspondence:**
Karthik Raman
kraman@iitm.ac.in

Specialty section:
This article was submitted to Synthetic Biology, a section of the journal Frontiers in Bioengineering and Biotechnology

Received: *18 September 2021*
Accepted: *02 December 2021*
Published: *07 January 2022*

Citation:
Raajaraam L and Raman K (2022) A Computational Framework to Identify Metabolic Engineering Strategies for the Co-Production of Metabolites. Front. Bioeng. Biotechnol. 9:779405. doi: 10.3389/fbioe.2021.779405

1 INTRODUCTION

Recent years have seen several advances in the usage of bioprocessing to produce a wide range of chemicals (Erickson et al., 2012). Microorganisms can produce diverse and complex products from simple carbon sources. Nevertheless, there are many challenges in designing economically feasible bioprocesses. The advancements in synthetic biology have enabled the metabolic engineering of organisms to improve yield and productivity (Yadav et al., 2019). Various computational strain design algorithms have been developed to identify the genetic manipulations required to over-produce a single product (Burgard et al., 2003; Rocha et al., 2008; Yang et al., 2011). Despite the increase in yield achieved through such rational strain design, the bioprocesses are unable to compete

with the traditional chemical processes in many cases (Cai and Bennett, 2011). This is due to two main reasons: 1) the cost of raw materials and 2) the maximum yield achievable for a given product in a given organism and environment is limited by the number of genetic manipulations that can be successfully implemented in a single strain (Silva et al., 2012). The former issue can be reduced by using agricultural waste as feedstock instead of a synthetic nutrient medium. The latter can be overcome by co-producing multiple products in the same bioprocess (da Silva et al., 2014).

Co-production equips us to exploit the system in a better fashion and produce more valuable products from the same raw materials. A high-value, low-volume chemical can be co-produced with a low-value, high-volume product in order to increase the economic feasibility, as in the case of riboflavin and butanol, respectively (Cai and Bennett, 2011). Co-production is essential when a cocktail of metabolites need to be produced together, rather than a single metabolite, as in the case of biofuels and fatty acids (Xin et al., 2018). A mixture of different alcohols or fatty acids of varying chain length need to be co-optimized in such cases. It can also balance carbon metabolism, as in the case of uridine, and acetoin (Fan et al., 2018). High carbon inflow towards uridine causes excess production of acetate, which hampers the growth of the organism. Conversion of acetate to acetoin prevents over-acidification of the nutrient medium and thereby improves growth and uridine production. There are many studies that have successfully achieved co-production of a variety of products with/without genetic manipulation of the organisms. Polyhydroxyalkanoates are a common class of metabolites that are co-produced with other metabolites (Li et al., 2017; Kumar and Kim, 2018; Yadav et al., 2021). Butanol and hydrogen have been co-produced in *Clostridium beijerinckii* (Zhang et al., 2021), and ethanol and xylitol have been co-produced in *Candida tropicalis* (Raj and Krishnan, 2020; de Souza Queiroz et al., 2021). The carbon source, nutrient medium, pH etc., are optimized in such cases to improve the yield of metabolites. Metabolic engineering can further expand the number of products that are co-produced and also improve their yield significantly. Multiple metabolites like ethanol, isopropanol, butanol and 2,3- butanediol have been co-produced by optimizing the acetone-butanol-ethanol (ABE) fermentation pathway in *Clostridium acetobutylicum* (Collas et al., 2012). Nisin and 3-phenyllactic acid, two antimicrobial agents, have been co-produced in *Lactococcus lactis* through genetic manipulation (Julien-Laferrière et al., 2016). Non-native metabolites can also be co-produced with other metabolites, as in the case of butanol and riboflavin, by engineering the heterologous pathway in *C. acetobutylicum* (Cai and Bennett, 2011).

Although many strain design algorithms have been successfully employed for metabolically engineering organisms to optimize a single product (Pharkya et al., 2003; Kumelj et al., 2019), few studies have applied it for co-production. The studies listed above only use existing literature and readily apparent deletion targets to achieve co-production. This limits the robustness of the bioprocesses that are designed. There is a lack of algorithms that can be easily applied to study co-production. In this study, we have extended the Flux Scanning based on Enforced Objective Flux (FSEOF) (Choi et al., 2010) algorithm to study co-production. Further, while deletion targets can be obtained for metabolites independently using existing algorithms like OptKnock (Burgard et al., 2003), OptGene (Rocha et al., 2008), there are very few algorithms that can identify amplification targets (Ranganathan et al., 2010). In order to identify amplification targets in addition to knock-out targets for co-optimizing a set of metabolites, we propose a new methodology, co-FSEOF, adapting the FSEOF algorithm. Co-FSEOF has a simple computational framework that can be easily modified, and it also provides the entire set of potential intervention strategies in a single run while many algorithms are sequential, returning one intervention target per run. The utility of the potential intervention strategies obtained was further assessed using Flux Variability Analysis (FVA). We applied co-FSEOF to evaluate all possible pairs of secretory metabolites in *Escherichia coli* and *Saccharomyces cerevisiae*. The different pairs of metabolites that can be co-produced through a single reaction deletion or amplification were obtained. This analysis helps us choose favorable pairs of metabolites for which higher-order intervention strategies can be obtained. We have demonstrated this by identifying the amplification targets, knock-out targets and mixed intervention strategies of size up to three to co-optimize the production of isobutanol and succinic acid in *S. cerevisiae*. Higher-order intervention strategies were able to achieve better yield with very little reduction in growth rate. Overall, our analyses provide an overall picture of the biosynthetic capabilities of an organism, particularly highlighting key interdependencies in metabolism.

2 METHODS

2.1 Flux Balance Analysis

FBA is a widely used steady-state constraint-based modelling approach to predict the metabolic capabilities of a variety of organisms (Varma and Palsson, 1994; Kauffman et al., 2003; Orth et al., 2010). The metabolic network of an organism, which comprises all reactions known to occur in the organism, is represented as a stoichiometric matrix S, of size $m \times n$, where m is the number of metabolites, and n is the number of reactions (**Figure 1A**). The entries in the jth column of S represent the stoichiometric coefficients of the metabolites that participate in the jth reaction. The minimum and maximum values of flux that any reaction can assume are constrained by the lower and upper bounds, respectively. The flux through a reaction under a given set of conditions, at steady-state, is calculated by solving a linear programming (LP) problem. The LP problem is formulated as:

$$\max_v \quad \boldsymbol{c}^T \boldsymbol{v}$$
$$\text{subject to } \boldsymbol{S}.\boldsymbol{v} = 0$$
$$\text{while } v_{l,i} \le v_i \le v_{u,i}, \forall i \in [1, n]$$

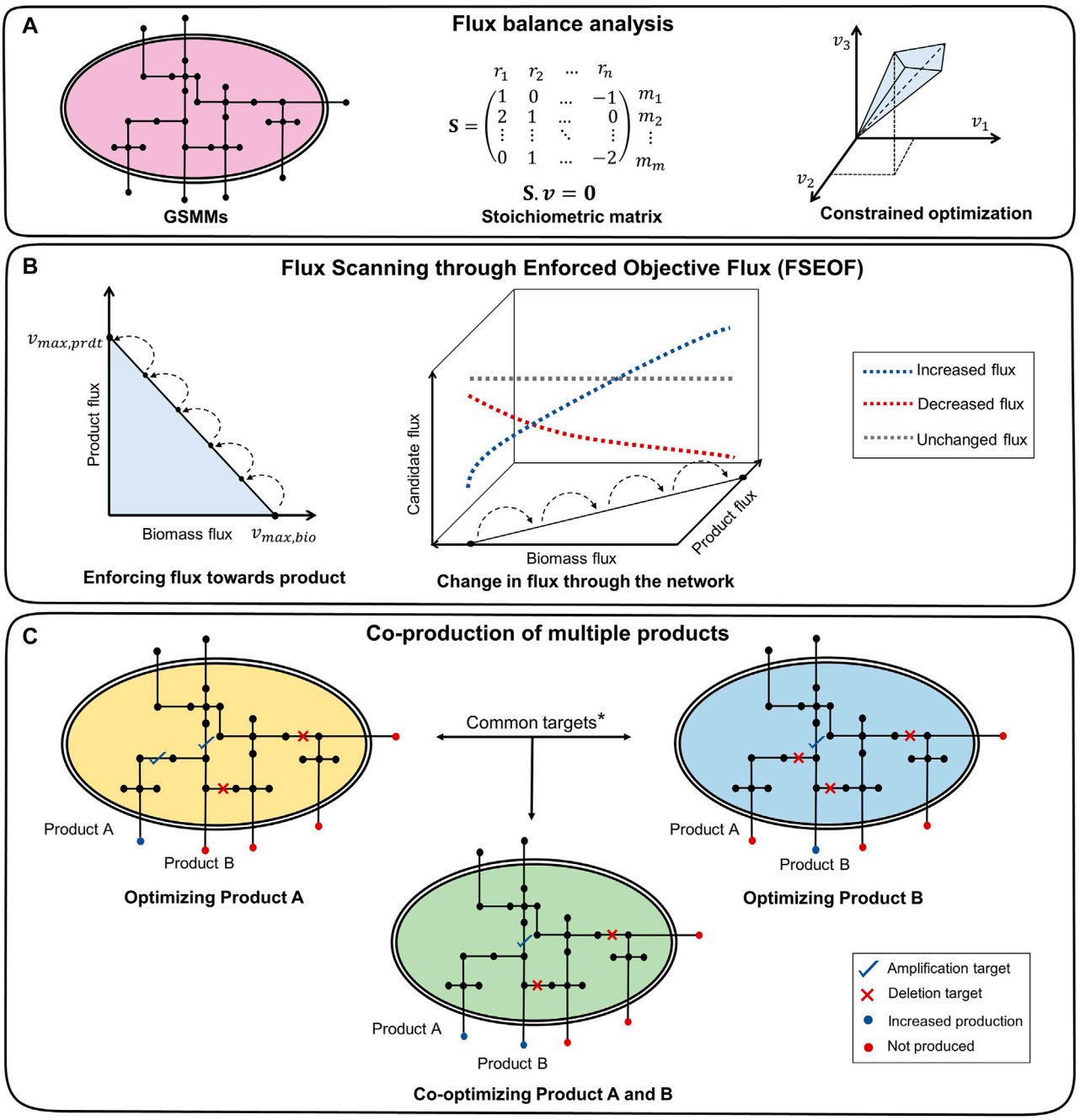

FIGURE 1 | Framework of co-FSEOF. **(A)** The GSMM is represented as a stoichiometric matrix, which is used for FBA. **(B)** The flux through the product is increased in steps, and flux changes through all other reactions are studied. The reactions that have increased flux with an increase in product flux are potential amplification targets. The reactions that have decreased flux are potential deletion targets, while those with unchanged or oscillatory fluxes are excluded. **(C)** The targets common to products A and B are the potential targets for co-optimization. *The union of all potential targets for products A and B is used for higher-order intervention strategies.

where c is a vector of weights denoting the contribution of each of the n reactions to the objective function, $\boldsymbol{v} \epsilon R^n$ is the vector of metabolic fluxes, $\boldsymbol{v_l}$ and $\boldsymbol{v_u}$ are vectors representing the lower and upper bounds for the reaction fluxes, respectively (Orth et al., 2010).

2.2 Flux Variability Analysis

FVA is used to identify the range of fluxes of each reaction that still satisfy the constraints, where two optimization problems are solved for each flux v_i of interest.

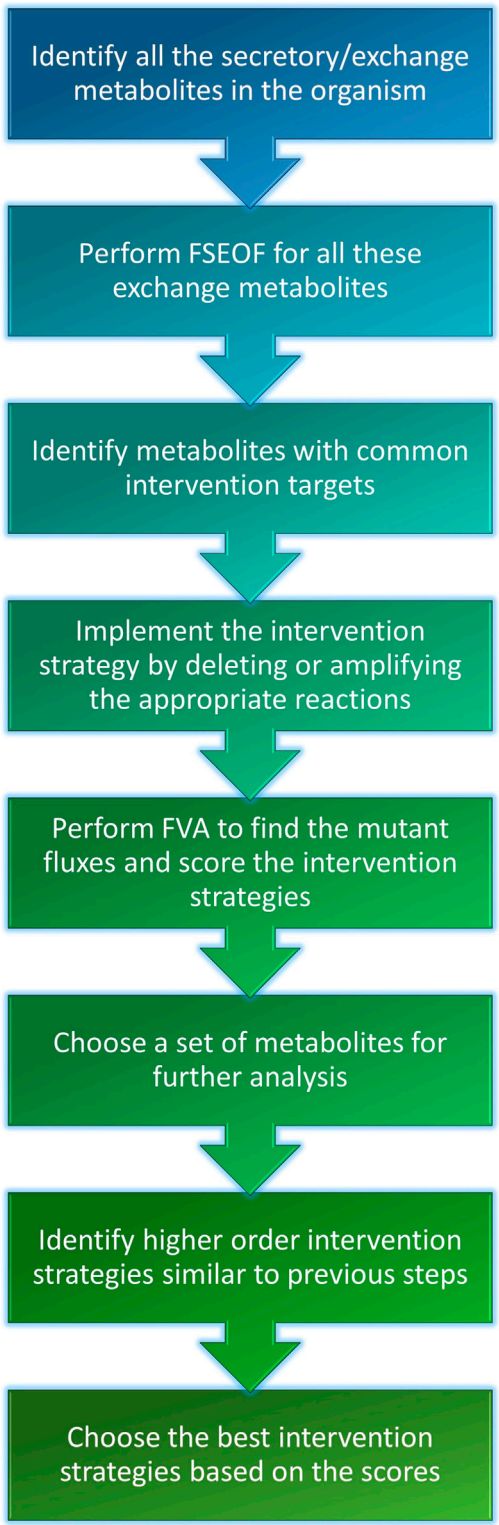

FIGURE 2 | Workflow of co-FSEOF. The figure illustrates succinctly, the key steps of the algorithm.

$$v_{j,max}/v_{j,min} = max_v/min_v \cdot v_j$$
$$\text{s.t. } \boldsymbol{S.v} = 0$$
$$\text{while } v_{l,i} \le v_i \le v_{u,i}\ ,\ \forall i \in [1,\ n]$$

where $v \epsilon R^n$ is the vector of metabolic fluxes, $v_{j,max}$ and $v_{j,min}$ are the maximum and minimum values of fluxes, respectively for each reaction flux v_j (Gudmundsson and Thiele, 2010).

2.3 Flux Scanning Based on Enforced Objective Flux

FSEOF (Choi et al., 2010) is a method used to identify potential reaction deletion and amplification targets in metabolic networks by observing the change in the reaction fluxes when the system moves from the wild-type flux of the target product to the theoretical maximum flux of the product (**Figure 1B**). The maximum biomass $v_{\max,bio}$ and maximum product $v_{\max,prdt}$ fluxes are obtained by performing FBA with the biomass reaction and the exchange reaction of the product as the objective, respectively. The flux of the target reaction, v_{prdt} is pinned to $x\%\ of\ v_{\max,prdt}$ $(x = 0 \rightarrow 100)$. The change in the flux of a reaction, v_j, is studied as the product flux, v_{prdt} is increased, and it is classified as a potential deletion or amplification target based on the decrease or increase in its flux, respectively. The reactions that undergo no change or oscillations in the fluxes are discarded from the set of potential intervention strategies. The set of potential intervention strategies obtained are assessed by simulating each intervention and performing FVA on the mutant.

2.4 Co-FSEOF: Co-Optimization of Metabolites

The Genome-Scale Metabolic Models (GSMMs) of *E. coli* iML1515 and *S. cerevisiae* iMM904 were obtained from the BiGG models database (http://bigg.ucsd.edu/) (Raj and Krishnan, 2020). The simulations were done with the following constraints on uptakes: −10 mmol/gDW/h glucose and −2 mmol/gDW/h oxygen for aerobic conditions and −10 mmol/gDW/h glucose and zero oxygen uptake for anaerobic conditions. Exchange and transport reactions were removed from the search space for FSEOF to increase the relevance of the results and to reduce the computational time. The potential intervention strategies for all secretory metabolites (metabolites that can be secreted into the medium) in the organism were obtained using FSEOF as described in **Section 2.3**. All possible pairs of secretory metabolites were examined for co-production by identifying their common intervention strategies which were obtained through FSEOF (**Figure 1C**). These common deletion or amplification targets constitute the potential intervention strategies for a set of metabolites. The implementation steps of the algorithm are summarized in **Figure 2**.

The reliability of the potential intervention targets is analyzed by comparing the flux values of biomass and product in the mutant with those of the wild-type organism. The mutant model is obtained by deleting the reaction in case of knock-out targets or

by fixing the flux bounds of the amplification target to its theoretical maximum. FVA is performed on this mutant model with biomass as objective to obtain the range of flux values for the products and biomass. Any reaction with more than a 5% increase in the maximum product flux and less than 75% decrease in biomass flux is considered a promising intervention strategy. FVA was performed using fastFVA to reduce the computational time (Gudmundsson and Thiele, 2010).

To obtain higher-order intervention strategies, the potential targets obtained earlier for a given set of metabolites were combined, and all possible combinations of intervention strategies of a certain size (up to three) were evaluated using FVA. The score for each product i (total number of products, n) and the overall score are calculated as

$$Score_i = \frac{\left(v_{prdt_i,mut} - v_{prdt_i,wt}\right)}{\left(v_{bio,wt} - v_{bio,mut}\right)}$$

$$Overall\ Score = \sum_{i=1}^{n} \left(Score_i\right)$$

where $v_{prdt_i,mut}$ and $v_{prdt_i,wt}$ are the mutant and wild-type maximum fluxes of the exchange reaction of the product i, and $v_{bio,mut}$ and $v_{bio,wt}$ are the mutant and wild-type fluxes of the biomass reaction. $Score_i$ denotes the score for the individual product while *overall score* denotes the cumulative score for the set of metabolites. All simulations were performed in MATLAB R2018a (MathWorks Inc., United States) using the COBRA Toolbox v3.0 (Heirendt et al., 2019) and IBM ILOG CPLEX 12.8 as the linear programming solver.

3 RESULTS

Metabolic engineering strategies for the co-production of all pairs of secreted metabolites in *E. coli* and *S. cerevisiae* were obtained using co-FSEOF as described in **Section 2.4**. We identified the intervention strategies required to optimize the co-production of metabolites in both aerobic and anaerobic conditions. Anaerobic conditions favor the co-production of more pairs of metabolites when compared to aerobic conditions. The intervention strategy for each pair of metabolites is scored as in **Section 2.4**. The best intervention strategy can be chosen using the *overall score*. In cases where one metabolite might be favored over the others, the individual scores, $Score_i$ can be used to choose the best intervention strategies. Some of the intervention strategies obtained have been successfully verified through experimental studies in literature. This shows the credibility of the intervention strategies obtained. We discuss a few of the industrially significant metabolites and their intervention strategies, along with supporting literature. We also propose many other intervention strategies, which form a ready short-list for experimental validation. We were able to identify other hitherto unexplored intervention strategies, which may be better alternatives to those in existing literature, further demonstrating the utility of the algorithm.

3.1 Co-Production in *Escherichia coli*

E. coli is one of the well-studied model organisms and has high-quality GSMMs available. The latest GSMM, *i*ML1515 (Monk et al., 2017), was used in this study, and the co-production of 337 secretory metabolites was studied in both aerobic and anaerobic conditions.

3.1.1 Aerobic Fermentation

Co-production of all pairs of metabolites was studied in *E. coli*, using co-FSEOF and FVA as described in **Section 2.3**, **2.4**. Out of ${}^{337}C_2$ pairs of secretory metabolites, only 237 could be successfully overproduced through deletion or amplification of a single reaction. The intervention strategies for a few industrially significant pairs of metabolites are listed in **Table 1**. One of the important pairs of metabolites that can be easily co-produced is L-lysine, a food additive and drug additive and cadaverine, which is essential for polyamide production. co-FSEOF was able to identify several reactions from the diaminopimelate pathway (DAP), which can be over-expressed to co-produce L-lysine and cadaverine. An experimental study by Xu et al. (2019) demonstrates the effect of engineering the DAP pathway in *E. coli* for the production of L-lysine. This indicates the reliability of the results obtained through our computational approach. Another significant result is the co-production of succinate and ethanol through the amplification of glyceraldehyde-3-phosphate dehydrogenase. Other studies have also successfully co-produced ethanol and succinate by other genetic manipulations (Liang et al., 2019).

3.1.2 Anaerobic Fermentation

Anaerobic conditions support the co-production of more metabolites when compared to aerobic conditions. More than 1,000 pairs of metabolites can be co-produced, out of which few are listed in **Table 2**. L-lysine and cadaverine can be co-produced under anaerobic conditions too. But the maximum flux achievable is lower when compared to aerobic conditions. The yield of metabolites like acetate, formate, and hexanoate can be co-optimized by deleting acetaldehyde dehydrogenase or alcohol dehydrogenase. We also found that succinate and lactate can be co-produced by the knock-out of pyruvate formate lyase. The effect of deletion of *pflB* gene encoding pyruvate formate lyase has been experimentally verified in *E. coli* for succinate production (Zhang et al., 2009) and lactate production (Utrilla et al., 2009) through separate studies. This shows that there are multiple co-production strategies available in the existing literature that can be easily utilized to design an efficient process.

3.2 Co-Production in *Saccharomyces cerevisiae*

Another industrially relevant and well-studied model organism is *S. cerevisiae*. Though heterologous pathways have not been analyzed in this study, one can easily modify the GSMM and apply co-FSEOF to identify co-production strategies for

TABLE 1 | Intervention strategies for co-production of pairs of metabolites in *E. coli* under aerobic conditions.

#	Product A	WT flux A	Product B	WT flux B	Intervention	Mutant product flux A	Mutant product flux B	Mutant biomass flux	Score A	Score B	Score A + B	KO/ Amp
1	L-lysine	*	1,5-Diamino pentane	*	Diaminopimelate decarboxylase	5.81	5.81	0.22	8.84	8.84	17.68	Amp
					Diaminopimelate epimerase	5.81	5.81	0.22	8.84	8.84	17.68	Amp
					Dihydrodipicolinate reductase	5.81	5.81	0.22	8.84	8.84	17.68	Amp
					Dihydrodipicolinate synthase	5.81	5.81	0.22	8.84	8.84	17.68	Amp
					Succinyl-diaminopimelate desuccinylase	5.81	5.81	0.22	8.84	8.84	17.68	Amp
					Tetrahydrodipicolinate succinylase	5.81	5.81	0.22	8.84	8.84	17.68	Amp
2	Succinate	*	Ethanol	*	Glyceraldehyde-3-phosphate dehydrogenase	12.86	15.84	0.22	19.56	24.10	43.67	Amp
3	Spermidine	*	5-Methylthio-D-ribose	*	Adenosylmethionine decarboxylase	2.01	2.01	0.22	3.06	3.06	6.12	Amp
					Methylthioadenosine nucleosidase	2.01	2.01	0.22	3.06	3.06	6.12	Amp
					Spermidine synthase	2.01	2.01	0.22	3.06	3.06	6.12	Amp
4	Xanthine	*	D-Lactate	*	Glyceraldehyde-3-phosphate dehydrogenase	8.90	15.84	0.22	13.55	24.10	37.65	Amp
5	Glycine	*	L-Asparagine	*	Glyceraldehyde-3-phosphate dehydrogenase	20.91	11.82	0.22	31.80	17.99	49.79	Amp
6	Fe-enterobactin	*	Enterobactin	*	2,3-Dihydro-2,3-dihydroxybenzoate dehydrogenase	1.29	1.29	0.22	1.97	1.97	3.93	Amp
					Isochorismatase	1.29	1.29	0.22	1.97	1.97	3.93	Amp
7	Pyruvate	*	L-Asparagine	*	Glyceraldehyde-3-phosphate dehydrogenase	18.01	11.82	0.22	27.39	17.99	45.38	Amp

*WT, wild type; *, less than 10^{-5} mmol/gDW/h.*

TABLE 2 | Intervention strategies for co-production of pairs of metabolites in *E. coli* under anaerobic conditions.

#	Product A	WT flux A	Product B	WT flux B	Intervention	Mutant product flux A	Mutant product flux B	Mutant biomass flux	Score A	Score B	Score A + B	KO/ Amp
1	Acetate	8.83	Formate	18.22	Acetaldehyde dehydrogenase	18.18	36.79	0.12	237.95	472.31	710.26	KO
					Alcohol dehydrogenase	18.18	36.79	0.12	237.95	472.31	710.26	KO
2	Succinate	0.05	D-Lactate	$3.76x10^{-4}$	Glyceraldehyde-3-phosphate dehydrogenase	14.98	19.41	0.04	126.78	164.92	291.71	Amp
					Acetaldehyde dehydrogenase	9.07	18.12	0.12	229.50	461.04	690.55	KO
					Alcohol dehydrogenase	9.07	18.12	0.12	229.50	461.04	690.55	KO
					Pyruvate formate lyase	0.49	17.76	0.12	10.57	426.65	437.22	KO
3	L-Alanine	*	Xanthine	*	Glyceraldehyde-3-phosphate dehydrogenase	13.56	0.97	0.04	115.18	8.23	123.41	Amp
4	Spermidine	*	5-Methylthio-D-ribose	*	Adenosylmethionine decarboxylase	0.64	0.64	0.04	5.46	5.46	10.93	Amp
					Methylthioadenosine nucleosidase	0.64	0.64	0.04	5.46	5.46	10.93	Amp
					Spermidine synthase	0.64	0.64	0.04	5.46	5.46	10.93	Amp
5	L-Aspartate	*	L-Glutamate	*	Glyceraldehyde-3-phosphate dehydrogenase	6.03	4.52	0.04	51.19	38.39	89.59	Amp
6	L-Lysine	*	1,5-Diamino pentane	*	Diaminopimelate decarboxylase	2.72	2.72	0.04	23.04	23.04	46.07	Amp
					Diaminopimelate epimerase	2.72	2.72	0.04	23.04	23.04	46.07	Amp
					Dihydrodipicolinate synthase	2.72	2.72	0.04	23.04	23.04	46.07	Amp
					Succinyl-diaminopimelate desuccinylase	2.72	2.72	0.04	23.04	23.04	46.07	Amp
					Tetrahydrodipicolinate succinylase	2.72	2.72	0.04	23.04	23.04	46.07	Amp
7	Acetate	8.83	Hexanoate	*	Acetaldehyde dehydrogenase	18.18	4.53	0.12	237.95	115.26	353.21	KO
					Alcohol dehydrogenase	18.18	4.53	0.12	237.95	115.26	353.21	KO

*WT, wild type; *, less than 10^{-5} mmol/gDW/h.*

TABLE 3 | Intervention strategies for co-production of pairs of metabolites in *S. cerevisiae* under aerobic conditions.

#	Product A	WT flux A	Product B	WT flux B	Intervention	Mutant product flux A	Mutant product flux B	Mutant biomass flux	Score A	Score B	Score A + B	KO/ Amp
1	Ethanol	15.81	L-Alanine	$1.69x10^{-4}$	Sedoheptulose 1,7-bisphosphate D-glyceraldehyde-3-phosphate-lyase	18.45	0.15	0.07	12.22	0.71	12.93	Amp
					Phosphofructokinase (s7p)	18.45	0.15	0.07	12.22	0.71	12.93	Amp
2	Acetate	3.55×10^{-3}	2,3-Butanediol	$3.21x10^{-4}$	Pyruvate dehydrogenase	1.48	0.25	0.28	230.94	38.48	269.42	KO
					Enolase	10.71	10.27	0.07	49.61	47.61	97.22	Amp
					Fructose-bisphosphate aldolase	10.70	10.27	0.07	49.62	47.64	97.26	Amp
					Glyceraldehyde-3-phosphate dehydrogenase	10.71	10.27	0.07	49.61	47.61	97.22	Amp
					Triose-phosphate isomerase	10.70	10.27	0.07	49.62	47.64	97.26	Amp
3	Isobutyl alcohol	*	Succinate	*	Pyruvate decarboxylase	7.63	5.45	0.19	79.29	56.66	135.95	KO
					Enolase	9.56	12.97	0.07	44.30	60.10	104.40	Amp
					Glyceraldehyde-3-phosphate dehydrogenase	9.56	12.97	0.07	44.30	60.13	104.43	Amp
					Triose-phosphate isomerase	9.56	12.97	0.07	44.33	60.17	104.50	Amp
4	2-Methylpropanal	*	Isobutyl alcohol	*	3-Methyl-2-oxobutanoate decarboxylase	6.50	9.36	0.07	30.14	43.39	73.54	Amp
					Acetolactate synthase mitochondrial	6.50	9.36	0.07	30.14	43.40	73.54	Amp
					Dihydroxy acid dehydratase 2,3-dihydroxy-3-methylbutanoate mitochondrial	6.50	9.36	0.07	30.14	43.40	73.54	Amp
					Enolase	8.95	9.56	0.07	41.47	44.30	85.77	Amp
					Glyceraldehyde-3-phosphate dehydrogenase	8.95	9.56	0.07	41.47	44.30	85.77	Amp
					Acetohydroxy acid isomeroreductase mitochondrial	6.50	9.36	0.07	30.14	43.40	73.54	Amp
					Triose-phosphate isomerase	8.94	9.56	0.07	41.49	44.33	85.82	Amp
5	L-Glutamate	*	2-Oxoglutarate	*	Citrate synthase	2.93	1.95	0.07	13.58	9.05	22.63	Amp
					Enolase	4.50	4.04	0.07	20.85	18.73	39.58	Amp
					Fructose-bisphosphate aldolase	4.50	4.04	0.07	20.86	18.73	39.60	Amp
					Glyceraldehyde-3-phosphate dehydrogenase	4.50	4.04	0.07	20.85	18.73	39.58	Amp
					Isocitrate dehydrogenase	2.99	2.00	0.07	13.87	9.25	23.12	Amp
					Triose-phosphate isomerase	4.50	4.04	0.07	20.86	18.73	39.60	Amp
6	Acetate	3.55×10^{-3}	Pyruvate	$3.24x10^{-4}$	Pyruvate dehydrogenase	1.48	0.25	0.28	230.94	38.48	269.42	KO
					Aspartate-semialdehyde dehydrogenase	8.79	11.85	0.07	41.14	55.49	96.63	Amp
					Enolase	10.71	14.42	0.07	49.61	66.83	116.44	Amp
					Fructose-bisphosphate aldolase	10.70	14.41	0.07	49.62	66.85	116.47	Amp
					Glyceraldehyde-3-phosphate dehydrogenase	10.71	14.42	0.07	49.61	66.83	116.44	Amp
					Triose-phosphate isomerase	10.70	14.41	0.07	49.62	66.85	116.47	Amp
7	4-Aminobutanoate	*	L-Serine	*	Glyceraldehyde-3-phosphate dehydrogenase	4.77	6.98	0.07	22.10	32.34	54.44	Amp
					Triose-phosphate isomerase	4.77	6.97	0.07	22.11	32.35	54.45	Amp
8	L-Alanine	$1.69x10^{-4}$	L-Cysteine	*	Glucose-6-phosphate dehydrogenase	10.60	1.20	0.07	49.11	5.56	54.67	Amp
					Phosphogluconate dehydrogenase	10.60	1.20	0.07	49.11	5.56	54.67	Amp
					6-phosphogluconolactonase	10.60	1.20	0.07	49.11	5.56	54.67	Amp
					Ribulose-5-phosphate-3-epimerase	10.60	1.20	0.07	49.11	5.56	54.67	Amp
					Transketolase	10.60	1.20	0.07	49.12	5.56	54.68	Amp
					Ribose-5-phosphate isomerase	18.16	2.21	0.08	85.44	10.40	95.84	Amp
9	sn-Glycero-3-phosphocholine	*	L-Methionine	*	Methionine synthase	0.02	2.19	0.07	0.11	10.17	10.27	Amp
					5,10-Methylene-tetrahydrofolate reductase	0.02	2.19	0.07	0.11	10.17	10.27	Amp
					Ribose-5-phosphate isomerase	0.66	1.71	0.08	3.11	8.03	11.14	Amp
10	2-Methylbutyl acetate	*	2-Methyl-1-butanol	*	Ribose-5-phosphate isomerase	3.00	4.42	0.08	14.13	20.78	34.92	Amp

*WT, wild type; *, less than 10^{-5} mmol/gDW/h.*

TABLE 4 | Intervention strategies for co-production of pairs of metabolites in *S. cerevisiae* under anaerobic conditions.

#	Product A	WT flux A	Product B	WT flux B	Intervention	Mutant product flux A	Mutant product flux B	Mutant biomass flux	Score A	Score B	Score A + B	KO/ Amp
1	2-Methyl-1-butanol	*	Isobutyl alcohol	*	Malic enzyme NADP mitochondrial	0.03	9.64	0.05	0.20	61.30	61.51	Amp
2	Isobutyl alcohol	*	Pyruvate	*	Pyruvate decarboxylase	8.73	5.66	0.11	88.74	57.57	146.31	KO
					Enolase	9.68	9.97	0.05	61.59	63.45	125.03	Amp
					Fructose-bisphosphate aldolase	9.68	9.96	0.05	61.67	63.47	125.14	Amp
					Glyceraldehyde-3-phosphate dehydrogenase	9.68	9.97	0.05	61.60	63.45	125.05	Amp
					Triose-phosphate isomerase	9.68	9.96	0.05	61.66	63.47	125.13	Amp
3	Formate	$6.26x10^{-4}$	Spermidine	*	Adenosylmethionine decarboxylase	1.22	1.22	0.05	7.76	7.76	15.52	Amp
					Aspartate transaminase	1.21	1.21	0.05	7.75	7.76	15.51	Amp
					2,3-Diketo-5-methylthio-1-phosphopentane degradation	1.22	1.22	0.05	7.76	7.76	15.52	Amp
					5-Methylthio-5-deoxy-D-ribulose-1-phosphate dehydratase	1.22	1.22	0.05	7.76	7.76	15.52	Amp
					5-Methylthioadenosine phosphorylase	1.22	1.22	0.05	7.76	7.76	15.52	Amp
					5-Methylthioribose-1-phosphate isomerase	1.22	1.22	0.05	7.76	7.76	15.52	Amp
					Spermidine synthase	1.22	1.22	0.05	7.76	7.76	15.52	Amp
					2-Keto-4-methylthiobutyrate transamination	1.22	1.22	0.05	7.76	7.76	15.52	Amp
4	4-Amino butanoate	*	Isobutyl acetate	*	Enolase	2.84	2.91	0.05	18.04	18.50	36.53	Amp
					Fructose-bisphosphate aldolase	2.84	2.90	0.05	18.11	18.50	36.61	Amp
					Glyceraldehyde-3-phosphate dehydrogenase	2.85	2.91	0.05	18.11	18.50	36.61	Amp
					Triose-phosphate isomerase	2.84	2.90	0.05	18.11	18.50	36.61	Amp
5	2-Methyl-1-butanol	*	Glycine	*	Aspartate kinase	0.05	4.55	0.05	0.32	28.95	29.26	Amp
					Glucose-6-phosphate dehydrogenase	0.08	4.15	0.05	0.52	26.39	26.91	Amp
					Phosphogluconate dehydrogenase	0.08	4.15	0.05	0.52	26.39	26.91	Amp
					Homoserine dehydrogenase NADH irreversible	0.05	4.55	0.05	0.32	28.95	29.26	Amp
					Homoserine kinase	0.05	4.55	0.05	0.32	28.91	29.22	Amp
					6-phosphogluconolactonase	0.08	4.15	0.05	0.52	26.39	26.91	Amp
					Ribulose-5-phosphate-3-epimerase	0.08	4.15	0.05	0.52	26.39	26.91	Amp
					Ribose-5-phosphate isomerase	3.31	4.01	0.06	21.52	26.04	47.56	Amp
					Threonine synthase	0.05	4.55	0.05	0.32	28.91	29.22	Amp
					Transketolase	0.08	4.15	0.05	0.52	26.39	26.91	Amp
					Transketolase	0.08	4.15	0.05	0.52	26.39	26.91	Amp
6	Isobutyl alcohol	*	Succinate	0.67	Pyruvate decarboxylase	8.73	6.70	0.11	88.74	61.27	150.02	KO
7	L-Glutamate	*	Xanthine	*	Fructose-bisphosphate aldolase	2.81	0.95	0.05	17.90	6.04	23.94	Amp
					Glyceraldehyde-3-phosphate dehydrogenase	2.81	0.95	0.05	17.90	6.04	23.93	Amp
					Triose-phosphate isomerase	2.81	0.95	0.05	17.90	6.04	23.94	Amp
8	Sorbitol	*	L-Methionine	*	Ribose-5-phosphate isomerase	5.61	1.28	0.06	36.45	8.29	44.74	Amp
9	2,3-Butanediol	*	L-Serine	*	Fructose-bisphosphate aldolase	9.30	4.74	0.05	59.21	30.19	89.40	Amp
					Glyceraldehyde-3-phosphate dehydrogenase	9.30	4.74	0.05	59.19	30.19	89.37	Amp
					Triose-phosphate isomerase	9.30	4.74	0.05	59.21	30.19	89.40	Amp

*WT, wild type; *, less than 10^{-5} mmol/gDW/h.*

heterologous metabolites. Since *S. cerevisiae* is a better candidate for recombinant protein production, it is essential to study co-production in yeast (Bill, 2014). It can also produce more complex metabolites when compared to *E. coli* and is, therefore, a favorable candidate for bio-production. The latest GSMM iMM904 (Mo et al., 2009) was used, and the ability to optimize the co-production of 164 secretory metabolites was studied in both aerobic and anaerobic conditions.

3.2.1 Aerobic Fermentation

We found that many industrially important metabolites like ethanol and L-alanine, and 4-aminobutanoate and L-serine can be co-produced in *S. cerevisiae* under aerobic conditions. We were also able to co-optimize isobutyl alcohol and 2-methyl propanal, which are long-chain alcohols that are used as biofuels. The deletion of pyruvate dehydrogenase increases the production of pyruvate and acetate, as shown in **Table 3**. Although the deletion of pyruvate dehydrogenase has not been experimentally verified as yet, a similar study has been carried out in *E. coli* (Moxley and Eiteman, 2021). In this study, it has been shown that the deletion of the genes encoding pyruvate dehydrogenase improves pyruvate production (Moxley and Eiteman, 2021). In addition to pyruvate dehydrogenase, co-FSEOF was able to identify several other amplification targets, which can also improve the production of pyruvate and acetate.

3.2.2 Anaerobic Fermentation

As in the case of *E. coli,* anaerobic fermentation enables the co-production of more pairs of metabolites in *S. cerevisiae* when compared to aerobic fermentation. 2-methyl-1-butanol, which is an important solvent used in the manufacture of pesticides and paints and isobutyl alcohol, which is a biofuel, can be co-produced by the amplification of malic enzyme, as shown in **Table 4**. Formate, which is used in dyeing and printing, can be co-produced with spermidine, a metabolite increasingly studied for its anti-ageing properties (Minois, 2014), through the amplification of a number of reactions. These strategies not only include readily apparent reactions that are involved in spermidine synthesis like spermidine synthase and adenosylmethionine decarboxylase but also provide some non-intuitive strategies like the amplification of aspartate transaminase or 2-keto-4-methylthiobutyrate transaminase. We also found that the deletion of pyruvate decarboxylase improves the production of succinate, isobutyl alcohol and pyruvate. The effect of deletion of pyruvate decarboxylase has been studied in *S. cerevisiae,* and the improvement in the production of pyruvate (van Maris et al., 2004) and succinate (Zahoor et al., 2019) has been verified experimentally in separate studies in literature.

3.2.3 Higher-Order Intervention Strategies—Co-Production of Isobutanol and Succinate

Higher-order intervention strategies can increase the maximum yield achievable for any product with a little difference in growth rate when compared to single interventions. But they are more cumbersome to identify, as the problem becomes time-consuming and computationally expensive. Instead of identifying higher-order targets for all metabolites in an organism, we have used the previous analysis to explore the metabolic capabilities of the organism and chose one set of metabolites to demonstrate the power of higher-order intervention strategies.

Isobutanol is a long-chain alcohol that is an attractive biofuel (Nanda et al., 2017). Succinic acid is an important metabolite essential for the production of various other products like biodegradable polymers, fatty acids, butyrolactone and tetrahydrofuran (Akhtar et al., 2014). The co-production of isobutanol and succinate has been proposed as a sustainable and economical process by Xu et al. (2018). They have discussed the development of various strains for the production of isobutanol and succinate separately. They emphasize how the co-production of isobutanol and succinate is not only of economic significance, but the high amount of carbon dioxide released from long-chain alcohol fermentation can be used for succinate production, and is hence also of ecological importance. But the article does not discuss any strategy to co-optimize the production of isobutanol and succinate.

Here we identified the higher-order intervention strategies (size up to three) for co-production of isobutanol and succinate in *S. cerevisiae* in aerobic conditions. More than 3,700 interventions can improve the yield of both the metabolites when compared to the wild-type strain. **Table 5** lists a few examples of each type of intervention strategy obtained, which are also represented in **Figure 3**. Though most of the amplification and deletion targets are integral components of the target product and by-product synthesis respectively, co-FSEOF is also able to find intervention targets in distant pathways like those in pentose phosphate pathway, shikimate pathway, and nucleotide metabolism. This shows the ability of the algorithm to identify non-intuitive targets. Also, a number of the targets predicted here are also found in experimental studies reported in literature. For example, the deletion of pyruvate decarboxylase has been shown to improve the production of isobutanol by Kondo et al. (2012). Zahoor et al. (2019) have shown that both pyruvate decarboxylase deletion and fumarase deletion can increase the production of succinate. This shows the dependability of the results obtained using the algorithm.

4 DISCUSSION

Chemical processes based on fossil fuels are cheaper when compared to bioprocesses, which leads to reluctance in the adoption of sustainable bioprocesses in industries. To improve the economic feasibility of a bioprocess, we can optimize the process variables and/or genetically engineer the microbes (Dzurendova et al., 2020). Even then, in some cases, the bioprocess might be less lucrative when compared to their chemical counterparts (Zhang et al., 2021). In such cases, we can co-produce multiple metabolites to improve the economic feasibility and efficiency of a bioprocess. For example, in the case of biofuels and fatty acids, we need to design processes that can support the production of multiple metabolites of similar nature (Xin et al., 2018). Co-production also ensures better utilization of

TABLE 5 | Higher-order intervention strategies for co-production of isobutanol and succinate in *S. cerevisiae* under aerobic conditions.

#	Intervention 1	Intervention 2	Intervention 3	A ⊕/K ⊖	Mutant flux 1	Mutant flux 2	Biomass flux	Score A	Score B	Score A + B
1	Glyceraldehyde-3-phosphate dehydrogenase (GAPD)	Pyruvate kinase (PYK)	NA	⊕ ⊕	7.19	8.60	0.20	81.73	97.87	179.59
2	Enolase (ENO)	Pyruvate kinase (PYK)	NA	⊕ ⊕	7.13	8.60	0.20	81.08	97.87	178.95
3	Glutamate-5-kinase (GLU5K)	Phosphoglycerate dehydrogenase (PGCD)	Pyruvate decarboxylase (PYRDC)	⊖ ⊖ ⊖	7.96	5.80	0.19	79.81	58.12	137.93
4	Fumarase (FUMm)	Phosphoserine phosphatase (PSP_L)	Pyruvate decarboxylase (PYRDC)	⊖ ⊖ ⊖	7.95	5.78	0.19	79.78	58.05	137.84
5	Aldehyde dehydrogenase (ALCD23x)	Glycerol-3-phosphate dehydrogenase (G3PD1iR)	NA	⊕ ⊖	2.99	2.52	0.22	43.76	36.77	80.54
6	Succinate CoA ligase ADP forming (SUCOASm)	Pyruvate decarboxylase (PYRDC)	NA	⊕ ⊖	7.63	5.45	0.19	79.31	56.69	136.00
7	Acetolactate synthase (ACLSm)	Oxoglutarate dehydrogenase lipoamide (AKGDam)	Guanylate kinase (GK2)	⊕ ⊕ ⊖	4.72	6.89	0.15	34.51	50.38	84.89
8	Citrate synthase (CSm)	Dihydroxy-acid dehydratase (DHAD1im)	Prephenate dehydrogenase (PPND)	⊕ ⊕ ⊖	4.73	6.98	0.14	32.31	47.71	80.02
9	Aldehyde dehydrogenase (ALCD23x)	Ribonucleoside-diphosphate reductase (RNDR1)	Ribulose 5-phosphate 3-epimerase (RPE)	⊕ ⊖ ⊖	2.99	2.48	0.22	43.84	36.32	80.16
10	Succinate CoA ligase ADP forming (SUCOASm)	Phosphoserine phosphatase (PSP_L)	Pyruvate decarboxylase (PYRDC)	⊕ ⊖ ⊖	7.95	5.78	0.19	79.78	58.05	137.84

⊕, *Amplification of reaction;* ⊖, *Knock-out of reaction.*

microbial capabilities, and better balance in the carbon metabolism (Fan et al., 2018). While there are multiple computational tools and algorithms to identify intervention strategies for a single product, there is a lack of readily appliable algorithms for co-production. As a result, almost no co-production study in existing literature was found to use computational algorithms to aid rational strain design. All of the studies rely on previous findings or readily apparent strategies to achieve co-production. This limits the intervention strategies designed.

In this study, we present co-FSEOF, by adapting the effective FSEOF algorithm to study the co-optimization of a set of metabolites. FSEOF is a well-established constraint-based modelling algorithm, which has been used to reliably predict metabolic engineering strategies for a variety of systems (Choi et al., 2010; Boghigian et al., 2012; Badri et al., 2019; Srinivasan et al., 2019). It has a simple and efficient framework and can identify both deletion and amplification targets. Flux Coupling Analysis (FCA) is yet another interesting algorithm that can identify which metabolites can be coupled together. But very few metabolites are innately coupled without interventions. Moreover, it excludes all the reactions that do not carry flux under a given set of conditions from the analysis. This affects the applicability of FCA because these reactions, though not coupled, can have an effect on target production in the presence of other interventions. co-FSEOF is able to identify more combinations of products that can be co-produced and also provides a wider range of intervention strategies for a given set of metabolites.

Using co-FSEOF, we examined the co-production of multiple pairs of metabolites, and both deletion and amplification targets were obtained in *E. coli* and *S. cerevisiae* under both aerobic and anaerobic conditions. Anaerobic fermentation enabled the co-production of a higher number of metabolites when compared to aerobic fermentation in both organisms. This could be due to the incomplete respiration in the absence of oxygen that leads to the formation of multiple by-products. Also, *S. cerevisiae* produces more industrially significant metabolites when compared to *E. coli*. Some of these proposed intervention strategies have been verified experimentally by other studies in literature, as mentioned in **Section 3**. This shows the efficacy of the algorithm in furnishing reliable targets. In addition to readily apparent intervention strategies, co-FSEOF also provides non-intuitive intervention strategies that are present in auxiliary biochemical pathways (as discussed in **Section 3.2.2**, **3.2.3**).

The co-optimization analysis for all possible pairs of metabolites in the network is intended to be exploratory in order to give a larger picture of the metabolic capabilities of the organism. This analysis showed that around 200 pairs could be co-optimized in *E. coli* under aerobic conditions, and around 1,000 pairs of metabolites could be co-optimized in the other cases. An important class of metabolites observed in the analysis are alcohols such as ethanol, isobutanol, and 2,3-butanediol, which can be co-produced using various interventions. Co-optimization can thus enable the efficient production of biofuels (Collas et al., 2012). We can explore the metabolic capabilities of the organism to identify all possible pairs of metabolites that can be co-produced. Following this, important and

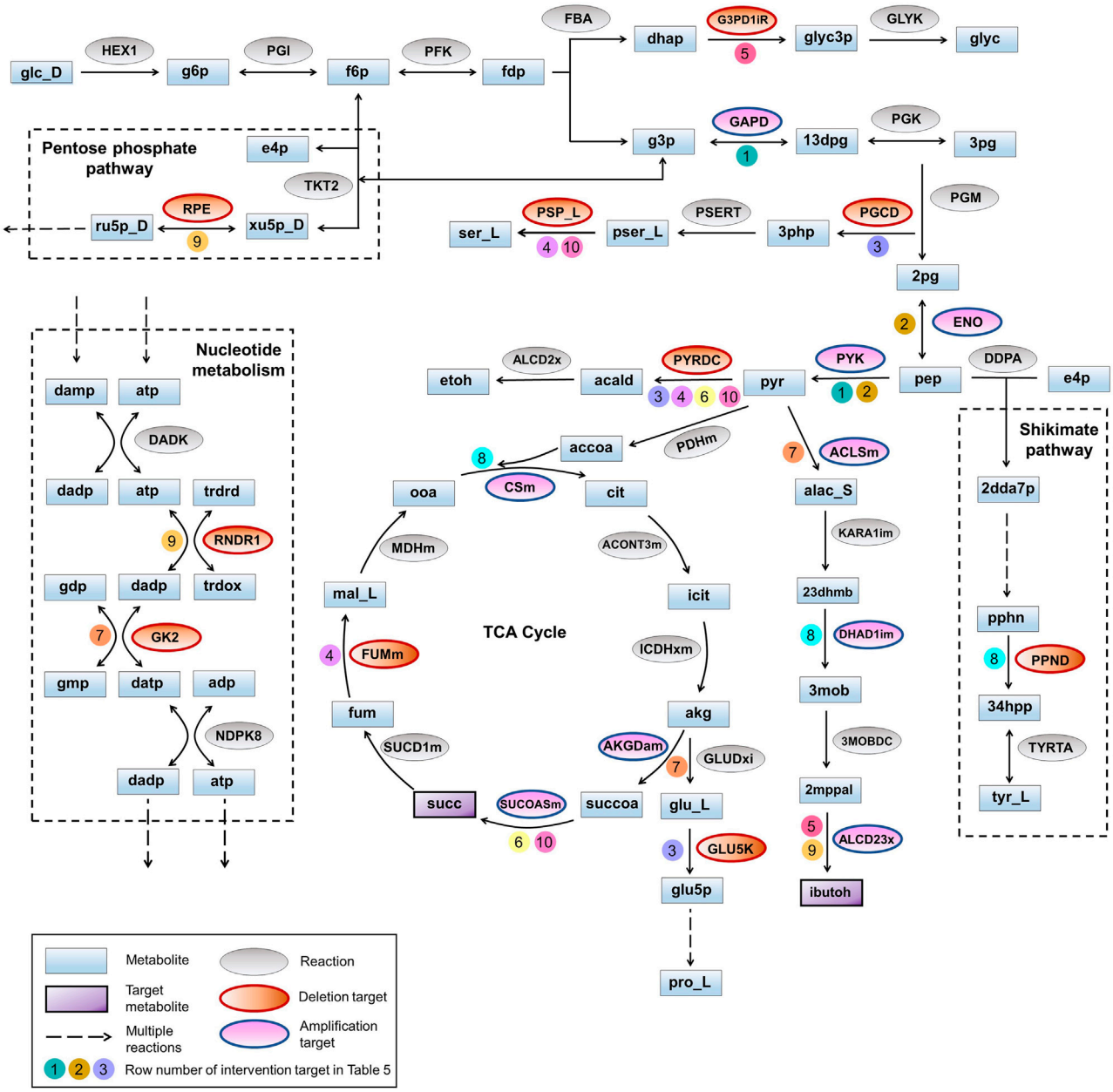

FIGURE 3 | Pathway diagram for co-production of isobutanol and succinate. The pathways for production of isobutanol and succinate are represented along with the intervention strategies listed in **Table 5**. Auxiliary pathways that are not directly related to the biosynthesis of target products but contain intervention strategies are shown within dotted rectangles. Co-factors and other small molecules are not depicted for better clarity. Numbers on the arrows point to row numbers in **Table 5**.

commercially valuable pairs of metabolites can be further studied to obtain higher-order intervention strategies, as shown in **Section 3.2.3**. Exploring the higher-order strategies can expand the efficiency of the intervention targets obtained. Since the evaluation of higher-order intervention strategies is laborious and computationally expensive, we have limited the size to a maximum of three manipulations at a time. It not only enhances yield, but also provides alternate routes to achieve a similar yield. The advantageous strategies can be chosen based on the ease of manipulation in an experimental setup in such cases.

The evaluation of the results is carried out using FVA, which ensures the robustness of the targets obtained. While FBA provides one optimal solution from the solution space, FVA gives the entire range of values the flux can take up. This is a significant difference that sets co-FSEOF apart from other existing algorithms like OptKnock (Burgard et al., 2003) and OptReg (Pharkya and Maranas, 2006). Also, the algorithm validates and returns all the intervention strategies in a single run, contrary to the existing algorithms, most of which are sequential and require a separate run for each strategy obtained. The set of intervention strategies

validated through FVA can be short-listed for experimental verification using the scores. The *overall score* can be used to compare the effectiveness of different intervention strategies. The score is designed to incorporate both increase in product flux and decrease in biomass flux, so that both biomass and product production are favored in the mutant. Moreover, co-FSEOF uses biomass as the objective throughout the analysis, and the effect of the intervention strategies on product synthesis is studied when the organism optimizes growth. Thereby, the intervention strategies result in the co-optimization of product production and biomass formation. An intervention strategy with better *overall score* ensures better product synthesis along with good biomass formation. If one product is more favored than the others economically or otherwise, we can use the individual scores $Score_i$ to choose the appropriate strategy for the process that is formulated. The products can be chosen based on their economic value, or ease of co-production. One drawback of co-production is the cost associated with downstream processing. But this can be overcome by choosing easily separable products or choosing metabolites such that one is accumulated in the cell and one is secreted out, as in the case of polyhydroxy butyrate and succinate, respectively (Kang et al., 2010). However, this problem does not occur in the case of biofuels where the alcohol mixture is optimized for and therefore does not require extensive separation of the products. Co-FSEOF not only identifies intervention strategies for co-production of a given set of metabolites, but also allows us to explore the different combinations of products that can be co-produced in an easy and efficient manner.

5 CONCLUSION

Co-production can open new avenues for the sustainable production of chemicals. Designing bioprocesses for co-production using laboratory experiments alone is cumbersome and can result in sub-optimal strategies. co-FSEOF empowers us to explore and exploit microbial systems in a better fashion. It can be used to computationally study and optimize co-production by identifying intervention strategies for multiple metabolites and thereby improve the efficiency of bioprocesses. It should be noted that the co-optimization analysis was limited to pairs of metabolites to reduce the computational time. Nevertheless, co-FSEOF can be easily extended to co-optimize a more extensive set of metabolites. To conclude, this study can be used to identify various genetic manipulations that can co-optimize a set of products, which might be challenging to achieve through pure experimentation. It provides a novel and critical approach to study co-production computationally. We hope this study will aid the design and development of more sustainable bioprocesses.

DATA AVAILABILITY STATEMENT

Publicly available datasets were analyzed in this study. This data can be found here: http://bigg.ucsd.edu/. All models used in this work and the codes used for our analysis are available at https://github.com/RamanLab/co-FSEOF.

AUTHOR CONTRIBUTIONS

Conceptualization—LR, KR; Funding—KR; Writing—original draft—LR; Writing—review and editing—LR, KR. Signed by all authors as follows: Lavanya Raajaraam (LR), Karthik Raman (KR)* *Corresponding author.

ACKNOWLEDGMENTS

LR acknowledges the HTRA fellowship from the Ministry of Education, Government of India. KR acknowledges support from the Science and Engineering Board (SERB) MATRICS Grant MTR/2020/000490.

REFERENCES

Akhtar, J., Idris, A., and Abd Aziz, R. (2014). Recent Advances in Production of Succinic Acid from Lignocellulosic Biomass. *Appl. Microbiol. Biotechnol.* 98 (3), 987–1000. doi:10.1007/s00253-013-5319-6

Badri, A., Raman, K., and Jayaraman, G. (2019). Uncovering Novel Pathways for Enhancing Hyaluronan Synthesis in Recombinant *Lactococcus Lactis*: Genome-Scale Metabolic Modeling and Experimental Validation. *Processes* 7 (6), 343. doi:10.3390/pr7060343

Bill, R. M. (2014). Playing Catch-Up with *Escherichia coli*: Using Yeast to Increase success Rates in Recombinant Protein Production Experiments. *Front. Microbiol.* 5, 85. doi:10.3389/fmicb.2014.00085

Boghigian, B. A., Armando, J., Salas, D., and Pfeifer, B. A. (2012). Computational Identification of Gene Over-expression Targets for Metabolic Engineering of Taxadiene Production. *Appl. Microbiol. Biotechnol.* 93 (5), 2063–2073. doi:10.1007/s00253-011-3725-1

Burgard, A. P., Pharkya, P., and Maranas, C. D. (2003). Optknock: A Bilevel Programming Framework for Identifying Gene Knockout Strategies for Microbial Strain Optimization. *Biotechnol. Bioeng.* 84 (6), 647–657. doi:10.1002/bit.10803

Cai, X., and Bennett, G. N. (2011). Improving the *Clostridium Acetobutylicum* Butanol Fermentation by Engineering the Strain for Co-production of Riboflavin. *J. Ind. Microbiol. Biotechnol.* 38 (8), 1013–1025. doi:10.1007/s10295-010-0875-6

Choi, H. S., Lee, S. Y., Kim, T. Y., and Woo, H. M. (2010). In Silico Identification of Gene Amplification Targets for Improvement of Lycopene Production. *Appl. Environ. Microbiol.* 76 (10), 3097–3105. doi:10.1128/aem.00115-10

Collas, F., Kuit, W., Clément, B., Marchal, R., López-Contreras, A. M., and Monot, F. (2012). Simultaneous Production of Isopropanol, Butanol, Ethanol and 2,3-butanediol by *Clostridium Acetobutylicum* ATCC 824 Engineered Strains. *AMB Expr.* 2 (1), 45. doi:10.1186/2191-0855-2-45

da Silva, T. L., Gouveia, L., and Reis, A. (2014). Integrated Microbial Processes for Biofuels and High Value-Added Products: the Way to Improve the Cost Effectiveness of Biofuel Production. *Appl. Microbiol. Biotechnol.* 98 (3), 1043–1053. doi:10.1007/s00253-013-5389-5

de Souza Queiroz, S., Jofre, F. M., dos Santos, H. A., Hernández-Pérez, A. F., and de Almeida Felipe, M. D. G. (2021). Xylitol and Ethanol Co-production from Sugarcane Bagasse and Straw Hemicellulosic Hydrolysate Supplemented with Molasses. *Biomass Conv. Bioref.* 1–10. doi:10.1007/s13399-021-01493-y

Dzurendova, S., Zimmermann, B., Kohler, A., Tafintseva, V., Slany, O., Certik, M., et al. (2020). Microcultivation and FTIR Spectroscopy-Based Screening Revealed a Nutrient-Induced Co-production of High-Value Metabolites in Oleaginous *Mucoromycota* Fungi. *Plos One* 15 (6), e0234870. doi:10.1371/journal.pone.0234870

Erickson, B., Nelsonand Winters, P. (2012). Perspective on Opportunities in Industrial Biotechnology in Renewable Chemicals. *Biotechnol. J.* 7 (2), 176–185. doi:10.1002/biot.201100069

Fan, X., Wu, H., Jia, Z., Li, G., Li, Q., Chen, N., et al. (2018). Metabolic Engineering of *Bacillus Subtilis* for the Co-production of Uridine and Acetoin. *Appl. Microbiol. Biotechnol.* 102 (20), 8753–8762. doi:10.1007/s00253-018-9316-7

Gudmundsson, S., and Thiele, I. (2010). Computationally Efficient Flux Variability Analysis. *BMC Bioinformatics* 11 (1), 489. doi:10.1186/1471-2105-11-489

Heirendt, L., Arreckx, S., Pfau, T., Mendoza, S. N., Richelle, A., Heinken, A., et al. (2019). Creation and Analysis of Biochemical Constraint-Based Models Using the COBRA Toolbox v.3.0. *Nat. Protoc.* 14 (3), 639–702. doi:10.1038/s41596-018-0098-2

Julien-Laferrière, A., Bulteau, L., Parrot, D., Marchetti-Spaccamela, A., Stougie, L., Vinga, S., et al. (2016). A Combinatorial Algorithm for Microbial Consortia Synthetic Design. *Sci. Rep.* 6 (1), 29182. doi:10.1038/srep29182

Kang, Z., Gao, C., Wang, Q., Liu, H., and Qi, Q. (2010). A Novel Strategy for Succinate and Polyhydroxybutyrate Co-production in *Escherichia coli*. *Bioresour. Technol.* 101 (19), 7675–7678. doi:10.1016/j.biortech.2010.04.084

Kauffman, K. J., Prakash, P., and Edwards, J. S. (2003). Advances in Flux Balance Analysis. *Curr. Opin. Biotechnol.* 14 (5), 491–496. doi:10.1016/j.copbio.2003.08.001

Kondo, T., Tezuka, H., Ishii, J., Matsuda, F., Ogino, C., and Kondo, A. (2012). Genetic Engineering to Enhance the Ehrlich Pathway and Alter Carbon Flux for Increased Isobutanol Production from Glucose by *Saccharomyces cerevisiae*. *J. Biotechnol.* 159 (1), 32–37. doi:10.1016/j.jbiotec.2012.01.022

Kumar, P., and Kim, B. S. (2018). Valorization of Polyhydroxyalkanoates Production Process by Co-synthesis of Value-Added Products. *Bioresour. Technol.* 269, 544–556. doi:10.1016/j.biortech.2018.08.120

Kumelj, T., Sulheim, S., Wentzel, A., and Almaas, E. (2019). Predicting Strain Engineering Strategies Using iKS1317: A Genome-Scale Metabolic Model of *Streptomyces Coelicolor*. *Biotechnol. J.* 14 (4), e1800180. doi:10.1002/biot.201800180

Li, T., Elhadi, D., and Chen, G.-Q. (2017). Co-Production of Microbial Polyhydroxyalkanoates with Other Chemicals. *Metab. Eng.* 43, 29–36. doi:10.1016/j.ymben.2017.07.007

Liang, C. Y., Xu, J. L., Xu, H. J., Qi, W., Zhang, Y., Luo, W., et al. (2019). Gene Cloning and Characterization of an Organic Solvent-Stimulated β-glucosidase and its Application for the Co-production of Ethanol and Succinic Acid. *Cellulose* 26 (15), 8237–8248. doi:10.1007/s10570-019-02477-y

Minois, N. (2014). Molecular Basis of the 'Anti-Aging' Effect of Spermidine and Other Natural Polyamines - A Mini-Review. *Gerontology* 60 (4), 319–326. doi:10.1159/000356748

Mo, M. L., Palsson, B. Ø., and Herrgård, M. J. (2009). Connecting Extracellular Metabolomic Measurements to Intracellular Flux States in Yeast. *BMC Syst. Biol.* 3 (1), 37. doi:10.1186/1752-0509-3-37

Monk, J. M., Lloyd, C. J., Brunk, E., Mih, N., Sastry, A., King, Z., et al. (2017). iML1515, a Knowledgebase that Computes *Escherichia coli* Traits. *Nat. Biotechnol.* 35 (10), 904–908. doi:10.1038/nbt.3956

Moxley, W. C., and Eiteman, M. A. (2021). Pyruvate Production by *Escherichia coli* by Use of Pyruvate Dehydrogenase Variants. *Appl. Environ. Microbiol.* 87 (13), e00487–21. doi:10.1128/aem.00487-21

Nanda, S., Golemi-Kotra, D., McDermott, J. C., Dalai, A. K., Gökalp, I., and Kozinski, J. A. (2017). Fermentative Production of Butanol: Perspectives on Synthetic Biology. *New Biotechnol.* 37, 210–221. doi:10.1016/j.nbt.2017.02.006

Orth, J. D., Thiele, I., and Palsson, B. Ø. (2010). What Is Flux Balance Analysis? *Nat. Biotechnol.* 28 (3), 245–248. doi:10.1038/nbt.1614

Pharkya, P., and Maranas, C. D. (2006). An Optimization Framework for Identifying Reaction Activation/inhibition or Elimination Candidates for Overproduction in Microbial Systems. *Metab. Eng.* 8 (1), 1–13. doi:10.1016/j.ymben.2005.08.003

Pharkya, P., Burgard, A. P., and Maranas, C. D. (2003). Exploring the Overproduction of Amino Acids Using the Bilevel Optimization Framework OptKnock. *Biotechnol. Bioeng.* 84 (7), 887–899. doi:10.1002/bit.10857

Raj, K., and Krishnan, C. (2020). Improved Co-production of Ethanol and Xylitol from Low-Temperature Aqueous Ammonia Pretreated Sugarcane Bagasse Using Two-Stage High Solids Enzymatic Hydrolysis and *Candida tropicalis*. *Renew. Energ.* 153, 392–403. doi:10.1016/j.renene.2020.02.042

Ranganathan, S., Suthers, P. F., and Maranas, C. D. (2010). OptForce: An Optimization Procedure for Identifying All Genetic Manipulations Leading to Targeted Overproductions. *Plos Comput. Biol.* 6 (4), e1000744. doi:10.1371/journal.pcbi.1000744

Rocha, I., Maia, P., Rocha, M., and Ferreira, E. C. (2008). *OptGene – A Framework for* in Silico *Metabolic Engineering* in 10th International Conference on Chemical and Biological Engineering (Portugal: University of Minho), 218–219.

Silva, F., Queiroz, J. A., and Domingues, F. C. (2012). Evaluating Metabolic Stress and Plasmid Stability in Plasmid DNA Production by *Escherichia coli*. *Biotechnol. Adv.* 30 (3), 691–708. doi:10.1016/j.biotechadv.2011.12.005

Srinivasan, A., S, V., Raman, K., and Srivastava, S. (2019). Rational Metabolic Engineering for Enhanced Alpha-Tocopherol Production in *Helianthus Annuus* Cell Culture. *Biochem. Eng. J.* 151, 107256. doi:10.1016/j.bej.2019.107256

Utrilla, J., Gosset, G., and Martinez, A. (2009). ATP Limitation in a Pyruvate Formate Lyase Mutant of *Escherichia coli* MG1655 Increases Glycolytic Flux to D-Lactate. *J. Ind. Microbiol. Biotechnol.* 36 (8), 1057–1062. doi:10.1007/s10295-009-0589-9

van Maris, A. J. A., Geertman, J.-M. A., Vermeulen, A., Groothuizen, M. K., Winkler, A. A., Piper, M. D. W., et al. (2004). Directed Evolution of Pyruvate Decarboxylase-Negative *Saccharomyces cerevisiae*, Yielding a C 2 -Independent, Glucose-Tolerant, and Pyruvate-Hyperproducing Yeast. *Appl. Environ. Microbiol.* 70 (1), 159–166. doi:10.1128/aem.70.1.159-166.2004

Varma, A., and Palsson, B. O. (1994). Metabolic Flux Balancing: Basic Concepts, Scientific and Practical Use. *Nat. Biotechnol.* 12 (10), 994–998. doi:10.1038/nbt1094-994

Xin, F., Dong, W., Jiang, Y., Ma, J., Zhang, W., Wu, H., et al. (2018). Recent Advances on Conversion and Co-production of Acetone-Butanol-Ethanol into High Value-Added Bioproducts. *Crit. Rev. Biotechnol.* 38 (4), 529–540. doi:10.1080/07388551.2017.1376309

Xu, C., Zhang, J., Zhang, Y., Guo, Y., Xu, H., and Xu, J. (2018). Long Chain Alcohol and Succinic Acid Co-production Process Based on Full Utilization of Lignocellulosic Materials. *Curr. Opin. Green Sustain. Chem.* 14, 1–9. doi:10.1016/j.cogsc.2018.04.012

Xu, J.-Z., Ruan, H.-Z., Liu, L.-M., Wang, L.-P., and Zhang, W.-G. (2019). Overexpression of Thermostable Meso-Diaminopimelate Dehydrogenase to Redirect Diaminopimelate Pathway for Increasing L-Lysine Production in *Escherichia coli*. *Sci. Rep.* 9 (1), 2423. doi:10.1038/s41598-018-37974-w

Yadav, A. N., Kour, D., Rana, K. L., Yadav, N., Singh, B., Chauhan, V. S., et al. (2019). "Metabolic Engineering to Synthetic Biology of Secondary Metabolites Production," in *New and Future Developments in Microbial Biotechnology and Bioengineering*. Editors VK Gupta and A Pandey, 279–320. doi:10.1016/b978-0-444-63504-4.00020-7

Yadav, B., Talan, A., Tyagi, R. D., and Drogui, P. (2021). Concomitant Production of Value-Added Products with Polyhydroxyalkanoate (PHA) Synthesis: A Review. *Bioresour. Technol.* 337, 125419. doi:10.1016/j.biortech.2021.125419

Yang, L., Cluett, W. R., and MahadevanEMILiO, R. (2011). EMILiO: A Fast Algorithm for Genome-Scale Strain Design. *Metab. Eng.* 13 (3), 272–281. doi:10.1016/j.ymben.2011.03.002

Zahoor, A., Küttner, F. T. F., Blank, L. M., and Ebert, B. E. (2019). Evaluation of Pyruvate decarboxylase-negativeSaccharomyces Cerevisiaestrains for the Production of Succinic Acid. *Eng. Life Sci.* 19 (10), 711–720. doi:10.1002/elsc.201900080

Zhang, X., Jantama, K., Shanmugam, K. T., and Ingram, L. O. (2009). Reengineering *Escherichia coli* for Succinate Production in Mineral Salts Medium. *Appl. Environ. Microbiol.* 75 (24), 7807–7813. doi:10.1128/aem.01758-09

Zhang, Y., Li, J., Meng, J., Sun, K., and Yan, H. (2021). A Neutral Red Mediated Electro-Fermentation System of *Clostridium Beijerinckii* for Effective Co-production of Butanol and Hydrogen. *Bioresour. Technol.* 332, 125097. doi:10.1016/j.biortech.2021.125097

Conflict of Interest: The authors declare that the research was conducted in the absence of any commercial or financial relationships that could be construed as a potential conflict of interest.

Publisher's Note: All claims expressed in this article are solely those of the authors and do not necessarily represent those of their affiliated organizations, or those of the publisher, the editors and the reviewers. Any product that may be evaluated in this article, or claim that may be made by its manufacturer, is not guaranteed or endorsed by the publisher.

frontiers in Bioengineering and Biotechnology

ORIGINAL RESEARCH
published: 10 January 2022
doi: 10.3389/fbioe.2021.794331

Optimization of a Two-Species Microbial Consortium for Improved Mcl-PHA Production From Glucose–Xylose Mixtures

Yinzhuang Zhu[1†], *Mingmei Ai*[1†] *and Xiaoqiang Jia*[1,2,3*]

[1]Department of Biochemical Engineering, School of Chemical Engineering and Technology, Tianjin University, Tianjin, China, [2]Frontier Science Center for Synthetic Biology and Key Laboratory of Systems Bioengineering (MOE), School of Chemical Engineering and Technology, Tianjin University, Tianjin, China, [3]Collaborative Innovation Center of Chemical Science and Engineering, Tianjin, China

OPEN ACCESS

Edited by:
Shuobo Shi,
Beijing University of Chemical Technology, China

Reviewed by:
Warren Blunt,
National Research Council Canada (NRC-CNRC), Canada
Suchada Chanprateep Napathorn,
Chulalongkorn University, Thailand

***Correspondence:**
Xiaoqiang Jia
xqjia@tju.edu.cn

[†]*These authors have contributed equally to this work and share first authorship*

Specialty section:
This article was submitted to Synthetic Biology, a section of the journal Frontiers in Bioengineering and Biotechnology

Received: *13 October 2021*
Accepted: *20 December 2021*
Published: *10 January 2022*

Citation:
Zhu Y, Ai M and Jia X (2022) Optimization of a Two-Species Microbial Consortium for Improved Mcl-PHA Production From Glucose–Xylose Mixtures. Front. Bioeng. Biotechnol. 9:794331. doi: 10.3389/fbioe.2021.794331

Polyhydroxyalkanoates (PHAs) have attracted much attention as a good substitute for petroleum-based plastics, especially mcl-PHA due to their superior physical and mechanical properties with broader applications. Artificial microbial consortia can solve the problems of low metabolic capacity of single engineered strains and low conversion efficiency of natural consortia while expanding the scope of substrate utilization. Therefore, the use of artificial microbial consortia is considered a promising method for the production of mcl-PHA. In this work, we designed and constructed a microbial consortium composed of engineered *Escherichia coli* MG1655 and *Pseudomonas putida* KT2440 based on the "nutrition supply–detoxification" concept, which improved mcl-PHA production from glucose-xylose mixtures. An engineered *E. coli* that preferentially uses xylose was engineered with an enhanced ability to secrete acetic acid and free fatty acids (FFAs), producing 6.44 g/L acetic acid and 2.51 g/L FFAs with 20 g/L xylose as substrate. The mcl-PHA producing strain of *P. putida* in the microbial consortium has been engineered to enhance its ability to convert acetic acid and FFAs into mcl-PHA, producing 0.75 g/L mcl-PHA with mixed substrates consisting of glucose, acetic acid, and octanoate, while also reducing the growth inhibition of *E. coli* by acetic acid. The further developed artificial microbial consortium finally produced 1.32 g/L of mcl-PHA from 20 g/L of a glucose–xylose mixture (1:1) after substrate competition control and process optimization. The substrate utilization and product synthesis functions were successfully divided into the two strains in the constructed artificial microbial consortium, and a mutually beneficial symbiosis of "nutrition supply–detoxification" with a relatively high mcl-PHA titer was achieved, enabling the efficient accumulation of mcl-PHA. The consortium developed in this study is a potential platform for mcl-PHA production from lignocellulosic biomass.

Keywords: MCL-PHA, artificial microbial consortium, engineered *Escherichia coli*, engineered *Pseudomonas putida*, xylose

INTRODUCTION

Due to environmental problems such as energy waste and "white pollution" caused by petroleum-based plastics, the search for biodegradable alternatives to petroleum-based plastics has received increasing attention (Muneer et al., 2020). Polyhydroxyalkanoates (PHAs) are among the most well-studied biodegradable materials. Their polymer properties are similar to petroleum-based plastics, including low crystallinity, high tensile strength, high elongation at break, and low glass transition temperature (Chen and Patel, 2012), while also offering good biodegradability and biocompatibility, which makes them an excellent substitute for petroleum-based plastics (Raza et al., 2018). PHA is a polyester produced by microorganisms as energy storage particles in cells under nutritionally limited conditions (Lee, 1996), first discovered in *Bacillus megaterium* in 1926 (Lemoigne, 1926). All types of PHA have similar structures but offer diversity in the monomer carbon chain length and side-chain groups, resulting in different material properties of various PHAs. Based on the repeat unit composition, more than 150 different PHA monomers have been identified so far, derived from hundreds of microorganisms (Agnew and Pfleger, 2013). There are many ways to classify PHA. According to the number of carbon atoms in the constituent monomers, PHA can be divided into short-chain-length polyhydroxyalkanoate (scl-PHA) composed of monomers with three to five carbon atoms, medium-chain-length polyhydroxyalkanoate (mcl-PHA) composed of monomers with 6–14 carbon atoms, and long-chain-length polyhydroxyalkanoate (lcl-PHA) composed of monomers with more than 15 carbon atoms (Singh and Mallick, 2009; Li et al., 2021). PHAs can also be classified according to the types of monomers, with homopolymers contain only one monomer, and copolymers containing more than one monomer. In terms of the physical properties, most scl-PHA has high crystallinity, brittleness, and hardness (Koning, 1995), except for individual monomers such as 4HB and 3HV, and et al. (Cavalheiro et al., 2013); while mcl-PHA is a thermoplastic, with low crystallinity, T_m values between 40 to 60°C, T_g values between −50 and −25°C, low tensile strength and high elongation at break (Kessler and Witholt, 1998).

Mcl-PHA has more diverse structures, as well as more flexible physical and mechanical properties, which can meet the needs of a broader range of engineering applications and realize material function customization (Chen and Wang, 2013). Previous studies found that mcl-PHA has better biocompatibility and biodegradability (Zhao et al., 2003a; Misra et al., 2006). In biological tissue engineering, PHA copolymers containing medium-chain length monomers exhibited higher biocompatibility than PHB (Liang et al., 2008). In medical applications, the impact of degradation products produced from PHA materials in cells is crucial. Several studies have proven that the biodegradability of PHA is affected by their physicochemical properties such as functional groups, affinity, hydrophobicity, structural order, and crystallinity (Zhao et al., 2002; Zhao et al., 2003b). Generally, the degradation ability of polymers decreases with the increase of crystallinity. Therefore, mcl-PHA with lower crystallinity and Tm has good biodegradability. In general, mcl-PHA has broader application prospects due to its better physical and mechanical properties, together with its environmental friendliness (Lee, 2006).

With the development of metabolic engineering and synthetic biology, natural (such as *Pseudomonas*) or non-natural (such as *E. coli*) PHA-producing strains can be engineered starting from the gene regulatory networks by regulating metabolic pathways, introducing the PHA synthesis pathway (Klinke et al., 1999; Zhuang et al., 2014), designing and synthesizing artificial cells, and building a promising metabolic platform for improved mcl-PHA accumulation (Borrero-de Acuna et al., 2014). Perhaps there are two main pathways to synthesize mcl-PHA in microorganisms, including the fatty acid β-oxidation pathway that metabolizes "related" carbon sources such as fatty acids and the fatty acid *de novo* synthesis pathway that uses "unrelated" carbon sources such as sugars (Tortajada et al., 2013). Huijberts et al. used the isotope labeling method to prove that when mcl-PHA was synthesized in *P. putida* KT2442, the fatty acid *de novo* synthesis pathway and fatty acid β-oxidation pathway were active at the same time but worked independently (Huijberts et al., 1994). At present, the related research on the production of mcl-PHA by single strains through the regulation of the above-mentioned metabolic pathways have been fully demonstrated. However, the limitation of a single engineered strain's metabolic capacity results in a limited range of available substrates, high production costs, and low accumulation of mcl-PHA, which further hinders its large-scale production, popularization, and application. In recent years, microbial consortia that can complete the arduous task using compartmentalized metabolic pathways in two or more strains have received more attention. Using waste-activated sludge (WAS) to combine the PHA production process with the sewage treatment process can reduce costs (Liu et al., 2013; Valentino et al., 2015; Jayakrishnan et al., 2021). However, the natural diverse microbial consortium has a longer domestication cycle and is poorly controllable, leading to disadvantages compared with a single engineered strain (Morgan-Sagastume et al., 2015). Compared with a single engineered strain and natural mixed microbial consortia to produce PHA, an artificial microbial consortium can solve the limitation of the metabolic capacity of a single engineered strain and the low conversion efficiency of natural mixed microbial consortia.

In previous research, our laboratory used a modular construction strategy to develop a co-culture consortium composed of engineered *P. putida* KT2440 and *E. coli* MG1655 that can synthesize mcl-PHA from "unrelated" carbon sources (Yang et al., 2019; Liu et al., 2020). To avoid growth competition, the four genes *ptsG*, *manZ*, *atpFH,* and *envR* were knocked out in *E. coli* (shown as ①, ②, ③, and ④ in **Figure 1**) (Liu et al., 2020), the engineered *P. putida* KT2440 overexpressed the *acs* gene to promote the utilization of acetic acid and increase the accumulation of mcl-PHA (shown as ⑤ in **Figure 1**) (Yang et al., 2019). The microbial consortium composed of *E. coli* Δ4 and KT2440-acs efficiently utilized mixed sugars (glucose and xylose) and corn straw hydrolysate to produce mcl-PHA titers of 0.541 and 0.434 g/L, respectively (Liu et al., 2020). However, the conversion efficiency from the

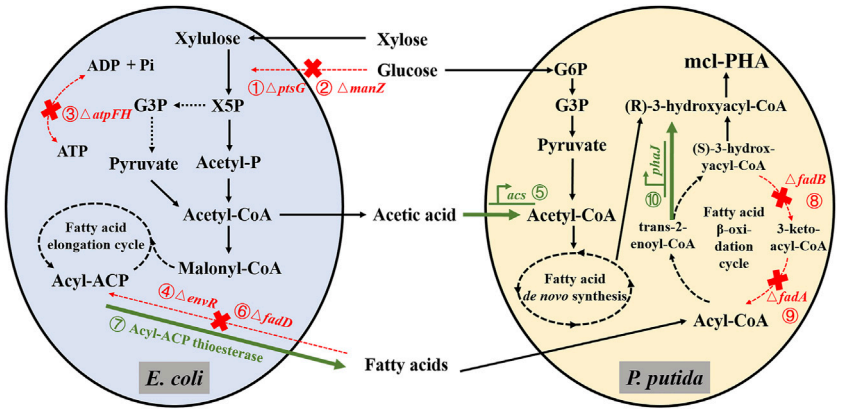

FIGURE 1 | Schematic diagram of metabolic engineering for the production of mcl-PHA from a mixture of xylose and glucose by the microbial consortium based on the concept of "nutrient supply-detoxification" (Acronyms: X5P, Xylulose 5-phosphate; G3P, Glyceraldehyde-3-phosphate; Acetyl-P, Acetyl Phosphate; G6P, Glucose-6-Phosphate. The red crosses in the biosynthetic pathway indicate the deletion of corresponding genes. The bold green arrows indicate the overexpression of corresponding genes. The related genetic engineering represented by ①, ②, ③, and ④ was completed by (Liu et al., 2020), and the corresponding genetic engineering represented by ⑤ was completed by (Yang et al., 2019). The related genetic engineering represented by ⑥, ⑦, ⑧, ⑨, and ⑩ was conducted in this work).

substrate to intermediate metabolites and final product was still limited, and the microbial consortium required further optimization.

In this work, we further optimized this previously developed microbial consortium to improve the production of mcl-PHA from xylose and glucose, "unrelated" carbon sources, by knocking out the *fadD* gene of *E. coli* while heterologously expressing the gene encoding the acyl carrier protein thioesterase from the castor plant (*Ricinus communis*), and knocking out the *fadA* and *fadB* genes in the β-oxidation pathway of *P. putida* while overexpressing the *phaJ* gene (shown as ⑥, ⑦, ⑧, ⑨, and ⑩ in **Figure 1**). Engineering *E. coli*, as the xylose-utilizing strain in our design, was capable of improved xylose utilization to produce acetic acid and FFAs, which act as intermediate metabolites of the microbial consortium. In the *P. putida*, we blocked a part of the β-oxidation pathway and improved the conversion efficiency of FFAs into mcl-PHA while relieving the growth inhibitory effects of acetic acid and FFAs on *E. coli*. Based on the above design, we reconstructed the artificial microbial consortium and then optimized its aerobic cultivation process, resulting in a significant improvement of the production of mcl-PHA and the efficiency of substrate conversion with mixed sugars (xylose and glucose). The successful construction of the microbial consortium based on the "nutrition supply–detoxification" concept provides insights for converting lignocellulose into high value-added compounds.

MATERIALS AND METHODS

Bacterial Strains, Plasmids, and Reagents

The bacterial strains and plasmids used in this study are listed in **Supplementary Table S1**. *E. coli* MG1655 was donated by Dr. Tao Chen of Tianjin University, and *E. coli* Δ4 was stored in our laboratory. *P. putida* KT2440 (ATCC 47054) was obtained from the American type culture collection (Manassas, VA, United States). *E. coli* S17-1 was stored in our laboratory. The plasmid pBBR1MCS-2 was donated by Dr. Yingjin Yuan of Tianjin University, China. The plasmids pTKS/CS and pTKRED were donated by Dr. Tao Chen of Tianjin University. The plasmids pET28a and pK18mobsacB were stored in our laboratory. Xylose (99% purity) was purchased from Yuanye (Shanghai, China). Acetate (HPLC grade) was purchased from Concord Tech (China). Glucose (AR) was purchased from Yuanli Chemical (Tianjin, China). DNA manipulating agents, including restriction endonucleases and T4 DNA ligase, were purchased from Thermo Scientific (Beijing, China). Phanta Max Super-Fidelity DNA polymerase and Taq for polymerase chain reaction (PCR) were purchased from Vazyme (Nanjing, China). PCR primers were synthesized by GENEWIZ (Suzhou, China) and are listed in **Supplementary Table S2**.

Plasmid and Strain Construction

E. coli MG1655 and *E. coli* Δ4 derivatives were used to construct the engineered strain for the biosynthesis of acetic acid and FFAs. According to the gene knockout method described previously (Lin et al., 2014), knockout of the *fadD* gene on the chromosomes of *E. coli* MG1655 and *E. coli* Δ4 through scarless chromosomal gene deletion strategy (**Supplementary Figure S1**). The primers tet-f and tet-r were used to amplify the tetracycline resistance gene and the I-SceI gene recognition sites at both ends, using pTKS/CS as the template. Using the genome of *E. coli* MG1655 as the template, the primer pairs *fadD* up-f/*fadD* up-r and *fadD* down-f/*fadD* down-r were used to amplify the 200 bp up and downstream flanking sequences of the *fadD* gene. The up-tet-down fragment was fused using overlap extension PCR and introduced into *E. coli* MG1655 and *E. coli* Δ4 by electrotransformation. The knockout strains *E. coli* ΔD and *E. coli* Δ4D were obtained after two rounds of resistance screening. Furthermore, pET28a was used as a vector to construct a heterologous expression vector using the T3

promoter and tac promoter to induce the expression of acyl carrier protein thioesterase. The original ricinoleoyl carrier protein sequence (GenBank: NM_001323748.1, **Supplementary Appendix SA**) was codon-optimized for *E. coli* (**Supplementary Appendix SB**) and synthesized by Genecreate (China). The primers RBS-ACP-f and ACP-r were used to amplify the ricinoleoyl carrier protein thioesterase gene fragment and add the ribosome binding site (RBS) in front of the fragment. The primers T3-ACP-f1/T3-ACP-f2/T3-ACP-f3 and ACP-r were then used to insert the T3 promoter and restriction sites on both sides of the sequence by multiplex PCR. Similarly, the primers tac-ACP-f1/tac-ACP-f2/tac-ACP-f3/tac-ACP-f4 and ACP-r were used for multiplex PCR to insert the tac promoter and restriction sites on both sides of the sequence. The amplified fragments were cloned into pET28a by restriction enzyme digestion and ligation to obtain the acyl carrier protein thioesterase expression vectors pET-T3-ACP and pET-tac-ACP, which were verified by DNA sequencing. The expression vectors were introduced into the target strain by electrotransformation to obtain the corresponding engineered strains.

P. putida KT2440 was used to construct the engineered strain for mcl-PHA synthesis, acetic acid, and FFAs utilization. Homologous recombination was used to knock out the *fadA* and *fadB* genes in the fatty acid β-oxidation pathway. The pK18mobsacB suicide plasmid was selected as the gene knockout vector, and the target gene was successfully knocked out through two rounds of homologous recombination. Using the genome of *P. putida* KT2440 as a template, specific primers were used to amplify 500 bp homology arms at the left and right ends of the gene to be knocked out. The homology arm fragments were ligated into the vector pK18mobsacB by restriction enzyme digestion and ligation to construct the knockout plasmids pK18-*fadA* and pK18-*fadB*, which were then transferred from *E. coli* S17-1 into *P. putida* KT2440 via intergeneric conjugation, and the knockout strain *P. putida* KTΔA was obtained through two homologous rounds of recombination and resistance screening. The same method was used to additionally knock out the *fadB* gene in *P. putida* KTΔA, resulting in the engineered strain *P. putida* KTΔAB. Furthermore, pBBR1MCS-2 was used to construct a vector for the co-expression of *acs* and *phaJ* genes using the T3 promoter and a synthetic RBS. Using *P. puti*da KT2440 as a template, the primer pairs acs-f/r and phaJ-f/r were used to amplify the *acs* and *phaJ* coding sequences, which were then cloned into pBBR1MCS-2 by restriction enzyme digestion and ligation to obtain p2-*acs-phaJ*. The expression vector p2-*acs-phaJ* was verified by restriction digestion and sequencing, and introduced into *P. putida* KT2440 and *P. putida* KTΔAB by electrotransformation, respectively.

Culture Medium and Growth Conditions

Luria Bertani (LB) medium was used for strain preservation and seed culture preparation. All fermentation (aerobic fermentation) processes were carried out in M9 medium (12.8 g/L Na_2HPO_4 $7H_2O$, 3 g/L KH_2PO_4, 1 g/L NH_4Cl, 0.5 g/L NaCl, and 0.24 g/L $MgSO_4$), which was autoclaved and subsequently supplement with the required content of filter-sterilized glucose and/or xylose, and a trace element solution containing 6.0 mg/L $FeSO_4{\cdot}7H_2O$, 2.7 mg/L $CaCO_3$, 2.0 mg/L $ZnSO_4{\cdot}H_2O$, 1.16 mg/L $MnSO_4{\cdot}H_2O$, 0.37 mg/L $CoSO_4{\cdot}7H_2O$, 0.33 mg/L $CuSO_4{\cdot}5H_2O$, and 0.08 mg/L H_3BO_3. Where appropriate, 50 μg/ml kanamycin, 100 μg/ml chloramphenicol, and 2 mM Isopropyl β-D-1-thiogalactopyranoside (IPTG) were added. For the shake flask fermentations, single colonies of *E. coli* and *P. putida* were grown in 5 ml of culture medium in test tubes overnight at 30 °C and 220 rpm. The overnight cultures were used to inoculate 500 ml shake flasks containing 50 ml of M9 medium at a seed ratio of 1%, and fermented at 30°C and 220 rpm. For bioreactor fermentation, the overnight cultures were transferred at an inoculation ratio of 1%–100 ml of fresh LB medium and cultivated at 30°C and 220 rpm for 12 h to prepare the seed cultures. The seed cultures were used to inoculate a 5 L bioreactor (Bailun, Shanghai, China) with 2 L of M9 medium at a seed ratio of 0.5%, and the fermentation was carried out at 30 °C. Sterile air was delivered at a flow rate of two vvm, and the dissolved oxygen level was kept above 25% of air saturation by controlling the stirring speed. The pH was kept constant via the automatic addition of 0.5 M H_2SO_4 and 1.0 M KOH or 25% aqueous ammonia. Fed-batch strategies in bioreactor were performed to analyze the ability of engineered *P. putida* to produce mcl-PHA using acetic acid, with *P. putida* KT2440 as the control. The total concentration of acetic acid was quantified as 25 g/L through two feeds. Samples are taken at every interval to detect the concentration of acetic acid during the cultivation process to determine the feeding time. The fermentation experiments in the manuscript were conducted in triplicates, and data were shown as the mean values ± standard deviations (SD).

Extraction and Analysis of Mcl-PHA

The extraction and analysis of PHA were described previously (Poblete-Castro et al., 2013). Briefly, an appropriate amount of culture solution was taken and the cells were harvested by centrifugation at 4°C and 8,000 rpm for 10 min and washed with distilled water. The washed bacteria were then frozen at −80°C and lyophilized for 24 h. Then, an appropriate amount of bacteria was weighed after drying, placed in a reactor containing 2 ml of esterification solution and 2 ml of chloroform, and esterified at 100°C for 4 h. The esterification solution was 3% sulfuric acid in methanol, and benzoic acid was added as an internal standard. After the esterification reaction was completed, pure water was added to the reaction mixture at room temperature, mixed evenly, and left standing for stratification. The lower organic phase was passed through a filter membrane to obtain the sample to be tested. The PHA was quantified by gas chromatography, with an injection volume of 1 μL. The starting temperature of the chromatographic separation column (Agilent HP-5) was 80°C and maintained for 1.5min, followed by ramp to 140°C at 30°C/min. Then the temperature was increased to 240°C at 40°C/min and kept at 240°C for 4 min, and the entire program lasted 10 min. The PHA monomer was characterized by gas chromatography-mass spectrometry. The starting temperature of the chromatographic separation column (Agilent HP-FFAP) was 50 °C and was maintained for 5 min. The temperature was then increased to 220°C at 5°C/min and kept for 20 min. The inlet

temperature was 220°C, the ion source temperature was 230°C, and the interface temperature was 220°C.

Analytical Methods

Cell optical density was measured at a wavelength of 600 nm (OD_{600}) with UV-1200 spectrophotometer (Mapada, China). The OD_{600} value of two bacteria in the microbial consortium culture process was analyzed using the colony counting method (Liu X. et al., 2018; Liu et al., 2020). Based on the characteristics of kanamycin and chloramphenicol resistance in *E. coli* Δ4D (T3) and *P. putida* KTΔAB (p2-acs-phaJ), both *E. coli* Δ4D (T3) and *P. putida* KTΔAB (p2-acs-phaJ) are resistant to kanamycin, while *P. putid*a KTΔAB (p2-acs-phaJ) is also resistant to chloramphenicol. The first step is to test the quantitative relationship between the number of colonies of the two bacteria and their OD_{600}, respectively. Diluting the bacterial liquids with different OD_{600} to the appropriate multiples and spreading them on the corresponding resistant plates, the quantitative relationships between OD_{600} and the number of colonies of the two bacteria was obtained as: for *E. coli* Δ4D (T3), $1OD_{600} = 0.42 \times 10^9$ CFU/ml; for *P. putida* KTΔAB (p2-acs-phaJ), $1OD_{600} = 0.20 \times 10^7$ CFU/ml. Secondly, the co-culture solutions of different periods were diluted to a certain multiple and then coated on plates with kanamycin and chloramphenicol resistance, respectively. The OD_{600} of the two bacteria in the co-culture can be calculated then, based on the different characteristics of resistance in *E. coli* Δ4D (T3) and *P. putida* KTΔAB (p2-acs-phaJ), and the above quantitative relationships.

Acetate, glucose, and xylose were quantified in the culture supernatant using an Ultimate 3000 HPLC (Dionex, Sunnyvale, CA, United States) equipped with an Aminex HPX-87H ion-exchange column (Bio-Rad, United States) operating at 65 °C and a differential refraction detector, with 5 mM H_2SO_4 as the mobile phase at a flow rate of 0.6 ml/min. Extraction and detection of fatty acids were performed as described previously (Eiteman and Altman, 2006). Briefly, 2 ml of fermentation broth was centrifuged at 12,000 rpm for 5 min, and the supernatant was collected. Then, 200 μL of glacial acetic acid and 150 mg of internal standard (undecanoic acid) were added to the supernatant, mixed with 2 ml of extractant (n-hexane: chloroform = 4: 1 v/v), and shaken thoroughly. After standing still, the above-mentioned mixed solution was placed in the inner lining of the reactor, and allowed to stand overnight in a fume hood. After the organic reagents were completely volatilized, 1 ml of esterification solution (chloroform: methanol: sulfuric acid = 10: 8.5: 1.5, v/v) was added, the reactor was sealed and placed in an oven at 100 °C for 1 h. After the reaction was completed, pure water was added to the reaction mixture at room temperature, mixed evenly, and left standing for stratification. The lower organic phase was passed through a filter membrane to obtain the sample to be tested. The fatty acids were quantified by gas chromatography, with an injection volume of 1 μL. The starting temperature of the chromatographic separation column (Agilent HP-5) was 60 °C and maintained for 3min. Then the temperature was increased to 250 °C at 10°C/min and kept at 250 °C for 10 min, and the entire program lasted 30 min.

RESULTS AND DISCUSSION

The Division of Labor and Collaborative Design of the Artificial Microbial Consortium

Previous studies have shown that adding fatty acid as external substrates will significantly increase the titer of mcl-PHA synthesis by *P. putida* and the final yield (Wang and Nomura, 2010). As FFAs are the preferred carbon source for *P. putida* to synthesize mcl-PHA, their toxicity to cells and production costs must be considered as a priority. Therefore, we aimed to start the synthesis from the main sugars in the cheap substrate cellulosic hydrolysate, such as xylose and glucose. However, pure cultures of *P. putida* cannot co-utilize glucose and xylose to produce mcl-PHA. To overcome this, we introduced an engineered *E. coli* in which the four genes *ptsG*, *manZ*, *atpFH,* and *envR* were knocked out, while further strengthened its functions, and co-cultured it with engineered *P. putida* to form a microbial consortium to produce mcl-PHA from glucose and xylose. As shown in **Figure 1**, based on the construction principle of division of labor, when synthetic co-cultures are used to perform complex tasks, the functions of the two strains in the microbial consortium are distinguished. The two strains are independent but play complementary roles in the microbial consortium, which we call "nutrition supply–detoxification" (Liu et al., 2020). We further strengthened this interaction by designing an engineered *E. coli* with increased secretion of long-chain FFAs. Then, by weakening the β-oxidation of fatty acids in *P. putida* while strengthening its acetic acid utilization capacity, it was able to efficiently produce mcl-PHA. As for the co-culture design, we conducted the performance tests on all engineered *P. putida* and engineered *E. coli* after each step of genetic modification, which indirectly reflects the effect of each genetic operation on the synthesis of the target product. The optimized microbial consortium based on the "nutrition supply–detoxification" concept is expected to enable the industrial production of mcl-PHA from glucose-xylose mixtures.

The Performance of Engineered *E. coli* in the Production of Acetic Acid and FFAs

Engineering *E. coli* for the Production of Acetic Acid and FFAs

Unlike most strains that naturally produce fatty acids, *E. coli* usually does not accumulate fatty acids in the cell. In the fatty acid metabolic pathway of *E. coli*, the *fadD* gene encodes a long-chain fatty acid coenzyme A ligase that plays a vital role in the activation and secretion of fatty acids. Voelker and Davies found that engineering *E. coli* MG1655 with a mutation in the *fadD* gene was significantly different from other strains in terms of FFA titer and type, producing up to 2.0 g/L of FFAs in shake-flask culture (Voelker and Davies, 1994). Therefore, we knocked out the *fadD* gene in wild-type *E. coli* MG1655 and engineering *E. coli* Δ4, resulting in the strains *E. coli* ΔD and engineering *E. coli* Δ4D respectively. Li et al. further modified the MG1655 mutant strain

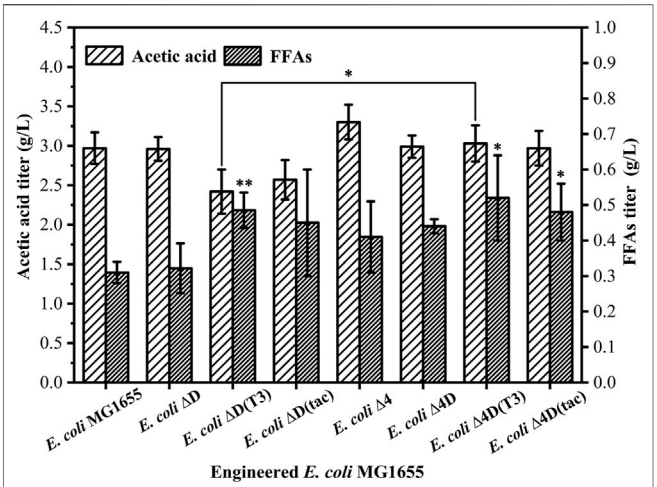

FIGURE 2 | Comparison of the ability of engineered *E. coli* to produce acetic acid and FFAs in shake flasks, and the cultivation time was 60 h. The error bars indicate the standard deviation of triplicate experiments. $^{*}p < 0.05$; $^{**}p < 0.01$; $^{***}p < 0.001$; ns, no significance.

by knocking out the *fadD* gene and simultaneously expressing an exogenous acyl sulfide lipase gene (Li et al., 2012). The resulting strain was able to use xylose as the sole carbon source to produce 2.62 g/L of FFAs. The lack of an acyl carrier protein thioesterase gene in *E. coli* results in poor secretion of fatty acids. The transfer of acyl carrier protein thioesterase into *E. coli* can disrupt the elongation cycle of fatty acids and promote the extracellular secretion of fatty acids. Studies have confirmed that acyl carrier protein thioesterases can be divided into FatA and FatB thioesterase families according to their substrate specificity. FatA thioesterase has activity on unsaturated acyl carrier protein, while FatB thioesterase has stronger activity on saturated acyl carrier protein (Salas and Ohlrogge, 2002). In addition, acyl carrier protein thioesterases from different sources have different activities on acyl carrier proteins with fatty acids of varying chain lengths (Yuan et al., 1995). Zhang et al. confirmed that heterologous expression of the acyl carrier protein thioesterase gene from the castor plant (*Ricinus communis*) in *E. coli* can increase the production of extracellular FFAs to 2.0 g/L (Zhang et al., 2011). We codon-optimized the acyl carrier protein thioesterase gene sequence from the castor plant and used a T3 promoter and tac promoter to induce expression, respectively.

Preliminary tests on acetic acid and FFAs production in engineered *E. coli* and the parental strain (**Figure 2**) showed the strains engineered based on *E. coli* Δ4 have a stronger ability to produce acetic acid than *E. coli* MG1655. As expected, the strain with only the *fadD* gene knocked out showed the same result. In a comprehensive comparison, the engineered strains with *fadD* gene knockout and expression of the exogenous acyl carrier protein thioesterase gene produced more FFAs. *E. coli* Δ4D (T3) and *E. coli* Δ4D (tac) produced about 3.0 g/L acetic acid and 0.5 g/L FFAs. There is no statistical difference as *E. coli* MG1655 as the control, so the degree of enhancement was not ideal. By comparing the OD_{600} of *E. coli* MG1655 and engineered strains at the end of cultivation, it was found that the OD_{600} of *E. coli* MG1655 was 2.29, while the OD_{600} of *E. coli* Δ4D (T3) and *E. coli* Δ4D (tac) was only 1.62 and 1.69 respectively (**Supplementary Figure S2**). Hence, the growth of the engineered strains was worse than that of wild-type bacteria. At the same time, we measured the residual amount of xylose in the fermentation broth, and found that the five strains *E. coli* MG1655, *E. coli* ΔD, *E. coli* ΔD (T3), *E. coli* ΔD (tac), and *E. coli* Δ4 completely consumed xylose, while *E. coli* Δ4D, *E. coli* Δ4D (T3), and *E. coli* Δ4D (tac) still had approximately 2.8 g/L of residual xylose (**Supplementary Figure S2**). The excessive accumulation of acetic acid may have an inhibitory effect on the fermentation system of the strain. On the one hand, acetic acid will cause the pH to drop and thus form an inhibitory effect. On the other hand, when the pH is close to the pKa of acetate (approximately 4.76), more of the acetate would be in its protonated form so that toxic concentrations of acetic acid itself may cause more potent inhibition. We hypothesized that the accumulation of acetic acid produced by the strains in the shake flask cultivation system caused the system's pH to decrease, inhibiting the growth of the bacteria and the utilization of xylose. The pH of the cultivation broth was tested, and the pH was around 4.65, which partially confirmed our hypothesis and maybe explained why the engineered strain was unable to reach its full potential in the shake flask cultivation system.

Fermentation of Engineered *E. coli* to Produce Acetic Acid and FFA

Bioreactors can be used to control the dynamic balance of pH in the fermentation system, effectively avoiding the negative effects of excessive acetic acid accumulation in the fermentation environment, which leads to a decrease in pH and inhibits bacterial growth. As shown in **Figure 3A**, during the same fermentation time, the wild-type bacteria initially consumed xylose quickly, which may be caused by the excessive growth of the initial biomass of the wild-type bacteria. By contrast, *E. coli* Δ4D (T3) and *E. coli* Δ4D (tac) showed faster xylose consumption in the middle of the fermentation, and at this time, the production of acetic acid was also quicker. The output of FFAs and acetic acid at the end of the fermentation is shown in **Figure 3B**. The acetic acid output of *E. coli* MG1655 was 2.27 g/L, while *E. coli* Δ4D (T3) and *E. coli* Δ4D (tac) produced 5.67 and 3.86 g/L of acetic acid, respectively. It can be seen that the engineered strain *E. coli* Δ4D (T3) has an outstanding ability to produce acetic acid. However, *E. coli* Δ4D (tac) and *E. coli* Δ4D (T3) produced 2.87 g/L and 2.42 g/L FFAs, respectively. Compared with *E. coli* MG1655, the corresponding titers were increased 4.6 and 4.0 times. Consistent with previous studies, heterologous expression of the acyl carrier protein thioesterase gene of the castor plant in *E. coli* enhanced its ability to secrete FFAs outside the cell.

The engineered strains *E. coli* Δ4D (T3) and *E. coli* Δ4D (tac) were compared with *E. coli* MG1655 in the bioreactor fermentation to obtain acetic acid and FFAs, the production was greatly improved. This confirmed the effect of bacterial growth on the production of acetic acid and FFAs. From the perspective of the culture medium, the limitation of nitrogen source is an essential factor affecting the growth of bacteria. We

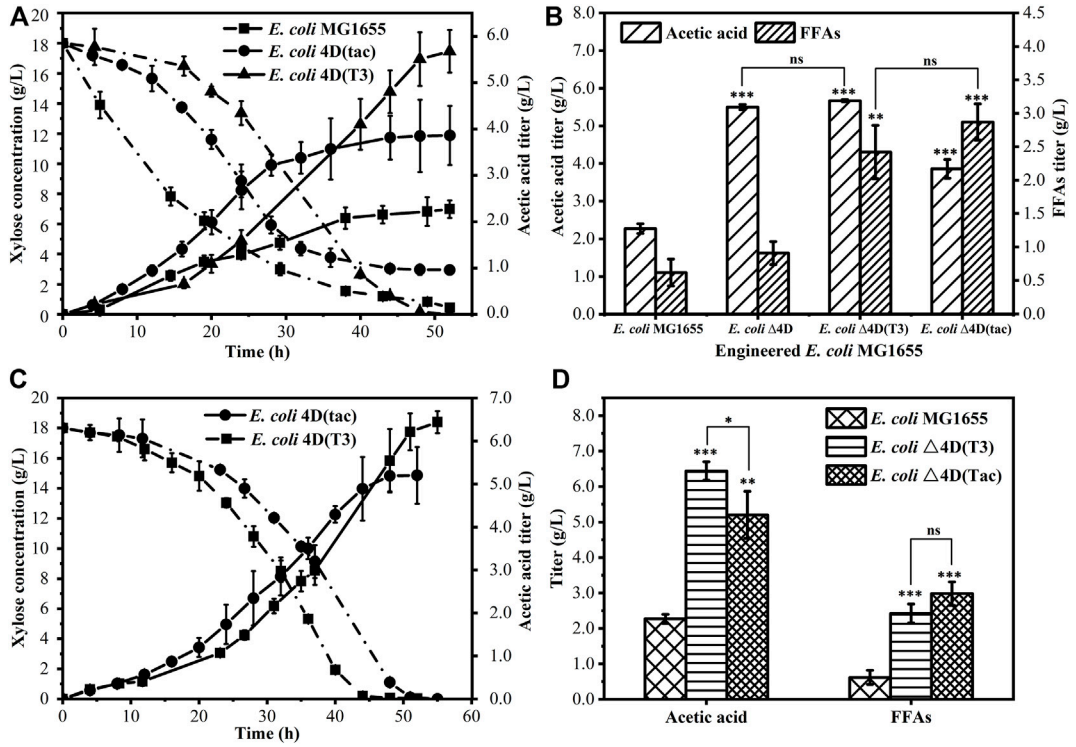

FIGURE 3 | Production of acetic acid and fatty acids by engineered *E. coli* in a bioreactor **(A)** Process diagram of *E. coli* MG1655, *E. coli* Δ4D (T3), and *E. coli* Δ4D (tac) using xylose to produce acetic acid in a bioreactor **(B)** acetic acid and FFAs titer obtained by fermentation of *E. coli* MG1655 and engineered *E. coli*, and the cultivation time was 55 h **(C)** Process diagram of *E. coli* Δ4D (T3) and *E. coli* Δ4D (tac) using xylose to produce acetic acid in a bioreactor after optimization of the nitrogen source **(D)** Comparison of the titers of acetic acid and FFAs obtained by fermentation of *E. coli* MG1655 and engineered *E. coli*, and the cultivation time was 55 h. The error bars indicate the standard deviation of triplicate experiments. $^{*}p < 0.05$; $^{**}p < 0.01$; $^{***}p < 0.001$; ns, no significance.

changed the pH-adjusting solution from 1M KOH to 25% aqueous ammonia to provide sufficient nitrogen. As shown in **Figure 3C**, the engineered strain's xylose consumption phase was shortened after switching of pH control, while the titer of acetic acid obtained by fermentation was increased. At the end of fermentation, the acetic acid output of *E. coli* Δ4D (T3) and *E. coli* Δ4D (tac) was raised to 6.44 and 5.20 g/L, respectively, while the FFAs yields were similar to those obtained before optimization (**Figure 3D**). The main extracellular FFAs included n-hexanoic acid, n-heptanoic acid, n-octanoic acid, n-decanoic acid, and n-dodecanoic acid. The switching of pH control improved the growth of engineered strains in the fermentation process, which accelerated the degradation of xylose and its conversion into acetic acid. These results show that both engineered *E. coli* Δ4D (T3) and *E. coli* Δ4D (tac) can efficiently use xylose to produce acetic acid and FFAs. After switching of pH control, the acetic acid production of *E. coli* Δ4D (T3) was 3.0 times higher than that of wild-type bacteria, and the output of FFAs was about 4.0 times higher than that of wild-type bacteria. However, *E. coli* Δ4D (tac) requires the addition of IPTG as inducer during the fermentation process, and considering the limitations of adding IPTG during large-scale fermentation and its effect on the fermentation costs, the engineered strain *E. coli* Δ4D (T3) was a better option for constructing the microbial consortium.

Engineering *P. putida* to Produce Mcl-PHA

Engineered *P. putida* Uses Acetic Acid to Accumulate Mcl-PHA

Based on the collaborative design of the microbial consortium for mutual benefit and symbiosis, the available carbon sources of *P. putida* include the initial substrate glucose, as well as the acetic acid and FFAs provided by the engineered *E. coli*. As "unrelated" carbon sources, glucose and acetic acid can be converted into mcl-PHA through the fatty acid synthesis pathway via acetyl-CoA as an immediate precursor. Therefore, strengthening the acetic acid assimilation pathway and promoting its conversion into acetyl-CoA can encourage the accumulation of mcl-PHA. In the previous study by (Yang et al., 2019), overexpression of the *acs* gene in *P. putida* KT2440 increased the strain's ability to utilize acetate and promoted the conversion of acetate into mcl-PHA. Therefore, we also overexpressed the *acs* gene. FFAs are "related" carbon sources for the synthesis of mcl-PHA through fatty acid β-oxidation in *P. putida*. Weakening the fatty acid β-oxidation pathway can redirect the carbon flux toward PHA precursors, which is beneficial to increase the production of mcl-PHA (Salvachua et al., 2020; Zhao et al., 2020). Studies have confirmed that knocking out the *fadA* and *fadB* genes in the fatty acid β-oxidation pathway of *P. putida* leads to the conversion of most fatty acids into 3-hydroxyacyl-CoA for the synthesis of PHA, rather than them being oxidized into acetyl-CoA, thereby

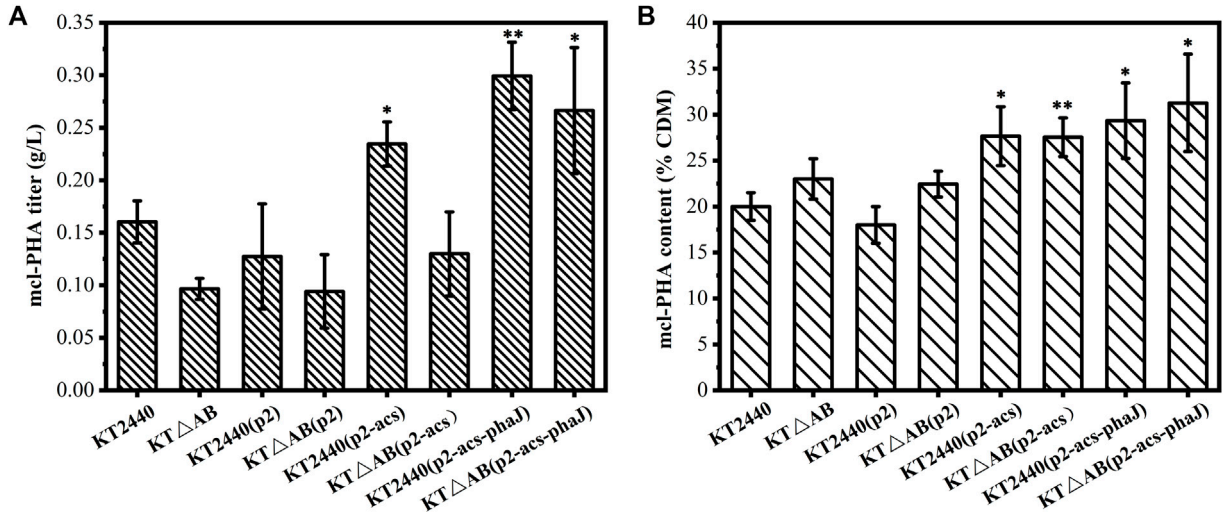

FIGURE 4 | Comparison of the production of mcl-PHA by engineered *P. putida* in shake-flask fermentation with acetic acid as the sole carbon source, and the cultivation time was 60 h **(A)** The titer of mcl-PHA **(B)** Intracellular content of mcl-PHA. The error bars indicate the standard deviation of triplicate experiments. $^{*}p < 0.05$; $^{**}p < 0.01$; $^{***}p < 0.001$; ns, no significance.

significantly improving the conversion rate of the substrates into mcl-PHA (Wang et al., 2009; Chung et al., 2011; Liu et al., 2011). Therefore, the two previously identified genes encoding 3-hydroxyacyl-CoA dehydrogenase (*fadB*) and 3-ketoacyl-CoA thiolase (*fadA*) were knocked out in *P. putid*a KT2440, resulting in engineered strain KTΔAB. On the other hand, the relationship between fatty acid β-oxidation and PHA synthesis can still be established through enoyl-coenzyme A hydratase (PhaJ). In fatty acid β-oxidation, PhaJ can hydrate the intermediate 2-trans-enoyl-CoA to generate the mcl -PHA precursor (R)-3-hydroxyacyl-CoA. The overexpression of the *phaJ* gene in *P. putida* leads to an increase in the accumulation of mcl-PHA, illustrating the critical role of this enzyme in linking fatty acid β-oxidation with PHA synthesis from "related" carbon sources.

The mcl-PHA production capacity of the engineered *P. putida* was tested with acetic acid as the sole source in shake flasks. As shown in **Figure 4A**, the engineered strains *P. putida* KT2440 (p2-acs-phaJ) and *P. putida* KTΔAB (p2-acs-phaJ) showed efficient utilization of acetic acid and accumulated 0.30 and 0.27 g/L of mcl-PHA. Compared with the production of mcl-PHA by *P. putida* KT2440 (0.16 g/L), this is a dramatic improvement. Thus, the overexpression of the *acs* and *phaJ* genes increased the output of mcl-PHA by the engineered strains, which was consistent with previous studies. The intracellular content of mcl-PHA in the engineered strains in which the *fadA* and *fadB* genes were knocked out was higher. *P. putida* KTΔAB (p2-acs-phaJ) accumulated mcl-PHA equivalent to 31.27% of the dry cell mass (CDM), which was significantly higher than in *P. putida* KT2440 (**Figure 4B**). However, the gene knockout caused a delay in the biomass accumulation of the strain. The consequent reduction of biomass resulted in a slightly lower final mcl-PHA titer compared to the engineered strains without a knock out of the *fadA* and *fadB* genes. Similarly, the metabolic burden stemming from the propagation of plasmid vectors will slightly reduce the accumulation of mcl-PHA indicating that the biomass of engineered strains is highly correlated with the accumulation of mcl-PHA.

A comparative experiment was conducted in a bioreactor to reduce the environmental impact such as oxygen limitation and the inhibitory effect of acetic acid on the biomass of the strains. *P. putida* KT2440 and *P. putida* KTΔAB (p2-acs-phaJ) were grown with acetic acid as the sole carbon source for fed-batch fermentation. By detecting the concentration of acetic acid in the system, *P. putida* KT2440 was fed with acetic acid at 15 and 30 h, and *P. putida* KTΔAB (p2-acs-phaJ) was fed at 33 and 51 h. As shown in **Figure 5**, *P. putida* KTΔAB (p2-acs-phaJ) exhibited a lag in biomass accumulation compared with *P. putida* KT2440, so the fermentation time was 5 h longer than in *P. putida* KT2440. However, the biomass obtained by the two strains by the end of the bioreactor fermentation was similar. The intracellular PHA content of *P. putida* KTΔAB (p2-acs-phaJ) (43.48% of CDM) was twice that of *P. putida* KT2440 (21.81% of CDM). The final titer of mcl-PHA was 0.70 g/L, which was twice that of *P. putida* KT2440. Therefore, a series of genetic modifications of *P. putida* greatly increased its ability to use acetic acid to produce mcl-PHA. In addition, *P. putida* KTΔAB (p2-acs-phaJ) has similar yields (about 0.03 g/g) of mcl-PHA obtained by using the different concentration of acetic acid in the shake flask (**Figure 4A**) and the bioreactor (**Figure 5**), which may indicate that the limitation of oxygen in shake flask culture has less influence on the accumulation of mcl-PHA.

Engineering *P. putida* to Produce Mcl-PHA by Fermentation With Mixed Substrates

Previous studies have shown that FFAs are the preferred substrate of *P. putida* to achieve large amounts of PHA accumulation in the cell. The PHA polymer exhibits an even-numbered carbon chain length unless there are odd-chain length fatty acids in the substrate (Ma et al., 2009), which illustrates the critical role of

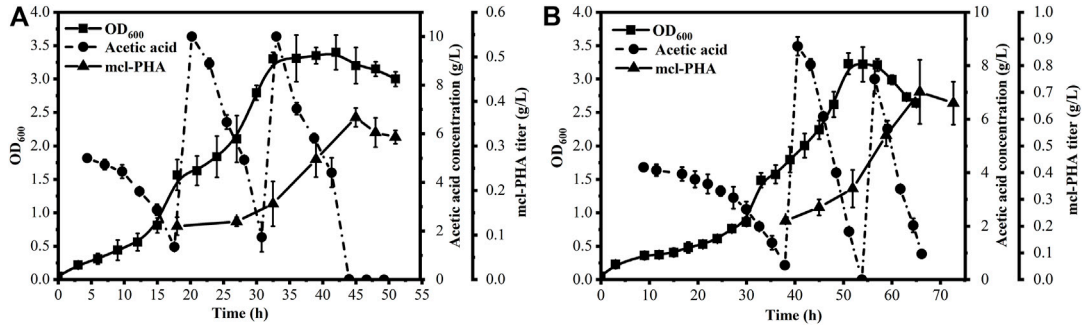

FIGURE 5 | *P. putida* KT2440 **(A)** and the engineered strain *P. putida* KTΔAB (p2-acs-phaJ) **(B)** were used to produce mcl-PHA from acetic acid as the sole substrate in a bioreactor through fed-batch strategy. The error bars indicate the standard deviation of triplicate experiments.

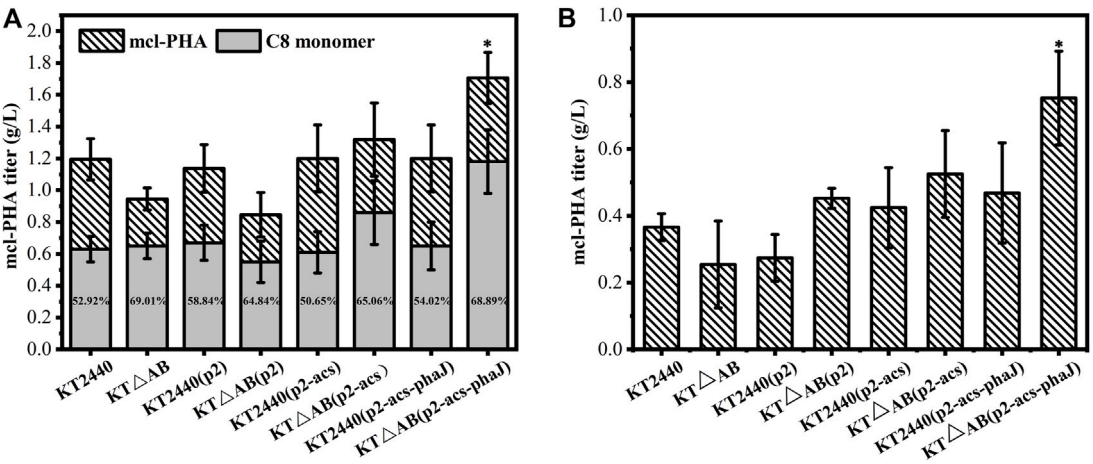

FIGURE 6 | The engineered strain *P. putida* KTΔAB (p2-acs-phaJ) was used to produce mcl-PHA by fermentation with mixed substrates **(A)** *P. putida* KTΔAB (p2-acs-phaJ) was used to produce mcl-PHA in a two-step fermentation with a mixed substrate comprising 10 g/L glucose and 2 g/L octanoate **(B)** *P. putida* KTΔAB (p2-acs-phaJ) was cultured with 5 g/L glucose and 5 g/L acetic acid as a substrate for 24 h, after which 2 g/L octanoate was added, and the fermentation was continued for 72 h to measure the final mcl-PHA titer. The error bars indicate the standard deviation of triplicate experiments. *$p < 0.05$; **$p < 0.01$; ***$p < 0.001$; ns, no significance.

fatty acid β-oxidation in the synthesis of mcl-PHA by *P. putida*. *P. putida* KT2440 could degrade octanoate into acyl-CoA and use the β-oxidation pathway to synthesize C6 or C8 R-3-hydroxyacyl-CoA as the β-oxidation intermediates, which are mcl-PHA precursors. While knocking out the *fadA* and *fadB* genes weakens the β-oxidation pathway, it promotes C8 R-3-hydroxyacyl-CoA to become more mcl-PHA precursors. Therefore, the content of the C8 monomer in mcl-PHA accumulated by engineered *P. putida* using octanoate may be higher than that of *P. putida* KT2440. In the microbial consortium, engineered *E. coli* provides *P. putida* with the optimal metabolites for accumulation of mcl-PHA that medium- and long-chain fatty acids. We observed the utilization of FFAs by engineered *P. putida* in a two-step fermentation with glucose and octanoate are the only carbon sources in the medium. As shown in **Figure 6A**, the mcl-PHA titer of the engineered *P. putida* with a knockout of the β-oxidation-related genes was lower than that of *P. putida* KT2440, which is suspected to be related to growth inhibition. Ultimately the mcl-PHA titer of the fully engineered strain *P. putida* KTΔAB (p2-acs-phaJ) reached 1.71 g/L. The synthesized mcl-PHA monomer is composed of 3-hydroxyhexanoate (C6), 3-hydroxyoctanoate (C8), 3-hydroxydecanoate (C10), 3-hydroxydodecanoate (C12), and 3-hydroxytetradecanoate (C14) (**Supplementary Table S3**). Predictably, octanoate causes the C8 monomer to become the main component of the polymer composition. Further comparing the C8 monomer content of mcl-PHA, the average C8 monomer in mcl-PHA of the engineered strains with modified β-oxidation related genes accounted for 66.95% of the total compared to the unmodified engineered strains (54.11%). Similarly, the C8 monomer in the mcl-PHA accumulated by *P. putida* KTΔAB (p2-acs-phaJ) accounted for 68.89% of the total. Consistent with our expectations, modification of the β-oxidation pathway can improve the conversion efficiency of FFAs to synthesize mcl-PHA precursors and then mcl-PHA. To test the engineered *P. putida* to

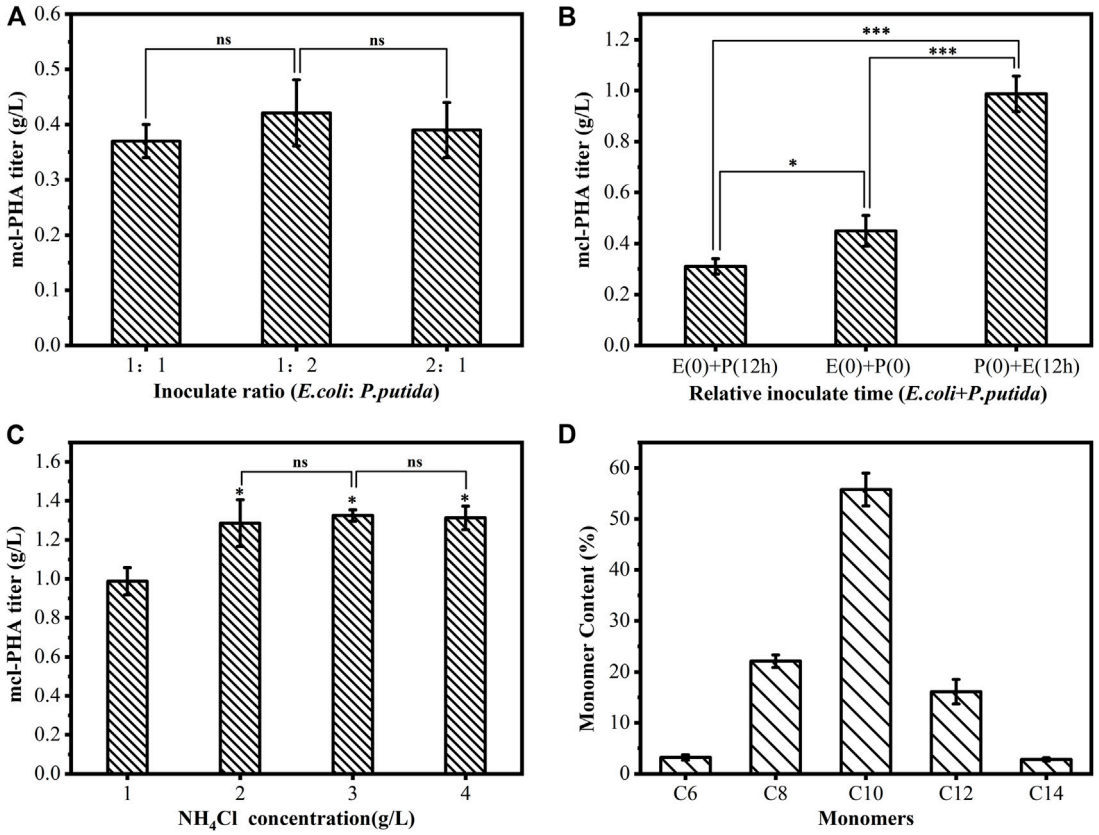

FIGURE 7 | The artificial microbial consortium with optimized inoculation ratio, inoculation time, and nitrogen source was used to convert a mixture of glucose and xylose (mass ratio = 1:1) into mcl-PHA in the bioreactor, and the cultivation time was 60 h **(A)** Different inoculation ratios (vol/vol) **(B)** Different relative inoculation times; E (0) + P (12 h), *P. putida* inoculated 12 h after inoculation with *E. coli*; E (0) + P (0), Simultaneous inoculation of *E. coli* and *P. putida*; P (0) + E (12 h), *E. coli* inoculated 12 h after inoculation with *P. putida* **(C)** Different nitrogen source concentrations **(D)** The monomer composition of mcl-PHA produced by the microbial consortium. The error bars indicate the standard deviation of triplicate experiments. *$p < 0.05$; **$p < 0.01$; ***$p < 0.001$; ns, no significance.

produce mcl-PHA in the microbial consortium, the substrate utilization mechanism of the microbial consortium was simulated at the shake flask level. Acetic acid was added as one of the mixed substrates based on the above research. As shown in **Figure 6B**, the engineered strain *P. putida* KTΔAB (p2-acs-phaJ) was able to produce 0.75 g/L mcl-PHA, which was twice that of *P. putida* KT2440 (0.37 g/L). It can be seen that the engineered *P. putida* can effectively use the mixed substrates of the microbial consortium to produce mcl-PHA, which includes glucose, as well as the acetic acid and FFAs secreted by *E. coli*.

Construction of the Microbial Consortium to Produce Mcl-PHA From a Glucose-Xylose Mixture

The microbial consortium uses xylose and glucose, the main components of cellulosic hydrolysate, as substrates to produce mcl-PHA. Based on our design principle, two engineered strains were designed and extensively tested to construct a mutually beneficial symbiosis. Ideally, *E. coli* Δ4D (T3) in the microbial consortium should preferentially metabolize xylose, and *P. putida* KTΔAB (p2-acs-phaJ) metabolizes glucose to avoid substrate competition, thereby ensuring the stability of the microbial consortium. However, the artificial microbial consortium for the production of mcl-PHA is dynamic. Coordinating the interactions in the microbial consortium and the synergistic growth of the two strains is essential for optimizing the co-culture strategy. Therefore, the relative inoculation ratio (the volume ratio of the seed liquid), inoculation time, and nitrogen source concentration of the microbial consortium were optimized. Firstly, the two strains in the microbial consortium were added at different inoculation ratios (*E. coli*: *P. putida* = 1:1, *E. coli*: *P. putida* = 1:2, *E. coli*: *P. putida* = 2:1). As shown in **Figure 7A**, at an *E. coli*: *P. putida* ratio of 1:2, the maximum mcl-PHA titer produced by the microbial consortium was 0.42 g/L. However, the mcl-PHA titers were not statistically different under different inoculation ratios, which may be that the relatively fast-growing strains quickly reached equilibrium in the co-culture. According to the plate counting assay, *E. coli* was the dominant strain in the microbial consortium at the end of the fermentation at three different inoculation ratios. Because mcl-PHA is an intracellular product, the biomass accumulation of *P. putida* may affect the production of mcl-PHA in co-culture. If *P. putida* becomes the dominant strain in the co-culture system,

it will increase the output of mcl-PHA. Therefore, the glucose and xylose consumption was measured in the microbial consortium with an *E. coli*: *P. putida* inoculation ratio of 1:2. As shown in **Supplementary Figure S3**, all glucose was consumed after 20 h of fermentation, with 6.24 g/L residual xylose remaining at this time. This result indicated that there may still be carbon catabolite repression and competition between the two strains for glucose in the co-culture. In the microbial consortium, *E. coli* Δ4D (T3) prefers to metabolize xylose but still consumes glucose, which causes the glucose to be consumed first, and *E. coli* becomes the dominant strain in the microbial consortium by the end of the fermentation.

The relative inoculation time of the two strains (*E. coli* was added to the fermentation medium 12 h before *P. putida* inoculation, 12 h after *P. putida* inoculation, and at the same time with *P. putida* inoculation) may have a significant impact on the microbial consortium. As shown in **Figure 7B**, the co-culture system that was first inoculated with *E. coli* produced 0.31 g/L of mcl-PHA, while the co-culture system in which *E. coli* was added to the medium 12 h after *P putida* inoculated produced 0.99 g/L of mcl-PHA. The results of plate colony counting showed that the adjustment of the relative inoculation time of the two strains reversed the status of the dominant strain in the microbial consortium. Thus, inoculation with *P. putida* before adding *E. coli* avoids the competition between the two strains for glucose. It promotes *P. putida* to become the dominant strain in the co-culture system while also weakening the inhibitory effect of acetic acid and FFAs secreted by *E. coli* into the co-culture system on its own growth. The two strains grew cooperatively, and the mcl-PHA output of the system was increased.

P. putida in the microbial consortium is a functional strain that produces mcl-PHA. *P. putida* accumulates mcl-PHA in the cell under the conditions of limited nitrogen and abundant carbon sources. However, supplementing with good nitrogen sources is beneficial to the growth of *E. coli* and the secretion of acetic acid and FFAs. Based on the difference in the nitrogen source requirements of the two strains in the microbial consortium, the concentration of the nitrogen source in the medium of the co-culture system was optimized. As shown in **Figure 7C**, when the concentration of NH_4Cl reached 3.0 g/L, the co-culture system produced 1.32 g/L of mcl-PHA and a further increase of the NH_4Cl concentration did not increase the output of mcl-PHA. However, when the nitrogen source concentration was 1.0 g/L, there may be nitrogen limitation, which caused the mcl-PHA titer to be lower than that at other nitrogen source concentrations. The monomer composition analysis of mcl-PHA produced by the microbial consortium is shown in **Figure 7D**. The polymer contained C6, C8, C10, C12, and C14 monomers, whereby the C14 monomers were partially unsaturated, and C10 monomers were the most abundant, accounting for 55.76% of the total content of mcl-PHA. In addition to mcl-PHA containing monomers with 6–14 carbon atoms, it also contains small amounts of C16 and C16:1 unsaturated long-chain monomers. These lcl-monomers were not observed in the pure culture of *P. putida*, which may be caused by the engineered *P. putida* using undetected lcl-FFAs secreted by *E. coli* to form lcl-PHA monomers. The microbial consortium based on the concept of "nutrient supply-detoxification" can therefore effectively use the "unrelated" carbon sources glucose and xylose to produce mcl-PHA by coordinating the metabolic communication and interaction between the two strains.

PERSPECTIVES

From the perspective of synthetic biology goals and tasks, artificial microbial consortia are suitable for more complex tasks and are more robust to environmental changes than pure cultures. At present, the relevant research on the synthesis of PHA by microbial consortia is mostly focused on the screening of unique microorganisms that can cooperate with each other to accumulate PHA using cheap substrates. However, most of them produce scl-PHA or copolymers (**Table 1**). Rebocho et al. co-cultured *Cupriavidus necator* DSM 428 and *Pseudomonas citronellolis* NRRL B-2504, using apple pulp extract rich in sugars such as fructose and glucose as the substrate, which resulted in a PHA blend with a titer of 1.85 g/L, containing about 48 wt% of P (3HB) and 52 wt% of mcl-PHA (Rebocho et al., 2020). Generally, the synthesis of mcl-PHA is highly dependent on the substrate. Although a single metabolically engineered strain can increase the titer, it still must be supplied with FFAs rich substrates, such as waste oil or simple FFAs. In addition to its own substrate cost, it is limited by the strain's ability to decompose fats and the robustness of production during large-scale fermentation. Microorganisms in nature often adapt to complex environments by forming interactive symbiotic communities and the division of labor between strains (Agapakis et al., 2012). Targeted design and construction of microbial consortia can achieve tasks that cannot be accomplished by purely cultured microorganisms or improve the metabolic functions of multi-cell systems (Jones and Wang, 2018). Research has shown that *P. putida* can be introduced into microbial consortia as an excellent mcl-PHA producing strain (Huang et al., 2016). At present, artificial microbial consortia are widely used to overcome the shortcomings of the pure culture process to synthesize natural products (Jones et al., 2016; Zhang and Wang, 2016; Liu Y. et al., 2018), and high value-added chemicals (Zhang et al., 2015; Zhang and Stephanopoulos, 2016; Liu X. et al., 2018).

The synthesis of PHA by a microbial consortium composed of two microorganisms has been extensively studied. The cooperation between the strains allows the possibility to expand the range of available substrates and improves PHA production. Different metabolic functions are carried out in different strains, and they cooperate well with each other to complete the entire task. The interaction of the two strains in the microbial consortium will ultimately affect the production efficiency of the target product. The main challenge facing artificial microbial consortia is the difficulty of maintaining a stable ratio of individually engineered strains in the system during co-culture, and this balance can be disrupted by growth competition and metabolic pressures. We proposed a strategy to design and construct a microbial consortium that synthesizes

TABLE 1 | Research on artificial consortia for PHA synthesis.

Strains	Substrates	Type of PHA	Titer (g/L)	Yield* (g/g)	References
P. putida KT2440 + *E. coli* MG1655	Glucose + xylose	mcl-PHA	1.32	0.07	This study
P. putida KT2440 + *E. coli* MG1655	Glucose + xylose	mcl-PHA	0.54	0.03	Liu et al. (2020)
P. putida KT2440 + *E. coli* MG1655	Corn straw hydrolysate	mcl-PHA	0.43	0.02	Liu et al. (2020)
Ralstonia eutropha H16 + *Bacillus subtilis* 5119	Sucrose	scl-PHA	2.30	0.08	Bhatia et al. (2018)
Cupriavidus necator DSM 428 + *Pseudomonas citronellolis* NRRL B-2504	Apple pulp wastes	P (3HB) and mcl-PHA	1.85	0.11	Rebocho et al. (2020)
Saccharophagus degradans 2–40 + *Bacillus cereus*	Xylan	scl-PHA	0.27	N.A.	Sawant et al. (2017)
Cupriavidus necator IPT 026 + *Xanthomonas campestris* IBSBF 1867	Palm oil	scl-PHA	6.43	0.05	Rodrigues et al. (2019)
Aeromonas hydrophila ATCC7966 + *Acinetobacter junii* BP25	Acetic acid + butyric acid	scl-PHA	2.64	N.A.	Anburajan et al. (2019)
Synechococcus elongatus cscB + *Pseudomonas putida cscAB*	CO_2	mcl-PHA	0.16	N.A.	Loewe et al. (2017)
Synechococcus elongatus PCC 7942+ *Escherichia coli*	CO_2	scl-PHA	N.A.	N.A.	Hays et al. (2017)
Synechococcus elongatus PCC 7942+ *Azotobacter vinelandii* AV3	CO_2	scl-PHA	N.A.	N.A.	Smith and Francis, (2016)

*Values were calculated based on visible data of the original paper with unified to two decimal places; * the yield coefficient is the ratio of the final PHA, titer to the substrate concentration consumed; N.A., not available.*

mcl-PHA from a mixed substrate comprising glucose and xylose based on the "nutrition supply–detoxification" concept (**Figure 1**). The artificial microbial consortium realized the production of mcl-PHA using "unrelated" carbon sources as substrates without the need for external FFAs. This microbial consortium can efficiently produce mcl-PHA with a maximum titer of 1.32 g/L (**Figure 7C**), and the yield (0.07 g/g) was increased nearly 2.3 times compared with the previous study (0.03 g/g) (**Table 1**). In addition, the properties of mcl-PHA can be referred the previous study (Liu et al., 2020), because the monomer compositions of the two are very similar. We further knocked out the *fadD* gene and heterologously expressed an acyl carrier protein thioesterase gene in the *E. coli* mutant strain, which improved the engineered *E. coli* to secrete acetic acid and FFAs. Enhancing the function of *E. coli* is critical for the accumulation of mcl-PHA by *P. putida* in the microbial consortium. Acetic acid and FFAs are used as intermediate metabolic substances between the two strains in the microbial consortium. The ability of *P. putida* to utilize acetic acid and FFAs will directly affect the overall productivity and the conversion efficiency of the initial substrate. Therefore, we weakened the fatty acid β-oxidation and enhanced the acetic acid assimilation pathways of *P. putida*, which increased the production of mcl-PHA and relieved the inhibition of bacterial growth caused by the accumulation of large amounts of acetic acid. However, acetic acid is less important for the intracellular accumulation of mcl-PHA by *P. putida* KT2240 than FFAs, which are the main substrate for PHA accumulation. Rerouting the carbon flux from fatty acid synthesis toward the synthesis of mcl-PHA is a potential strategy to improve the synthesis of mcl-PHA in strains using "unrelated" carbon sources such as acetic acid. In addition, *P. putida* could be further engineered a more ideal PHA production cell factory through various methods, including weakening competing pathways (Wang et al., 2011), strengthening the PHA synthesis pathway (Tobin et al., 2007), modifying the cell size (Liang et al., 2021), and eliminating PHA consumption (Cai et al., 2009). All these approaches can improve the overall production efficiency of mcl-PHA by the microbial consortium.

Competition between the two strains in the microbial consortium for glucose is inevitable. Therefore, we introduced an engineered *E. coli* that preferentially uses xylose. When the microbial consortium uses a composite substrate with a 1:1 mass ratio of glucose and xylose, it can still maintain stable production of mcl-PHA, which shows that the microbial consortium can effectively utilize xylose. This brings us further in the development of microbial consortia to expand the range of substrate utilization. Lignocellulose is the largest biomass resource in nature, and its main components include cellulose, hemicellulose, and lignin (Yang et al., 2007). Following hydrolysis, lignocellulosic biomass mainly yields glucose and a small amount of xylose. Lignocellulose has already been used in the synthesis of PHA (Sandhya et al., 2013; Kucera et al., 2018). The primary method is to convert lignocellulose into fermentable sugars through various ways and then use sugar components to carry out biological fermentation to synthesize PHA (de Souza et al., 2020). However, most studies produced the relatively low-value PHB, and there are few reports on the synthesis of mcl-PHA from lignocellulosic sugars. Researchers have introduced xylose utilization genes into *P. putida* KT2440 to construct an engineered strain that can use xylose to accumulate biomass, but it could not produce mcl-PHA (Le Meur et al., 2012). Here, we were able to use xylose directly through the microbial consortium, and the yield of mcl-PHA has been dramatically improved. Therefore, lignocellulose can be used as a potential substrate for microbial consortia. Using cheap lignocellulosic sugars as a carbon source reduces the production cost compared to fatty acids. Therefore, Using the microbial consortium as a microbial cell factory to produce mcl-PHA offers clear economic advantages.

The biosynthesis results of the co-cultures with different inoculation times have significant differences, indicating that the development of control strategies for fed-batch culture may boost the utilization of mixed sugars to an even higher

level, thus maximize the co-culture's capability of producing mcl-PHA. The two strains in the microbial consortium developed in this study have different substrate preferences, and there is a one-way energy transfer between them. Therefore, when scaling up the microbial consortium to fed-batch, according to the inoculation time verified in the previous period, we consider prioritizing the inoculation of *P. putida* and promoting the accumulation of *P. putida* biomass through the flow of glucose addition mode. Then, at a specific time, xylose was fed, and *E. coli* were inoculated simultaneously to secrete the intermediate metabolites acetic acid and FFAs. The right proportion and feed concentration of mixed sugars to maintain energy metabolism for growth, the secretion of intermediate metabolites, and product formation enable higher productivity of mcl-PHA in co-culture. What needs to be ensured is that the feed concentration should be sufficient to maintain the accumulation of mcl-PHA and not allow it to be decomposed by depolymerase. In addition, prolonging a particular phase of batch culture favors mcl-PHA formation due to the interaction between the two strains. For example, ensuring enough biomass of *P. putida*, optimizing the C/N ratio in the fed-batch stage to promote the secretion of intermediate metabolites may increase the synthesis of mcl-PHA. In short, this requires us to find an equilibrium between maximizing the synthesis of mcl-PHA and the threshold of mixed sugar ratio, feed concentration, and C/N ratio in the fed-batch co-culture phase.

CONCLUSION

We optimized a previously developed microbial consortium composed of engineered *E. coli* and *P. putida* to produce mcl-PHA from a mixed substrate of glucose and xylose. We knocked out the *fadD* gene in the genome of *E. coli* Δ4 and expressed an exogenous acyl carrier protein thioesterase gene. The resulting engineered *E. coli* Δ4D (T3) was fermented to produce acetic acid and FFAs with xylose as the sole carbon source, and it exhibited 3.0 and 4.0 fold higher titers than the wild-type bacteria, respectively. *P. putida* KTΔAB (p2-acs-phaJ) has an improved acetic acid assimilation pathway and fatty acid β-oxidation pathway, which enabled the synthesis of mcl-PHA from glucose, acetic acid, and FFAs, while solving the growth inhibition of *E. coli* caused by the accumulation of acetic acid in the culture broth. Finally, we conducted competition control and fermentation optimization for the microbial consortium. The two strains avoided substrate competition and formed a mutually beneficial symbiosis based on the concept of "nutrient supply-detoxification". The microbial consortium was able to effectively use the mixed substrate of glucose and xylose, the main components of lignocellulosic hydrolysates, to produce mcl-PHA, with a maximum titer of 1.32 g/L. This represents a notable 2.3-fold increase of the mcl-PHA yield compared with previous studies. The further development of the microbial consortium was effective in improving the efficiency of substrate conversion. These results demonstrated that the microbial consortium has excellent potential to produce mcl-PHA from lignocellulosic hydrolysates.

DATA AVAILABILITY STATEMENT

The original contributions presented in the study are included in the article/**Supplementary Material**, further inquiries can be directed to the corresponding author.

AUTHOR CONTRIBUTIONS

YZ and MA performed all experiments, analyzed the data, and wrote the manuscript. XJ conceived the idea, designed the experiments, and modified the manuscript.

FUNDING

The authors wish to acknowledge the financial support provided by the National Key Research and Development Program of China (Project No. 2018YFA0902100) and the National Natural Science Foundation of China (No. 22178262, No. 21576197).

ACKNOWLEDGMENTS

The authors are grateful for the kind donation of *Escherichia coli* MG1655, the plasmids pTKS/CS and pTKRED from Prof. Tao Chen at Tianjin University, and the plasmid pBBR1MCS-2 from Prof. Yingjin Yuan at Tianjin University.

SUPPLEMENTARY MATERIAL

The Supplementary Material for this article can be found online at: https://www.frontiersin.org/articles/10.3389/fbioe.2021.794331/full#supplementary-material

REFERENCES

Agapakis, C. M., Boyle, P. M., and Silver, P. A. (2012). Natural Strategies for the Spatial Optimization of Metabolism in Synthetic Biology. *Nat. Chem. Biol.* 8 (6), 527–535. doi:10.1038/nchembio.975

Agnew, D. E., and Pfleger, B. F. (2013). Synthetic Biology Strategies for Synthesizing Polyhydroxyalkanoates from Unrelated Carbon Sources. *Chem. Eng. Sci.* 103, 58–67. doi:10.1016/j.ces.2012.12.023

Anburajan, P., Naresh Kumar, A., Sabapathy, P. C., Kim, G.-B., Cayetano, R. D., Yoon, J.-J., et al. (2019). Polyhydroxy Butyrate Production by *Acinetobacter Junii* BP25, *Aeromonas Hydrophila* ATCC 7966, and Their Co-culture Using a Feast and Famine Strategy. *Bioresour. Technology* 293, 122062. doi:10.1016/j.biortech.2019.122062

Bhatia, S. K., Yoon, J.-J., Kim, H.-J., Hong, J. W., Gi Hong, Y., Song, H.-S., et al. (2018). Engineering of Artificial Microbial Consortia of *Ralstonia Eutropha* and *Bacillus Subtilis* for Poly(3-Hydroxybutyrate-Co-3-Hydroxyvalerate) Copolymer Production from Sugarcane Sugar

without Precursor Feeding. *Bioresour. Technology* 257, 92–101. doi:10.1016/j.biortech.2018.02.056

Borrero-de Acuña, J. M., Bielecka, A., Häussler, S., Schobert, M., Jahn, M., Wittmann, C., et al. (2014). Production of Medium Chain Length Polyhydroxyalkanoate in Metabolic Flux Optimized *Pseudomonas Putida*. *Microb. Cel Fact* 13. doi:10.1186/1475-2859-13-88

Cai, L., Yuan, M., Liu, F., Jian, J., and Chen, G. (2009). Enhanced Production of Medium-Chain-Length Polyhydroxyalkanoates (PHA) by PHA Depolymerase Knockout Mutant of *Pseudomonas Putida* KT2442. *Bioresour. Technology* 100 (7), 2265–2270. doi:10.1016/j.biortech.2008.11.020

Cavalheiro, J. M. B. T., Pollet, E., Diogo, H. P., Cesário, M. T., Avérous, L., de Almeida, M. C. M. D., et al. (2013). On the Heterogeneous Composition of Bacterial Polyhydroxyalkanoate Terpolymers. *Bioresour. Technology* 147, 434–441. doi:10.1016/j.biortech.2013.08.009

Chen, G.-Q., and Patel, M. K. (2012). Plastics Derived from Biological Sources: Present and Future: A Technical and Environmental Review. *Chem. Rev.* 112 (4), 2082–2099. doi:10.1021/cr200162d

Chen, G.-q., and Wang, Y. (2013). Medical Applications of Biopolyesters Polyhydroxyalkanoates. *Chin. J. Polym. Sci.* 31 (5), 719–736. doi:10.1007/s10118-013-1280-1

Chung, A.-L., Jin, H.-L., Huang, L.-J., Ye, H.-M., Chen, J.-C., Wu, Q., et al. (2011). Biosynthesis and Characterization of Poly(3-Hydroxydodecanoate) by β-Oxidation Inhibited Mutant of Pseudomonas Entomophila L48. *Biomacromolecules* 12 (10), 3559–3566. doi:10.1021/bm200770m

de Souza, L., Y., M., and Shivakumar, S. (2020). Bioconversion of Lignocellulosic Substrates for the Production of Polyhydroxyalkanoates. *Biocatal. Agric. Biotechnol.* 28, 101754. doi:10.1016/j.bcab.2020.101754

Eiteman, M. A., and Altman, E. (2006). Overcoming Acetate in *Escherichia coli* Recombinant Protein Fermentations. *Trends Biotechnol.* 24 (11), 530–536. doi:10.1016/j.tibtech.2006.09.001

Hays, S. G., Yan, L. L. W., Silver, P. A., and Ducat, D. C. (2017). Synthetic Photosynthetic Consortia Define Interactions Leading to Robustness and Photoproduction. *J. Biol. Eng.* 11. doi:10.1186/s13036-017-0048-5

Huang, L., Liu, C., Liu, Y., and Jia, X. (2016). The Composition Analysis and Preliminary Cultivation Optimization of a PHA-Producing Microbial Consortium with Xylose as a Sole Carbon Source. *Waste Management* 52, 77–85. doi:10.1016/j.wasman.2016.03.020

Huijberts, G. N., de Rijk, T. C., de Waard, P., and Eggink, G. (1994). 13C Nuclear Magnetic Resonance Studies of Pseudomonas Putida Fatty Acid Metabolic Routes Involved in Poly(3-Hydroxyalkanoate) Synthesis. *J. Bacteriol.* 176 (6), 1661–1666. doi:10.1128/jb.176.6.1661-1666.1994

Jayakrishnan, U., Deka, D., and Das, G. (2021). Waste as Feedstock for Polyhydroxyalkanoate Production from Activated Sludge: Implications of Aerobic Dynamic Feeding and Acidogenic Fermentation. *J. Environ. Chem. Eng.* 9 (4), 105550. doi:10.1016/j.jece.2021.105550

Jones, J. A., Vernacchio, V. R., Sinkoe, A. L., Collins, S. M., Ibrahim, M. H. A., Lachance, D. M., et al. (2016). Experimental and Computational Optimization of an *Escherichia coli* Co-culture for the Efficient Production of Flavonoids. *Metab. Eng.* 35, 55–63. doi:10.1016/j.ymben.2016.01.006

Jones, J. A., and Wang, X. (2018). Use of Bacterial Co-cultures for the Efficient Production of Chemicals. *Curr. Opin. Biotechnol.* 53, 33–38. doi:10.1016/j.copbio.2017.11.012

Kessler, B., and Witholt, B. (1998). Synthesis, Recovery and Possible Application of Medium-Chain-Length Polyhydroxyalkanoates: A Short Overview. *Macromol. Symp.* 130, 245–260. doi:10.1002/masy.19981300122

Klinke, S., Ren, Q., Witholt, B., and Kessler, B. (1999). Production of Medium-Chain-Length Poly(3-Hydroxyalkanoates) from Gluconate by Recombinant *Escherichia coli*. *Appl. Environ. Microbiol.* 65 (2), 540–548. doi:10.1128/aem.65.2.540-548.1999

Koning, G. d. (1995). Physical Properties of Bacterial poly((R)-3-hydroxyalkanoates). *Can. J. Microbiol.* 41 (13), 303–309. doi:10.1139/m95-201

Kucera, D., Pernicová, I., Kovalcik, A., Koller, M., Mullerova, L., Sedlacek, P., et al. (2018). Characterization of the Promising Poly(3-Hydroxybutyrate) Producing Halophilic Bacterium *Halomonas Halophila*. *Bioresour. Technology* 256, 552–556. doi:10.1016/j.biortech.2018.02.062

Le Meur, S., Zinn, M., Egli, T., Thöny-Meyer, L., and Ren, Q. (2012). Production of Medium-Chain-Length Polyhydroxyalkanoates by Sequential Feeding of Xylose and Octanoic Acid in Engineered *Pseudomonas Putida* KT2440. *BMC Biotechnol.* 12. doi:10.1186/1472-6750-12-53

Lee, S. Y. (1996). Bacterial Polyhydroxyalkanoates. *Biotechnol. Bioeng.* 49 (1), 1–14. doi:10.1002/(SICI)1097-0290(19960105)49:1<1:AID-BIT1>3.0.CO;2-P

Lee, S. Y. (2006). Deciphering Bioplastic Production. *Nat. Biotechnol.* 24 (10), 1227–1229. doi:10.1038/nbt1006-1227

Lemoigne, M. (1926). Produits de deshydration et de polymerisation de l'acide β-oxybutyrique. *Bull. Soc. Chim. Biol.* 8, 770–782.

Li, M., Ma, Y., Zhang, X., Zhang, L., Chen, X., Ye, J. W., et al. (2021). Tailor-Made Polyhydroxyalkanoates by Reconstructing Pseudomonas Entomophila. *Adv. Mater.* 33 (41), 2102766. doi:10.1002/adma.202102766

Li, M., Zhang, X., Agrawal, A., and San, K.-Y. (2012). Effect of Acetate Formation Pathway and Long Chain Fatty Acid CoA-Ligase on the Free Fatty Acid Production in *E. coli* Expressing Acy-ACP Thioesterase from Ricinus communis. *Metab. Eng.* 14 (4), 380–387. doi:10.1016/j.ymben.2012.03.007

Liang, P., Zhang, Y., Ma, T., and Yang, C. (2021). Improve the Ability of *Pseudomonas Putida* KT2440 Mutant KTU-U13 to Produce PHA by Regulating the Expression of Cell Morphology-Related Genes. *Acta Scientiarum Naturalium Universitatis Nankaiensis* 54 (2), 37–44.

Liang, Y.-S., Zhao, W., and Chen, G.-Q. (2008). Study on the Biocompatibility of Novel Terpolyester Poly(3-Hydroxybutyrate-Co-3-Hydroxyvalerate-Co-3-Hydroxyhexanoate). *J. Biomed. Mater. Res.* 87A (2), 441–449. doi:10.1002/jbm.a.31801

Lin, Z., Xu, Z., Li, Y., Wang, Z., Chen, T., and Zhao, X. (2014). Metabolic Engineering of *Escherichia coli* for the Production of Riboflavin. *Microb. Cel Fact* 13. doi:10.1186/s12934-014-0104-5

Liu, C., Wang, H., Xing, W., and Wei, L. (2013). Composition Diversity and Nutrition Conditions for Accumulation of Polyhydroxyalkanoate (PHA) in a Bacterial Community from Activated Sludge. *Appl. Microbiol. Biotechnol.* 97 (21), 9377–9387. doi:10.1007/s00253-013-5165-6

Liu, Q., Luo, G., Zhou, X. R., and Chen, G.-Q. (2011). Biosynthesis of Poly(3-Hydroxydecanoate) and 3-hydroxydodecanoate Dominating Polyhydroxyalkanoates by β-oxidation Pathway Inhibited Pseudomonas Putida. *Metab. Eng.* 13 (1), 11–17. doi:10.1016/j.ymben.2010.10.004

Liu, X., Li, X.-B., Jiang, J., Liu, Z.-N., Qiao, B., Li, F.-F., et al. (2018a). Convergent Engineering of Syntrophic *Escherichia coli* Coculture for Efficient Production of Glycosides. *Metab. Eng.* 47, 243–253. doi:10.1016/j.ymben.2018.03.016

Liu, Y., Tu, X., Xu, Q., Bai, C., Kong, C., Liu, Q., et al. (2018b). Engineered Monoculture and Co-culture of Methylotrophic Yeast for De Novo Production of Monacolin J and Lovastatin from Methanol. *Metab. Eng.* 45, 189–199. doi:10.1016/j.ymben.2017.12.009

Liu, Y., Yang, S., and Jia, X. (2020). Construction of a "nutrition Supply-Detoxification" Coculture Consortium for Medium-Chain-Length Polyhydroxyalkanoate Production with a Glucose-Xylose Mixture. *J. Ind. Microbiol. Biotechnol.* 47 (3), 343–354. doi:10.1007/s10295-020-02267-7

Löwe, H., Hobmeier, K., Moos, M., Kremling, A., and Pflüger-Grau, K. (2017). Photoautotrophic Production of Polyhydroxyalkanoates in a Synthetic Mixed Culture of *Synechococcus Elongatus* cscB and *Pseudomonas Putida* cscAB. *Biotechnol. Biofuels* 10. doi:10.1186/s13068-017-0875-0

Ma, L., Zhang, H., Liu, Q., Chen, J., Zhang, J., and Chen, G.-Q. (2009). Production of Two Monomer Structures Containing Medium-Chain-Length Polyhydroxyalkanoates by β-oxidation-impaired Mutant of Pseudomonas Putida KT2442. *Bioresour. Technology* 100 (20), 4891–4894. doi:10.1016/j.biortech.2009.05.017

Misra, S. K., Valappil, S. P., Roy, I., and Boccaccini, A. R. (2006). Polyhydroxyalkanoate (PHA)/inorganic Phase Composites for Tissue Engineering Applications. *Biomacromolecules* 7 (8), 2249–2258. doi:10.1021/bm060317c

Morgan-Sagastume, F., Hjort, M., Cirne, D., Gérardin, F., Lacroix, S., Gaval, G., et al. (2015). Integrated Production of Polyhydroxyalkanoates (PHAs) with Municipal Wastewater and Sludge Treatment at Pilot Scale. *Bioresour. Technology* 181, 78–89. doi:10.1016/j.biortech.2015.01.046

Muneer, F., Rasul, I., Azeem, F., Siddique, M. H., Zubair, M., and Nadeem, H. (2020). Microbial Polyhydroxyalkanoates (PHAs): Efficient Replacement of Synthetic Polymers. *J. Polym. Environ.* 28 (9), 2301–2323. doi:10.1007/s10924-020-01772-1

Poblete-Castro, I., Binger, D., Rodrigues, A., Becker, J., Martins dos Santos, V. A. P., and Wittmann, C. (2013). In-silico-driven Metabolic Engineering of

Pseudomonas Putida for Enhanced Production of Poly-Hydroxyalkanoates. *Metab. Eng.* 15, 113–123. doi:10.1016/j.ymben.2012.10.004

Raza, Z. A., Abid, S., and Banat, I. M. (2018). Polyhydroxyalkanoates: Characteristics, Production, Recent Developments and Applications. *Int. Biodeterioration Biodegradation* 126, 45–56. doi:10.1016/j.ibiod.2017.10.001

Rebocho, A. T., Pereira, J. R., Neves, L. A., Alves, V. D., Sevrin, C., Grandfils, C., et al. (2020). Preparation and Characterization of Films Based on a Natural P(3HB)/mcl-PHA Blend Obtained through the Co-culture of *Cupriavidus Necator* and *Pseudomonas Citronellolis* in Apple Pulp Waste. *Bioengineering* 7 (2), 34. doi:10.3390/bioengineering7020034

Rodrigues, P. R., Assis, D. J., and Druzian, J. I. (2019). Simultaneous Production of Polyhydroxyalkanoate and Xanthan Gum: From Axenic to Mixed Cultivation. *Bioresour. Technology* 283, 332–339. doi:10.1016/j.biortech.2019.03.095

Salas, J. J., and Ohlrogge, J. B. (2002). Characterization of Substrate Specificity of Plant FatA and FatB Acyl-ACP Thioesterases. *Arch. Biochem. Biophys.* 403 (1), 25–34. doi:10.1016/s0003-9861(02)00017-6

Salvachúa, D., Rydzak, T., Auwae, R., De Capite, A., Black, B. A., Bouvier, J. T., et al. (2020). Metabolic Engineering of *Pseudomonas Putida* for Increased Polyhydroxyalkanoate Production from Lignin. *Microb. Biotechnol.* 13 (1), 290–298. doi:10.1111/1751-7915.13481

Sandhya, M., Aravind, J., and Kanmani, P. (2013). Production of Polyhydroxyalkanoates from *Ralstonia Eutropha* Using Paddy Straw as Cheap Substrate. *Int. J. Environ. Sci. Technol.* 10 (1), 47–54. doi:10.1007/s13762-012-0070-6

Sawant, S. S., Salunke, B. K., and Kim, B. S. (2017). Enhanced Agarose and Xylan Degradation for Production of Polyhydroxyalkanoates by Co-culture of Marine Bacterium, Saccharophagus Degradans and its Contaminant, Bacillus Cereus. *Appl. Sci.* 7 (3), 225. doi:10.3390/app7030225

Singh, A. K., and Mallick, N. (2009). Exploitation of Inexpensive Substrates for Production of a Novel SCL-LCL-PHA Co-polymer by *Pseudomonas aeruginosa* MTCC 7925. *J. Ind. Microbiol. Biotechnol.* 36 (3), 347–354. doi:10.1007/s10295-008-0503-x

Smith, M. J., and Francis, M. B. (2016). A Designed *A. Vinelandii-S. Elongatus* Coculture for Chemical Photoproduction from Air, Water, Phosphate, and Trace Metals. *ACS Synth. Biol.* 5 (9), 955–961. doi:10.1021/acssynbio.6b00107

Tobin, K. M., O'Leary, N. D., Dobson, A. D. W., and O'Connor, K. E. (2007). Effect of Heterologous Expression ofphaG[(R)-3-hydroxyacyl-ACP-CoA Transferase] on Polyhydroxyalkanoate Accumulation from the Aromatic Hydrocarbon Phenylacetic Acid inPseudomonasspecies. *Fems Microbiol. Lett.* 268 (1), 9–15. doi:10.1111/j.1574-6968.2006.00607.x

Tortajada, M., da Silva, L. F., and Prieto, M. A. (2013). Second-generation Functionalized Medium-Chain-Length Polyhydroxyalkanoates: the Gateway to High-Value Bioplastic Applications. *Int. Microbiol.* 16 (1), 1–15. doi:10.2436/20.1501.01.175

Valentino, F., Morgan-Sagastume, F., Fraraccio, S., Corsi, G., Zanaroli, G., Werker, A., et al. (2015). Sludge Minimization in Municipal Wastewater Treatment by Polyhydroxyalkanoate (PHA) Production. *Environ. Sci. Pollut. Res.* 22 (10), 7281–7294. doi:10.1007/s11356-014-3268-y

Voelker, T. A., and Davies, H. M. (1994). Alteration of the Specificity and Regulation of Fatty Acid Synthesis of *Escherichia coli* by Expression of a Plant Medium-Chain Acyl-Acyl Carrier Protein Thioesterase. *J. Bacteriol.* 176 (23), 7320–7327. doi:10.1128/jb.176.23.7320-7327.1994

Wang, H.-h., Li, X.-t., and Chen, G.-Q. (2009). Production and Characterization of Homopolymer Polyhydroxyheptanoate (P3HHp) by a *fadBA* Knockout Mutant *Pseudomonas Putida* KTOY06 Derived from *P. Putida* KT2442. *Process Biochem.* 44 (1), 106–111. doi:10.1016/j.procbio.2008.09.014

Wang, H.-h., Zhou, X.-r., Liu, Q., and Chen, G.-Q. (2011). Biosynthesis of Polyhydroxyalkanoate Homopolymers by *Pseudomonas Putida*. *Appl. Microbiol. Biotechnol.* 89 (5), 1497–1507. doi:10.1007/s00253-010-2964-x

Wang, Q., and Nomura, C. T. (2010). Monitoring Differences in Gene Expression Levels and Polyhydroxyalkanoate (PHA) Production in *Pseudomonas Putida* KT2440 Grown on Different Carbon Sources. *J. Biosci. Bioeng.* 110 (6), 653–659. doi:10.1016/j.jbiosc.2010.08.001

Yang, H., Yan, R., Chen, H., Lee, D. H., and Zheng, C. (2007). Characteristics of Hemicellulose, Cellulose and Lignin Pyrolysis. *Fuel* 86 (12-13), 1781–1788. doi:10.1016/j.fuel.2006.12.013

Yang, S., Li, S., and Jia, X. (2019). Production of Medium Chain Length Polyhydroxyalkanoate from Acetate by Engineered *Pseudomonas Putida* KT2440. *J. Ind. Microbiol. Biotechnol.* 46 (6), 793–800. doi:10.1007/s10295-019-02159-5

Yuan, L., Voelker, T. A., and Hawkins, D. J. (1995). Modification of the Substrate Specificity of an Acyl-Acyl Carrier Protein Thioesterase by Protein Engineering. *Proc. Natl. Acad. Sci.* 92 (23), 10639–10643. doi:10.1073/pnas.92.23.10639

Zhang, H., Li, Z., Pereira, B., and Stephanopoulos, G. (2015). Engineering E. coli-E. coli Cocultures for Production of Muconic Acid from Glycerol. *Microb. Cel Fact* 14. doi:10.1186/s12934-015-0319-0

Zhang, H., and Stephanopoulos, G. (2016). Co-culture Engineering for Microbial Biosynthesis of 3-amino-benzoic Acid in *Escherichia coli*. *Biotechnol. J.* 11 (7), 981–987. doi:10.1002/biot.201600013

Zhang, H., and Wang, X. (2016). Modular Co-culture Engineering, a New Approach for Metabolic Engineering. *Metab. Eng.* 37, 114–121. doi:10.1016/j.ymben.2016.05.007

Zhang, X., Li, M., Agrawal, A., and San, K.-Y. (2011). Efficient Free Fatty Acid Production in *Escherichia coli* Using Plant Acyl-ACP Thioesterases. *Metab. Eng.* 13 (6), 713–722. doi:10.1016/j.ymben.2011.09.007

Zhao, F., He, F., Liu, X., Shi, J., Liang, J., Wang, S., et al. (2020). Metabolic Engineering of *Pseudomonas Mendocina* NK-01 for Enhanced Production of Medium-Chain-Length Polyhydroxyalkanoates with Enriched Content of the Dominant Monomer. *Int. J. Biol. Macromolecules* 154, 1596–1605. doi:10.1016/j.ijbiomac.2019.11.044

Zhao, K., Deng, Y., and Chen, G. Q. (2003a). Effects of Surface Morphology on the Biocompatibility of Polyhydroxyalkanoates. *Biochem. Eng. J.* 16 (2), 115–123. doi:10.1016/s1369-703x(03)00029-9

Zhao, K., Deng, Y., Chun Chen, J., and Chen, G.-Q. (2003b). Polyhydroxyalkanoate (PHA) Scaffolds with Good Mechanical Properties and Biocompatibility. *Biomaterials* 24 (6), 1041–1045. doi:10.1016/s0142-9612(02)00426-x

Zhao, K., Yang, X., Chen, G.-Q., and Chen, J.-C. (2002). Effect of Lipase Treatment on the Biocompatibility of Microbial Polyhydroxyalkanoates. *J. Mater. Science-Materials Med.* 13 (9), 849–854. doi:10.1023/a:1016596228316

Zhuang, Q., Wang, Q., Liang, Q., and Qi, Q. (2014). Synthesis of Polyhydroxyalkanoates from Glucose that Contain Medium-Chain-Length Monomers via the Reversed Fatty Acid β-oxidation Cycle in *Escherichia coli*. *Metab. Eng.* 24, 78–86. doi:10.1016/j.ymben.2014.05.004

Conflict of Interest: The authors declare that the research was conducted in the absence of any commercial or financial relationships that could be construed as a potential conflict of interest.

Publisher's Note: All claims expressed in this article are solely those of the authors and do not necessarily represent those of their affiliated organizations, or those of the publisher, the editors and the reviewers. Any product that may be evaluated in this article, or claim that may be made by its manufacturer, is not guaranteed or endorsed by the publisher.

frontiers in Bioengineering and Biotechnology

ORIGINAL RESEARCH
published: 13 January 2022
doi: 10.3389/fbioe.2021.808258

Enhanced 3-Hydroxypropionic Acid Production From Acetate *via* the Malonyl-CoA Pathway in *Corynebacterium glutamicum*

Zhishuai Chang[1†], Wei Dai[1†], Yufeng Mao[1,2], Zhenzhen Cui[1], Zhidan Zhang[2], Zhiwen Wang[1], Hongwu Ma[2] and Tao Chen[1]**

[1]*Frontier Center for Synthetic Biology and Key Laboratory of Systems Bioengineering of the Ministry of Education, School of Chemical Engineering and Technology, Department of Biochemical Engineering and Technology, Tianjin University, Tianjin, China,* [2]*Key Laboratory of Systems Microbial Biotechnology, Tianjin Institute of Industrial Biotechnology, Chinese Academy of Sciences, Tianjin, China*

OPEN ACCESS

Edited by:
Shuobo Shi,
Beijing University of Chemical Technology, China

Reviewed by:
Hui Wu,
East China University of Science and Technology, China
Yunying Zhao,
Jiangnan University, China

***Correspondence:**
Hongwu Ma
ma_hw@tib.cas.cn
Tao Chen
chentao@tju.edu.cn

†These authors have contributed equally to this work and share first authorship

Specialty section:
This article was submitted to Synthetic Biology, a section of the journal Frontiers in Bioengineering and Biotechnology

Received: *03 November 2021*
Accepted: *16 December 2021*
Published: *13 January 2022*

Citation:
Chang Z, Dai W, Mao Y, Cui Z, Zhang Z, Wang Z, Ma H and Chen T (2022) Enhanced 3-Hydroxypropionic Acid Production From Acetate via the Malonyl-CoA Pathway in Corynebacterium glutamicum. Front. Bioeng. Biotechnol. 9:808258. doi: 10.3389/fbioe.2021.808258

Acetate is an economical and environmental-friendly alternative carbon source. Herein, the potential of harnessing *Corynebacterium glutamicum* as a host to produce 3-hydroxypropionic acid (3-HP) from acetate was explored. First, the expression level of malonyl-CoA reductase from *Chloroflexus aurantiacus* was optimized through several strategies, strain Cgz2/sod-N-C* showed an MCR enzyme activity of 63 nmol/mg/min and a 3-HP titer of 0.66 g/L in flasks. Next, the expression of citrate synthase in Cgz2/sod-N-C* was weakened to reduce the acetyl-CoA consumption in the TCA cycle, and the resulting strain Cgz12/sod-N-C* produced 2.39 g/L 3-HP from 9.32 g/L acetate. However, the subsequent deregulation of the expression of acetyl-CoA carboxylase genes in Cgz12/sod-N-C* resulted in an increased accumulation of intracellular fatty acids, instead of 3-HP. Accordingly, cerulenin was used to inhibit fatty acid synthesis in Cgz14/sod-N-C*, and its 3-HP titer was further increased to 4.26 g/L, with a yield of 0.50 g 3-HP/g-acetate. Finally, the engineered strain accumulated 17.1 g/L 3-HP in a bioreactor without cerulenin addition, representing the highest titer achieved using acetate as substrate. The results demonstrated that *Corynebacterium glutamicum* is a promising host for 3-HP production from acetate.

Keywords: 3-hydroxypropionic acid, acetate, *Corynebacterium glutamicum*, metabolomics analysis, fed-batch fermentation, metabolic engineering, malonyl-CoA pathway

INTRODUCTION

3-Hydroxypropionic acid (3-HP) is an important chemical raw material. It has been broadly used in agriculture, food, and materials (Schwarz et al., 2004), which could be attributed to its capability to produce various chemicals like 1,3-propanediol and acrylic acid (Kumar et al., 2013) and its significant market value. It is worth mentioning that 3-HP has been listed as one of the top high value-added chemicals for development both in 2004 and 2010 by the U.S. Department of Energy (Werpy et al., 2004; Bozell and Petersen, 2010). Bioconversion of 3-HP has already been extensively

Abbreviations: MCR, malonyl-CoA reductase; TCA, tricarboxylic, acid; CS, citrate synthase; ACC, acetyl-CoA carboxylase.

TABLE 1 | 3-HP titers and yields of different substrates.

Organism	Carbon source	Operational technique	Titer (g/L)	Yield (g/g)	References
Corynebacterium glutamicum[a]	Glucose	Fed-batch, 5-L bioreactor	62.6	0.51	Chen et al. (2017)
Klebsiella pneumoniae[a]	Glycerol	Fed-batch, 5-L bioreactor	102.6	-	Zhao et al. (2019)
Escherichia coli[a]	Acetate	Whole-cell biocatalysis	15.8	0.71	Lai et al. (2021)
Corynebacterium glutamicum[a]	Acetate	Fed-batch, 5-L bioreactor	17.1	0.10	This study
Halomonas bluephagenesis[a]	1,3-Propanediol	Fed-batch, 7-L bioreactor	154	0.93	Jiang et al. (2021)
Escherichia coli[a]	Fatty acids	Fed-batch, 5-L bioreactor	52	1.56	Liu et al. (2019)

[a]*Engineered microorganisms.*

studied in many organisms, such as *Escherichia coli*, *Klebsiella pneumoniae*, and *Saccharomyces cerevisiae* (Rathnasingh et al., 2010; Chen et al., 2014; Zhao et al., 2019), and a variety of substrates have been exploited to produce 3-HP (**Table 1**). So far, the highest 3-HP titer was achieved in *Halomonas bluephagenesis*, which accumulated 154 g/L 3-HP in a 7-L bioreactor using 1,3-propanediol as substrate (Jiang et al., 2021). *Corynebacterium glutamicum* is generally recognized as safe (GRAS) with strong robustness (Richmond, 1999), which is also endowed with a broad spectrum of substrates such as xylose, glycerol, and starch (Gopinath et al., 2011). Meanwhile, it has been successfully exploited to produce various kinds of valuable chemicals, like L-glutamate, L-lysine, succinate, and acetoin with high productivities, some of which have been industrialized (Becker and Wittmann, 2012; Mao et al., 2017; Mao et al., 2018; Lu et al., 2020).

Acetic acid, a kind of non-food resource, has attracted much attention until now. It could be produced both from cheap chemical synthesis and wasted organic raw materials, which makes it a green and recyclable substrate. Although acetate is toxic and unfavorable for many microorganisms as substrate, it has been exploited to produce various kinds of organic acids such as succinate (Niu et al., 2018), itaconic acid (Noh et al., 2018), and 3-HP (Lee et al., 2018). It is worth mentioning that acetate could act as the sole carbon source in *C. glutamicum* ATCC 13032, when more than 6-fold of acetyl-CoA would be accumulated compared to glucose (Wendisch et al., 1997; Wendisch et al., 2000), which would be advantageous for 3-HP production through the malonyl-CoA pathway. Currently, only few research studies have focused on 3-HP production via acetate, the majority of which used *E. coli* as the host. Lee et al. (2018) modified an *E. coli* strain for 3-HP production, and it could produce 3 g/L 3-HP from 8.98 g/L acetate in shake flasks. A recombinant *E. coli* strain produced 7.3 g/L 3-HP with a yield of 0.39 g-3-HP/g-acetate in a 2.5-L bioreactor, using a two-stage strategy whereby glucose was used for cell growth and acetate for 3-HP formation (Lama et al., 2021). Recently, a whole-cell biocatalysis method was used for 3-HP production from acetate by using an engineered *E. coli* strain LNY07(M*DA), and 15.8 g/L 3-HP was produced with a yield of 0.71 g-3-HP/g-acetate (Lai et al., 2021). These studies proved the feasibility of 3-HP production from acetate.

In our previous study, it was demonstrated that *C. glutamicum* is a promising 3-HP producer which produced 3.77 g/L 3-HP from a mixture of glucose and acetate via the malonyl-CoA pathway with cerulenin addition (Chang et al., 2020). In this study, we aimed to enhance the ability of *C. glutamicum* to efficiently produce 3-HP using acetate as the sole substrate (**Figure 1**). First, the expression level of malonyl-CoA reductase (MCR) was optimized to increase its activity and 3-HP accumulation in strain Cgz2. Second, gradient weakening of the expression level of citrate synthase (CS) was undertaken to save more acetyl-CoA for malonyl-CoA formation. Afterward, deregulation of acetyl-CoA carboxylase (ACC) was performed in order to increase the synthesis of malonyl-CoA. Meanwhile, metabolomics analysis was conducted to shed light on the changes of key intracellular metabolites among the engineered strains. Based on these strategies, the best strain Cgz14/sod-N-C* accumulated 4.26 g/L 3-HP with a yield of 0.50 g/g-acetate in flask cultivation with cerulenin addition. In fed-batch cultivation, the strain produced 17.1 g/L 3-HP in a 5-L bioreactor without addition of cerulenin. As far as we know, this is the highest 3-HP titer achieved by fed-batch fermentation using acetate as substrate.

MATERIALS AND METHODS

Construction of Plasmids and *C. glutamicum* Mutant Strains

The original strain was *C. glutamicum* ATCC 13032. All the plasmids and strains used in this study are listed in **Table 2**. All primers used in this study are listed in **Supplementary Table S1**. *E. coli* DH5α was used as the host for plasmid construction. All DNA manipulations including restriction enzyme digestion and vector isolation were carried out using standard protocols. The *mcr* gene encoding MCR (NCBI-protein ID: AAS20429.1) was synthesized by GENEWIZ (Suzhou, China), and three reported point mutations (N940V, K1106W, S1114R) were introduced to increase enzyme activity (Liu et al., 2016). To construct plasmid pEC-*mcr*, gene *mcr* was amplified by PCR, followed by digesting and ligating to corresponding sites of vector pEC-XK99E. Plasmids pEC-*mcr**, pEC-N-C, pEC-N-C*, and pEC-C*-N were constructed analogously. To construct plasmid pEC-mbp-*mcr**, gene *mcr** was amplified with a forward primer containing mbp sequence, after which the resulting fragment was digested and ligated to corresponding sites of vector pEC-XK99E. Plasmid pEC-his-*mcr** was constructed analogously. To construct plasmid pEC-sod-N-C*, the promoter and RBS sequence of gene *sod* were amplified from the *C. glutamicum*

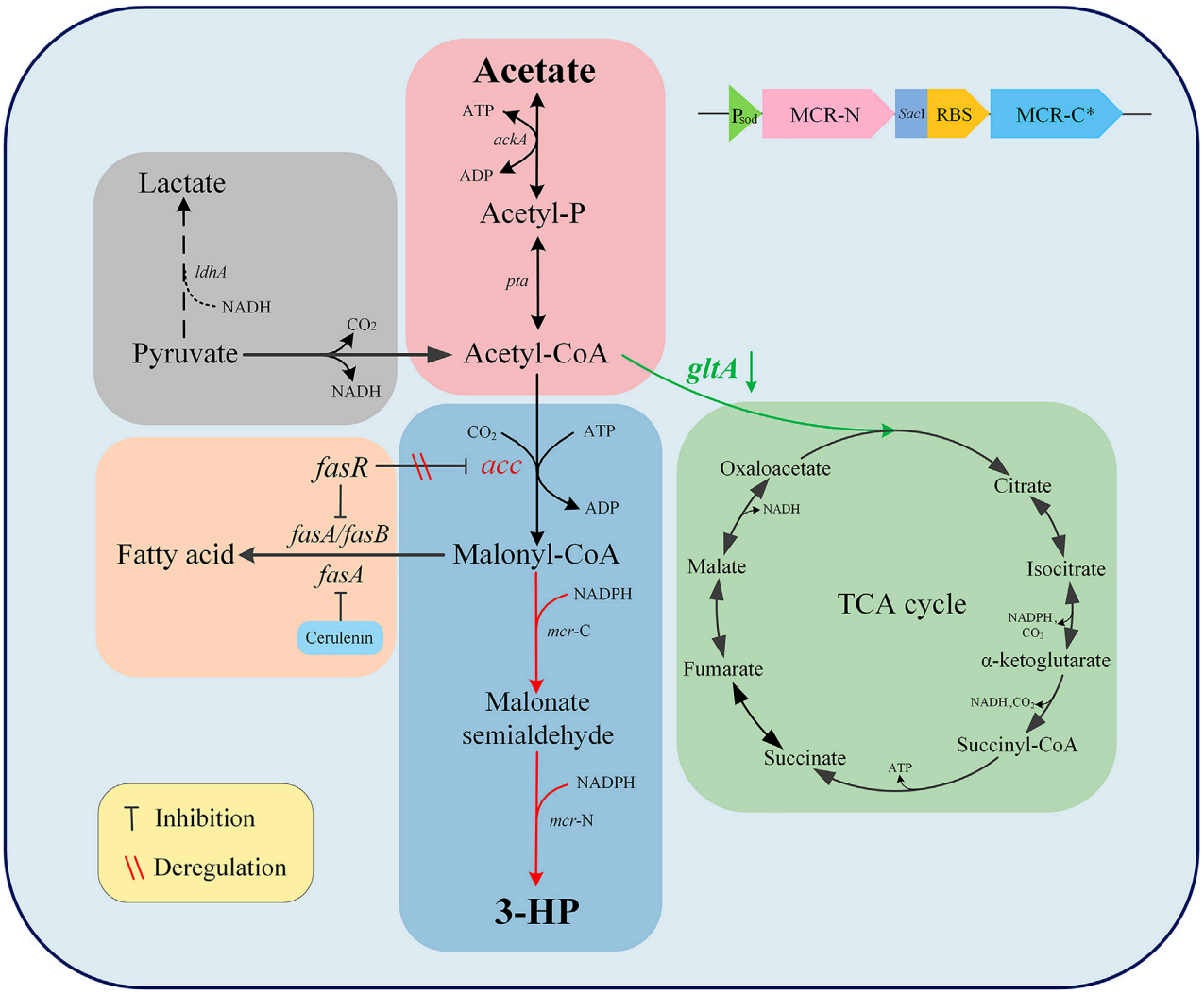

FIGURE 1 | Schematic diagram of 3-HP biosynthetic route in *Corynebacterium glutamicum via* acetate assimilation. Black arrows indicate the native pathways of *C. glutamicum*, red arrows indicate genes which were overexpressed or introduced, green arrows indicate genes which were weakened, and dotted arrows indicate genes which were deleted. Acetyl-P, acetyl phosphate; 3-HP, 3-hydroxypropionic acid; *ldhA*, lactate dehydrogenase; *ackA*, acetate kinase A; *pta*, acetyl phosphate transferase; *acc*, acetyl-CoA carboxylase; *mcr*-C, C-terminal of malonyl-CoA reductase; *mcr*-N, N-terminal of malonyl-CoA reductase; *fasA*, fatty acid synthetase A; *fasB*, fatty acid synthetase B; *fasR*, fatty acid repressor; *gltA*, citrate synthase.

ATCC 13032 genome and fused with the N-C* sequence which was amplified from pEC-N-C*. The resulting fragment and the linear fragment of pEC-XK99E without promoter P_{trc} and gene *lacIq* were digested and ligated to construct the vector. The plasmid pEC-H36-N-C* was constructed analogously. To construct plasmid pEC-sod*-mbp-N-C*, N-C* sequence was amplified with a forward primer containing mbp sequence. The resulting fragment, along with the linear fragment of pEC-sod-N-C*, was digested and ligated to construct the vector. All constructs used the RBS sequence AAAGGAGGACAACC, except for genes placed right behind P_{sod}, whose RBS sequences were the same as that of gene *sod* in *C. glutamicum* ATCC 13032. Plasmids without promoter substitution need isopropyl-β-D-1-thiogalactopyranoside (IPTG) to induce expression.

Genome editing of *C. glutamicum* was achieved via a two-step homologous recombination using suicide plasmid pD-*sacB*. For replacing the native promoter of *gltA*, the vector pD-*sacB*-P1-*gltA* was constructed as follows: Both the upstream and downstream sequences of *gltA* promoter were amplified by PCR and fused with promoter P1, followed by digesting and ligating to corresponding sites of vector pD-*sacB*. The plasmids pD-*sacB*-P5-*gltA* and pD-*sacB*-P7-*gltA* were constructed analogously.

To introduce mutations into *fasO* sites of *accBC* and *accD1*, the vector pD-*sacB*-*fasO*(M)-*accBC* was constructed as follows: the flanking regions of the *fasO* site of *accBC* with relevant modifications were amplified and fused using PCR, after which the fused fragment was digested and ligated to corresponding sites of vector pD-*sacB*. The plasmid pD-*sacB*-*fasO*(M)-*accD1* was constructed analogously.

TABLE 2 | Bacterial strains and plasmids used in this study.

Strains and plasmids	Description	Source
Strains		
Escherichia coli DH5α	Host for plasmid construction	Invitrogen
ATCC 13032	*C. glutamicum* wild type, biotin auxotrophic	ATCC[a]
Cgz2	ATCC 13032 Δ*ldhA*	Zhu et al. (2014)
Cgz8	Cgz2 P1-*gltA*	This study
Cgz9	Cgz2 P5 *gltA*	This study
Cgz10	Cgz2 P7-*gltA*	This study
Cgz11	Cgz8 with the replacement of *gltA* initiation codon ATG by GTG	This study
Cgz12	Cgz8 with the replacement of *gltA* initiation codon ATG by TTG	This study
Cgz13	Cgz2 with mutated *fasO* sequences upstream of *accBC* and *accD1*	This study
Cgz14	Cgz12 with mutated *fasO* sequences upstream of *accBC* and *accD1*	This study
Cgz2/*mcr*	Cgz2 harboring plasmid pEC-*mcr*	This study
Cgz2/*mcr**	Cgz2 harboring plasmid pEC-*mcr**	This study
Cgz2/mbp-*mcr**	Cgz2 harboring plasmid pEC-mbp-*mcr**	This study
Cgz2/his-*mcr**	Cgz2 harboring plasmid pEC-his-*mcr**	This study
Cgz2/N-C	Cgz2 harboring plasmid pEC-N-C	This study
Cgz2/N-C*	Cgz2 harboring plasmid pEC-N-C*	This study
Cgz2/C*-N	Cgz2 harboring plasmid pEC-C*-N	This study
Cgz2/H36-N-C*	Cgz2 harboring plasmid pEC-H36-N-C*	This study
Cgz2/sod-N-C*	Cgz2 harboring plasmid pEC-sod-N-C*	This study
Cgz2/sod-mbp-N-C*	Cgz2 harboring plasmid pEC-sod-mbp-N-C*	This study
Cgz8/sod-N-C*	Cgz8 harboring plasmid pEC-sod-N-C*	This study
Cgz9/sod-N-C*	Cgz9 harboring plasmid pEC-sod-N-C*	This study
Cgz10/sod-N-C*	Cgz10 harboring plasmid pEC-sod-N-C*	This study
Cgz11/sod-N-C*	Cgz11 harboring plasmid pEC-sod-N-C*	This study
Cgz12/sod-N-C*	Cgz12 harboring plasmid pEC-sod-N-C*	This study
Cgz13/sod-N-C*	Cgz13 harboring plasmid pEC-sod-N-C*	This study
Cgz14/sod-N-C*	Cgz14 harboring plasmid pEC-sod-N-C*	This study
Plasmids		
pEC-XK99E	Kan^{R} [b], *E. coli/C. glutamicum* shuttle vector	Kirchner and Tauch (2003)
pEC-*mcr*	Kan^{R}, pEC-XK99E containing gene *mcr* from *C. aurantiacus* (codon optimized)	This study
pEC-*mcr**	Kan^{R}, pEC-XK99E containing mutated gene *mcr* (N940V K1106W S1114R)	This study
pEC-mbp-*mcr**	Kan^{R}, pEC-*mcr** with mbp tag sequence inserted between promoter and RBS	This study
pEC-his-*mcr**	Kan^{R}, pEC-*mcr** with his tag sequence inserted between promoter and RBS	This study
pEC-N-C	Kan^{R}, pEC-XK99E containing separated *mcr* gene, *mcr*-N and *mcr*-C	This study
pEC-N-C*	Kan^{R}, pEC-N-C with mutated *mcr*-C	This study
pEC-C*-N	Kan^{R}, pEC-N-C* with the order of *mcr*-C* and *mcr*-N exchanged	This study
pEC-H36-N-C*	Kan^{R}, pEC-N-C* with P_{trc} substituted by P_{H36}	This study
pEC-sod-N-C*	Kan^{R}, pEC-N-C* with P_{trc} substituted by P_{sod}	This study
pEC-sod-mbp-N-C*	Kan^{R}, pEC-sod-N-C* with mbp tag sequence inserted between promoter and RBS	This study
pEC-mbp-N-C*	Kan^{R}, pEC-N-C* with mbp tag sequence inserted between promoter and RBS	This study
pD-*sacB*	Kan^{R}, vector for in-frame deletion	Zhu et al. (2013)
pD-*sacB*-P1-*gltA*	pD-*sacB* containing P_{P1} and *gltA* flanks	This study
pD-*sacB*-P5-*gltA*	pD-*sacB* containing P_{P5} and *gltA* flanks	This study
pD-*sacB*-P7-*gltA*	pD-*sacB* containing P_{P7} and *gltA* flanks	This study
pD-*sacB*-P1-GTG-*gltA*	pD-*sacB*-P1-*gltA* with translation initiation codon ATG substituted by GTG	This study
pD-*sacB*-P1-TTG-*gltA*	pD-*sacB*-P1-*gltA* with translation initiation codon ATG substituted by TTG	This study
pD-*sacB*-*fasO*(M)-*accBC*	pD-*sacB* containing the flanking sequences of *fasO* site upstream of *accBC* for mutating *fasO*	This study
pD-*sacB*-*fasO*(M)-*accD1*	pD-*sacB* containing the flanking sequences of *fasO* site upstream of *accD1* for mutating *fasO*	This study

[a]*American Type Culture Collection.*
[b]*Kanamycin resistance.*

Culture Conditions

For the cultivation of the plasmid host, *E. coli* DH5α was incubated at 37°C and 220 rpm in test tubes containing 5 ml LB medium; 40 μg/ml kanamycin was added to the medium if needed.

For the shake flask cultivation of various recombinant *C. glutamicum* strains, a single colony was used to inoculate 5 ml BHI broth (74 g/L) in a test tube for overnight pre-cultivation, after which 1 ml of the seed was used to inoculate 50 ml CGIII medium (10 g/L yeast extract, 10 g/L tryptone, 21 g/L MOPS, 2.5 g/L NaCl, pH 7.0) with 20 g/L glucose in a 250-ml flask. When OD_{600} reached 15–20, the culture was used to inoculate 50 ml CGXII-YA medium (10 g/L yeast extract, 14 g/L sodium acetate, 20 g/L $(NH_4)_2SO_4$, 5 g/L urea, 1 g/L KH_2PO_4, 1 g/L K_2HPO_4,

0.25 g/L $MgSO_4·7H_2O$, 21 g/L MOPS, 10 mg/L $CaCl_2$, 10 mg/L $FeSO_4·7H_2O$, 0.1 mg/L $ZnSO_4·7H_2O$, 0.2 mg/L $CuSO_4·5H_2O$, 20 μg/L $NiCl_2·H_2O$, 0.2 mg/L biotin, pH 7.0) in a 250-ml flask to an initial OD_{600} of 0.5. Then 25 μg/ml kanamycin and 1 mM isopropyl-β-D-1-thiogalactopyranoside (IPTG) at 0 h were added to the medium if needed. And 15 μM cerulenin was added to the medium at 12 h if needed. All fermentations were performed at 30°C and 220 rpm.

The seed used for fed-batch cultivation was prepared in the same way, and 200 ml seed cultured in CGIII medium was used to inoculate CGXII-YB medium (20 g/L yeast extract, 1.4 g/L sodium acetate, 20 g/L $(NH_4)_2SO_4$, 5 g/L urea, 1 g/L KH_2PO_4, 1 g/L K_2HPO_4, 0.25 g/L $MgSO_4·7H_2O$, 10 mg/L $CaCl_2$, 10 mg/L $FeSO_4·7H_2O$, 0.1 mg/L $ZnSO_4·7H_2O$, 0.2 mg/L $CuSO_4·5H_2O$, 20 μg/L $NiCl_2·H_2O$, 0.2 mg/L biotin, pH 7.0) to a working volume of 2 L in a 5-L bioreactor (Baoxing Bio, Shanghai, China). Temperature was set at 30 °C, and air flow rate was set at 1 vvm. The initial agitation speed was 300 rpm, which was set to adjust automatically to maintain dissolved oxygen above 30% of saturation. Pure acetate was added automatically into the broth to maintain pH at 7.0, and an adequate amount of sodium acetate was added externally when needed.

Analytical Methods

Cell growth was monitored by measuring the optical density at 600 nm (OD_{600}). Organic acids were quantified using a high-performance liquid chromatography (HPLC) system (Agilent Technologies, CA, United States) equipped with a cation-exchange column (HPX-87H; BioRad, CA, United States), as described previously (Mao et al., 2017; Mao et al., 2018). And 5 mM H_2SO_4 was used as mobile phase at a flow rate of 0.4 ml/min, and temperature of the column was set at 65°C. All data represent the average values and standard deviations from three independent replicates.

Enzyme Activity Assays

To extract crude enzyme, *C. glutamicum* strains were cultured in CGXII-YA medium till the exponential growth phase. Procedures of crude enzyme extraction were followed as previously described (Lu et al., 2020). Total protein concentrations were determined using a Bradford assay kit (CWBiotech, Beijing, China).

For measuring the enzyme activity of MCR, the procedures were followed as previously described (Liu et al., 2013) with incubation temperature changed to 30 °C. The enzyme activity of MCR was calculated according to the oxidation rate of NADPH.

For measuring the enzyme activity of CS, the procedures were followed as previous described (Eikmanns et al., 1994). The enzyme activity of CS was calculated according to the formation rate of coenzyme A.

Metabolome Analysis

Procedures for extraction of intracellular metabolites are listed in the **Supplementary Material**. Intracellular metabolites were analyzed using an ultra-performance liquid chromatography (UPLC) system (Nexera 30A, Shimadzu, Kyoto, Japan) coupled with a mass spectrometer (TripleTOF™ 5600, Applied Biosystem Sciex, United States) in negative electrospray ionization (ESI) mode. Most of the metabolites were identified with LC equipped with a SeQuant ZIC-HILIC column (100 × 2.1 mm, 3.5 μm, Merck, Germany). Then 10 mM ammonium acetate and 100% acetonitrile were used as mobile phases A and B, respectively, and the flow rate was set at 0.2 ml/min with a gradient as follows: 0–3 min, 90% B; 3–6 min, 90–60% B; 6–25 min, 60–50% B; 25–30 min, 50% B; 30–30.5 min, 50–90% B; and 30.5–38 min, 90% B. The relative content of metabolites was normalized to cell density.

Real-Time Quantitative PCR

To extract RNA, *C. glutamicum* strains were cultured in CGXII-YA medium till the exponential growth phase. Procedures of total RNA extraction and qRT-PCR were followed as previously described (Zhu et al., 2013). The transcriptional level of 16S ribosomal RNA of *C. glutamicum* was used as an internal reference. Each targeted gene of a strain was measured three times.

RESULTS AND DISCUSSION

Optimization of the Expression Level of Malonyl-CoA Reductase

Corynebacterium glutamicum can assimilate acetate as the sole carbon substrate. More precursor acetyl-CoA would be supplemented when acetate was utilized, rather than glucose, which could be beneficial to 3-HP production via malonyl-CoA pathway. However, *C. glutamicum* is not a natural 3-hydroxypropionic acid (3-HP) producer due to the lack of the malonyl-CoA reductase (MCR). Therefore, the *mcr** gene encoding a bifunctional malonyl-CoA reductase mutant (N940V, K1106W, S1114R) (Liu et al., 2016) from *Chloroflexus aurantiacus* was inserted into shuttle vector pEC-XK99E, resulting in pEC-*mcr**. Then, several strategies were used to increase the expression level of MCR (**Figure 2A**): the sequences of mbp-tag and his-tag, which could increase the expression level of target protein by destabilizing the secondary structures of mRNA (Fang et al., 2018), were inserted upstream of the RBS of *mcr**, resulting in expression plasmids pEC-mbp-*mcr** and pEC-his-*mcr**, respectively; the N-terminal half with malonate semialdehyde (MSA) reductase (MCR-N) activity and the C-terminal half with malonyl-CoA reductase (MCR-C) activity (Liu et al., 2013) were separately expressed in different sort orders, yielding plasmids pEC-N-C, pEC-N-C*, and pEC-C*-N; and stronger promoters P_{H36} (Yim et al., 2013) and P_{sod} were used to express N-terminal and C-terminal halves, resulting in pEC-H36-N-C* and pEC-sod-N-C*, respectively. The vector pEC-*mcr* which contains unmutated *mcr* gene was also constructed as control. All plasmids were separately introduced into Cgz2, generating a series of strains (**Table 2**). An optimization of IPTG induction strength was conducted, and an induction time and concentration of 0 h and 1 mM were found to be ideal for MCR expression (**Supplementary Figure S1**). Both MCR enzyme activities and 3-HP titers of the constructed strains were determined.

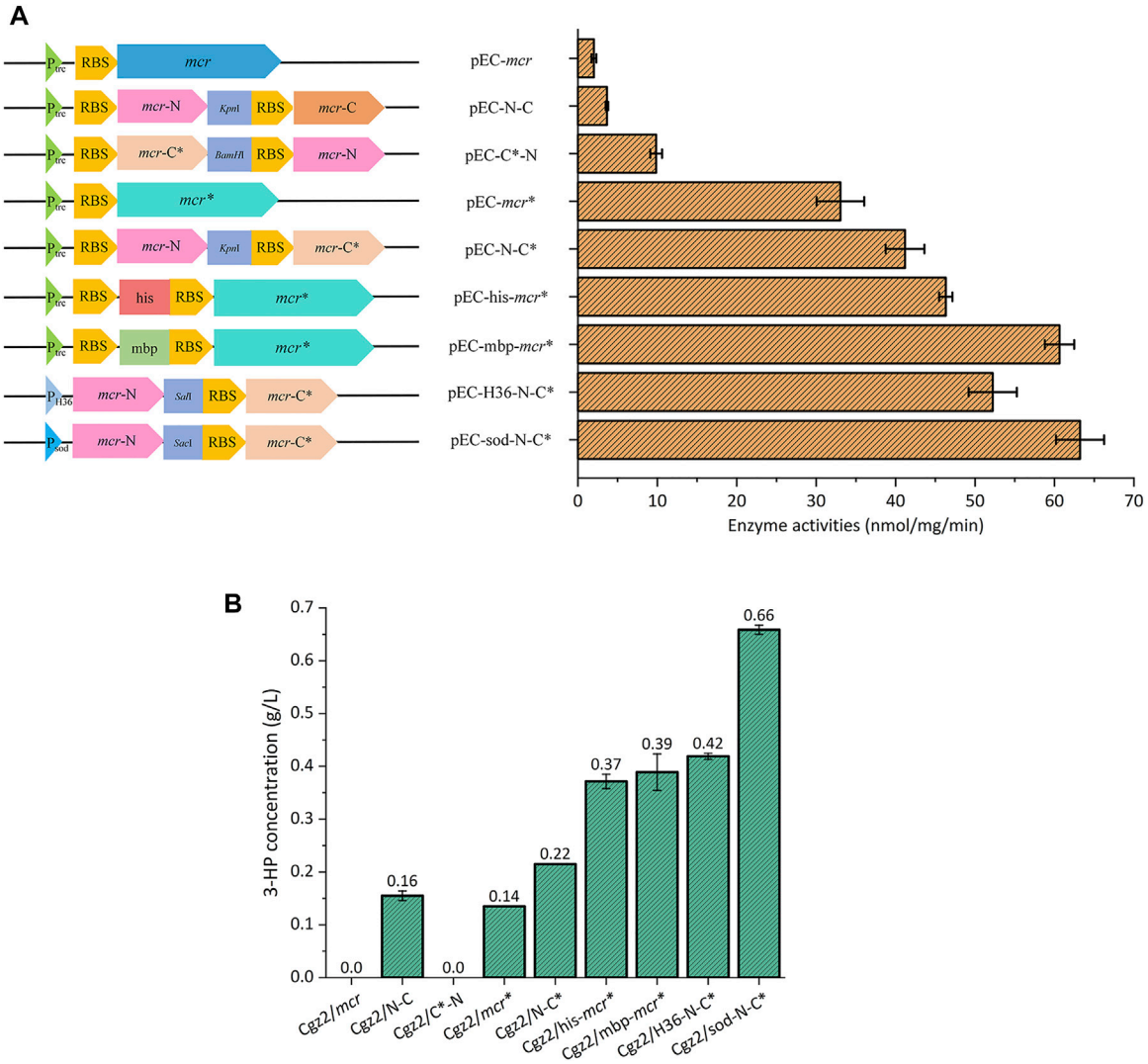

FIGURE 2 | Overviews of a series of *mcr* overexpression plasmids and their applications in 3-HP production. **(A)** Schematic drawing of different *mcr* overexpression plasmids, and their respective MCR enzyme activities. **(B)** 3-HP concentrations of Cgz2 series strains.

As is shown in **Figure 2A**, Cgz2/*mcr* showed neglectable MCR activity (2 nmol/mg/min), which explained the undetectable 3-HP in the medium. MCR activity of Cgz2/*mcr** was increased to 33 nmol/mg/min, which was 15.5-fold higher than Cgz2/*mcr*, and 0.14 g/L 3-HP (**Figure 2B**) was accumulated by this strain in 48 h. When mbp-tag and his-tag were introduced, the corresponding strains Cgz2/mbp-*mcr** and Cgz2/his-*mcr** both showed an obvious increase in MCR enzyme activity and 3-HP titer. The better producer Cgz2/mbp-*mcr** accumulated 0.42 g/L 3-HP. Strain Cgz2/N-C* possessing both mutation and dissection showed higher catalytic efficiency (41 nmol/mg/min), and 3-HP titer was also increased to 0.22 g/L. It was reported that C-terminal half was the rate-limiting part (Liu et al., 2016); therefore, it is reasonable to deduce that placing *mcr*-C* into the first place of the operon would improve its expression level as a similar case was reported (Liu et al., 2019). However, an obvious decline of catalytic activity (9.9 nmol/mg/min) in Cgz2/C*-N was observed, resulting in the vanishment of 3-HP (**Figure 2B**). Both strains Cgz2/sod-N-C* (63 nmol/mg/min) and Cgz2/H36-N-C* (52 nmol/mg/min) showed much increased MCR enzyme activity. The best strain Cgz2/sod-N-C* produced 0.66 g/L 3-HP after 48 h cultivation in flasks (**Supplementary Figure S2**). Cell growth was not severely retarded when acetate was used as the sole carbon source, and the biomass of Cgz2/sod-N-C* reached 23.8 OD_{600}. The results illustrated the successful optimization of MCR expression in *C. glutamicum*.

The mbp-tag and his-tag were shown to improve the enzyme activity of MCR and the overall 3-HP production under the control of promoter P_{trc}. The mRNA secondary structure analysis showed that the insertion of mbp-tag and his-tag increased the minimum free energy (MFE) from -36.15 kJ/mol to -27.24 kJ/mol and -24.8 kJ/mol, respectively (**Supplementary Figure S3**), which connoted the effectiveness of mbp-tag and his-tag in destabilizing the mRNA secondary structure. Moreover, transcriptional levels

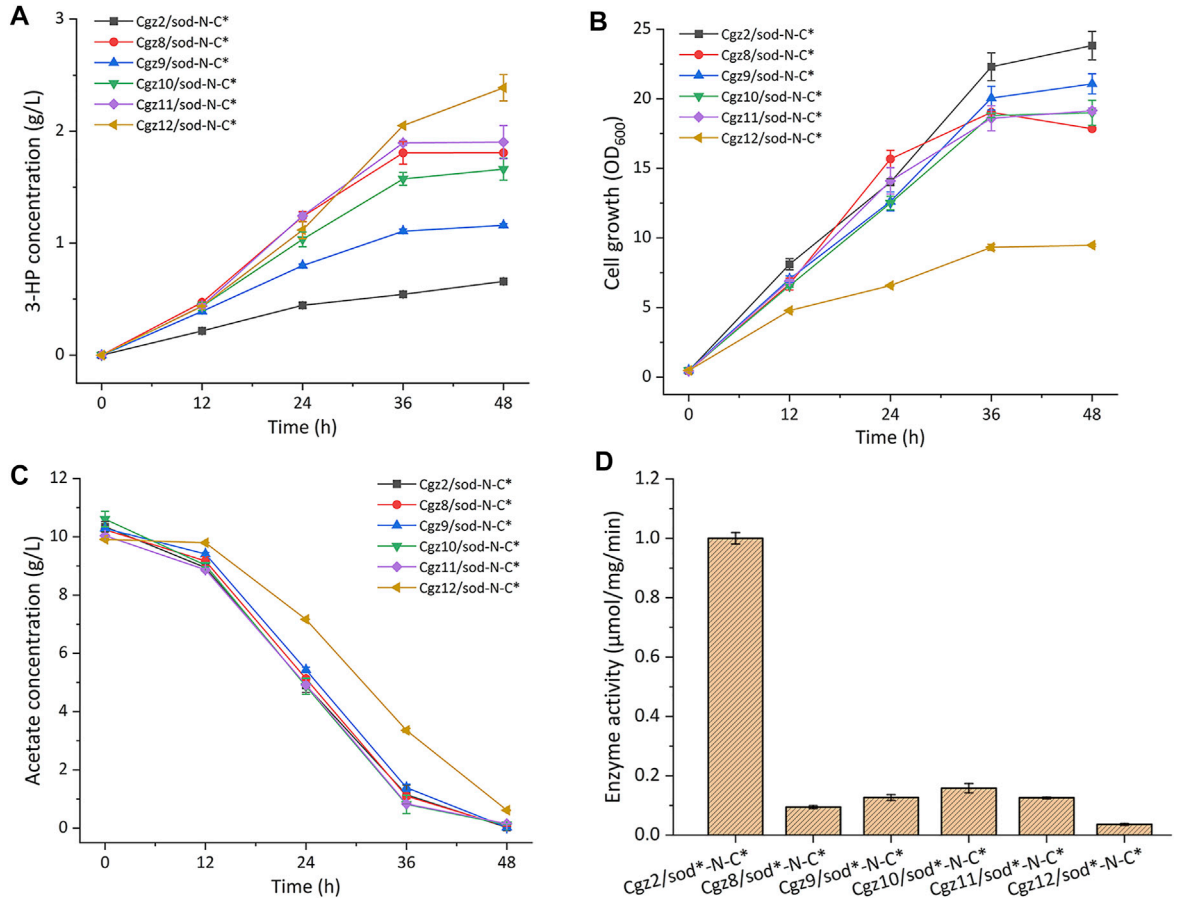

FIGURE 3 | Characterizations of citrate synthase (CS) modified recombinant strains. **(A)** 3-HP production, **(B)** cell growth (OD_{600}), **(C)** acetate consumption, and **(D)** CS enzyme activities.

of *mcr** were also measured by RT-PCR. As shown in **Supplementary Figure S4**, mRNA levels of gene *mcr** in Cgz2/his-*mcr** and Cgz2/mbp-*mcr** were slightly increased, which were 13.0 and 12.4% higher than that of Cgz2/*mcr**, respectively. However, the enzyme activities of MCR in Cgz2/his-*mcr** and Cgz2/mbp-*mcr** were, respectively, 40.2 and 83.4% higher than the activity of Cgz2/*mcr**. The results demonstrated that the increased enzyme activities of MCR in Cgz2/his-*mcr** and Cgz2/mbp-*mcr** were mainly caused by destabilization of mRNA secondary structure of *mcr**, which facilitated the translation initiation of MCR. Naturally, the better mbp-tag was also inserted in pEC-sod-N-C* and then introduced into strain Cgz2, resulting in strain Cgz2/sod-mbp-N-C*. Minimum free energy of pEC-sod-mbp-N-C* also increased from -30.2 kJ/mol to -25.25 kJ/mol compared to pEC-sod-N-C* (**Supplementary Figure S5**); however, 3-HP production was not boosted as expected (**Supplementary Figure S6**). It was presumed that insertion of tag could only enhance the expression level of *mcr*-N, leaving the rate-limiting *mcr*-C* unaffected, which was of no help to 3-HP production. Strain Cgz2/mbp-N-C* under the control of promoter P_{trc} was also constructed to vindicate our presumption. As expected, 3-HP titer of Cgz2/mbp-N-C* did not increase comparing with strain Cgz2/N-C* (data not shown). Therefore, Cgz2/sod-N-C* was selected for further modification.

Knockdown of Gene *gltA* Boosts the Production of 3-HP

Acetyl-CoA is the indirect key precursor for 3-HP synthesis, whose availability would extensively affect malonyl-CoA pool and 3-HP production. It was reported that when glucose was replaced with acetate as the sole carbon source, acetyl-CoA concentration in *C. glutamicum* was increased by about 5-fold, and the majority of which was depleted through the TCA cycle (Wendisch et al., 1997; Wendisch et al., 2000). In order to save more acetyl-CoA for 3-HP synthesis, we tried to reduce the flux of TCA by downregulating the expression of the *gltA* gene, which encodes citrate synthase (CS).

Three weak promoters P_1, P_5, and P_7 with different strengths (1, 6, and 13% relative strength of promoter P_{trc}, respectively) were selected from a promoter library constructed in our previous work (Zhang et al., 2018) and used to replace the native promoter of *gltA*, respectively. Then plasmid pEC-sod-N-C* was introduced into the engineered strains, yielding strains Cgz8/

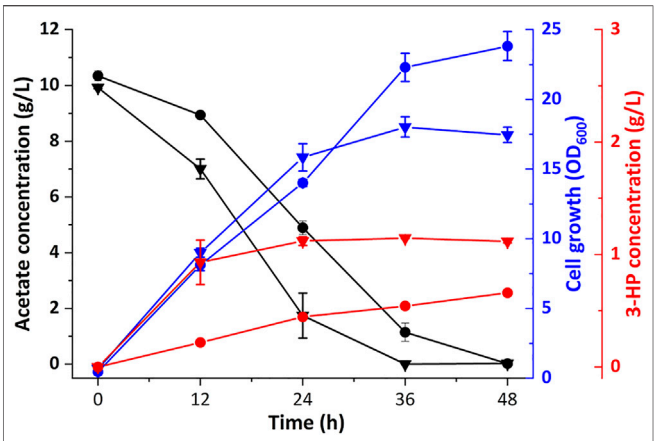

FIGURE 4 | Effect delineations of deregulation of *acc*. Time profiles of cell growth (OD_{600}), acetate, and 3-HP concentrations of recombinant strains Cgz2/sod-N-C* and Cgz13/sod-N-C*. Circles indicate strain Cgz2/sod-N-C*. Triangles indicate strain Cgz13/sod-N-C*.

sod-N-C*, Cgz9/sod-N-C*, and Cgz10/sod-N-C*. The cultivation results indicated that all the three strains exhibited significantly increased 3-HP titer, and the best producer Cgz8/sod-N-C* accumulated 1.81 g/L 3-HP, which was 1.74-fold higher than that of the control strain Cgz2/sod-N-C*, while strains Cgz9/sod-N-C* and Cgz10/sod-N-C* produced 1.16 g/L and 1.66 g/L 3-HP, respectively (**Figure 3A**). Meanwhile, the maximum biomass of all the three strains decreased to different extents, among which Cgz8/pEC-sod-N-C* (OD_{600} 17.85) exhibited the highest biomass reduction (25.1%) compared with Cgz2/sod-N-C* (**Figure 3B**). No difference in acetate consumption was observed among the strains, suggesting the acetate transport and utilization systems were not affected (**Figure 3C**).

Since P_{P1} is the weakest promoter in the library (Zhang et al., 2018), the start codon ATG of *gltA* was replaced with GTG and TTG, respectively, to further decrease the expression level of CS in Cgz8/sod-N-C*, generating strains Cgz11/sod-N-C* and Cgz12/sod-N-C*. As expected, cell growth of Cgz11/sod-N-C* slightly declined to 16.65 OD_{600}, and 1.90 g/L 3-HP was detected, which was similar to Cgz8/sod-N-C* (**Figure 3A**). The 3-HP titer of Cgz12/sod-N-C* showed a more distinct increase of 32.04%, reaching 2.39 g/L with a yield of 0.26 g-3-HP/g-acetate in 48 h (**Figure 3A**), which were, respectively, 2.62-fold and 3.06-fold higher than those of strain Cgz2/sod-N-C*. Accordingly, the maximal biomass of Cgz12/sod-N-C* was further decreased to an OD_{600} of 9.48, which decreased by 60% compared to Cgz2/sod-N-C* (**Figure 3B**). The acetate consumption rate was also negatively affected by the decreased cell growth, and 0.61 g/L residual acetate was detected after the fermentation (**Figure 3C**).

In order to prove that it was the reduction of CS enzyme activity that escalated 3-HP production, CS enzyme activities of relevant strains were analyzed. CS activities were sharply decreased by 90.6, 84.2, and 87.3%, respectively, when promoters P_1, P_5, and P_7 were used. The detected CS activities were in line with the trends of 3-HP production and cell growth (**Figure 3D**). Thereinto, CS enzyme activity of the best producer Cgz12/sod-N-C* with the start codon TTG for *gltA* was reduced to merely 3.62% of the control. The results demonstrated that the reduced CS activity contributed significantly to 3-HP accumulation.

Deregulation of the Expression of *acc* Genes Elevated 3-HP Production

Malonyl-CoA is the direct precursor for 3-HP synthesis and is converted from acetyl-CoA. This reaction was catalyzed by acetyl-CoA carboxylase (ACC)—a heterodimer comprising subunits AccBC and AccD1 (Gande et al., 2007). It was reported that the two subunits were strictly regulated by transcriptional repressor FasR via binding with the *fasO* motifs of *accBC* and *accD1* (Nickel et al., 2010). Since FasR is also a negative regulator for the genes involving fatty acid synthesis pathway, which is the dominating competitive pathway of 3-HP synthesis, we chose to deregulate the expression of *acc* genes by eliminating the *fasO* sequences, instead of deleting *fasR*.

The *fasO* sequences of *accBC* and *accD1* in Cgz2/sod-N-C* were substituted, as previously reported (Milke et al., 2019), generating strain Cgz13/sod-N-C*. As shown in **Figure 4**, strain Cgz13/sod-N-C* produced 1.12 g/L 3-HP in 24 h and the titer remained about the same (1.19 g/L) in 36 h as a result of the depletion of acetate in the medium, which was 1.80 times as Cgz2/sod-N-C*. Meanwhile, 3-HP yield also increased to 0.12 g-3-HP/g-acetate. Noteworthily, 3-HP productivity was increased from 18.54 mg/L/h to 46.64 mg/L/h during 0–24 h. Likewise, the acetate assimilation rate of Cgz13/sod-N-C* reached 0.34 g/L/h, which was increased by 47.8% compared with strain Cgz2/sod-N-C* (0.23 g/L/h). The cell growth rates of the two strains were similar within 24 h. However, the final OD_{600} of strain Cgz13/sod-N-C* in 36 h was only 18.0, 24% lower than that of strain Cgz2/sod-N-C*. It was concluded that deregulation of the repression of the *acc* genes could efficiently redirect more acetyl-CoA toward 3-HP production.

Combination of the Strategies of *gltA* Knockdown and Deregulation of the Expression of *acc* Genes

Both the knockdown of *gltA* and deregulation of the expression of *acc* genes were effective in promoting 3-HP production. Hence, mutations of *acc* genes were introduced into strain Cgz12/sod-N-C*, generating strain Cgz14/sod-N-C*. However, no obvious differences in final 3-HP titer, cell growth, and acetate consumption rate were observed between the two strains (**Supplementary Figure S7**). The transcription levels of *accBC* and *accD1* were then analyzed by RT-PCR to verify the effect of *acc* genes deregulation. As shown in **Supplementary Figure S8**, the transcription levels of genes *accBC* and *accD1* in strain Cgz14/sod-N-C* were, respectively, 2.7 times and 3.0 times as those of strain Cgz12/sod-N-C*, illustrating the fact that the two *acc* genes were deregulated by *fasO* mutations.

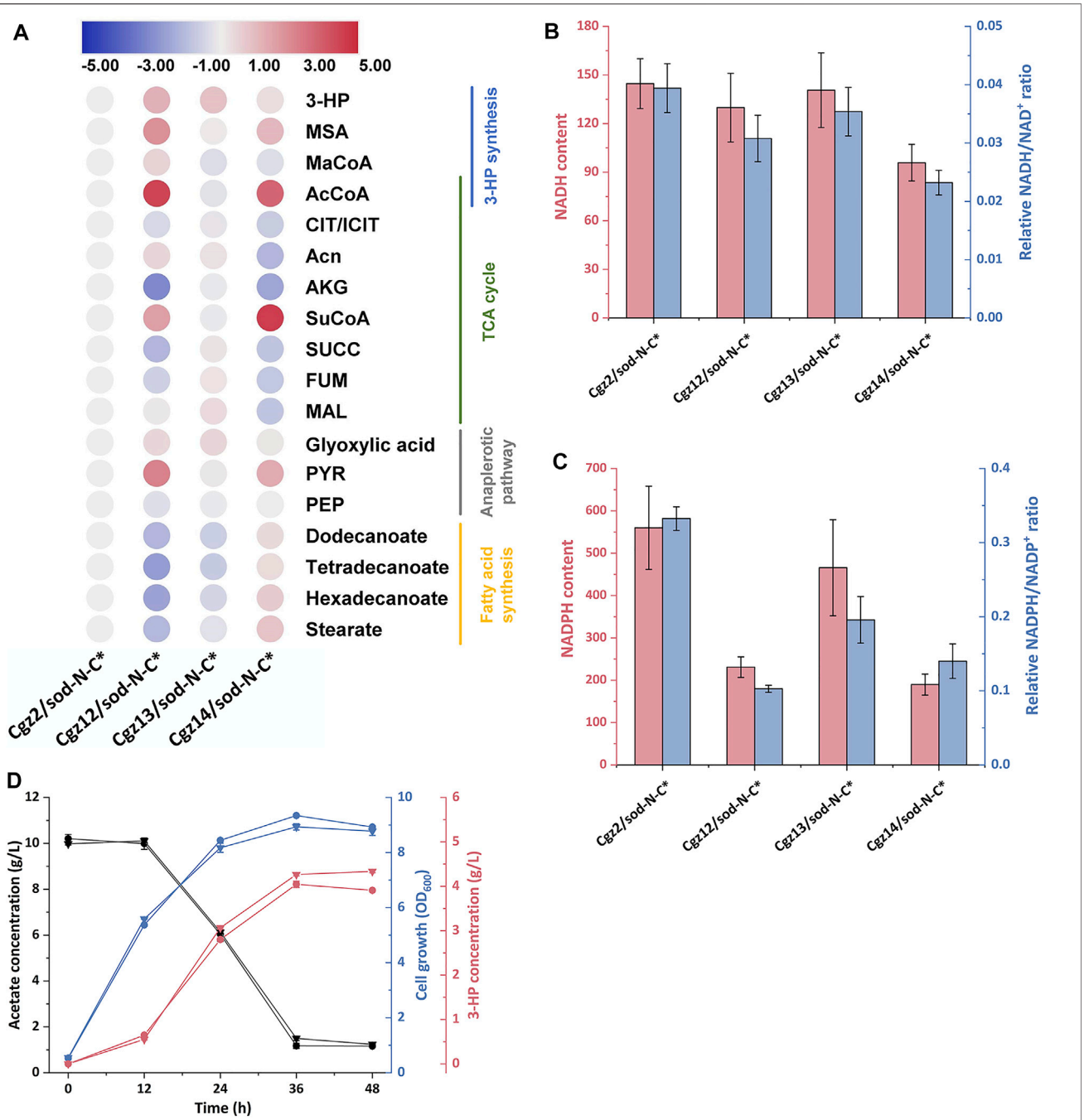

FIGURE 5 | Changes of intracellular metabolites in response to different genetic manipulations. **(A)** Heat map (log_2 fold change) showing the changes of intracellular metabolites involving central carbon metabolism in strains Cgz2/sod-N-C*, Cgz12/sod-N-C*, Cgz13/sod-N-C*, and Cgz14/sod-N-C* at 12 h. "#" indicates metabolites that could not be distinguished in LC-MS. Comparison of intracellular **(B)** relative NADH content and NADH/NAD^+ ratio, and **(C)** relative NADPH content and NADPH/$NADP^+$ ratio in strains Cgz2/sod-N-C*, Cgz12/sod-N-C*, Cgz13/sod-N-C*, and Cgz14/sod-N-C* at 12 h. **(D)** Time profile of cell growth (OD_{600}), acetate, and 3-HP concentrations of Cgz12/sod-N-C* and Cgz14/sod-N-C* with addition of 15 μM cerulenin at 12 h.

The combination of the two strategies did not promote 3-HP production further as expected. Considering the enzyme activities of MCR were similar in Cgz2/sod-N-C* and Cgz12/sod-N-C*, it could be deduced that supply of acetyl-CoA coordinated well with the MCR activity in Cgz2/sod-N-C*. However, when CS was weakened and acetyl-CoA consumption in the TCA cycle was decreased in strain Cgz12/sod-N-C*, its MCR activity or NADPH supply became the rate-limiting factor for 3-HP production. Future endeavors should focus on further optimization of MCR expression and increase the supply of cofactor NADPH.

Quantification of the Intracellular Metabolites *via* Metabolomics Analysis

To elucidate the changes of intracellular metabolites behind the improvement of 3-HP titers and give instructions to future strain improvement, intracellular metabolites of strains Cgz2/sod-N-C*, Cgz12/sod-N-C*, Cgz13/sod-N-C*, and Cgz14/sod-N-C* were extracted and analyzed. When comparing Cgz12/sod-N-C* with Cgz2/sod-N-C*, it was shown that attenuating CS had a significant influence on metabolites involving several pathways (**Figure 5A**). Acetyl-CoA, the main substrate for CS, was increased by 18-fold in Cgz12/sod-N-C* and consequently increased concentrations of metabolites involving 3-HP synthesis (53, 411 and 181% higher for malonyl-CoA, MSA and 3-HP, respectively). This result demonstrated that the knockdown of *gltA* directed more acetyl-CoA into the 3-HP synthesis pathway in Cgz12/sod-N-C*. However, the significantly piled up acetyl-CoA and MSA suggested the activities of ACC and MCR-N might be the limiting steps for 3-HP production. On the other hand, metabolites in the major competing route, TCA cycle, were decreased in different degrees (30, 84, 62, and 39% lower for citrate/isocitrate, α-ketoglutarate, succinate, and fumarate, respectively). Moreover, intracellular levels of cofactors NADH and NADPH were also influenced by the decreased flux through the TCA cycle as the intracellular NADH content and NADH/NAD^+ ratio were decreased by 10 and 22%, respectively; meanwhile, the NADPH content and NADPH/$NADP^+$ ratio were decreased by 59 and 69%, respectively (**Figures 5B,C**). The reduced concentrations of these metabolites were highly correlated with the reduced maximal cell biomass of Cgz12/sod-N-C*.

The detailed intracellular metabolites in Cgz14/sod-N-C* were also compared with Cgz12/sod-N-C* to analyze the metabolic response of deregulating *acc* genes. As shown in **Figure 5A**, the concentrations of metabolites along the 3-HP synthesis pathway obviously declined (44, 50, 51, and 54% lower for acetyl-CoA, malonyl-CoA, MSA, and 3-HP, respectively). On the contrary, the concentrations of the main fatty acids were much higher in Cgz14/sod-N-C* (270, 463, 560, and 414% higher for dodecanoate, tetradecanoate, hexadecanoate, and stearate, respectively). This result indicated more acetyl-CoA was directed into fatty acids, instead of 3-HP synthesis pathway in Cgz14/sod-N-C*. However, the phenomenon was not observed in Cgz13/sod-N-C* when compared with its control strain Cgz2/sod-N-C* (**Figure 5A**). Deregulating *acc* genes in two different hosts (Cgz2/sod-N-C* and Cgz12/sod-N-C*) led to different metabolic responses, and the exact reason for which was undetermined. It was reported that the K_m value for NADPH of MCR from *Chloroflexus aurantiacus* was 25 μM (Hugler et al., 2002), which was much higher than the corresponding value (4.5 μM) of fatty acid synthase from *C. glutamicum* (Agira et al., 1984). Therefore, it was deduced that the difference might be caused by the different NADPH and NADH levels (or NADPH/$NADP^+$ and NADH/NAD^+ ratios) in the two hosts, and malonyl-CoA might tend to be metabolized by fatty acid synthesis pathway under a lower intracellular NADPH level (**Figure 5C**). Moreover, concentrations of metabolites in TCA were decreased to different extents in Cgz14/sod-N-C* (19, 75, 17, and 54% lower for citrate/isocitrate, aconitate, fumarate, and malate, respectively), which showed that the deregulation of the expression of *acc* genes further reduced the amount of acetyl-CoA metabolized in TCA cycle. The NADPH level in Cgz14/sod-N-C* was further decreased by 18%, indicating the NADPH availability in Cgz14/sod-N-C* needs to be improved to increase 3-HP synthesis.

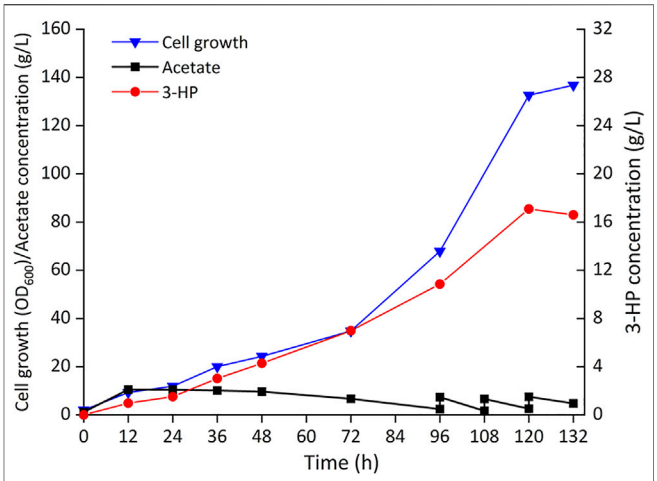

FIGURE 6 | Time profiles of cell growth (OD_{600}), acetate, and 3-HP concentrations during the fed-batch culture of recombinant strain Cgz14/sod-N-C* in a 5-L bioreactor. Pure acetate was added automatically into the broth to maintain pH at 7.0; 14 g sodium acetate was added externally at 96, 108, and 120 h.

In view of the fact that the increased supply of malonyl-CoA in Cgz14/sod-N-C* was mainly directed to fatty acids synthesis, cerulenin was used to inhibit fatty acid synthesis to explore its potential in 3-HP production with Cgz12/sod-N-C* as control. As shown in **Figure 5D**, the 3-HP titer and yield of Cgz14/sod-N-C* reached 4.26 g/L and 0.50 g-3-HP/g-acetate, which were 5.4 and 12.2% higher than strain Cgz12/sod-N-C*. The addition of cerulenin resulted in an increase of 81 and 108% in 3-HP titer and yield compared to those without cerulenin addition, and 3-HP productivity was also significantly increased from 50 mg/L/h to 120 mg/L/h during 0–36 h. The results demonstrated that Cgz14/sod-N-C* is a promising host for 3-HP production from acetate. However, the high cost of cerulenin renders its application unsuitable for large-scale production. Therefore, besides further increasing MCR activity, future endeavors should also be made to inhibit fatty acid synthesis properly, which can save both malonyl-CoA and NADPH for 3-HP production.

Fed-Batch Fermentation in a 5 L Bioreactor

To further evaluate the ability of 3-HP production from acetate, Cgz14/sod-N-C* was cultured in a 5-L bioreactor without cerulenin addition. As shown in **Figure 6**, a titer of 17.1 g/L 3-HP was obtained in 120 h with a production rate of 140 mg/L/

h and a yield of 0.10 g-3-HP/g-acetate. Cell growth was slow in the first 72 h, after which cells grew faster with a specific growth rate of 0.028 h^{-1} till 120 h, reaching an OD_{600} of 132.6. The yield of 3-HP in bioreactor decreased by 61.5% compared with that of the same strain in shake flasks, which might be caused by increased carbon flow toward cell growth in the bioreactor, indicating the conditions for fed-batch fermentation could be further optimized.

Strain Cgz14/sod-N-C* produced 4.26 g/L 3-HP from 8.52 g/L acetate with cerulenin addition in shake flasks, and 17.1 g/L 3-HP using acetate as substrate without addition of cerulenin in bioreactor, which is the highest titer achieved using acetate as substrate. The performance of the engineered *C. glutamicum* strain proved its potential in 3-HP production from acetate.

CONCLUSION

This is the first report on engineering *C. glutamicum* to sufficiently assimilate acetate as the sole substrate to produce 3-HP. With optimization of MCR expression and weakening of CS expression, 3-HP titer of strain Cgz12/sod-N-C* was increased to 2.39 g/L. With the subsequent deregulation of ACC and addition of cerulenin, strain Cgz14/sod-N-C* produced 4.26 g/L 3-HP with a yield of 0.50 g/g-acetate. Furthermore, Cgz14/sod-N-C* accumulated 17.1 g/L 3-HP without addition of cerulenin in a 5 L bioreactor. The results demonstrate that *C. glutamicum* is a promising host for 3-HP production from acetate.

DATA AVAILABILITY STATEMENT

The original contributions presented in the study are included in the article/**Supplementary Material**; further inquiries can be directed to the corresponding authors.

AUTHOR CONTRIBUTIONS

TC and ZCH designed the study. ZCH and WD wrote the manuscript. ZCH, WD, YM, ZCU, ZZ, and ZW performed the experiments and analyzed the results. TC and HM supervised the project and critically revised the manuscript. All authors gave final approval of the version to be submitted, and read and approved the final manuscript version.

FUNDING

This work was financially supported by the National Natural Science Foundation of China (NSFC-21776208 and NSFC-21621004) and the Tianjin Synthetic Biotechnology Innovation Capacity Improvement Project (TSBICIP-PTJS-001).

SUPPLEMENTARY MATERIAL

The Supplementary Material for this article can be found online at: https://www.frontiersin.org/articles/10.3389/fbioe.2021.808258/full#supplementary-material

REFERENCES

Agira, N., Maruyama, K., and Kawaguchi, A. (1984). Comparative Studies of Fatty Acid Synthases of Corynebacteria. *J. Gen. Appl. Microbiol.* 30, 87–95.

Becker, J., and Wittmann, C. (2012). Bio-based Production of Chemicals, Materials and Fuels - *Corynebacterium glutamicum* as Versatile Cell Factory. *Curr. Opin. Biotechnol.* 23 (4), 631–640. doi:10.1016/j.copbio.2011.11.012

Bozell, J. J., and Petersen, G. R. (2010). Technology Development for the Production of Biobased Products from Biorefinery Carbohydrates-The US Department of Energy's "Top 10" Revisited. *Green. Chem.* 12 (4), 539–554. doi:10.1039/b922014c

Chang, Z., Dai, W., Mao, Y., Cui, Z., Wang, Z., and Chen, T. (2020). Engineering *Corynebacterium glutamicum* for the Efficient Production of 3-Hydroxypropionic Acid from a Mixture of Glucose and Acetate via the Malonyl-CoA Pathway. *Catalysts* 10 (2), 203. doi:10.3390/catal10020203

Chen, Y., Bao, J., Kim, I.-K., Siewers, V., and Nielsen, J. (2014). Coupled Incremental Precursor and Co-factor Supply Improves 3-Hydroxypropionic Acid Production in *Saccharomyces cerevisiae*. *Metab. Eng.* 22, 104–109. doi:10.1016/j.ymben.2014.01.005

Chen, Z., Huang, J., Wu, Y., Wu, W., Zhang, Y., and Liu, D. (2017). Metabolic Engineering of *Corynebacterium glutamicum* for the Production of 3-Hydroxypropionic Acid from Glucose and Xylose. *Metab. Eng.* 39, 151–158. doi:10.1016/j.ymben.2016.11.009

Eikmanns, B. J., Thum-Schmitz, N., Eggeling, L., Ludtke, K.-U., and Sahm, H. (1994). Nucleotide Sequence, Expression and Transcriptional Analysis of the *Corynebacterium glutamicum gltA* Gene Encoding Citrate Synthase. *Microbiology* 140 (8), 1817–1828. doi:10.1099/13500872-140-8-1817

Fang, H., Li, D., Kang, J., Jiang, P., Sun, J., and Zhang, D. (2018). Metabolic Engineering of *Escherichia coli* for De Novo Biosynthesis of Vitamin B12. *Nat. Commun.* 9, 4917. doi:10.1038/s41467-018-07412-6

Gande, R., Dover, L. G., Krumbach, K., Besra, G. S., Sahm, H., Oikawa, T., et al. (2007). The Two Carboxylases of *Corynebacterium glutamicum* Essential for Fatty Acid and Mycolic Acid Synthesis. *J. Bacteriol.* 189 (14), 5257–5264. doi:10.1128/JB.00254-07

Gopinath, V., Murali, A., Dhar, K. S., and Nampoothiri, K. M. (2011). *Corynebacterium glutamicum* as a Potent Biocatalyst for the Bioconversion of Pentose Sugars to Value-Added Products. *Appl. Microbiol. Biotechnol.* 93 (1), 95–106. doi:10.1007/s00253-011-3686-4

Hügler, M., Menendez, C., Schägger, H., and Fuchs, G. (2002). Malonyl-Coenzyme A Reductase from *Chloroflexus aurantiacus*, a Key Enzyme of the 3-Hydroxypropionate Cycle for Autotrophic CO_2 Fixation. *J. Bacteriol.* 184 (9), 2404–2410. doi:10.1128/Jb.184.9.2404-2410.2002

Jiang, X.-R., Yan, X., Yu, L.-P., Liu, X.-Y., and Chen, G.-Q. (2021). Hyperproduction of 3-Hydroxypropionate by *Halomonas bluephagenesis*. *Nat. Commun.* 12 (1), 1513. doi:10.1038/s41467-021-21632-3

Kirchner, O., and Tauch, A. (2003). Tools for Genetic Engineering in the Amino Acid-Producing Bacterium *Corynebacterium glutamicum*. *J. Biotechnol.* 104 (1-3), 287–299. doi:10.1016/S0168-1656(03)00148-2

Kumar, V., Ashok, S., and Park, S. (2013). Recent Advances in Biological Production of 3-Hydroxypropionic Acid. *Biotechnol. Adv.* 31 (6), 945–961. doi:10.1016/j.biotechadv.2013.02.008

Lai, N., Luo, Y., Fei, P., Hu, P., and Wu, H. (2021). One Stone Two Birds: Biosynthesis of 3-Hydroxypropionic Acid from CO_2 and Syngas-Derived Acetic Acid in *Escherichia coli*. *Synth. Syst. Biotechnol.* 6 (3), 144–152. doi:10.1016/j.synbio.2021.06.003

Lama, S., Kim, Y., Nguyen, D. T., Im, C. H., Sankaranarayanan, M., and Park, S. (2021). Production of 3-Hydroxypropionic Acid from Acetate Using Metabolically-Engineered and Glucose-Grown *Escherichia coli*. *Bioresour. Technol.* 320 (Pt A), 124362. doi:10.1016/j.biortech.2020.124362

Lee, J., Cha, S., Kang, C., Lee, G., Lim, H., and Jung, G. (2018). Efficient Conversion of Acetate to 3-Hydroxypropionic Acid by Engineered *Escherichia coli*. *Catalysts* 8 (11), 525. doi:10.3390/catal8110525

Liu, C., Wang, Q., Xian, M., Ding, Y., and Zhao, G. (2013). Dissection of Malonyl-Coenzyme A Reductase of *Chloroflexus aurantiacus* Results in Enzyme Activity Improvement. *Plos One* 8 (9), e75554. doi:10.1371/journal.pone.0075554

Liu, C., Ding, Y., Zhang, R., Liu, H., Xian, M., and Zhao, G. (2016). Functional Balance between Enzymes in Malonyl-CoA Pathway for 3-Hydroxypropionate Biosynthesis. *Metab. Eng.* 34, 104–111. doi:10.1016/j.ymben.2016.01.001

Liu, B., Xiang, S., Zhao, G., Wang, B., Ma, Y., Liu, W., et al. (2019). Efficient Production of 3-Hydroxypropionate from Fatty Acids Feedstock in *Escherichia coli*. *Metab. Eng.* 51, 121–130. doi:10.1016/j.ymben.2018.10.003

Lu, L., Mao, Y., Kou, M., Cui, Z., Jin, B., Chang, Z., et al. (2020). Engineering Central Pathways for Industrial-Level (3*R*)-Acetoin Biosynthesis in *Corynebacterium glutamicum*. *Microb. Cel. Fact.* 19, 102. doi:10.1186/s12934-020-01363-8

Mao, Y., Fu, J., Tao, R., Huang, C., Wang, Z., Tang, Y.-J., et al. (2017). Systematic Metabolic Engineering of *Corynebacterium glutamicum* for the Industrial-Level Production of Optically Pure D-(−)-Acetoin. *Green. Chem.* 19 (23), 5691–5702. doi:10.1039/c7gc02753b

Mao, Y., Li, G., Chang, Z., Tao, R., Cui, Z., Wang, Z., et al. (2018). Metabolic Engineering of *Corynebacterium glutamicum* for Efficient Production of Succinate from Lignocellulosic Hydrolysate. *Biotechnol. Biofuels* 11 (1), 95. doi:10.1186/s13068-018-1094-z

Milke, L., Kallscheuer, N., Kappelmann, J., and Marienhagen, J. (2019). Tailoring *Corynebacterium glutamicum* towards Increased Malonyl-CoA Availability for Efficient Synthesis of the Plant Pentaketide Noreugenin. *Microb. Cel Fact* 18, 71. doi:10.1186/s12934-019-1117-x

Nickel, J., Irzik, K., Van Ooyen, J., and Eggeling, L. (2010). The TetR-type Transcriptional Regulator FasR of *Corynebacterium glutamicum* Controls Genes of Lipid Synthesis during Growth on Acetate. *Mol. Microbiol.* 78 (1), 253–265. doi:10.1111/j.1365-2958.2010.07337.x

Niu, H., Li, R., Wu, J., Cai, Z., Yang, D., Gu, P., et al. (2018). Production of Succinate by Recombinant *Escherichia coli* Using Acetate as the Sole Carbon Source. *3 Biotech.* 8 (10), 421. doi:10.1007/s13205-018-1456-z

Noh, M. H., Lim, H. G., Woo, S. H., Song, J., and Jung, G. Y. (2018). Production of Itaconic Acid from Acetate by Engineering Acid-Tolerant *Escherichia coli* W. *Biotechnol. Bioeng.* 115 (3), 729–738. doi:10.1002/bit.26508

Rathnasingh, C., Raj, S. M., Jo, J.-E., and Park, S. (2009). Development and Evaluation of Efficient Recombinant *Escherichia coli* strains for the Production of 3-Hydroxypropionic Acid from Glycerol. *Biotechnol. Bioeng.* 104 (4), 729–39. doi:10.1002/bit.22429

Richmond, J. Y. (1999). *Biosafety in Microbiological and Biomedical Laboratories*. United States: National Institutes of Health.

Schwarz, M., Köpcke, B., Weber, R., Sterner, O., and Anke, H. (2004). 3-Hydroxypropionic Acid as a Nematicidal Principle in *Endophytic fungi*. *Phytochemistry* 65 (15), 2239–2245. doi:10.1016/j.phytochem.2004.06.035

Wendisch, V. F., Spies, M., Reinscheid, D. J., Schnicke, S., Sahm, H., and Eikmanns, B. J. (1997). Regulation of Acetate Metabolism in *Corynebacterium glutamicum* : Transcriptional Control of the Isocitrate Lyase and Malate Synthase Genes. *Arch. Microbiol.* 168 (4), 262–269. doi:10.1007/s002030050497

Wendisch, V. F., De Graaf, A. A., Sahm, H., and Eikmanns, B. J. (2000). Quantitative Determination of Metabolic Fluxes during Coutilization of Two Carbon Sources: Comparative Analyses with *Corynebacterium glutamicum* during Growth on Acetate and/or Glucose. *J. Bacteriol.* 182 (11), 3088–3096. doi:10.1128/JB.182.11.3088-3096.2000

Werpy, T., Holladay, J., and White, J. (2004). *Top Value Added Chemicals from Biomass: I. Results of Screening for Potential Candidates from Sugars and Synthesis Gas*. United States: Pacific Northwest National Lab. doi:10.2172/926125

Yim, S. S., An, S. J., Kang, M., Lee, J., and Jeong, K. J. (2013). Isolation of Fully Synthetic Promoters for High-Level Gene Expression in *Corynebacterium glutamicum*. *Biotechnol. Bioeng.* 110 (11), 2959–2969. doi:10.1002/bit.24954

Zhang, S., Liu, D., Mao, Z., Mao, Y., Ma, H., Chen, T., et al. (2018). Model-based Reconstruction of Synthetic Promoter Library in *Corynebacterium glutamicum*. *Biotechnol. Lett.* 40 (5), 819–827. doi:10.1007/s10529-018-2539-y

Zhao, P., Ma, C., Xu, L., and Tian, P. (2019). Exploiting Tandem Repetitive Promoters for High-Level Production of 3-Hydroxypropionic Acid. *Appl. Microbiol. Biotechnol.* 103 (10), 4017–4031. doi:10.1007/s00253-019-09772-5

Zhu, N., Xia, H., Wang, Z., Zhao, X., and Chen, T. (2013). Engineering of Acetate Recycling and Citrate Synthase to Improve Aerobic Succinate Production in *Corynebacterium glutamicum*. *PLoS One* 8 (4), e60659. doi:10.1371/journal.pone.0060659

Zhu, N., Xia, H., Yang, J., Zhao, X., and Chen, T. (2014). Improved Succinate Production in *Corynebacterium glutamicum* by Engineering Glyoxylate Pathway and Succinate Export System. *Biotechnol. Lett.* 36 (3), 553–560. doi:10.1007/s10529-013-1376-2

Conflict of Interest: The authors declare that the research was conducted in the absence of any commercial or financial relationships that could be construed as a potential conflict of interest.

Publisher's Note: All claims expressed in this article are solely those of the authors and do not necessarily represent those of their affiliated organizations, or those of the publisher, the editors, and the reviewers. Any product that may be evaluated in this article, or claim that may be made by its manufacturer, is not guaranteed or endorsed by the publisher.

frontiers in Bioengineering and Biotechnology

REVIEW
published: 20 January 2022
doi: 10.3389/fbioe.2022.833920

Synthetic Biology-Driven Microbial Production of Resveratrol: Advances and Perspectives

Chao Feng[1], Jing Chen[1], Wenxin Ye[1], Kaisen Liao[1], Zhanshi Wang[1], Xiaofei Song[2,3†] and Mingqiang Qiao[2,4*†]*

[1]Department of Urology, Tongde Hospital of Zhejiang Province, Hangzhou, China, [2]The Key Laboratory of Molecular Microbiology and Technology, Ministry of Education, College of Life Sciences, Nankai University, Tianjin, China, [3]The Key Laboratory of Bioorganic Synthesis of Zhejiang Province, College of Biotechnology and Bioengineering, Zhejiang University of Technology, Hangzhou, China, [4]College of Life Sciences, Shanxi University, Taiyuan, China

OPEN ACCESS

Edited by:
Shuobo Shi,
Beijing University of Chemical Technology, China

Reviewed by:
Jiazhang Lian,
Zhejiang University, China
Quanli Liu,
Chalmers University of Technology, Sweden
Yajie Wang,
Westlake University, China

***Correspondence:**
Xiaofei Song
xiaofei@zjut.edu.cn
Mingqiang Qiao
qiaomq@nankai.edu.cn

[†]These authors have contributed equally to this work

Specialty section:
This article was submitted to Synthetic Biology, a section of the journal Frontiers in Bioengineering and Biotechnology

Received: 12 December 2021
Accepted: 05 January 2022
Published: 20 January 2022

Citation:
Feng C, Chen J, Ye W, Liao K, Wang Z, Song X and Qiao M (2022) Synthetic Biology-Driven Microbial Production of Resveratrol: Advances and Perspectives. Front. Bioeng. Biotechnol. 10:833920. doi: 10.3389/fbioe.2022.833920

Resveratrol, a bioactive natural product found in many plants, is a secondary metabolite and has attracted much attention in the medicine and health care products fields due to its remarkable biological activities including anti-cancer, anti-oxidation, anti-aging, anti-inflammation, neuroprotection and anti-glycation. However, traditional chemical synthesis and plant extraction methods are impractical for industrial resveratrol production because of low yield, toxic chemical solvents and environmental pollution during the production process. Recently, the biosynthesis of resveratrol by constructing microbial cell factories has attracted much attention, because it provides a safe and efficient route for the resveratrol production. This review discusses the physiological functions and market applications of resveratrol. In addition, recent significant biotechnology advances in resveratrol biosynthesis are systematically summarized. Furthermore, we discuss the current challenges and future prospects for strain development for large-scale resveratrol production at an industrial level.

Keywords: resveratrol, physiological function, microorganism, metabolic engineering, synthetic biology

INTRODUCTION

Resveratrol has been universally found in a variety of plants including berries, bilberries, peanuts, grapes and even ferns since it was initially extracted from the root of white hellebore (Veratrum grandiflorum) in 1940 (Lim et al., 2011; Jeandet et al., 2012; Li et al., 2015). In plants, resveratrol, the *de novo* synthetic phytoalexin, acts as a protector against pathogen invasion and infection (Tian and Liu, 2020). It is known that two isomeric forms exist in nature, including *cis*- and *trans*-resveratrol, but the *trans* isomer is the primary biologically-active form. The anti-tumor properties of resveratrol in multiple human organs or systems, include breast (Sinha et al., 2016), cervical (Liu Q et al., 2020), uterine (Sexton et al., 2006), blood (Breuss et al., 2019), kidney (Den Hartogh and Tsiani, 2019), liver (Jakubczyk et al., 2020), eye (Bola et al., 2014), bladder (Almeida and Silva, 2021), thyroid (Giuliani et al., 2017), esophageal (Zhou et al., 2003), prostate (Zaffaroni and Beretta, 2021), brain (Kiskova et al., 2020), lung (Feng et al., 2016), skin (Ravikumar et al., 2019), gastric (Zulueta et al., 2015), colon (Li et al., 2019), head and neck (Shrotriya et al., 2015), bone (Chen et al., 2019), ovarian (Sirotkin et al., 2020), and cervical (Sun et al., 2021), and have been extensively studied over the last few decades (Baur and Sinclair, 2006). Moreover, as a plant secondary metabolite, resveratrol has also been noted for many pharmacological applications such as an anti-oxidant, anti-inflammatory, anti-

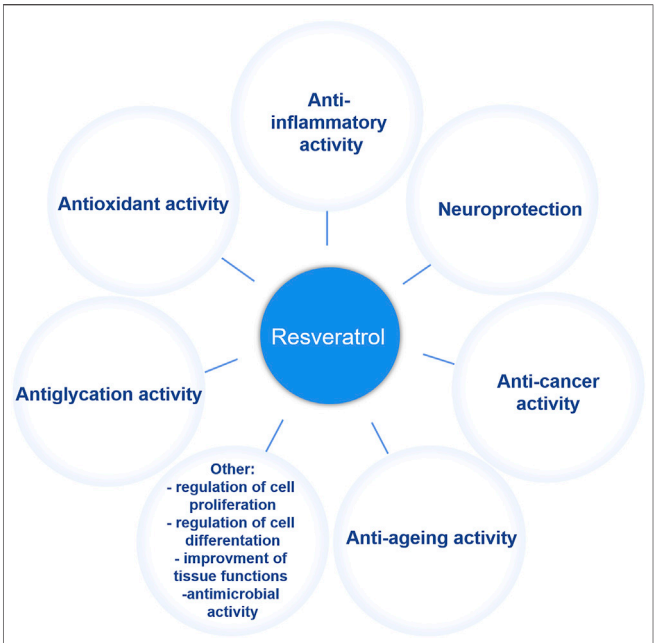

FIGURE 1 | Physiological function of resveratrol.

aging, and neuroprotective agent, as well as for many other properties (Rauf et al., 2018) (**Figure 1**). However, the effects of resveratrol, especially its clinical effects on human health, currently must be further verified and studied because of a limited number of human studies and small cohort sizes. Nevertheless, considering its various physiological activities, resveratrol has attracted much attention in the pharmaceutical, cosmetic and many other industries. Because of an increasing demand in all walks of life, large-scale resveratrol production is urgently needed.

It is difficult to meet the current industry demand for resveratrol by extracting and purifying it from plants, due to the complex process, high production cost and low yield (Sáez-Sáez et al., 2020). Although resveratrol production can currently be increased by employing chemical synthesis, the complex production process, the requirement for toxic solvents and the production of byproducts limits large-scale production (Shrestha et al., 2019). It is noteworthy that the use of microorganisms has made significant contributions to the biosynthesis of pharmaceutical and industrial compounds in recent decades, because of its low production cost, high efficiency, high product purity and simple genetic operation process, and it is considered to have a promising potential for the production of natural products (Cravens et al., 2019). *De novo* resveratrol biosynthesis via metabolic engineering and synthetic biology in microorganisms provides a feasible way to produce resveratrol, and this has attracted worldwide interest (Liu et al., 2019; He et al., 2020; Liu Z et al., 2020; Yuan et al., 2020; Costa et al., 2021). This review discusses the current status and progress of resveratrol production in recent years, as well as optimization strategies for related hosts, pathways and enzymes for resveratrol production. Hopefully in the next few years, researchers will continue to improve process engineering strategies, and increasingly utilize metabolic and protein engineering to meet a series of more complex biosynthetic challenges.

MICROORGANISM HOSTS FOR RESVERATROL PRODUCTION

Many properties should be considered when selecting hosts for natural products production. Due to a long history of research, microorganisms have been widely chosen because of mature techniques such as gene editing and large-scale fermentation, particularly for metabolic engineering (Yang et al., 2021). With the increasing demand for resveratrol, many studies have focused on heterologous resveratrol production in prokaryotes such as *Escherichia coli*, *Corynebacterium glutamicum* and *Streptomyces venezuelae*, and in eukaryotes, including *Saccharomyces cerevisiae* and *Yarrowia lipolytica* (Dudnik et al., 2018; Cravens et al., 2019). **Table 1** presents studies using metabolically engineered strains to produce resveratrol.

YEAST HOSTS

Yeasts are considered as a more suitable platform than bacteria for the expression of natural products, because of their ability to carry out eukaryotic post-translational modifications and feasibility of genetic manipulation (Madzak, 2015; Braga et al., 2018a). Yeasts and plants have a similar endoplasmic reticulum, an intracellular compartment to support eukaryotic and membrane protein biosynthesis (Rainha et al., 2020). *S. cerevisiae* is a Generally Regarded As Safe (GRAS) organism that is widely used for pharmaceutical products and food markets because of its safety, and it is more commonly used for resveratrol production than other host species (Fletcher et al., 2016; Pereira et al., 2019). Becker et al. (2003) reconstructed for the first time a biochemical pathway in a microorganism to produce resveratrol and obtained a titer of 0.00145 mg/L resveratrol in yeast. The biosynthesis of resveratrol via a tyrosine intermediate has been achieved in *S. cerevisiae*; this was a first time demonstration of the possibility of *de novo* resveratrol biosynthesis from glucose. By using a pull-push-block strain engineering strategy, 800 mg/L resveratrol was produced by the engineered host strains (Li et al., 2015; Li et al., 2016). Yuan et al. (2020) constructed a consortium system for *de novo* resveratrol biosynthesis and obtained 36 mg/L resveratrol. *Y. lipolytica*, another yeast, has been widely concentrated in industrial area for more than 50 years because of its high production capacity for organic acids, which are widely used in diverse research areas (Ma et al., 2020) (Madzak, 2018). Gu et al. (2020) created resveratrol-producing strains of *Y. lipolytica*, in which could produce 12.67 ± 2.23 mg/L of resveratrol with glucose as the substrate. He et al. (2020) engineered *Y. lipolytica* as a vehicle for high-level resveratrol production and obtained 0.43 g/L resveratrol by exploiting the tyrosine and the phenylalanine branches of the pathway. Recently, Sáez-Sáez et al. (2020) tried to improve the resveratrol titer in *Y. lipolytica* by metabolic engineering,

TABLE 1 | Biosynthesis of resveratrol in engineered microorganisms.

Microbial host	Pathway genes (source)	Pathway/Host engineering	Substrate	Titer (mg/L)	References
S. cerevisiae W303-1A	4CL1 (*A. thaliana*) STS (*A. hypogaea*)	PAD1 knockout	*p*-Coumaric acid	3.1	Shin et al. (2011)
S. cerevisiae WAT11	TAL (*R. sphaeroides*) 4CL:STS, 4CL1 (*A. thaliana*)-STS (*V.vinifera*) fusion enzyme	Expression of araE transporter (*E. coli*)	Tyrosine *p*-Coumaric acid Grape Juice	3.1 2.3 3.44	Wang et al. (2011)
S. cerevisiae W303-1A	PAL (*R. toruloides*) C4H, 4CL1 (*A. thaliana*) STS (*A. hypogaea*)	Overexpression of ACC1	Tyrosine	5.8	Shin et al. (2012)
S. cerevisiae WAT11	4CL1 (*A. thaliana*) STS (*V. vinifera*)	Synthetic scaffold	*p*-Coumaric acid	14.4	Wang and Yu, (2012)
S. cerevisiae WAT11	4CL:STS, 4CL1 (*A. thaliana*)-STS (*V. vinifera*) fusion enzyme	Overexpression of AAE13	*p*-Coumaric acid	Up to 3.7	Wang et al. (2014)
S. cerevisiae EC1118	4CL (*A. thaliana*) STS (*V. vinifera*)	—	*p*-coumaric acid	8.249	Sun et al. (2015)
S. cerevisiae CEN.PK102-5B	TAL (*H. aurantiacus*) TAL (*F. johnsoniae*) 4CL1 and 4CL2 (*A. thaliana*) RS (*V. vinifera*)	Overexpression of ARO4fbr,ARO7fbr, and ACC1	Glucose (Fed-batch) Ethanol (Fed-batch)	415.65 531.41	Li et al. (2015)
S. cerevisiae CEN.PK102-5B	PAL2, C4H, 4CL2 (*A. thaliana*) VST1 (*V. vinifera*)	Overexpression of ARO4fbr, ARO7fbr, ACC1, CYB5 (*S.cerevisiae*), ATR2 *A. thaliana*), ACS (*S. enterica*), and deletion of aro10	Glucose (Fed-batch) Ethanol (Fed-batch)	812 755	Li et al. (2016)
Y. lipolytica	4CL (*N. tabacum*) STS (*A. hypogaea*)	Overexpression of:ACC1, PEX10	*p*-Coumaric acid	48.7	Palmer et al. (2020)
Y. lipolytica Po1d (wt), derived from W29	TAL (*F. johnsoniae*) PAL (*V. vinifera*) C4H, 4CL1 (*A. thaliana*) VST (*V. vinifera*)	—	Glycerol	430	He et al. (2020)
Y. lipolytica ST6512 (W29)	TAL (*F. johnsoniae*) 4CL1 (*A. thaliana*) VST1 (*V. vinifera*)	Overexpression of:ARO4fbr and ARO7fbr	Glucose Glucose (Fed-batch)	409 12,355	Sáez-Sáez et al. (2020)
C. glutamicum DelAro3	STS (*A. hypogaea*) 4CL (*P. crispum*)	Deletion of *phdB, pcaF* and *pobA*	*p*-Coumaric acid *p*-coumaric acid + cerulenin	12 158	Kallscheuer et al. (2016)
C. glutamicum DelAro4	TAL (*F. johnsoniae*) 4CL (*Petroselinum*) STS (*A. hypogaea*) *aroH* (*E. coli*)	Deletion of *phdB, pcaF, qsuB* and *pobA*	Glucose Glucose + cerulenin Glucose (40 g/L) Glucose (80 g/L) Glucose (Fed-batch)	12 59 4 12 7	Braga et al. (2018b)
E.coli BW27784	4CL (*A. thaliana*) STS (*A. hypogaea*) 4CL (*A. thaliana*) STS (*V. vinifera*) 4CL (*P. crispum*) STS (*A. hypogaea*) 4CL (*P. crispum*) STS (*V. vinifera*) 4CL (*A. thaliana*) STS (*V. vinifera*)	—	*p*-Coumaric acid	404 1,380 142 610 2,340	Lim et al. (2011)
E. coli C41 (DE3)	TAL (*Saccharothrix espanaensis*) 4CL (*Streptomyces coelicolor*)	—	*p*-Coumaric acid	1.4	Choi et al. (2011)
E. coli BL21 (DE3)	TAL (*R. glutinis*) 4CL (*P. crispum*) STS (*V. vinifera*) *matB* and *matC* (*R. trifolii*)	—	Tyrosine	35.02	Wu et al. (2013)

(Continued on following page)

TABLE 1 | (*Continued*) Biosynthesis of resveratrol in engineered microorganisms.

Microbial host	Pathway genes (source)	Pathway/Host engineering	Substrate	Titer (mg/L)	References
E. coli C41 (DE3)	TAL (*S. espanaensis*) 4-CL (*S. coelicolor*) STS (*A. hypogaea*)	—	Glucose	5.2	Kang et al. (2014)
E. coli BW27784	4CL (*A. thaliana*) STS (*A. hypogaea*)	—	*p*-Coumaric acid	160	Afonso et al. (2015)
E. coli BL21 (DE3)	TAL (*S. espanaensis*) 4-CL (*A. thaliana*) STS (*A. hypogaea*)	—	Tyrosine	114.2	Wang et al. (2015)
E. coli BW25113	4CL2 (*P.crispum*) STS (*V. vinifera*)	—	*p*-Coumaric acid	268.2	Yang et al. (2015)
E. coli BW25113 (DE3)	TAL (*R. glutinis*) 4CL (*P. crispum*) STS (*V. vinifera*)	Inactivation of *tyr*R and deletion of *trp*ED by chromosomal integration	Glucose	4.6	Liu et al. (2016)
E.coli W (pheA-) Rg	TAL (*R. glutinis*) *tktAfbr* and *aroGfbr* (*E. coli*)	Deletion of *phe*A	Glycerol	22.58	Camacho-Zaragoza et al. (2016)
E.coli W-Vv	4CL (*S. coelicolor*) STS (*V. vinifera*)				
E. coli BL21 (DE3)	TAL (*Trichosporon cutaneum*) 4CL (*P. crispum*) STS (*V. vinifera*) *matB* and *matC* (*R. trifolii*) *tyrAfbr* and *aroGfbr* (*E.coli K12*)	Down-regulation of *fabD, fabH, fabB, fabF, fabI*	Glucose	304.5	Wu et al. (2017)

resulting in 12.4 ± 0.3 g/L resveratrol, which is the highest titer for *de novo* resveratrol production up to now.

BACTERIAL HOSTS

E. coli has been the subject of industrial interest for resveratrol production because of its fast growth the availability of advanced technology for its genetic manipulation and synthetic biology (Braga et al., 2018a). Furthermore, tyrosine and *p*-coumaric acid, the basic precursors of resveratrol, are the critical for increasing production, and are easily assessable and improved in *E. coli via* multiple metabolic engineering strategies (Shrestha et al., 2019). Additionally, *E. coli* is more suitable for resveratrol production than yeast because of its high tolerance to *p*-coumaric acid, another advantage (Shin et al., 2011; Huang et al., 2013) (Donnez et al., 2009). Recently, Zhang et al. identified stilbene synthase as the limiting enzyme via a novel probabilistic computational model and improved the final resveratrol titer from 62.472 mg/L to 172.799 mg/L, proving the model useful for predicting and improving biological production (Cotner et al., 2021).

Engineered *C. glutamicum* has also been employed as a vehicle for resveratrol production. Kallscheuer et al. (2016) introduced TAL from *Flavobacterium johnsoniae* into a strain of *C. glutamicum* for resveratrol production; 60 mg/L resveratrol was produced when using glucose as the carbon source. They further achieved 5 mg/L *trans*-resveratrol in *C. glutamicum* from 4-hydroxybenzoate, which is the first time a phenylpropanoid was synthesized from 4-hydroxybenzoic acid other than aromatic amino acids and ammonia lyase (Kallscheuer et al., 2017). Milke et al. (2019) constructed a recombinant *C. glutamicum* stain and increased the titer of resveratrol to 112 mg/L by modulating the central carbon metabolism of the host strain.

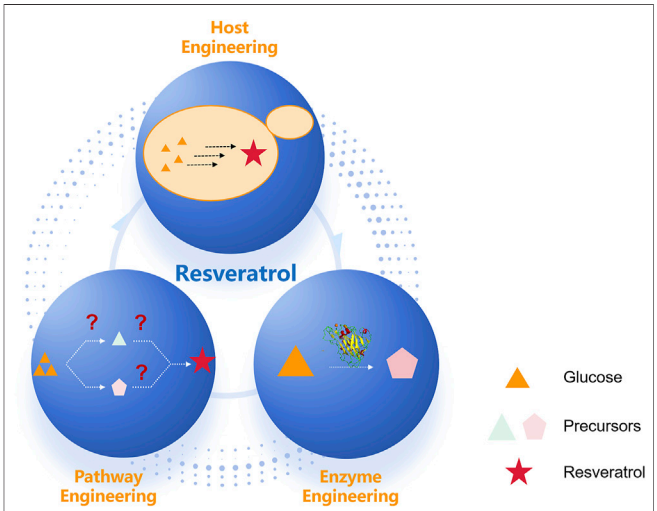

FIGURE 2 | Metabolic engineering at multiple levels has enabled engineering of increasingly complex heterologous resveratrol pathways. Heterologous resveratrol production in a microbial host can involve engineering at three different scales: host, pathway, and enzyme.

Engineered *S. venezuelae* has also been employed to produce resveratrol. Park and others reported resveratrol synthesis by expressing the heterologous phenylpropanoid biosynthetic pathway genes in *S. venezuelae* for the first time, although they only obtained 0.4 mg/L of resveratrol (Park et al., 2009). Likewise, the use of other organisms such as *Lactobacillus lactis* and *Aspergillus niger* has also been reported for resveratrol bioproduction (Chong et al., 2012).

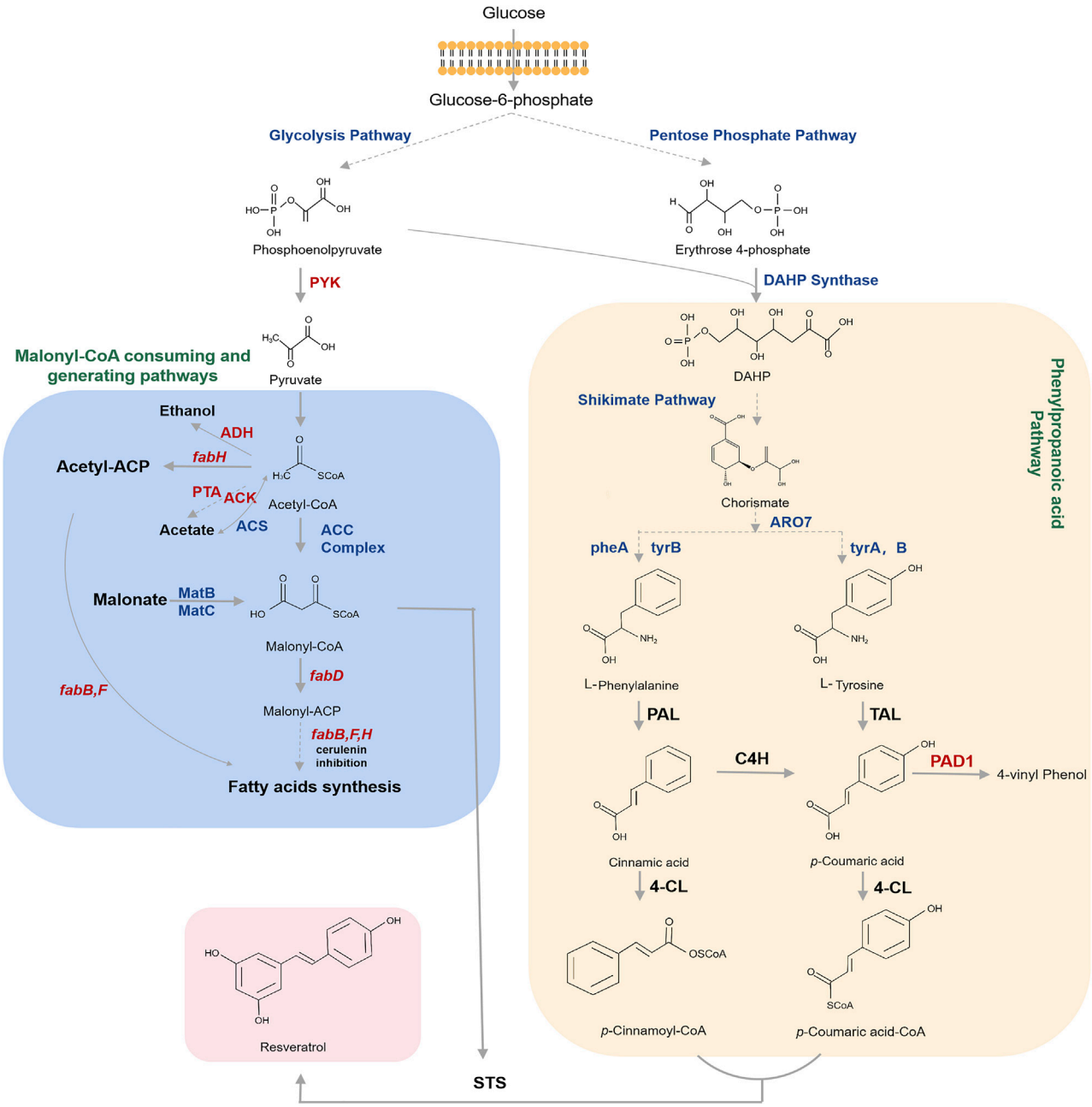

FIGURE 3 | Biosynthetic pathway for resveratrol starting from glucose. The pathways for generating precursors of resveratrol biosynthesis such as phenylpropanoyl-CoAs and malonyl-CoA are highlighted. Dotted arrows refer to multiple steps. Genes and enzymes in blue are targets for overexpression. Genes and enzymes in red are targets for knockout or inhibition. Note that the malonate is externally supplied. DAHP Synthase, 3-deoxy- D-arabinoheptulosonate-7-phosphate (DAHP) synthase; DAHP, 3-deoxy-D arabinoheptulosonate 7- phosphate; ARO7, chorismate mutase; ARO7, chorismate mutase; tyrA/pheA, genes that encode the chorismate mutase protein; tyrB, gene that encodes the tyrosine aminotransferase; PAL, phenylalanine ammonia lyase; TAL, tyrosine ammonia-lyase; C4H, cinnamate 4-hydroxylase; PAD, phenyl acrylic acid decarboxylase; 4CL, 4-coumaroyl-coA ligase; STS, stilbene synthase; PYK, pyruvate kinase; Acetyl-CoA, acetyl-coenzyme A; ADH, alcohol dehydrogenases; fabH, gene that encodes 3-oxoacyl carrier protein synthase III; PTA, phosphate acetyltransferase; ACK, acetate kinase; ACS: acetyl-CoA synthase; Acetyl-ACP, acetyl-acyl carrier protein; ACC complex, acetyl-coA carboxylase multienzyme complex; Malonyl-CoA, malonylcoenzyme A; MatB, malonyl-CoA synthetase; MatC, malonate carrier protein; fabD, gene that encodes the malonyl-CoA-acyl carrier protein transacylase; Malonyl-ACP, malonyl-acyl carrier protein; fabB/fabF, genes that encode the beta-ketoacyl-acp synthase I/II protein.

METABOLIC ENGINEERING TO ENHANCE RESVERATROL PRODUCTION

The design-build-test cycle (DBT cycle) has been widely used in metabolic engineering for the production of plant natural products (Nielsen and Keasling, 2016). In DBT iterative engineering cycles, host engineering includes the sufficient provision of precursor via precursor metabolites overproduction. Pathway engineering includes biosynthesis via a heterologous route to produce natural products, and enzyme engineering includes directed evolution to improve the properties of key rate-limiting enzymes (Cravens et al., 2019) (**Figure 2**). The rapid development of synthetic biology and enabling technology has accelerated DBT iterative engineering cycles, which have been widely employed for the engineering of resveratrol biosynthesis.

HOST ENGINEERING

In recent years, significant progress toward high-level resveratrol production has been achieved by microbial metabolic engineering. Nevertheless, an insufficient precursor supply (i.e., aromatic amino acids and malonyl-CoA) is still the main rate-limiting factor for resveratrol production in heterologous hosts. Thus, increasing the precursor supply via genetic manipulation of the host strain is considered a fundamental strategy for resveratrol bioproduction (van Summeren-Wesenhagen and Marienhagen, 2013; Milke et al., 2018).

As shown in **Figure 3**, resveratrol is produced from the aromatic amino acids L-phenylalanine (L-Phe) or L-tyrosine (L-Tyr). The metabolic engineering of the shikimic acid pathway primarily regulates the carbon flux into chorismate, followed by L-Phe and L-Tyr (Jiang et al., 2005; Rodriguez et al., 2015). Frequently-used strategies to increase the biosynthetic flux of the shikimic acid pathway are the elimination of enzyme feedback inhibition and the regulation of transcription. Furthermore, extending the supply and availability of erythrose-4-phosphate (E4P) and phosphoenolpyruvate (PEP) are the primary methods for improving chorismate production (Bulter et al., 2003; Lütke-Eversloh and Stephanopoulos, 2007). Significant strategies have been developed to enhance the production of aromatic amino acids or derived phenylpropanoic acids in microorganisms (Juminaga et al., 2012; Zhang and Stephanopoulos, 2013; Rodriguez et al., 2015). For example, Juminaga et al. (2012) reported the biosynthesis of resveratrol by encoding the key enzymes for converting E4P and PEP to L-Tyr, which significantly increased L-Tyr production to 80% of the theoretical yield.

Malonyl-CoA also serves as an important precursor for resveratrol biosynthesis. Moreover, malonyl-CoA is mostly used as an essential intermediate for fatty acid biosynthesis to support cell growth, so only a limited level of malonyl-CoA remains for resveratrol biosynthesis, which is a major challenge in resveratrol production. Therefore, two prime strategic steps have been utilized in order to expand the intracellular malonyl-CoA pool in microorganisms: 1) repressing fatty acid biosynthesis to inhibit malonyl-CoA consumption; 2) expanding the cytoplasmic malonyl-CoA pool by carboxylation of acetyl-CoA carboxylase (ACC), which can increase the amount of acetyl-CoA carboxylation to malonyl-CoA. Zha et al. (2009) found that overexpression of ACC increased the concentration of malonyl-CoA in *E. coli*. In addition, deleting genes encoding competing pathways, such as *pta* and *ackA,* which are involved in the degradation of acetyl-CoA into acetic acid, and the *adhE* gene, which is involved in ethanol production, can achieve significant effects (Finzel et al., 2015). Yang et al. (2015) revealed that blocking malonyl-CoA consumption and the deletion of the *fab* genes were lethal in microorganisms. Thus, three procedures have been carried out to inhibit malonyl-CoA consumption: 1) inhibiting FabB and FabF by adding the antibiotic cerulenin (Lim et al., 2011; Lu et al., 2016); 2) using antisense RNA to repress the *fab* operon, especially the *fabD* genes (Wu et al., 2014; Yang et al., 2015); 3) using CRISPRi technology to inhibit the *fab* gene and direct the carbon flux toward malonyl-CoA (Wu et al., 2015; Liang et al., 2016). Furthermore, another significant approach is to introduce biosynthetic pathway genes for malonate assimilation, such as *matB* and *matC*, into the system. (Shin et al., 2011).

PATHWAY ENGINEERING

By introducing the entire biosynthetic pathway into microorganisms, efficient synthesis of resveratrol from precursors (L-Phe or L-Tyr) or low-cost materials (such as glucose, ethanol or glycerol) can be realized, which is a great help for *de novo* biosynthesis or biotransformation of resveratrol (Jeandet et al., 2012; Li et al., 2016; Chen et al., 2020). The biosynthetic pathway for resveratrol is shown in **Figure 3**. The secondary metabolite phenylpropanoid route is the major metabolic pathway for resveratrol biosynthesis (Lu et al., 2016). The first step in resveratrol biosynthesis is the production of phenylpropanoic acids (i.e., *p*-coumaric acid and cinnamic acid) through nonoxidative deamination via tyrosine ammonia lyase (TAL) and L-phenylalanine ammonia lyase (PAL), which are then converted to *p*-coumaroyl-CoA and cinnamoyl-CoA by 4-coumarate-CoA ligase (4CL). Cinnamic acid can also be hydroxylated with the assistance of cinnamic acid-4-hydroxylase (C4H) to form *p*-coumaric acid. Finally, malonyl-CoA is condensed with *p*-coumaroyl-CoA to produce resveratrol, catalyzed by stilbene synthases (STSs) (van Summeren-Wesenhagen and Marienhagen, 2015; Milke et al., 2018). The main objective for the engineering of this pathway is to efficiently convert the aromatic amino acids to phenylpropyl by introducing hyper-active ammonia lyases such as PAL or TAL (Huang et al., 2013; Zhang and Stephanopoulos, 2013), which is a bottleneck in the resveratrol production from glucose (Yang et al., 2015; Kallscheuer et al., 2016). Liu et al. (2016) introduced TAL, 4CL and STS genes into *E. coli* strain and obtained 4.6 mg/L of resveratrol from glucose. Soon after, Wu et al. (2017) applied multiple metabolic engineering approaches to produce resveratrol from glucose in *E. coli*. However, the low activity of TAL and PAL enzymes is still the main obstacle for introducing the entire *de novo* pathway into the microorganism.

ENZYME ENGINEERING

As mentioned above, in many cases the function of one or a few key enzymes acts as a bottleneck in the overall metabolic fluxes, which are considered as the rate-limiting steps. Microorganisms cannot produce enough targeted product because of enzymes that have limited turnover or poor expression (Song et al., 2017; Song et al., 2018; Lian et al., 2018). Therefore, protein engineering, particularly directed evolution, has become one of the most powerful and widespread tools for engineering improved or novel functions in enzymes (Wu et al., 2013; Wang et al., 2021). Researchers employed protein engineering of 4CL and STS in *E. coli* for higher and more efficient resveratrol production (Becker et al., 2003; Zhang et al., 2015). Likewise, a yeast host harboring codon-optimized TAL and fused 4CL and STS, which allowed the production of 1.06 mg/L resveratrol without the use of L-Tyr (Wang et al., 2011). Moreover, the robustness of the rate-limiting enzymes or the metabolic activity of pathways can be optimized *in vivo* via metabolite-responsive biosensors (Skjoedt et al., 2016). Xiong et al. (2017) selected resveratrol hyper-producers rapidly and efficiently by reapplying the TtgR regulatory protein to a resveratrol-responsive biosensor in *E. coli*. Compared to the wild type, 4CL variants displayed improved catalytic properties for the production of this aromatic compound.

PRODUCTION PROCESS OPTIMIZATION TO INCREASE RESVERATROL SYNTHESIS

The balance and optimization of microbial growth and product formation have been identified as essential for increasing resveratrol production. In order to satisfy the world's sustainable demand, researchers have conducted some important studies for large-scale industrial production. Braga et al. (2018b) observed that increasing the glucose concentration from 40 g/L to 80 g/L resulted in a resveratrol titer that increased from 4 mg/L to 12 mg/L, which demonstrated that proper culture conditions, i.e., substrate concentration, were essential for the resveratrol production in *C. glutamicum* (Braga et al., 2018b).

In order to optimize and construct recombinant strains, the metabolic burden caused by the competition between natural metabolism and chemical production pathways (including chemical precursors, energy molecules and reduction equivalents) is one of the most important challenges to be urgently faced and resolved. Considering that polyphenols such as resveratrol are produced through complex biosynthetic pathways, the concept of co-culture has gained increasing attention in recent years. Through co-culture, that is, using multiple strains to produce different products or metabolize different substrates, it is feasible to co-produce resveratrol. Furthermore, the entire pathway can be divided and introduced into each strain as an entire module (Zhou et al., 2015). Yuan et al. (2020) recently described an approach utilizing a co-culture of *E. coli*–*S. cerevisiae* to produce resveratrol, with a final titer of 36 mg/L using glucose as a carbon source. To alleviate the metabolic burden of a single host, researchers divided the labor among artificial microbial communities using a cell consortium strategy (Yuan et al., 2020).

There are many other obstacles to resveratrol production in microbial hosts, such as the high cost of precursors and precursor toxicity. Researchers recently attempted to overcome these difficulties by using engineered strains to obtain low-cost and sustainable substrates and by using fed-batch cultures to reduce the toxicity of precursors (Wu et al., 2017) (Watts et al., 2006; Huang et al., 2013; Zhang and Stephanopoulos, 2013).

CONCLUSION AND FUTURE PERSPECTIVES

As of now, the efforts and results mentioned above have demonstrated the feasibility of converting microorganism hosts into cell factories to produce resveratrol, which can be achieved by grafting exogenous biosynthetic pathways into the endogenous metabolic network of cells. However, the current problem is that although they have promising potential for development and popularization, at present the performance of most engineered strains cannot achieve the goals required for industrial production. How to use microorganisms as vehicles to produce resveratrol more economically is still an important challenge. Multiple factors, including the cytotoxicity of end products, the low activity and stability of catalytic enzymes, and metabolic imbalances at the biosynthetic pathway level and across the cellular network, are challenges for the advancement of cell growth, the rate of production, product titer and yield to a certain degree. Furthermore, the production process is also hampered by the lack of critical, basic information about the interactions and regulation of metabolic networks, which require more time to discover and verify the contribution of potential biosynthetic pathways for resveratrol production. However, with the recent rapid development of metabolic engineering principles, it is expected that novel and reliable solutions will be found that will break the shackles that hinder industrial biological resveratrol production.

The cellular adaptation and metabolic stability of engineered cell factories has frequently been affected by heterologous chemicals, which are tremendously cytotoxic during the process of biosynthesis and long-term accumulation. Consequently, some approaches, including adaptive laboratory evolution (ALE) (Sandberg et al., 2019) and the multi-functional genome-wide CRISPR (MAGIC) system (Lian et al., 2019), have been designed to reduce the toxicity of products while maximizing the potency and yield of chemical products. For instance, Pereira et al. (2019) recently investigated through ALE experiments the mechanism of tolerance of *S. cerevisiae* to the cellular stress imposed by inhibiting concentrations of dicarboxylic acids. Lian et al. (2019) improved furfural tolerance in yeast using the MAGIC system; a method that identifies complex phenotypic genetic determinants that have not been previously identified, especially those interacting synergistically when disturbed to different levels of expression. The novel strategies mentioned above represent a promising alternative strategy to improve the resveratrol production capability of microbial hosts.

In order to alleviate the rate-limiting steps, protein engineering, especially directed evolution, has been applied to improve enzyme properties. It is particularly worth noting that machine learning has been increasingly utilized for protein engineering. Luo et al.

developed a high-performance method called Evolutionary Context-Integrated Neural Network (ECNet), providing generalization from low-order mutants to higher-order mutants, which can predict protein function levels from sequence to protein engineering process (Luo et al., 2021). Besides, recent advances in the development of sequence-based, MD-based, structure-based, and machine learning-based computational tools will promote the identification of the beneficial mutations and accelerate the protein engineering process by creating smaller but smarter libraries to enhance the robustness of catalytic enzymes (Huang et al., 2016). Moreover, attention should be paid to a combinatorial method to guide every precursor and metabolite towards the large-scale resveratrol production. Additionally, for resveratrol biosynthesis processes based on a microbial platform, the application of complete biosynthetic and related knowledge of molecular biology, including the entire genome, transcriptome, proteome and metabolome, will be promising for the improvement of the production efficiency and yield of resveratrol.

In summary, the goal of efficient resveratrol production in microbial hosts can be advanced by the integration of multiple tools such as metabolic engineering, systems and synthetic biology for strain design, as well as by improving process engineering strategies. By using such strategies, heterologous resveratrol production can be competitive with existing chemical synthesis and plant extraction processes, which will be a better choice to achieve the goal of sustainable resveratrol production.

AUTHOR CONTRIBUTIONS

CF wrote the manuscript. JC, WY, KL, and ZW searched the literatures. XS and MQ designed the review. All authors revised and approved the manuscript.

ACKNOWLEDGMENTS

We thank Ligang Ren (Department of Urology, Tongde Hospital of Zhejiang province, Hangzhou, Zhejiang, P.R.China) for his support and encouragement.

REFERENCES

Afonso, M. S., Ferreira, S., Domingues, F. C., and Silva, F. (2015). Resveratrol Production in Bioreactor: Assessment of Cell Physiological States and Plasmid Segregational Stability. *Biotechnol. Rep.* 5, 7–13. doi:10.1016/j.btre.2014.10.008

Almeida, T. C., and Silva, G. N. d. (2021). Resveratrol Effects in Bladder Cancer: A Mini Review. *Genet. Mol. Biol.* 44, e20200371. doi:10.1590/1678-4685-GMB-2020-0371

Baur, J. A., and Sinclair, D. A. (2006). Therapeutic Potential of Resveratrol: the *In Vivo* Evidence. *Nat. Rev. Drug Discov.* 5, 493–506. doi:10.1038/nrd2060

Becker, J., Armstrong, G., Vandermerwe, M., Lambrechts, M., Vivier, M., and Pretorius, I. (2003). Metabolic Engineering of for the Synthesis of the Wine-Related Antioxidant Resveratrol. *FEMS Yeast Res.* 4 (1), 79–85. doi:10.1016/s1567-1356(03)00157-0

Bola, C., Bartlett, H., and Eperjesi, F. (2014). Resveratrol and the Eye: Activity and Molecular Mechanisms. *Graefes Arch. Clin. Exp. Ophthalmol.* 252, 699–713. doi:10.1007/s00417-014-2604-8

Braga, A., Ferreira, P., Oliveira, J., Rocha, I., and Faria, N. (2018a). Heterologous Production of Resveratrol in Bacterial Hosts: Current Status and Perspectives. *World J. Microbiol. Biotechnol.* 34, 122. doi:10.1007/s11274-018-2506-8

Braga, A., Oliveira, J., Silva, R., Ferreira, P., Rocha, I., Kallscheuer, N., et al. (2018b). Impact of the Cultivation Strategy on Resveratrol Production from Glucose in Engineered *Corynebacterium Glutamicum*. *J. Biotechnol.* 265, 70–75. doi:10.1016/j.jbiotec.2017.11.006

Breuss, J., Atanasov, A., and Uhrin, P. (2019). Resveratrol and its Effects on the Vascular System. *Ijms* 20, 1523. doi:10.3390/ijms20071523

Bulter, T., Bernstein, J. R., and Liao, J. C. (2003). A Perspective of Metabolic Engineering Strategies: Moving up the Systems Hierarchy. *Biotechnol. Bioeng.* 84, 815–821. doi:10.1002/bit.10845

Camacho-Zaragoza, J. M., Hernández-Chávez, G., Moreno-Avitia, F., Ramírez-Iñiguez, R., Martínez, A., Bolívar, F., et al. (2016). Engineering of a Microbial Coculture of *Escherichia coli* Strains for the Biosynthesis of Resveratrol. *Microb. Cel Fact* 15, 163. doi:10.1186/s12934-016-0562-z

Chen, G., Xia, H., Zhang, Z.-g., and Yu, H.-l. (2019). Resveratrol in Management of Bone and Spinal Cancers. *Nat. Prod. Res.* 33, 516–526. doi:10.1080/14786419.2017.1389936

Chen, R., Yang, S., Zhang, L., and Zhou, Y. J. (2020). Advanced Strategies for Production of Natural Products in Yeast. *iScience* 23, 100879. doi:10.1016/j.isci.2020.100879

Choi, O., Wu, C.-Z., Kang, S. Y., Ahn, J. S., Uhm, T.-B., and Hong, Y.-S. (2011). Biosynthesis of Plant-specific Phenylpropanoids by Construction of an Artificial Biosynthetic Pathway in *Escherichia coli*. *J. Ind. Microbiol. Biotechnol.* 38, 1657–1665. doi:10.1007/s10295-011-0954-3

Chong, Y., Yan, A., Yang, X., Cai, Y., and Chen, J. (2012). An Optimum Fermentation Model Established by Genetic Algorithm for Biotransformation from Crude Polydatin to Resveratrol. *Appl. Biochem. Biotechnol.* 166, 446–457. doi:10.1007/s12010-011-9440-7

Costa, C. E., Møller-Hansen, I., Romaní, A., Teixeira, J. A., Borodina, I., and Domingues, L. (2021). Resveratrol Production from Hydrothermally Pretreated Eucalyptus Wood Using Recombinant Industrial *Saccharomyces cerevisiae* Strains. *ACS Synth. Biol.* 10, 1895–1903. doi:10.1021/acssynbio.1c00120

Cotner, M., Zhan, J., and Zhang, Z. (2021). A Computational Metabolic Model for Engineered Production of Resveratrol in *Escherichia coli*. *ACS Synth. Biol.* 10, 1992–2001. doi:10.1021/acssynbio.1c00163

Cravens, A., Payne, J., and Smolke, C. D. (2019). Synthetic Biology Strategies for Microbial Biosynthesis of Plant Natural Products. *Nat. Commun.* 10, 2142. doi:10.1038/s41467-019-09848-w

Den Hartogh, D. J., and Tsiani, E. (2019). Health Benefits of Resveratrol in Kidney Disease: Evidence from *In Vitro* and *In Vivo* Studies. *Nutrients* 11, 1624. doi:10.3390/nu11071624

Donnez, D., Jeandet, P., Clément, C., and Courot, E. (2009). Bioproduction of Resveratrol and Stilbene Derivatives by Plant Cells and Microorganisms. *Trends Biotechnology* 27, 706–713. doi:10.1016/j.tibtech.2009.09.005

Dudnik, A., Gaspar, P., Neves, A. R., and Forster, J. (2018). Engineering of Microbial Cell Factories for the Production of Plant Polyphenols with Health-Beneficial Properties. *Cpd* 24, 2208–2225. doi:10.2174/1381612824666180515152049

Feng, Y., Zhou, J., and Jiang, Y. (2016). Resveratrol in Lung Cancer- a Systematic Review. *J. BUON* 21, 950–953.

Finzel, K., Lee, D. J., and Burkart, M. D. (2015). Using Modern Tools to Probe the Structure-Function Relationship of Fatty Acid Synthases. *ChemBioChem* 16, 528–547. doi:10.1002/cbic.201402578

Fletcher, E., Krivoruchko, A., and Nielsen, J. (2016). Industrial Systems Biology and its Impact on Synthetic Biology of Yeast Cell Factories. *Biotechnol. Bioeng.* 113, 1164–1170. doi:10.1002/bit.25870

Giuliani, C., Iezzi, M., Ciolli, L., Hysi, A., Bucci, I., Di Santo, S., et al. (2017). Resveratrol Has Anti-thyroid Effects Both *In Vitro* and *In Vivo*. *Food Chem. Toxicol.* 107, 237–247. doi:10.1016/j.fct.2017.06.044

Gu, Y., Ma, J., Zhu, Y., Ding, X., and Xu, P. (2020). Engineering *Yarrowia Lipolytica* as a Chassis for *De Novo* Synthesis of Five Aromatic-Derived Natural Products and Chemicals. *ACS Synth. Biol.* 9, 2096–2106. doi:10.1021/acssynbio.0c00185

He, Q., Szczepańska, P., Yuzbashev, T., Lazar, Z., and Ledesma-Amaro, R. (2020). *De Novo* production of Resveratrol from Glycerol by Engineering Different Metabolic Pathways in *Yarrowia Lipolytica*. *Metab. Eng. Commun.* 11, e00146. doi:10.1016/j.mec.2020.e00146

Huang, P.-S., Boyken, S. E., and Baker, D. (2016). The Coming of Age of *De Novo* Protein Design. *Nature* 537, 320–327. doi:10.1038/nature19946

Huang, Q., Lin, Y., and Yan, Y. (2013). Caffeic Acid Production Enhancement by Engineering a Phenylalanine Over-producingEscherichia Colistrain. *Biotechnol. Bioeng.* 110, 3188–3196. doi:10.1002/bit.24988

Jakubczyk, K., Skonieczna-Żydecka, K., Kałduńska, J., Stachowska, E., Gutowska, I., and Janda, K. (2020). Effects of Resveratrol Supplementation in Patients with Non-Alcoholic Fatty Liver Disease-A Meta-Analysis. *Nutrients* 12, 2435. doi:10.3390/nu12082435

Jeandet, P., Delaunois, B., Aziz, A., Donnez, D., Vasserot, Y., Cordelier, S., et al. (2012). Metabolic Engineering of Yeast and Plants for the Production of the Biologically Active Hydroxystilbene, Resveratrol. *J. Biomed. Biotechnol.* 2012, 1–14. doi:10.1155/2012/579089

Jiang, H., Wood, K. V., and Morgan, J. A. (2005). Metabolic Engineering of the Phenylpropanoid Pathway in *Saccharomyces cerevisiae*. *Appl. Environ. Microbiol.* 71, 2962–2969. doi:10.1128/AEM.71.6.2962-2969.2005

Juminaga, D., Baidoo, E. E. K., Redding-Johanson, A. M., Batth, T. S., Burd, H., Mukhopadhyay, A., et al. (2012). Modular Engineering of L-Tyrosine Production in *Escherichia coli*. *Appl. Environ. Microbiol.* 78, 89–98. doi:10.1128/AEM.06017-11

Kallscheuer, N., Vogt, M., and Marienhagen, J. (2017). A Novel Synthetic Pathway Enables Microbial Production of Polyphenols Independent from the Endogenous Aromatic Amino Acid Metabolism. *ACS Synth. Biol.* 6, 410–415. doi:10.1021/acssynbio.6b00291

Kallscheuer, N., Vogt, M., Stenzel, A., Gätgens, J., Bott, M., and Marienhagen, J. (2016). Construction of a *Corynebacterium Glutamicum* Platform Strain for the Production of Stilbenes and (2S)-Flavanones. *Metab. Eng.* 38, 47–55. doi:10.1016/j.ymben.2016.06.003

Kang, S.-Y., Lee, J. K., Choi, O., Kim, C. Y., Jang, J.-H., Hwang, B. Y., et al. (2014). Biosynthesis of Methylated Resveratrol Analogs through the Construction of an Artificial Biosynthetic Pathway in *E. coli*. *BMC Biotechnol.* 14, 67. doi:10.1186/1472-6750-14-67

Kiskova, T., Kubatka, P., Büsselberg, D., and Kassayova, M. (2020). The Plant-Derived Compound Resveratrol in Brain Cancer: A Review. *Biomolecules* 10, 161. doi:10.3390/biom10010161

Li, D., Wang, G., Jin, G., Yao, K., Zhao, Z., Bie, L., et al. (2019). Resveratrol Suppresses colon Cancer Growth by Targeting the AKT/STAT3 Signaling Pathway. *Int. J. Mol. Med.* 43, 630–640. doi:10.3892/ijmm.2018.3969

Li, M., Kildegaard, K. R., Chen, Y., Rodriguez, A., Borodina, I., and Nielsen, J. (2015). *De Novo* production of Resveratrol from Glucose or Ethanol by Engineered *Saccharomyces cerevisiae*. *Metab. Eng.* 32, 1–11. doi:10.1016/j.ymben.2015.08.007

Li, M., Schneider, K., Kristensen, M., Borodina, I., and Nielsen, J. (2016). Engineering Yeast for High-Level Production of Stilbenoid Antioxidants. *Sci. Rep.* 6, 36827. doi:10.1038/srep36827

Lian, J., Mishra, S., and Zhao, H. (2018). Recent Advances in Metabolic Engineering of *Saccharomyces cerevisiae*: New Tools and Their Applications. *Metab. Eng.* 50, 85–108. doi:10.1016/j.ymben.2018.04.011

Lian, J., Schultz, C., Cao, M., HamediRad, M., and Zhao, H. (2019). Multi-functional Genome-wide CRISPR System for High Throughput Genotype-Phenotype Mapping. *Nat. Commun.* 10, 5794. doi:10.1038/s41467-019-13621-4

Liang, J.-l., Guo, L.-q., Lin, J.-f., He, Z.-q., Cai, F.-j., and Chen, J.-f. (2016). A Novel Process for Obtaining Pinosylvin Using Combinatorial Bioengineering in *Escherichia coli*. *World J. Microbiol. Biotechnol.* 32, 102. doi:10.1007/s11274-016-2062-z

Lim, C. G., Fowler, Z. L., Hueller, T., Schaffer, S., and Koffas, M. A. G. (2011). High-yield Resveratrol Production in Engineered *Escherichia coli*. *Appl. Environ. Microbiol.* 77, 3451–3460. doi:10.1128/AEM.02186-10

Liu, Q., Liu, Y., Chen, Y., and Nielsen, J. (2020). Current State of Aromatics Production Using Yeast: Achievements and Challenges. *Curr. Opin. Biotechnol.* 65, 65–74. doi:10.1016/j.copbio.2020.01.008

Liu, Q., Yu, T., Li, X., Chen, Y., Campbell, K., Nielsen, J., et al. (2019). Rewiring Carbon Metabolism in Yeast for High Level Production of Aromatic Chemicals. *Nat. Commun.* 10, 4976. doi:10.1038/s41467-019-12961-5

Liu, X., Lin, J., Hu, H., Zhou, B., and Zhu, B. (2016). De Novobiosynthesis of Resveratrol by Site-specific Integration of Heterologous Genes inEscherichia Coli. *FEMS Microbiol. Lett.* 363, fnw061. doi:10.1093/femsle/fnw061

Liu, Z., Li, Y., She, G., Zheng, X., Shao, L., Wang, P., et al. (2020). Resveratrol Induces Cervical Cancer HeLa Cell Apoptosis through the Activation and Nuclear Translocation Promotion of FOXO3a. *Pharmazie* 75, 250–254. doi:10.1691/ph.2020.0386

Lu, Y., Shao, D., Shi, J., Huang, Q., Yang, H., and Jin, M. (2016). Strategies for Enhancing Resveratrol Production and the Expression of Pathway Enzymes. *Appl. Microbiol. Biotechnol.* 100, 7407–7421. doi:10.1007/s00253-016-7723-1

Luo, Y., Jiang, G., Yu, T., Liu, Y., Vo, L., Ding, H., et al. (2021). ECNet Is an Evolutionary Context-Integrated Deep Learning Framework for Protein Engineering. *Nat. Commun.* 12, 5743. doi:10.1038/s41467-021-25976-8

Lütke-Eversloh, T., and Stephanopoulos, G. (2007). L-tyrosine Production by Deregulated Strains of *Escherichia coli*. *Appl. Microbiol. Biotechnol.* 75, 103–110. doi:10.1007/s00253-006-0792-9

Ma, J., Gu, Y., Marsafari, M., and Xu, P. (2020). Synthetic Biology, Systems Biology, and Metabolic Engineering of *Yarrowia Lipolytica* toward a Sustainable Biorefinery Platform. *J. Ind. Microbiol. Biotechnol.* 47, 845–862. doi:10.1007/s10295-020-02290-8

Madzak, C. (2018). Engineering *Yarrowia Lipolytica* for Use in Biotechnological Applications: A Review of Major Achievements and Recent Innovations. *Mol. Biotechnol.* 60, 621–635. doi:10.1007/s12033-018-0093-4

Madzak, C. (2015). *Yarrowia Lipolytica*: Recent Achievements in Heterologous Protein Expression and Pathway Engineering. *Appl. Microbiol. Biotechnol.* 99, 4559–4577. doi:10.1007/s00253-015-6624-z

Milke, L., Aschenbrenner, J., Marienhagen, J., and Kallscheuer, N. (2018). Production of Plant-Derived Polyphenols in Microorganisms: Current State and Perspectives. *Appl. Microbiol. Biotechnol.* 102, 1575–1585. doi:10.1007/s00253-018-8747-5

Milke, L., Ferreira, P., Kallscheuer, N., Braga, A., Vogt, M., Kappelmann, J., et al. (2019). Modulation of the central Carbon Metabolism of Corynebacterium Glutamicum Improves malonyl-CoA Availability and Increases Plant Polyphenol Synthesis. *Biotechnol. Bioeng.* 116, 1380–1391. doi:10.1002/bit.26939

Nielsen, J., and Keasling, J. D. (2016). Engineering Cellular Metabolism. *Cell* 164, 1185–1197. doi:10.1016/j.cell.2016.02.004

Palmer, C. M., Miller, K. K., Nguyen, A., and Alper, H. S. (2020). Engineering 4-Coumaroyl-CoA Derived Polyketide Production in Yarrowia Lipolytica through a β-oxidation Mediated Strategy. *Metab. Eng.* 57, 174–181. doi:10.1016/j.ymben.2019.11.006

Park, S. R., Yoon, J. A., Paik, J. H., Park, J. W., Jung, W. S., Ban, Y.-H., et al. (2009). Engineering of Plant-specific Phenylpropanoids Biosynthesis in *Streptomyces Venezuelae*. *J. Biotechnol.* 141, 181–188. doi:10.1016/j.jbiotec.2009.03.013

Pereira, R., Wei, Y., Mohamed, E., Radi, M., Malina, C., Herrgård, M. J., et al. (2019). Adaptive Laboratory Evolution of Tolerance to Dicarboxylic Acids in *Saccharomyces cerevisiae*. *Metab. Eng.* 56, 130–141. doi:10.1016/j.ymben.2019.09.008

Rainha, J., Gomes, D., Rodrigues, L. R., and Rodrigues, J. L. (2020). Synthetic Biology Approaches to Engineer Saccharomyces cerevisiae towards the Industrial Production of Valuable Polyphenolic Compounds. *Life* 10, 56. doi:10.3390/life10050056

Rauf, A., Imran, M., Butt, M. S., Nadeem, M., Peters, D. G., and Mubarak, M. S. (2018). Resveratrol as an Anti-cancer Agent: A Review. *Crit. Rev. Food Sci. Nutr.* 58, 1428–1447. doi:10.1080/10408398.2016.1263597

Ravikumar, P., Katariya, M., Patil, S., Tatke, P., and Pillai, R. (2019). Skin Delivery of Resveratrol Encapsulated Lipidic Formulation for Melanoma Chemoprevention. *J. microencapsulation* 36, 1–17. doi:10.1080/02652048.2019.1649481

Rodriguez, A., Kildegaard, K. R., Li, M., Borodina, I., and Nielsen, J. (2015). Establishment of a Yeast Platform Strain for Production of *P*-Coumaric Acid through Metabolic Engineering of Aromatic Amino Acid Biosynthesis. *Metab. Eng.* 31, 181–188. doi:10.1016/j.ymben.2015.08.003

Sáez-Sáez, J., Wang, G., Marella, E. R., Sudarsan, S., Cernuda Pastor, M., and Borodina, I. (2020). Engineering the Oleaginous Yeast *Yarrowia Lipolytica* for High-Level Resveratrol Production. *Metab. Eng.* 62, 51–61. doi:10.1016/j.ymben.2020.08.009

Sandberg, T. E., Salazar, M. J., Weng, L. L., Palsson, B. O., and Feist, A. M. (2019). The Emergence of Adaptive Laboratory Evolution as an Efficient Tool for Biological Discovery and Industrial Biotechnology. *Metab. Eng.* 56, 1–16. doi:10.1016/j.ymben.2019.08.004

Sexton, É., Van Themsche, C., LeBlanc, K., Parent, S., Lemoine, P., and Asselin, E. (2006). Resveratrol Interferes with AKT Activity and Triggers Apoptosis in Human Uterine Cancer Cells. *Mol. Cancer* 5, 45. doi:10.1186/1476-4598-5-45

Shin, S.-Y., Han, N. S., Park, Y.-C., Kim, M.-D., and Seo, J.-H. (2011). Production of Resveratrol from *P*-Coumaric Acid in Recombinant *Saccharomyces cerevisiae* Expressing 4-coumarate:coenzyme A Ligase and Stilbene Synthase Genes. *Enzyme Microb. Technol.* 48, 48–53. doi:10.1016/j.enzmictec.2010.09.004

Shin, S.-Y., Jung, S.-M., Kim, M.-D., Han, N. S., and Seo, J.-H. (2012). Production of Resveratrol from Tyrosine in Metabolically Engineered *Saccharomyces cerevisiae*. *Enzyme Microb. Technol.* 51, 211–216. doi:10.1016/j.enzmictec.2012.06.005

Shrestha, A., Pandey, R. P., and Sohng, J. K. (2019). Biosynthesis of Resveratrol and Piceatannol in Engineered Microbial Strains: Achievements and Perspectives. *Appl. Microbiol. Biotechnol.* 103, 2959–2972. doi:10.1007/s00253-019-09672-8

Shrotriya, S., Agarwal, R., and Sclafani, R. A. (2015). A Perspective on Chemoprevention by Resveratrol in Head and Neck Squamous Cell Carcinoma. *Adv. Exp. Med. Biol.* 815, 333–348. doi:10.1007/978-3-319-09614-8_19

Sinha, D., Sarkar, N., Biswas, J., and Bishayee, A. (2016). Resveratrol for Breast Cancer Prevention and Therapy: Preclinical Evidence and Molecular Mechanisms. *Semin. Cancer Biol.* 40-41, 209–232. doi:10.1016/j.semcancer.2015.11.001

Sirotkin, A., Kádasi, A., Balaží, A., Kotwica, J., Alwasel, S., and Harrath, A. H. (2020). The Action of Benzene, Resveratrol and Their Combination on Ovarian Cell Hormone Release. *Folia Biol. (Praha)* 66, 67–71.

Skjoedt, M. L., Snoek, T., Kildegaard, K. R., Arsovska, D., Eichenberger, M., Goedecke, T. J., et al. (2016). Engineering Prokaryotic Transcriptional Activators as Metabolite Biosensors in Yeast. *Nat. Chem. Biol.* 12, 951–958. doi:10.1038/nchembio.2177

Song, X., Li, Y., Wu, Y., Cai, M., Liu, Q., Gao, K., et al. (2018). Metabolic Engineering Strategies for Improvement of Ethanol Production in Cellulolytic *Saccharomyces cerevisiae*. *FEMS yeast Res.* 18 (8), foy090. doi:10.1093/femsyr/foy090

Song, X., Liu, Q., Mao, J., Wu, Y., Li, Y., Gao, K., et al. (2017). POT1-mediated δ-integration Strategy for High-Copy, Stable Expression of Heterologous Proteins in Saccharomyces cerevisiae. *FEMS yeast Res.* 17 (6), fox064. doi:10.1093/femsyr/fox064

Sun, P., Liang, J.-L., Kang, L.-Z., Huang, X.-Y., Huang, J.-J., Ye, Z.-W., et al. (2015). Increased Resveratrol Production in Wines Using Engineered Wine strainsSaccharomyces cerevisiaeEC1118 and Relaxed Antibiotic or Auxotrophic Selection. *Biotechnol. Prog.* 31, 650–655. doi:10.1002/btpr.2057

Sun, X., Fu, P., Xie, L., Chai, S., Xu, Q., Zeng, L., et al. (2021). Resveratrol Inhibits the Progression of Cervical Cancer by Suppressing the Transcription and Expression of HPV E6 and E7 Genes. *Int. J. Mol. Med.* 47, 335–345. doi:10.3892/ijmm.2020.4789

Tian, B., and Liu, J. (2020). Resveratrol: a Review of Plant Sources, Synthesis, Stability, Modification and Food Application. *J. Sci. Food Agric.* 100, 1392–1404. doi:10.1002/jsfa.10152

van Summeren-Wesenhagen, P. V., and Marienhagen, J. (2015). Metabolic Engineering of *Escherichia coli* for the Synthesis of the Plant Polyphenol Pinosylvin. *Appl. Environ. Microbiol.* 81, 840–849. doi:10.1128/AEM.02966-14

van Summeren-Wesenhagen, P. V., and Marienhagen, J. (2013). Putting Bugs to the Blush. *Bioengineered* 4, 355–362. doi:10.4161/bioe.23885

Wang, S., Zhang, S., Xiao, A., Rasmussen, M., Skidmore, C., and Zhan, J. (2015). Metabolic Engineering of *Escherichia coli* for the Biosynthesis of Various Phenylpropanoid Derivatives. *Metab. Eng.* 29, 153–159. doi:10.1016/j.ymben.2015.03.011

Wang, Y., Chen, H., and Yu, O. (2014). A Plant Malonyl-CoA Synthetase Enhances Lipid Content and Polyketide Yield in Yeast Cells. *Appl. Microbiol. Biotechnol.* 98, 5435–5447. doi:10.1007/s00253-014-5612-z

Wang, Y., Halls, C., Zhang, J., Matsuno, M., Zhang, Y., and Yu, O. (2011). Stepwise Increase of Resveratrol Biosynthesis in Yeast *Saccharomyces cerevisiae* by Metabolic Engineering. *Metab. Eng.* 13, 455–463. doi:10.1016/j.ymben.2011.04.005

Wang, Y., Xue, P., Cao, M., Yu, T., Lane, S. T., and Zhao, H. (2021). Directed Evolution: Methodologies and Applications. *Chem. Rev.* 121, 12384–12444. doi:10.1021/acs.chemrev.1c00260

Wang, Y., and Yu, O. (2012). Synthetic Scaffolds Increased Resveratrol Biosynthesis in Engineered Yeast Cells. *J. Biotechnol.* 157, 258–260. doi:10.1016/j.jbiotec.2011.11.003

Watts, K. T., Lee, P. C., and Schmidt-Dannert, C. (2006). Biosynthesis of Plant-specific Stilbene Polyketides in Metabolically Engineered *Escherichia coli*. *BMC Biotechnol.* 6, 22. doi:10.1186/1472-6750-6-22

Wu, J., Du, G., Chen, J., and Zhou, J. (2015). Enhancing Flavonoid Production by Systematically Tuning the central Metabolic Pathways Based on a CRISPR Interference System in *Escherichia coli*. *Sci. Rep.* 5, 13477. doi:10.1038/srep13477

Wu, J., Liu, P., Fan, Y., Bao, H., Du, G., Zhou, J., et al. (2013). Multivariate Modular Metabolic Engineering of *Escherichia coli* to Produce Resveratrol from L-Tyrosine. *J. Biotechnol.* 167, 404–411. doi:10.1016/j.jbiotec.2013.07.030

Wu, J., Yu, O., Du, G., Zhou, J., and Chen, J. (2014). Fine-tuning of the Fatty Acid Pathway by Synthetic Antisense RNA for Enhanced (2S)-Naringenin Production from L-Tyrosine in *Escherichia coli*. *Appl. Environ. Microbiol.* 80, 7283–7292. doi:10.1128/AEM.02411-14

Wu, J., Zhou, P., Zhang, X., and Dong, M. (2017). Efficient *De Novo* Synthesis of Resveratrol by Metabolically Engineered *Escherichia coli*. *J. Ind. Microbiol. Biotechnol.* 44, 1083–1095. doi:10.1007/s10295-017-1937-9

Xiong, D., Lu, S., Wu, J., Liang, C., Wang, W., Wang, W., et al. (2017). Improving Key Enzyme Activity in Phenylpropanoid Pathway with a Designed Biosensor. *Metab. Eng.* 40, 115–123. doi:10.1016/j.ymben.2017.01.006

Yang, H., Zhang, X., Liu, Y., Liu, L., Li, J., Du, G., et al. (2021). Synthetic Biology-Driven Microbial Production of Folates: Advances and Perspectives. *Bioresour. Technol.* 324, 124624. doi:10.1016/j.biortech.2020.124624

Yang, Y., Lin, Y., Li, L., Linhardt, R. J., and Yan, Y. (2015). Regulating Malonyl-CoA Metabolism via Synthetic Antisense RNAs for Enhanced Biosynthesis of Natural Products. *Metab. Eng.* 29, 217–226. doi:10.1016/j.ymben.2015.03.018

Yuan, S.-F., Yi, X., Johnston, T. G., and Alper, H. S. (2020). *De Novo* resveratrol Production through Modular Engineering of an *Escherichia Coli-Saccharomyces cerevisiae* Co-culture. *Microb. Cel Fact* 19, 143. doi:10.1186/s12934-020-01401-5

Zaffaroni, N., and Beretta, G. L. (2021). Resveratrol and Prostate Cancer: The Power of Phytochemicals. *Cmc* 28, 4845–4862. doi:10.2174/0929867328666201228124038

Zha, W., Rubin-Pitel, S. B., Shao, Z., and Zhao, H. (2009). Improving Cellular Malonyl-CoA Level in *Escherichia coli* via Metabolic Engineering. *Metab. Eng.* 11, 192–198. doi:10.1016/j.ymben.2009.01.005

Zhang, E., Guo, X., Meng, Z., Wang, J., Sun, J., Yao, X., et al. (2015). Construction, Expression, and Characterization of Arabidopsis thaliana 4CL and Arachis hypogaea RS Fusion Gene 4CL:RS in *Escherichia coli*. *World J. Microbiol. Biotechnol.* 31, 1379–1385. doi:10.1007/s11274-015-1889-z

Zhang, H., and Stephanopoulos, G. (2013). Engineering *E. coli* for Caffeic Acid Biosynthesis from Renewable Sugars. *Appl. Microbiol. Biotechnol.* 97, 3333–3341. doi:10.1007/s00253-012-4544-8

Zhou, H.-B., Yan, Y., Sun, Y. N., and Zhu, J. R. (2003). Resveratrol Induces Apoptosis in Human Esophageal Carcinoma Cells. *Wjg* 9, 408–411. doi:10.3748/wjg.v9.i3.408

Zhou, K., Qiao, K., Edgar, S., and Stephanopoulos, G. (2015). Distributing a Metabolic Pathway Among a Microbial Consortium Enhances Production of Natural Products. *Nat. Biotechnol.* 33, 377–383. doi:10.1038/nbt.3095

Zulueta, A., Caretti, A., Signorelli, P., and Ghidoni, R. (2015). Resveratrol: A Potential Challenger against Gastric Cancer. *Wjg* 21, 10636–10643. doi:10.3748/wjg.v21.i37.10636

Conflict of Interest: The authors declare that the research was conducted in the absence of any commercial or financial relationships that could be construed as a potential conflict of interest.

Publisher's Note: All claims expressed in this article are solely those of the authors and do not necessarily represent those of their affiliated organizations, or those of the publisher, the editors and the reviewers. Any product that may be evaluated in this article, or claim that may be made by its manufacturer, is not guaranteed or endorsed by the publisher.

frontiers in Bioengineering and Biotechnology

ORIGINAL RESEARCH
published: 14 February 2022
doi: 10.3389/fbioe.2022.843843

Glucose-Derived Raspberry Ketone Produced via Engineered *Escherichia coli* Metabolism

Shunsuke Masuo, Chisa Saga, Kurumi Usui, Yuma Sasakura, Yukie Kawasaki and Naoki Takaya*

Faculty of Life and Environmental Sciences, Microbiology Research Center for Sustainability, University of Tsukuba, Tsukuba, Japan

The demand for raspberry ketone (RK) as a plant-based natural flavoring agent is high, but natural RK is one of the most expensive flavor compounds due to its limited content in plants. Here, we produced RK *de novo* from simple carbon sources in *Escherichia coli.* We genetically engineered *E. coli* metabolism to overproduce the metabolic precursors tyrosine and *p*-coumaric acid and increase RK production. The engineered *E. coli* produced 19.3- and 1.9 g/L of tyrosine and *p*-coumaric acid from glucose, respectively. The *p*-coumaric acid CoA ligase from *Agrobacterium tumefaciens* and amino acid substituted benzalacetone synthase of *Rhemu palmatum* (Chinese rhubarb) were overexpressed in *E. coli* overproducing *p*-coumaric acid. The overexpression of *fabF*, encoding β-ketoacyl-acyl carrier protein synthetase II increased intracellular malonyl-CoA, the precursor of benzalacetone synthase for RK biosynthesis, and improved RK production. Fed-batch cultures given glucose as a carbon source produced 62 mg/L of RK under optimized conditions. Our production system is inexpensive and does not rely on plant extraction; thus, it should significantly contribute to the flavor and fragrance industries.

Keywords: raspberry ketone, flavor agent, microbial production, plant secondary metabolite, metabolic engieering

OPEN ACCESS

Edited by:
Jingyu Wang,
Westlake Institute for Advanced Study (WIAS), China

Reviewed by:
Jifeng Yuan,
Xiamen University, China
Jian Zha,
Shaanxi University of Science and Technology, China

***Correspondence:**
Naoki Takaya
takaya.naoki.ge@u.tsukuba.ac.jp

Specialty section:
This article was submitted to Synthetic Biology, a section of the journal Frontiers in Bioengineering and Biotechnology

Received: *27 December 2021*
Accepted: *18 January 2022*
Published: *14 February 2022*

Citation:
Masuo S, Saga C, Usui K, Sasakura Y, Kawasaki Y and Takaya N (2022) Glucose-Derived Raspberry Ketone Produced via Engineered Escherichia coli *Metabolism. Front. Bioeng. Biotechnol. 10:843843. doi: 10.3389/fbioe.2022.843843*

1 INTRODUCTION

The raspberry phenylbutanoid ketone 4-(4-hydroxyphenyl)butan-2-one (RK) is a natural flavor in plants such as raspberries, grapes, peaches, and rhubarb. The berry flavor of RK with a low odor threshold is used as a food additive to create various aromas such as cherry, strawberry, kiwi and other fruits (Beekwilder et al., 2007; Bredsdorff et al., 2015; Sun et al., 2021). The alleged health benefits of RK include weight reduction (Morimoto et al., 2005; Wang et al., 2012) and skin lightening (Harada et al., 2008) and it is in high demand in the supplements and cosmetics industries (Milke et al., 2020; Vandamme and Soetaert, 2002). As the demand for RK is second only to vanillin, the potential of RK in the natural flavor market RK is 6–10 million Euros (Feron and Wache 2005). However, RK is difficult to cost-effectively produce from plants due to low contents. For example, raspberries contain only 1 to 4 mg/kg of RK (Larsen et al., 1991; Beekwilder et al., 2007), and extraction costs are high (Böker et al., 2001). Thus, the market for naturally occurring RK as a flavoring agent is United States $3,000–$20,000/kg (Milke et al., 2020). Chemically synthesized RK (Malkar and Yadav 2019) is not regarded as a natural flavor by United States and EU regulations, and it is essentially unacceptable to some consumers. However, microbial fermentation is an alternative strategy that allows inexpensive mass production of RK without the need for extraction from plants.

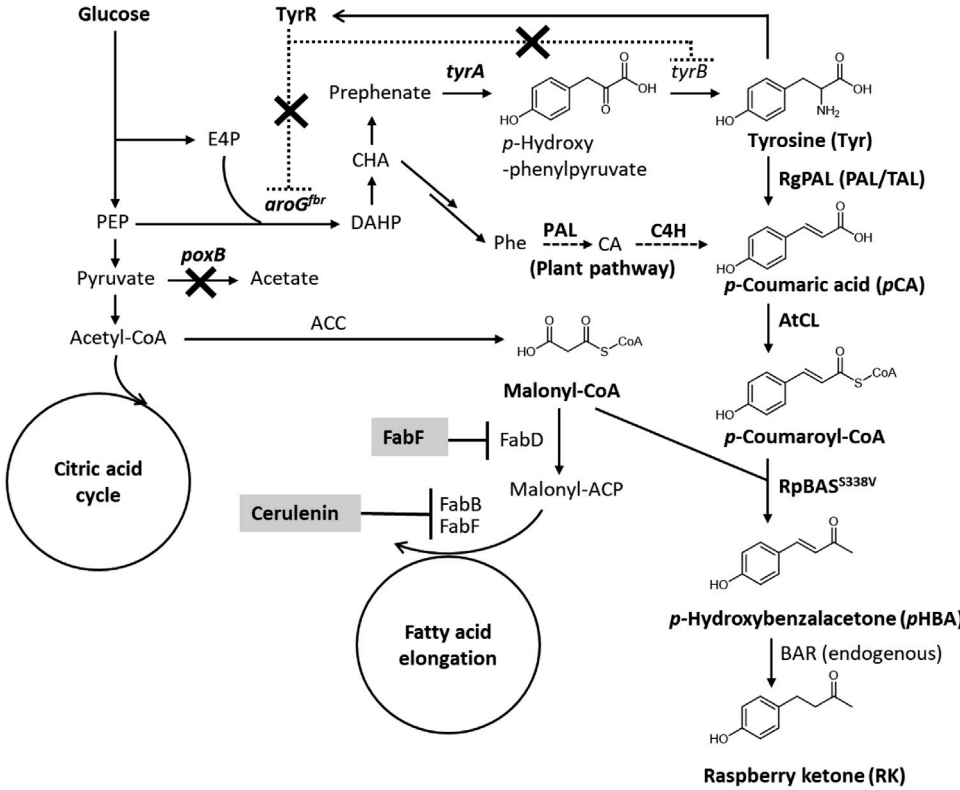

FIGURE 1 | Metabolic network for RK biosynthesis from glucose in engineered *E. coli*. ACC, acetyl-CoA carboxylase; ACP, acyl carrier protein; aroG^{fbr}, feedback resistant isozyme of DAHP synthase; BAR, benzalacetone reductase; BAS, benzalacetone synthase; CA, cinnamic acid; CL, 4-coumarate CoA ligase; C4H, cinnamate-4-hydroxylase; DAHP, 3-deoxy-D-arabino-heptulosonate 7-phosphate; E4P, erythrose 4-phosphate; FabB, β-ketoacyl-ACP synthase I; FabD, malonyl-CoA-ACP transacylase; FabF, β-ketoacyl-ACP synthase II; PAL, phenylalanine ammonia lyase; PEP, phosphoenolpyruvate; Phe, phenylalanine; *poxB*, pyruvate oxidase; TAL, tyrosine ammonia lyase; *tyrA*, chorismate mutase/prephenate dehydrogenase; *tyrB*, tyrosine aminotransferase; TyrR, transcriptional repressor of aromatic amino acid biosynthesis genes.

The RK biosynthesis pathways and mechanisms in raspberries and rhubarb have been investigated (Borejsza-Wysocki and Hrazdina 1994; Abe et al., 2001). The pathway starts from *p*-coumaroyl-CoA (**Figure 1**), which is a ubiquitous intermediate of the plant lignin biosynthetic pathway. During RK synthesis, the non-oxidative deamination of phenylalanine is catalyzed by phenylalanine ammonia lyase (PAL) and followed by hydroxylation and CoA-activation catalyzed by cinnamate-4-hydroxylase (C4H) and *p*-coumarate CoA ligase (CL) to produce *p*-coumaroyl-CoA. Thereafter, *p*-coumaroyl-CoA is condensed with malonyl-CoA to generate *p*-hydroxybenzalacetone by the activity of benzalacetone synthase (BAS), which is a type III polyketide synthase. The resulting *p*-hydroxybenzalacetone is reduced by the NADPH-dependent benzalacetone reductase (BAR) to yield RK (**Figure 1**).

Microbial RK has been produced using genetically manipulated microorganisms such as yeast, *Escherichia coli* and other bacteria (Lee at al. 2016; Wang et al., 2019; Milke et al., 2020). The common approach converts *p*-coumaric acid as a starting material to RK in host cells producing heterogenous CL, BAS and BAR that originate from plants. Host *E. coli* and *Corynebacterium glutamicum* cells convert *p*-coumaric acid to RK with titers of 91.0 and 99.8 mg/l, respectively (Wang et al., 2019; Milke et al., 2020). However, few efforts have been made to produce RK *de novo* using renewable carbon sources. One exception is a wine yeast that generates plant PAL, C4H, and the synthetic CL and BAS fusion enzyme, and this yeast produces 3.5 mg/l of RK in grape juice medium (Lee at al. 2016), which is far lower than that yielded using *p*-coumaric acid as the raw material. The low titer could be due to the low availability of *p*-coumaroyl-CoA and malonyl-CoA that are substrates of BAS, the key enzyme of RK biosynthesis. Here, we showed that improving *p*-coumaric acid and malonyl-CoA availability significantly increased the productivity of microbial *de novo* RK synthesis. We constructed *E. coli* that generated abundant *p*-coumaric acid and malonyl-CoA by metabolic engineering and chemical stimulation. After gene selection and stepwise culture optimization, our recombinant *E. coli* produced RK biosynthesis enzymes and fermented glucose to produce 62 mg/L of RK.

2 MATERIALS AND METHODS

2.1 Strains, Materials, and Instrumentation

Supplementary Table S1 lists the strains used in this study. We produced RK and constructed plasmids using *E. coli* BL21 (DE3)

and *E. coli* JM109 (Novagen, Madison, WI, United States), respectively. We purchased 4-coumaroyl-CoA from Sigma–Aldrich (St. Louis, MO, United States) and L-tyrosine, *p*-coumaric acid, and *p*-hydroxybenzalacetone from Wako Chemicals (Tokyo, Japan). Plasmids were constructed using KOD One PCR Master Mix (Toyobo, Osaka, Japan), restriction enzymes (Takara Bio Inc., Shiga, Japan), Ligation high Ver. 2 (Toyobo) and NEBuilder HiFi DNA Assembly Master Mix (New England Biolabs Inc., Ipswich, MA, United States). Metabolites were analyzed by high-performance liquid chromatography (HPLC) using a 1200 infinity photodiode array detector (Agilent Technologies Inc., Santa Clara, CA, United States), and by LC-ESI-MS/MS and GC-MS using LCMS-8045 and QP-2010 mass spectrometers (both from Shimadzu, Kyoto, Japan).

2.2 Plasmid Construction and *E. coli* Gene Knockout

Supplementary Table S2 lists the plasmids used in this study. Nucleotide fragments of the *tyrA* gene were amplified by PCR using *E. coli* MG1655 genomic DNA and primers (**Supplementary Table S3**), digested with NcoI and BamHI, and cloned into pETduet-1 (Novagen) that was also digested with these enzymes to generate pET-tyrA. Plasmid pET-FevV for producing TAL (*fevV* from *Streptomyces* sp. WK-5344), was provided by Dr. Kawaguchi (Kawaguchi et al., 2017). Nucleotide sequences of the PAL genes of *Camellia sinensis* (Matsumoto et al., 1994) and *Lithospermum erythrorhizon* (Yazaki et al., 1995) were optimized according to *E. coli* codon usage (accession numbers; MZ439822 and MZ439823, Cspal and Lepal), synthesized and cloned into pUC57 (Genscript Biotech Corp., Piscataway, NJ, United States) to generate pUC-Cspal and pUC-Lepal. These plasmids were digested with NdeI and EcoRI and the resulting PAL gene fragments were cloned into pET-28b (Novagen) to obtain pET-Cspal and pET-Lepal, respectively. Plasmid pET28a-*pal* (Zhu et al., 2013) was digested with NdeI and XhoI to obtain *Rhodotorula glutinis* PAL gene fragments, and these were cloned into pRSFduet-1 (Novagen) to generate pRSF-Rgpal. The *Agrobacterium tumefaciens* 4-coumarate CoA ligase gene (Atu1416) was amplified by PCR using *A. tumefaciens* C58 genomic DNA and primers (**Supplementary Table S3**), digested with EcoRI and SalI, and cloned into pCDFduet-1 (Novagen) to generate pCDF-AtCL. The *Rubus idaeus* and *Rhemu palmatum* BAS genes were codon optimized (accession numbers; MZ439820 and MZ439821), synthesized, and cloned into pEX-A2 to obtain pEX-RiBAS and pEX-RpBAS (Eurofins Genomics Inc., Tokyo, Japan), respectively. We mutated BAS genes using QuickChange Site-directed Mutagenesis Kits (Agilent Technologies) and primers (**Supplementary Table S3**) to generate pEX-RiBAS^{S338V} pEX-RpBAS^{S331V}. The DNA fragments of RiBAS and RpBAS genes were digested with NdeI and XhoI and cloned into pCDF-AtCL to generate pCDF-AtCL-RiBAS, pCDF-AtuCL-RpBAS, pCDF-AtCL-RiBAS^{S338V} and pCDF-AtuCL-RpBAS^{S331V}, respectively. We amplified *fabF* by PCR using *E. coli* MG1655 genomic DNA and primers (**Supplementary Table S3**), then assembled it with pET28b that was digested with NcoI and XhoI to generate pET-fabF. Fragments of DNA containing the T7lac promoter, *fabF*, and T7 terminator sequences were amplified by PCR using pET-fabF and primers (**Supplementary Table S3**), then assembled with pCDF-AtCL-RpBAS that was digested with PacI to generate pCDF-AtCL-RpBAS-fabF. The *tyrR* and *poxB* genes of BL21 (DE3) were disrupted using the Red/ET recombination system (Gene Bridges, Heidelberg, Germany) with the described primers (**Supplementary Table S3**) to generate ΔtyrR and ΔpoxB strains (Masuo et al., 2016).

2.3 Fermentation

Recombinant *E. coli* BL21 (DE3) strains were cultured in 3 ml of LB medium, then 2 ml portions were inoculated into 500-ml conical flasks containing 100 ml of fermentation medium (10 g glucose, 10 g tryptone, 5 g yeast extract, 24 g Na_2HPO_4, 12 g KH_2PO_4, 0.5 g NaCl, 1 g NH_4Cl, 0.5 g $MgSO_4$ $7H_2O$, 15 mg $CaCl_2$, 50 mg thiamine-HCl and 2 ml of trace element solution/L; Fujita et al., 2013) or modified fermentation medium (10 g glucose, 10 g tryptone, 5 g yeast extract, 12 g Na_2HPO_4, 6 g KH_2PO_4, 42 g MOPS, 0.5 g NaCl, 10 g (NH4) 2SO4, 0.5 g $MgSO_4$ $7H_2O$, 15 mg $CaCl_2$, 50 mg thiamine-HCl and 2 ml of trace element solution/L). The flasks were rotary-shaken at 120 rpm and 30°C for 3 h under aerobic conditions unless otherwise stated. When the OD_{600} reached 0.6, 0.5 mM isopropyl-β-D-thiogalactoside (IPTG) was added, then the cells were further incubated for the indicated amounts of time. Fed-batch cultures in a 1.0-L BMJ-01 fermenter (Biott, Tokyo, Japan) containing 0.5 L of fermentation or modified fermentation medium were agitated at 550 rpm, 30°C, and aerated at 1.0 L/min. When the OD_{600} reached 0.6, 0.1 mM IPTG was added. Peristaltic pumps fed the cultures with 500 g/L of glucose when the glucose concentration dipped below 1.5 g/L. The pH was monitored using an electrode and maintained between 7.0 and 7.1 by adding 10% NH_4OH.

2.4 Bioconversion

Escherichia coli BL21 (DE3) harboring either pET-FevV, pET-28a-*pal*, pET-Cspal or pET-Lepal was cultured in 3 ml of LB medium, then 2 ml portions were inoculated into 100 ml of LB medium and rotary-shaken at 120 rpm at 30°C under aerobic conditions. When the OD_{600} of the cultures reached 0.6, the cultures were incubated for 18 h with 0.5 mM IPTG, then the cells were sedimented by centrifugation at 3,000 × g for 10 min. The cells were washed with 50 mM Tris-HCl (pH 7.0), suspended in 50 mM Tris-HCl (pH 8.0) containing 1.8 g/L of tyrosine and incubated at 30°C with agitation at 120 rpm.

2.5 GC-MS Analysis

Culture supernatants were acidified with formic acid and extracted twice with equal amounts ethyl acetate. The ethyl acetate was evaporated, then the extracts were dissolved in methanol and analyzed by GC-MS equipped with a ZB-5MS capillary column (30 m × 0.32 mm internal diameter × 0.25-μm film thickness: Phenomenex, Torrance, CA, United States). The injection and ion-source temperatures were 250 and 200°C,

respectively. The linear velocity of the carrier helium gas was 45 cm/s. The oven temperature was controlled at 40°C for 4 min, increased to 250°C at a rate of 12°C/min, then maintained at 250°C for 7 min.

2.6 Determination of Metabolite Concentrations

Tyrosine and *p*-coumaric acid were quantified using HPLC and a TSKgel® ODS-100V column (4.6 mm × 25 cm, particle size 3 μm, Tosoh, Tokyo, Japan). The initial mobile phase comprised 95%: 5% 10 mM ammonium formate (pH 7.0): acetonitrile for 8 min, followed by an increase to 50% acetonitrile for 6 min and maintained for 2 min. The flow rate of 0.8 ml min^{-1} and the column temperature of 30°C were maintained throughout the analysis.

We quantified RK and intermediates using the multiple-reaction monitoring mode on the LC-ESI-MS/MS under the following conditions: capillary voltage, 4.5 kV; desolvation line, 250°C; heat block, 400°C; nebulizer nitrogen gas 3 L/min; drying gas, 10 L/min. Compounds of interest were separated by the LC system equipped with a 150 × 2.1 mm ACQUITY UPLC CSH™ C_{18} 2.1 × 150 mm (Waters, Corp., Milford, MA United States) with particle and pore sizes of 1.7 μm and 130 Å, respectively. The initial mobile phase was solvent A (0.025% formic acid) for 4 min. The concentration of solvent B (acetonitrile) was increased to 50% for 11 min, then maintained for 1 min. The column was re-equilibrated for 4 min. Malonyl-CoA was separated using 5 mM ammonium formate (pH 7.0) containing 50% acetonitrile as the mobile phase in isocratic mode. The flow rate of 0.4 ml min^{-1} and the column temperature at 40°C were maintained throughout the analysis. The MRM-transitions were *m*/*z* 180.05 to 163.15 (for tyrosine, negative ion mode), *m*/*z* 163.05 to 119.05 (*p*-coumaric acid, negative ion mode), *m*/*z* 165.05 to 147.10 (p-hydroxybenzalacetone, positive ion mode), *m*/*z* 854.05 to 303.00 (malonyl-CoA, positive ion mode) and *m*/*z* 165.10 to 107.10 (RK, positive ion mode). The dwell time, Q1 pre-bias, collision energy and Q3 pre-bias were set at 100 ms, 20 V, 14 eV, 17 V for tyrosine, 100 ms, 17 V, 14 eV, 21 V for *p*-coumaric acid, 100 ms, −12vV, −12 eV, −15 V for *p*-hydroxybenzalacetone, 100 ms, −34 V, −41 eV, −30 V for malonyl-CoA, and 100 ms, −14 V, −12 eV, −11 V for RK.

3 RESULTS

3.1 Metabolic Engineering of *E. coli* to Produce *p*-Coumaric Acid

We initially generated *E. coli* that overproduced tyrosine, the precursor of *p*-coumaric acid to construct a microbial *de novo* RK synthesis system (**Figure 1**). A feedback resistant mutant of 3-deoxy-D-arabinoheptulosonate-7-phosphate (DAHP) synthase (*aroG*^{fbr}) and the chorismate mutase/prephenate dehydrogenase gene (*tyrA*) were overexpressed in *E. coli* BL21 (DE3) with the native *aroG* and T7 promoters, respectively (**Figure 1**). The resulting strain produced 0.4 ± 0.1 g/L of tyrosine in the modified M9 medium, whereas the parental *E. coli* BL21 (DE3) almost did not (**Supplementary Figure S1**). Another potential parental strain,

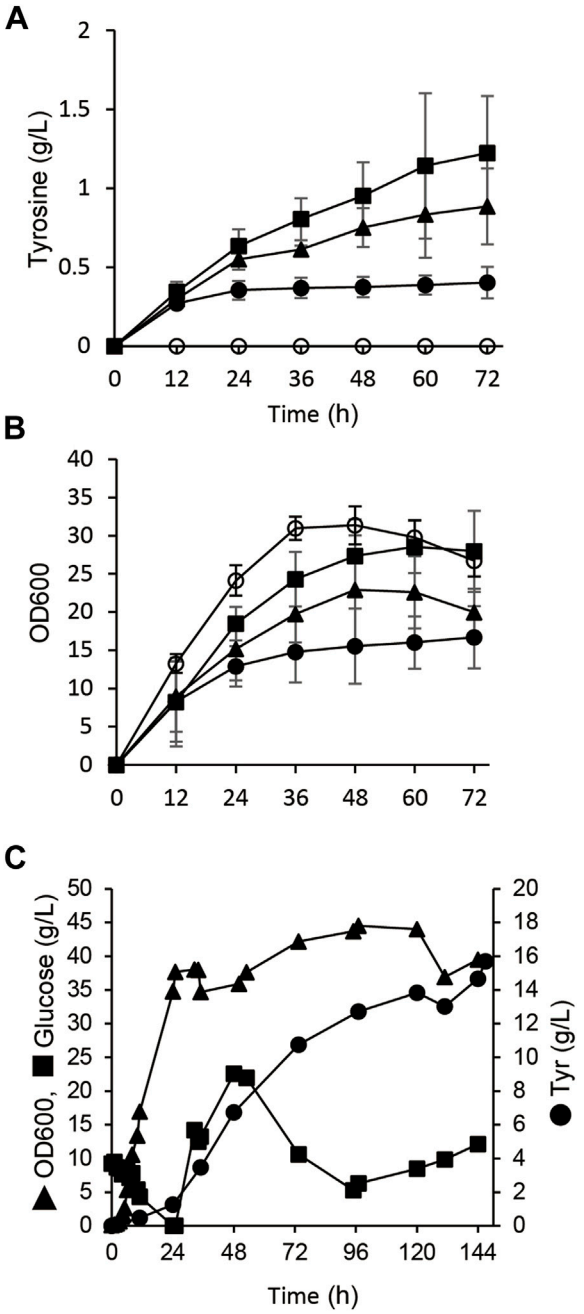

FIGURE 2 | Tyrosine production from glucose by *E. coli* with engineered metabolism. **(A,B)** Time-dependent tyrosine production **(A)** and growth **(B)** of *E. coli* BL21 (DE3) (closed circles), *ΔpoxB* (closed triangles) and *ΔtyrR* (closed squares) harboring pET-tyrA and pACYC-aroG^{fbr} in fermentation medium at 30°C. *E. coli* BL21 (DE3) harboring pET and pACYC empty plasmids was analyzed as a control (open squares). **(C)** Fed-batch cultures of *ΔtyrR* harboring pET-tyrA and pACYC-aroG^{fbr} in jar fermenters containing 0.5 L of fermentation medium at 30°C and pH 7.1 (maintained by 10% ammonium) were incubated for 24 h, then fed with glucose (0.8 g/L/h). Error bars indicate standard deviation (*n* = 3).

TABLE 1 | Tyrosine production from glucose by *E. coli* gene deletion mutants.

Strain	Growth rate (h^{-1})	Tyr production (g/L)	Tyr production rate (g/L/h)	Yield (%)
Wild-type (pET-duet, pACYC184)	0.90 ± 0.25	<0.01	<0.00002	n.d.
Wild-type (pET-tyrA, pACYC-aroG4)	0.38 ± 0.08	0.40 ± 0.08	0.007 ± 0.001	1.9
ΔpoxB (pET-tyrA, pACYC-aroG4)	0.52 ± 0.12	0.89 ± 0.08	0.021 ± 0.003	3.8
ΔtyrR (pET-tyrA, pACYC-aroG4)	0.85 ± 0.08	1.2 ± 0.1	0.024 ± 0.002	5.1

Wild-type E. coli *BL21 (DE3), ΔpoxB and ΔtyrR harboring pET-tyrA and pACYC-aroG4 were cultured in fermentation medium. Growth and tyrosine production rates were calculated from changes in OD_{600} and tyrosine concentrations during culture for 12 and 24 h. The yield was calculated from amounts of tyrosine produced and glucose consumed after 96 h of culture. n.d.: not determined.*

TABLE 2 | Bioconversion of tyrosine to *p*-coumaric acid by *E. coli* harboring PAL expression plasmids.

PAL/TAL	*p*-Coumaric acid produced (g/L)	*p*-Coumaric acid production rate (g/L/h)	Conversion efficiency (%)
FevV	1.1 ± 0.1	0.095 ± 0.008	66
RgPAL	1.6 ± 0.2	0.80 ± 0.04	89
CsPAL	0.27 ± 0.01	0.05 ± 0.01	17
LePAL	1.5 ± 0.1	0.50 ± 0.06	88

Escherichia coli *BL21 (DE3) cells (10 mg wet weight), harboring pET-FevV (Kawaguchi et al., 2017), pET28a*-pal *(Zhu et al., 2013), pET-CspaI or pET-LepaI, were each incubated in 1 ml of 100 mM Tris-HCl (pH 8.5) containing 1.8 g/l of tyrosine. Production rates were calculated from the amount of p-coumaric acid produced during the first 0.5 h of incubation.*

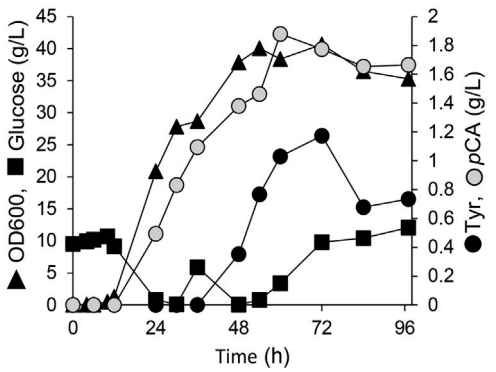

FIGURE 3 | Production of *p*-coumaric acid by *E. coli*. Fed-batch cultures of AT2 strain in jar fermenters containing 0.5 L of fermentation medium at 30°C and pH 7.1 (maintained by 10% ammonium) were incubated for 24 h, then fed with glucose (0.8 g/L/h).

E. coli NST37 (DE3)/*ΔpheLA*, which has an enhanced shikimate pathway (Masuo et al., 2016), produced less tyrosine after the same genetic modification (**Supplementary Figure S1B**). The *poxB* gene deletion mutant (*ΔpoxB*) harboring $aroG^{fbr}$ and *tyrA* expression plasmids produced 0.9 ± 0.2 g/L of tyrosine in the 72-h flask culture (**Figure 2A** and **Table 1**). Deletion of *poxB* encoding the pyruvate oxidase that synthesizes acetate from pyruvate (Causey et al., 2004), led to a positive effect on tyrosine production probably due to the altered carbon flux including acetate, phosphoenolpyruvate, and erythrose-4-phosphate generation (**Figure 1**).

A gene deletion mutant of *tyrR* (*ΔtyrR*), which encodes a transcriptional repressor of aromatic amino acid biosynthesis genes (Pittard et al., 2005), harboring the $aroG^{fbr}$ and *tyrA* expression plasmids (strain AT1) produced 1.2 ± 0.3 g/L of tyrosine in flask cultures. The production titer of AT1 was 3.0-fold higher than that of parental BL21 (DE3) strain (**Figure 2A** and **Table 1**). Growth defect caused by $aroG^{fbr}$ and *tyrA* overexpression was restored by gene disruption of *tyrR* (**Figures 2A,B**). Fed-batch cultures of AT1 with stepwise additions of glucose avoided excessive glucose accumulation in the jar fermenters. The culture generated 15.7 g/L tyrosine with a production yield of 7.4% vs glucose (**Figure 2C**). Precipitates that appeared on the inner walls of fermentation vessels (**Supplementary Figure S2B**), contained 1.9 g of tyrosine, and the total amount produced was 19.3 g/L. The culture generated low levels of acetate (<1.0 g L^{-1}; **Supplementary Figure S2A**), indicating decreased metabolic flow of glucose to acetate, which resulted in increased tyrosine production.

To convert the produced tyrosine to *p*CA, we employed tyrosine ammonia lyase (TAL) or bifunctional PAL that deaminate phenylalanine and tyrosine. We cloned TAL or PAL genes derived from yeast, plant or bacteria into the pRSFduet1 vector under the control of the T7 promoter and the resulting plasmids were introduced into BL21 (DE3). These strains converted tyrosine into *p*CA (**Table 2**). The *E. coli* producing *Rodotorura glutinis* PAL (RgPAL) had the highest yield, conversion rate and efficiency, and was deemed adequate for *p*CA synthesis *de novo*. We introduced the RgPAL expression plasmid into the AT1 strain and the resulting AT2 strain produced 1.9 g/L of *p*CA from glucose in a fed-batch culture under optimized conditions over a period of 60 h (**Figure 3**). The culture accumulated >1.0 g/L tyrosine, indicating that PAL reaction limits *p*CA production.

3.2 RK Production by *p*-Coumaric Acid Producing *E. coli*.

We used AT2 as a heterologous expression host to construct the RK pathway. We expressed both the genes for AtCL and RiBAS,

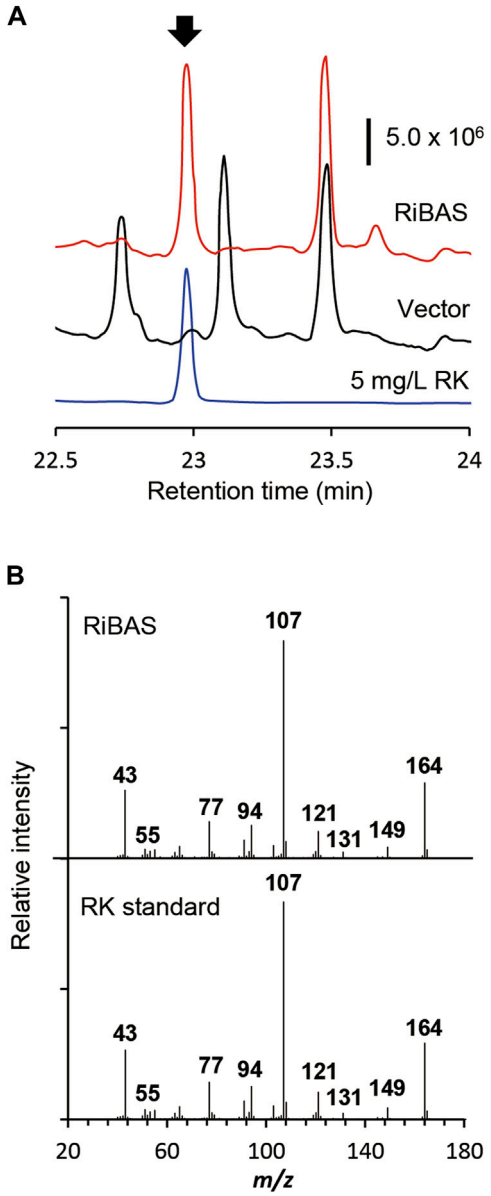

FIGURE 4 | Production of RK from glucose by *E. coli* expressing 4CL and BAS. **(A)** GC-MS profile of extracts of cultured *E. coli* AT2 harboring pCDF-Atu4CL-RiBAS (RiBAS) or pCDFduet-1 (Vector). Arrow, peak of standard RK. **(B)** Gas chromatography-mass spectrometry fragmentation patterns of peaks at 23 min (arrow in **(A)**).

derived from *Agrobacterium tumefaciens* C58 (Campillo et al., 2014) and *Rubus idaeus* BAS (Zheng and Hrazdina, 2008) in the AT2 strain under the control of T7lac promoter. The resulting AT2Ri strain was cultured in modified M9 medium for 169 h and its metabolites were extracted with ethyl acetate and analyzed by GC-MS (**Figure 4A**). The ion peaks had the same retention time and fragmentation ion pattern as standard RK in the metabolites of AT2Ri, but not AT2 (**Figures 4A,B**). The AT2Ri strain produced 0.44 mg L^{-1} of RK from glucose for 76 h, whereas is considerable amount of *p*CA remaining in the culture supernatant (**Table 3**), implied insufficient BAS activities in the cells. Substituting serine 331 with valine in BAS from *Rhemu palmatum* (RpBAS) increases the catalytic activity (Abe et al., 2007). Alignment of the amino acid sequences showed that this serine residue was conserved in RiBAS (**Supplementary Figure S3**). The corresponding mutants of RiBAS ($RiBAS^{S338V}$), RpBAS, and mutated $RpBAS^{S331V}$, together with AtCL, were introduced into AT2, respectively. The resulting AT2Rp and AT2RpSV strains, expressing RpBAS and $RpBAS^{S331V}$, produced 28 and 29 mg/L of RK from glucose as the raw material after 76 h, respectively. These yields were 60-fold higher than that of AT2Ri (**Table 3**). The AT2Rp and AT2RpSV strains accumulated less *p*CA than AT2Ri, indicating that conversion of *p*CA to RK is more efficient with RpBAS and $RpBAS^{S331V}$. Our study showed that the mutations in RpBAS and RiBAS had little effect on cellular RK production (**Table 3**), probably due to the pH dependence of BAS activity (Abe et al., 2007). Less *p*-hydroxybenzalacetone accumulated in cultured AT2RpSV (**Table 3**), implying sufficient BAR activities in this strain under appropriate culture conditions.

3.3 Genetic and Chemical Manipulation Increased Intracellular Malonyl-CoA and RK Production.

The overexpression of *fabF*, which encodes β-ketoacyl carrier protein synthase II, inhibits FabD activity and hence fatty acid elongation (**Figure 1**), and resulted in cellular accumulation of malonyl-CoA in *E. coli* (Subrahmanyam and Cronan 1998; Kassab et al., 2019). The AT3 strain that was the AT2 strain overexpressing in under the control of T7 lac promoter, accumulated 2.2-fold more malonyl-CoA than AT2 (**Figure 5A**). We constructed a plasmid to overexpress *fabF* along with the AtCL and $RpBAS^{S331V}$ genes and introduced it into AT2 to generate AT3RpSV, which produced 24 mg/L of RK

TABLE 3 | Raspberry ketone production by *E. coli* expressing different BAS genes.

Gene	Tyrosine (mg/l)	*p*-Coumaric acid (mg/l)	*p*-Hydroxybenzalacetone (mg/l)	Raspberry ketone (mg/l)
RiBAS	31.3 ± 1.9	142.6 ± 8.3	0.04 ± 0.01	0.44 ± 0.02
RpBAS	6.4 ± 0.5	<0.1	3.44 ± 0.32	28.38 ± 3.52
RiBAS (S338V)	27.6 ± 1.8	353.4 ± 17.6	0.07 ± 0.01	0.29 ± 0.02
RpBAS (S331V)	<0.1	0.6 ± 0.1	0.46 ± 0.08	29.19 ± 2.32

AT2 harboring BAS expression plasmids were cultured in modified fermentation medium containing 1% glucose for 76 h, then concentrations of compounds were determined by LC-MS.

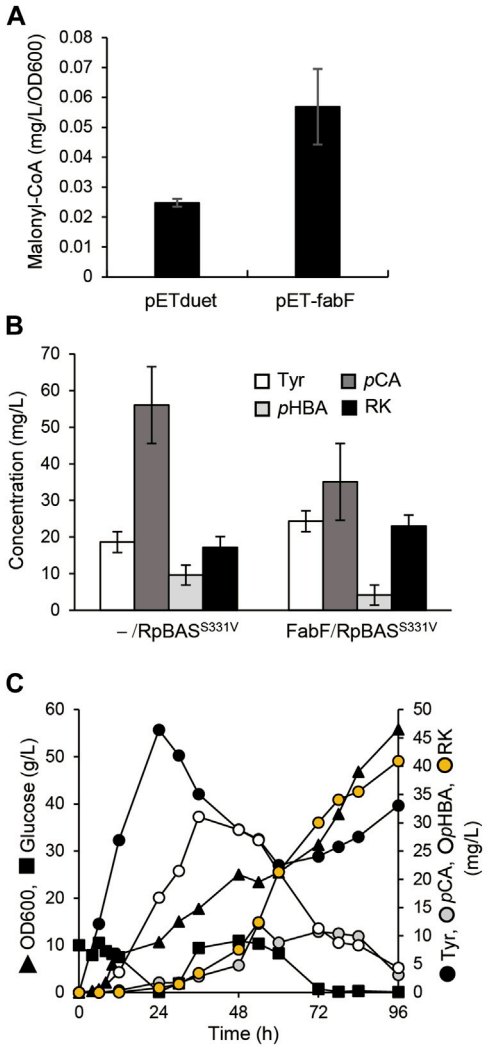

FIGURE 5 | Overexpression of FabF increased intracellular malonyl-CoA and RK production. **(A)** Intracellular malonyl-CoA concentration in *ΔtyrR* strain harboring pETduet-1 or pET-fabF incubated in modified fermentation medium at 30°C for 60 h. **(B)** Concentrations of RK and intermediates in cultured AT2 strain harboring pCDF-Atu4CL-RpBAS^{S331V} (-/RpBAS^{S331V}) or pCDF-Atu4CL-RpBAS^{S331V}-fabF (FabF/RpBAS^{S331V} (AT3RpSV strain). Strains were incubated in modified fermentation medium at 30°C for 60 h. **(C)** Fed-batch cultures of AT3RpSV in jar fermenters containing 0.5 L of fermentation medium were incubated for 24 h at 30°C and pH 7.1 (maintained by 10% ammonium), then fed with glucose (0.8 g/L/h). Error bars indicate standard deviation (n = 3).

when cultured for 60 h in modified fermentation medium (**Figure 5B**). The production titer of AT3RpSV was 1.4-fold higher than that of AT2RpSV, indicating that the increased cellular malonyl-CoA levels improved the amount of malonyl-CoA available for RK production. We optimized aeration conditions, culture media, and IPTG concentrations for RK production by AT3RpSV (**Supplementary Figure S4**). Fed-batch cultured AT3RpSV under controlled glucose addition produced 41 mg/L of RK with a production yield of 0.08% (vs glucose, **Figure 5C**).

Cerulenin binds to ACP synthase to block its interaction with malonyl-CoA and inhibits fatty acid biosynthesis. Adding cerulenin to bacterial cultures thus accumulates high levels of intracellular malonyl-CoA (Davis et al., 2000). We simultaneously added IPTG and various concentrations of cerulenin to AT3RpSV cultures. The AT3RpSV strain produced 1.6-fold RK (54 mg/L) when cultured with 0.1 mM cerulenin than those without cerulenin (**Figure 6A**). Fed-batch cultures of AT3RpSV with 0.1 mM cerulenin in 1-L jar fermenters produced 62 mg/L of RK under optimized culture conditions, which increased the yield (**Figure 6B**) up to 0.12% vs glucose.

4 DISCUSSION

We constructed a microbial platform that produced RK from glucose. Genetically engineering *E. coli* metabolism and subsequent PAL optimization resulted in the respective production of 19.3 and 1.9 g/L of Tyr and *p*CA from glucose (**Figures 2**, **3**). A strain producing *p*CA harbored plasmids to express CL and BAS generated RK from glucose (**Figure 4**). Increasing cellular malonyl-CoA by genetic and chemical

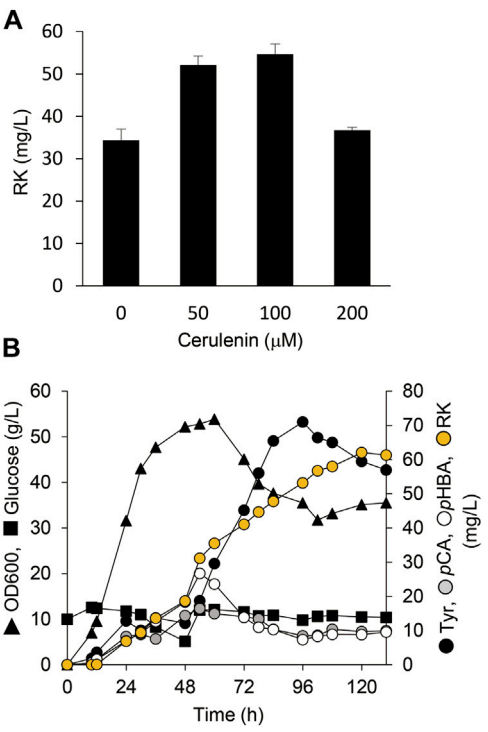

FIGURE 6 | Cerulenin addition increased *E. coli* RK production. **(A)** Production of RK by AT3RpSV cultured in modified fermentation medium containing various concentrations of cerulenin at 30°C for 60 h. **(B)** Fed-batch cultures of AT3RpSV were incubated in jar fermenters containing 0.5 L of fermentation medium at 30°C and pH 7.1 (maintained by 10% ammonium). Cerulenin (100 mM) was added after incubation for 10 h and the cultures were fed with glucose (0.8 g/L/h) after incubation for 24 h. Error bars indicate standard deviation (n = 3).

manipulation improved the RK yield (**Figures 5**, **6**). Finally, fed-batch culture under optimal conditions fermented 62 mg/L of RK from glucose (**Figure 6**). Currently, the use of cerulenin is a disadvantage for cost-saving RK production. Notably, our platform produces 41 mg/L of RK without the cerulenin, which is 12-times more than the previous fermenting process (Lee et al., 2016).

During biosynthesis, BAS conjugates *p*-coumaroyl-CoA and malonyl-CoA, which are respectively synthesized *via* the phenylpropanoid and fatty acid synthesis pathways (**Figure 1**). The efficient production of RK from glucose in a heterologous host requires the optimal production of these substrates. Due to difficulties achieving this, published reports describing microbial RK production are limited to those in which phenylpropanoid *p*CA was the raw material (Lee at al. 2016; Wang et al., 2019; Milke et al., 2020). The present study engineered the phenylpropanoid- and fatty acid synthesis pathways using genetic and chemical approaches, as well as fermentation, and optimized *p*CA levels and malonyl-CoA supplies in *E. coli*.

The engineered AT2 strain fermented glucose to produce 1.9 g/L of *p*CA during culture for 60 h (**Figure 3**). This amount exceeded that produced by any previous *E. coli* system (Flourat et al., 2021). Not only is *p*CA important as an aromatic precursor of bioactive substances such as stilbenoids, flavonoids and curcuminoids (Katsuyama et al., 2008; Trantas et al., 2009), but it is also a raw material for thermo-tolerant plastics (Kaneko et al., 2006). Our platform could thus facilitate the production of these valuable compounds.

The culture supernatant of the AT2 strain still contained a large amount of tyrosine (>1.0 g/L), and this strain yielded 10-fold less *p*CA than AT1 (**Figures 2**, **3**). This implied insufficient conversion of tyrosine to *p*CA, and that enhancing RgPAL production improves the generation of *p*CA and RK. The tyrosine conversion rate of RgPAL to *p*CA reached 0.8 g of *p*CA/L/h under resting-cell reactions (**Table 2**). This was much higher than the calculated maximum rate of 0.07 g of *p*CA/L/h generated by fermenting AT2 cells (**Figure 3**). This indicates that fine-tuning cellular metabolic flux further improves productivity.

The availability of intracellular malonyl-CoA was increased by FabF overexpression and cerulenin, which improved RK production *de novo* (**Figures 5**, **6**). This implied that increasing the intracellular flux for malonyl-CoA synthesis would improve RK production. Another strategy might be to overproduce acetyl-CoA carboxylase that converts intracellular acetyl-CoA to malonyl-CoA (**Figure 1**), which is supported by the following findings. Excessive acetyl-CoA carboxylase production results in a 100-fold increase in intracellular malonyl-CoA levels (Davis et al., 2000). Overexpressed acetyl-CoA carboxylase combined with engineering the metabolism of the glycolytic system and the TCA cycle, results in 4- and 5.6-fold increases, respectively, in the amounts of intracellular malonyl-CoA and naringenin, a plant-specific secondary metabolite derived from malonyl-CoA (Xu et al., 2011).

This study used multiple plasmids for expressing heterologous genes. Although this approach allows rapid construction of recombinant *E. coli*, several issues should be addressed before applied to large-scale fermentation that includes stability of plasmids, cost of antibiotics, and stable enzyme production. Genomic integration of the introduced genes should be a possible approach to solve these issues. CRISPR/Cas9 or λ-Red recombination systems enable scarless genome engineering in *E. coli* (Pyne et al., 2015; Bayer et al., 2021; Vo et al., 2021) and must be powerful tools for this purpose. These approaches improve our RK fermentation system to a more stable and economically friendly one.

In conclusion, this study established a microbial system that produced useful amounts of RK at low cost, and within a reasonable time frame. The present supply of RK derived from plants is limited and extraction is costly. Our straightforward batch fermentation system offers an inexpensive and efficient alternative to extracting RK from plants based on a simple carbon source that should significantly contribute to the flavor and fragrance industries.

DATA AVAILABILITY STATEMENT

The datasets presented in this study can be found in online repositories. The names of the repository/repositories and accession number(s) can be found in the article/**Supplementary Material**.

AUTHOR CONTRIBUTIONS

SM and NT conceived and designed research. SM, CS, KU, YS and YK conducted experiments. SM, CS, KU and YS analyzed data. SM and NT wrote the manuscript. All authors read and approved the manuscript.

FUNDING

This study was supported by the Japan Society for the Promotion of Science KAKENHI Grants-in-Aid for Scientific Research (17K15257), Japan Science and Technology Agency CREST (JPMJCR13B) and a Japan Science and Technology Agency ERATO Project Grant (JPMJER1502).

ACKNOWLEDGMENTS

We thank Norma Foster for critical reading of the manuscript.

SUPPLEMENTARY MATERIAL

The Supplementary Material for this article can be found online at: https://www.frontiersin.org/articles/10.3389/fbioe.2022.843843/full#supplementary-material

REFERENCES

Abe, I., Takahashi, Y., Morita, H., and Noguchi, H. (2001) Benzalacetone Synthase. *Eur. J. Biochem.* 268(11):3354–3359. doi:10.1046/j.1432-1327.2001.02255.x

Abe, T., Morita, H., Noma, H., Kohno, T., Noguchi, H., and Abe, I. (2007) Structure Function Analysis of Benzalacetone Synthase from *Rheum Palmatum*. *Bioorg. Med. Chem. Lett.* 17(11):3161–3166. doi:10.1016/j.bmcl.2007.03.029

Bayer, C. N., Rennig, M., Ehrmann, A. K., and Nørholm, M. H. H. (2021) A Standardized Genome Architecture for Bacterial Synthetic Biology (SEGA). *Nat. Commun.* 12(1):5876. doi:10.1038/s41467-021-26155-5

Beekwilder, J., van der Meer, I. M., Sibbesen, O., Broekgaarden, M., Qvist, I., Mikkelsen, J. D., et al. (2007) Microbial Production of Natural Raspberry Ketone. *Biotechnol. J.* 2:1270–1279. doi:10.1002/biot.200700076

Boker, A., Fischer, M., and Berger, R. G. (2001) Raspberry Ketone from Submerged Cultured Cells of the Basidiomycete Nidula Niveo-Tomentosa *Biotechnol. Prog.* 17(3):568–572. doi:10.1021/bp010011b

Borejsza-Wysocki, W., Goers, S. K., McArdle, R. N., and Hrazdina, G. (1992) (p-Hydroxyphenyl)butan-2-one Levels in Raspberries Determined by Chromatographic and Organoleptic Methods. *J. Agric. Food Chem.* 40: 1176–1177. doi:10.1021/jf00019a018

Borejsza-Wysocki, W., and Hrazdina, G. (1994) Biosynthesis of *P*-Hydroxyphenylbutan-2-One in Raspberry Fruits and Tissue Cultures. *Phytochemistry* 35(3):623–628. doi:10.1016/S0031-9422(00)90575-2

Bredsdorff, L., Wedebye, E. B., Nikolov, N. G., Hallas-Møller, T., and Pilegaard, K. (2015) Raspberry Ketone in Food Supplements - High Intake, Few Toxicity Data - A Cause for Safety Concern? *Regul. Toxicol. Pharmacol.* 73(1):196–200. doi:10.1016/j.yrtph.2015.06.022

Campillo, T., Renoud, S., Kerzaon, I., Vial, L., Baude, J., Gaillard, V., et al. (2014) Analysis of Hydroxycinnamic Acid Degradation in *Agrobacterium Fabrum* Reveals a Coenzyme A-dependent, Beta-Oxidative Deacetylation Pathway. *Appl. Environ. Microbiol.* 80(11):3341–3349. doi:10.1128/AEM.00475-14

Causey, T. B., Shanmugam, K. T., Yomano, L. P., and Ingram, L. O. (2004) Engineering *Escherichia coli* for Efficient Conversion of Glucose to Pyruvate. *Proc. Natl. Acad. Sci.* 101(8):2235–2240. doi:10.1073/pnas.0308171100

Davis, M. S., Solbiati, J., and Cronan, J. E., Jr (2000) Overproduction of Acetyl-CoA Carboxylase Activity Increases the Rate of Fatty Acid Biosynthesis in *Escherichia coli J. Biol. Chem.* 275(37):28593–28598. doi:10.1074/jbc.M004756200

Feron, G., Mauvais, G., Martin, F., Sémon, E., and Blin-Perrin, C. 2007, Microbial Production of 4-hydroxybenzylidene Acetone, the Direct Precursor of Raspberry Ketone, *Lett. Appl. Microbiol.*, 45) *"Microbial Production of Food Flavour," in Food Biotech*, eds K. Shetty, A. L. Pometto, and G. Paliyath (New York, NY: M. Dekker Inc.), 29–35. doi:10.1111/j.1472-765X.2007.02147.x

Flourat, A. L., Combes, J., Bailly-Maitre-Grand, C., Magnien, K., Haudrechy, A., Renault, J. H., et al. (2021) Accessing P -Hydroxycinnamic Acids: Chemical Synthesis, Biomass Recovery, or Engineered Microbial Production? *ChemSusChem* 14(1):118–129. doi:10.1002/cssc.202002141

Fujita, T., Nguyen, H. D., Ito, T., Zhou, S., Osada, L., Tateyama, S., et al. (2013) Microbial Monomers Custom-Synthesized to Build True Bio-Derived Aromatic Polymers. *Appl. Microbiol. Biotechnol.* 97(20):8887–8894. doi:10.1007/s00253-013-5078-4

Harada, N., Okajima, K., Narimatsu, N., Kurihara, H., and Nakagata, N. (2008) Effect of Topical Application of Raspberry Ketone on Dermal Production of Insulin-like Growth Factor-I in Mice and on Hair Growth and Skin Elasticity in Humans. *Growth Horm. IGF Res.* 18:335–344. doi:10.1016/j.ghir.2008.01.005

Kaneko, T., Thi, T. H., Shi, D. J., and Akashi, M. (2006) Environmentally Degradable, High-Performance Thermoplastics from Phenolic Phytomonomers. *Nat. Mater* 5(12):966–970. doi:10.1038/nmat1778

Kassab, E., Fuchs, M., Haack, M., Mehlmer, N., and Brueck, T. B. (2019) Engineering *Escherichia coli* FAB System Using Synthetic Plant Genes for the Production of Long Chain Fatty Acids. *Microb. Cel Fact.* 18(1):163. doi:10.1186/s12934-019-1217-7

Katsuyama, Y., Matsuzawa, M., Funa, N., and Horinouchi, S. (2008) Production of Curcuminoids by *Escherichia coli* Carrying an Artificial Biosynthesis Pathway. *Microbiology (Reading)* 154(9):2620–2628. doi:10.1099/mic.0.2008/018721-0

Kawaguchi, H., Katsuyama, Y., Danyao, D., Kahar, P., Nakamura-Tsuruta, S., Teramura, H., et al. (2017) Caffeic Acid Production by Simultaneous Saccharification and Fermentation of Kraft Pulp Using Recombinant *Escherichia coli Appl. Microbiol. Biotechnol.* 101(13):5279–5290. doi:10.1007/s00253-017-8270-0

Kim, M., Baek, H. S., Lee, M., Park, H., Shin, S. S., Choi, D. W., et al. (2016) Rhododenol and Raspberry Ketone Impair the normal Proliferation of Melanocytes through Reactive Oxygen Species-dependent Activation of GADD45. *Toxicol. Vitro* 32:339–346. doi:10.1016/j.tiv.2016.02.003

Larsen, M., Poll, L., Callesen, O., and Lewis, M. (1991) Relations between the Content of Aroma Compounds and the Sensory Evaluation of 10 Raspberry Varieties (Rubus idaeusL). *Acta Agriculturae Scand.* 41:447–454. doi:10.1080/00015129109439927

Lee, D., Lloyd, N. D. R., Pretorius, I. S., and Borneman, A. R. (2016) Heterologous Production of Raspberry Ketone in the Wine Yeast *Saccharomyces cerevisiae* via Pathway Engineering and Synthetic Enzyme Fusion. *Microb. Cel Fact* 15:49. doi:10.1186/s12934-016-0446-2

Malkar, R. S., and Yadav, G. D. (2019) Selectivity Engineering in One Pot Synthesis of Raspberry Ketone: Crossed Aldol Condensation of P -Hydroxybenzaldehyde and Acetone and Hydrogenation over Novel Ni/Zn-La Mixed Oxide. *ChemistrySelect* 4:2140–2152. doi:10.1002/slct.201804060

Masuo, S., Zhou, S., Kaneko, T., and Takaya, N. (2016) Bacterial Fermentation Platform for Producing Artificial Aromatic Amines. *Sci. Rep.* 6:25764 doi:10.1038/srep25764

Matsumoto, S., Takeuchi, A., Hayatsu, M., and Kondo, S. (1994) Molecular Cloning of Phenylalanine Ammonia-Lyase cDNA and Classification of Varieties and Cultivars of tea Plants (*Camellia Sinensis*) Using the tea PAL cDNA Probe. *Theoret. Appl. Genet.* 89(6):671–675. doi:10.1007/BF00223703

Milke, L., Mutz, M., and Marienhagen, J. (2020) Synthesis of the Character Impact Compound Raspberry Ketone and Additional Flavoring Phenylbutanoids of Biotechnological Interest with *Corynebacterium Glutamicum*. *Microb. Cel Fact* 19:92. doi:10.1186/s12934-020-01351-y

Morimoto, C., Satoh, Y., Hara, M., Inoue, S., Tsujita, T., and Okuda, H. (2005) Anti-obese Action of Raspberry Ketone. *Life Sci.* 77:194–204. doi:10.1016/j.lfs.2004.12.029

Pittard, J., Camakaris, H., and Yang, J. (2005) The TyrR Regulon. *Mol. Microbiol.* 55(1):16–26. doi:10.1111/j.1365-2958.2004.04385.x

Pyne, M. E., Moo-Young, M., Chung, D. A., and Chou, C. P. (2015) Coupling the CRISPR/Cas9 System with Lambda Red Recombineering Enables Simplified Chromosomal Gene Replacement in *Escherichia coli*. *Appl. Environ. Microbiol.* 81(15):5103–5114. doi:10.1128/AEM.01248-15

Subrahmanyam, S., and Cronan, J. E., Jr (1998) Overproduction of a Functional Fatty Acid Biosynthetic Enzyme Blocks Fatty Acid Synthesis in *Escherichia coli J. Bacteriol.* 180(17):4596–4602. doi:10.1128/JB.180.17.4596-4602.1998

Sun, L., Xin, F., and Alper, H. S. (2021) Bio-synthesis of Food Additives and Colorants-A Growing Trend in Future Food. *Biotechnol. Adv.* 47:107694. doi:10.1016/j.biotechadv.2020.107694

Trantas, E., Panopoulos, N., and Ververidis, F. (2009) Metabolic Engineering of the Complete Pathway Leading to Heterologous Biosynthesis of Various Flavonoids and Stilbenoids in *Saccharomyces cerevisiae*. *Metab. Eng.* 11(6): 355–366. doi:10.1016/j.ymben.2009.07.004

Vandamme, E. J., and Soetaert, W. (2002) Bioflavours and Fragrances via Fermentation and Biocatalysis. *J. Chem. Technol. Biotechnol.* 77:1323–1332. doi:10.1002/jctb.722

Vo, P. L. H., Ronda, C., Klompe, S. E., Chen, E. E., Acree, C., Wang, H. H., et al. (2021) CRISPR RNA-Guided Integrases for High-Efficiency, Multiplexed Bacterial Genome Engineering. *Nat. Biotechnol.* 39(4):480–489. doi:10.1038/s41587-020-00745-y

Wang, C., Zheng, P., and Chen, P. (2019) Construction of Synthetic Pathways for Raspberry Ketone Production in Engineered *Escherichia coli*. *Appl. Microbiol. Biotechnol.* 103(9):3715–3725. doi:10.1007/s00253-019-09748-5

Wang, L., Meng, X., and Zhang, F. (2012) Raspberry Ketone Protects Rats Fed High-Fat Diets against Nonalcoholic Steatohepatitis. *J. Med. Food* 15:495–503. doi:10.1089/jmf.2011.1717

Xu, P., Ranganathan, S., Fowler, Z. L., Maranas, C. D., and Koffas, M. A. G. (2011) Genome-scale Metabolic Network Modeling Results in Minimal Interventions that Cooperatively Force Carbon Flux towards Malonyl-CoA. *Metab. Eng.* 13(5):578–587. doi:10.1016/j.ymben.2011.06.008

Yazaki, K., Kataoka, M., Honda, G., Severin, K., and Heide, L. (1997) cDNA Cloning and Gene Expression of Phenylalanine Ammonia-Lyase

inLithospermum Erythrorhizon. *Biosci. Biotechnol. Biochem.* 61(12): 1995–2003. doi:10.1271/bbb.61.1995

Zheng, D., and Hrazdina, G. (2008) Molecular and Biochemical Characterization of Benzalacetone Synthase and Chalcone Synthase Genes and Their Proteins from Raspberry (*Rubus Idaeus* L.). *Arch. Biochem. Biophys.* 470(2):139–145. doi:10.1016/j.abb.2007.11.013

Zhu, L., Cui, W., Fang, Y., Liu, Y., Gao, X., and Zhou, Z. (2013) Cloning, Expression and Characterization of Phenylalanine Ammonia-Lyase from *Rhodotorula Glutinis*. *Biotechnol. Lett.* 35(5):751–756. doi:10.1007/s10529-013-1140-7

Conflict of Interest: The authors declare that the research was conducted in the absence of any commercial or financial relationships that could be construed as a potential conflict of interest.

Publisher's Note: All claims expressed in this article are solely those of the authors and do not necessarily represent those of their affiliated organizations, or those of the publisher, the editors and the reviewers. Any product that may be evaluated in this article, or claim that may be made by its manufacturer, is not guaranteed or endorsed by the publisher.

frontiers in Bioengineering and Biotechnology

REVIEW
published: 25 February 2022
doi: 10.3389/fbioe.2022.841443

Natural 5-Aminolevulinic Acid: Sources, Biosynthesis, Detection and Applications

Meiru Jiang[1†], *Kunqiang Hong*[1†], *Yufeng Mao*[2], *Hongwu Ma*[2], *Tao Chen*[1] *and Zhiwen Wang*[1*]

[1]*Frontier Science Center for Synthetic Biology (Ministry of Education), Key Laboratory of Systems Bioengineering (Ministry of Education), SynBio Research Platform, Collaborative Innovation Center of Chemical Science and Engineering (Tianjin), School of Chemical Engineering and Technology, Tianjin University, Tianjin, China,* [2]*Key Laboratory of System Microbial Biotechnology, Tianjin Institute of Industrial Biotechnology, Chinese Academy of Sciences, Tianjin, China*

5-Aminolevulinic acid (5-ALA) is the key precursor for the biosynthesis of tetrapyrrole compounds, with wide applications in medicine, agriculture and other burgeoning fields. Because of its potential applications and disadvantages of chemical synthesis, alternative biotechnological methods have drawn increasing attention. In this review, the recent progress in biosynthetic pathways and regulatory mechanisms of 5-ALA synthesis in biological hosts are summarized. The research progress on 5-ALA biosynthesis via the C4/C5 pathway in microbial cells is emphasized, and the corresponding biotechnological design strategies are highlighted and discussed in detail. In addition, the detection methods and applications of 5-ALA are also reviewed. Finally, perspectives on potential strategies for improving the biosynthesis of 5-ALA and understanding the related mechanisms to further promote its industrial application are conceived and proposed.

Keywords: 5-aminolevulinic acid, biosynthetic pathway, metabolic engineering, detection, application

OPEN ACCESS

Edited by:
Shuobo Shi,
Beijing University of Chemical Technology, China

Reviewed by:
Liang Quanfeng,
Shandong University, China
Zhen Kang,
Jiangnan University, China

****Correspondence:***
Zhiwen Wang
zww@tju.edu.cn

[†]These authors have contributed equally to this work

Specialty section:
This article was submitted to Synthetic Biology, a section of the journal Frontiers in Bioengineering and Biotechnology

Received: *22 December 2021*
Accepted: *20 January 2022*
Published: *25 February 2022*

Citation:
Jiang M, Hong K, Mao Y, Ma H, Chen T and Wang Z (2022) Natural 5-Aminolevulinic Acid: Sources, Biosynthesis, Detection and Applications. Front. Bioeng. Biotechnol. 10:841443. doi: 10.3389/fbioe.2022.841443

1 INTRODUCTION

5-Aminolevulinic acid (5-ALA), also known as δ-aminolevulinic acid, is an oxygen- and nitrogen-containing hydrocarbon. It is the common precursor of all tetrapyrrole compounds, including chlorophyll, heme and vitamin B_{12} (Kang et al., 2012). It can be synthesized by plants, animals, bacteria and fungi. There are two biosynthetic pathways of it in nature, C4 pathway and C5 pathway respectively. Since it is an endogenous substance that is non-toxic to humans and animals and is easily degraded in the environment without residues, 5-ALA has received widespread attentions in recent years. 5-ALA can be converted into protoporphyrin IX, which is a powerful photosensitizer to cause photosensitive effect (Wang X. F. et al., 2020). Therefore, 5-ALA is successfully used in the treatment of tumors and others diseases (Millesi et al., 2016; Pepa et al., 2020; Suero Molina et al., 2021; Ubbink et al., 2021). 5-ALA is also used as an animal feed additive to improve iron status and immune response in livestock (Wang et al., 2009; Hendawy et al., 2019; Direkbusarakom et al., 2021). It also has functions in higher plants, such as stimulating physiochemical processes, regulating plant

Abbreviations: 5-ALA, 5-aminolevulinic acid; ALAS, 5-aminolevulinic acid synthase; pyridoxal PLP, 5′-phosphate; GluTS, glutamyl–tRNA synthetase; GluTR, glutamyl-tRNA reductase; GSA, L-glutamic acid 1-semialdehyde; GSA-AM, glutamate-1-semialdehyde aminotransferase; ALAD, 5-aminolevulinate dehydratase; OdhI, oxoglutarate dehydrogenase inhibitor; GS, glutamate dehydrogenase; asRNAs, antisense RNA; PMP, pyridoxamine 5′-phosphate; PEP, phosphoenolpyruvate; ROS, reactive oxygen species; LA, levulinic acid; 5′-UTRs; 5′-untranslated regions; CRISPRi, CRISPR interference.

growth and development in seed germination, vegetative growth and fruit coloring (Wu et al., 2018). With the continuous discovery of biological functions of 5-ALA, its synthesis and related regulatory mechanisms have attracted increasing attention, which led to further research and progress.

Compared with chemical methods, the biosynthesis of 5-ALA has many advantages as green, sustainable, renewable, and inexpensive technology (Kang et al., 2012). Researchers have made major breakthroughs in the study of synthesis mechanisms of 5-ALA and fermentation process optimization for its biosynthesis over the past 20 years. A number of different microbial hosts were used to produce 5-ALA, including *Escherichia coli* (Zhao and Zhai, 2019), *Corynebacterium glutamicum* (Feng et al., 2016) and *Saccharomyces cerevisiae* (Hara et al., 2019). Recently, the highest titer of biosynthetic 5-ALA reached 18.5 g/L in *C. glutamicum*, which was achieved via evaluation of 5-ALA synthetases from different sources, regulating intracellular activities of 5-ALA synthetase and phosphoenolpyruvate carboxylase, and optimization of the fermentation medium (Chen et al., 2020). In the process of microbial 5-ALA production, the optimization strategies of biosynthetic pathways or metabolic networks based on genome-scale metabolic network models also play an important role in the biosynthesis of 5-ALA by solving the problems of precursor supply (Ren et al., 2018; Hara et al., 2019), proper expression of 5-ALA synthase (Yu et al., 2019; Chen et al., 2020), and regulating the expression levels of key enzymes in downstream pathways (Zhou et al., 2019; Sakurai et al., 2021). Additionally, the detection technologies applied for different samples have also made great progress (Hara et al., 2019; Ren et al., 2018; Tan Z. J. et al., 2019). Previous applications and synthetic methods have been reviewed in detail before in earlier (Kang et al., 2012; Liu et al., 2014; Kang et al., 2017). However, a review focusing on the metabolic engineering strategies to improve 5-ALA production and systematic summary of detection methods with recent advances has not been reported. Therefore, it is of great significance to provide a comprehensive review on 5-ALA for its further synthesis, detection and application.

In this paper, we summarized the recent progress in the research on the biosynthetic pathways and regulatory mechanisms of 5-ALA. The research progress on 5-ALA synthesis in microbial cells is emphasized, and design strategies for obtaining efficient production hosts are analyzed and discussed in detail. Additionally, 5-ALA detection methods as well as its applications in agriculture, medicine and food additives are also reviewed. Finally, possible solutions are proposed to increase our understanding of the regulatory mechanisms and biosynthesis of 5-ALA.

2 BIOSYNTHESIS AND MOLECULAR REGULATION OF 5-AMINOLEVULINIC ACID

In 1953, 5-ALA was firstly discovered in duck blood (Shemin and Russell, 1953). In the following years, more and more studies proved the existence of 5-ALA synthesis in many animals and higher plants (Harel and Klein, 1972; Samuel and Paul, 1974). Although many efforts have been made to improve the yield of 5-ALA (Ano et al., 1999; Hama and Hase, 1978), its yield was still very low in plants. Some microorganisms in nature also have the ability to synthesize 5-ALA, such as photosynthetic bacteria, which were the first host organisms to synthesize 5-ALA (Sasaki et al., 1987). It is undeniable that some photosynthetic bacteria liking *Rhodobacter sphaeroides* show significant advantages on yield compared to animals and plants (Kamiyama et al., 2000), but its strict requirement demand on fermentation conditions are not conducive to subsequent large-scale industrial production. Therefore, the development of engineered strains for directional produce 5-ALA is in the core of the research in 5-ALA biosynthesis. At present, *Corynebacterium glutamicum*, *Escherichia coli* and *Saccharomyces cerevisiae* are the most commonly used strains for biosynthesis of 5-ALA by metabolic engineering strategies. Additionally, *Streptomyces coelicolor*, *Propionibacterium acidipropionici* (Kiatpapan et al., 2011), *Shewanella oneidensis* (Yi and Ng, 2021) and *Bacillus subtilis* (Liu et al., 2020) have also been attempted to synthesis 5-ALA recently (**Supplementary Table S1**).

2.1 Biosynthetic Pathway of 5-Aminolevulinic Acid

5-ALA was confirmed as the common precursor of tetrapyrrole compounds and was found in many organisms. Two natural 5-ALA biosynthesis pathways are known to date. One is the C4 pathway (Shemin pathway), which was firstly reported by Shemin and Russell (1953). It exists in animals, yeast, some protozoa and purple non-sulfur photosynthetic bacteria. In this pathway, glycine and succinyl-CoA are condensed to 5-ALA under the catalysis of 5-aminolevulinic acid synthase (ALAS), with pyridoxal 5′-phosphate (PLP) as the cofactor (**Figure 1**) (Sasaki et al., 2002). Succinyl-CoA is synthesized by methylmalonyl-CoA mutase, which utilizes vitamin B_{12} as an essential co-factor (38). The other is the C5 pathway (Beale pathway), which starts from the discovery of 5-ALA in *Chlorella vulgaris* by Beale (Beale, 1970). Glutamate produced via the TCA cycle acts as the substrate of the C5 pathway (Kang et al., 2012). The C5 pathway is mainly present in higher plants, algae, and many bacteria. The pathway starts with the ligation of tRNA and glutamate to generate L-glutamyl–tRNA, catalyzed by glutamyl–tRNA synthetase (GluTS) (**Figure 1**). The NADPH-dependent glutamyl-tRNA reductase (GluTR) reduces the carboxyl group of Glu–tRNA to a formyl group, which enables the conversion of L-Glu–tRNA into L-glutamic acid 1-semialdehyde (GSA). In the last step, 5-ALA is created through transamination by glutamate-1-semialdehyde aminotransferase (GSA-AM) (Moser et al., 2001). The enzymes involved in this pathway, GluTS, GluTR and GSA-AM, are encoded by the genes *gltX*, *hemA* (homonymic with the ALAS gene of the C4 pathway) and *hemL*, respectively. However, a few microorganisms have both C4 and C5 pathways with *Euglena gracilis* being a well-known example (Weinstein and Beale, 1983).

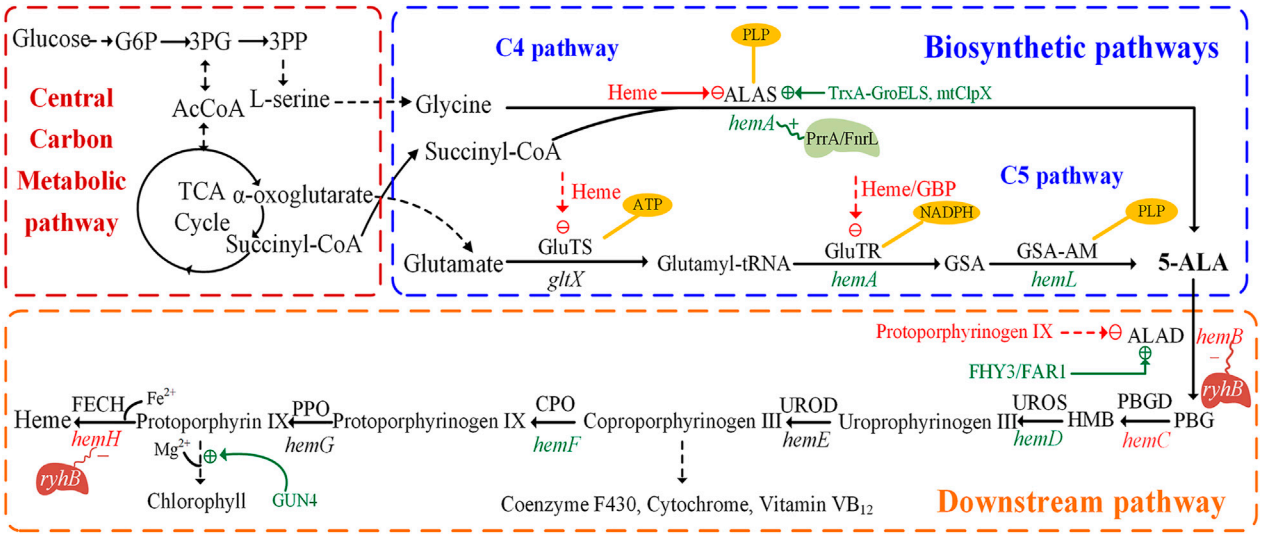

FIGURE 1 | Biosynthetic pathways and downstream pathways of 5-aminolevulinic acid. The figure is divided into three parts: central carbon metabolic pathways, biosynthetic pathways and downstream pathways. The dashed green line indicates positive regulation, the dashed red line indicates feedback inhibition. The genes in green or red represent the enzymes that are positive or negative for 5-aminolevulinic acid accumulation, respectively. The polygons represent transcriptional regulators and red or blue represent positive/negative regulation. PBGD, porphobilinogen deaminase; UROS, uroporphyrinogen III synthase; UROD, uroporphyrinogen decarboxylase; CPO, coproporphyrinogen oxidase; PPO, protoporphyrinogen oxidase; FECH, ferrochelatase; FHY3, Far-red Elongated Hypocotyl 3; FAR1, Far-red Impaired Response 1; mitochondrial ClpX (mtClpX); 3PG, 3-phosphoglycerate.

2.2 Regulation of 5-Aminolevulinic Acid Biosynthesis

2.2.1 Main Regulation Mechanism of the C4 Pathway

In the C4 pathway, 5-ALA is formed by ALAS, encoded by the *hemA* or *hemT* gene, which catalyzes the condensation of succinyl-CoA and glycine. The *hemA* gene provides most of the ALAS activity, much more than *hemT* (Neidle and Kaplan, 1993; Zeilstra-Ryalls and Kaplan, 1995). ALAS is a rate-limiting enzyme for 5-ALA biosynthesis, and the synthesis of this enzyme is itself highly regulated via feedback regulation of the *hemA* and *hemT* genes (Sasaki et al., 1995). The transcription of *hemA* from its two promoters is regulated by the DNA-binding proteins FnrL and PrrA in *R. sphaeroides* (**Figure 1**), which might be the only transcription factors involved in the oxygen responsiveness of *hemA* (Fales et al., 2002; Ranson-Olson and Zeilstra-Ryalls, 2008). Furthermore, the enzymatic activity of ALAS is subject to feedback inhibition by the end-product heme (Tian et al., 2011). Another important protein, mitochondrial ClpX, directly stimulates 5-ALA synthase in *S. cerevisiae* by catalyzing the incorporation of its cofactor, pyridoxal 5' phosphate (Kardon et al., 2020).

2.2.2 Main Regulation Mechanism of the C5 Pathway

In the C5 pathway, 5-ALA is derived from a transfer RNA (tRNA)-bound glutamate in three enzymatic steps. In some bacteria, the GluTS complexed with ATP and $tRNA^{Glu}$, as well as its five domains for substrate or cofactor recognition (Zn^{2+}, Mg^{2+}, ATP, glutamate and tRNA) and catalytic activity have been studied (Dubois et al., 2009). In *E. coli*, GluTS is responsible for the formation of glutamyl-tRNA and 5-ALA synthesis (Beale et al., 1975). The regulation of GluTS activity is multi-dimensional and complex. Its activity is regulated by intracellular heme levels (Levican et al., 2007) (**Figure 1**). GluTR was proved to be the key enzyme of the C5 pathway, forming a tight complex with GSA-AM to protect the highly reactive intermediate GSA-AM (Moser et al., 2001). The activated glutamate is converted to GSA by the NADPH dependent GluTR enzyme, which in turn is quickly converted to 5-ALA by GSA-AM. In addition, GluTR is regulated at the posttranscriptional and protein levels (Woodard and Dailey, 1995; Wang et al., 1999). When the concentration of heme is sufficient, the activity of GluTR is strongly inhibited to reduce the synthesis of 5-ALA. Furthermore, the complex of heme and GluTR-binding protein also inhibits the interaction between GBP and GluTR, causing the deregulation of GluTR (Richter et al., 2019).

Similar but more complex regulation mechanisms also exist in higher plants. Feedback inhibition plays an important regulative role in 5-ALA synthesis via the C5 pathway. It was reported that GluTR is the target of FLU protein in higher plants (Zhang M. et al., 2015). The negative regulator, FLU protein, has been proposed to have a synergetic role in the chlorophyll branch, similar to the function of heme (Kauss et al., 2012). The transcription factors like Far-red Elongated Hypocotyl 3 (FHY3) and Far-red Impaired Response 1 (FAR1) have a positive regulative role in chlorophyll biosynthesis since they can bind and activate the expression of *hemB* (encodes ALAD), thereby upregulating the synthesis of 5-ALA in higher plants (Tang et al., 2012).

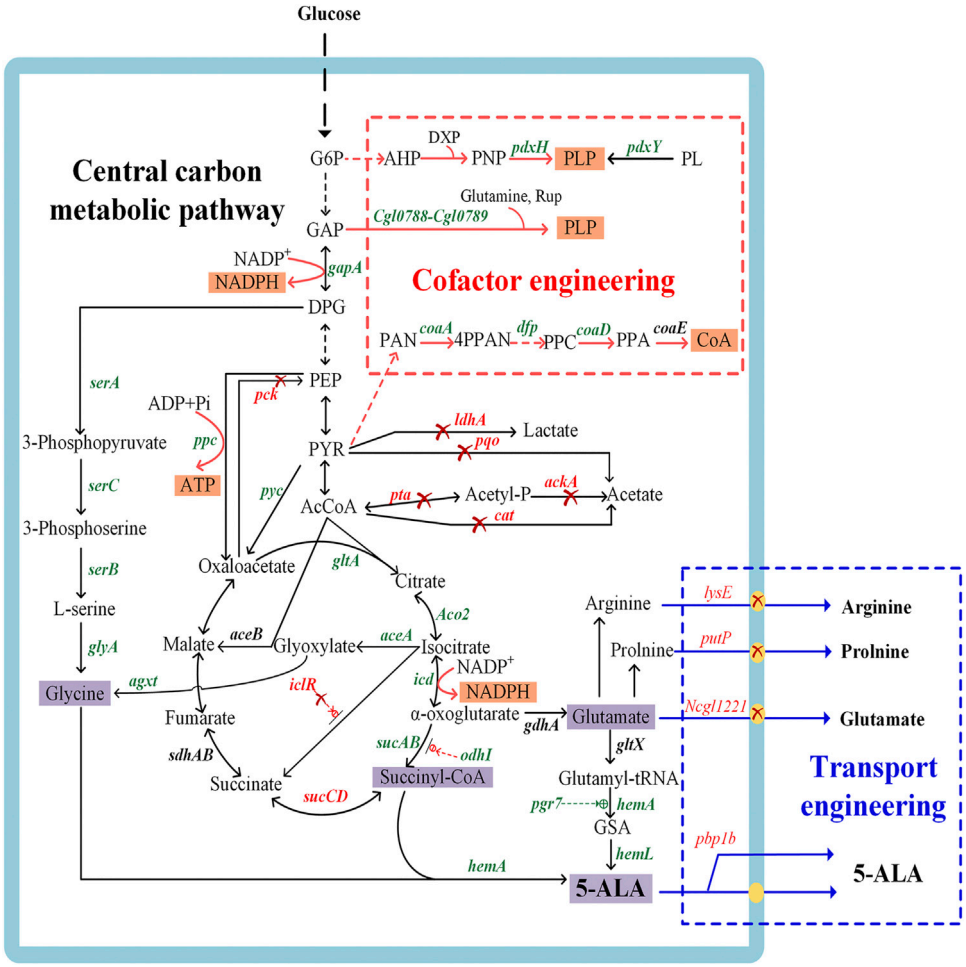

FIGURE 2 | Genetic manipulations in metabolic engineering strategies for 5-aminolevulinic acid biosynthesis. The genes in green or red represent the enzymes that should be overexpressed or inactivated to accelerate 5-ALA accumulation, respectively. The red cross indicates that the pathways are disrupted, the dashed green line indicates positive regulation, and the dashed red line indicates feedback inhibition. *pdxH*, encoding pyridoxal 5-phosphate synthase; *pdxY*, pyridoxal kinase; *Cgl0788-Cgl0789*, pyridoxal 5′-phosphate synthase gene; *gapA*, encoding glyceraldehyde 3-phosphate dehydrogenase; *serA*, encoding 3-phosphoglycerate dehydrogenase; *serB*, encoding phosphoserine phosphatase; *serC*, encoding phosphoserine aminotransferase; *glyA*, encoding serine hydroxymethyl transferase; *coaA*, encoding pantothenate kinase; *dfp*, encoding dephospho-CoA kinase; *coaD*, encoding pantetheine-phosphate adenylyltransferase; *coaE*, encoding dephospho-CoA kinase; *ppc*, encoding phosphoenolpyruvate carboxylase; *pyc*, encoding pyruvate carboxylase; *pck*, encoding phosphoenolpyruvate carboxykinase; *gltA*, encoding citrate synthase; *ldhA*, encoding L-lactate dehydrogenase; *pqo*, encoding pyruvate:menaquinone oxidoreductase; *pta*, encoding phosphotransacetylase; *ackA*, encoding acetate kinase; *cat*, encoding acetyl-CoA:CoA transferase; *ACO2*, encoding aconitase; *icd*, encoding isocitrate dehydrogenase; *sucAB*, encoding α-oxoglutarate dehydrogenase; *odhI*, encoding α-oxoglutarate dehydrogenase inhibitor; *sucCD*, encoding succinyl-CoA synthetase; *aceA*, encoding isocitrate lyase; *aceB,* encoding malate synthase; *iclR*, encoding the transcriptional regulator of glyoxylate cycle genes *aceBAK*; *gdhA*, encoding glutamate dehydrogenase; *gltX*, encoding glutamyl-tRNA synthetase; *hemA*, encoding glutamyl-tRNA reductase; *hemL*, encoding glutamate-1-semialdehyde aminotransferase; *pgr7*, encoding *hem1* stimulator protein; *hemA*, encoding 5-aminolevulinate synthase; *rhtA*, encoding serine/threonine transporter; *lysE*, encoding lysine/arginine transporter; *putP*, encoding L-proline transporter; *Ncgl1221*, encoding glutamate transporter; *agxt*, encoding glyoxylate aminotransferase from *Homo sapiens*. G6P, glucose-6-phosphate; 3PP, 3-phosphoserine; GAP, glyceraldehyde 3-phosphate; DPG, 1,3-bisphosphoglyceric acid; PEP, phosphoenolpyruvate; PYR, pyruvic acid; AcCoA, acetyl-CoA; AHP, 3-hydroxy-1-aminoacetone phosphate; DXP, deoxyxylulose 5-phosphate; PNP, pyridoxine 5′-phosphate; PL, pyridoxal; Rup, ribulose 5-phosphate; PAN, pantothenate; 4PPAN, 4′-phosphopantothenate; PPC, 4′-phosphopantethenine; PPA, dephpspho-CoA; CoA, coenzyme A; ADK, adenylate kinase; HK, hexokinase; ZWF, glucose-6-phosphate dehydrogenase; PGL, phosphogluconolactonase; GND, 6-phosphogluconate dehydrogenase; R5P, D-ribulose 5-phosphate.

3 METABOLIC ENGINEERING STRATEGIES FOR 5-AMINOLEVULINIC ACID BIOSYNTHESIS

A number of metabolic engineering strategies have been developed with the aim to establish an industrially sustainable biosynthesis route for 5-ALA (**Figure 2**), including engineering of key enzymes, redistribution of central carbon fluxes toward precursors, blockage of downstream pathways, cofactor engineering, and transporter engineering. The recent research on improving 5-ALA biosynthesis is summarized in **Supplementary Table S1**.

3.1 Engineering of Key Enzymes for 5-Aminolevulinic Acid Biosynthesis

3.1.1 5-Aminolevulinate Synthase in the C4 Pathway

ALAS is the key enzyme for 5-ALA synthesis via the C4 pathway, and its isoenzymes are encoded by different redundant genes (Kang et al., 2012). Tai et al. (1988) identified the two genes *hemA* and *hemT* as potentially encoding ALAS in *R. sphaeroides*, which was further confirmed by Neidle et al., as well as Neidle and Kaplan (1993). Compared with the *hemT* gene, the expression of *hemA* is more sensitive to feedback inhibition by heme in wild-type *R. sphaeroides* 2.4.9 (Stoian et al., 2018). When the expression of *hemA* is inhibited, *hemT* starts to play an alternative role in 5-ALA synthesis. In addition, *hemO* is another redundant gene that also encodes ALAS and can support the synthesis of 5-ALA in *R. sphaeroides* (Zhang et al., 2013). Engineered *E. coli* overexpressing the *hemO* gene produced 6.3 g/L of 5-ALA, which was higher than the 5.7 g/L of the strain overexpressing *hemA* (Zhang et al., 2013). Moreover, both ALAS activity and its affinity for substrates in the host cell influence the synthesis of 5-ALA. For example, overexpression of the *hemA* gene from *R. palustris* ATCC 17001 yielded a 5-ALA titer of 3.8 g/L, which was 15.2% and 18.9% higher than those produced by two other ALAS genes in *C. glutamicum* (Chen et al., 2020).

To decrease the feedback inhibition by heme and increase the thermostability of ALAS, the enzyme was modified using different strategies. For example, the H29R and H15K ALAS mutants were screened from several single variants by computer-assisted rational design (Tan Z. J. et al., 2019). The 5-ALA levels of *C. glutamicum* strains expressing the mutants respectively increased by 6 and 22 compared with the strain expressing wild-type ALAS (Tan Z. J. et al., 2019). To enhance the soluble protein expression, Yu et al. (2019) used TrxA and its chaperone GroELS to improve the activity of ALAS (**Figure 1**). Recently, Yu et al. (2022) further biosynthesized 5-ALA by integrating and co-expressing *groELS* and *hemA* in chromosome. The final 5-ALA titer increased to 15.6 g/L after supplying ferric ion and optimizing the glucose-glycerol as a mixed carbon source. In addition, the transcription of *hemA* was found to be influenced by changes of the cellular redox state (Zeilstra-Ryalls and Kaplan, 1996). Most importantly, the expression strength of ALAS should be maintained at a moderate level in case of an imbalance between 5-ALA synthesis and the TCA cycle (Chen et al., 2020). In conclusion, reliving the complex feedback inhibition of ALAS and maintaining moderate expression levels are the key to achieving high productivity of 5-ALA.

3.1.2 Glutamyl-tRNA Reductase and Glutamate-1-semialdehyde Aminotransferase in the C5 Pathway

GluTR (encoded by *hemA*) and GSA-AM (encoded by *hemL*) are two charging enzymes in the C5 pathway (**Figure 2**). GluTR is the key enzyme forming a tight complex with GSA-AM to protect the highly reactive intermediate GSA-AM (Moser et al., 2001). GluTR activity is also inhibited by heme and further influences the synthesis of 5-ALA. However, it has been reported that a C170A mutant of HemA from *Salmonella enterica* is not influenced by heme (Jones and Elliott, 2010). Although this work was a breakthrough in eliminating feedback inhibition from heme, the influence of the C170A mutant to 5-ALA synthesis was still unknown. Subsequently, HemA mutants from different sources with higher activity and stability were screened to increase the production of 5-ALA combined with HemL in *E. coli* and *C. glutamicum* (Kang et al., 2011a; Yu et al., 2015; Zhang et al., 2017; Ko et al., 2019). To increase the expression level of the two genes *hemA* and *hemL*, different metabolic engineering strategies were applied with good results, including promoter engineering (Noh et al., 2017), transcriptional regulation with synthetic 5′-untranslated regions (5′-UTRs) (Noh et al., 2017) and RBS engineering (Zhang and Ye, 2018; Zhang J. L. et al., 2019) (**Figure 3**). Recently, the engineered strain *E. coli* Transetta GTR/GBP co-overexpressing the stimulator protein GBP (encoded by *pgr7*) could produce 3.08 g/L of 5-ALA, representing a 2.37-increase compared to overexpression of *hemA1* alone (Zhao and Zhai, 2019). In general, overexpression of the two genes *hemA* and *hemL* both contributes to the biosynthesis of 5-ALA. Further exploring the mechanisms that control these two genes and reducing other influencing factors are effective strategies for increasing the production of 5-ALA.

3.2 Enhancing Precursor Supply by Redistributing the Fluxes of Central Carbon Metabolism

3.2.1 Metabolic Engineering of Central Carbon Metabolic Pathways for Supplying Precursors in the C4 Pathway

5-ALA is produced by the condensation of succinyl-CoA and glycine in the C4 pathway (**Figure 2**). Previous studies found that addition of the precursors succinyl-CoA and glycine was conducive to enhancing the production of 5-ALA (Choi et al., 1999; Liu et al., 2010), which indicated that the supply of these two precursors might be the main bottleneck of 5-ALA synthesis. Consequently, many metabolic engineering studies have been undertaken in different microorganisms to increase the supply of these precursors (**Figure 2**). Further advances will make it possible to directly regulate the metabolic flux toward succinyl-CoA and glycine.

There are two main strategies to improve the intracellular succinyl-CoA pool. One relies on reinforcing the carbon flux toward the TCA cycle. For example, overexpression of *gltA* (encoding citrate synthase), *ppc* (encoding phosphoenolpyruvate carboxylase) and *pyc* (encoding pyruvate carboxylase), together with the deletion of *pck* (encoding phosphoenolpyruvate carboxykinase), can redirect the carbon flux towards the TCA cycle (Feng et al., 2016). Combined with the knockout of by-product pathways that produce acetate and lactate, the production of 5-ALA by engineered *C. glutamicum* was further increased from 1.44 to 2.07 g/L (Feng et al., 2016). However, high overexpression levels of target genes in central carbon metabolic pathways might interfere with the synthesis of 5-ALA and destroy the balance between complicated pathways. Recently,

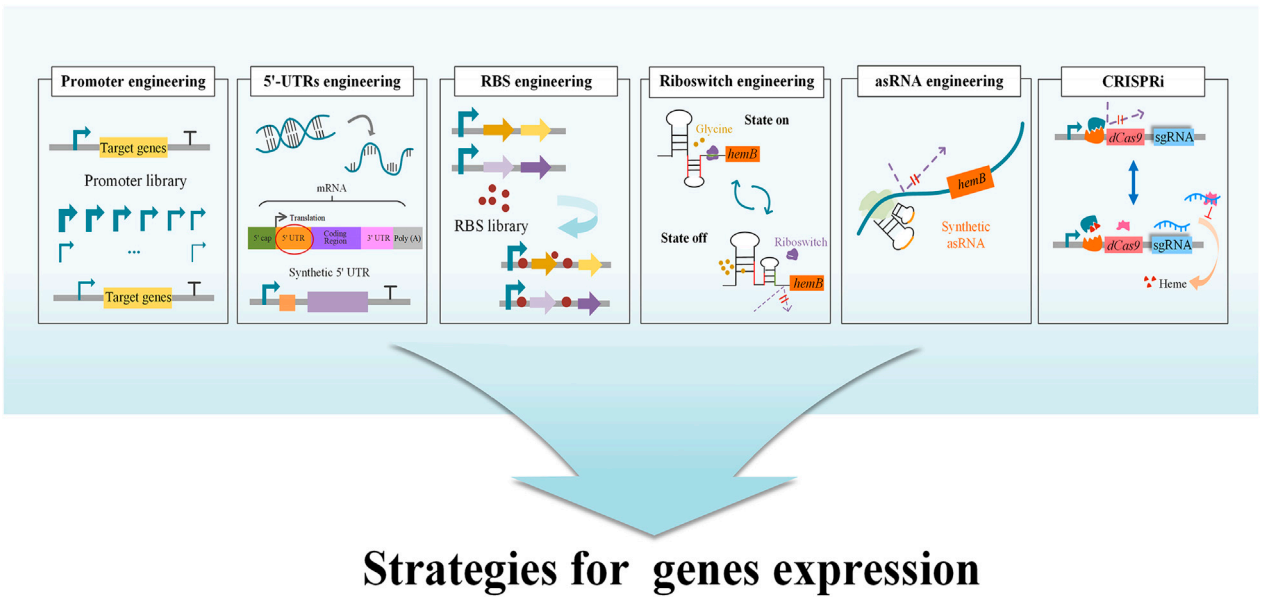

FIGURE 3 | Strategies for tuning the expression and regulation of genes. Tuning gene expression and regulation requires a balance between cell growth and a specific biological activity in order to transform the original system within the microbial cells into one that generates the target product. The strategies include several methods, such as CRISPRi, Riboswitch engineering, Synthetic asRNA engineering, RBS engineering. Promoter engineering, 5′-UTR engineering and RBS library can be used to optimize the expression of the target genes, and thereby increase the biosynthesis of 5-ALA. In riboswitch engineering, a glycine-OFF riboswitch was utilized to dynamically downregulate ALAD expression in the presence of glycine, while small amounts of glycine allow *hemB* to be expressed normally (Zhou et al., 2019). Using CRISPRi technology, a heme-responsive regulatory system was developed to control the concentration of heme dynamically and precisely. At low heme concentration, the regulatory system hinders the expression of CRISPRi (Zhang et al., 2020a).

overexpression of *ppc* resulted in decreased accumulation of 5-ALA while an obvious elevation of production (34.1% higher than control) could be achieved by finer tuning using a moderate RBS (Chen et al., 2020). Another approach relies on strengthening the metabolic flux from the TCA cycle to the precursor of 5-ALA synthesis. Succinyl-CoA synthetase, encoded by *sucCD*, catalyzes the reversible reaction between succinate and succinyl-CoA. The inactivation of *sucCD* can redirect the carbon flux toward the 5-ALA synthesis branch rather than the reductive TCA cycle (Yang et al., 2016; Ding et al., 2017). And cutting down glutamate biosynthesis pathway (encoded by *gdhA*) increased the flux from α-oxoglutarate to succinyl-CoA, which increased the 5-ALA titer 2-fold compared to the control (Ge F. et al., 2021). Apart from preventing the flux to the reductive TCA cycle, reinforcing the gene expression in the oxidative arm of the TCA cycle is equally significant for the synthesis 5-ALA. For example, the overexpression of *ACO2* (encoding aconitase) in the oxidative-arm of the TCA cycle could enhance the 5-ALA yield in *S. cerevisiae* (Hara et al., 2019). In *C. glutamicum* CgS1, overexpressing α-oxoglutarate dehydrogenase (encoded by *sucAB*) caused a 6% increase of the 5-ALA titer, while isocitrate dehydrogenase (encoded by *icd*) had a negative effect in this case (Yang et al., 2016). These results indicated that the regulation of multiple genes in the TCA cycle is relatively complex, and a design based on genome-scale metabolic network model is a more effective approach for increasing 5-ALA production.

Glycine is another precursor in the C4 pathway and it limits the yield of 5-ALA. The supply of glycine is a well-known bottleneck for the high-level production of 5-ALA, and this problem is mainly solved by adding exogenous glycine in the fermentation process (Fu et al., 2010; Kang et al., 2010; Kang et al., 2011b). Some experts also attempted to provide glycine for 5-ALA biosynthesis via metabolic engineering strategies (**Figure 2**). 3-phosphoglycerate dehydrogenase (encoded by *serA*) is the first enzyme of the glycine synthesis pathway and is tightly regulated via feedback inhibition by L-serine analogues, which could be released by mutations (Ding et al., 2017). The level of 5-ALA in a *C. glutamicum* strain overexpressing $serA^{\Delta 197}$, *serB* and *serC* increased by 70% compared to the parental strain with an unmodified glycine synthesis pathway (Zou et al., 2017). Recently, an unnatural pathway for the production of 5-ALA was construct by introducing the *agxt* gene from *Homo sapiens* to transform glyoxylate into glycine and finally realize 5-ALA synthesis without glycine addition (Ren et al., 2018). The proposed new approach is particularly useful to circumvent the problem of precursor supply, which was difficult to be engineered. In addition, our own research demonstrated the moderate amounts of glycine indeed improve 5-ALA synthesis (Zou et al., 2017), while excessive glycine poisons the host cells and influences the final yield (Sasaki et al., 2002; Fu et al., 2010). Therefore, it is necessary to continuously maintain an appropriate concentration of glycine in order to realize high productivity of 5-ALA.

3.2.2 Metabolic Engineering of Central Carbon Metabolic Pathways for Providing Precursors to the C5 Pathway

Glutamate is the precursor of the C5 pathway, mainly produced from α-oxoglutarate by glutamate dehydrogenase (GS) (encoded by *gdhA*). To improve the supply of glutamate, the carbon flux from the TCA cycle or glyoxylate cycle is redistributing towards α-oxoglutarate (**Figure 2**). The carbon flux of the TCA cycle was diverted to glutamate by overexpressing the *gltA* gene, deleting *sucA* (encoding α-oxoglutarate dehydrogenase), and precisely regulating the glyoxylate cycle using an appropriate transcription strength of *aceA* (encoding isocitrate lyase) in an engineered *E. coli* overexpressing $hemA^M$ and *hemL*, generating the flux-optimized strain WSAL4 (Noh et al., 2017). The level of 5-ALA was increased 3.6-fold compared to the control strain. In addition, repressing the transformation of α-oxoglutarate to succinyl-CoA and overexpressing an oxoglutarate dehydrogenase inhibitor (OdhI) reinforced the supply of glutamate in *C. glutamicum* (Ko et al., 2019). Double-mutated OdhI with eliminated phosphorylation and inhibited oxoglutarate dehydrogenase activity was further used to synthesize 5-ALA.The 5-ALA production of the double-mutated OdhI strain increased to 2.1 g/L, which was much higher than the 0.35 g/L of the strain expressing wild-type OdhI (Ko et al., 2019). Moreover, Zhang et al. dynamically regulated the expression of *odhA* (α-ketoglutarate dehydrogenase complex E1 subunit gene) with the strategies of auto-inducible metabolic engineering by a growth-regulated promoter P_{CP_2836}, which increased the production of 5-ALA by 1-fold (Zhang C. L. et al., 2020).

Repressing glutamate degradation and transport is also an alternative strategy. Recent studies reported that inactivation of a glutamate-transporter membrane protein (encoded by *Ncgl1221*) could drastically decrease the secretion of glutamate (Zhang and Ye, 2018) and promote the accumulation of intracellular 5-ALA in *C. glutamicum* (Chen et al., 2015; Zhang and Ye, 2018) (**Figure 2**). There are also other glutamate transport proteins, such as GltP, GltJ, GltK, GltL and GltS, which are strongly related to the intracellular glutamate concentration (Zhao and Zhai, 2019). Moreover, deleting the transport proteins of the downstream by-products of glutamate, proline and arginine also promoted the synthesis for 5-ALA (Zhang and Ye, 2018).

3.3 Regulated Expression of Key Genes in Downstream Pathways

Tetrapyrrole compounds are produced from 5-ALA in specific downstream pathways and are important for physiological and metabolic activities of organisms. The expression levels of downstream genes affect enzymes activity and transcription of the 5-ALA biosynthesis pathway as well as cell growth. In other words, regulated expression of key genes in downstream pathways is conducive to further increase 5-ALA production.

ALAD is the first enzyme in the biosynthetic pathways of heme, chlorophyll and other essential porphyrins. They all start from 5-ALA in the downstream pathway and ALAD has a close relationship with final accumulation of 5-ALA. The metabolic intermediate protoporphyrinogen IX inhibits the expression of ALAD and further influences the accumulation of 5-ALA (**Figure 1**) (Zhang J. L. et al., 2015; Zhang et al., 2016). Many studies have attempted to improve the concentration of 5-ALA by inhibiting the expression of ALAD to reduce the intracellular utilization of 5-ALA (Ding et al., 2017; Yu et al., 2015). As ALAD is an important enzyme catalyzing the first step in the synthesis of many essential porphyrins, the complete loss of ALAD activity has a negative impact on cell growth. The replacements of the initiation codon or promoter to regulate ALAD expression at the transcriptional and translational levels is another validated measure to realize the balance between cell growth and 5-ALA biosynthesis. After altering the most preferred initiation codon AUG into GUG in *E. coli*, the production of 5-ALA significantly increased from 1.31 to 1.76 g/L (Ding et al., 2017). Promoter engineering is another effective way to directly downregulate ALAD expression at the transcriptional level by replacing its promoter with constitutive promoters and stationary-phase promoters (**Figure 3**). A strain in which the stationary-phase promoter *fliCp* was introduced displayed superior performance, and the final production of 5-ALA was 2.68 g/L (increased by 11% over the control strain) (Zhang J. L. et al., 2019). Additionally, a glycine-OFF riboswitch from *Clostridium pasteurianum*, Apt2#82, was utilized to dynamically downregulate ALAD expression in the presence of glycine, resulting in an 11% improvement of 5-ALA production in recombinant *E. coli* (Zhou et al., 2019) (**Figure 3**). It is reported that the antisense RNA (asRNAs) of *hemB* could decrease its' mRNA level by 50%, and the production of 5-ALA was increased by 17.6% (Ge F. L. et al., 2021) (**Figure 3**). In a recent research, CRISPR interference (CRISPRi) was used to repress the expression of *hemB*, and the titer of 5-ALA increased 3.7 fold compared to the control (Miscevic et al., 2021). However, weakening the activity of ALAD cannot guarantee the elevation of production (Xie et al., 2003; Zhang J. L. et al., 2019), implying that ALAD has an appropriate range of activity and advanced research should be carried on.

The combinatorial perturbation of multiple genes in the downstream pathway has attracted widespread attention, with most studies focusing on engineered *E. coli*. Among several genes in the downstream pathway, the upregulation of *hemD* and *hemF* facilitated the accumulation of 5-ALA, while the overexpression of *hemB*, *hemG* and *hemH* had no effect (Zhang J. L. et al., 2019). The expression of *hemD* and *hemF* with moderate intensity, as well as overexpression of *hemA* and *hemL* increased the production of 5-ALA in recombinant *E. coli* LADF-6 to 3.25 g/L, 3.78-fold higher than the parental strain (Zhang J. L. et al., 2015). Recent studies indicated that the iron regulator small RNA *ryhB* distinctly downregulates the transcription of *hemB* and *hemH*, perturbing the accumulation of heme and 5-ALA (**Figure 1**) (Li et al., 2014). Subsequently, further studies investigated the transcriptional regulatory mechanism of *ryhB* in relation to other genes of the heme synthesis pathway. It was demonstrated that both overexpression of *hemD* and *hemF* downregulated the transcription of *ryhB*, while overexpression of *hemB* resulted in an unexpected increase (Zhang et al., 2016). In addition, a heme-responsive regulatory system (**Figure 3**) was

designed and constructed by CRISPRi to dynamically and precisely control the downstream pathways for 5-ALA synthesis (Zhang et al., 2020a). In this work, a H149D mutant was obtained by semi-rational design with site saturated mutagenesis of HrtR from *Lactococcus lactis*, and used as a biosensor to dynamically regulate the expression of *hemC* and *hemH* in the downstream pathways, which resulted in a 5-ALA titer of up to 5.35 g/L 5-ALA in batch-cultures of *E. coli* (Zhang et al., 2020a).

Thus, the biosynthesis of 5-ALA interacts with heme synthesis in downstream pathways and the deeper regulation is complex and ambiguous. Therefore, the simple deletion or overexpression of genes may not be able to produce a high yield of 5-ALA, and more elaborate regulatory strategies need to be developed to achieve a balance between cell growth and 5-ALA biosynthesis.

3.4 Cofactor Engineering

The supply of cofactors immediately impacts the production of metabolic products and the modification in cofactor engineering can accelerate the yield of targeted products, such as acetoin and 2,3-butanediol (Yang et al., 2017). During the synthesis of 5-ALA, the conversion of substances and the activation of enzymes mostly relies on cofactors such as pyridoxal PLP, coenzyme A, NADPH/NADP, etc. The supply of sufficient cofactors is of great significance to ensure the flow of electrons, activation of enzymes and maintenance of their stability. Currently, studies on cofactor supply mainly focus on the strengthening of the pyridoxal 5′-phosphate and coenzyme A supply by exogenous addition and metabolic pathway engineering, and also few involves the metabolic engineering of ATP and NAD(P)H (**Figure 2**).

3.4.1 Pyridoxal 5′-Phosphate

Pyridoxal 5′-phosphate (PLP) is a biologically active form of vitamin B_6 that can catalyze many enzymatic and non-enzymatic reactions (Heyl et al., 1951; Hayashi et al., 1990). At the same time, PLP is also an essential cofactor involved in both the C4 and C5 pathways. The key residues of these enzymes that interact with PLP are suspected to undergo extensive movements and contribute to the formation and stabilization of the functional conformation at the active sites (Brown et al., 2018). In the C4 pathway, ALAS condenses two precursors into 5-ALA with the assistance of PLP as an important cofactor. Firstly, PLP combines with glycine to form a covalent adduct, and further triggers transaldimination in the microenvironment. Then the PLP-glycine adduct releases CO_2 to synthesize 5-ALA by decarboxylation or deprotonation with the participation of succinyl-CoA (Kang et al., 2012). The interplay of the PLP cofactor with the protein moiety determines and modulates the multi-intermediate reaction cycle of ALAS (Stojanovski et al., 2019). At the same time, PLP binding induces re-ordering of active sites and key residues to achieve the active conformation of the enzyme according to the crystal structure of ALAS (Brown et al., 2018). GSA-AM is the last enzyme in the C5 pathway and also depends on PMP/PLP to synthesize 5-ALA. In view of structural similarity with ALAS, GSA-AM has been hypothesized to be the evolutionary precursor of ALAS (Schulze et al., 2006). One proposed reaction mechanism supported by kinetic studies posits that PLP is initially present as pyridoxamine 5′-phosphate (PMP) (Pugh et al., 1992). GSA is converted to 5-ALA via the intermediate 4,5-diaminovalerate along with the conversion of PMP into PLP (Li et al., 2018).

It was confirmed that the addition of PLP has a positive effect on 5-ALA production (Zhang J. L. et al., 2019). Subsequently, the supply of PLP was reinforced by slightly strengthening the native PLP pathway, and the titer of 5-ALA was increased by 7% to 2.86 g/L in the C5 pathway (Zhang J. L. et al., 2019). In a recent research, the overexpression of *Cgl0788-Cgl0789* operon (encoding pyridoxal 5′-phosphate synthase) in engineered *C. glutamicum* also improved the production of 5-ALA by 15.6% (Yan et al., 2020), which proved that the metabolic modification of PLP pathway promoted the production of 5-ALA (**Figure 2**). Similarly, PLP is also important in the C4 pathway and removing PLP led to complete loss of enzyme activity (Choi et al., 1999; Liu et al., 2010). Given the obvious efficiency of PLP in the C5 pathway, we speculate that it also may have a significant positive effect on 5-ALA synthesis in the C4 pathway, which is confirmed by a recent research. After integrating the gene encoding pyridoxal kinase (PdxY) into the chromosome and coexpressing ALAS from *R. capsulatus*, the 5-ALA titer of recombinant *E. coil* increased 4.33-fold to 1.99 g/L (Xue et al., 2021).

3.4.2 Coenzyme A

Coenzyme A (CoA) is another essential cofactor in numerous biosynthetic pathways, such as the synthesis of pantothenate (vitamin B_5), cysteine, and ATP (Takagi et al., 2010). Moreover, CoA has a direct relationship with the synthesis of succinyl-CoA, indicating that perturbation of CoA metabolism might have a distinct influence on 5-ALA.

Pantothenate kinase (encoded by *coaA*) is an essential protein in the CoA biosynthesis pathway and it is regulated via feedback inhibition by CoA (Song and Jackowski, 1992; Rock et al., 2000). The overexpression of *coaA* in recombinant *C. glutamicum* led to a 10% increase of 5-ALA production (Yang et al., 2016). The synthesis of CoA from pantothenate involves a four-step enzymatic process, whereby the reactions catalyzed by pantothenate kinase and phospho-pantetheine adenylyl transferase (encoded by *coaD*) are major rate-limiting steps (Vadali et al., 2004; Lee et al., 2013). The effects of all genes in the CoA synthetic pathway on 5-ALA was confirmed, and it was demonstrated that upregulating all the genes of the CoA synthesis pathway, except for *coaE* (encoding dephospho-CoA kinase), is beneficial to the accumulation of 5-ALA (Ding et al., 2017). The production of 5-ALA reached 1.00 g/L (increased by 45.1%) by co-overexpressing the $coaA^M$, *dfp* and *coaD* genes (Ding et al., 2017) (**Figure 2**).

3.4.3 ATP and NAD(P)H

As cofactor, ATP and NAD(P)H directly participate in the transmission of energy and the transport of electrons to influence the yield of 5-ALA (Ren et al., 2018). The strains are capable of synthesizing these cofactors, while their own

regeneration is generally insufficient for the overproduction of 5-ALA. Accounting for the importance of cofactors for growth and production, it was assumed that enhancing cofactor regeneration pathways may facilitate increased 5-ALA production. In the biosynthesis of 5-ALA in the C5 pathway, the reactions catalyzed by GluTS and GluTR are respectively ATP and NADPH dependent (**Figure 1**). The appropriate overexpression of phosphoenolpyruvate (PEP) carboxykinase (PCK, encoded by *pckA*) from *Mannheiemia succiniciproducens*, which can irreversibly convert PEP to oxaloacetate and generates ATP, increased the production of 5-ALA by 12.7% (Zhang C. L. et al., 2020). In order to improve the pool of NADPH, isocitrate dehydrogenase (IDH, encoded by *icd*) and $NADP^+$- dependent glyceraldehyde 3-phosphate dehydrogenase (GAPDH, encoded by *gapA*) were successively overexpressed, and the production of 5-ALA respectively increased 13.5% and 26.7% compared with the control (Zhang C. L. et al., 2020) (**Figure 2**). Although few research concerned on increasing ATP flux by metabolic engineering strategies, the potential positive effect on increasing the yield of 5-ALA deserves further attention from researchers in the future.

3.5 Accelerated Transport of Intracellular 5-Aminolevulinic Acid

High-level synthesis of target products may be harmful to the microbial host cells and further inhibit the production of the target product to some extent. 5-ALA is one of the typical representatives, which easily result in the accumulation of reactive oxygen species (ROS) that has toxic effects on cells. It is therefore critical to improve 5-ALA production by accelerating intracellular 5-ALA transfer to the extracellular environment, alleviating the cytotoxicity.

Because its physical properties are close to those of proteinogenic amino acids, different transport proteins with the ability to transport amino acids and their analogues have been used to improve the production of 5-ALA (**Figure 2**) (Moser et al., 2001). The serine/threonine transporter RhtA has been widely used in numerous recombinant strains and exhibited excellent results in increasing the extracellular 5-ALA concentration. Kang et al. firstly applied the *rhtA* gene in 5-ALA synthesis and successfully demonstrated its feasibility for further improvement of production (Kang et al., 2011a). Recently, overexpressing *rhtA* with a T7 system composed of orthogonal T7RNA polymerase and the T7 promoter increased 5-ALA production 40-fold in *E. coli* (Tan S. I. et al., 2019). Introduction of *rhtA* into the high-yield recombinant *C. glutamicum* AL-OI** increased production of 5-ALA by 28% over the control (Ko et al., 2019). Interestingly, the expression level of *rhtA* was upregulated 17-fold in the high-yield *E. coli* Transetta GTR/GBP co-expressing *HemA1* and *pgr7* from *A. thaliana* (Zhao and Zhai, 2019). The timely and effective transport of 5-ALA outside the cell is of great significance for the continuous synthesis of 5-ALA. It is undeniable that RhtA is not the only protein that can transport 5-ALA. However, only few export proteins have been found, and the discovery of transporters remains a great challenge.

A second strategy for facilitating the transport of 5-ALA relies on changing the permeability of the cell wall. Penicillin inhibits the synthesis of cell wall components by restraining the activity of penicillin-binding proteins and further benefits the accumulation of 5-ALA (Laneelle et al., 2013; Ramzi et al., 2015). However, the exogenous addition of penicillin not only increases the production cost but is also not environmentally friendly. Our previous study directly influenced the synthesis of the cell wall by deleting the non-essential high molecular-weight penicillin-binding protein genes *pbp1a*, *pbp1b*, and *pbp2b* individually, and all were positive for the production of 5-ALA with increases of 13.53, 29.47, and 22.22%, respectively (Feng et al., 2016), demonstrating the vital role of cell wall permeability for extracellular 5-ALA accumulation.

3.6 Cell-free Metabolic Engineering *in vitro*

The production of 5-ALA *in vivo* is limited by low volumetric productivity, byproduct losses and complex fermentation processes. Moreover, the producer strains tend to be exposed to the toxic effects of ROS, which affects the normal growth of the cells (Zeng et al., 2015). To address these limitations, cell-free metabolic engineering that utilizes purified enzymes or crude cell extracts to synthesize 5-ALA was proposed (Dudley et al., 2015).

In an early study using cell-free extracts of recombinant *E. coli* with the addition of succinate, glycine, LA and ATP, the production of 5-ALA reached 22.6 mM (2.96 g/L) *in vitro* (Van Der Werf and Zeikus, 1996). By contrast, the same recombinant strain from which the cell extract was prepared was only able to produce 2.25 mM (0.30 g/L) 5-ALA *in vivo*, which illustrates the great potential for high-level 5-ALA production *in vitro*. Limited by the relatively lower enzyme activities of cell extracts and complex engineered of recombinant strains, researchers were continually looking for more efficient and commercially viable approaches for 5-ALA synthesis. With the purification of the key enzymes in the metabolic pathway and elucidation of their structure and mechanism (Brown et al., 2018), it is possible to produce 5-ALA using a cell-free multi-enzyme catalysis system. Meng et al. (Meng et al., 2016) firstly constructed a cell-free multi-enzyme catalysis system based on the C4 pathway using the substrates succinic acid, glycine, and polyphosphate, catalyzed by the three enzymes, ALAS, succinyl-CoA synthase and polyphosphate kinase. Although the final titer of 5-ALA reached only 5.4 mM (0.71 g/L), the study demonstrated the possibility of cell-free multienzymatic synthesis. Subsequently, a cell-free semi-permeable process based on the C5 pathway was realized using glucose, sodium polyphosphate, ATP, NADPH, glutamate and nine enzymes (Zhao et al., 2019). Similar to previous research, the yield of 5-ALA was very low and the cost was very high, but this cell-free semi-permeable system firstly realized the recycling of enzymes and high-value cofactors for 5-ALA biosynthesis. In spite of the challenges faced by current studies, the considerable potential to realize commercial *in vitro* production by cell-free metabolic engineering cannot be ignored.

4 DETECTION OF 5-ALA

Detection of 5-ALA is important for the study of synthetic pathways, metabolic mechanisms and applications of 5-ALA. In order to more easily measure the quantity of 5-ALA, detection methods based on Ehrlich's reagent, fluorescent protein-based detection systems, liquid chromatography tandem-mass spectrometry (LC–MS/MS), high performance liquid chromatography (HPLC) and gas chromatography-mass spectrometry (GC–MS) have been developed.

4.1 Ehrlich's Reagent Method

Ehrlich's reagent was firstly used for the quantification of 5-ALA. It produces an adduct, that can be detected colorimetrically at 553 nm (Mauzerall and Granick, 1956; Tomokuni and Ogata, 1972). This method involves cell collection, extraction of intracellular components, and the Ehrlich reaction, which requires about 30 min for each sample (Mauzerall and Granick, 1956; Tomokuni and Ogata, 1972). Ehrlich's reagent, as a classic detection method, has been widely accepted and used to measure the 5-ALA content, but the method suffers from severe sample background interference, in addition to being time-consuming and laborious.

4.2 Fluorescence Spectroscopy

5-ALA is stable only under acidic conditions. Currently, it is mostly sold in the form of hydrochloride and there is need for a simpler approach. The conversion of chemicals into easily detectable signals such as color or fluorescence has been a powerful tool for *de novo* metabolite monitoring and *in vitro* small molecule detection. Chung et al. (2005) proposed a combination of *hemA* with a green fluorescent protein gene (*egfp*) to realize the characterization and investigation of extracellular 5-ALA. Although the concentration of 5-ALA is reflected in the fluorescence intensity, the precise concentration of 5-ALA still depends on Ehrlich's reagent. Recently, a fluorescence-based whole-cell system was developed for the simultaneous detection and production of 5-ALA in recombinant *E. coli* (Tan S. I. et al., 2019). In this method, a constitutive 5-ALA production strain with *R. sphaeroides* HemA (RshemA) and a fusion of super-folder-green fluorescent protein was established with an optimized promoter, medium, and fusion sites. The *de novo* quantification of intracellular and extracellular 5-ALA by monitoring the fluorescence of sfGFP fused to *RshemA* was also explored using dual promoters and dual plasmids (Tan S. I. et al., 2019). Additionally, to increase the understanding of the regulatory mechanism of 5-ALA in higher organisms, matrix isopotential synchronous fluorescence spectrometry and the first derivative technique were combined for the direct determination of δ-ALA in urine samples (Ajmal et al., 2019). The fluorescent derivatization of 5-ALA was based on the Hantzsch reaction. Matrix-isopotential synchronous fluorescence spectra were recorded along a matrix-isopotential trajectory, which combines the points of equal intensity in theoretical 3D contours. Maximum sensitivity and appropriate selectivity were ensured by the study of the experimental variables in the d-ALA bands, centered at its excitation and emission maxima (392.6 and 464.5 nm) (Ajmal et al., 2019). This method was comparable to conventional high performance liquid chromatography-fluorescence, with a detection limit of 5.4 ppb and lower linear-range limit of 18 ppb. These methods have improved effectiveness, enabling real-time detection with outstanding sensitivity, which is of great significance for ALA synthesis, detection and studies of the underlying metabolic mechanism.

4.3 Chromatography

Compared with a microbial fermentation broth with high 5-ALA content, samples with low 5-ALA concentrations such as blood, urine or tissue require more sensitive detection technology. The LC–MS/MS method was developed to simultaneously determine 5-ALA concentrations in fluids or tissues after solid-phase extraction, butanol derivatization, and quantification by selective reaction monitoring using $^{13}C_5$, ^{15}N-ALA and 2,4-$^{13}C_2$-PBG internal standards (Zhang et al., 2011; Dogan et al., 2019). The assay was highly sensitive for 5-ALA (LLOQ = 0.05-0.005 μM), and required ~4 h from extraction to results. Later, a HPLC and GC–MS test method for 5-ALA detection was also developed (Ren et al., 2018; Hara et al., 2019) to obtain the real 5-ALA levels in microbial fermentation broth. Although these methods are sensitive and practical, more research is still needed to improve 5-ALA detection and decrease the assay costs.

5 BIOLOGICAL EFFECTS AND APPLICATIONS OF 5-AMINOLEVULINIC ACID

5.1 Plant Growth Regulators, Herbicides and Insecticides in Agriculture

To date, 5-ALA has been demonstrated to act as a metabolic intermediate and also as a growth regulator in plant cultivation. It is regarded as a plant growth promoting hormone since many studies found that it could regulate the growth and development of higher plants. Instead of only focusing on the effects of 5-ALA on plant, more and more researchers began to use omics to explain its mechanism (Zheng et al., 2021). The role of 5-ALA in stimulating physiochemical processes in higher plants under stress, regulating plant growth and development in seed germination, vegetative growth and fruit coloring has been reviewed by Wu et al., in 2019 (Wu et al., 2018). Here, we mainly discussed the latest studies on its role in plant growth as well as the amelioration of the effects caused by various abiotic stresses.

5-ALA can selectively kill weeds without affecting monocotyledonous wheat and corn crops (Rebeiz et al., 1984). Therefore, a large amount of 5-ALA is used in plants or pests to exert the effects of herbicides and insecticides (Sasikala et al., 1994). For example, two different types of agricultural herbicides have been produced based on the principle that 5-ALA is necessary for plant life and cannot be synthesized in the dark. "Norfluron" can inhibit Glu-tRNA gene expression and prevent 5-ALA synthesis, resulting in a lack of 5-ALA leading to plant death (Kumar et al., 1999). Acifluorfen-methyl is a product that

deregulates 5-ALA synthesis leading to a large accumulation of 5-ALA, thereby inhibiting the synthesis of heme and porphyrin compounds (Gullner and Dodge, 2000). However, higher concentrations required in herbicides and insecticides made it difficult to popularize the application or 5-ALA in this field based on current prices.

The abiotic stresses caused by environment, such as drought, salinity, high or low temperature, cause great losses to crop yields and social and economic aspects, and 5-ALA is helpful to alleviate these problems effectively. With the foliage application of 5-ALA at 75 mg/L, the activities of catalase, ascorbate peroxidase and superoxide dismutase of sunfower (*Helianthus annuus* L.) enhanced by 157.1, 90 and 80% under drought stress than no 5-ALA addition (Sher et al., 2021). It is reported that exogenous addition of a suitable concentration of 5-ALA can effectively alleviate weak light stress in tobacco seedlings (Li et al., 2019) and damages induced by UV-B in *Cajanus cajan* L. seedlings (Gupta and Prasad, 2021). Moreover, 5-ALA has shown a significant effect on alleviating abiotic stress caused by low temperature (Yan et al., 2020) and salinity (Islam et al., 2021; Wu et al., 2021) and so on in plants, which were summarized in detail in a recent review (Rhaman et al., 2021).

5.2 Photosensitizers and Cosmetics

Many studies have investigated fluorescence-guided resection of malignant tumors based on 5-ALA and protoporphyrin IX accumulation in tumors. This approach has become a well-established technique to facilitate greater extent of resection resulting in improved progression free survival (Stummer et al., 1998; Stummer et al., 2000; Pichlmeier et al., 2008; Stummer and Kamp, 2009; Rapp et al., 2012; Hadjipanayis et al., 2015; Guyotat et al., 2016). Additionally, 5-ALA was used with varying success in tumors such as meningiomas, medulloblastomas, ependymomas, and metastatic carcinoma (Millesi et al., 2016;Zhang C. et al., 2019; Wainwright et al., 2019). Other applications in medicine are being constantly developed, in addition to the applications related to cancer. Recently, there have been some excellent reviews covering the research progress on 5-ALA-based treatment of tumors (Wainwright et al., 2019; Zhang C. et al., 2019), and will not be repeated here.

Photodynamic therapy (PDT) with 5-ALA has been demonstrated as an effective treatment for severe acne in medical and cosmetic field (Itoh et al., 2000; Gold and Goldman, 2004), and recent studies have further researched the concentration of 5-ALA administration in different cases (Serini et al., 2019; Zhang et al., 2020b). Additionally, 5-ALA or its derivatives and ferric citrate compounds also are the main ingredient of disease prevention and improvement agent. A recent research demonstrated that 5-ALA combined with sodium ferric citrate could effectively improve aerobic capacity and voluntary exercise training achievement in older women over 75 years (Masuki et al., 2016; Ichihara et al., 2021). 5-ALA was also developed as a combined therapeutic-diagnostic agent in dentistry based on the strong dual modality of 5-ALA as lethal to cariogenic bacteria through photodynamic inactivation and enhancing LIF intensity for identification of dental caries (Lashkari et al., 2019). However, 5-ALA has a complex mechanism of action in the body, and the metabolic mechanism of 5-ALA conversion is still unclear. These unresolved issues led to a more prudent acceptance process of related products containing 5-ALA.

5.3 Promising Animal Feed Additives

It was found that adding appropriate amounts of 5-ALA to animal feed can significantly improve their growth. In invertebrate aquaculture, dietary administration of 5-ALA effectively improved the immune system, ATP levels and acute hepatopancreatic necrosis disease resistance in pacific white shrimp (Direkbusarakom et al., 2021). Dankook University studied the effects of 5-ALA on the growth performance, blood status, and immune system of weaned piglets, sows, broilers and hens in South Korea. These results showed that adding appropriate amounts of 5-ALA to the diet can increase the hemoglobin concentration and iron in the serum, the levels of lymphocyte subsets, the quality of immune organs and the immune performance of these animals (Chen Y. J. et al., 2008; Chen Y. et al., 2008; Wang et al., 2009). Similarly, 5-ALA had the same effect on cows (Hendawy et al., 2019). Our own recent research work tried to efficiently enrich feed with 5-ALA by developing a solid-state fermentation process based on *S. cerevisiae* (Mao et al., 2020). In this work, 5-ALA not only plays a role in improving the animal's growth performance and immune system, but yeast cells can be used as feed protein to provide nutrition for animals. In summary, it was concluded that 5-ALA could indeed be used as an animal feed additive to improve the iron status and immune response in livestock, which was also reviewed recently by Hendawy et al. recently (Hendawy et al., 2020).

6 DISCUSSION AND OUTLOOK

6.1 Exploration of Production Hosts With Natural Advantages

According to the Comprehensive Enzyme Information System of BRENDA, there are 147 known organisms with 5-aminolevulinate synthesis ability, and we can assume that many natural hosts have not yet been developed to synthesize 5-ALA. In the future, high-yield production of 5-ALA can be achieved by fully screening natural hosts with innate advantages in 5-ALA synthesis. Furthermore, efficient 5-ALA synthesis can also be achieved through further metabolic engineering to transform the current model strains to give full play to their natural advantages. For example, *C. glutamicum* can naturally accumulate amino acids and lacks a glycine cleavage pathway, making it a highly attractive potential biosynthetic host (Jorgensen et al., 2012). It was shown that the activation of native antioxidant defense systems alleviated the deregulation of ROS metabolism due to 5-ALA accumulation and further improved 5-ALA tolerance and synthesis (Zhu et al., 2019). Therefore, hosts such as *C. glutamicum* and *S. cerevisiae* with the advantages of natural resistance to high concentrations of organic acids can be further explored as chassis cells for 5-ALA

synthesis. Fully exploiting and utilizing the natural advantages of hosts to build a 5-ALA artificial cell factory may be an effective way to synthesize 5-ALA.

6.2 In-Depth Analysis and Understanding of Relevant Mechanisms of 5-ALA Biosynthesis

Although the synthesis and application of 5-ALA has been extensively studied, there are still some challenges that need to be resolved, such as the regulation and transport mechanisms in 5-ALA biosynthesis and the metabolic mechanisms related to 5-ALA application. First, the feedback regulation of ALAS or GluTR by heme exists in plants, animals and microorganisms, and influences the 5-ALA biosynthesis and host cell growth. In addition, feed-back regulation by downstream products in plant cells regulates the biosynthesis of 5-ALA in an opposite manner. However, the mechanism of feedback regulation by these factors and heme has not been elucidated. Secondly, the cellular transport capacity is also crucial for 5-ALA biosynthesis, which has been proved in previous research (Feng et al., 2016). However, Transport mechanisms of 5-ALA are not fully clear and need to be studied further. Detailed knowledge of the metabolic mechanisms of 5-ALA will resolve the safety issues and improve its industrial applications.

6.3 Improving 5-Aminolevulinic Acid Synthesis Using Artificial Microbial Consortia

Recently, a growing fraction of research has transitioned towards employing a modular co-culture engineering strategy using multiple microbes growing together to facilitate a "divide-and-conquer" approach for chemical biosynthesis. Artificial microbial consortia have been constructed and applied to produce bio-based chemicals (Lu et al., 2019), natural products (Wang R. F. et al., 2020) and bioenergy (Jiang et al., 2019). According to the latest research progress on metabolic engineering for the synthesis of 5-ALA (**Supplementary Table S1**), the high-level production 5-ALA through the C4 pathway requires the exogenous addition of glycine in all cases. Moreover, our research group confirmed the effect of the addition of different glycine concentrations on the synthesis of 5-ALA in *C. glutamicum* (Zou et al., 2017), and the supply of glycine is the key limiting factor for 5-ALA synthesis in the C4 pathway (Ren et al., 2018). However, the addition of glycine not only increases the cost of the product, but the toxic effects of high glycine concentrations on the cells will also inhibit the growth of engineered bacteria and reduce the production efficiency. Moreover, 5-ALA is synthesized from the precursors glycine and succinyl-CoA in the C4 pathway, whose balanced supply is the key to the efficient synthesis of 5-ALA. To achieve precise control of the two precursors and the efficient synthesis of 5-ALA, synthetic microbial consortia can be constructed by placing the synthesis pathway modules of glycine and succinyl-CoA into different engineered strains. Based on the flexible optimization of the metabolic module within a single strain, combined with the adjustment of the inoculation volume and fermentation process of the microbial consortia, the artificial microbial consortia may be used as a potential method to synthesize 5-ALA. This approach can save costs and reduce the burden imposed on the cellular metabolism, solve the problem of flux optimization of nonlinear synthetic pathways, and achieve precise control of synthetic pathways.

AUTHOR CONTRIBUTIONS

ZW, MJ and KH contributed to the writing of the article. MJ and KH were responsible for the writing and arrangement of the article, YM, HM, and TC were responsible for the structure design of the article. All authors contribute to the revision, reading and approval of manuscripts.

FUNDING

This work was supported by the National Key Research and Development Program of China (2018YFA0901300) and National Natural Science Foundation of China (NSFC-21776209 and NSFC-21621004) and Natural Science Foundation of Tianjin (No. 19JCYBJC21100).

SUPPLEMENTARY MATERIAL

The Supplementary Material for this article can be found online at: https://www.frontiersin.org/articles/10.3389/fbioe.2022.841443/full#supplementary-material

Supplementary Table S1 | Recent researches on the biosynthesis of 5-aminolevulinic acid *in vivo* or *in vitro*.

REFERENCES

Ajmal, M., Shindi, A. A. F., Liu, Y.-H., Zhao, Y., Wu, P.-P., Wei, J.-W., et al. (2019). Derivative Matrix-Isopotential Synchronous Spectrofluorimetry: a Solution for the Direct Determination of Urinary δ-aminolevulinic Acid. *New J. Chem.* 43 (46), 18092–18097. doi:10.1039/c9nj04261j

Ano, A., Funahashi, H., Nakao, K., and Nishizawa, Y. (1999). Effect of Glycine on 5-Aminolevulinic Acid Biosynthesis in Heterotrophic Culture of *Chlorella regularis* Ya-603. *J. Biosci. Bioeng.* 88 (1), 57–60. doi:10.1016/S1389-1723(99)80176-5

Beale, S. I., Gough, S. P., and Granick, S. (1975). Biosynthesis of Delta-Aminolevulinic Acid from the Intact Carbon Skeleton of Glutamic Acid in Greening Barley. *Proc. Natl. Acad. Sci.* 72 (7), 2719–2723. doi:10.1073/pnas.72.7.2719

Beale, S. I. (1970). The Biosynthesis of δ-Aminolevulinic Acid in Chlorella. *Plant Physiol.* 45 (4), 504–506. doi:10.1104/pp.45.4.504

Brown, B. L., Kardon, J. R., Sauer, R. T., and Baker, T. A. (2018). Structure of the Mitochondrial Aminolevulinic Acid Synthase, a Key Heme Biosynthetic Enzyme. *Structure* 26 (4), 580–589. doi:10.1016/j.str.2018.02.012

Chen, J., Wang, Y., Guo, X., Rao, D., Zhou, W., Zheng, P., et al. (2020). Efficient Bioproduction of 5-Aminolevulinic Acid, a Promising Biostimulant and

Nutrient, from Renewable Bioresources by Engineered *Corynebacterium glutamicum*. *Biotechnol. Biofuels.* 13 (1), 41. doi:10.1186/s13068-020-01685-0

Chen, M., Chen, X., Wan, F., Zhang, B., Chen, J., and Xiong, Y. (2015). Effect of Tween 40 and DtsR1 on L-Arginine Overproduction in *Corynebacterium crenatum*. *Microb. Cel Fact.* 14, 119. doi:10.1186/s12934-015-0310-9

Chen, Y. J., Kim, I. H., Cho, J. H., Min, B. J., Yoo, J. S., and Wang, Q. (2008). Effect of δ-aminolevulinic Acid on Growth Performance, Nutrient Digestibility, Blood Parameters and the Immune Response of Weanling Pigs Challenged with *Escherichia coli* Lipopolysaccharide. *Livestock Sci.* 114 (1), 108–116. doi:10.1016/j.livsci.2007.04.015

Chen Y, Y., Kim, I., Cho, J., Yoo, J., Kim, H., and Shin, S. (2008). Utilization of δ-aminolevulinic Acid for Livestock: Blood Characteristics and Immune Organ Weight in Broilers. *J. Anim. Feed Sci.* 17 (2), 215–223. doi:10.22358/jafs/66601/2008

Choi, C., Hong, B.-S., Sung, H.-C., Lee, H.-S., and Kim, J.-H. (1999). Optimization of Extracellular 5-Aminolevulinic Acid Production from *Escherichia coli* Transformed with ALA Synthase Gene of *Bradyrhizobium japonicum*. *Biotechnol. Lett.* 21, 551–554. doi:10.1023/A:1005520007230

Choi, H. P., Lee, Y. M., Yun, C. W., and Sung, H. C. (2008). Extracellular 5-Aminolevulinic Acid Production by *Escherichia coli* Containing the *Rhodopseudomonas palustris* KUGB306 *hemA* Gene. *J. Microbiol. Biotechnol.* 18 (6), 1136–1140. doi:10.1007/s12275-008-0038-x

Chung, S.-Y., Seo, K.-H., and Rhee, J. I. (2005). Influence of Culture Conditions on the Production of Extra-cellular 5-Aminolevulinic Acid (ALA) by Recombinant *E. coli*. *Process Biochem.* 40 (1), 385–394. doi:10.1016/j.procbio.2004.01.024

Cui, Z., Jiang, Z., Zhang, J., Zheng, H., Jiang, X., Gong, K., et al. (2019). Stable and Efficient Biosynthesis of 5-Aminolevulinic Acid Using Plasmid-free *Escherichia coli*. *J. Agric. Food Chem.* 67 (5), 1478–1483. doi:10.1021/acs.jafc.8b06496

Cui, Z., Zhu, Z., Zhang, J., Jiang, Z., Liu, Y., Wang, Q., et al. (2021). Efficient 5-Aminolevulinic Acid Production through Reconstructing the Metabolic Pathway in SDH-Deficient *Yarrowia lipolytica*. *Biochem. Eng. J.* 174, 108125. doi:10.1016/j.bej.2021.108125

Della Pepa, G. M., Ius, T., La Rocca, G., Gaudino, S., Isola, M., Pignotti, F., et al. (2020). 5-Aminolevulinic Acid and Contrast-Enhanced Ultrasound: The Combination of the Two Techniques to Optimize the Extent of Resection in Glioblastoma Surgery. *Neurosurg.* 86 (6), E529–E540. doi:10.1093/neuros/nyaa037

Ding, W., Weng, H., Du, G., Chen, J., and Kang, Z. (2017). 5-Aminolevulinic Acid Production from Inexpensive Glucose by Engineering the C4 Pathway in *Escherichia coli*. *J. Ind. Microbiol. Biotechnol.* 44 (8), 1127–1135. doi:10.1007/s10295-017-1940-1

Direkbusarakom, S., Kinoshita, H., Pooljun, C., Saeng-ngern, S., and Wuthisuthimethavee, S. (2021). 5-Aminolevulinic Acid's Effects on Immune-Related Gene Expression and Acute Hepatopancreatic Necrosis Disease (AHPND) Protection in Pacific White Shrimp *Litopenaeus vannamei*. *Fish. Pathol.* 55 (4), 125–131. doi:10.3147/jsfp.55.125

Dogan, O., Serdar, M. A., Murat, K., Sonmez, C., İspir, E., Serteser, M., et al. (2019). A Simple Method for Quantification of Five Urinary Porphyrins, Porphobilinogen and 5-Aminolevulinic Acid, Using Liquid Chromatography Tandem Mass Spectrometry. *Ind. J. Clin. Biochem.* 34 (1), 82–88. doi:10.1007/s12291-017-0716-8

Dubois, D. Y., Blais, S. P., Huot, J. L., and Lapointe, J. (2009). A C-Truncated Glutamyl-tRNA Synthetase Specific for tRNA (Glu) Is Stimulated by its Free Complementary Distal Domain: Mechanistic and Evolutionary Implications. *Biochemistry* 48 (25), 6012–6021. doi:10.1021/bi801690f

Dudley, Q. M., Karim, A. S., and Jewett, M. C. (2015). Cell-Free Metabolic Engineering: Biomanufacturing Beyond the Cell. *Biotechnol. J.* 10 (1), 69–82. doi:10.1002/biot.201400330

Fales, L., Nogaj, L., and Zeilstra-Ryalls, J. (2002). Analysis of the Upstream Sequences of the *Rhodobacter sphaeroides* 2.4.1 *hemA* Gene: *In Vivo* Evidence for the Presence of Two Promoters that Are Both Regulated by. *fnrl. Photosynth. Res.* 74 (2), 143–151. doi:10.1023/A:1020947308227

Feng, L., Zhang, Y., Fu, J., Mao, Y., Chen, T., Zhao, X., et al. (2016). Metabolic Engineering of *Corynebacterium glutamicumfor* Efficient Production of 5-aminolevulinic Acid. *Biotechnol. Bioeng.* 113 (6), 1284–1293. doi:10.1002/bit.25886

Fu, W., Lin, J., and Cen, P. (2007). 5-Aminolevulinate Production with Recombinant *Escherichia coli* Using a Rare Codon Optimizer Host Strain. *Appl. Microbiol. Biotechnol.* 75 (4), 777–782. doi:10.1007/s00253-007-0887-y

Fu, W., Lin, J., and Cen, P. (2008). Enhancement of 5-Aminolevulinate Production with Recombinant *Escherichia coli* Using Batch and Fed-Batch Culture System. *Bioresour. Technol.* 99 (11), 4864–4870. doi:10.1016/j.biortech.2007.09.039

Fu, W., Lin, J., and Cen, P. (2010). Expression of a *hemA* Gene from *Agrobacterium radiobacter* in a Rare Codon Optimizing *Escherichia coli* for Improving 5-Aminolevulinate Production. *Appl. Biochem. Biotechnol.* 160 (2), 456–466. doi:10.1007/s12010-008-8363-4

Ge, F., Li, X., Ge, Q., Zhu, D., Li, W., Shi, F., et al. (2021). Modular Control of Multiple Pathways of *Corynebacterium glutamicum* for 5-Aminolevulinic Acid Production. *AMB Expr.* 11 (1), 179. doi:10.1186/s13568-021-01335-0

Ge, F., Wen, D., Ren, Y., Chen, G., He, B., Li, X., et al. (2021). Downregulating of *hemB* via Synthetic Antisense RNAs for Improving 5-Aminolevulinic Acid Production in *Escherichia coli*. *3 Biotech.* 11 (5), 230. doi:10.1007/s13205-021-02733-8

Gold, M. H., and Goldman, M. P. (2004). 5-Aminolevulinic Acid Photodynamic Therapy: Where We Have Been and where We Are Going. *Dermatol. Surg.* 30 (8), 1077–1084. doi:10.1111/j.1524-4725.2004.30331.x

Gullner, G., and Dodge, A. D. (2000). Accumulation of Glutathione in Pea Leaf Discs Exposed to the Photooxidative Herbicides Acifluorfen and 5-Aminolevulinic Acid. *J. Plant Physiol.* 156 (1), 111–117. doi:10.1016/s0176-1617(00)80280-1

Gupta, D., and Prasad, S. M. (2021). Priming with 5-Aminolevulinic Acid (ALA) Attenuates UV-B Induced Damaging Effects in Two Varieties of *Cajanus cajan* L. Seedlings by Regulating Photosynthetic and Antioxidant Systems. *South Afr. J. Bot.* 138, 129–140. doi:10.1016/j.sajb.2020.12.009

Guyotat, J., Pallud, J., Armoiry, X., Pavlov, V., and Metellus, P. (2016). 5-Aminolevulinic Acid-Protoporphyrin IX Fluorescence-Guided Surgery of High-Grade Gliomas: A Systematic Review. *Adv. Tech. Stand. Neurosurg.* 2016 (43), 61–90. doi:10.1007/978-3-319-21359-0_3

Hadjipanayis, C. G., Widhalm, G., and Stummer, W. (2015). What Is the Surgical Benefit of Utilizing 5-Aminolevulinic Acid for Fluorescence-Guided Surgery of Malignant Gliomas? *Neurosurgery* 77 (5), 663–673. doi:10.1227/neu.0000000000000929

Hama, O. T., and Hase, E. (1978). Blue light effect on chlorophyll formation in chlorella protothecoides. *Photochem. Photobiol.* 27, 199–202. doi:10.1016/B978-0-08-022677-4.50018-6

Hara, K. Y., Saito, M., Kato, H., Morikawa, K., Kikukawa, H., Nomura, H., et al. (2019). 5-Aminolevulinic Acid Fermentation Using Engineered *Saccharomyces cerevisiae*. *Microb. Cel Fact.* 18 (1), 194. doi:10.1186/s12934-019-1242-6

Harel, E., and Klein, S. (1972). Light Dependent Formation of δ-aminolevulinic Acid in Etiolated Leaves of Higher Plants. *Biochem. Biophysical Res. Commun.* 49 (2), 364–370. doi:10.1016/0006-291x(72)90419-6

Hayashi, H., Wada, H., Yoshimura, T., Esaki, N., and Soda, K. (1990). Recent Topics in Pyridoxal 5'-Phosphate Enzyme Studies. *Annu. Rev. Biochem.* 59, 87–110. doi:10.1146/annurev.bi.59.070190.000511

Hendawy, A. O., Khattab, M. S., Sugimura, S., and Sato, K. (2020). Effects of 5-Aminolevulinic Acid as a Supplement on Animal Performance, Iron Status, and Immune Response in Farm Animals: A Review. *Animals* 10 (8), 1352–1415. doi:10.3390/ani10081352

Hendawy, A. O., Shirai, M., Takeya, H., Sugimura, S., Miyanari, S., Taniguchi, S., et al. (2019). Effects of 5-Aminolevulinic Acid Supplementation on Milk Production, Iron Status, and Immune Response of Dairy Cows. *J. Dairy Sci.* 102 (12), 11009–11015. doi:10.3168/jds.2018-15982

Heyl, D., Luz, E., Harris, S. A., and Folkers, K. (1951). Phosphates of the Vitamin B_6 Group. I. The Structure of Codecarboxylase. *J. Am. Chem. Soc.* 73, 3430–3433. doi:10.1021/ja01151a126

Ichihara, Y., Masuki, S., Uchida, K., Takahashi, K., Nakajima, M., and Nose, H. (2021). Effects of 5-Aminolevulinic Acid with Iron Supplementation on Respiratory Responses to Graded Cycling and Interval Walking Training Achievement in Older Women over 75 yrs. *Exp. Gerontol.* 150, 111356. doi:10.1016/j.exger.2021.111356

Itoh, Y., Ninomiya, Y., Tajima, S., and Ishibashi, A. (2000). Photodynamic Therapy for Acne Vulgaris with Topical 5-Aminolevulinic Acid. *Arch. Dermatol.* 136 (9), 1093–1095. doi:10.1001/archderm.136.9.1093

Jiang, Y., Wu, R., Zhou, J., He, A., Xu, J., Xin, F., et al. (2019). Recent Advances of Biofuels and Biochemicals Production from Sustainable Resources Using Co-cultivation Systems. *Biotechnol. Biofuels.* 12, 155. doi:10.1186/s13068-019-1495-7

Jones, A. M., and Elliott, T. (2010). A Purified Mutant *HemA* Protein from *Salmonella enterica* Serovar Typhimurium Lacks Bound Heme and Is Defective for Heme-Mediated Regulation *In Vivo*. *FEMS Microbiol. Lett.* 307 (1), 41–47. doi:10.1111/j.1574-6968.2010.01967.x

Jørgensen, M. G., Nielsen, J. S., Boysen, A., Franch, T., Møller-Jensen, J., and Valentin-Hansen, P. (2012). Small Regulatory RNAs Control the Multi-Cellular Adhesive Lifestyle of *Escherichia coli*. *Mol. Microbiol.* 84 (1), 36–50. doi:10.1111/j.1365-2958.2012.07976.x

Kamiyama, H., Hotta, Y., Tanaka, T., Nishikawa, S., and Sasaki, K. (2000). Production of 5-Aminolevulinic Acid by a Mutant Strain of a Photosynthetic Bacteria. *J. Biosci. Bioeng.* 78 (2), 48–55.

Kang, Z., Ding, W., Gong, X., Liu, Q., Du, G., and Chen, J. (2017). Recent Advances in Production of 5-Aminolevulinic Acid Using Biological Strategies. *World J. Microbiol. Biotechnol.* 33 (11), 200. doi:10.1007/s11274-017-2366-7

Kang, Z., Gao, C., Wang, Q., Liu, H., and Qi, Q. (2010). A Novel Strategy for Succinate and Polyhydroxybutyrate Co-production in *Escherichia coli*. *Bioresour. Technol.* 101 (19), 7675–7678. doi:10.1016/j.biortech.2010.04.084

Kang, Z., Wang, Y., Gu, P., Wang, Q., and Qi, Q. (2011a). Engineering *Escherichia coli* for Efficient Production of 5-Aminolevulinic Acid from Glucose. *Metab. Eng.* 13 (5), 492–498. doi:10.1016/j.ymben.2011.05.003

Kang, Z., Wang, Y., Wang, Q., and Qi, Q. (2011b). Metabolic Engineering to Improve 5-Aminolevulinic Acid Production. *Bioengineered bugs* 2 (6), 342–345. doi:10.4161/bbug.2.6.17237

Kang, Z., Zhang, J., Zhou, J., Qi, Q., Du, G., and Chen, J. (2012). Recent Advances in Microbial Production of δ-aminolevulinic Acid and Vitamin B_{12}. *Biotechnol. Adv.* 30 (6), 1533–1542. doi:10.1016/j.biotechadv.2012.04.003

Kardon, J. R., Moroco, J. A., Engen, J. R., and Baker, T. A. (2020). Mitochondrial ClpX Activates an Essential Biosynthetic Enzyme through Partial Unfolding. *Elife* 9, e54387. doi:10.7554/eLife.54387

Kauss, D., Bischof, S., Steiner, S., Apel, K., and Meskauskiene, R. (2012). FLU, a Negative Feedback Regulator of Tetrapyrrole Biosynthesis, Is Physically Linked to the Final Steps of the Mg^{++} -branch of This Pathway. *FEBS Lett.* 586 (3), 211–216. doi:10.1016/j.febslet.2011.12.029

Kiatpapan, P., and Murooka, Y. (2001). Construction of an Expression Vector for Propionibacteria and its Use in Production of 5-Aminolevulinic Acid by *Propionibacterium freudenreichii*. *Appl. Microbiol. Biotechnol.* 56 (1-2), 144–149. doi:10.1007/s002530100603

Kiatpapan, P., Phonghatsabun, M., Yamashita, M., Murooka, Y., and Panbangred, W. (2011). Production of 5-Aminolevulinic Acid by *Propionibacterium acidipropionici* TISTR442. *J. Biosci. Bioeng.* 111 (4), 425–428. doi:10.1016/j.jbiosc.2010.11.019

Ko, Y. J., You, S. K., Kim, M., Lee, E., Shin, S. K., Park, H. M., et al. (2019). Enhanced Production of 5-Aminolevulinic Acid via Flux Redistribution of TCA Cycle toward L-Glutamate in *Corynebacterium glutamicum*. *Biotechnol. Bioproc. E.* 24 (6), 915–923. doi:10.1007/s12257-019-0376-z

Kumar, M. A., Chaturvedi, S., and Söll, D. (1999). Selective Inhibition of *hemA* Gene Expression by Photooxidation in *Arabidopsis thaliana*. *Phytochemistry* 51 (7), 847–851. doi:10.1016/s0031-9422(99)00114-4

Lanéelle, M.-A., Tropis, M., and Daffé, M. (2013). Current Knowledge on Mycolic Acids in *Corynebacterium glutamicum* and Their Relevance for Biotechnological Processes. *Appl. Microbiol. Biotechnol.* 97 (23), 9923–9930. doi:10.1007/s00253-013-5265-3

Lashkari, S. M., Kariminezhad, H., Amani, H., Mataji, P., and Rahimnejad, M. (2019). Introduction of 5-Aminolevulinic Acid as a Theranostics Agent in Dentistry. *Photodiagnosis Photodynamic Ther.* 25, 336–343. doi:10.1016/j.pdpdt.2019.01.021

Lee, M. J., Kim, H. J., Lee, J. Y., Kwon, A. S., Jun, S. Y., Kang, S. H., et al. (2013). Effect of Gene Amplifications in Porphyrin Pathway on Heme Biosynthesis in a Recombinant *Escherichia coli*. *J. Microbiol. Biotechnol.* 23 (5), 668–673. doi:10.4014/jmb.1302.02022

Levican, G., Katz, A., de Armas, M., Nunez, H., and Orellana, O. (2007). Regulation of a Glutamyl-tRNA Synthetase by the Heme Status. *Proc. Natl. Acad. Sci.* 104 (9), 3135–3140. doi:10.1073/pnas.0611611104

Li, F., Wang, Y., Gong, K., Wang, Q., Liang, Q., and Qi, Q. (2014). Constitutive Expression of *RyhB* Regulates the Heme Biosynthesis Pathway and Increases the 5-aminolevulinic Acid Accumulation in *Escherichia coli*. *FEMS Microbiol. Lett.* 350 (2), 209–215. doi:10.1111/1574-6968.12322

Li, N., Shahid, M., Zong, X., Lv, J., Wang, D., Saleem, A., et al. (2019). Exogenously Applied 5-Aminolevulinic Acid Mediated Physiochemical Regulations Ameliorate Weak Light Stress in Tobacco Seedlings. *Bangladesh J. Bot.* 48 (2), 353–358. doi:10.3329/BJB.V48I2.47681

Li, S., Lou, X., Xu, Y., Teng, X., Che, S., Liu, R., et al. (2018). Crystal Structure of a Glutamate-1-Semialdehyde-Aminomutase from *Pseudomonas aeruginosa* Pao1. *Biochem. Biophysical Res. Commun.* 500 (3), 804–809. doi:10.1016/j.bbrc.2018.04.163

Lin, J., Fu, W., and Cen, P. (2009). Characterization of 5-Aminolevulinate Synthase from *Agrobacterium radiobacter*, Screening New Inhibitors for 5-Aminolevulinate Dehydratase from *Escherichia coli* and Their Potential Use for High 5-Aminolevulinate Production. *Bioresour. Technol.* 100 (7), 2293–2297. doi:10.1016/j.biortech.2008.11.008

Liu, J., Ye, Z., Wu, H., Liu, J., and Gong, Y. (2020). Overexpression of *hemA* and *hemL* in *Bacillus subtilis* Promotes Overexpression of 5-aminolevulinic Acid. *Ijar* 54 (10), 1235–1240. doi:10.18805/ijar.B-1193

Liu, S., Zhang, G., Li, J., Li, X., and Zhang, J. (2016). Optimization of Biomass and 5-Aminolevulinic Acid Production by *Rhodobacter sphaeroides* ATCC17023 via Response Surface Methodology. *Appl. Biochem. Biotechnol.* 179 (3), 444–458. doi:10.1007/s12010-016-2005-z

Liu, S., Zhang, G., Li, X., and Zhang, J. (2014). Microbial Production and Applications of 5-Aminolevulinic Acid. *Appl. Microbiol. Biotechnol.* 98 (17), 7349–7357. doi:10.1007/s00253-014-5925-y

Liu, X. X., Wang, L., Wang, Y. J., and Cai, L. L. (2010). D-glucose Enhanced 5-Aminolevulinic Acid Production in Recombinant *Escherichia coli* Culture. *Appl. Biochem. Biotechnol.* 160 (3), 822–830. doi:10.1007/s12010-009-8608-x

Lu, H., Villada, J. C., and Lee, P. K. H. (2019). Modular Metabolic Engineering for Biobased Chemical Production. *Trends Biotechnol.* 37 (2), 152–166. doi:10.1016/j.tibtech.2018.07.003

Mao, Y., Chen, Z., Lu, L., Jin, B., Ma, H., Pan, Y., et al. (2020). Efficient Solid-State Fermentation for the Production of 5-Aminolevulinic Acid Enriched Feed Using Recombinant *Saccharomyces cerevisiae*. *J. Biotechnol.* 322, 29–32. doi:10.1016/j.jbiotec.2020.06.001

Masuki, S., Morita, A., Kamijo, Y.-i., Ikegawa, S., Kataoka, Y., Ogawa, Y., et al. (2016). Impact of 5-Aminolevulinic Acid with Iron Supplementation on Exercise Efficiency and Home-Based Walking Training Achievement in Older Women. *J. Appl. Physiol.* 120 (1), 87–96. doi:10.1152/japplphysiol.00582.2015

Mauzerall, D., and Granick, S. (1956). THE OCCURRENCE AND DETERMINATION OF δ-AMINOLEVULINIC ACID AND PORPHOBILINOGEN IN URINE. *J. Biol. Chem.* 219 (1), 435–446. doi:10.1016/s0021-9258(18)65809-0

Meng, Q., Zhang, Y., Ju, X., Ma, C., Ma, H., Chen, J., et al. (2016). Production of 5-Aminolevulinic Acid by Cell Free Multi-Enzyme Catalysis. *J. Biotechnol.* 226, 8–13. doi:10.1016/j.jbiotec.2016.03.024

Millesi, M., Kiesel, B., Mischkulnig, M., Martínez-Moreno, M., Wöhrer, A., Wolfsberger, S., et al. (2016). Analysis of the Surgical Benefits of 5-ALA-Induced Fluorescence in Intracranial Meningiomas: Experience in 204 Meningiomas. *Jns* 125 (6), 1408–1419. doi:10.3171/2015.12.Jns151513

Miscevic, D., Mao, J. Y., Kefale, T., Abedi, D., Moo-Young, M., and Perry Chou, C. (2021). Strain Engineering for High-level 5-aminolevulinic Acid Production in *Escherichia coli*. *Biotechnol. Bioeng.* 118 (1), 30–42. doi:10.1002/bit.27547

Moser, J., Schubert, W. D., Beier, V., Bringemeier, I., Jahn, D., and Heinz, D. W. (2001). V-shaped Structure of Glutamyl-tRNA Reductase, the First Enzyme of tRNA-Dependent Tetrapyrrole Biosynthesis. *EMBO J.* 20 (23), 6583–6590. doi:10.1093/emboj/20.23.6583

Neidle, E. L., and Kaplan, S. (1993). Expression of the *Rhodobacter sphaeroides hemA* and *hemT* Genes, Encoding Two 5-Aminolevulinic Acid Synthase Isozymes. *J. Bacteriol.* 175 (8), 2292–2303. doi:10.1128/jb.175.8.2292-2303.1993

Noh, M. H., Lim, H. G., Park, S., Seo, S. W., and Jung, G. Y. (2017). Precise Flux Redistribution to Glyoxylate Cycle for 5-Aminolevulinic Acid Production in *Escherichia coli*. *Metab. Eng.* 43 (Part A), 1–8. doi:10.1016/j.ymben.2017.07.006

Pichlmeier, U., Bink, A., Schackert, G., Stummer, W., and Grp, A. G. S. (2008). Resection and Survival in Glioblastoma Multiforme: An Rtog Recursive

Partitioning Analysis of Ala Study Patients. *Neuro-Oncology* 10 (6), 1025–1034. doi:10.1215/15228517-2008-052

Pugh, C. E., Harwood, J. L., and John, R. A. (1992). Mechanism of Glutamate Semialdehyde Aminotransferase. Roles of Diamino- and Dioxo-Intermediates in the Synthesis of Aminolevulinate. *J. Biol. Chem.* 267, 1584–1588. doi:10.1016/S0021-9258(18)45985-6

Ramzi, A. B., Hyeon, J. E., Kim, S. W., Park, C., and Han, S. O. (2015). 5-Aminolevulinic Acid Production in Engineered *Corynebacterium glutamicum* via C5 Biosynthesis Pathway. *Enzyme Microb. Technol.* 81, 1–7. doi:10.1016/j.enzmictec.2015.07.004

Ranson-Olson, B., and Zeilstra-Ryalls, J. H. (2008). Regulation of the *Rhodobacter sphaeroides* 2.4.1 *hemA* Gene by PrrA and FnrL. *J. Bacteriol.* 190 (20), 6769–6778. doi:10.1128/JB.00828-08

Rapp, M., Klingenhöfer, M., Felsberg, J., Steiger, H., Stummer, W., and Sabel, M. (2012). Fluorescence-Guided Resection of Spinal Metastases of Malignant Glioma: Report of 2 Cases. *J. Neurol. Surg. A. Cent. Eur. Neurosurg.* 73 (2), 103–105. doi:10.1055/s-0032-1309068

Rebeiz, C. A., Montazer-Zouhoor, A., Hopen, H. J., and Wu, S. M. (1984). Photodynamic Herbicides: 1. Concept and Phenomenology. *Enzyme Microb. Technol.* 6, 390–396. doi:10.1016/0141-0229(84)90012-7

Ren, J., Zhou, L., Wang, C., Lin, C., Li, Z., and Zeng, A.-P. (2018). An Unnatural Pathway for Efficient 5-Aminolevulinic Acid Biosynthesis with Glycine from Glyoxylate Based on Retrobiosynthetic Design. *ACS Synth. Biol.* 7 (12), 2750–2757. doi:10.1021/acssynbio.8b00354

Rhaman, M. S., Imran, S., Karim, M. M., Chakrobortty, J., Mahamud, M. A., Sarker, P., et al. (2021). 5-Aminolevulinic Acid-Mediated Plant Adaptive Responses to Abiotic Stress. *Plant Cel Rep* 40 (8), 1451–1469. doi:10.1007/s00299-021-02690-9

Richter, A. S., Banse, C., and Grimm, B. (2019). The GluTR-Binding Protein Is the Heme-Binding Factor for Feedback Control of Glutamyl-tRNA Reductase. *Elife* 8, e46300. doi:10.7554/eLife.46300

Robyul Islam, M., Naznin, T., Rani Gupta, D., Ashraful Haque, M., Hasanuzzaman, M., and Motiar Rohman, M. (2020). Insight into 5-Aminolevulinic Acid-Induced Modulation of Cellular Antioxidant Metabolism to Confer Salinity and Drought Tolerance in Maize. *Biocell* 44 (4), 713–730. doi:10.32604/BIOCELL.2020.011812

Rock, C. O., Calder, R. B., Karim, M. A., and Jackowski, S. (2000). Pantothenate Kinase Regulation of the Intracellular Concentration of Coenzyme A. *J. Biol. Chem.* 275 (2), 1377–1383. doi:10.1074/jbc.275.2.1377

Saikeur, A., Choorit, W., Prasertsan, P., Kantachote, D., and Sasaki, K. (2009). Influence of Precursors and Inhibitor on the Production of Extracellular 5-Aminolevulinic Acid and Biomass by *Rhodopseudomonas palustris* KG31. *Biosci. Biotechnol. Biochem.* 73 (5), 987–992. doi:10.1271/bbb.80682

Sakurai, Y., Ngwe Tun, M. M., Kurosaki, Y., Sakura, T., Inaoka, D. K., Fujine, K., et al. (2021). 5-Amino Levulinic Acid Inhibits SARS-CoV-2 Infection *In Vitro*. *Biochem. Biophysical Res. Commun.* 545, 203–207. doi:10.1016/j.bbrc.2021.01.091

Samuel, I. B., and Paul, A. C. (1974). The Biosynthesis of 5-Aminolevulinic Acid in Higher Plants. *Plant Physiol.* 53, 297–303.

Sasaki, K., Ikeda, S., Nishizawa, Y., and Hayashi, M. (1987). Production of 5-Aminolevulinic Acid by Photosynthetic Bacteria. *J. Ferment. Bioeng.* 65 (5), 511–515. doi:10.1016/0385-6380(87)90109-9

Sasaki, K., Marquez, F. J., Nishio, N., and Nagai, S. (1995). Promotive Effect of 5-Aminolevulinic Acid on the Growth and Photosynthesis of *Spirulina platensis*. *J. Ferment. Bioeng.* 79(5), 453–457. doi:10.1016/0922-338X(95)91261-3

Sasaki, M., Watanabe, T., and Tanaka, T. K. (2002). Biosynthesis, Biotechnological Production and Applications of 5-Aminolevulinic Acid. *Appl. Microbiol. Biotechnol.* 58 (1), 23–29. doi:10.1007/s00253-001-0858-7

Sasikala, C., Ramana, C. V., and Rao, P. R. (1994). 5-Aminolevulinic Acid: A Potential Herbicide/Insecticide from Microorganisms. *Biotechnol. Frog.* 10, 451–459. doi:10.1021/bp00029a001

Sattayasamitsathit, S., and Prasertsan, P. (2014). Improvement of 5-Aminolevulinic Acid Production by *Rubrivivax benzoatilyticus* PS-5 with Self-Flocculation by Co-fermentation of Precursors and Volatile Fatty Acids under pH-Controlled Conditions. *Ann. Microbiol.* 64 (1), 385–389. doi:10.1007/s13213-013-0637-6

Schulze, J. O., Schubert, W. D., Moser, J., Jahn, D., and Heinz, D. W. (2006). Evolutionary Relationship between Initial Enzymes of Tetrapyrrole Biosynthesis. *J. Mol. Biol.* 358 (5), 1212–1220. doi:10.1016/j.jmb.2006.02.064

Serini, S. M., Cannizzaro, M. V., Dattola, A., Garofalo, V., Del Duca, E., Ventura, A., et al. (2019). The Efficacy and Tolerability of 5-Aminolevulinic Acid 5% Thermosetting Gel Photodynamic Therapy (PDT) in the Treatment of Mild-To-Moderate Acne Vulgaris. A Two-Center, Prospective Assessor-Blinded, Proof-Of-Concept Study. *J. Cosmet. Dermatol.* 18 (1), 156–162. doi:10.1111/jocd.12670

Shemin, D., and Russell, C. S. (1953). 5-Aminolevulinic Acid, its Role in the Biosynthesis of Porphyrins and Purines. *J. Am. Chem. Soc.* 75 (19), 4873–4874. doi:10.1021/ja01115a546

Sher, A., Tahira, A. S., Sattar, A., Nawaz, A., Qayyum, A., Hussain, S., et al. (2021). Foliage Application of 5-Aminolevulinic Acid Alleviates Drought Stress in Sunflower (*Helianthus annuus* L.) through Improving Stay Green and Antioxidant Enzymes Activities. *Acta Physiol. Plant* 43 (2), 22. doi:10.1007/s11738-020-03189-8

Song, W. J., and Jackowski, S. (1992). Cloning, Sequencing, and Expression of the Pantothenate Kinase (*CoaA*) Gene of *Escherichia coli*. *J. Bacteriol.* 172 (20), 6411–6417. doi:10.1111/j.1365-2672.1992.tb04989.x10.1128/jb.174.20.6411-6417.1992

Sonhom, R., Thepsithar, C., and Jongsareejit, B. (2012). High Level Production of 5-Aminolevulinic Acid by *Propionibacterium acidipropionici* Grown in a Low-Cost Medium. *Biotechnol. Lett.* 34 (9), 1667–1672. doi:10.1007/s10529-012-0943-2

Stoian, N., Kaganjo, J., and Zeilstra-Ryalls, J. (2018). Resolving the Roles of the *Rhodobacter sphaeroides hemA* and *hemT* 5-Aminolevulinic Acid Synthases. *Mol. Microbiol.* 110 (6), 1011–1029. doi:10.1111/mmi.14133

Stojanovski, B. M., Hunter, G. A., Na, I., Uversky, V. N., Jiang, R. H. Y., and Ferreira, G. C. (2019). 5-Aminolevulinate Synthase Catalysis: The Catcher in Heme Biosynthesis. *Mol. Genet. Metab.* 128 (3), 178–189. doi:10.1016/j.ymgme.2019.06.003

Stummer, W., and Kamp, M. A. (2009). The Importance of Surgical Resection in Malignant Glioma. *Curr. Opin. Neurobiol.* 22 (6), 645–649. doi:10.1097/WCO.0b013e3283320165

Stummer, W., Novotny, A., Stepp, H., Goetz, C., Bise, K., and Reulen, H. J. (2000). Fluorescence-Guided Resection of Glioblastoma Multiforme by Using 5-Aminolevulinic Acid-Induced Porphyrins: A Prospective Study in 52 Consecutive Patients. *J. Neurosurg.* 93 (6), 1003–1013. doi:10.3171/jns.2000.93.6.1003

Stummer, W., Stocker, S., Wagner, S., Stepp, H., Fritsch, C., Goetz, C., et al. (1998). Intraoperative Detection of Malignant Gliomas by 5-Aminolevulinic Acid-Induced Porphyrin Fluorescence. *Neurosurgery* 42 (3), 518–525. doi:10.1097/00006123-199803000-00017

Suero Molina, E., Kaneko, S., Black, D., and Stummer, W. (2021). 5-Aminolevulinic Acid-Induced Porphyrin Contents in Various Brain Tumors: Implications Regarding Imaging Device Design and Their Validation. *Neurosurgery* 89 (6), 1132–1140. doi:10.1093/neuros/nyab361

Tai, T. N., Moore, M. D., and Kaplan, S. (1988). Cloning and Characterization of the 5-Aminolevulinate Synthase Gene(s) from *Rhodobacter sphaeroides*. *Gene* 70, 139–151. doi:10.1016/0378-1119(88)90112-6

Takagi, M., Tamaki, H., Miyamoto, Y., Leonardi, R., Hanada, S., Jackowski, S., et al. (2010). Pantothenate Kinase from the Thermoacidophilic Archaeon *Picrophilus torridus*. *J. Bacteriol.* 192 (1), 233–241. doi:10.1128/JB.01021-09

Tan, S. I., You, S. C., Shih, I. T., and Ng, I. S. (2019). Quantification, Regulation and Production of 5-Aminolevulinic Acid by Green Fluorescent Protein in Recombinant *Escherichia coli*. *J. Biosci. Bioeng.* 129 (4), 387–394. doi:10.1016/j.jbiosc.2019.10.005

Tan, Z. J., Zhao, J., Chen, J. Z., Rao, D. M., Zhou, W. J., Chen, N., et al. (2019). Enhancing Thermostability and Removing Hemin Inhibition of *Rhodopseudomonas palustris* 5-Aminolevulinic Acid Synthase by Computer-Aided Rational Design. *Biotechnol. Lett.* 41 (1), 181–191. doi:10.1007/s10529-018-2627-z

Tang, W. J., Wang, W. Q., Chen, D. Q., Ji, Q., Jing, Y. J., Wang, H. Y., et al. (2012). Transposase-Derived Proteins FHY3/FAR1 Interact with Phytochrome-Interacting Factor1 to Regulate Chlorophyll Biosynthesis by Modulating *hemB1* during Deetiolation in *Arabidopsis*. *Plant Cell* 24 (5), 1984–2000. doi:10.1105/tpc.112.097022

Tian, Q., Li, T., Hou, W. H., Zheng, J. Y., Schrum, L. W., and Bonkovsky, H. L. (2011). Lon Peptidase 1 (LONP1)-dependent Breakdown of Mitochondrial 5-Aminolevulinic Acid Synthase Protein by Heme in Human Liver Cells. *J. Biol. Chem.* 286 (30), 26424–26430. doi:10.1074/jbc.M110.215772

Tomokuni, K., and Ogata, M. (1972). Simple Method for Determination of Urinary Daminolevulinic Acid as an Index of Lead Exposure. *Clin. Chem.* 18 (1534), e1536. doi:10.1093/clinchem/18.12.1534

Tran, N. T., Pham, D. N., and Kim, C. J. (2019). Production of 5-Aminolevulinic Acid by Recombinant *Streptomyces coelicolor* Expressing *hemA* from *Rhodobacter sphaeroides*. *Biotechnol. Bioproc. E* 24 (3), 488–499. doi:10.1007/s12257-018-0484-1

Ubbink, R., Prens, E. P., and Mik, E. G. (2021). Quantitative Intracellular Oxygen Availability before and after 5-Aminolevulinic Acid Skin Photodynamic Therapy. *Photodiagn Photodyn* 36, 102599. doi:10.1016/j.pdpdt.2021.102599

Vadali, R. V., Bennett, G. N., and San, K. Y. (2004). Cofactor Engineering of Intracellular CoA/Acetyl-CoA and its Effect on Metabolic Flux Redistribution in *Escherichia coli*. *Metab. Eng.* 6 (2), 133–139. doi:10.1016/j.ymben.2004.02.001

Van Der Werf, M. J., and Zeikus, J. G. (1996). 5-Aminolevulinate Production by *Escherichia coli* Containing the *Rhodobacter sphaeroides hemA* Gene. *Appl. Environ. Microbiol.* 62 (19), 3560–3566. doi:10.1128/AEM.62.10.3560-3566.1996

Wainwright, J. V., Endo, T., Cooper, J. B., Tominaga, T., and Schmidt, M. H. (2019). The Role of 5-Aminolevulinic Acid in Spinal Tumor Surgery: A Review. *J. Neurooncol.* 141 (3), 575–584. doi:10.1007/s11060-018-03080-0

Wang, J. P., Kim, H. J., Chen, Y. J., Yoo, J. S., Cho, J. H., Kang, D. K., et al. (2009). Effects of Delta-Aminolevulinic Acid and Vitamin C Supplementation on Feed Intake, Backfat, and Iron Status in Sows. *J. Anim. Sci.* 87 (11), 3589–3595. doi:10.2527/jas.2008-1489

Wang, L. Y., Elliott, M., and Elliott, T. (1999). Conditional Stability of the HemA Protein (Glutamyl-tRNA Reductase) Regulates Heme Biosynthesis in *Salmonella typhimurium*. *J. Bacteriol.* 181 (4), 1211–1219. doi:10.1128/jb.181.4.1211-1219.1999

Wang, R. F., Zhao, S. J., Wang, Z. T., and Koffas, M. A. G. (2020). Recent Advances in Modular Co-culture Engineering for Synthesis of Natural Products. *Curr. Opin. Biotechnol.* 62, 65–71. doi:10.1016/j.copbio.2019.09.004

Wang, X. F., Tian, Y., Liao, X., Tang, Y. X., Ni, Q. Q., Sun, J., et al. (2020). Enhancing Selective Photosensitizer Accumulation and Oxygen Supply for High-Efficacy Photodynamic Therapy toward Glioma by 5-Aminolevulinic Acid Loaded Nanoplatform. *J. Mol. Cel Cardiol.* 565, 483–493. doi:10.1016/j.jcis.2020.01.020

Weinstein, J. D., and Beale, S. I. (1983). Separate Physiological Roles and Subcellular Compartments for Two Tetrapyrrole Biosynthetic Pathways in *Euglena gracilis*. *J. Biol. Chem.* 258 (11), 6799–6807. doi:10.1016/S0021-9258(18)32293-2

Woodard, S. I., and Dailey, H. A. (1995). Regulation of Heme Biosynthesis in *Escherichia coli*. *Arch. Biochem. Biophys.* 316 (1), 110–115. doi:10.1006/abbi.1995.1016

Wu, Y., Liao, W. B., Dawuda, M. M., Hu, L., and Yu, J. H. (2018). 5-Aminolevulinic Acid (AlA) Biosynthetic and Metabolic Pathways and its Role in Higher Plants: A Review. *Plant Growth Regul.* 87 (2), 357–374. doi:10.1007/s10725-018-0463-8

Wu, Y., Liu, N., Hu, L. L., Liao, W. B., Tang, Z., Xiao, X., et al. (2021). 5-Aminolevulinic Acid Improves Morphogenesis and Na^+ Subcellular Distribution in the Apical Cells of *Cucumis sativus* L. Under Salinity Stress. *Front. Plant Sci.* 12, 636121. doi:10.3389/fpls.2021.636121

Xie, L., Hall, D., Eiteman, M. A., and Altman, E. (2003). Optimization of Recombinant Aminolevulinate Synthase Production in *Escherichia coli* Using Factorial Design. *Appl. Microbiol. Biotechnol.* 63 (3), 267–273. doi:10.1007/s00253-003-1388-2

Xue, C., Yu, T. H., and Ng, I. S. (2021). Engineering Pyridoxal Kinase PdxY-Integrated *Escherichia coli* Strain and Optimization for High-Level 5-Aminolevulinic Acid Production. *J. Taiwan Inst. Chem. Eng.* 120, 49–58. doi:10.1016/j.jtice.2021.03.017

Yan, F., Jiang, W. H., Qu, D., Fu, J., and Zhao, X. (2020). Effects of Exogenous 5-Aminolevulinic Acid on Photosynthetic and Physiological Characteristics of Tea Plants under Low Temperature Stress. *J. Tea Sci.* 40 (5), 597–606. doi:10.13305/j.cnki.jts.2020.05.004

Yang, J., Zhu, L., Fu, W. Q., Lin, Y. J., Lin, J. P., and Cen, P. L. (2013). Improved 5-Aminolevulinic Acid Production with Recombinant *Escherichia coli* by a Short-Term Dissolved Oxygen Shock in Fed-Batch Fermentation. *Chin. J. Chem. Eng.* 21 (11), 1291–1295. doi:10.1016/s1004-9541(13)60627-8

Yang, P., Liu, W. J., Cheng, X. L., Wang, J., Wang, Q., and Qi, Q. S. (2016). A New Strategy for Production of 5-Aminolevulinic Acid in Recombinant *Corynebacterium glutamicum* with High Yield. *Appl. Environ. Microbiol.* 82 (9), 2709–2717. doi:10.1128/AEM.00224-16

Yang, T. W., Rao, Z. M., Zhang, X., Xu, M. J., Xu, Z. H., and Yang, S. T. (2017). Metabolic Engineering Strategies for Acetoin and 2,3-Butanediol Production: Advances and Prospects. *Crit. Rev. Biotechnol.* 37 (8), 990–1005. doi:10.1080/07388551.2017.1299680

Yi, Y. C., and Ng, I. S. (2021). Redirection of Metabolic Flux in *Shewanella oneidensis* MR-1 by CRISPRi and Modular Design for 5-Aminolevulinic Acid Production. *Bioresour. Bioproc.* 8 (1), 13. doi:10.1186/s40643-021-00366-6

Yu, T.-H., Tan, S.-I., Yi, Y.-C., Xue, C., Ting, W.-W., Chang, J.-J., et al. (2022). New Insight into the Codon Usage and Medium Optimization toward Stable and High-Level 5-Aminolevulinic Acid Production in *Escherichia coli*. *Biochem. Eng. J.* 177, 108259. doi:10.1016/j.bej.2021.108259

Yu, T. H., Yi, Y. C., Shih, I. T., and Ng, I. S. (2019). Enhanced 5-Aminolevulinic Acid Production by Co-expression of Codon-Optimized *hemA* Gene with Chaperone in Genetic Engineered *Escherichia coli*. *Appl. Biochem. Biotechnol.* 19 (1), 299–312. doi:10.1007/s12010-019-03178-9

Yu, X. L., Jin, H. Y., Liu, W. L., Wang, Q., and Qi, Q. S. (2015). Engineering *Corynebacterium glutamicum* to Produce 5-Aminolevulinic Acid from Glucose. *Microb. Cel Fact.* 14, 183. doi:10.1186/s12934-015-0364-8

Zeilstra-Ryalls, J. H., and Kaplan, S. (1996). Control of *hemA* Expression in *Rhodobacter sphaeroides* 2.4.1: Regulation through Alterations in the Cellular Redox State. *J. Bacteriol.* 178 (4), 985–993. doi:10.1128/jb.178.4.985-993.1996

Zeilstra-Ryalls, J. H., and Kaplan, S. (1995). Regulation of 5-Aminolevulinic Acid Synthesis in *Rhodobacter sphaeroides* 2.4.1: The Genetic Basis of Mutant H-5 Auxotrophy. *J. Bacteriol.* 177 (10), 2760–2768. doi:10.1128/jb.177.10.2760-2768.1995

Zeng, X., Chen, X. S., Gao, Y., Ren, X. D., Wang, L., and Mao, Z. G. (2015). Continuously High Reactive Oxygen Species Generation Decreased the Specific ε-Poly-L-Lysine Formation Rate in Fed-Batch Fermentation Using Glucose and Glycerol as a Mixed Carbon Source. *Process. Biochem.* 50 (12), 1993–2003. doi:10.1016/j.procbio.2015.09.012

Zhang, B., and Ye, B. C. (2018). Pathway Engineering in *Corynebacterium glutamicum* S9114 for 5-Aminolevulinic Acid Production. *3 Biotech.* 8 (5), 247. doi:10.1007/s13205-018-1267-2

Zhang, C., Boop, F. A., and Ruge, J. (2019). The Use of 5-Aminolevulinic Acid in Resection of Pediatric Brain Tumors: A Critical Review. *J. Neurooncol.* 141 (3), 567–573. doi:10.1007/s11060-018-03004-y

Zhang, C. L., Li, Y. J., Zhu, F. Z., Li, Z. X., Lu, N., Li, Y. H., et al. (2020). Metabolic Engineering of an Auto-Regulated *Corynebacterium glutamicum* Chassis for Biosynthesis of 5-Aminolevulinic Acid. *Bioresour. Technol.* 318, 124064. doi:10.1016/j.biortech.2020.124064

Zhang, J. L., Kang, Z., Chen, J., and Du, G. C. (2015). Optimization of the Heme Biosynthesis Pathway for the Production of 5-Aminolevulinic Acid in *Escherichia coli*. *Sci. Rep.* 5, 8584. doi:10.1038/srep08584

Zhang, J. L., Kang, Z., Ding, W. W., Chen, J., and Du, G. C. (2016). Integrated Optimization of the *In Vivo* Heme Biosynthesis Pathway and the *In Vitro* Iron Concentration for 5-Aminolevulinate Production. *Appl. Biochem. Biotechnol.* 178 (6), 1252–1262. doi:10.1007/s12010-015-1942-2

Zhang, J. L., Rang, Z., Qian, S. D., Qiu, L., Chen, J., and Du, G. C. (2018). Construction of Recombinant *Saccharomyces cerevisiae* for Production of 5-Aminolevulinic Acid. *J. Food Sci. Biotechnol.* 37, 232–239. doi:10.3969/j.issn.1673-1689.2018.03.002

Zhang, J. L., Weng, H. J., Zhou, Z. X., Du, G. C., and Kang, Z. (2019). Engineering of Multiple Modular Pathways for High-Yield Production of 5-Aminolevulinic Acid in *Escherichia coli*. *Bioresour. Technol.* 274, 353–360. doi:10.1016/j.biortech.2018.12.004

Zhang, J. L., Yasuda, M., Desnick, R. J., Balwani, M., Bishop, D., and Yu, C. L. (2011). A LC-MS/MS Method for the Specific, Sensitive, and Simultaneous Quantification of 5-Aminolevulinic Acid and Porphobilinogen. *J. Chromatogr. B.* 879 (24), 2389–2396. doi:10.1016/j.jchromb.2011.06.034

Zhang, J., Wang, Z. G., Su, T. Y., Sun, H. H., Zhu, Y., Qi, Q. S., et al. (2020a). Tuning the Binding Affinity of Heme-Responsive Biosensor for Precise and Dynamic Pathway Regulation. *iScience* 23 (5), 101067. doi:10.1016/j.isci.2020.101067

Zhang, J., Weng, H., Ding, W., and Kang, Z. (2017). N-terminal Engineering of Glutamyl-tRNA Reductase with Positive Charge Arginine to Increase

5-Aminolevulinic Acid Biosynthesis. *Bioengineered* 8 (4), 424–427. doi:10.1080/21655979.2016.1230572

Zhang, J., Zhang, X. H., He, Y., Wu, X. Y., Huang, J. M., Huang, H. Q., et al. (2020b). Photodynamic Therapy for Severe Facial Acne Vulgaris with 5% 5-Aminolevulinic Acid vs 10% 5-Aminolevulinic Acid: A Split-Face Randomized Controlled Study. *J. Cosmet. Dermatol.* 19 (2), 368–374. doi:10.1111/jocd.13038

Zhang, L. L., Chen, J. Z., Chen, N., Sun, J. B., Zheng, P., and Ma, Y. H. (2013). Cloning of Two 5-Aminolevulinic Acid Synthase Isozymes *hemA* and *hemO* from *Rhodopseudomonas palustris* with Favorable Characteristics for 5-Aminolevulinic Acid Production. *Biotechnol. Lett.* 35 (5), 763–768. doi:10.1007/s10529-013-1143-4

Zhang, M., Zhang, F. L., Fang, Y., Chen, X. M., Chen, Y. H., Zhang, W. X., et al. (2015). The Non-canonical Tetratricopeptide Repeat (TPR) Domain of Fluorescent (FLU) Mediates Complex Formation with Glutamyl-tRNA Reductase. *J. Biol. Chem.* 290 (28), 17559–17565. doi:10.1074/jbc.M115.662981

Zhang, X., Zhang, J., Xu, J. S., Zhao, Q., Wang, Q., and Qi, Q. S. (2018). Engineering *Escherichia coli* for Efficient Coproduction of Polyhydroxyalkanoates and 5-Aminolevulinic Acid. *J. Ind. Microbiol. Biotechnol.* 45 (1), 43–51. doi:10.1007/s10295-017-1990-4

Zhao, A. G., Ding, R. W., and Zhai, M. Z. (2019). Multi-Enzymatic Recycling of ATP and NADPH for the Synthesis of 5-Aminolevulinic Acid Using a Semipermeable Reaction System. *Biosci. Biotechnol. Biochem.* 83 (12), 2213–2219. doi:10.1080/09168451.2019.1648204

Zhao, A. G., and Zhai, M. Z. (2019). Production of 5-Aminolevulinic Acid from Glutamate by Overexpressing *hemA1* and *Pgr7* from *Arabidopsis thaliana* in *Escherichia coli*. *World J. Microbiol. Biotechnol.* 35 (11), 175. doi:10.1007/s11274-019-2750-6

Zheng, J., Liu, L. B., Tao, H. H., An, Y. Y., and Wang, L. J. (2021). Transcriptomic Profiling of Apple Aalli with a Focus on the Key Genes for ALA-Induced Anthocyanin Accumulation. *Front. Plant Sci.* 12, 640606. doi:10.3389/fpls.2021.640606

Zhou, L., Ren, J., Li, Z., Nie, J., Wang, C., and Zeng, A. P. (2019). Characterization and Engineering of a Clostridium Glycine Riboswitch and its Use to Control a Novel Metabolic Pathway for 5-Aminolevulinic Acid Production in *Escherichia coli*. *ACS Synth. Biol.* 8 (10), 2327–2335. doi:10.1021/acssynbio.9b00137

Zhu, C. C., Chen, J. Z., Wang, Y., Wang, L. X., Guo, X., Chen, N., et al. (2019). Enhancing 5-Aminolevulinic Acid Tolerance and Production by Engineering the Antioxidant Defense System of *Escherichia coli*. *Biotechnol. Bioeng.* 116 (8), 2018–2028. doi:10.1002/bit.26981

Zou, Y. L., Chen, T., Feng, L. L., Zhang, S. H., Xing, D. X., and Wang, Z. W. (2017). Enhancement of 5-Aminolevulinic Acid Production by Metabolic Engineering of the Glycine Biosynthesis Pathway in *Corynebacterium glutamicum*. *Biotechnol. Lett.* 39 (9), 1369–1374. doi:10.1007/s10529-017-2362-x

Conflict of Interest: The authors declare that the research was conducted in the absence of any commercial or financial relationships that could be construed as a potential conflict of interest.

Publisher's Note: All claims expressed in this article are solely those of the authors and do not necessarily represent those of their affiliated organizations, or those of the publisher, the editors, and the reviewers. Any product that may be evaluated in this article, or claim that may be made by its manufacturer, is not guaranteed or endorsed by the publisher.

frontiers in Bioengineering and Biotechnology

ORIGINAL RESEARCH
published: 02 March 2022
doi: 10.3389/fbioe.2021.816980

YALIcloneNHEJ: An Efficient Modular Cloning Toolkit for NHEJ Integration of Multigene Pathway and Terpenoid Production in *Yarrowia lipolytica*

Ya-Wen Li[1], Cai-Ling Yang[1], Qi Shen[1], Qian-Qian Peng[1], Qi Guo[2], Zhi-Kui Nie[3], Xiao-Man Sun[1], Tian-Qiong Shi[1], Xiao-Jun Ji[2]* and He Huang[1,4]*

[1]School of Food Science and Pharmaceutical Engineering, Nanjing Normal University, Nanjing, China, [2]College of Biotechnology and Pharmaceutical Engineering, Nanjing Tech University, Nanjing, China, [3]Jiangxi New Reyphon Biochemical Co., Ltd., Salt and Chemical Industry, Xingan, China, [4]College of Pharmaceutical Sciences, Nanjing Tech University, Nanjing, China

OPEN ACCESS

Edited by:
Shuobo Shi,
Beijing University of Chemical Technology, China

Reviewed by:
Su Tianyuan,
Shandong University, China
Zhuobin Liang,
Shenzhen Bay Laboratory, China
Zongjie Dai,
Tianjin Institute of Industrial Biotechnology (CAS), China

***Correspondence:**
Tian-Qiong Shi
tqshi@njnu.edu.cn
Xiao-Jun Ji
xiaojunji@njtech.edu.cn

Specialty section:
This article was submitted to Synthetic Biology, a section of the journal Frontiers in Bioengineering and Biotechnology

Received: *17 November 2021*
Accepted: *29 December 2021*
Published: *02 March 2022*

Citation:
Li Y-W, Yang C-L, Shen Q, Peng Q-Q, Guo Q, Nie Z-K, Sun X-M, Shi T-Q, Ji X-J and Huang H (2022) YALIcloneNHEJ: An Efficient Modular Cloning Toolkit for NHEJ Integration of Multigene Pathway and Terpenoid Production in Yarrowia lipolytica. *Front. Bioeng. Biotechnol. 9:816980. doi: 10.3389/fbioe.2021.816980*

Non-homologous end-joining (NHEJ)-mediated random integration in *Yarrowia lipolytica* has been demonstrated to be an effective strategy for screening hyperproducer strains. However, there was no multigene assembly method applied for NHEJ integration, which made it challenging to construct and integrate metabolic pathways. In this study, a Golden Gate modular cloning system (YALIcloneNHEJ) was established to develop a robust DNA assembly platform in *Y. lipolytica*. By optimizing key factors, including the amounts of ligase and the reaction cycles, the assembly efficiency of 4, 7, and 10 fragments reached up to 90, 75, and 50%, respectively. This YALIcloneNHEJ system was subsequently applied for the overproduction of the sesquiterpene (-)-α-bisabolol by constructing a biosynthesis route and enhancing the flux in the mevalonate pathway. The resulting strain produced 4.4 g/L (-)-α-bisabolol, the highest titer reported in yeast to date. Our study expands the toolbox of metabolic engineering and is expected to enable a highly efficient production of various terpenoids.

Keywords: *Y. lipolytica*, (-)-α-bisabolol, sesquiterpene, Golden Gate cloning, non-homologous end-joining

INTRODUCTION

The monocyclic sesquiterpene (-)-α-bisabolol has important applications in the fields of medicine, food, and biofuels (Han et al., 2016; Lim et al., 2021)—for example, Melo et al. (2017) found that oral formulations of (-)-α-bisabolol can reduce oral injury in rodents to a certain extent. Tabari and Tehrani (2017) were the first to explore the potential mechanism of the pharmacological properties of (-)-α-bisabolol, showing that it could interact with the neurotransmitter γ-aminobutyric acid, exhibiting anxiolytic and sedative effects. In previous studies, (-)-α-bisabolol was mainly produced through plant extraction, but this method is limited due to low extraction efficiency and high cost (Lim et al., 2021). In recent years, with the fast development of synthetic biology, microbial fermentation has become increasingly more popular in the synthesis of natural products (Luo

Abbreviations: ERG10, acetoacetyl-CoA thiolase; ERG13, hydroxymethylglutaryl-CoA synthase; tHMG1, truncated hydroxymethylglutaryl-CoA reductase; ERG12, mevalonate kinase; ERG8, phosphomevalonate kinase; ERG19, mevalonate diphosphate decarboxylase; IDI, isopentenyl diphosphate isomerase; ERG20, geranyl/farnesyl diphosphate synthase; PCR, polymerase chain reaction.

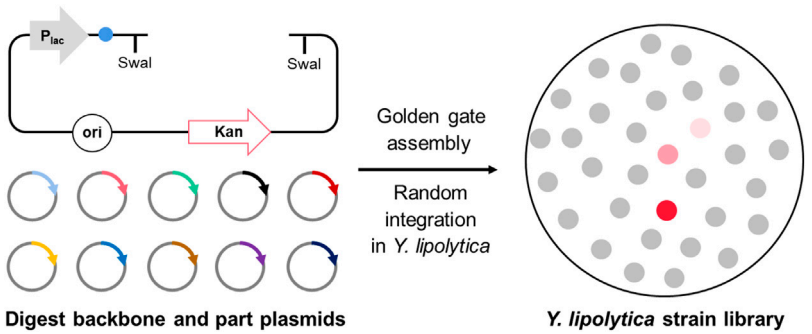

GRAPHICAL ABSTRACT |

et al., 2015; Ledesma-Amaro and Nicaud, 2016; Chae et al., 2017). The synthesis of (-)-α-bisabolol has been previously achieved in *Escherichia coli* with the highest titer of 23.4 g/L (Lim et al., 2021). However, due to the possible infection risk of *E. coli* by bacteriophage, lots of researchers preferred to use fungi as the host to synthesize (-)-α-bisabolol—for example, some researchers attempted to use *Saccharomyces cerevisiae* to synthesize (-)-α-bisabolol heterologously. When a (-)-α-bisabolol synthase from *Matricaria recutita* was expressed, the titer was only 8 mg/L (Son et al., 2014). Introducing a truncated *HMG1* gene coding for HMG-CoA reductase, *ERG10* encoding acetyl-CoA thiolase, and *ACS1* gene coding for acetyl-CoA synthetase into *S. cerevisiae* genome, the titer increased to 124 mg/L (Kim et al., 2021). In order to improve the level, metabolic engineering strategies, including optimizing the mevalonate pathway and the lipid synthesis pathway, were adopted. The (-)-α-bisabolol titer was improved from 8 to 364 mg/L in yeast (Ma et al., 2021). Nevertheless, the production of (-)-α-bisabolol in fungi is still very low (**Table 1**).

The non-conventional oleaginous yeast *Yarrowia lipolytica* is a generally-recognized-as-safe organism, and it has gradually become a promising host for the synthesis of various terpene chemicals (Ma et al., 2019; Li et al., 2021). Compared with *S. cerevisiae* and *Escherichia coli*, *Y. lipolytica* has many natural advantages, including a sufficient intracellular acetyl-CoA/cofactor supply, no phage infection risk, and no Crabtree effect (Cao et al., 2017; Tang et al., 2021). Therefore, *Y. lipolytica* has great potential as a robust chassis for biosynthesizing terpenes.

Although episomal plasmids containing centromeric sequences or autonomously replicating sequences have been developed for *Y. lipolytica*, they are usually unstable and have a low copy number (Dulermo et al., 2017). Consequently, the genetic manipulation of *Y. lipolytica* for metabolic engineering applications mainly relies on homologous recombination (HR)-mediated chromosomal integration (Larroude et al., 2018). However, this method is limited by low integration efficiency, especially in the case of long DNA fragments encoding multi-gene transcription units. Cui et al. (2019) systematically investigated a genomic integration method based on non-homologous end-joining (NHEJ) in *Y. lipolytica*. In comparison with homologous recombination, NHEJ has many unique advantages, including high integration efficiency and no need for a homologous template (Liu et al., 2019). Moreover, the heterologous DNA can be randomly inserted into the chromosome, which results in a library of multilocus integrants that can facilitate the screening of hyperproducer strains (Ye et al., 2012; Friedlander et al., 2016; Cui et al., 2021). However, there was no multigene plasmid construction method for NHEJ-based integration, which made it challenging to construct and integrate metabolic pathways in *Y. lipolytica*. Golden Gate is a gene cloning method using type IIS restriction endonucleases, which enables the modular assembly of customized DNA building blocks (Sarkari et al., 2017; Tong et al., 2021). By designing various features of the building block, including promoters with a highly variable strength of expression and terminators with a rigorously variable control of mRNA half-life, the Golden Gate assembly method can be applied into the combinatorial expression of multiple genes or the construction of gene libraries with variable intensities—for example, Celińska et al. (2017) designed a Golden Gate assembly system to create HR-mediated multigene integration for *Y. lipolytica*. Subsequently, the Golden Gate-based promoter shuffling was used to identify the best promoter set for the production of β-carotene (Larroude et al., 2017). The β-carotene titer could reach 6.5 g/L in *Y. lipolytica*, which is the highest yield currently reported in the literature. In addition, this assembly

TABLE 1 | (-)-α-Bisabolol production in yeast.

Strains	Titer (mg/L)	Productivity (mg L^{-1} h^{-1})	References
S. cerevisiae	8	-	Son et al. (2014)
S. cerevisiae DtEMA	124	2.1	Kim et al. (2021)
Y. lipolytica Po1f-2BtHE-S-R8	364.23	3.04	Ma et al. (2021)
Y. lipolytica LYW7-3	4,400	26.20	This work

TABLE 2 | Strains used in this study.

Strains	Genotype or properties	Sources
E. coli DH5α	supE44 ΔlacU169 (φ80 lacZ ΔM15) hsdR17 recA1 endA1 gyrA96 thi-1 relA1	Ktsm-life
Po1h	MatA, leu2-270:LEU, ura3-302, xpr2-322, axp-2	Madzak et al. (2004)
LYW1-1~ LYW1-12	Po1h with integrated fragment of linearized plasmid pGGYL1-HTBX	This work
LYW2-1~ LYW2-12	LYW1-11 with integrated fragment of linearized plasmid pGGYL3-HTitY-Gi12S-G19L	This work
LYW3-1~ LYW3-12	LYW2-11 with integrated fragment of linearized plasmid pGGYL3-HT10X-G13M-GIL	This work
LYW4-1~ LYW4-12	LYW3-5 with integrated fragment of linearized plasmid pGGYL2-HG8M-T20Y	This work
LYW5-1~ LYW5-12	LYW4-2 with integrated fragment of linearized plasmid pGGYL1-HTitX	This work
LYW6-1~ LYW6-12	LYW4-2 with integrated fragment of linearized plasmid pGGYL2-HTitX-EtL	This work
LYW7-1~ LYW7-12	LYW6-3 with integrated fragment of linearized plasmid pGGYL2-HTiBS-TBY	This work

method also has the characteristics of low cost and convenient operation. Therefore, we aimed to establish a Golden Gate library specifically for NHEJ integration in *Y. lipolytica*.

In this work, we first adapted the Golden Gate method for NHEJ-based random integration in *Y. lipolytica*, which can be applied for the rapid assembly of up to 10 fragments. Using this approach, we rapidly optimized the biosynthetic pathway of (-)-α-bisabolol and realized a titer of 4.4 g/L, the highest (-)-α-bisabolol titer reported in yeast to date. This study expands the synthetic biology toolbox for DNA assembly and integration, greatly facilitating the genetic manipulation of the non-conventional yeast *Y. lipolytica*.

MATERIALS AND METHODS

Strains, Media, and Culture Conditions

E. coli DH5α was used for plasmid construction. The strains with plasmids encoding gene fragments were cultivated at 37°C in lysogeny broth (LB) medium supplemented with 100 μg/ml ampicillin, while the strains with the backbone plasmids with or without assembled building blocks were cultivated at 37°C in LB supplemented with 50 μg/ml kanamycin, 40 μg/ml X-Gal, and 0.05 μM IPTG. The Po1h (uracil auxotrophy) and other *Y. lipolytica* strains were cultivated at 30°C with shaking at 240 rpm in YPD medium for seed culture (20 g/L peptone, 10 g/L yeast extract, and 20 g/L glucose). Subsequently, the seed cultures were transferred into the fermentation medium YPDE (20 g/L peptone, 10 g/L yeast extract, and 60 g/L glucose) at an initial OD_{600} of ~0.1, followed by a fermentation period of 4 days. An upper organic phase comprising 10 ml dodecane was added to 40 ml YPDE medium after 24 h to capture the (-)-α-bisabolol. The synthetic SC-URA solid medium (20 g/L glucose, 6.7 g/L yeast nitrogen base without amino acids, and 2.5% agar) was used to screen yeast transformants. YPD medium supplemented with 1.2 g/L 5-fluoroorotic acid and 20 g/L agar was used to remove the *URA3* counter-selection marker (Gao et al., 2017).

Construction of Building Block Plasmids and Backbone Plasmids

The sequence of (-)-α-bisabolol synthase (*MrBBS*, AIG92846.1) from *Matricaria recutita* (Son et al., 2014) was codon-optimized for *Y. lipolytica* and synthesized by Tsingke Biotech Co., Ltd. Building blocks including promoters, coding genes, and terminators were amplified from the *Y. lipolytica* genome and then cloned into plasmid pUC-T7-FCC1 (Shi et al., 2019). Each building block in the building block plasmids was flanked with *Bsa*I recognition sites and predesigned 4-bp overhangs, in which the internal *Bsa*I recognition sites have been removed by synonymous mutations. The backbone plasmid PGGYL1-3 was derived from pUC19, in which (1) the ampicillin resistance gene was substituted with a kanamycin resistance gene, (2) the internal *Bsa*I site in pUC19 was removed by loop PCR, and (3) *lacZ* flanked with *Bsa*I and 4-bp overhangs was cloned into pUC19. All building block plasmids and backbone plasmids were constructed using the ClonExpress® MultiS One Step Cloning Kit (Vazyme Biotech Co., Ltd., Nanjing, China). All plasmids used in this study and the sequences of building blocks and backbone plasmids are listed in **Supplementary Tables S1, S2**.

Yeast Transformation and Strain Construction

The Frozen-EZ Yeast Transformation II Kit was used for *Y. lipolytica* transformation (Shi et al., 2021). A flow chart summarizing the construction of *Y. lipolytica* strains is shown in **Figure 5B**. All *Y. lipolytica* strains constructed in this study are listed in **Table 2**.

Golden Gate Assembly Protocol

The Golden Gate assembly mainly relies on the restriction enzyme *Bsa*I (NEB, R3733L) and T4 DNA Ligase (Takara, 2011A; NEB, M0202T; Vazyme, C301-01). The reaction conditions were based on a previously published protocol (Celińska et al., 2017). The backbone and building block plasmids were first digested with *Bsa*I, and the DNA concentration of each assembly piece was measured. Assembly reaction systems of 20 μl contained 100 ng of the linearized backbone plasmid, equimolar amounts of the other assembly pieces, 2 μl of 10× Takara T4 Buffer, 1 μl of *Bsa*I, Takara T4 Ligase, and ddH_2O. The assembly reaction was performed in a PCR thermocycler as follows: (3 min at 37°C, 4 min at 16°C) × 60 reaction cycles (or 90 and 120), followed by 5 min at 50°C and 5 min at 80°C. After that, 20 μl of the reaction mixture was used to transform 100 μl of *E. coli* DH5α competent cells.

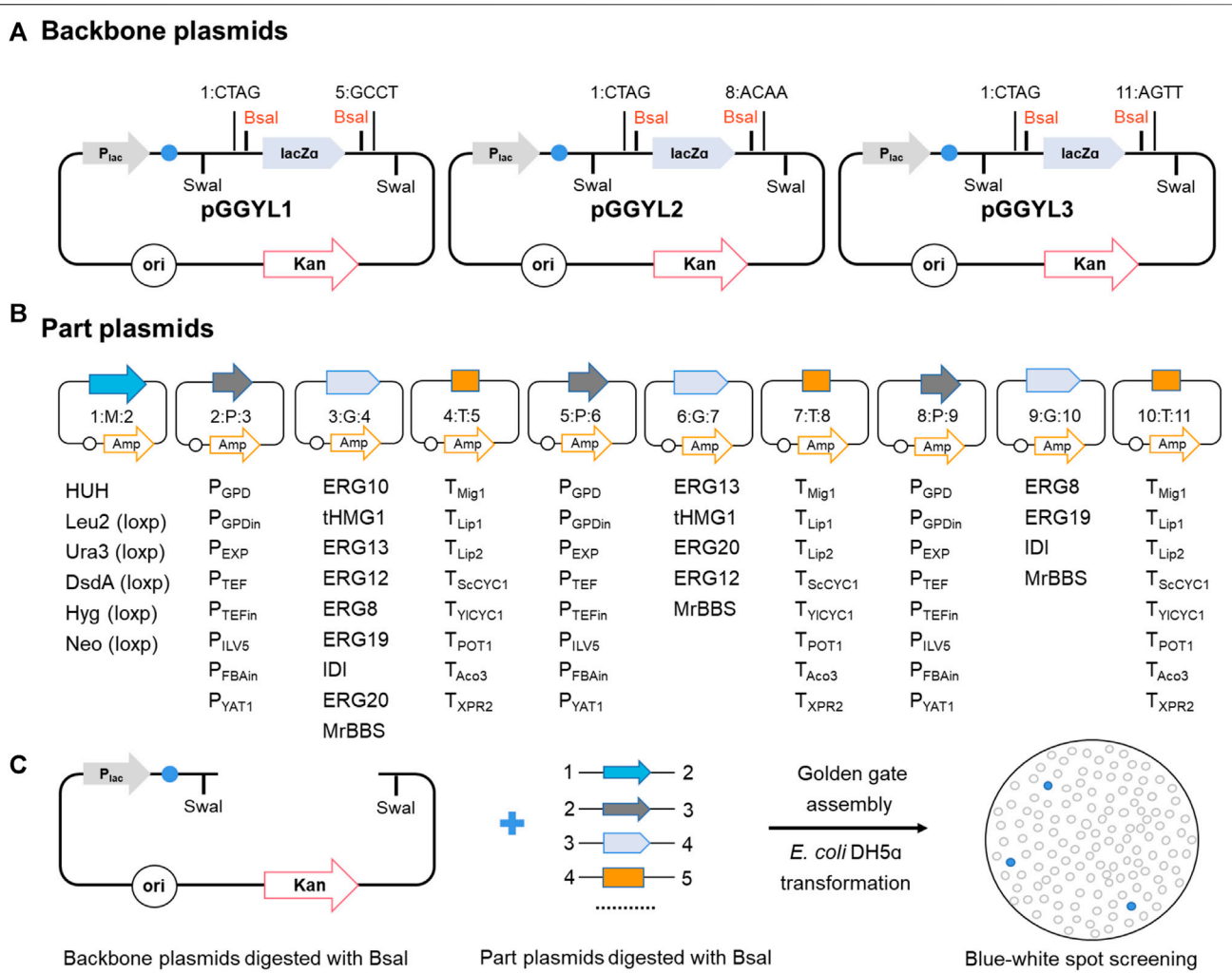

FIGURE 1 | Non-homologous end-joining (NHEJ) integration-based Golden Gate cloning toolkit dedicated to *Yarrowia lipolytica*. **(A)** The backbone plasmid pGGYL1-3 was designed for the assembly of 4, 7, and 10 DNA fragments covering 1–3 transcription units, respectively. *Swa*I recognition sites were included to cut the assembled selection marker and transcription unit for *Y. lipolytica* transformation. **(B)** Building blocks, including the selection marker, promoters, coding gene, and terminator, were cloned into pUC57-T7-FCC1 to generate building block plasmids. The building blocks were flanked with predesigned 4-bp overhangs. The *Bsa*I cleavage sequences at the junction sites of two building blocks were designed to be complementary with each other (each assigned a number from 1 to 11). **(C)** Schematic diagram of the NHEJ integration-based Golden Gate cloning toolkit. The backbone and building block plasmids were digested with *Bsa*I, assembled in one step, and used to transform *Escherichia coli* DH5α. White colonies were picked for verification.

In this study, the quantification of assembly efficiency was carried out on blue and white spot screening plates. Strains with successful ligation products were white in color, but white colonies could also be mis-joined or false positives. Therefore, PCR analysis and Sanger sequencing were required. In brief, 24 white colonies on the plates were picked randomly. Primer F (5′ to 3′: TCTCCCCGCGCGTTGGCCGATT) and primer R (5′ to 3′: GTCTCGCGCGTTTCGGTGATG) were designed to target the outside regions of *Swa*I in the plasmids (**Figures 2A**, **3A**, **4A**). First, the PCR results obtained by colony PCR and DNA gel electrophoresis were used to select the possibly positive colonies. Subsequently, the 4-bp overhangs in the assembled plasmids (extracted from possibly positive colonies) were sequenced to rule out the possibility of mis-joined or false positive cases. The final assembly efficiency is the ratio of the number of successfully assembled spots to the total white spots (24 colonies). The quantification of transformation efficiency was the ratio of the number of total white spots on the plates to the linearized backbone plasmid (100 ng).

Finally, the successfully assembled plasmid was linearized by restriction digestion with *Swa*I and used to transform *Y. lipolytica* for random integration.

Analytical Methods

In order to determine the (-)-α-bisabolol titer, the standard curve was measured by diluting the standard with dodecane to yield concentrations of 0.001, 0.002, 0.004, 0.008, 0.02, 0.04, 0.06, 0.08,

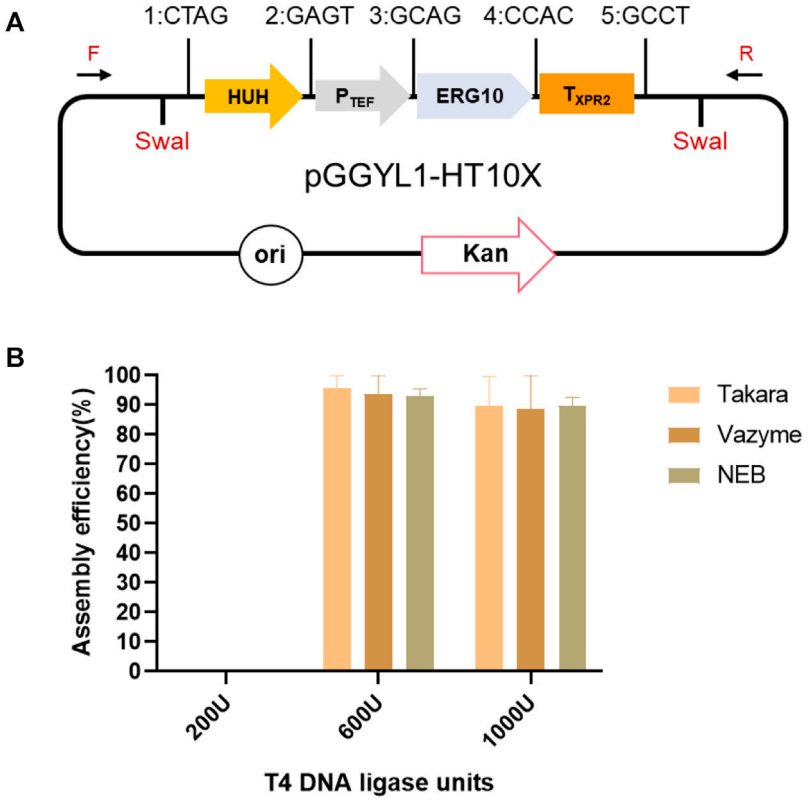

FIGURE 2 | Assembly of four fragments using YALIcloneNHEJ. **(A)** Schematic representation of the completely assembled plasmid pGGYL1-HT10X. **(B)** Assembly efficiency using different amounts of T4 DNA ligase from three commercial suppliers. The primers F/R were used to amplify the assembled fragments.

0.10, 0.20, 0.40, 0.60, 0.80, and 1.00 g/L and analyzed by gas chromatography–mass spectrometry. The dodecane phase and the fermentation broth were centrifuged at 5,000 g for 5 min. The upper dodecane phase was filtered through a 0.22-μm-pore-size membrane and analyzed on a QP2020NX instrument (Shimadzu, Japan) equipped with an HP-5MS column (30 m × 320 μm × 0.5 μm). The oven program consisted of a ramp at 20°C/min to 280°C for 20 min, with N_2 as the carrier gas at a flow rate of 1.14 ml/min. The retention time of (-)-α-bisabolol was 12.24 min. The cell pellet was washed twice with distilled water and lyophilized for further analysis.

5-L Fermentation

An inoculum comprising 5 ml of a pre-culture in YPD was first transferred into 45 ml of fresh YPD medium. After 24 h of cultivation at 28°C and 240 rpm, 20 ml of the culture was transferred into 180 ml of YPD in a 500-ml shake flask and cultivated under the same conditions for 18 h. Then, 200 ml of the resulting seed culture was used to inoculate a 5-L bioreactor (T&J-Atype, Shanghai, China) containing 2 L of medium for fed-batch fermentation. The initial fermentation medium consisted of 60 g/L glucose, 40 g/L peptone, and 20 g/L yeast extract. The temperature, dissolved oxygen, and agitation speed were maintained at 30°C, 1 vvm, and 600 rpm, respectively. The pH was controlled at 7.0 by automatically adding 3 M potassium hydroxide or 3 M sulfuric acid. When the glucose concentration fell below 2 g/L, feed solution containing 800 g/L glucose was added to reach a glucose concentration of 80 g/L in the bioreactor. The (-)-α-bisabolol titer, glucose content, and OD_{600} were measured every 12 h.

RESULTS AND DISCUSSION

Preparing the Modular Parts for Golden Gate Assembly

NHEJ was recently found to be a promising method for chromosomal integration in *Y. lipolytica* (Cui et al., 2021). However, there is currently no modular assembly tool for the construction of multi-gene biosynthetic pathways applied for NHEJ integration, which makes genetic manipulation time-consuming and laborious. Therefore, we constructed a Golden Gate library for terpene production in *Y. lipolytica*.

The library consists of a total of 75 backbone plasmids and the building block plasmids. Three backbone plasmids—pGGYL1, pGGYL2, and pGGYL3—can be used for the ligation of 4, 7, and 10 fragments, respectively (**Figure 1A**). In order to make the subsequent transformant screening more convenient, a lacZ expression box was inserted between the *Bsa*I sites in the pGGYL1-3 plasmid for blue–white colony screening.

The 72 building block plasmids contain genetic parts, such as selection markers, promoters, protein-coding gene sequences, and terminators. Each building block is flanked with respective *Bsa*I recognition sites and predesigned 4-bp overhangs (from 1 to 11).

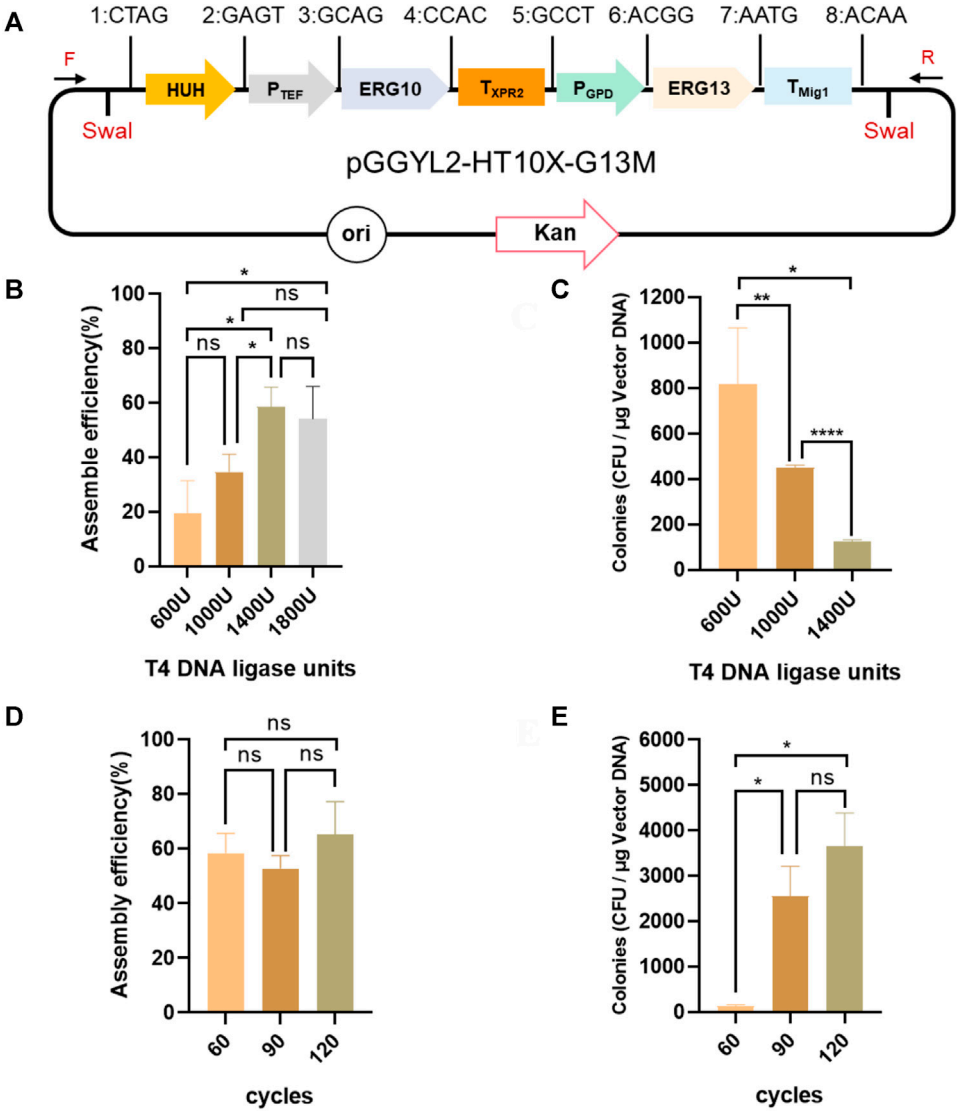

FIGURE 3 | Assembly of seven fragments using YALIcloneNHEJ. **(A)** Schematic representation of the completely assembled plasmid pGGYL2-HT10X-G13M. **(B)** The effect of different amounts of Takara T4 DNA ligase on the assembly efficiency of seven DNA fragments. **(C)** The effect of different amounts of Takara T4 DNA ligase on the number of transformants. **(D)** Assembly efficiency using different numbers of reaction cycles with 1,400 U of T4 DNA ligase. **(E)** Number of transformants using different numbers of reaction cycles with 1,400 U of T4 DNA ligase. The primer F/R was used to amplify the assembled fragments.

The *Bsa*I cleavage sequences at the junction sites of two building blocks are designed to be complementary with each other. As shown in **Figure 1B**, eight endogenous promoters (P_{GPD}, P_{GPDin}, P_{EXP}, P_{TEF}, P_{TEFin}, P_{ILV5}, P_{FBAin}, and P_{YAT}) and nine terminators (T_{Mig1}, T_{Lip1}, T_{Lip2}, T_{ScCYC1}, T_{YICYC1}, T_{TEF}, T_{POT1}, T_{Aco3}, and T_{XPR2}) with different transcriptional and termination strengths in *Y. lipolytica* were selected in order to regulate the gene expression effectively (Curran et al., 2015; Dulermo et al., 2017; Holkenbrink et al., 2018). Eight genes (*tHMG1*, *IDI*, *ERG8*, *ERG10*, *ERG12*, *ERG13*, *ERG19*, and *ERG20*) from the mevalonate (MVA) pathway were selected as building blocks to enhance the terpene biosynthesis flux. Six selection markers, including *hisG-URA3-hisG* (*HUH*), *LEU2* (β-isopropylmalate dehydrogenase), *HPH* (hygromycin B phosphotransferase), *NEO* (aminoglycoside phosphotransferase), *URA3* (orotidine-5′-phosphate decarboxylase), and *DsdA* (D-serine ammonia-lyase), were selected to be used in different auxotrophic or non-auxotrophic strains of *Y. lipolytica*. Among these, *LEU*, *HPH*, *NEO*, *URA3*, and *DsdA* were flanked with loxp tags (locus of X cross-over in P1) to make the markers recyclable. Furthermore, to ensure efficient assembly, the internal *Bsa*I and *Swa*I recognition sites inside the building blocks were removed by introducing synonymous mutations. After the assembly reaction was finished and the DNA was introduced into *E. coli* DH5α, white colonies were screened for identification of successfully assembled plasmid by multiplex PCR and Sanger sequencing (**Figure 1C**).

The successfully constructed plasmid can be digested with *Swa*I. After the target fragment is recovered, it can be used to transform *Y. lipolytica* for random integration.

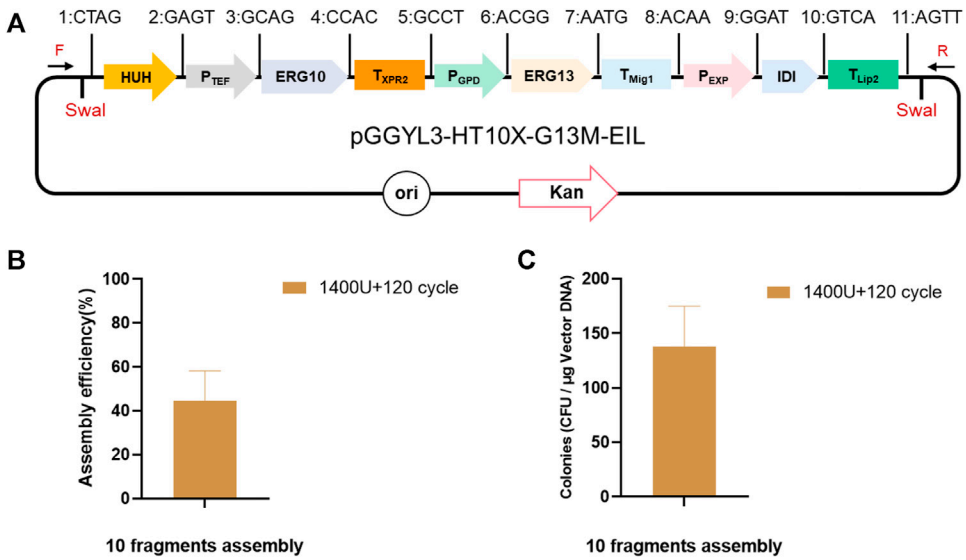

FIGURE 4 | Assembly of 10 fragments using YALIcloneNHEJ. **(A)** Schematic representation of the completely assembled plasmid pGGYL3-HT10X-G13M-EIL. **(B)** Assembly efficiency with 1,400 U of T4 DNA ligase and 120 reaction cycles. **(C)** Number of transformants with 1,400 U of T4 DNA ligase and 120 reaction cycles. The primer F/R was used to amplify the assembled fragments.

Optimization of the Assembly Efficiency

It was previously reported that the assembly efficiency decreased with an increasing number of ligation fragments (Marillonnet and Werner, 2015). Therefore, the DNA ligation conditions were subsequently optimized to maximize the assembly efficiency of 4, 7, and 10 fragments.

Considering that T4 DNA ligase has a direct effect on assembly efficiency (Potapov et al., 2018), T4 ligases from three different producers (Takara, NEB, and Vazyme) were selected, and their assembly efficiency was compared when four fragments (*HUH*, P_{TEF}, *ERG10*, and T_{XPR2}) were assembled (**Figure 2A**). When 200 U of enzyme was used, no successful assembly cases were found, indicating that the enzyme amount was too low to support the ligation reaction. Therefore, the T4 DNA ligase amount was increased to 600 and 1,000 U, respectively. It was found that the assembly efficiency of four fragments could reach more than 90% with all three enzymes (**Figure 2B**). Taking into account the lower price of T4 DNA ligase from Takara, this enzyme was used for further experiments.

Subsequently, the assembly efficiency of seven fragments (*HUH*, P_{TEF}, *ERG10*, T_{XPR2}, P_{GPD}, *ERG13*, and T_{Mig1}) was verified under the same conditions (**Figure 3A**). However, the assembly efficiency reached only 19.4 ± 9.8%, indicating that 600 U of T4 DNA ligase may not be enough for the assembly of seven fragments (**Figure 3B**). Therefore, the ligase amounts were increased to 1,000 and 1,400 U. It was found that the assembly efficiency was improved with increased ligase amounts, and the highest reached 58.5 ± 5.2%. Therefore, the ligase amounts were further increased to 1,800 U, but there was no further increase of efficiency (**Figure 3B**). In addition, although the assembly efficiency was highest with 1,400 U of T4 ligase, it came at the cost of a decreased number of transformants (**Figure 3C**). Consequently, it was significant to search for an approach to balance the assembly efficiency and the number of transformants. By increasing the number of ligation cycles with 1,400 U of T4 ligase from the original 60 cycles to 90 and 120 cycles, it was found that, although the assembly efficiency was not be improved (**Figure 3D**), the number of transformants increased a remarkable 20 times from 133 ± 21 to 3,655 ± 515 cfu/μg vector (**Figure 3E**). Due to the fact that the transformation efficiency of circular plasmid is dozens of times higher than that of linear plasmid in *E. coli*, we thus speculated that when the number of ligation cycles was increased, multigene fragments (which could not be assembled as a circular plasmid in a short time) assembled successfully in an extended period of time. Therefore, the number of transformants was improved significantly. In brief, increasing the number of ligation cycles can be a good strategy for improving the efficiency of Golden Gate assembly.

Finally, the optimized ligation conditions (1,400 U, 120 cycles) were used for the assembly of 10 fragments (*HUH*, P_{TEF}, *ERG10*, T_{XPR2}, P_{GPD}, *ERG13*, T_{Mig1}, P_{EXP}, *IDI*, and T_{Lip2}), and the assembly length reached 13.8 kb (**Figure 4A**). In this case, the number of transformants still reached 1,380 ± 30 cfu/μg vector, with more than 44.5 ± 11.2% assembly efficiency (**Figures 4B,C**), which was high enough for plasmid assembly and verification.

These results demonstrate that, with careful optimization of ligation conditions, Golden Gate can efficiently assemble 10 DNA fragments *via* a simple one-step ligation reaction, which achieved the simultaneous assembly and expression of three genes.

Constructing a Baseline (-)-α-Bisabolol Production Strain by Randomly Integrating the *MrBBS* Cassette

After the Golden Gate library for NHEJ integration was successfully constructed, we sought to use the library to quickly construct an (-)-α-bisabolol-overproducing strain.

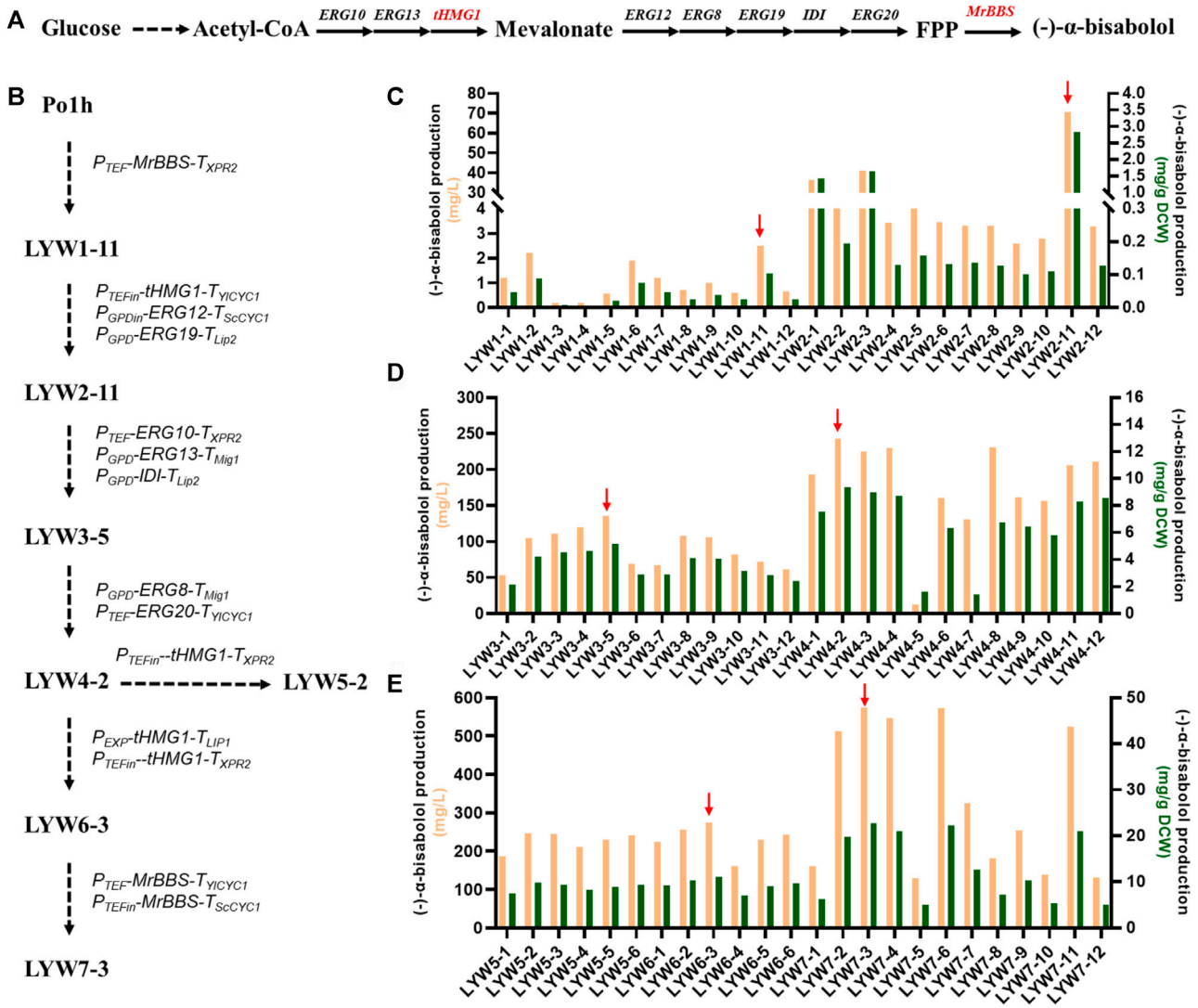

FIGURE 5 | Overproduction of (-)-α-bisabolol by optimizing the mevalonate pathway. **(A)** (-)-α-Bisabolol biosynthesis pathway. **(B)** Flow chart describing the construction of engineered *Yarrowia lipolytica* strains. **(C)** (-)-α-Bisabolol titer after randomly integrating *MrBBS* into Po1h and *tHMG1* as well as *ERG12* and *ERG19* into LYW1-11. **(D)** (-)-α-Bisabolol titer after randomly integrating *ERG10*, *ERG13*, and *IDI* into LYW2-11 and *ERG8* and *ERG20* into LYW3-5. **(E)** (-)-α-Bisabolol titer after randomly integrating a single copy or two copies of *tHMG1* into LYW4-2 and two copies of *MrBBS* into LYW6-3. The red arrow indicates the best-performing strain.

(-)-α-Bisabolol is synthesized by *MrBBS* from the precursor farnesyl diphosphate (FPP), which is an intermediate of the MVA pathway (**Figure 5A**) (Sarrade-Loucheur et al., 2020; Kim et al., 2021). Therefore, we first verified whether *MrBBS* was functional in *Y. lipolytica*. We chose the strain Po1h derived from W29 as the host (Nicaud et al., 2002; Madzak et al., 2004). Subsequently, the plasmid pGGYL1-HTBX containing the selection marker *HUH* and *MrBBS* expression cassette was constructed using YALIcloneNHEJ. After the plasmid was linearized by digestion with *Swa*I, the *HUH* and *MrBBS* expression cassettes were recovered and used to transform *Y. lipolytica* protoplasts for random chromosomal integration. Twelve transformants (designated LYW1-1 to LYW1-12) were picked randomly to test the yield of (-)-α-bisabolol after 4 days of fermentation. It was found that all picked strains were able to produce (-)-α-bisabolol, indicating 100% integration efficiency (**Figure 5C**). Among these, the highest titer of strain LYW1-11 reached 2.5 mg/L, corresponding to a yield of 0.103 mg/g dry cell weight (DCW). Therefore, the LYW1-11 strain was selected for further optimization.

Improving the (-)-α-Bisabolol Titer by Iteratively Integrating an Entire MVA Pathway

Although (-)-α-bisabolol could be synthesized heterologously in *Y. lipolytica*, the titer was still too low to meet the demands of

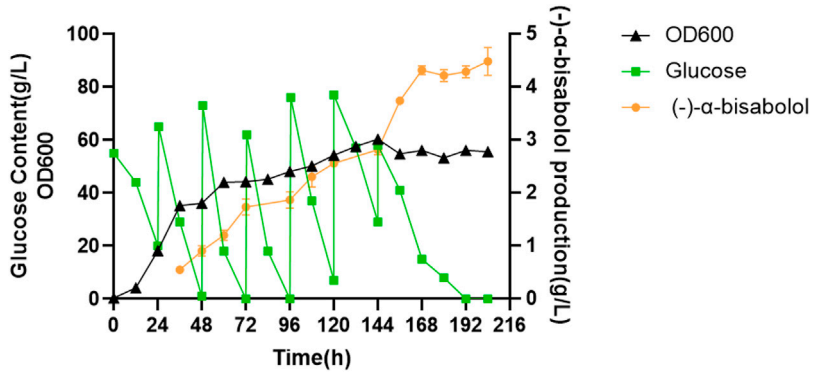

FIGURE 6 | Fed-batch bioreactor fermentation for (-)-α-bisabolol production.

industrial production. Previous studies have demonstrated that enhancement of the MVA pool favors the accumulation of related terpene products (Yang et al., 2016; Liu et al., 2020). Therefore, eight genes in the MVA pathway for the synthesis of FPP from acetyl-CoA, including *ERG10*, *ERG13*, truncated *HMG1* (*tHMG1*), *ERG12*, *ERG8*, *ERG19*, *IDI*, and *ERG20*, were overexpressed to push the carbon flux from acetyl-CoA towards (-)-α-bisabolol. The eight genes were placed under the control of a series of strong constitutive promoters and divided into three sets by Golden Gate assembly: (1) P_{TEFin}-*tHMG1*-T_{YlCYC1}, P_{GPDin}-*ERG12*-T_{ScCYC1}, and P_{GPD}-*ERG19*-T_{Lip2}, (2) P_{TEF}-*ERG10*-T_{XPR2}, P_{GPD}-*ERG13*-T_{Mig1}, and P_{GPD}-*IDI*-T_{Lip2}, and (3) P_{GPD}-*ERG8*-T_{Mig1} and P_{TEF}-*ERG20*-T_{YlCYC1}. Subsequently, the three sets were iteratively integrated into strain LYW1-11, and 12 transformants were randomly picked after each round of integration to test the (-)-α-bisabolol titer. The best-performing strains were selected for the next iterative round of transformation.

As shown in **Figure 5C**, LYW2-11 produced the highest (-)-α-bisabolol titer among 12 randomly picked strains (70.6 mg/L, 2.83 mg/g DCW). When *tHMG1*, *ERG12*, and *ERG19* were first introduced to LYW1-11, the titer of the resulting strain was 28-fold higher compared with the control strain LYW1-1. After that, *ERG10*, *ERG13*, and *IDI* were integrated into the best-performing strain LYW2-11. The (-)-α-bisabolol titer among the eight picked strains in this round exceeded that of LYW2-11, and the highest (-)-α-bisabolol titer of LYW3-5 can reach 135.3 mg/L (5.16 mg/g DCW), a 91.6% increase compared with the parental strain (**Figure 5D**). Based on this excellent result, the last two genes of the MVA pathway, *ERG8* and *ERG20*, were integrated into LYW3-5. The best-performing strain LYW4-2 produced 242.6 mg/L (9.34 mg/g DCW) (-)-α-bisabolol, a further 79.3% increase compared with LYW3-5 (**Figure 5D**).

Following three rounds of random integration of an entire MVA pathway, the (-)-α-bisabolol titer was increased from 2.5 to 242.6 mg/L, a nearly 97-fold improvement, which indicated that dredging the MVA pool by NHEJ-based random integration was an effective strategy for (-)-α-bisabolol overproduction. This method could also be applied to the production of other terpenoids in *Y. lipolytica* in the future.

Optimizing the Copy Number of the Cassettes Encoding the Rate-Limiting Enzymes *tHMG1* and *MrBBS*

In terpenoid biosynthesis, *tHMG1* is generally considered a key rate-limiting enzyme which irreversibly reduces 3-hydroxy-3-methyl glutaryl coenzyme A to mevalonate (Gao et al., 2017). Therefore, *tHMG1* was first overexpressed. A single copy of *tHMG1* and two copies of *tHMG1* under the control of strong promoters were individually introduced into strain LYW4-2. Six strains (designated LYW5-1 to LYW5-6 and LYW6-1 to LYW6-6) were respectively picked, but none showed a significantly improved (-)-α-bisabolol. The best-performing strain LYW6-3 could produce 275.3 mg/L (11.03 mg/g DCW) (-)-α-bisabolol, which was 13.48% higher than the titer of LYW4-2 (**Figure 5E**). These results indicated that the expression level of *tHMG1* was high enough, and this reaction was no longer a limiting step. Terpenoid synthases are also generally considered key rate-limiting enzymes because they directly convert the precursor skeleton into various terpenoid products (Li et al., 2021). Thus, in order to increase the titer, two copies of *MrBBS* under the control of strong promoters were introduced into strain LYW6-3. It was found that 6 of 12 randomly picked transformations produced higher (-)-α-bisabolol titers than the control strain LYW6-3. In particular, strain LYW7-3 produced 573.7 mg/L (22.71 mg/g DCW) (-)-α-bisabolol in shake flasks, which was a 108.4% improvement over LYW6-3 (**Figure 5E**). To our best knowledge, this is the highest shake-flask titer of (-)-α-bisabolol reported in yeast so far.

In addition, the stability of the selected strains used for the next round of transformation, including LYW1-11, LYW2-11, LYW3-5, LYW4-2, LYW5-2, LYW6-3, and the final optimized strain LYW7-3, was also investigated. After 10 generations of continuous subculture, the (-)-α-bisabolol titer was not significantly lower than that of the first generation, which indicated that the engineered strains were genetically stable (**Supplementary Figure S1**).

In summary, terpenoid production could be significantly improved by dredging the MVA pathway. In addition, a mutant library can be quickly constructed based on NHEJ integration to screen hyperproducer strains.

High-Density Fermentation

In order to explore the potential of LYW7-3 for large-scale production of (-)-α-bisabolol, we carried out fed-batch fermentation experiments in a 5-L bioreactor. As shown in **Figure 6**, cell growth entered the stationary phase at about 60 h. After that, the cell growth was relatively slow, and the highest OD_{600} value reached 60.40 after 144 h of fermentation. However, (-)-α-bisabolol increased continuously, reaching 4.4 g/L after 168 h, which corresponds to a productivity of 26.2 mg L^{-1} h^{-1}. After that, the titer remained basically unchanged. To the best of our knowledge, this is the highest (-)-α-bisabolol titer reported in yeast to date. These results showed that terpenoid biosynthesis could be boosted through high-density fermentation. What is more, engineering *Y. lipolytica* for terpenoid production quickly by using an efficient NHEJ integration-based modular cloning toolkit is a powerful new strategy, which can be used for a highly efficient production of various terpenoids in the near future.

CONCLUSION

In this study, we build a Golden Gate cloning toolkit YALIcloneNHEJ, which could assemble 4, 7, and 10 fragments simultaneously with high efficiency in one step. Using this toolkit, we constructed a (-)-α-bisabolol biosynthesis route in *Y. lipolytica*. After randomly integrating an entire MVA pathway and optimizing the copy number of rate-limiting enzymes *tHMG1* and *MrBBS*, the (-)-α-bisabolol titer in the resulting strain LYW7-3 reached 4.4 g/L, the highest (-)-α-bisabolol titer reported in yeast. Our study expands the toolbox for metabolic engineering in *Y. lipolytica* and is expected to be used for a highly efficient production of various terpenoids since all plasmids can be shared by the community.

DATA AVAILABILITY STATEMENT

The original contributions presented in the study are included in the article/**Supplementary Material**. Further inquiries can be directed to the corresponding authors.

AUTHOR CONTRIBUTIONS

T-QS designed the experiments. T-QS, Y-WL, C-LY, QS, Q-QP, and QG performed the experiments. T-QS, X-JJ, X-MS, and HH analyzed the data and wrote the manuscript. T-QS and Z-KN revised the manuscript.

FUNDING

This work was financially supported by the National Key Research and Development Program of China (No.2019YFA0904900), the Natural Science Foundation of Jiangsu Province (BK20210573), the National Science Fund for Excellent Young Scholars of China (21922806), the Key Research and Development Project of Jiangxi Province (20181BBF60029), and the Science and Technology Innovation High-end talent (Youth) Project of Jiangxi Province (jxsq2019201089).

SUPPLEMENTARY MATERIAL

The supplementary material for this article can be found online at: https://www.frontiersin.org/articles/10.3389/fbioe.2021.816980/full#supplementary-material

REFERENCES

Cao, X., Wei, L.-J., Lin, J.-Y., and Hua, Q. (2017). Enhancing Linalool Production by Engineering Oleaginous Yeast *Yarrowia Lipolytica*. *Bioresour. Tech.* 245, 1641–1644. doi:10.1016/j.biortech.2017.06.105

Celińska, E., Ledesma-Amaro, R., Larroude, M., Rossignol, T., Pauthenier, C., and Nicaud, J. M. (2017). Golden Gate Assembly System Dedicated to Complex Pathway Manipulation in *Yarrowia Lipolytica*. *Microb. Biotechnol.* 10, 450–455. doi:10.1111/1751-7915.12605

Chae, T. U., Choi, S. Y., Kim, J. W., Ko, Y.-S., and Lee, S. Y. (2017). Recent Advances in Systems Metabolic Engineering Tools and Strategies. *Curr. Opin. Biotechnol.* 47, 67–82. doi:10.1016/j.copbio.2017.06.007

Cui, Z., Zheng, H., Zhang, J., Jiang, Z., Zhu, Z., Liu, X., et al. (2021). A CRISPR/Cas9-Mediated, Homology-independent Tool Developed for Targeted Genome Integration in Yarrowia Lipolytica. *Appl. Environ. Microbiol.* 87, e02666–20. doi:10.1128/AEM.02666-20

Cui, Z., Jiang, X., Zheng, H., Qi, Q., and Hou, J. (2019). Homology-independent Genome Integration Enables Rapid Library Construction for Enzyme Expression and Pathway Optimization inYarrowia Lipolytica. *Biotechnol. Bioeng.* 116, 354–363. doi:10.1002/bit.26863

Curran, K. A., Morse, N. J., Markham, K. A., Wagman, A. M., Gupta, A., and Alper, H. S. (2015). Short Synthetic Terminators for Improved Heterologous Gene Expression in Yeast. *ACS Synth. Biol.* 4, 824–832. doi:10.1021/sb5003357

Dulermo, R., Brunel, F., Dulermo, T., Ledesma-Amaro, R., Vion, J., Trassaert, M., et al. (2017). Using a Vector Pool Containing Variable-Strength Promoters to Optimize Protein Production in Yarrowia Lipolytica. *Microb. Cell Fact* 16, 31. doi:10.1186/s12934-017-0647-3

Friedlander, J., Tsakraklides, V., Kamineni, A., Greenhagen, E. H., Consiglio, A. L., MacEwen, K., et al. (2016). Engineering of a High Lipid Producing *Yarrowia Lipolytica* Strain. *Biotechnol. Biofuels* 9, 77. doi:10.1186/s13068-016-0492-3

Gao, S., Tong, Y., Zhu, L., Ge, M., Zhang, Y., Chen, D., et al. (2017). Iterative Integration of Multiple-Copy Pathway Genes in Yarrowia Lipolytica for Heterologous β-carotene Production. *Metab. Eng.* 41, 192–201. doi:10.1016/j.ymben.2017.04.004

Han, G. H., Kim, S. K., Yoon, P. K., Kang, Y., Kim, B. S., Fu, Y., et al. (2016). Fermentative Production and Direct Extraction of (-)-α-Bisabolol in Metabolically Engineered *Escherichia coli*. *Microb. Cel. Fact.* 15, 185. doi:10.1186/s12934-016-0588-2

Holkenbrink, C., Dam, M. I., Kildegaard, K. R., Beder, J., Dahlin, J., Doménech Belda, D., et al. (2018). EasyCloneYALI: CRISPR/Cas9-based Synthetic Toolbox for Engineering of the Yeast *Yarrowia Lipolytica*. *Biotechnol. J.* 13, e1700543. doi:10.1002/biot.201700543

Kim, T. Y., Park, H., Kim, S.-K., Kim, S.-J., and Park, Y.-C. (2021). Production of (−)-α-Bisabolol in Metabolically Engineered *Saccharomyces cerevisiae*. *J. Biotechnol.* 340, 13–21. doi:10.1016/j.jbiotec.2021.08.008

Larroude, M., Celinska, E., Back, A., Thomas, S., Nicaud, J.-M., and Ledesma-Amaro, R. (2017). A Synthetic Biology Approach to Transform Yarrowia Lipolytica into a Competitive Biotechnological Producer of β-carotene. *Biotechnol. Bioeng.* 115, 464–472. doi:10.1002/bit.26473

Larroude, M., Rossignol, T., Nicaud, J.-M., and Ledesma-Amaro, R. (2018). Synthetic Biology Tools for Engineering *Yarrowia Lipolytica*. *Biotechnol. Adv.* 36 (8), 2150–2164. doi:10.1016/j.biotechadv.2018.10.004

Ledesma-Amaro, R., and Nicaud, J.-M. (2016). *Yarrowia Lipolytica* as a Biotechnological Chassis to Produce Usual and Unusual Fatty Acids. *Prog. Lipid Res.* 61, 40–50. doi:10.1016/j.plipres.2015.12.001

Li, Z.-J., Wang, Y.-Z., Wang, L.-R., Shi, T.-Q., Sun, X.-M., and Huang, H. (2021). Advanced Strategies for the Synthesis of Terpenoids in *Yarrowia Lipolytica*. *J. Agric. Food Chem.* 69, 2367–2381. doi:10.1021/acs.jafc.1c00350

Lim, H. S., Kim, S. K., Woo, S.-G., Kim, T. H., Yeom, S.-J., Yong, W., et al. (2021). (−)-α-Bisabolol Production in Engineered *Escherichia coli* Expressing a Novel (−)-α-Bisabolol Synthase from the Globe Artichoke Cynara Cardunculus Var. Scolymus. *J. Agric. Food Chem.* 69 (30), 8492–8503. doi:10.1021/acs.jafc.1c02759

Liu, H., Wang, F., Deng, L., and Xu, P. (2020). Genetic and Bioprocess Engineering to Improve Squalene Production in *Yarrowia Lipolytica*. *Bioresour. Tech.* 317, 123991. doi:10.1016/j.biortech.2020.123991

Liu, Y., Jiang, X., Cui, Z., Wang, Z., Qi, Q., and Hou, J. (2019). Engineering the Oleaginous Yeast Yarrowia Lipolytica for Production of α-farnesene. *Biotechnol. Biofuels* 12, 296. doi:10.1186/s13068-019-1636-z

Luo, Y., Li, B.-Z., Liu, D., Zhang, L., Chen, Y., Jia, B., et al. (2015). Engineered Biosynthesis of Natural Products in Heterologous Hosts. *Chem. Soc. Rev.* 44, 5265–5290. doi:10.1039/c5cs00025d

Ma, Y.-R., Wang, K.-F., Wang, W.-J., Ding, Y., Shi, T.-Q., Huang, H., et al. (2019). Advances in the Metabolic Engineering of *Yarrowia Lipolytica* for the Production of Terpenoids. *Bioresour. Tech.* 281, 449–456. doi:10.1016/j.biortech.2019.02.116

Ma, Y., Li, W., Mai, J., Wang, J., Wei, Y., Ledesma-Amaro, R., et al. (2021). Engineering Yarrowia Lipolytica for Sustainable Production of the Chamomile Sesquiterpene (−)-α-Bisabolol. *Green. Chem.* 23, 780–787. doi:10.1039/d0gc03180a

Madzak, C., Gaillardin, C., and Beckerich, J.-M. (2004). Heterologous Protein Expression and Secretion in the Non-conventional Yeast *Yarrowia Lipolytica*: a Review. *J. Biotechnol.* 109, 63–81. doi:10.1016/j.jbiotec.2003.10.027

Marillonnet, S., and Werner, S. (2015). Assembly of Multigene Constructs Using golden Gate Cloning. *Methods Mol. Biol.* 1321, 269–284. doi:10.1007/978-1-4939-2760-9_19

Melo, L. T., Duailibe, M. A. B., Pessoa, L. M., da Costa, F. N., Vieira-Neto, A. E., de Vasconcellos Abdon, A. P., et al. (2017). (−)-α-Bisabolol Reduces Orofacial Nociceptive Behavior in Rodents. *Naunyn-schmiedeberg's Arch. Pharmacol.* 390, 187–195. doi:10.1007/s00210-016-1319-2

Nicaud, J.-M., Madzak, C., Broek, P., Gysler, C., Duboc, P., Niederberger, P., et al. (2002). Protein Expression and Secretion in the yeastYarrowia Lipolytica. *FEMS Yeast Res.* 2, 371–379. doi:10.1111/j.1567-1364.2002.tb00106.x

Potapov, V., Ong, J. L., Kucera, R. B., Langhorst, B. W., Bilotti, K., Pryor, J. M., et al. (2018). Comprehensive Profiling of Four Base Overhang Ligation Fidelity by T4 DNA Ligase and Application to DNA Assembly. *ACS Synth. Biol.* 7, 2665–2674. doi:10.1021/acssynbio.8b00333

Sarkari, P., Marx, H., Blumhoff, M. L., Mattanovich, D., Sauer, M., and Steiger, M. G. (2017). An Efficient Tool for Metabolic Pathway Construction and Gene Integration for *Aspergillus niger*. *Bioresour. Tech.* 245, 1327–1333. doi:10.1016/j.biortech.2017.05.004

Sarrade-Loucheur, A., Ro, D.-K., Fauré, R., Remaud-Siméon, M., and Truan, G. (2020). Synthetic Derivatives of (+)-Epi-α-Bisabolol Are Formed by Mammalian Cytochromes P450 Expressed in a Yeast Reconstituted Pathway. *ACS Synth. Biol.* 9, 368–380. doi:10.1021/acssynbio.9b00399

Shi, T.-Q., Gao, J., Wang, W.-J., Wang, K.-F., Xu, G.-Q., Huang, H., et al. (2019). CRISPR/Cas9-based Genome Editing in the Filamentous Fungus *Fusarium Fujikuroi* and its Application in Strain Engineering for Gibberellic Acid Production. *ACS Synth. Biol.* 8 (2), 445–454. doi:10.1021/acssynbio.8b00478

Shi, T. Q., Li, Y. W., Zhu, L., Tong, Y. Y., Yang, J., Fang, Y. M., et al. (2021). Engineering the Oleaginous Yeast *Yarrowia Lipolytica* for β-farnesene Overproduction. *Biotechnol. J.* 16, e2100097. doi:10.1002/biot.202100097

Son, Y.-J., Kwon, M., Ro, D.-K., and Kim, S.-U. (2014). Enantioselective Microbial Synthesis of the Indigenous Natural Product (−)-α-Bisabolol by a Sesquiterpene Synthase from Chamomile (Matricaria Recutita). *Biochem. J.* 463, 239–248. doi:10.1042/bj20140306

Tabari, M. A., and Tehrani, M. A. B. (2017). Evidence for the Involvement of the GABAergic, but Not Serotonergic Transmission in the Anxiolytic-like Effect of Bisabolol in the Mouse Elevated Plus Maze. *Naunyn-schmiedeberg's Arch. Pharmacol.* 390, 1041–1046. doi:10.1007/s00210-017-1405-0

Tang, W.-Y., Wang, D.-P., Tian, Y., Fan, X., Wang, C., Lu, X.-Y., et al. (2021). Metabolic Engineering of *Yarrowia Lipolytica* for Improving Squalene Production. *Bioresour. Tech.* 323, 124652. doi:10.1016/j.biortech.2020.124652

Tong, Y., Zhou, J., Zhang, L., and Xu, P. (2021). A Golden-Gate Based Cloning Toolkit to Build Violacein Pathway Libraries in *Yarrowia Lipolytica*. *ACS Synth. Biol.* 10, 115–124. doi:10.1021/acssynbio.0c00469

Yang, X., Nambou, K., Wei, L., and Hua, Q. (2016). Heterologous Production of α-farnesene in Metabolically Engineered Strains of Yarrowia Lipolytica. *Bioresour. Tech.* 216, 1040–1048. doi:10.1016/j.biortech.2016.06.028

Ye, R. W., Sharpe, P. L., and Zhu, Q. (2012). Bioengineering of Oleaginous Yeast *Yarrowia Lipolytica* for Lycopene Production. *Methods Mol. Biol.* 898, 153–159. doi:10.1007/978-1-61779-918-1_9

Conflict of Interest: Z-KN was employed by Jiangxi New Reyphon Biochemical Co., Ltd.

The remaining authors declare that the research was conducted in the absence of any commercial or financial relationships that could be construed as a potential conflict of interest.

Publisher's Note: All claims expressed in this article are solely those of the authors and do not necessarily represent those of their affiliated organizations or those of the publisher, the editors, and the reviewers. Any product that may be evaluated in this article or claim that may be made by its manufacturer is not guaranteed or endorsed by the publisher.

frontiers in Bioengineering and Biotechnology

ORIGINAL RESEARCH
published: 18 March 2022
doi: 10.3389/fbioe.2022.838732

Transporter-Driven Engineering of a Genetic Biosensor for the Detection and Production of Short-Branched Chain Fatty Acids in *Saccharomyces cerevisiae*

Ryoma Miyake[1,2,3,4], *Hua Ling*[1,2,3], *Jee Loon Foo*[1,2,3], *Nobutake Fugono*[4] *and Matthew Wook Chang*[1,2,3]*

[1]NUS Synthetic Biology for Clinical and Technological Innovation (SynCTI), National University of Singapore, Singapore, Singapore, [2]Synthetic Biology Translational Research Programme, Yong Loo Lin School of Medicine, National University of Singapore, Singapore, Singapore, [3]Department of Biochemistry, Yong Loo Lin School of Medicine, National University of Singapore, Singapore, Singapore, [4]Science & Innovation Center, Mitsubishi Chemical Corporation, Yokohama, Japan

Biosensors can be used for real-time monitoring of metabolites and high-throughput screening of producer strains. Use of biosensors has facilitated strain engineering to efficiently produce value-added compounds. Following our recent work on the production of short branched-chain fatty acids (SBCFAs) in engineered *Saccharomyces cerevisiae*, here we harnessed a weak organic acid transporter Pdr12p, engineered a whole-cell biosensor to detect exogenous and intracellular SBCFAs and optimized the biosensor's performance by varying *PDR12* expression. We firstly constructed the biosensor and evaluated its response to a range of short-chain carboxylic acids. Next, we optimized its sensitivity and operational range by deletion and overexpression of *PDR12*. We found that the biosensor responded to exogenous SBCFAs including isovaleric acid, isobutyric acid and 2-methylbutanoic acid. *PDR12* deletion enhanced the biosensor's sensitivity to isovaleric acid at a low concentration and *PDR12* overexpression shifted the operational range towards a higher concentration. Lastly, the deletion of *PDR12* improved the biosensor's sensitivity to the SBCFAs produced in our previously engineered SBCFA-overproducing strain. To our knowledge, our work represents the first study on employing an ATP-binding-cassette transporter to engineer a transcription-factor-based genetic biosensor for sensing SBCFAs in *S. cerevisiae*. Our findings provide useful insights into SBCFA detection by a genetic biosensor that will facilitate the screening of SBCFA-overproducing strains.

Keywords: short branched-chain fatty acids, weak organic acids, transporter, genetic biosensor, promoter, *Saccharomyces cerevisiae*

OPEN ACCESS

Edited by:
Shihui Yang,
Hubei University, China

Reviewed by:
Xinqing Zhao,
Shanghai Jiao Tong University, China
Jifeng Yuan,
Xiamen University, China

***Correspondence:**
Matthew Wook Chang
bchcmw@nus.edu.sg

Specialty section:
This article was submitted to Synthetic Biology, a section of the journal Frontiers in Bioengineering and Biotechnology

Received: *18 December 2021*
Accepted: *28 February 2022*
Published: *18 March 2022*

Citation:
Miyake R, Ling H, Foo JL, Fugono N and Chang MW (2022) Transporter-Driven Engineering of a Genetic Biosensor for the Detection and Production of Short-Branched Chain Fatty Acids in Saccharomyces cerevisiae. Front. Bioeng. Biotechnol. 10:838732. doi: 10.3389/fbioe.2022.838732

INTRODUCTION

Carboxylic acids are used as platform chemicals for manufacturing a variety of industrial products such as plastics, solvents, polymers and serve as "building blocks" for pharmaceuticals, fragrances, foods and other valuable products (Sauer et al., 2008). In the industry, carboxylic acids are produced from petrochemicals, which has brought concerns about unsustainability and environmental pollution. Therefore, there are strong interests in developing economical and environmentally

friendly routes to produce carboxylic acids using microbial hosts (Chen and Nielsen, 2016). Isovaleric acid (IVA), isobutyric acid (IBA) and 2-methylbutanoic acid (2MBA) are representative short branched-chain fatty acids (SBCFAs) containing a methyl branch located on one or two carbon atoms (Yu et al., 2016). IVA derivatives are used as drugs, e.g., anticonvulsant and sedative and flavourings (Suerbaev et al., 2012; Wang et al., 2018). IBA derivatives are used as plastics, flavorings, fragrances, textile auxiliaries, surfactants and plasticizers (Zhang et al., 2011; Lang et al., 2014; Hammer et al., 2020). 2MBA is used for the synthesis of pharmaceuticals and flavoring (Kwon et al., 2000). Recently, several microorganisms, including *Saccharomyces cerevisiae*, *Pseudomonas putida* and *Bacillus licheniformis*, have been engineered to produce these SBCFAs (Lang et al., 2014; Yu et al., 2016; Shi et al., 2019). However, their production level in the engineered microbes is still low.

Genetic biosensors can be developed and used to facilitate strain engineering and optimization by biosensor-assisted high-throughput screening (HTS) of microbes for high SBCFA producers. Typically, a genetic biosensor consists of an allosterically regulated transcription factor (TF), which binds a specific ligand and associates with a target promoter to regulate the expression of a reporter gene (Teo and Chang, 2015; Taylor et al., 2016; Chen et al., 2018; Xia et al., 2019; D'Ambrosio et al., 2020; Hossain et al., 2020). For constructing an SBCFA biosensor, the weak organic acid-activated TF, War1p, from *S. cerevisiae* is a suitable candidate. War1p is constitutively expressed and binds to the weak organic acid response (War) element in the *PDR12* promoter (pPDR12) (Kren et al., 2003; Gregori et al., 2008). When it binds to a weak organic acid, War1p is phosphorylated and conformationally changed to activate the expression of *PDR12* (Mollapour and Piper, 2012). Based on this inducible system, Baumann et al. have developed a genetic biosensor which consists of War1p and pPDR12 coupled with green fluorescent protein (GFP) to detect short- and medium-chain fatty acids in *S. cerevisiae*, in which the fatty acid sensing was decoupled from the production using a two-cell sensor system (Baumann et al., 2018). Compared to the two-cell sensor system, a one-cell sensor system that produces and senses SBCFAs is favored for HTS of SBCFA-producing strains (Lim et al., 2018).

Optimizations are commonly needed to achieve desired properties of the genetic biosensors such as dynamic and operational ranges for the effective detection of target compounds (Hossain et al., 2020). The main strategies for such optimization include tuning of the TF's receptor level, engineering of the DNA binding domain, the promoter's upstream region, operator sequence or the 5′-untranslated region of the reporter gene and control of the target chemical level. For instance, Snoek et al. have reported that the evolution-guided engineering of the ligand binding domain of a bacterial TF (BenM) in *S. cerevisiae* led to a 15-fold increase in sensitivity and a 40-fold change in operational range (Snoek et al., 2020). Dabirian et al. have inserted the binding sites into various positions in the core promoter region of five native promoters in *S. cerevisiae*, which led to a higher sensitivity of malonyl-CoA-responsive TF (FapR) (Dabirian et al., 2019). Williams et al. have developed a pPDR12-based genetic biosensor to detect p-hydroxybenzoic acid and propionic acid through a positive-feedback activation of War1p by promoter engineering (Williams et al., 2017). Reduction of the intracellular level of target chemical by activating an exporter shifts the operational range of an allosteric TF-based biosensor in *E. coli* (Raman et al., 2014). In yeast, the ATP-binding-cassette (ABC) transporter Pdr12p plays roles in regulating the intracellular level of weak organic acids by export and its expression is selectively induced by weak organic acids (Piper et al., 1998; Hatzixanthis et al., 2003). Therefore, we hypothesized that tuning of *PDR12* expression could be employed to optimize the properties of genetic biosensors for the detection of weak organic acids such as SBCFAs.

In this study, we aimed to develop a genetic biosensor to detect SBCFAs (exemplified by IVA, IBA and 2MBA) produced by our previously engineered *S. cerevisiae* strain (Yu et al., 2016). To this end, we firstly constructed a biosensor based on the War1p TF and pPDR12 and characterized its substrate spectrum. Furthermore, we optimized its sensitivity and operational range by deletion and overexpression of *PDR12* in the engineered SBCFA-overproducing strain. This study provides useful insights into SBCFA detection by a one-cell biosensor system that can potentially facilitate the HTS of SBCFA-overproducing strains.

MATERIALS AND METHODS

Plasmids and Strains

Plasmids and strains used in this study are shown in **Table 1**. Oligonucleotide primers (**Supplementary Table S1**) were synthesized by Integrated DNA Technologies (Singapore). Chemically competent *Escherichia coli* TOP10 was used for subcloning. The transformants were selected on LB agar plates with 100 μg/mL ampicillin.

Chemicals and Reagents

The Q5 high-fidelity DNA polymerase, NEBuilder HiFi DNA Assembly Cloning Kit, Restriction enzymes, T4 DNA ligase and PCR reagents were purchased from New England Biolabs (Beverly, MA, United States). QIAquick Gel Extraction Kit, QIAprep Spin Miniprep Kit and RNeasy Mini Kit were purchased from Qiagen (Valencia, CA, United States). Peptone was purchased from Oxoid Ltd. (Basingstoke, Hampshire, UK). Dropout SC amino acid mixture formulation (without Uracil) for *S. cerevisiae* growth media was purchased from MP Biomedicals (Santa Ana, CA, United States). All other reagents were purchased from Sigma Aldrich (St. Louis, MO, United States) or Tokyo Chemical Industry Co., Ltd. (Tokyo, Japan) unless otherwise stated.

Construction of the SBCFA Biosensor

To construct the SBCFA biosensor, a GFP reporter gene was cloned under the control of pPDR12 which is inducible by weak organic acids. Specifically, pPDR12 was amplified by PCR from the genomic DNA of *S. cerevisiae* BY4741 using primers PDR12p-f with a *Sac*I site and PDR12p-r (**Supplementary Table S1**). The GFP gene was amplified from pKT127

TABLE 1 | Plasmids and strains used in this study.

Plasmids/ Strains	Description	Source
Plasmids		
pESC-URA	AmpR, URA3, 2-micron ori	Agilent
pUG72	AmpR, *loxP–URA3–loxP*	Gueldener et al. (2002)
pUG72-TEF1	pUG72 carrying P_{TEF1}	Yu et al. (2016)
pSH69	AmpR, hpnMX, Cre under P_{GAL1} control	Hegemann and Heick, (2011)
pPDR12-GFP	pESC-URA carrying P_{PDR12} and yEGFP	This study
Strains		
E. coli		
E. coli TOP10	F– *mcrA* Δ (*mrr-hsdRMS-mcrBC*) ϕ80*lacZ*ΔM15 ΔlacX74 recA1 *araD*139 Δ(*ara-leu*)7697 *galU galK rpsL*(*Str*^{R}) *endA1 nupG*	Invitrogen
S. cerevisiae		
BY4741	MATa *his3Δ1 leu2Δ0 met15Δ0 ura3Δ0*	ATCC
4G-ΔADH6	BY4741 with overexpressed *BAT1*, *ARO10*, *ALD2*, *ALD5* and disrupted *ADH6*	Yu et al. (2016)
TOE01	BY4741 with overexpressed *PDR12*	This study
TDL01	BY4741 with disrupted *PDR12*	This study
TDL02	4G-ΔADH6 with disrupted *PDR12*	This study
BY4741-S_{LCA}	BY4741 with pPDR12-GFP	This study
4G-ΔADH6-S_{LCA}	4G-ΔADH6 with pPDR12-GFP	This study
TOE01-S_{LCA}	TOE01 with pPDR12-GFP	This study
TDL01-S_{LCA}	TDL01 with pPDR12-GFP	This study
TDL02-S_{LCA}	TDL02 with pPDR12-GFP	This study

harboring the yEGFP gene (Accession No. MK178572) (Sheff and Thorn, 2004) using primers yEGFP-f and yEGFP-r with an *Xho*I site. pESC-URA was digested with *Sac*I and *Xho*I. The amplified pPDR12, *yEGFP* and the digested pESC-URA fragment were purified and assembled by NEBuilder to yield the SBCFA biosensor namely pPDR12-GFP. The sequence of the biosensor plasmid was confirmed by Sanger sequencing (1st Base, Singapore).

Deletion and Overexpression of *PDR12* in *S. cerevisiae*

To tune the expression of *PDR12* gene and study its effect on the biosensor's behavior, *PDR12* was deleted and over-expressed in *S. cerevisiae*. Briefly, the *PDR12* gene deletion was carried out using the Cre-LoxP system (Gueldener et al., 2002). The plasmid pUG72 (carrying the loxP–*URA3*–loxP cassette) was used to generate the gene deletion cassette and its derivative plasmid namely pUG72-TEF1 (carrying the strong constitutive promoter pTEF1) was used to replace the pPDR12 with pTEF1 in the chromosome (Yu et al., 2016). The plasmid pSH69 (carrying pGAL1-CRE) which contains a hygromycin B resistance gene was used for marker rescue (Hegemann and Heick, 2011).

To delete the *PDR12* gene, the *URA3* selection marker flanked by loxP sites was amplified from pUG72 by PCR using primers PDR12-Del-f and PDR12-Del-r, which contained a 42 bp homology to the integration site of *PDR12* gene (**Supplementary Table S1**). The obtained DNA fragments were purified and transformed into BY4741 and the SBCFA-overproducing strain 4G-ΔADH6 using a modified yeast transformation method (Gietz and Schiestl, 2007; Ling et al., 2015). The transformants were selected on solid defined medium lacking uracil (SCD-U) and confirmed by colony PCR using the primers PDR12-CheGD-f PDR12-CheGD-r (**Supplementary Figure S1**). The obtained strains were transformed with the CRE recombinase-expressing plasmid pSH69 and grown on YPD plates containing 200 μg/mL hygromycin B (YPDH) to remove the *URA3* marker gene between the loxP sites. The obtained strains were evaluated by PCR to confirm removal of the *URA3* gene and designated as TDL01 (derived from BY4741) and TDL02 (derived from 4G-ΔADH6).

The replacement of the native promoter of *PDR12* gene (pPDR12) to *TEF1* promoter (pTEF1) was carried out using the same procedure as described for *PDR12* deletion. The pTEF1 was amplified by using primers PDR12-pTEF1-F and PDR12-pTEF1-R and pGU72-TEF1 as a template. The promoter replacement in the obtained transformants were confirmed by PCR with the primers TEFp-UP-f and PDR12-CheTEFp-r (**Supplementary Figure S1**). After marker rescue, the obtained strains were evaluated by PCR with primers PDR12-CheTEFp-f and PDR12-CheTEFp-r to confirm removal of the *URA3* gene. The confirmed strain was used for transformation with the constructed SBCFA biosensor as described above.

Detection of Exogenous SBCFAs by the SBCFA Biosensor

Prior to the detection of exogenous SBCFAs, the strains harboring the SBCFA biosensor pPDR12-GFP were grown in SCD-U with 100 mM potassium phosphate buffer (KPB, pH6.5) overnight at 30°C with shaking at 200 rpm. The overnight culture was diluted to OD_{600} of 0.1 in 2 mL of fresh medium and grown until the OD_{600} reached 0.4–0.6. The cells were centrifuged and resuspended in fresh SCD-U with 100 mM KPB (pH6.5) and 100 μL of cells was transferred to each well in black 96-well plates with clear flat bottom. Subsequently, 90 μL of fresh SCD-U with

KPB was mixed with 10 μL of SBCFAs (**Supplementary Table S2**) to final concentrations of 0.05–10 mM, where the SBCFA stocks were prepared at 1 M in 70% ethanol and pH neutralized with sodium hydroxide solution. The SBCFA stocks were diluted to 1–200 mM using sterile water before adding into the microplate wells.

To measure the fluorescence signal of the SBCFA biosensor, the samples described as above in the 96-well plate were incubated at 30°C with shaking at 600 rpm in a Synergy H1 plate reader (BioTek, VT, United States). The cell density (OD_{600}) was measured at 600 nm and the fluorescence signal was measured with excitation at 470 nm and emission at 515 nm every 30 min. The fluorescence intensity was normalized to OD_{600} and the normalized fluorescence intensity was compared between the conditions with and without SBCFAs. The EC_{50} (50% effective concentration) values were calculated by nonlinear regression using GraphPad Prism version 9 software (Graph Pad Software, CA, United States).

Detection of Intracellularly Produced SBCFAs by the SBCFA Biosensor

Besides the detection of exogenous SBCFAs, the intracellular SBCFAs produced by our previous SBCFAs-overproducing strain 4G-ΔADH6 was detected. The strains were cultivated in SCD-U medium at 30°C with shaking at 220 rpm overnight. The overnight culture was re-inoculated to an initial OD_{600} of 0.05 in 25 mL fresh SCD-U with 100 mM KPB (pH6.5) and grown under the same conditions in 250 mL shake flasks. For time course experiments, culture samples were collected every 12 h to determine the SBCFA levels and cell density (OD_{600}) was measured by a spectrophotometer BioPhotometer Plus (Eppendorf, Germany). The culture samples were diluted by SCD-U with KPB to adjust the cell concentration and the fluorescence intensity was measured on a Synergy H1 microplate reader and normalized to the cell density (Jung et al., 2021) as described above.

Gas Chromatography/Mass Spectrometry Analysis of SBCFAs

GC analysis of SBCFAs was performed using methods modified from previous studies (Teo et al., 2015; Yu et al., 2016; Ng et al., 2020). One milliliter of yeast culture was collected and centrifuged to obtain the supernatant. To quantify the SBCFAs in the supernatant, 0.4 mL of 10% hydrochloric acid–methanol (v/v) and heptadecanoic acid (C17:0) at a final concentration of 1 mM as an internal standard were added to 0.8 mL culture supernatant and the mixtures were vortexed for 2 min and incubated at 62°C for 3 h to methylate the SBCFAs. SBCFA standards (IVA, 2MBA, IBA) at 0.5 and 2.0 mM added to SCD-URA medium were extracted and methylated as describe above. To the reaction mixtures, 0.2 mL hexane was added, and the resulting fatty acid methyl esters (FAMEs) were extracted by vortexing for 2 min and phase separation by centrifugation. The organic extracts containing FAMEs were then subjected to GC/MS analysis using a 7890B GC system with an Agilent 5977A MSD and an HP-5MS column. The method for GC/MS analysis was as follows: oven temperature with initial hold at 45°C for 3 min, ramp to 50°C at 10°C/min and hold for 3 min, ramp to 280°C at 50°C/min and hold for 5 min. Helium was used as the carrier gas and set at a constant pressure of 13.8 psi. The injector was maintained at 250°C and the ion source temperature was set to 230°C. The injection volume was 1.0 μL in a splitless mode. FAMEs of the respective SBCFAs were identified by their retention time and the mass spectra of FAME standards. Data analysis was performed using the Agilent Enhanced Data Analysis software. Given that 2MBA and IVA are isomers that have the same mass spectrum and retention time, they were quantified as a mixture.

RESULTS AND DISCUSSION

Construction and Characterization of the SBCFA Biosensor

We have previously engineered *S. cerevisiae* to produce SBCFAs that comprise IVA, IBA and 2MBA (Yu et al., 2016). Here, to construct a genetic biosensor to detect SBCFAs in *S. cerevisiae*, we designed a biosensor that consists of 1) War1p, a TF that phosphorylates upon binding to weak organic acids (e.g., hexanoic acid, heptanoic acid and octanoic acid), 2) pPDR12, which is activated by the phosphorylated War1p and 3) a yeast-enhanced GFP gene (*yEGFP*) under the control of pPDR12. To ensure a higher copy number of the target genes, we cloned the aforementioned genetic elements into a high-copy plasmid pESC-URA and introduced the resulting biosensor (namely S_{LCA}) into *S. cerevisiae* strains (BY4741, TOE01, TDL01, TDL02, 4G-ΔADH6) to obtain the biosensor strains (BY4741-S_{LCA}, TOE01-S_{LCA}, TDL01-S_{LCA}, TDL02-S_{LCA}, 4G-ΔADH6-S_{LCA}).

To determine a suitable condition for sensing SBCFAs, we measured and compared the fluorescence intensity of BY4741-S_{LCA} in SCD-U medium under buffered pH (at pH6.5 and pH7.4) and unbuffered (at pH4.5) pH conditions added with IBA and IVA, respectively. **Supplementary Figure S2** shows that SLCA with a starting pH4.5 and unbuffered had a higher background than that when the pH was buffered to 6.5 and 7.4 without SBCFAs, suggesting that the low pH effect can be mitigated by maintaining the pH at about 7.0. The background fluorescence without pH buffering increased with incubation, whereas it remained low and constant under the buffered pH condition. It was found that under the unbuffered condition, the pH dropped from pH4.5 to pH3.5 after overnight incubation and under the buffered condition the pH remained above pH6.0. The higher fluorescence background under the unbuffered condition (pH 4.5) was likely due to the higher concentration of proton than that at pH 6.0. The undissociated weak organic acids can pass through the plasma membrane by passive diffusion under an acidic condition and free weak organic acids can be taken up by active transport at a physiological condition near pH7 (Casal et al., 2008). The uptaking efficiency of the former is generally more efficient than the latter (Borrull et al., 2015). We hypothesized that the whole-cell biosensor BY4741-SLCA would give a higher response at pH6.5 and pH7.4 than at

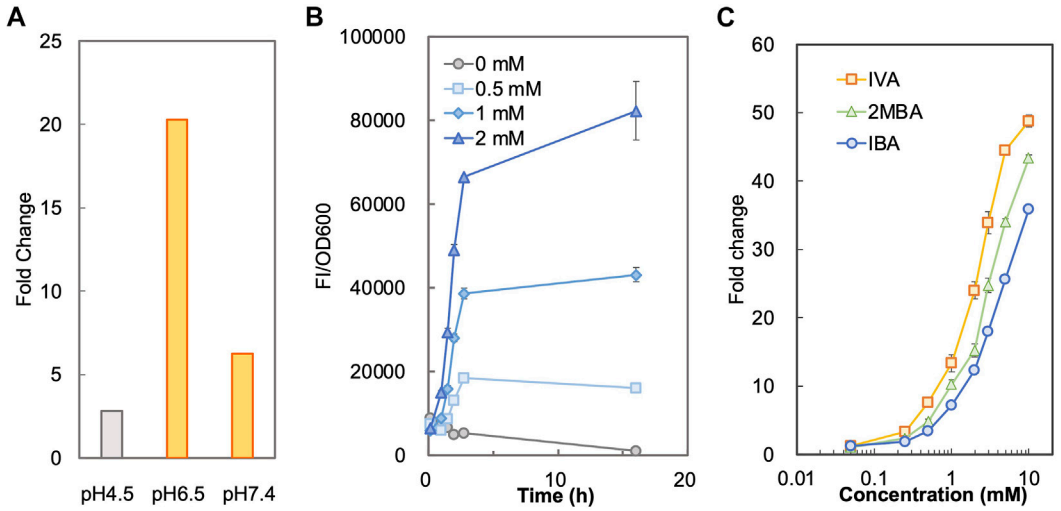

FIGURE 1 | Characterization of biosensor BY4741-S_{LCA}. **(A)** Responses of BY4741-S_{LCA} cells (fold changes) to IBA under different pH conditions. BY4741-S_{LCA} cells were grown in SCD-U medium under buffered (at pH6.5 and pH7.4) or unbuffered (at pH4.5) pH conditions. GFP fluorescence was measured after incubation with 1.0 mM IBA and normalized to cell density (OD600). The fluorescence of control without the IBA supply was normalized to its cell density and set to 1. **(B)** Time-course fluorescence intensity of BY4741-S_{LCA} cells in response to IBA supplied into the medium. BY4741-S_{LCA} cells were incubated in the buffered SCD medium (pH 6.5) with IBA supply (at 0.5, 1, and 2 mM). The fluorescence was measured and normalized to cell density (OD600). **(C)** Dose-dependent responses of BY4741-S_{LCA} cells to respective SBCFA, i.e. IVA, 2MBA and IBA after a 3-h incubation. FI, fluorescence intensity. Values are means of three independent experiments. An error bar represents a standard deviation of three independent experiments.

pH4.5. This was proven by a 7.3-fold and 2.3-fold higher fold-change (FC) of fluorescence intensity towards IBA under the buffered pH at 6.5 (FC 20.3) and 7.4 (FC 6.3) than that when unbuffered (FC 2.8) at about 3 h (**Figure 1A**). **Supplementary Figure S2B** also shows that the time-course responses (FC) to IVA at pH6.5 (FC 37.0) and 7.4 (FC 14.9) are significantly higher than at pH4.5 (FC 3.9) at about 3 h. Given higher fluorescence from at pH6.5 than pH7.4, the medium buffered at pH6.5 was chosen for biosensing SBCFAs in this study.

Next, under the condition with the pH buffered to 6.5, we characterized the operational range of BY4741-S_{LCA} against individual SBCFAs (IVA, 2MBA, IBA) fed at various concentrations. We firstly determined the minimal incubation time required for the S_{LCA} to respond to the SBCFAs till the signal remained stable. Using IBA as an example, we found that there was a time-dependent exponential increase in the fluorescence signal against 0.5–2.0 mM of IBA till about 3 h. Afterwards, there was a slight decrease of signal from control (without IBA) (**Figure 1B**), which showed a 10-fold increase in cell density and a 2-fold increase in fluorescence (**Supplementary Figure S3**). This result suggests that a 3-h incubation is required prior to measuring the biosensor's signal.

To determine the correlation of SBCFA doses to the signal, we exposed the BY4741-S_{LCA} to IVA, 2MBA and IBA fed at various concentrations (0.05–10 mM) and measured the fluorescence signal. In **Figure 1C**, with a 3-h incubation, BY4741-S_{LCA} demonstrated a dose-dependent increase of the response (FC) against the respective SBCFAs ranging from 0.05 mM (~FC 2) to 10 mM (>FC 36). It is noted that, starting from 0.25 mM till 10 mM, the response from IVA was the highest (up to FC 49) amongst the three tested SBCFAs, suggesting that IVA is a preferred sensing target (EC_{50} 2.2) over 2MBA (up to FC 43, EC_{50} 3.6) and IBA (up to FC 36, EC_{50} 5.0). Our results show that our biosensor is suitable for screening SBCFA-overproducing strains that produce SBCFAs at 0.25–10 mM, including the engineered *S. cerevisiae* strain producing 4 mM SBCFAs (Yu et al., 2016).

Structurally, the branched chain of IBA (C4) and 2MBA (C5) is located at the α position, whereas IVA's (C5) branched chain is at the β position further from the carboxylic group. Given the differences in the branched-chain positions, the binding affinity of War1p to these SBCFAs will differ, depending on the varying binding tendency towards the structurally dissimilar carbon chain. It is known that War1p prefers binding to lipophilic weak acids over hydrophilic weak acids (Kim et al., 2019). Therefore, the differences in the binding efficacy of War1p to the SBCFAs could cause different responses of the biosensor. In addition, intracellular concentration of these SBCFAs could vary due to different import/export efficiency, hence causing variable responses of the biosensor.

Substrate Spectrum of the SBCFA Biosensor

Besides SBCFAs, we investigated the substrate spectrum of S_{LCA} against other representative industry-relevant short-chain weak organic acids, including short linear chain fatty acids and lipophilic carboxylic acid derivatives such as phenolic acids, methacrylic acid, hydroxy carboxylic acids, keto acid and branched-chain amino acid (Castano-Cerezo et al., 2019).

To determine if shorter linear chain fatty acids and the lipophilic carboxylic acids with various chemical groups (vinyl,

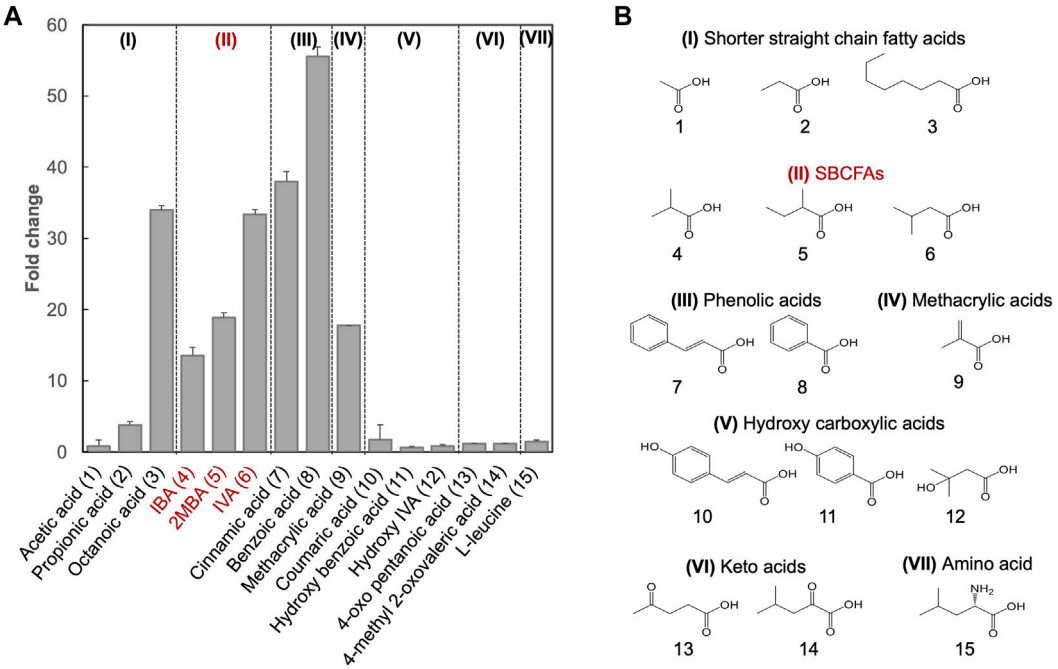

FIGURE 2 | Substrate spectral analysis of biosensor BY4741-S_{LCA}. **(A)** Responses of BY4741-S_{LCA} cells (fold change) to weak organic acids categorized based on the similarity of their chemical structures. GFP fluorescence was measured after overnight incubation at 30°C and normalized to cell density (OD600) and further to control without weak organic acid supply. Values are the means of three independent experiments, and an error bar represents a standard deviation of three independent experiments. **(B)** Molecular structures of the tested weak acids, comprising of shorter straight chain fatty acids (I), and lipophilic carboxylic acid derivatives including SBCFAs (II), phenolic acids (III), methacrylic acid (IV), hydroxy carboxylic acid (V), keto acids (VI) and amino acid Leucine (VII). Their numbers are indicated, and SBCFAs are highlighted in red.

methyl, oxo, phenyl, hydroxyl and amino) were substrates of the biosensor BY4741-S_{LCA}, we investigated its response to acetic (C2), propionic (C3) and octanoic (C8) acids and several lipophilic carboxylic acid derivatives (**Figure 2**). We found that S_{LCA} was responsive to propionic acid (FC 3.8) and octanoic acid (FC 34.0), but not acetic acid. This result suggests that the pPDR12-based genetic biosensor respond to linear chain fatty acids with 3 carbons (C3) and longer. In addition, the biosensor S_{LCA} showed a strong response (FC 40.0), consistent with a previous study (Baumann et al., 2018).

For methacrylic acid, a lipophilic carboxylic acid derivative with a vinyl group, a significant response was observed from the biosensor (FC 17.7). In line with previous studies (Hatzixanthis et al., 2003; Kren et al., 2003), the biosensor showed an FC 55.6 in response to benzoic acid (with a phenyl group) and an FC 38.0 in response to cinnamic acid (with a phenyl and a vinyl group). To our knowledge, this is the first evidence on sensing cinnamic acid using the pPDR12-based system in *S. cerevisiae*. We did not observe any responses (FC < 2.0) to the SBCFA's precursors including L-leucine (with an amino group) and 4-methyl 2-oxovalerate (with a methyl and an oxo group), as well as hydroxylated derivatives including hydroxy isovaleric acid, hydroxy benzoic acid and coumaric acid. **Supplementary Table S2** shows that some carboxylic acids (e.g., hydroxy isovaleric acid and 4-oxo pentanoic acid) have a relatively low hydrophobic constant (logP), i.e., a relatively low solubility in the medium. Interestingly, coumaric acid and hydroxy benzoic acid have high logP values. The lack of response to these compounds might be due to their low intracellular concentration caused either by low uptake, high efflux, or cellular metabolism (Barnhart-Dailey et al., 2019).

Optimization of the SBCFA Biosensor by *PDR12* Deletion and Overexpression

Given the role of transporters in regulating the intracellular level of SBCFAs (Piper et al., 1998; Nygard et al., 2014), we examined the effect of deleting and overexpressing an efflux pump gene *PDR12* on the S_{LCA}'s behaviors (sensitivity and operational range). We hypothesized that the deletion of *PDR12* would result in a higher intracellular level of SBCFAs than that in the wild-type cells and *vice versa* for *PDR12* overexpression.

Based on the above hypothesis, we sought to enhance the biosensor's sensitivity through *PDR12* deletion and to shift the operational range through *PDR12* overexpression (**Figure 4A**). Firstly, we deleted *PDR12* gene (**Supplementary Figure S1**) and examined its effect on cell growth in the presence of 15 mM IVA. We found that the *PDR12*-deficient strain (TDL01) had a slight growth retardation after 12 h in the absence of IVA. In the presence of IVA, TDL01 showed a significant growth retardation till the log-phase when it had a cell density comparable to its parental strain BY4741 (**Supplementary**

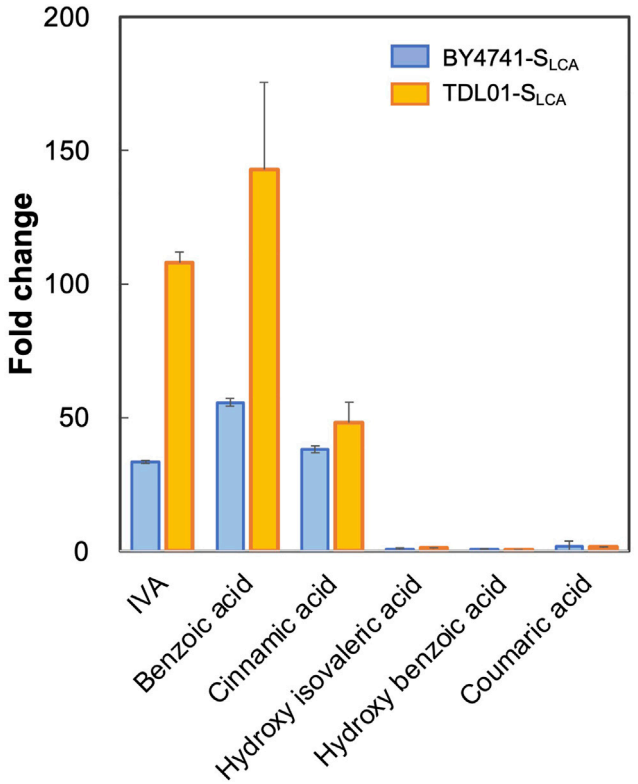

FIGURE 3 | Responses of biosensor TDL01-S_{LCA} with *PDR12* gene deletion to representative weak organic acid including IVA, benzoic acid, cinnamic acid, hydroxy isovaleric acid, hydroxy benzoic acid and coumaric acid. BY4741-S_{LCA} and TDL01-S_{LCA} cells were grown until the exponential phase. After a 16-h incubation in a buffered SCD-U medium (at pH6.5) with the supply of weak organic acids (2 mM each), GFP fluorescence was measured, and fold changes were calculated. Values are means of three independent experiments, and an error bar represents standard deviation of three independent experiments.

Figure S4). The significant growth retardation suggests a growth inhibition caused by the higher intracellular IVA accumulated in TDL01. Secondly, we introduced the biosensor plasmid pPDR12-GFP into TDL01 and measured the FC of the resulting strain TDL-S_{LCA}. TDL-S_{LCA} was found to have a response of FC 107.9 to 2 mM IVA, which is over 3-fold higher than BY4741 (FC 33.4). The increase in response to IVA in TDL-S_{LCA} confirms the significant improvement in sensitivity. In addition, there was an increase in response by about three times to 2 mM of benzoic acid and a slight increase against cinnamic acid. We observed no change in the response toward other carboxylic acids (i.e., hydroxyl isovaleric acid, hydroxyl benzoic acid and coumaric acid) (**Figure 3**). These results show that the *PDR12* deletion improves the sensitivity of the pPDR12-GFP biosensor to its target sensing substrates. Thirdly, to evaluate the operational range of the biosensor, we investigated its response to IVA at various doses in the *PDR12*-deficient (TDL01) and -overexpressing (TOE01) strains (**Figure 4B** and **Supplementary Figure S1**). Given a higher expression level of *PDR12* upon the replacement of pPDR12 with the TEF1 promoter (pTEF1) in *S. cerevisiae* (Yu et al., 2016), in the absence of exogenous IVA supply, the biosensor TOE01-S_{LCA} showed the lowest background fluorescence in SCD medium (**Supplementary Figure S5**). TOE01-S_{LCA} showed a shift of the operational range towards higher concentrations to exogenous IVA (2–25 mM) compared to BY4741-S_{LCA} (Control). Given that the response was not saturated at 25 mM IVA, there would be a continuing increase of the response to IVA at >25 mM. Thus, we speculated an operational range that is wider than 2–25 mM. TDL01-S_{LCA} showed a higher sensitivity (up to FC18.9) toward exogenous IVA (0.2–10 mM). EC_{50} of TDL01-S_{LCA} (1.3 mM) was 7.7-fold lower than that of BY4741-S_{LCA} (10 mM).

The higher sensitivity (TDL01-S_{LCA}) and wider operational range (TOE01-S_{LCA}) could be due to changes in export efficiency caused by *PDR12* overexpression and deletion. Our results suggest that maintenance of the appropriate intracellular level of target biochemical can be used to enhance the operational range or widen the sensitivity of a whole-cell biosensor. Whole-cell biosensors with various operational ranges or sensitivities are desired for pathway engineering and strain optimization. For instance, at the early stage of pathway engineering when the production level of target biochemical is low, a biosensor with a higher sensitivity like TDL01-S_{LCA} is favored for screening strain screening. On the other hand, at a later stage, a biosensor with a wider operational range like TOE01-S_{LCA} is suitable for optimizing the production to achieve a higher production level.

Sensing of SBCFAs in the SBCFAs-Overproducing Strain

After we studied S_{LCA}'s responses to exogenously supplied SBCFAs, we used it to sense SBCFAs in an SBCFA-overproducing strain. We previously engineered *S. cerevisiae* BY4741 (4G-ΔADH6) to overproduce SBCFAs at up to 3.7 mM SBCFAs (Yu et al., 2016). Given that the intracellular level of SBCFAs lies within the identified operational range of TDL01-S_{LCA} (0.2–10 mM), we employed the strategy of *PDR12* deletion for the biosensing. To this end, we deleted *PDR12* in 4G-ΔADH6, resulting in TDL02. Next, we introduced the pPDR12-GFP plasmid into 4G-ΔADH6, TDL02 and analyzed the fluorescence signals of the resulting strains 4G-ΔADH6-S_{LCA} and TDL02-S_{LCA}.

Figure 5A shows that the fluorescence signal of 4G-ΔADH6-S_{LCA} intensified with the increase in SBCFA production. The fluorescence signal of TDL02-S_{LCA} also showed an increase along with the SBCFA production, but up to 76.7% higher than 4G-ΔADH6-S_{LCA}. The fluorescence signal of both 4G-ΔADH6-S_{LCA} and TDL02-S_{LCA} showed a linear correlation to the produced SBCFAs (R^2 > 0.93) (**Figure 5B**). Given that the SBCFA production level is comparable in 4G-ΔADH6 and TDL02, the fluorescence signal suggests the biosensor S_{LCA} can monitor the SBCFA production real-time and the *PDR12* deletion enhances the sensitivity of the biosensor in the SBCFA-overproducing strain. The sensitivity enhancement is consistent with BY4741 and TDL01 with SBCFA supplementation. At 48 h, the signal of TDL02-S_{LCA} is slightly lower than

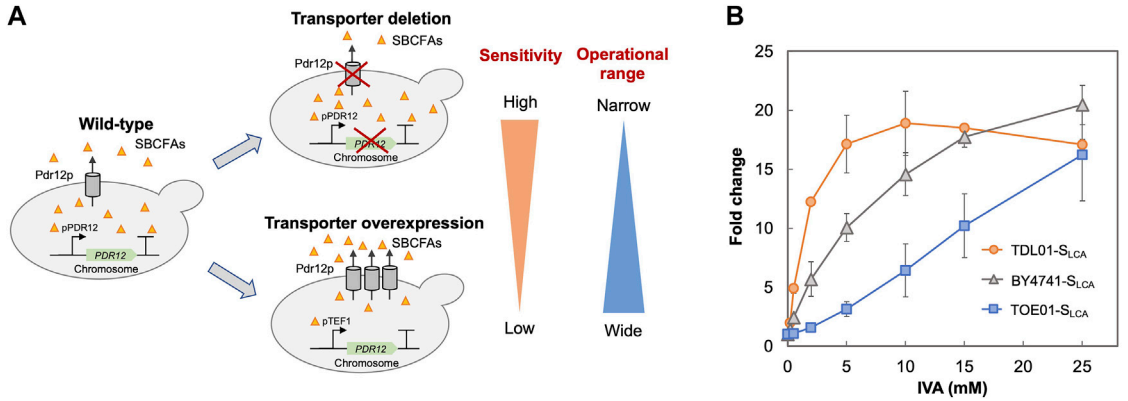

FIGURE 4 | Optimization of biosensor's sensitivity and operational range. **(A)** Schematic presentation of strategies employed to optimize the biosensor. The ABC transporter Pdr12p is known to regulate the intracellular level of weak organic acids by export. To improve the biosensor's sensitivity, an ABC transporter gene *PDR12* was deleted to increase the intracellular SBCFA level (TDL-S_{LCA}), which will increase the fluorescence. To extend the biosensor's operational range, *PDR12* was over-expressed under the control of a strong constitutive promoter pTEF1 to reduce the intracellular SBCFA level (TOE-S_{LCA}) through SBCFA export, which will enhance the SBCFA saturation level. **(B)** Dose-dependent responses of biosensors against IVA fed at 0.5, 2, 5, 10, and 25 mM. Their responses (fold change) were compared to control BY4741-S_{LCA}. Fluorescence was measured after a 5-h incubation with IVA. Values are the means of three independent experiments, and an error bar represents a standard deviation of three independent experiments.

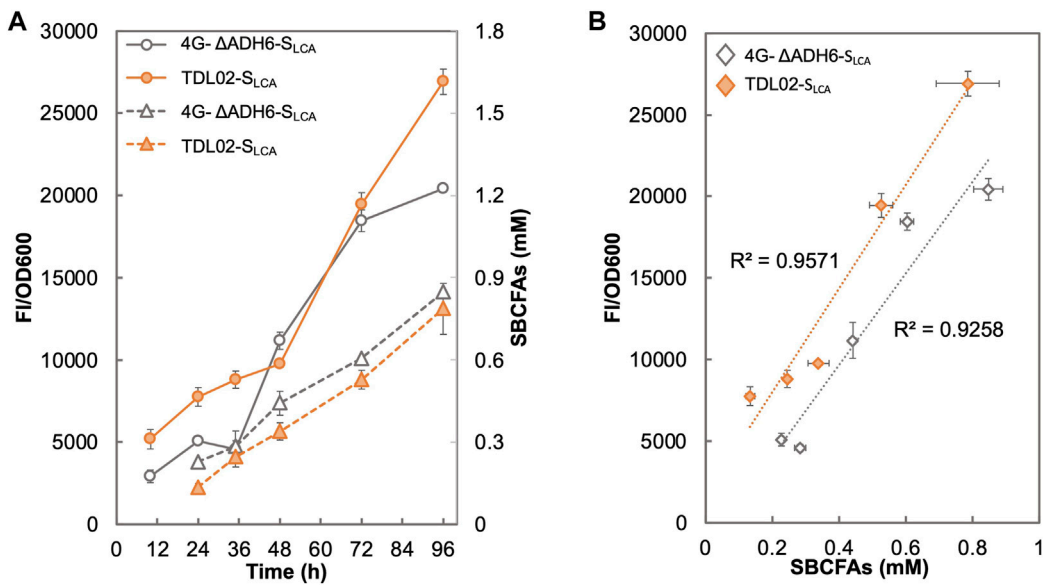

FIGURE 5 | Responses of SBCFA biosensor in a *S. cerevisiae* strain overproducing SBCFAs. *PDR12* was deleted in a previously engineered SBCFA-overproducing strain 4G-ΔADH6, resulting in strain TDL02. The biosensor S_{LCA} was introduced into TDL02 and 4G-ΔADH6 respectively. **(A)** The fluorescence (solid lines) and the over-produced SBCFAs (dotted lines) were measured after fermentation in buffered SCD-U (at pH6.5) medium for up to 96 h. **(B)** Correlation between GFP fluorescence with SBCFAs produced in 4G-ΔADH6-S_{LCA} and TDL02-S_{LCA}. Trendlines with respective R^2 value are shown in orange (4G-ΔADH6-S_{LCA}) and grey (TDL02-S_{LCA}). Values are the means of three independent experiments, and an error bar represents a standard deviation of three independent experiments.

4G-ΔADH6-S_{LCA}, likely due to a slightly lower SBCFA production in TDL02-S_{LCA} (0.34 mM) than 4G-ΔADH6-S_{LCA} (0.44 mM) (**Supplementary Figure S6**).

In terms of the biosensing substrates, TDL02-S_{LCA} and 4G-ΔADH6-S_{LCA} sensed the mixture of SBCFAs, where the fluorescence signal attributes to the responses from such a mixture of SBCFAs. However, the contribution of each SBCFA in the mixture to the fluorescence is still unclear. In addition, we observed a 3-fold lower SBCFA titer in both 4G-ΔADH6 and TDL02 and a lower proportion of IVA/2MBA than those reported in our previous study (Yu et al., 2016). Such changes in the production titer and SBCFA profiles could be due to the use of a defined medium SCD that allows the SBCFA production from glucose, whereas in our previous study, the SBCFAs were likely produced from glucose and branched-chain amino acids present in YPD medium. Nevertheless, the SBCFA levels obtained using SCD were shown to lie within the

operational range of our biosensor TDL01-S_{LCA} which allows real-time monitoring of the SBCFA production in the engineered strains.

CONCLUSION

In this study, we engineered a genetic biosensor based on War1p and pPDR12. The biosensor detected SBCFAs (e.g., IVA, IBA and 2MBA) that were exogenously fed and intracellularly produced by engineered *S. cerevisiae* strains. The biosensor's properties including sensitivity and operational range were optimized by varying the expression level of *PDR12* encoding an ABC transporter responsible for SBCFA export. Besides SBCFAs, the biosensor can also sense short linear chain fatty acids and lipophilic carboxylic acid derivatives. Our findings suggest that the engineered biosensor is potentially a useful tool for monitoring the production of biochemicals, such as IVA, IBA, 2MBA, benzoic acid, cinnamic acid, propionic acid and octanoic acid, and for screening and discovering high producer strains.

Given the low sensitivity observed when the SBCFAs were at low concentrations (<0.25 mM), future efforts could be focused on improving the sensitivity. One strategy could be to introduce a positive-feedback loop on War1p to enhance the sensitivity. Williams et al. reported that the promoter replacement of the *WAR1* promoter with pPDR12 in the genome, where War1p regulates its own expression in response to propionic acid (Williams et al., 2017), resulting in a dramatic increase in the sensitivity (from FC 3.6 to FC 10). In our current study, we confirmed an operational range of up to ~0.8 mM of the intracellularly produced SBCFA mixture. To effectively detect SBCFAs produced by a higher producer, the operational range could be further evaluated and improved through optimization of the binding affinity between SBCFAs and the receptor domain of War1p, DNA binding domain of War1p or WARE sequence of pPDR12 (Gregori et al., 2008).

DATA AVAILABILITY STATEMENT

The original contributions presented in the study are included in the article/**Supplementary Material**, further inquiries can be directed to the corresponding author.

AUTHOR CONTRIBUTIONS

RM designed and performed the study. RM and HL wrote the manuscript. HL, JF, NF, and MC analyzed the data and edited the manuscript. MC supervised the study. All authors have read and agreed to the published version of the manuscript.

FUNDING

This work was supported by Mitsubishi Chemical Corporation (2019-0449), the NUS Medicine Synthetic Biology Translational Research Programme (NUHSRO/2020/077/MSC/02/SB), the Summit Research Program of the National University Health System (NUHSRO/2016/053/SRP/05), the Synthetic Biology Initiative of the National University of Singapore (DPRT/943/09/14), the Synthetic Biology R&D Programme (SBP-P2, SBP-P7, SBP-P9), the U.S. Army (ARO/2019/74459LS) and the Ministry of Education, Singapore (NUHSRO/2020/046/T1/3). We thank Ms. Sofia Sigal-Passeck for assisting in strain characterization and fluorescence measurements.

SUPPLEMENTARY MATERIAL

The Supplementary Material for this article can be found online at: https://www.frontiersin.org/articles/10.3389/fbioe.2022.838732/full#supplementary-material

REFERENCES

Barnhart-Dailey, M. C., Ye, D., Hayes, D. C., Maes, D., Simoes, C. T., Appelhans, L., et al. (2019). Internalization and Accumulation of Model Lignin Breakdown Products in Bacteria and Fungi. *Biotechnol. Biofuels* 12, 175. doi:10.1186/s13068-019-1494-8

Baumann, L., Rajkumar, A. S., Morrissey, J. P., Boles, E., and Oreb, M. (2018). A Yeast-Based Biosensor for Screening of Short- and Medium-Chain Fatty Acid Production. *ACS Synth. Biol.* 7, 2640–2646. doi:10.1021/acssynbio.8b00309

Borrull, A., López-Martínez, G., Poblet, M., Cordero-Otero, R., and Rozès, N. (2015). New Insights into the Toxicity Mechanism of Octanoic and Decanoic Acids onSaccharomyces Cerevisiae. *Yeast* 32, 451–460. doi:10.1002/yea.3071

Casal, M., Paiva, S., Queirós, O., and Soares-Silva, I. (2008). Transport of Carboxylic Acids in Yeasts. *FEMS Microbiol. Rev.* 32, 974–994. doi:10.1111/j.1574-6976.2008.00128.x

Castaño-Cerezo, S., Fournié, M., Urban, P., Faulon, J. L., and Truan, G. (2019). Development of a Biosensor for Detection of Benzoic Acid Derivatives in *Saccharomyces cerevisiae*. *Front. Bioeng. Biotechnol.* 7, 372. doi:10.3389/fbioe.2019.00372

Chen, B., Lee, H. L., Heng, Y. C., Chua, N., Teo, W. S., Choi, W. J., et al. (2018). Synthetic Biology Toolkits and Applications in *Saccharomyces cerevisiae*. *Biotechnol. Adv.* 36, 1870–1881. doi:10.1016/j.biotechadv.2018.07.005

Chen, Y., and Nielsen, J. (2016). Biobased Organic Acids Production by Metabolically Engineered Microorganisms. *Curr. Opin. Biotechnol.* 37, 165–172. doi:10.1016/j.copbio.2015.11.004

D'Ambrosio, V., Pramanik, S., Goroncy, K., Jakočiūnas, T., Schönauer, D., Davari, M. D., et al. (2020). Directed Evolution of VanR Biosensor Specificity in Yeast. *Biotechnol. Notes* 1, 9–15. doi:10.1016/j.biotno.2020.01.002

Dabirian, Y., Li, X., Chen, Y., David, F., Nielsen, J., and Siewers, V. (2019). Expanding the Dynamic Range of a Transcription Factor-Based Biosensor in *Saccharomyces cerevisiae*. *ACS Synth. Biol.* 8, 1968–1975. doi:10.1021/acssynbio.9b00144

Gietz, R. D., and Schiestl, R. H. (2007). High-efficiency Yeast Transformation Using the LiAc/SS Carrier DNA/PEG Method. *Nat. Protoc.* 2, 31–34. doi:10.1038/nprot.2007.13

Gregori, C., Schüller, C., Frohner, I. E., Ammerer, G., and Kuchler, K. (2008). Weak Organic Acids Trigger Conformational Changes of the Yeast Transcription Factor War1 *In Vivo* to Elicit Stress Adaptation. *J. Biol. Chem.* 283, 25752–25764. doi:10.1074/jbc.m803095200

Gueldener, U., Heinisch, J., Koehler, G. J., Voss, D., and Hegemann, J. H. (2002). A Second Set of loxP Marker Cassettes for Cre-Mediated Multiple Gene Knockouts in Budding Yeast. *Nucleic Acids Res.* 30, e23. doi:10.1093/nar/30.6.e23

Hammer, S. K., Zhang, Y., and Avalos, J. L. (2020). Mitochondrial Compartmentalization Confers Specificity to the 2-ketoacid Recursive

Pathway: Increasing Isopentanol Production in *Saccharomyces cerevisiae*. *ACS Synth. Biol.* 9, 546–555. doi:10.1021/acssynbio.9b00420

Hatzixanthis, K., Mollapour, M., Seymour, I., Bauer, B. E., Krapf, G., Schüller, C., et al. (2003). Moderately Lipophilic Carboxylate Compounds Are the Selective Inducers of theSaccharomyces cerevisiaePdr12p ATP-Binding Cassette Transporter. *Yeast* 20, 575–585. doi:10.1002/yea.981

Hegemann, J. H., and Heick, S. B. (2011). Delete and Repeat: a Comprehensive Toolkit for Sequential Gene Knockout in the Budding Yeast *Saccharomyces cerevisiae*. *Methods Mol. Biol.* 765, 189–206. doi:10.1007/978-1-61779-197-0_12

Hossain, G. S., Saini, M., Miyake, R., Ling, H., and Chang, M. W. (2020). Genetic Biosensor Design for Natural Product Biosynthesis in Microorganisms. *Trends Biotechnol.* 38, 797–810. doi:10.1016/j.tibtech.2020.03.013

Jung, H., Ling, H., Tan, Y. Q., Chua, N. H., Yew, W. S., and Chang, M. W. (2021). Heterologous Expression of Cyanobacterial Gas Vesicle Proteins in *Saccharomyces cerevisiae*. *Biotechnol. J.* 16, e2100059. doi:10.1002/biot.202100059

Kim, M. S., Cho, K. H., Park, K. H., Jang, J., and Hahn, J.-S. (2019). Activation of Haa1 and War1 Transcription Factors by Differential Binding of Weak Acid Anions inSaccharomyces Cerevisiae. *Nucleic Acids Res.* 47, 1211–1224. doi:10.1093/nar/gky1188

Kren, A., Mamnun, Y. M., Bauer, B. E., Schüller, C., Wolfger, H., Hatzixanthis, K., et al. (2003). War1p, a Novel Transcription Factor Controlling Weak Acid Stress Response in Yeast. *Mol. Cell Biol* 23, 1775–1785. doi:10.1128/mcb.23.5.1775-1785.2003

Kwon, D. Y., Hong, Y.-J., and Yoon, S. H. (2000). Enantiomeric Synthesis of (S)-2-methylbutanoic Acid Methyl Ester, Apple Flavor, Using Lipases in Organic Solvent. *J. Agric. Food Chem.* 48, 524–530. doi:10.1021/jf990871w

Lang, K., Zierow, J., Buehler, K., and Schmid, A. (2014). Metabolic Engineering of Pseudomonas Sp. Strain VLB120 as Platform Biocatalyst for the Production of Isobutyric Acid and Other Secondary Metabolites. *Microb. Cell Fact* 13, 2. doi:10.1186/1475-2859-13-2

Lim, H. G., Jang, S., Jang, S., Seo, S. W., and Jung, G. Y. (2018). Design and Optimization of Genetically Encoded Biosensors for High-Throughput Screening of Chemicals. *Curr. Opin. Biotechnol.* 54, 18–25. doi:10.1016/j.copbio.2018.01.011

Ling, H., Pratomo Juwono, N. K., Teo, W. S., Liu, R., Leong, S. S. J., and Chang, M. W. (2015). Engineering Transcription Factors to Improve Tolerance against Alkane Biofuels in *Saccharomyces cerevisiae*. *Biotechnol. Biofuels* 8, 231. doi:10.1186/s13068-015-0411-z

Mollapour, M., and Piper, P. W. (2012). Activity of the Yeast Zinc-finger Transcription Factor War1 Is Lost with Alanine Mutation of Two Putative Phosphorylation Sites in the Activation Domain. *Yeast* 29, 39–44. doi:10.1002/yea.1915

Ng, T.-K., Yu, A.-Q., Ling, H., Pratomo Juwono, N. K., Choi, W. J., Leong, S. S. J., et al. (2020). Engineering *Yarrowia Lipolytica* towards Food Waste Bioremediation: Production of Fatty Acid Ethyl Esters from Vegetable Cooking Oil. *J. Biosci. Bioeng.* 129, 31–40. doi:10.1016/j.jbiosc.2019.06.009

Nygård, Y., Mojzita, D., Toivari, M., Penttilä, M., Wiebe, M. G., and Ruohonen, L. (2014). The Diverse Role of Pdr12 in Resistance to Weak Organic Acids. *Yeast* 31, 219–232. doi:10.1002/yea.3011

Piper, P., Mahe, Y., Thompson, S., Pandjaitan, R., Holyoak, C., Egner, R., et al. (1998). The Pdr12 ABC Transporter Is Required for the Development of Weak Organic Acid Resistance in Yeast. *EMBO J.* 17, 4257–4265. doi:10.1093/emboj/17.15.4257

Raman, S., Rogers, J. K., Taylor, N. D., and Church, G. M. (2014). Evolution-guided Optimization of Biosynthetic Pathways. *Proc. Natl. Acad. Sci. USA* 111, 17803–17808. doi:10.1073/pnas.1409523111

Sauer, M., Porro, D., Mattanovich, D., and Branduardi, P. (2008). Microbial Production of Organic Acids: Expanding the Markets. *Trends Biotechnol.* 26, 100–108. doi:10.1016/j.tibtech.2007.11.006

Sheff, M. A., and Thorn, K. S. (2004). Optimized Cassettes for Fluorescent Protein Tagging inSaccharomyces Cerevisiae. *Yeast* 21, 661–670. doi:10.1002/yea.1130

Shi, J., Zhan, Y., Zhou, M., He, M., Wang, Q., Li, X., et al. (2019). High-level Production of Short Branched-Chain Fatty Acids from Waste Materials by Genetically Modified *Bacillus Licheniformis*. *Bioresour. Technol.* 271, 325–331. doi:10.1016/j.biortech.2018.08.134

Snoek, T., Chaberski, E. K., Ambri, F., Kol, S., Bjørn, S. P., Pang, B., et al. (2020). Evolution-guided Engineering of Small-Molecule Biosensors. *Nucleic Acids Res.* 48, e3. doi:10.1093/nar/gkz954

Suerbaev, K. A., Chepaikin, E. G., and Zhaksylykova, G. Z. (2012). Hydromenthoxycarbonylation of Isobutylene in the Presence of Tetrakis(triphenylphosphine)palladium-Based Catalyst Systems. *Pet. Chem.* 52, 422–425. doi:10.1134/s0965544112060126

Taylor, N. D., Garruss, A. S., Moretti, R., Chan, S., Arbing, M. A., Cascio, D., et al. (2016). Engineering an Allosteric Transcription Factor to Respond to New Ligands. *Nat. Methods* 13, 177–183. doi:10.1038/nmeth.3696

Teo, W. S., and Chang, M. W. (2015). Bacterial XylRs and Synthetic Promoters Function as Genetically Encoded Xylose Biosensors inSaccharomyces Cerevisiae. *Biotechnol. J.* 10, 315–322. doi:10.1002/biot.201400159

Teo, W. S., Ling, H., Yu, A.-Q., and Chang, M. W. (2015). Metabolic Engineering of *Saccharomyces cerevisiae* for Production of Fatty Acid Short- and Branched-Chain Alkyl Esters Biodiesel. *Biotechnol. Biofuels* 8, 177. doi:10.1186/s13068-015-0361-5

Wang, Y., He, L., Pan, Q., Duan, C., and Wang, J. (2018). Effects of Basal Defoliation on Wine aromas: A Meta-Analysis. *Molecules* 23, 779. doi:10.3390/molecules23040779

Williams, T. C., Xu, X., Ostrowski, M., Pretorius, I. S., and Paulsen, I. T. (2017). Positive-feedback, Ratiometric Biosensor Expression Improves High-Throughput Metabolite-Producer Screening Efficiency in Yeast. *Synth. Biol. (Oxf)* 2, ysw002. doi:10.1093/synbio/ysw002

Xia, P.-F., Ling, H., Foo, J. L., and Chang, M. W. (2019). Synthetic Genetic Circuits for Programmable Biological Functionalities. *Biotechnol. Adv.* 37, 107393. doi:10.1016/j.biotechadv.2019.04.015

Yu, A.-Q., Pratomo Juwono, N. K., Foo, J. L., Leong, S. S. J., and Chang, M. W. (2016). Metabolic Engineering of *Saccharomyces cerevisiae* for the Overproduction of Short Branched-Chain Fatty Acids. *Metab. Eng.* 34, 36–43. doi:10.1016/j.ymben.2015.12.005

Zhang, K., Woodruff, A. P., Xiong, M., Zhou, J., and Dhande, Y. K. (2011). A Synthetic Metabolic Pathway for Production of the Platform Chemical Isobutyric Acid. *ChemSusChem* 4, 1068–1070. doi:10.1002/cssc.201100045

Conflict of Interest: Authors RM and NF were employed by company Mitsubishi Chemical Corporation.

The remaining authors declare that the research was conducted in the absence of any commercial or financial relationships that could be construed as a potential conflict of interest.

Publisher's Note: All claims expressed in this article are solely those of the authors and do not necessarily represent those of their affiliated organizations, or those of the publisher, the editors and the reviewers. Any product that may be evaluated in this article, or claim that may be made by its manufacturer, is not guaranteed or endorsed by the publisher.

frontiers in Bioengineering and Biotechnology

ORIGINAL RESEARCH
published: 31 March 2022
doi: 10.3389/fbioe.2022.837720

Comparison of the Unfolded Protein Response in Cellobiose Utilization of Recombinant Angel- and W303-1A-Derived Yeast Expressing β-Glucosidase

Shaolan Zou[1,2,3]*, *Yudie Jia*[1,2], *Qing He*[2], *Kun Zhang*[1,4], *Rui Ban*[2], *Jiefang Hong*[1,2,3]* and *Minhua Zhang*[1,2,3]

[1]Tianjin R&D Center for Petrochemical Technology, Tianjin University, Tianjin, China, [2]School of Chemical Engineering and Technology, Tianjin University, Tianjin, China, [3]Key Laboratory for Green Chemical Technology of Ministry of Education, Tianjin University, Tianjin, China, [4]School of Pharmaceutical Science and Technology, Tianjin University, Tianjin, China

OPEN ACCESS

Edited by:
Shuobo Shi,
Beijing University of Chemical Technology, China

Reviewed by:
Tsutomu Tanaka,
Kobe University, Japan
Jonathan Galazka,
National Aeronautics and Space Administration (NASA), United States
Guiyang Shi,
Jiangnan University, China

***Correspondence:**
Shaolan Zou
slzhou@tju.edu.cn
Jiefang Hong
hjf@tju.edu.cn

Specialty section:
This article was submitted to Synthetic Biology, a section of the journal Frontiers in Bioengineering and Biotechnology

Received: 17 December 2021
Accepted: 07 March 2022
Published: 31 March 2022

Citation:
Zou S, Jia Y, He Q, Zhang K, Ban R, Hong J and Zhang M (2022) Comparison of the Unfolded Protein Response in Cellobiose Utilization of Recombinant Angel- and W303-1A-Derived Yeast Expressing β-Glucosidase. Front. Bioeng. Biotechnol. 10:837720. doi: 10.3389/fbioe.2022.837720

The unfolded protein response (UPR) is one of the most important protein quality control mechanisms in cells. At least, three factors are predicted to activate the UPR in yeast cells during fermentation. Using UPRE-*lacZ* as a reporter, we constructed two indicator strains, KZ and WZ, based on Angel-derived K-a and W303-1A strains, respectively, and investigated their UPR response to tunicamycin, ethanol, and acetic acid. Then, four strains carrying plasmids BG-cwp2 and BG were obtained to realize the displaying and secretion of β-glucosidase, respectively. The results of cellobiose utilization assays indicated interactions between the UPR and the metabolic burden between the strain source, anchoring moiety, oxygen supply, and cellobiose concentration. Meanwhile, as expected, growth (OD_{600}), β-glucosidase, and β-galactosidase activities were shown to have a positive inter-relationship, in which the values of the KZ-derived strains were far lower than those of the WZ-derived strains. Additionally, extra metabolic burden by displaying over secreting was also much more serious in strain KZ than in strain WZ. The maximum ethanol titer of the four strains (KZ (BG-cwp2), KZ (BG), WZ (BG-cwp2), and WZ (BG)) in oxygen-limited 10% cellobiose fermentation was 3.173, 5.307, 5.495, and 5.486% (v/v), respectively, and the acetic acid titer ranged from 0.038 to 0.060% (v/v). The corresponding maximum values of the ratio of β-galactosidase activity to that of the control were 3.30, 5.29, 6.45, and 8.72, respectively. Under aerobic conditions with 2% cellobiose, those values were 3.79, 4.97, 6.99, and 7.67, respectively. A comparison of the results implied that β-glucosidase expression durably induced the UPR, and the effect of ethanol and acetic acid depended on the titer produced. Further study is necessary to identify ethanol- or acid-specific target gene expression. Taken together, our results indicated that the host strain W303-1A is a better secretory protein producer, and the first step to modify strain K-a for cellulosic ethanol fermentation would be to relieve the bottleneck of UPR capacity. The results of the present study will help to identify candidate host strains and optimize expression and fermentation by quantifying UPR induction.

Keywords: recombinant yeast, UPRE-*lacZ*, β-glucosidase, displaying and secreting, cellobiose, ethanol and acid, UPR response, metabolic burden

1 INTRODUCTION

Saccharomyces cerevisiae is one of the most widely used cell factories and is utilized in biotechnological processes including the production of heterologous proteins, biofuels, and chemicals of medical or industrial interest (Jouhten et al., 2016; Lian et al., 2018; Thak et al., 2020). In synthetic biology and metabolic engineering applications, yeast not only faces many kinds of stress, such as osmotic, heat, inhibitor, and nutrient starvation stress, but also endures a metabolic burden resulting from the heterologous production of enzymes to broaden the yeast's substrate or product range (Mattanovich et al., 2004; Wu et al., 2016; Brandt et al., 2021).

Protein synthesis, folding, and processing are tightly controlled and are sensitive to perturbation of endoplasmic reticulum (ER) homeostasis in all organisms. The unfolded protein response (UPR) is a conserved intracellular signaling pathway that regulates the transcription of ER homoeostasis-related genes (Dallbey et al., 2009; Young and Robinson, 2014). *S. cerevisiae* is a major model for studying UPR mechanisms. Research has focused on protein quality control pathways and mechanisms using endogenous or exogenous protein expression in yeast (Dallbey et al., 2009; Young and Robinson, 2014; Cedras et al., 2019; Sun and Brodsky, 2019). However, in recent years, other factors have been reported to induce the UPR (Navarro-Tapia et al., 2016; Kawazoe et al., 2017; Navarro-Tapia et al., 2018). Ethanol stress has been shown to alter membrane fluidity, which then activates the UPR; thus, ethanol tolerance might be improved by enhancing the UPR (Navarro-Tapia et al., 2016; Navarro-Tapia et al., 2018). Acetic acid has also been demonstrated to cause ER stress and lead to UPR (Kawazoe et al., 2017).

In fact, the UPR is so important that it is increasingly becoming a limiting factor in the exploitation of yeast. Quantification of UPR induction and modulation of the UPR and ER-Associated Degradation (ERAD) activity is increasingly applied in yeast synthetic biology and metabolic engineering (Cedras et al., 2019; Thak et al., 2020). However, current knowledge about the UPR pathway and its mechanism in yeast is inadequate, especially the regulatory role of the UPR underlying stress adaptation, the metabolic burden, and their mutual interaction.

In the bio-energy field, although *S. cerevisiae* is the preferred microorganism in various biofuel production configurations, its application in second-generation (2G) fermentation involving lignocellulose conversion remains challenging (Lian et al., 2018; Brandt et al., 2021). One of the key difficulties is the low titer of cellulase expression, which is reported to possibly be limited by the UPR or ERAD or both (Davison et al., 2020). Furthermore, because ethanol and acetic acid are constantly present, either as a target in the bio-energy field or as the main by-product in other application fields (Navarro-Tapia et al., 2016; Kawazoe et al., 2017; Navarro-Tapia et al., 2018), the role of ethanol and acetic acid and their mutual interaction with other activators in the UPR are also important.

β-Glucosidase is an essential and key component in lignocellulose bio-conversion and is also an important enzyme in medicine and industry (Bhatia et al., 2002; Wang et al., 2013; Ding et al., 2018). The expression of β-glucosidase in yeast leads to enzyme production or the production of whole cell biocatalysts for cellulosic ethanol fermentation (Wang et al., 2013; Ding et al., 2018; Cedras et al., 2019; Davison et al., 2020). The haploid strain K-a is derived from the diploid industrial yeast strain TH-AADY (Angel Yeast Co., Ltd., Yichang, China) and has been proven to have good ethanol fermentative performance and stress resistance. Thus, in this study, the enzyme BGLI (β-glucosidase) from *Aspergillus aculeatus* was selected as a reporter protein to investigate the effects on the UPR of genetically different host strains (industrial K-a and a laboratory strain W303-1A), heterologous enzyme expression, displaying or secreting mode, and fermentation conditions. Then, the unfolded protein response element (UPRE)-*lac*Z was used as a reporter gene to evaluate the UPR (Amberg and Huo, 2009; Dallbey et al., 2009). In the present study, the UPRE was a hybrid promoter and contained a 22-base pair sequences, which allows Hac1p (a UPR-associated transcription factor) binding to activate the UPR (Dallbey et al., 2009). Assays to measure β-galactosidase activity were performed to determine the UPR induction levels (Amberg and Huo, 2009). In addition, 2 and 10% cellobiose were used to observe the possible effects from metabolic products, including ethanol and acetic acid. The relative expression of several key target genes was further investigated. The results of this study are expected to assist in identifying candidate host strains and for optimizing the expression mode and fermentation condition by quantifying UPR induction.

2 MATERIALS AND METHODS

2.1 Strains, Plasmids, Media, and Growth Conditions

The microbial strains and plasmids used in this study are listed in **Table 1** (Wang et al., 2013; Ding et al., 2018; Lu et al., 2019; Zhang et al., 2020). *Escherichia coli* Top10 was used for recombinant DNA manipulation. Recombinant plasmids were constructed and amplified in Top10 cultivated at 37°C in a Luria-Bertani liquid medium or on Luria-Bertani agar (1% tryptone, 1% NaCl and 0.5% yeast extract, pH7.0). Ampicillin was used at a final concentration of 100 g/L. WZ, that was W303-1A (*leu* 2::UPRE-*lac*Z) (Zhang et al., 2020), was constructed by integrating the donor DNA fragment UPRE-*lac*Z into gene *leu* 2 site with the CRISPR-Cas9 method (Lu et al., 2019). The haploid yeast strain K-a, obtained by the sporulation of the commercial Angel yeast strain TH-AADY (diploid, Alcohol active dry yeast, Angel Yeast Co., Ltd., Yichang, China, http://www.angelyeast.com) and then counter selection on a 5′-FOA plate, was used as the host to express exogenous cellulases (Lu et al., 2019; Zou et al., 2021). Yeast strains were generally cultivated at 30°C in rich YPD or YPC medium (1% yeast extract, 2% peptone, 2% glucose or cellobiose), or basal CMG or CMC medium (6.7 g/L yeast nitrogen base without amino acids, 20 g/L glucose or cellobiose, and the appropriate amino acid and nucleic acid supplements) (Wang et al., 2013).

TABLE 1 | Microbial strains, plasmids, and primers used in this study.

Strains/plasmids/ primers	Essential properties	Source or reference
Escherichia coli Top10	F⁻ *mcr*A (*mrr-hsd* RMS-*mcr*BC)80 *lac*ZM15 *lac*X74 *rec*A1 *ara*139 (*ara-leu*)7,697 *gal*U *gal*K *rps*L (Str^R) *end*A1 *nup*G	In our lab
S. cerevisiae	*MAT*a *ade*2 *trp*1 *his*3 *can*1 *ura*3 *leu*2	In our lab
W303-1A		
WZ	W303-1A (*leu* 2:: UPRE-*lacZ*)	In our lab
WZ (YEplac195)	Strain WZ containing plasmid YEplac195	In our lab
K-a	*MAT*a *ura*3, derivative from the diploid industrial yeast strains TH-AADY (Angel Yeast, Yichang, China)	In our lab
K-a (YCplac33-Cas9)	Strain K-a containing plasmid YCplac33-Cas9	In our lab
WZ (BG)	Strain WZ containing plasmid YEplac195-P*tpi-xyn*2s-Aa BGL1-T*adh*I	In this study
WZ (BG-cwp2)	Strain WZ containing plasmid YEplac195-P*tpi-xyn*2s-Aa BGL1-*cwp*2-T*adh*I	In this study
KZ	K-a (*leu* 2::UPRE-*lacZ*)	In this study
KZ (YEplac195)	Strain KZ containing plasmid YEplac195	In this study
KZ (BG)	KZ containing plasmid YEplac195-P*tpi-xyn*2s-Aa BGL1- T*adh*I	In this study
KZ (BG-cwp2)	KZ containing plasmid YEplac195-P*tpi-xyn*2s-Aa BGL1- *cwp*2-T*adh*I	In this study
YCplac33-Cas9	*Amp*^{r}, *URA 3*, Cas 9, 5,603 bp (shown in **Figure 1** and **Supplementary Material Data Sheet 2**)	In our lab
pRS42H-gRNA	*Amp*^{r}, *hph N*T1 crRNA	In our lab
pRS42H-gLEU2	*Amp*^{r}, *hph N*T1, crRNA, 20 bp guide for *LEU* 2 gene (shown in **Figure 1** and **Supplementary Material Data Sheet 1**)	In our lab
YEplac195	*Amp*^{r}, *URA*3	In our lab
BG	YEplac195-P*tpi-xyn*2s-Aa BGL1-T*adh*I, β-glucosidase secreting expressing vector	In our lab Wang et al. (2013)
BG-*cwp*2	YEplac195-P*tpi-xyn*2s-Aa BGL1-*cwp2*-T*adh*I, β- glucosidase displaying expressing vector, containing 207 bp *cwp*2 sequence encoding an anchored peptide to display the expressed β-glucosidase on the cell surface	In our lab Ding et al. (2018)
Primer P1	5′ CACAATTTGCTAAAGGTACT 3′	Donor DNA synthesis
Primer P2	5′ CTTGTGATTCTTTGCACTTC 3′	
Primer P3	5′ TGACCAAGTTCGTAAATCTA 3′	Transformant identifying
Primer P4	5′ CCATCTCCACAATAGGCATA 3′	
HAC1-F	5′CTTTGTCGCCCAAGAGTATGCG3′	Product size 532/280 bp
HAC1-R	5′GTGATGAAGAAATCATTCAATTCAAATG3′	
ACT1-F	5′CAAACCGCTGCTCAATCTTC3′	Product size 150 bp
ACT1-R	5′AGTTTGGTCAATACCGGCAG3′	
IRE1-F	5′AAGGCATCCGTTGTTTTGGC3′	Product size 128 bp
IRE1-R	5′AGTCAGAACCGGCGTCAAAT 3′	
INO1-F	5′AGAGATTGCTCCTTCCACGA 3′	Product size 164 bp
INO1-R	5′ACTTGGTTTGTCCCGACTTG 3′	
ERO1-F	5′TGAAGGAGGCAGGCAAATCG 3′	Product size 150 bp
ERO1-R	5′TACCGTTAGAGGGCCTTGGA 3′	
HLJ1-F	5′ATTTGGGCCTTCTGCTTCCA 3′	Product size 127 bp
HLJ1-R	5′TGCTTGTTGTTGCTGCTGTC 3′	
LHS1-F	5′GCTCGTCAGGAGTTGCGTAT 3′	Product size 149 bp
LHS1-R	5′AGTAAAAGCCAAACGGCTGC 3′	
MPD1-F	5′CCCCCAATGAGGGTCCTTTT 3′	Product size 109 bp
MPD1-R	5′TCGTCGTGCTTGTTTCCTGA 3′	
KAR1-F	5′ATTCCACCAGCACCAAGAGG 3′	product size 85 bp
KAR1-R	5′CTGTGGCAGACACCTTCAGA 3′	

2.2 DNA Manipulation, Plasmid Construction, and Yeast Transformation

Standard molecular genetic techniques were used for nucleic acid manipulations (Sambrook and Russell, 2001). The primers and plasmids used were listed in **Figure 1**, **Table 1**, and **Supplementary Material**.

The procedure to construct an indicating strain K-a (*leu 2*:: UPRE-*lac*Z), also abbreviated as KZ, was shown as follows: 1) The primer pair P1/P2 was used to amplify 3,721 bp donor DNA fragment UPRE-*lac*Z by PCR with the genomic DNA of strain WZ as the template; 2) The aforementioned donor DNA and guide plasmid pRS42H-gLEU2 (**Table 1**) were co-transformed into the competent cells of strain K-a (YCplac33-Cas9) by the lithium acetate method (Gietz et al., 1995), and the screening plate used was CMG^{-LEU} with hygromycin B at the final concentration of 450 μg/mL; 3) The colonies grown on the aforementioned plates were copied to the plate YPD with tunicamycin and X-Gal (5-bromo-4-chloro-3-indolyl-beta-D-galacto-pyranoside). The blue colonies were further identified by PCR with genomic DNA as the template and the primers used were P3 and P4, which were all external to P1 and P2, respectively. The PCR products were predicted to be 4,327 and 795 bp for positive and negative colonies, respectively.

Plasmids YEplac195, BG, and BG-cwp2 (**Table 1**) were also transformed into the competent cells of the strains WZ and KZ by the lithium acetate method (Gietz et al., 1995). *URA3* was used as a selective marker and yeast transformants were screened in a CMG solid medium absent of uracil.

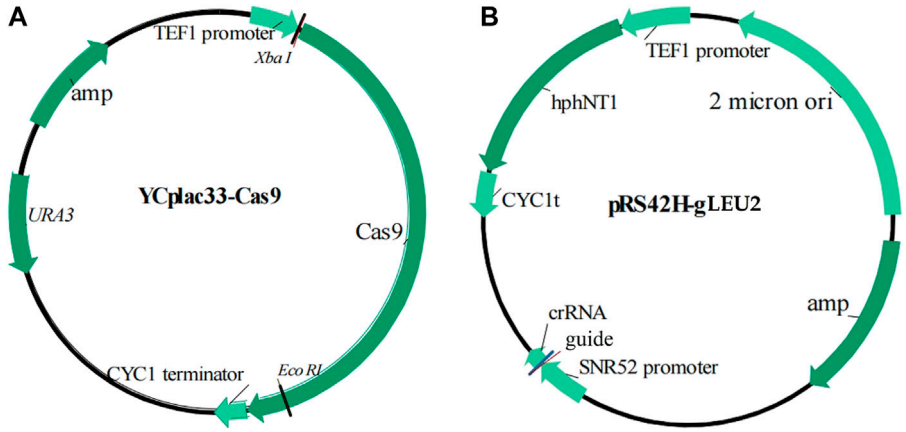

FIGURE 1 | Schematic illustration of plasmids. **(A)** YCplac33-Cas9; **(B)** pRS42H-gLEU2.

2.3 Growth and UPR Response Evaluation of Indicating Strains WZ and KZ in YPD With Different Additives

After being pre-cultivated twice in the YPD medium for 16–20 h at 30°C, the recombinant yeast indicator strains were grown aerobically to OD_{600} = 2.0 ± 0.1 in a fresh YPD medium with the initial OD_{600} value ~0.2 at 30°C and 220 rpm. 50 ml of the resultant cultures were aliquoted into 250 ml shake flasks, mixed with different reagents, sealed with Parafilm films and then continued to grow at 30°C and 150 rpm. These cultures were sampled at regular time points for growth and UPR response analysis.

Growth analysis was generally conducted by detecting the optical density of the culture at 600 nm (OD_{600}). UPR response analysis was carried out by β-galactosidase activity assay (Amberg and Huo, 2009). Protein content was measured with the Bradford protein assay kit according to the instruction book (Tiangen Biotech (Beijing) Co., Ltd.). One unit of activity (U) was defined as the amount of enzymes required to release 1 nmol of O-nitrophenol per minute under the assay condition.

2.4 Growth, β-Glucosidase and Ethanol Production, and UPR Response Evaluation of β-Glucosidase-Expressing Strains in Cellobiose

After being pre-cultivated in the CMG medium for 24 h, the recombinant yeast β-glucosidase-expressing strains were grown aerobically in a fresh medium for 24 h at 30°C. The resultant cells were collected by centrifugation, and these were washed twice with distilled water and then inoculated into 250 ml shake flasks containing 50 ml of rich media containing 2% or 10% cellobiose. The initial optical density at 600 nm (OD_{600}) of the medium was adjusted to 0.2. These cultures were allowed to grow aerobically at 30°C with shaking at 220 rpm, or anaerobically by sealing with Parafilm films at 30 C with shaking at 150 rpm. Samples were collected at regular time points for growth, β-glucosidase or/and β-galactosidase activity, sugar, and product analyses.

Growth and β-galactosidase activity analyses were carried out as aforementioned. If needed, the cell dry weight was further measured according to the reported method (Ding et al., 2013). β-Glucosidase activity was evaluated by using p-nitrophenyl- β-D-gluco-pyranoside (pNPG) as described previously (Wang et al., 2013). The supernatant and cells of the resultant cultures were separated by centrifugation before the cells were washed twice with distilled water and finally re-suspended in distilled water. The supernatant and the re-suspended cells were tested for activity. Then the total activity and the ratio of extracellular activity to total activity were calculated.

Sugar and product analysis was carried out by HPLC (Waters Alliance 2695) with RI-detection after the separation on a guard column (Cation-H Refill Cartridges) and an Aminex HPX-87H column (Bio-Rad), using 4 mM H_2SO_4 as the mobile phase with a flow rate of 0.6 ml/min at 40°C.

2.5 RNA Extraction, Reverse Transcription, and PCR and qPCR Methods

The broth for RNA extraction was sampled and stored at −80°C as soon as possible. Then, the total RNA was extracted with a TIANDZ Column Fungal RNAout Kit (Beijing TIANDZ Gene Technology Co., Ltd.) according to the manufacturer's instructions. Absorbance value determination, integrity analysis, reverse transcription reaction, and DNA pollution detection were all carried out according to the methods previously reported in our laboratory (Li et al., 2020).

The primers used for PCR and qPCR are described in **Table 1**. The product of the reverse transcription reaction was used for the amplification of the bands belonging to active/inactive *HAC1* ($HAC1^{i}$ and $HAC1^{u}$, respectively) with the pair of HAC1 primers (**Table 1**) (Kawazoe et al., 2017). Reactions were subjected to 30 PCR cycles of 95°C for 30 s, 54°C for 30 s and 72°C for 60 s. The PCR products were resolved on a 1.5% (w/v) agarose gel.

qPCR was carried out by using LightCycler 480 II and its corresponding software (Roche, Switzer-land) and ROCHE LightCycler@ 480 SYBR Green I Master and referring to the

manual for specific operation steps. A total volume of 20 μl and 25 ng nucleic acid templates were used and the nucleic acid source was the RNA extraction or cDNA from RNA extraction. The qPCR conditions were as follows: 95°C for 5 min, 40 cycles of 95°C for 20 s, 55°C for 20 s, and 72°C for 20 s. The constitutive reference gene *ACT*1 and the $2^{-\triangle\triangle CT}$ method was utilized to normalize the amount of mRNA and obtain the relative expression level of the targeted genes. Each data point was referred to the control strain samples. The results represent the average and standard deviation of three independent biological replicates. Specially, all evaluating and analyzing experiments in aforementioned sections were repeated at least three times with consistent results.

3 RESULTS

3.1 Amplification of the Donor DNA Fragment and Construction of Recombinant Indicating Strains and β-Glucosidase-Expressing Strains

In our previous work, we constructed the indicator strain W303-1A (*leu* 2::UPRE-*lac*Z, abbreviated as WZ) (Zhang et al., 2020) (**Figure 1**; **Table 1**), using the clustered regularly interspaced short palindromic repeats (CRISPR)-CRISPR associated protein nine (Cas9) method, with UPRE-*lac*Z as a reporter gene. Specifically, UPRE contains a 22 bp DNA sequence, 5′-GGAACTGGACAGCGTG TCGAAA-3′, and a 250 bp upstream sequence before the initial codon of the *CYC*1gene (Cox et al., 1993; Dallbey et al., 2009); and has *Lac*Z, a commonly used reporter (Cox et al., 1993). The 20 bp guide DNA sequence selected was 5′ TATTTACTTTGGTAAGAGAA 3′, corresponding to 423–442 nt of the *LEU*2 open reading frame (ORF), according to the design principle of the CRISPR-Cas9 method (DiCarlo et al., 2013). The PAM site sequence AGG, corresponding to 443–445 nt of the *LEU*2 ORF, was deleted and replaced by a UPRE-*lac*Z fragment in the genome of strain WZ. The resultant strain was selected by plating onto yeast potato dextrose (YPD) agar plates with tunicamycin and X-Gal. Tunicamycin induced the UPR, leading to the expression of *lac*Z, which enzyme catalyzes the substrate X-Gal to produce blue colonies. This phenotype indicated the existence and function of UPRE-*lac*Z fragment in cells.

In addition, we isolated and obtained the haploid strain K-a, derived from the diploid industrial yeast strain TH-AADY (Angel Yeast Co., Ltd., Yichang, China), and further proved that the CRISPR-Cas9 method was feasible in this strain (Lu et al., 2019). To conveniently design a guide sequence and integration site, auxotroph marker-encoding genes were sequenced, and the results proved that strain K-a contained the same DNA sequence of the *LEU2* ORF as that of the strain W303-1A. Therefore, the same strategy was carried out to construct the indicator strain KZ (**Figure 1**; **Table 1**; **Section 2.2**).

Furthermore, β-glucosidase-expressing strains were obtained by transforming β-glucosidase- Expressing plasmids BG and BG-cwp2 into strains WZ and KZ, respectively. As a control, the plasmid YEplac195 was also transformed. The results of the effect of secreting or displaying β-glucosidase using plasmids BG or BG-cwp2, respectively, has been reported previously (Wang et al., 2013; Ding et al., 2018).

3.2 Growth and UPR of Indicator Strains WZ and KZ in the Presence of Tunicamycin, Ethanol, and Acetic Acid

In YPD, no significant growth difference between the indicator strains and their host strains were observed (data not shown). Previous reports suggested that ethanol and acetic acid might induce a UPR during the fermentation process of cellobiose or lignocellulosic hydrolysates by the constructed β-glucosidase-expressing strains (Navarro-Tapia et al., 2016; Kawazoe et al., 2017; Navarro-Tapia et al., 2018; Cedras et al., 2019). Therefore, in the present study, ethanol and acetic acid, as well as tunicamycin as a control, were first selected to investigate the UPR in the indicator strains KZ and WZ. The growth data (**Figures 2A,B**) indicated that while the maximum OD_{600} value of KZ-1 was significantly lower than that of WZ-1, different additives inhibited growth by variable degrees. Acetic acid induced the highest growth inhibition and tunicamycin induced the lowest. In addition, the growth of strain KZ was inhibited to a lower extent than that of strain WZ, which implied that strain KZ has higher ethanol and acetic acid tolerance compared to strain WZ, which is in agreement with previous observations of the parental strains K-a and W303-1A (data unpublished).

The β-galactosidase activity data (**Figure 2C**) indicated that the UPR varied greatly according to the strains and additives, but did not seem to be related to growth. From high to low values, the β-galactosidase activity in the two strains in the presence of the additives was: tunicamycin > 8% ethanol (v/v) >5% ethanol (v/v) + 0.1% acetic acid (v/v) > 0.3% acetic acid (v/v). The ratio values of the latter two additives were 5.07–3.42 and 1.10–1.49 for strain KZ, and 1.99–2.57 and 1.46–2.15 for strain WZ, respectively. Thus, acetic acid showed only a slight activating effect.

In strain KZ, the β-galactosidase activity increased rapidly, peaked at about 2 h, and then decreased quickly. By contrast, the enzyme activity in strain WZ increased slowly and peaked at 16 h.

Taken together, these results demonstrated obvious differences in the rate and degree of the UPR between the strains. As a control, the β-galactosidase activity values of strain KZ and WZ in YPD were (10.65 ± 0.61)–(12.06 ± 0.59) and (22.2 ± 1.09)–(24.1 ± 1.35) U/mg protein, respectively.

3.3 Aerobic Growth, β-Glucosidase Production, and the UPR of β-Glucosidase-Expressing Strains in 2% Cellobiose

The catalytic activity of β-glucosidase toward cellobiose allows recombinant strains that express β-glucosidase to utilize cellobiose directly for growth and ethanol production. Here, 2% cellobiose medium, YPC, was first selected, and the aerobic growth, β-glucosidase, and β-galactosidase production of the

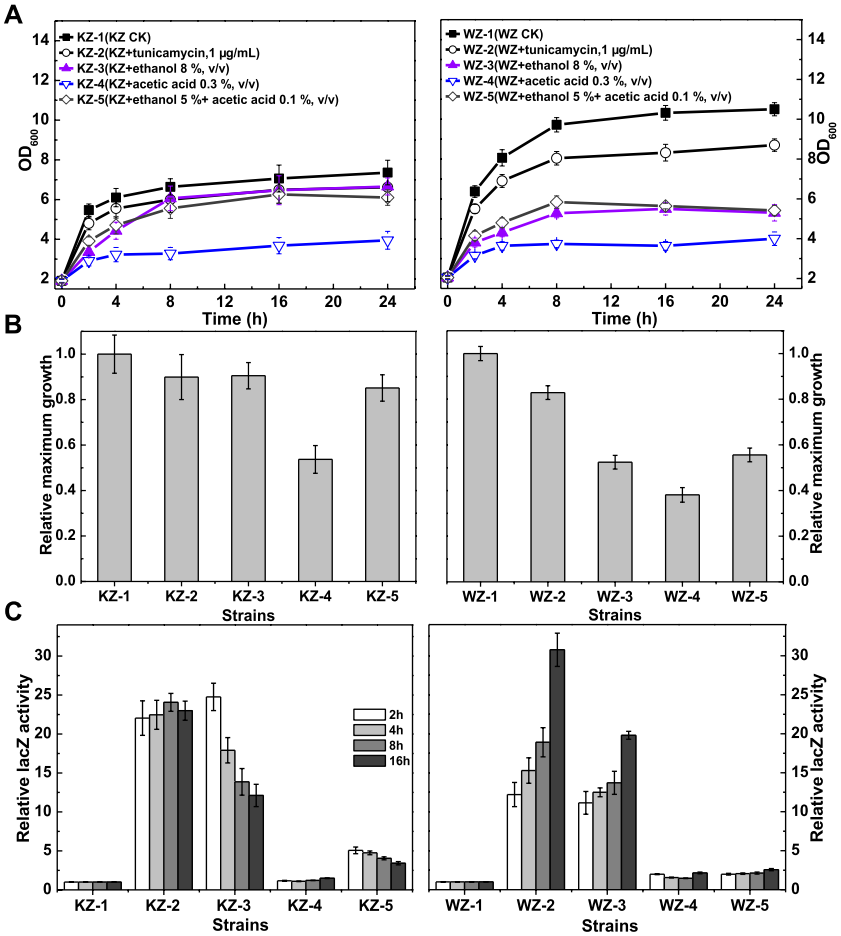

FIGURE 2 | The growth and β-galactosidase activity of strains KZ and WZ in the YPD medium with different additives. **(A)** The growth curve; **(B)** the ratio of maximum OD_{600} value to that of controls KZ-1 or WZ-1; and **(C)** the ratio of β-galactosidase activity to that of controls KZ-1 or WZ-1. The original data was shown in **Supplementary Material Table 1**.

recombinant strains were determined (**Figure 3**). As expected, the growth rates of strain WZ (BG-cwp2) and WZ (BG) were similar (Ding et al., 2018); however, the growth of strains KZ (BG-cwp2) and KZ (BG) differed (**Figure 3A**). Their OD_{600} values at 48 h, which were close to the maximum during the whole period, were 30.23 ± 1.08 WZ (BG-cwp2), 32.15 ± 1.41 WZ (BG), 17.00 ± 0.65 KZ (BG-cwp2), and 26.40 ± 1.14 KZ (BG), respectively.

Growth in the YPC medium depends on β-glucosidase production; therefore, the growth rate reflects the β-glucosidase production. **Figure 3B** shows that the total β-glucosidase activities of strains KZ (BG-cwp2) and KZ (BG) were also far lower than those of WZ (BG-cwp2) and WZ (BG), and their maximum activities were 0.035 ± 0.002 KZ (BG-cwp2), 0.047 ± 0.003 KZ (BG), 0.147 ± 0.008 WZ (BG-cwp2), and 0.323 ± 0.021 WZ (BG) U/ml/OD_{600}. Interestingly, the ratios of β-glucosidase activity of KZ (BG) to that of KZ (BG-cwp2) and WZ (BG) to that of WZ (BG-cwp2), were relatively stable. The differences in the ratios of extracellular activity between strains KZ (BG) and WZ (BG), or between KZ (BG-cwp2) and WZ (BG-cwp2), were also not significant, at (39.08 ± 2.15) %—(49.82 ± 2.11) % and (3.55 ± 0.21) %—(8.00 ± 0.37) %, respectively (**Figure 3C**).

Furthermore, the β-galactosidase activities of the four strains correlated positively with their corresponding β-glucosidase values; however, the relationship was not linear (**Figures 3B,D**). All the β-galactosidase values of strain KZ-based samples were much lower than those of strain WZ-based samples (**Figure 3D**). However, when the activity data were expressed as ratios to that of the control, and their difference was not significant (**Figure 3E**). The maximum ratio values of strain KZ (BG-cwp2), KZ (BG), WZ (BG-cwp2), and WZ (BG) were 3.79, 4.97, 6.99, and 7.67, respectively. This clearly showed that plasmid BG led to higher β-galactosidase as well as β-glucosidase activities than plasmid BG-cwp2 in both hosts. In addition, plasmid BG allowed the cells to reach the maximum value of β-galactosidase activity more quickly than did plasmid BG-cwp2.

HPLC analysis revealed that ethanol and acetic acid were produced, with maximum titers of 5.38–6.09 g/L and ≤0.302 g/L, respectively. According to the results from **Section 3.2**, we

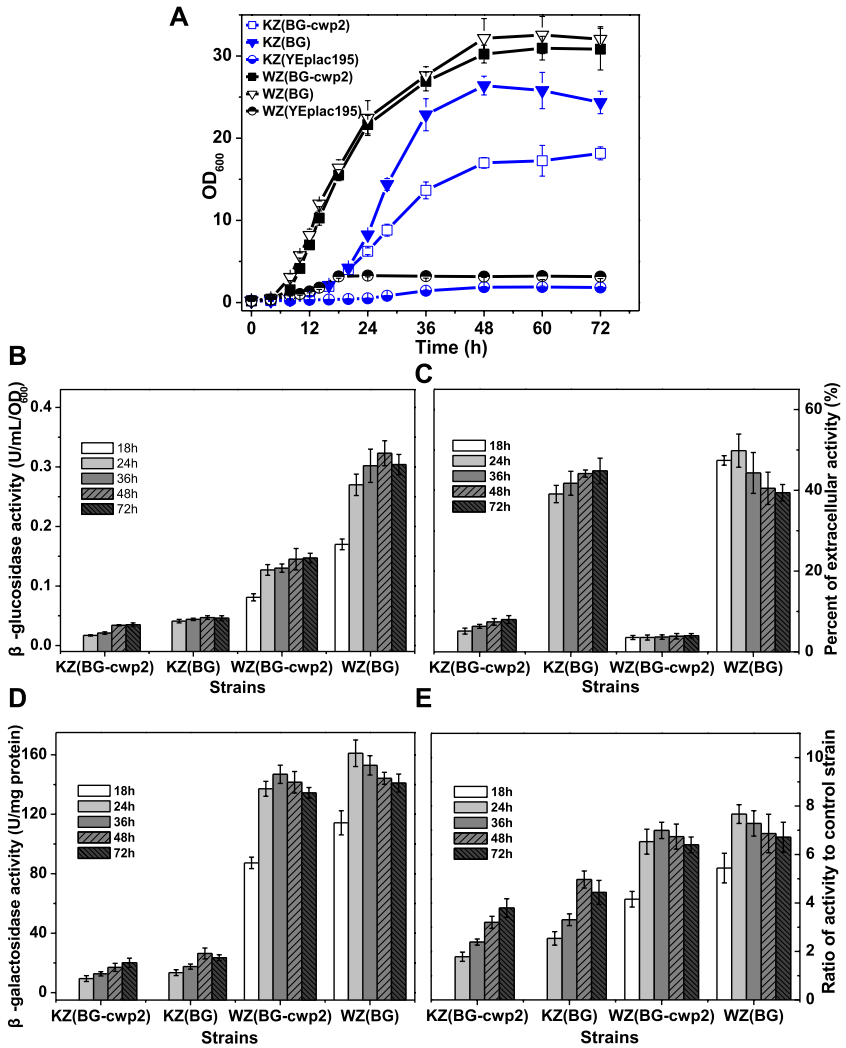

FIGURE 3 | The growth, β-glucosidase, and β-galactosidase activities of the recombinant strains aerobically in 2% cellobiose. **(A)** The growth curve; **(B)** total β-glucosidase activity (U/ml/OD_{600}), not detected for control strains KZ (YEplac195) and WZ (YEplac195); **(C)** the percent of extracellular β-glucosidase activity (%); **(D)** the β-galactosidase activity (U/mg protein); and **(E)** the ratio of β-galactosidase activity value of four strains to that of control strain KZ (YEplac195) and WZ (YEplac195), 5.30 ± 0.83 and 21.0 ± 0.95 U/mg protein, respectively. The original data was shown in **Supplementary Material Table 2**.

suspected that ethanol or acetic acid did not contribute to the UPR, because their concentrations in the fermentation culture were too low.

3.4 Oxygen-Limited Growth, β-Glucosidase and Ethanol Production, and the UPR of β-Glucosidase-Expressing Strains in 10% Cellobiose

Oxygen conditions greatly influences enzyme expression levels, cell growth, and fermentation performance. In addition, a high sugar concentration will lead to a high production of ethanol and other by-products. To observe the possible mutual interaction of UPR activation with exogenous gene expression, ethanol, and other by-products, we evaluated oxygen-limited growth, β-glucosidase activity, ethanol production, and β-galactosidase activity of the recombinant strains in media containing 10% cellobiose. The results are summarized in **Figure 4**, which indicated a significant effect of the strain source and displaying or secreting expression mode of the exogenous gene.

First, the results showed that strains WZ (BG-cwp2) and WZ (BG) could quickly produce sufficient β-glucosidase to utilize high cellobiose for growth and fermentation into ethanol and acetic acid (**Figures 4A–C**). In fact, the initial cellobiose concentration in media was measured by HPLC to be 93.3 ± 0.9 g/L. Strain WZ (BG-cwp2) and WZ (BG) exhausted cellobiose during 48–60 h and 24–36 h, respectively (**Figure 4F**). The maximum ethanol titer and yield reached 45.98 ± 2.31 g/L (5.495 ± 0.276%, v/v) and 91.7% (at 72 h) in WZ (BG-cwp2), and 45.91 ± 1.96 g/L (5.486 ± 0.234%, v/v) (72 h) and 91.5% in WZ (BG) (expressed as a percentage of the theoretical yield) (**Figure 4C**). At the same time, acetic acid was produced and reached the highest level of 0.631 g/L or 0.058% (v/v) in WZ (BG-

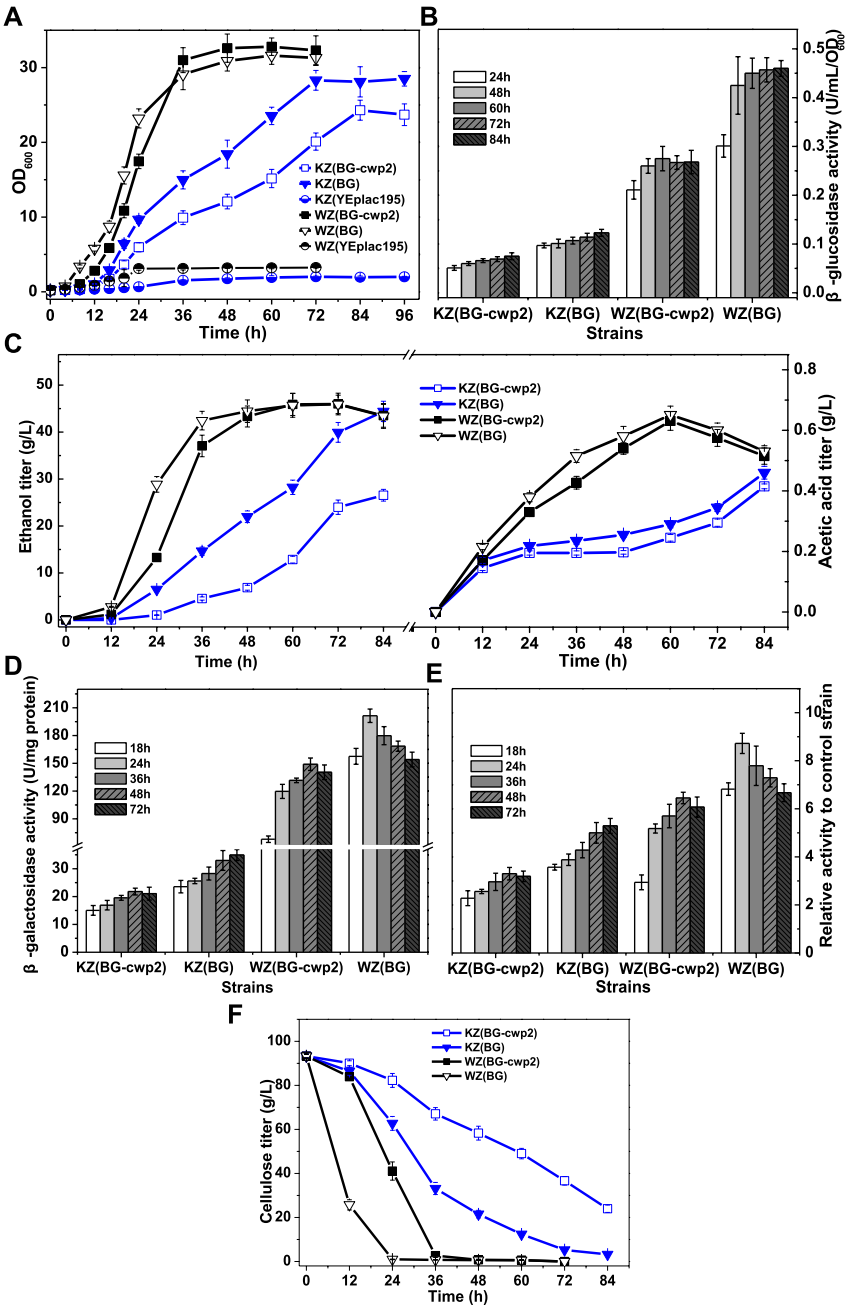

FIGURE 4 | The growth, sugar consumption, β-glucosidase, ethanol and acid production, and β-galactosidase activity of the recombinant strains anaerobically in 10% cellobiose. **(A)** The growth curve; **(B)** total β-glucosidase activity (U/ml/OD_{600}), not detected for control strains WZ (YEplac195) and KZ (YEplac195); **(C)** ethanol and acetic acid production; **(D)** the β-galactosidase activity (U/mg protein); **(E)** the ratio of β-galactosidase activity value of four strains to that of control strains KZ (YEplac195) and WZ (YEplac195), 6.60 ± 0.85 and 23.1 ± 0.93 U/mg protein, respectively; and **(F)** the cellobiose curve. The original data was shown in **Supplementary Material Table 3**.

cwp2), and 0.651 g/L or 0.060% (v/v) at 60 h in WZ (BG) (**Figure 4C**).

By contrast, the results showed that strains KZ (BG-cwp2) and KZ (BG) utilized cellobiose but grew slowly (**Figures 4A–C,F**), possibly because of insufficient enzyme supply (**Figure 4B**). In detail, their maximum values of OD_{600} reached 24.30 ± 1.34 in KZ (BG-cwp2) and 28.30 ± 1.32 in KZ (BG) at 84 and 72 h, respectively (**Figure 4A**). The cellobiose, ethanol, and acetic acid concentrations of strain KZ (BG-cwp2) at 84 h were 23.96 ± 1.67, 26.55 ± 1.26, and 0.415 ± 0.008 g/L, respectively. Those of strain KZ (BG) at 84 h were 3.21 ± 0.28,44.41 ± 2.16, and 0.460 ± 0.021 g/L, respectively (**Figures 4C,F**).

In our experience, a higher cellobiose content resulted in a higher β-glucosidase production level. In fact, the maximum values of total β-glucosidase activity from the four strains, KZ (BG-cwp2), KZ (BG), WZ (BG-cwp2), and WZ (BG), were 0.075 ± 0.007, 0.123 ± 0.006, 0.275 ± 0.015, and 0.460 ± 0.036 U/ml/OD_{600}, respectively (**Figure 4B**). Compared with those in 2% cellobiose media (**Figure 3B**), the maximum values increased by 2.14, 2.62, 1.87, and 1.42 times in 10% cellobiose media in the four strains, respectively (**Figure 4B**).

In 10% cellobiose, there was also a positive, but not linear, relationship between the β-glucosidase and β-galactosidase activities (**Figures 4B,D,E**). Similar to that in 2% cellobiose, the β-galactosidase values from strain KZ-based samples were lower than those of strain WZ-based samples (**Figures 4D,E**). The maximal ratio values of β-galactosidase activity of strain KZ (BG-cwp2), KZ (BG), WZ (BG-cwp2), and WZ (BG) became 3.30, 5.29, 6.45, and 8.72, respectively (**Figure 4E**). Therefore, the results suggested that anaerobic fermentation with 10% cellobiose increased the difference in β-galactosidase activity levels between strains KZ (BG-cwp2) and KZ (BG), or WZ (BG -cwp2) and WZ (BG). Additionally, strain WZ (BG) reached the maximum value of β-galactosidase activity the most quickly in both 2 and 10% cellobiose, at 24 and 48 h, respectively, after which, the values decreased.

The times taken by the three strains, WZ (BG), WZ (BG-cwp2), and KZ (BG) to produce ≥5% (v/v) ethanol, which is equal to 41.85 g/L ethanol, were 36, 48, and 84 h, respectively. At those times, the ethanol titers in the three strains were 5.07, 5.18, and 5.31% (v/v), respectively, and the acetic acid titers were 0.515, 0.540, and 0.460 g/L, corresponding to 0.047, 0.050, and 0.042% (v/v), respectively. Such ethanol and acetic acid titers were close to those of the group treated with 5% (v/v) ethanol +0.1% (v/v) acetic acid in **Section 3.2** (**Figure 2**) and would probably make a contribution to UPR signaling. It would be a challenge to determine the effect of ethanol or acetic acid on the UPR, because their titers varied with the course of fermentation, especially when the UPR had been induced by other factors, for example, exogenous protein expression.

3.5 Quantitative PCR of UPR Target Genes and *HAC1* mRNA Analysis

UPRE contains a 22 bp cis-acting element, that is, necessary and sufficient for the induction of the yeast *KAR2* (BiP) gene in response to unfolded proteins (Dallbey et al., 2009). In fact, UPRE-*lac*Z has often been used in UPR studies as a reporter gene (Dallbey et al., 2009; Navarro-Tapia et al., 2018). It has also been proven to respond to tunicamycin, ethanol, or acetic acid (**Figure 2**), in addition to β-glucosidase production (**Figure 3**). Therefore, it could provide a direct and quantitative comparison of UPR signaling from different inducers.

To investigate the effect and mechanism on the UPR of the abovementioned inducers, it is necessary to carry out molecular detection. The canonical UPR pathway genes in yeast cells include those encoding an ER membrane sensor, IreIp, a transcription factor, HacIp, and Kar2p. When activated by the accumulation of aberrant folded proteins in the ER, IreIp catalyzes the splicing of *HAC1* to activate hundreds of genes that restore the normal ER function. Kar2p acts as a chaperone to mediate protein folding in the ER and regulates the UPR *via* interaction with Ire1p (Dallbey et al., 2009). While no protein denaturation has been described at 6% or 8% ethanol, ethanol was reported to activate *INO1* gene expression and further enhance the UPR by membrane fluidification (Navarro-Tapia et al., 2016; Navarro-Tapia et al., 2018). *INO1* encodes an essential enzyme for inositol biosynthesis and is activated to restore lipid levels (Navarro-Tapia et al., 2018). Acetic acid was demonstrated to lead to the accumulation of misfolded proteins in the ER and the activation of Ire1p and Hac1p (Kawazoe et al., 2017). Therefore, in the present study, *HAC1* mRNA splicing and the expression of eight genes (**Table 1**) were analyzed by RNA extraction from the samples stored at −80°C in **Sections 3.2–3.4** experiments. An additional four genes involved in protein folding, *ERO1*, *LHS1*, *HLJ1*, and *MPD1* were assessed (Dallbey et al., 2009; Navarro-Tapia et al., 2018). The results are shown in **Figure 5**.

As expected, spliced *HAC1* mRNA was shown to accumulate by varying degrees, which correlated positively with the corresponding β-galactosidase values (**Figures 2C**, **4D**, **5A**,**B**). In fact, the spliced *HAC1* mRNA accumulation in the samples of strains WZ and KZ with 0.3% (v/v) acetic acid or 5% ethanol +0.1% acetic acid (v/v) was slight (**Figure 5A** and data not shown). This result was different from a previous report (Kawazoe et al., 2017). We hypothesized that the main causes were the differences in the strains, medium, and the initial OD_{600} value when exposed to stress. A similar phenomenon was also observed for strain KZ in the fermentation broth, especially in the presence of 2% cellobiose (data not shown).

The results in **Figures 5C–F** demonstrated the characteristic responses to the different inducers, which generally agreed with changes observed in previous articles (Navarro-Tapia et al., 2016; Kawazoe et al., 2017; Navarro-Tapia et al., 2018). The existence of ethanol led to *INO1* to be among the most activated genes. The expression of *KAR2* was relatively high and constant, as expected; however, *IRE1* only showed a slightly upregulated expression. In addition, the response of *LHS1* appeared to be specific for acetic acid and had a higher expression level than the other genes (**Figures 5C,D**).

The results in **Figures 5G–H** indicated that the expression levels of *INO1* and *KAR2* were significantly activated and upregulated in cells in the fermentation broth with 10% cellobiose. The times to obtain the highest level of *INO1* expression were 36 and 48 h for strains WZ (BG) and WZ (BG-cwp2), respectively, and the corresponding ethanol titers were 5.07, and 5.18% (v/v), respectively (**Figure 4**). Comparing all of the data under 10% cellobiose (**Figures 4**, **5**) with those under 2% cellobiose (**Figures 2**, **3**), allowed us to hypothesize that ethanol also contributes to UPR signaling over a certain titer range. For acetic acid, the data did not reveal its effect in the UPR in the fermentation broth, possibly because its titer was too low.

4 DISCUSSION

Although there has been a lot of research on protein quality control mechanisms and secretory recombinant protein

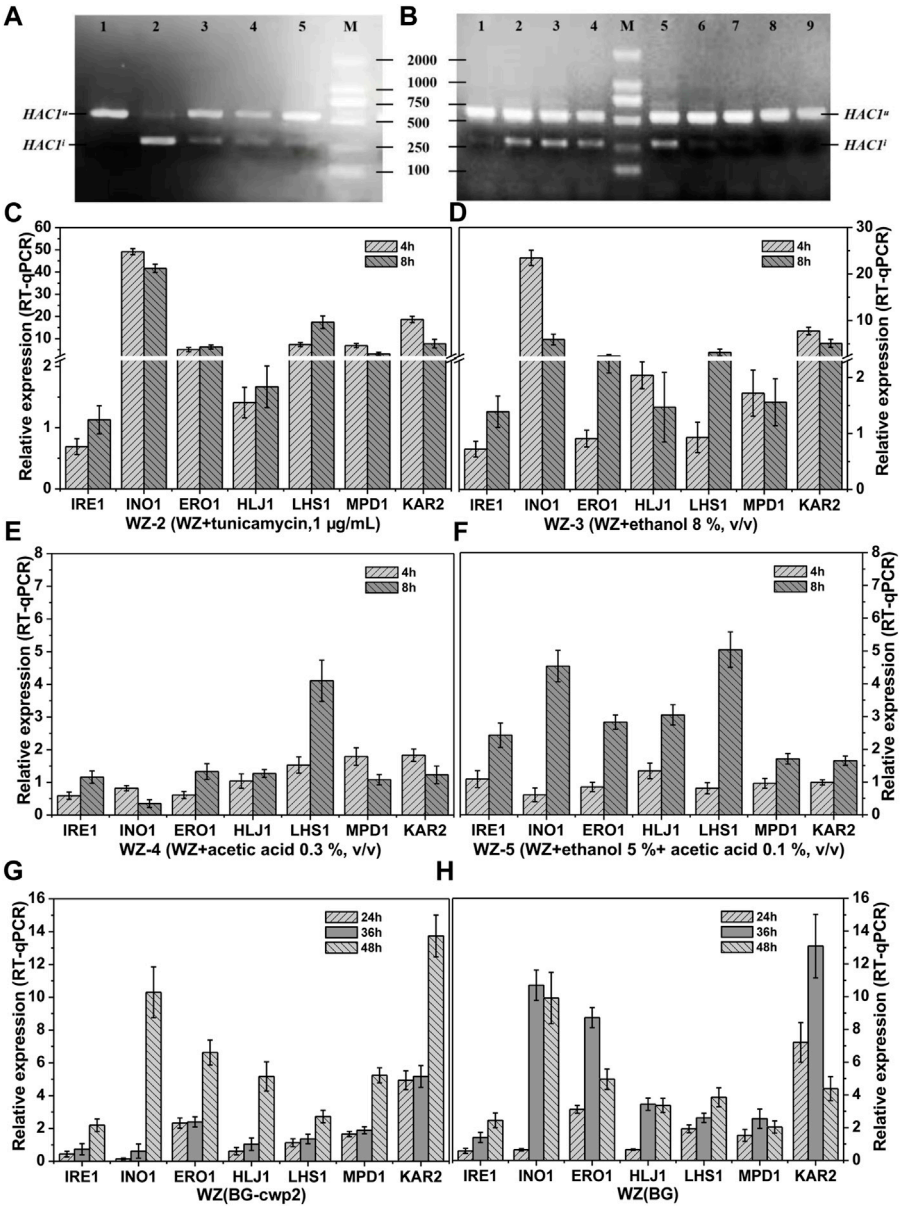

FIGURE 5 | *HAC1* mRNA splicing and relative expression of UPR target genes. *HAC1* mRNA splicing **(A)** and the relative expression level of UPR target genes **(C–F)** of strains WZ in YPD medium with different additives; *HAC1* mRNA splicing **(B)** and relative expression level of UPR target genes **(G–H)** of strains WZ (BG-cwp2) and WZ (BG) in 10% cellobiose. **(A)** lanes 1~5, WZ-1~WZ-5, 8 h; **(B)** lanes 1,8 and 9, 24, 36 and 48 h fermentation time of strain WZ (YEplac195); lanes 2~4, 24, 36 and 48 h fermentation time of strain WZ (BG); lanes 5~7, 24, 36 and 48 h fermentation time of strain WZ (BG-cwp2). Each data point was referred to the control strain samples, and the mRNA levels of the target genes were determined by qPCR after normalization with constitutive control *ACT1* gene. The results represent the average and standard deviation of three independent biological replicates. The original data was shown in **Supplementary Material Table 4**.

production in yeast (Orlean and Menon, 2007; Pittet and Conzelmann, 2007; Dallbey et al., 2009; Young and Robinson, 2014; Bao et al., 2017; Cedras et al., 2019; Sun and Brodsky, 2019; Davison et al., 2020; Thak et al., 2020), this study provides the first evaluation and direct comparison of the UPR during cellobiose utilization of recombinant haploid yeast derived from Angel and W303-1A strains expressing β-glucosidase under the same conditions. On the basis of quantifying UPR induction, we attempted to analyze all possible factors that contribute to UPR signaling in a specific fermentation system, and further investigated the interconnectedness and mutual influence on UPR among the inducers.

Although *S. cerevisiae* is reported to naturally have a relatively low secretory pathway capacity (Bao et al., 2017), there is still a significant difference in secretion capacity between different strains (Davison et al., 2020), which should be evaluated and exploited. Angel Yeast is widely used in large-scale industrial bio-ethanol production in China and is also among the world-famous

industrial yeast brands (http://www.angelyeast.com) (Zou et al., 2021), being an ideal candidate for lignocellulose conversion. However, Angel Yeast TH-AADY-derived haploid strains were repeatedly found to have much lower cellulase enzyme activity compared to the host strain W303-1A (Wang et al., 2013; Hong et al., 2014; Ding et al., 2018; Zou et al., 2021).

Therefore, one aim of this study was determining why the cellulase activity produced by Angel-derived strains is low, how it relates to UPR induction, and whether the UPR capacity is a limiting factor. The results of growth and UPR response evaluations of strains KZ and WZ in tunicamycin, ethanol, and acetic acid proved that strain KZ has a stronger resistance to those additives, and could more quickly activate and then inactivate the UPR (**Figure 2C**). By contrast, the results in 2% and 10% cellobiose both showed poorer β-glucosidase production and lower UPR signaling in KZ-based strains than in WZ-based strains, which led to a slower growth and a lower maximum OD_{600} value (**Figures 3**, **4**). The observed positive correlation between the two enzyme activities possibly implied a low processing capacity of the secretory pathway in the parental strain K-a, which implied a low threshold to activate the UPR to degrade unfolding proteins.

The second aim of this study was to observe how the displaying and secreting pattern of heterologous protein expression influenced the UPR and further determine if there is a relationship between the UPR and the metabolic burden, which has been reported to be an extra by displaying over secreting (Ding et al., 2018). Cellobiose cannot be transported into yeast, thus its utilization depends on the production of secreted enzymes; however, we observed a non-linear relationship between enzyme expression and biomass synthesis and/or product formation based on substrate utilization. The maximum value of β-glucosidase activity in WZ (BG) cells was 2.20 and 1.68 times the level of WZ (BG-cwp2) cells in 2% and 10% cellobiose, respectively (**Figures 3B**, **4B**). However, their growth and fermentation rates were very similar (**Figures 3A**, **4A,C**). Herein, the metabolic burden induced by β-glucosidase displaying over secreting seems to be low for the WZ-based strains. By contrast, while the maximum values of β-glucosidase activity in KZ (BG) cells were 1.35 and 1.64 times the level of KZ (BG-cwp2) cells in 2 and 10% cellobiose, respectively (**Figures 3B**, **4B**). There was a marked difference in their growth and fermentation rates (**Figures 3A**, **4A,C**), which demonstrated the existence of a significant metabolic burden, as reported previously (Ding et al., 2018).

Unexpectedly, only strains KZ (BG) and KZ (BG-cwp2) showed that the β-galactosidase activity was essentially proportional to the β-glucosidase activity, or were at least positively correlated. In other words, the UPR seems to have no direct relation to displaying or secreting, regardless of the oxygen supply or cellobiose concentration. However, this was not the case for strains WZ (BG) and WZ (BG-cwp2). Compared to the difference in β-glucosidase activity between strains WZ (BG-cwp2) and WZ (BG), the β-galactosidase activity of strain WZ (BG-cwp2) was similar to that of strain WZ (BG), and seemed to be abnormally high (**Figures 3D,E**, **4D,E**).

It is necessary to first analyze which factors induce UPR signaling. According to previous reports (Dallbey et al., 2009; Young and Robinson, 2014; Navarro-Tapia et al., 2016; Kawazoe et al., 2017; Navarro-Tapia et al., 2018; Cedras et al., 2019; Sun and Brodsky, 2019), it was speculated that there are at least three factors that activate the UPR in the cellobiose utilization system in this study, heterologous β-glucosidase expression, ethanol, and acetic acid production. However, only the combination of mild acetic acid stress (0.1% acetic acid) and mild ethanol stress (5% ethanol) was reported to induce the UPR, whereas neither mild ethanol stress nor mild acetic acid stress individually activated the UPR (Kawazoe et al., 2017). 6 or 8 % ethanol was observed to activate UPR but did not de-nature proteins (Navarro-Tapia et al., 2018). By contrast, a minimal ethanol titer of 4%–5% v/v is required to render distillation economically viable; however, ethanol concentrations in lignocellulose fermentations struggle to reach these concentrations (Brandt et al., 2021). Therefore, in this study, oxygen-limited 10% cellobiose fermentation was designed and ≥5% v/v maximum ethanol titers were obtained at the later stage of fermentation (**Figure 4C**).

In such a system, the switch from β-glucosidase expression to substrate utilization, and then biomass synthesis and by-product production, is supposed to influence the dynamics of the UPR. To detect the mRNA levels of both the UPR central components and UPR target genes, would help to reveal UPR inducers and response dynamics. Comparisons of the curves of enzyme activity, growth, substrate, and products in 2 and 10% cellobiose (**Figures 3**, **4**), and the relative expression level of different genes (**Figure 5**), made it reasonable to conclude that the constitutive heterologous expression would result in a durable UPR induction, and ethanol or acetic acid activation depends on the titer produced. In 10% cellobiose fermentation, the ethanol titer was up to 5% (v/v) and could induce high expression of the specific target gene *INO1* and should lead to UPR signaling. Regrettably, detection and analysis still could not differentiate and quantify the contribution of ethanol to UPR signaling in such a complex fermentation system. Such an analysis requires multi-faceted investigations.

An important issue is how and why the display and secretion pattern of β-glucosidase expression influenced UPR activation, especially in strain WZ cells. Undoubtedly, the key step is glycosylphosphatidylinositol (GPI) anchor addition, an essential maturation process of secretory proteins in the ER, which is also the first step to distinguish displaying from secreting of secretory proteins (Orlean and Menon, 2007; Pittet and Conzelmann, 2007). GPI lipids are synthesized in the ER and added onto proteins by a pathway comprising 12 steps, carried out by 23 gene products, 19 of which are essential (Pittet and Conzelmann, 2007). Thus, GPI anchoring of cell-surface proteins is the most complex and metabolically expensive lipid post-translational modification described to date (Orlean and Menon, 2007).

Consequently, the growth defect observed in this study was expected and was also similar to that reported previously (Ding et al., 2018; Brandt et al., 2021). The phenomenon that the defect was more serious in strain KZ (BG-cwp2) cells than that in strain WZ (BG-cwp2) cells supported the speculation that the growth defect stems from a combination of relatively low activity on cellobiose and the metabolic burden imposed by enzyme expression. In addition, anchoring moieties contribute to the

growth difference of the cell-surface-display-expressing strains under both aerobic and anaerobic conditions (Ding et al., 2018).

The results of the present study allowed us to cautiously speculate that the GPI anchoring process by an anchored peptide-encoding sequence (cwp2) in plasmid BG-cwp2 would bring about two results: 1) An increased expression of endogenous anchoring-related genes inside cells, which would boost UPR induction and make the resultant signal comparable to that during the secretion of β-glucosidase; 2) extra material and energy consumption, which would lead to biosynthesis stress and this lagged behind β-glucosidase expression in cells and cellobiose hydrolysis. Both of these pathways imposed a metabolic burden.

The maximum values of the ratio of β-galactosidase activity in aerobic 2% cellobiose culture were 3.79, 4.97, 6.99, and 7.67 for the four strains KZ (BG-cwp2), KZ (BG), WZ (BG-cwp2), and WZ (BG), respectively; whereas, those values in anaerobic 10% cellobiose culture changed to 3.30, 5.29, 6.45, and 8.72, respectively. Although β-glucosidase activity by all strains increased under anaerobic 10% cellobiose (**Figure 5**), it was still apparent that the difference in the ratio of β-galactosidase activity between strains KZ (BG-cwp2) and KZ (BG), and WZ (BG-cwp2) and WZ (BG), increased. One reason behind this might be attributed to biomass synthesis. The biomass yield (expressed as g of dry cell weight (DCW) /g sugar consumed) in anaerobic 10% cellobiose was determined to be only from one-third to one-fifth of the value under aerobic 2% cellobiose conditions (data not shown). This would greatly alleviate the aforementioned biosynthesis stress from GPI anchoring and also decrease UPR induction in KZ (BG-cwp2) or WZ (BG-cwp2) cells.

Therefore, the results of the present study indicated a mutual interaction of the UPR response and the metabolic burden that varied according to the host strain, protein expression level, displaying or secreting mode, and fermentation conditions. Undoubtedly, the host strain had the most significant effect. Here, the comparison of W303-1A- and K-a-derived strain demonstrated the relationship between secretory recombinant protein production and the UPR and metabolic burden. Low β-glucosidase production from KZ-derived strains should result in UPR and/or ERAD induction (Davison et al., 2020), and in turn, a low induction signal reflects a limited ER processing capacity in cells. Expensive displaying exacerbates the metabolic burden resulting from insufficient or slow enzymes and glucose substrate supply. By contrast, host strain W303-1A confers on its derived strains excellent enzyme productivity and secretory pathway capacity, and a subtle difference in the metabolic burden of displaying over secretion.

A key challenge for bioengineering or synthetic biology is to balance different traits for a specific application. It is apparent that strain W303-1A is more suitable for use as a host to produce secretory recombinant proteins than strain K-a. When it is necessary to express heterologous genes in strain K-a, to broaden its substrate range to take full advantage of its industrial traits for ethanol production, it will be necessary to first enhance the UPR and ERAD activity and modulate its secretory pathway capacity. In fact, recently, much progress has been made in strain K-a modification based on the results of this study in our laboratory.

In summary, this study illustrates the differences in resistance to ethanol or acetic acid and the UPR between indicator strains KZ and WZ. The results of cellobiose utilization assays demonstrated the interaction of the UPR and the metabolic burden according to the strain source, anchoring moiety, oxygen supply, and cellobiose concentration. The OD_{600} values and β-glucosidase and β-galactosidase activities were shown to correlate positively with each other; however, these values in the KZ-derived strains were far lower than those in the WZ-derived strains under the conditions tested. Meanwhile, the metabolic burden induced by displaying over secreting was also much more serious in strain KZ than in strain WZ. Comparisons of the results under two different conditions implied that β-glucosidase expression would provide a durable inducing effect on the UPR, whereas, the effect of ethanol and acetic acid depends on the titer produced, and could be identified by detecting the expression levels of key specifically targeted genes. The results indicated that host strain W303-1A is a better secretory protein producer. Moreover, the first step to modify strain K-a for cellulosic ethanol fermentation would to break the bottleneck of the UPR capacity.

DATA AVAILABILITY STATEMENT

The original contributions presented in this study are included in the article/**Supplementary Material**, further inquiries can be directed to the corresponding authors.

AUTHOR CONTRIBUTIONS

SZ, YJ, KZ, and JH performed experiments. JH, QH, and RB joined to write the manuscript and conceived the study. MZ coordinated the project.

FUNDING

This study was supported by the Tianjin Key Technology R&D Program (No. 18 YFZCNC01240), National Natural Science Foundation of China (No. 31470208), and National Key R&D Program of China (2019YFA0905600).

ACKNOWLEDGMENTS

The English writing was refined by Professor Weihui Wu at the College of Life Sciences, Nankai University, China.

SUPPLEMENTARY MATERIAL

The Supplementary Material for this article can be found online at: https://www.frontiersin.org/articles/10.3389/fbioe.2022.837720/full#supplementary-material

REFERENCES

Amberg, D. C., and Huo, K. K. (2009). *Experimental Guidelines on Yeast Genetic Methods*. 2nd edition. Beijing: Science Press.

Bao, J., Huang, M., Petranovic, D., and Nielsen, J. (2017). Moderate Expression of SEC16 Increases Protein Secretion by Saccharomyces C. *Appl. Environ. Microbiol.* 83, e03400–16. doi:10.1128/AEM.03400-16

Bhatia, Y., Mishra, S., and Bisaria, V. S. (2002). Microbial β-Glucosidases: Cloning, Properties, and Applications. *Crit. Rev. Biotechnol.* 22, 375–407. doi:10.1080/07388550290789568

Brandt, B. A., Jansen, T., Volschenk, H., Görgens, J. F., Van Zyl, W. H., and Den Haan, R. (2021). Stress Modulation as a Means to Improve Yeasts for Lignocellulose Bioconversion. *Appl. Microbiol. Biotechnol.* 105, 4899–4918. doi:10.1007/s00253-021-11383-y

Cedras, G., Kroukamp, H., Van Zyl, W. H., and Den Haan, R. (2019). The In Vivo Detection and Measurement of the Unfolded Protein Response in Recombinant Cellulase Producing Saccharomyces Cerevisiae Strains. *Biotechnol. Appl. Biochem.* 67, 82–94. doi:10.1002/bab.1819

Cox, J. S., Shamu, C. E., and Walter, P. (1993). Transcriptional Induction of Genes Encoding Endoplasmic Reticulum Resident Proteins Requires a Transmembrane Protein Kinase. *Cell* 73, 1197–1206. doi:10.1016/0092-8674(93)90648-A

Dallbey, R. E., Heijne, G. von., Wan, P., and Zhang, Y. Q. (2009). *Protein Targeting, Transport and Translocation*. Beijing: Science Press.

Davison, S. A., den Haan, R., and van Zyl, W. H. (2020). Exploiting Strain Diversity and Rational Engineering Strategies to Enhance Recombinant Cellulase Secretion by Saccharomyces Cerevisiae. *Appl. Microbiol. Biotechnol.* 104, 5163–5184. doi:10.1007/s00253-020-10602-2

DiCarlo, J. E., Norville, J. E., Mali, P., Rios, X., Aach, J., and Church, G. M. (2013). Genome Engineering in Saccharomyces Cerevisiae Using CRISPR-Cas Systems. *Nucleic Acids Res.* 41, 4336–4343. doi:10.1093/nar/gkt135

Ding, J., Liang, G., Zhang, K., Hong, J., Zou, S., Lu, H., et al. (2018). Extra Metabolic burden by Displaying over Secreting: Growth, Fermentation and Enzymatic Activity in Cellobiose of Recombinant Yeast Expressing β-Glucosidase. *Bioresour. Technol.* 254, 107–114. doi:10.1016/j.biortech.2017.12.030

Ding, W.-T., Zhang, G.-C., and Liu, J.-J. (2013). 3′ Truncation of the GPD1 Promoter in Saccharomyces Cerevisiae for Improved Ethanol Yield and Productivity. *Appl. Environ. Microbiol.* 79, 3273–3281. doi:10.1128/AEM.03319-12

Gietz, R. D., Schiestl, R. H., Willems, A. R., and Woods, R. A. (1995). Studies on the Transformation of Intact Yeast Cells by the LiAc/SS-DNA/PEG Procedure. *Yeast* 11, 355–360. doi:10.1002/yea.320110408

Hong, J., Yang, H., Zhang, K., Liu, C., Zou, S., and Zhang, M. (2014). Development of a Cellulolytic Saccharomyces Cerevisiae Strain with Enhanced Cellobiohydrolase Activity. *World J. Microbiol. Biotechnol.* 30, 2985–2993. doi:10.1007/s11274-014-1726-9

Jouhten, P., Boruta, T., Andrejev, S., Pereira, F., Rocha, I., and Patil, K. R. (2016). Yeast Metabolic Chassis Designs for Diverse Biotechnological Products. *Sci. Rep.* 6, 29694. doi:10.1038/srep29694

Kawazoe, N., Kimata, Y., and Izawa, S. (2017). Acetic Acid Causes Endoplasmic Reticulum Stress and Induces the Unfolded Protein Response in Saccharomyces Cerevisiae. *Front. Microbiol.* 8, 1192. doi:10.3389/fmicb.2017.01192

Li, J. M., Zhang, X. M., and Guo, J. H. (2020). Preliminary Optimization of RNA Extraction from Whole Course Cultures of a cAMP-Producing Yeast Strain. *Food Ferment. Industries* 46 (24), 1–8. doi:10.13995/j.cnki.11-1802/ts.024409

Lian, J., Mishra, S., and Zhao, H. (2018). Recent Advances in Metabolic Engineering of Saccharomyces Cerevisiae: New Tools and Their Applications. *Metab. Eng.* 50, 85–108. doi:10.1016/j.ymben.2018.04.011

Lu, H. Y., Li, J. M., Sun, S. F., Zhang, X. M., Ding, J. J., and Zou, S. L. (2019). Construction of an Auxotrophic Mutant from an Industrial Saccharomyces Cerevisiae Strain by CRISPR-Cas9 System. *Chin. J. Biotechnol.* 39, 67–74. doi:10.13523/j.cb.20191008

Mattanovich, D., Gasser, B., Hohenblum, H., and Sauer, M. (2004). Stress in Recombinant Protein Producing Yeasts. *J. Biotechnol.* 113, 121–135. doi:10.1016/j.jbiotec.2004.04.035

Navarro-Tapia, E., Nana, R. K., Querol, A., and Pérez-Torrado, R. (2016). Ethanol Cellular Defense Induce Unfolded Protein Response in Yeast. *Front. Microbiol.* 7, 1–12. doi:10.3389/fmicb.2016.00189

Navarro-Tapia, E., Querol, A., and Pérez-Torrado, R. (2018). Membrane Fluidification by Ethanol Stress Activates Unfolded Protein Response in Yeasts. *Microb. Biotechnol.* 11, 465–475. doi:10.1111/1751-7915.13032

Orlean, P., and Menon, A. K. (2007). Thematic Review Series: Lipid Posttranslational Modifications. GPI Anchoring of Protein in Yeast and Mammalian Cells, or: How We Learned to Stop Worrying and Love Glycophospholipids. *J. Lipid Res.* 48, 993–1011. doi:10.1194/jlr.R700002-JLR200

Pittet, M., and Conzelmann, A. (2007). Biosynthesis and Function of GPI Proteins in the Yeast Saccharomyces C. *Biochim. Biophys. Acta (Bba) - Mol. Cel Biol. Lipids* 1771, 405–420. doi:10.1016/j.bbalip.2006.05.015

Sambrook, J., and Russell, D. W. (2001). *Molecular Cloning: A Laboratory Manual*. 3rd edn. New York: Cold Spring Harbor Laboratory, Cold Spring Harbor.

Sun, Z., and Brodsky, J. L. (2019). Protein Quality Control in the Secretory Pathway. *J.Cell Biol.* 218, 3171–3187. doi:10.1083/jcb.201906047

Thak, E. J., Yoo, S. J., Moon, H. Y., and Kang, H. A. (2020). Yeast Synthetic Biology for Designed Cell Factories Producing Secretory Recombinant Proteins. *FEMS Yeast Res.* 20, foaa009. doi:10.1093/femsyr/foaa009

Wang, G., Liu, C., Hong, J., Ma, Y., Zhang, K., Huang, X., et al. (2013). Comparison of Process Configurations for Ethanol Production from Acid- and Alkali-Pretreated Corncob by Saccharomyces C Strains with and without β-Glucosidase Expression. *Bioresour. Technol.* 142, 154–161. doi:10.1016/j.biortech.2013.05.033

Young, C. L., and Robinson, A. S. (2014). Protein Folding and Secretion: Mechanistic Insights Advancing Recombinant Protein Production in S. C. *Curr. Opin. Biotechnol.* 30, 168–177. doi:10.1016/j.copbio.2014.06.018

Zhang, X. M., Guo, J. H., Hong, J. F., Lu, H. Y., Ding, J. J., Zou, S. L., et al. (2020). Evaluation of UPR Response in Yeast by Using UPRE-Lac Z as a Reporter Gene. *Chin. J. Biotechnol.* 40, 1–9. doi:10.13523/j.cb.2006036

Zou, S., Sun, S., Zhang, X., Li, J., Guo, J., Hong, J., et al. (2021). Repetitive δ-Integration of a Cellulase-Encoding Gene into the Chromosome of an Industrial Angel Yeast-Derived Strain by URA 3 Recycling. *Biotechnol. Appl. Biochem.* 68, 953–963. doi:10.1002/bab.1984

Conflict of Interest: The authors declare that the research was conducted in the absence of any commercial or financial relationships that could be construed as a potential conflict of interest.

frontiers | Frontiers in Bioengineering and Biotechnology

ORIGINAL RESEARCH
published: 25 April 2022
doi: 10.3389/fbioe.2022.888869

Engineering *Yarrowia lipolytica* to Produce Itaconic Acid From Waste Cooking Oil

Lanxin Rong[1], Lin Miao[1], Shuhui Wang[1], Yaping Wang[1], Shiqi Liu[1], Zhihui Lu[1], Baixiang Zhao[1], Cuiying Zhang[1], Dongguang Xiao[1], Krithi Pushpanathan[2], Adison Wong[2] and Aiqun Yu[1]**

[1]State Key Laboratory of Food Nutrition and Safety, Key Laboratory of Industrial Fermentation Microbiology of the Ministry of Education, Tianjin Key Laboratory of Industrial Microbiology, College of Biotechnology, Tianjin University of Science and Technology, Tianjin, China, [2]Food, Chemical and Biotechnology Cluster, Singapore Institute of Technology, Dover, Singapore

Itaconic acid (IA) is a high-value organic acid with a plethora of industrial applications. In this study, we seek to develop a microbial cell factory that could utilize waste cooking oil (WCO) as raw material for circular and cost-effective production of the abovementioned biochemical. Specifically, we expressed cis-aconitic acid decarboxylase (CAD) gene from *Aspergillus terreus* in either the cytosol or peroxisome of *Yarrowia lipolytica* and assayed for production of IA on WCO. To further improve production yield, the 10 genes involved in the production pathway of acetyl-CoA, an intermediate metabolite necessary for the synthesis of cis-aconitic acid, were individually overexpressed and investigated for their impact on IA production. To minimize off-target flux channeling, we had also knocked out genes related to competing pathways in the peroxisome. Impressively, IA titer up to 54.55 g/L was achieved in our engineered *Y. lipolytica* in a 5 L bioreactor using WCO as the sole carbon source.

Keywords: itaconic acid, *Y. lipolytica*, waste cooking oil, peroxisome, subcellular engineering

OPEN ACCESS

Edited by:
Hua Ling,
National University of Singapore, Singapore

Reviewed by:
Yuanda Song,
Shandong University of Technology, China
Xiao-Jun Ji,
Nanjing Tech University, China

****Correspondence:***
Adison Wong
adison.wong@singaporetech.edu.sg
Aiqun Yu
yuaiqun@tust.edu.cn

Specialty section:
This article was submitted to Synthetic Biology, a section of the journal Frontiers in Bioengineering and Biotechnology

Received: *03 March 2022*
Accepted: *04 April 2022*
Published: *25 April 2022*

Citation:
Rong L, Miao L, Wang S, Wang Y, Liu S, Lu Z, Zhao B, Zhang C, Xiao D, Pushpanathan K, Wong A and Yu A (2022) Engineering Yarrowia lipolytica to Produce Itaconic Acid From Waste Cooking Oil. Front. Bioeng. Biotechnol. 10:888869. doi: 10.3389/fbioe.2022.888869

INTRODUCTION

Carboxylic acids are important building blocks in the chemical industry. Among them, itaconic acid (IA) is favorably listed by the US Department of Energy as one of top 12 biochemical to be produced from renewable resources (Werpy and Petersen, 2004), with a forecasted market potential of $260 million in 2025 (Sriariyanun, 2019). IA is an unsaturated dicarboxylic acid that is characteristically stable in acidic, neutral and moderately alkaline conditions. Due to its advantageous properties, IA is often used as a co-monomer in the manufacture of synthetic fibers, coatings, adhesives, thickeners and binders (Willke and Vorlop, 2001; Zhao et al., 2018), and as substitutes for petrochemical-based acrylic or methacrylic acids (Nuss and Gardner, 2013). Traditionally, to meet the growing demand for IA, industries resort to fossil resources through petrochemical refinery processes to produce IA at scale. However, these methods often suffer from low efficiency and generate large amount of waste in the process, such as spent heavy metal catalysts and organic solvents (Krull et al., 2017). Furthermore, fossil resources are finite and will eventually be depleted. For these reasons, bio-based production of IA using microbial cell factories are increasingly being pursued.

Filamentous fungi such as *Aspergillus terreus* (Kuenz et al., 2012), *Ustilago maydis* (Geiser et al., 2016) and *Ustilago cynodontis* (Hosseinpour Tehrani et al., 2019b) have been demonstrated to naturally produce IA at high titers. In one example, the fermentation of *A. terreus* at industrial scale is able to generate a titer of 160 g/L IA (Krull et al., 2017), a value that is close to the theoretical yield. In

another example, up to 220 g/L IA was achieved by fermentation of *U. maydis* (Hosseinpour Tehrani et al., 2019a). Despite having high production titers, current bioprocesses involving filamentous fungi are not without challenges. Critically, the highly branched mycelial filaments of filamentous fungi give rise to high broth viscosity during fermentation, leading to poor aeration and mixing in stirred-tank bioreactors (Kubicek et al., 2011; Porro and Branduardi, 2017). Increasing impeller speed, on the other hand, is not an option due to the shear-sensitive nature of filamentous fungi. Moreover, fermentation of most filamentous fungi requires the addition of alkali to maintain a neutral pH condition which is a cause of concern as this increases the probability of bacterial contamination during cultivation (Cui et al., 2017; Li et al., 2021). To circumvent issues associated with filamentous fungi bioprocessing, scientists have applied systems metabolic engineering principles to enable heterologous production of IA in several strains of bacteria and yeasts (**Table 1**).

The industrial microbe *Yarrowia lipolytica* is an unconventional oleaginous yeast that is also classified by the US Food and Drug Administration as 'generally regarded as safe' (GRAS) (Zhao et al., 2021b). *Y. lipolytica* possesses unique physiological and metabolic features compared to the most widely used chassis strains *Escherichia coli* and *Saccharomyces cerevisiae*, which enhance its merits as a microbial cell factory (Liu et al., 2015). Firstly, *Y. lipolytica* has good tolerance for external environment stresses, such as low temperatures, high salt concentrations and acidic pH (Gonçalves et al., 2014). Secondly, the oleaginous yeast is able to utilize a myriad of carbon substrates for growth, including waste cooking oil (WCO) (Zinjarde, 2014; Pang et al., 2019; Li et al., 2022). This permits the valorization of waste streams and reduces the overall cost of production. Thirdly, *Y. lipolytica* is richly endowed with multiple pathways for the generation and accumulation of intracellular acetyl-CoA, which are important intermediaries of IA biosynthesis (Zhou et al., 2012; Ng et al., 2020). Finally, the yeast exhibits high tolerance for IA, thus allowing for accumulation of IA within (Zhao et al., 2019).

In our previous studies, we successfully engineered *Y. lipolytica* to produce limonene and bisabolene, where WCO was employed as the sole carbon source (Pang et al., 2019; Zhao et al., 2021b; Li et al., 2022). Motivated by earlier successes, we herein investigated the feasibility of producing IA from engineered *Y. lipolytica* on WCO (**Figure 1**). We expressed cis-aconitic acid decarboxylase (CAD) gene from *A. terreus* in either the cytosol or peroxisome of *Y. lipolytica* and assayed for production of IA in the extracellular supernatant. To further improve the final yield, the 10 genes involved in the production pathway of acetyl-CoA, an intermediate metabolite necessary for the synthesis of cis-aconitic acid, were each singly overexpressed. To minimize off-target flux channeling, we had also knocked out genes related to competing pathways in the peroxisome. Finally, IA titer up to 54.55 g/L was obtained in the engineered *Y. lipolytica* with a yield of 0.3 g/g WCO and a maximum productivity of 0.6 g/L/h without pH control in the 5 L bioreactor. At the time of writing, this is the highest titer of IA obtained with an engineered yeast cell factory.

MATERIALS AND METHODS

Strains, Plasmids, Primers, and Cultivation Media

The *E. coli* strain DH5α was used as the host in this study for the cloning and plasmid construction. *E. coli* strains were routinely cultured at 37°C in Luria-Bertani (LB) media (1% tryptone, 0.5% yeast extract, and 1% sodium chloride contained) or on LB agar plates supplemented with 100 μg/ml of ampicillin. *Y. lipolytica*

TABLE 1 | Representative examples of IA production in engineered microbial hosts.

Parental strain	Engineering strategy	Fermentation condition	Carbon source	Titer	References
E. coli	*CAD*↑, *CS*↑, *ICD*↓, *ICL*Δ, *PTA*Δ, *PYK*Δ, *SUCS*Δ	Fed-batch bioreactor	Glucose and glutamic acid	32.00 g/L	Harder et al. (2016)
	CAD↑, *ACO*↑, *ICD*Δ	Fed-batch bioreactor	LB + Glucose	4.34 g/L	Okamoto et al. (2014)
	CAD↑, *CS*↑, *ACO*↑, *PTA*Δ, *LDH*Δ	Bioreactor	LB + Glucose	0.69 g/L	Vuoristo et al. (2015)
S. cerevisiae	*CAD*↑, *ADE3*Δ, *BNA2*Δ, *TES1*Δ	Large-scale bioreactor	Glucose	0.17 g/L	Blazeck et al. (2014)
Halomonas bluephagenesis	*CAD*↑, *ACO*↑, *ICD*↓	Batch shake flask	Citrate	63.60 g/L	Zhang et al. (2021a)
Corynebacterium glutamicum	*CAD*↑, *MALE*↑, *ICD*↓	Shake flask	Glucose	7.80 g/L	Otten et al. (2015)
Pichia kudriavzevii	*CAD*↑, *MTT*↑, *ICD*Δ	Fed-batch bioreactor	Glucose	1.23 g/L	Sun et al. (2020)
Y. lipolytica	*CAD*↑, *ACO*↑, *AMPD*↓	Bioreactor	Glucose	4.60 g/L	Blazeck et al. (2015)
	CAD↑, *MTT*↑	Fed-batch bioreactor	Glucose	22.02 g/L	Zhao et al. (2019)
	CAD-ePTS1↑, *POT1*↑, *ICL*Δ	Bioreactor	Waste cooking oil	54.55 g/L	This study

↑, *Gene overexpression;* ↓, *gene knockdown;* Δ, *gene knockout;* CAD, *cis-aconitic acid decarboxylase gene;* CS, *citrate synthase gene;* ICD, *isocitrate dehydrogenase gene;* ICL, *isocitrate lyase gene;* PTA, *phosphate acetyltransferase gene;* PYK, *pyruvate kinase gene;* SUCS, *succinyl-CoA synthetase gene;* ACO, *aconitase gene;* LDH, *lactate dehydrogenase gene;* ADE3, *cytoplasmic trifunctional C1-tetrahydrofolate (THF) synthase gene;* BNA2, *a putative tryptophan 2,3-dioxygenase or indoleamine 2,3-dioxygenase gene;* TES1, *peroxisomal acyl-CoA, thioesterase gene; MALE, maltose-binding protein gene;* MTT, *mitochondrial tricarboxylate transporter gene;* AMPD, *adenosine monophosphate deaminase gene;* POT1, *peroxisomal thiolase gene.*

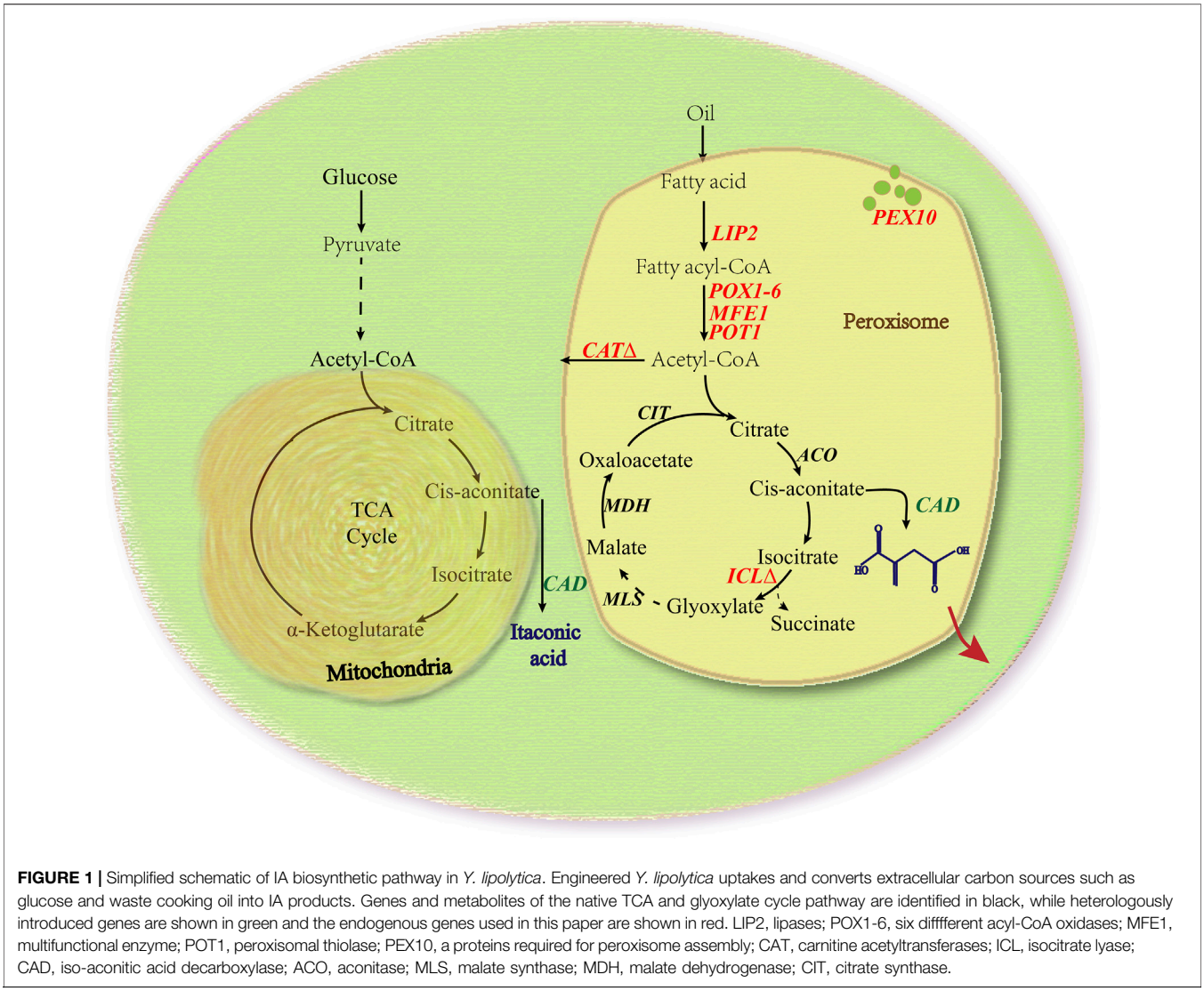

FIGURE 1 | Simplified schematic of IA biosynthetic pathway in *Y. lipolytica*. Engineered *Y. lipolytica* uptakes and converts extracellular carbon sources such as glucose and waste cooking oil into IA products. Genes and metabolites of the native TCA and glyoxylate cycle pathway are identified in black, while heterologously introduced genes are shown in green and the endogenous genes used in this paper are shown in red. LIP2, lipases; POX1-6, six diffffferent acyl-CoA oxidases; MFE1, multifunctional enzyme; POT1, peroxisomal thiolase; PEX10, a proteins required for peroxisome assembly; CAT, carnitine acetyltransferases; ICL, isocitrate lyase; CAD, iso-aconitic acid decarboxylase; ACO, aconitase; MLS, malate synthase; MDH, malate dehydrogenase; CIT, citrate synthase.

Po1g *KU70*Δ was used as the base strain in this study, which has been generated from the parental strain Po1g (a commonly used host strain for protein expression). This strain was used as it is known that the rate of precise homologous recombination (HR) increased substantially for deletion of the *KU70* gene in Po1g (Yu et al., 2016). Routine cultivation of *Y. lipolytica* strains was carried out at 30°C in YPD medium (1% yeast extract, 2% peptone and 2% dextrose contained) while the yeast synthetic complete medium (YNB) (0.67% yeast nitrogen base without amino acids, 2% glucose, 1.5% bacto agar) lacking the appropriate nutrients was used for the screening of transformants. The fermentation experiment used YPO medium containing WCO (1% yeast extract, 2% peptone, 1.18% WCO and 0.2% tween-80 contained), and the initial pH of cultivation media was 5.73. Among them, the amount of WCO added is calculated based on the same C atoms as glucose in YPD medium. The strains and plasmids used in this study are listed in **Supplementary Table S1**. The PCR primers used in this study were synthesized by Genewiz (Jiangsu, China) and are listed in **Supplementary Table S2**.

Plasmid Construction

The *Y. lipolytica* expression vector pYLEX1 used in this study possesses the strong promoter hp4d, and its detailed information was provided in Li et al. (2021). Using primers CAD1-F/R and CAD2-F/R that were synthesized according to the existing sequence (GenBank ID: AB326105.1) in NCBI GenBank, two fragments of the *CAD* gene without introns were amplified from the *A. terreus* HAT418 genome and cloned into pYLEX1 to yield pYLEX1-CAD through adapted homologous recombination. The construction process of plasmid pYLEX1-CAD is depicted in **Supplementary Figure S1**. The sequences of the oligonucleotides used to amplify all the genes are listed in **Supplementary Table S2** in the Additional file. Subsequently, the expression cassettes of other gene candidates were cloned into pYLEX1-CAD individually (**Supplementary Figure S2**). All recombinant plasmids were constructed using the One Step Cloning Kit from Vazyme Biotech Co., Ltd. (Nanjing, China). Transformants were plated on LB-ampicillin agar plates and incubated overnight at 37°C. Single colonies were inoculated into LB-ampicillin and cultured overnight

at 37°C with shaking at 225 rpm. Plasmids were isolated, and the genes were verified by DNA sequencing.

Following that, all plasmids were linearized using the *Spe* I enzyme and then transformed into the *Y. lipolytica* Po1g *KU70*Δ competent cells using lithium acetate/single-stranded vector DNA/polyethylene glycol method. The linearized plasmids introduced were integrated at the pBR322 locus of the strain Po1g *KU70*Δ. After 2 to 3 days of culture, the positive *Y. lipolytica* transformants were selected on YNB-LEU plates and subsequently confirmed by genomic DNA PCR analysis (Yu et al., 2016). Accordingly, in this study, the engineered *Y. lipolytica* Po1g *KU70*Δ strain was used as the host for all genetic modifications with gene knockouts and chromosomal expression constructs introduced *via* engineered pYLEX1 plasmids.

Yeast Cultivation

Seed inoculum of *Y. lipolytica* were first cultured in a 20 ml tube with 5 ml YPD medium and incubated for 24 h in a shaking incubator set at 30°C and 220 rpm. Next, a 250 ml flask was filled with 50 ml YPO medium and inoculated at the seeding density of OD_{600} 0.1. The inoculated finished shake flasks were grown in a shaking incubator set at 30°C and 220 rpm. Fermented yeast cultures were collected on the fourth day and analyzed by GC-MS to determine and identify the IA content.

Gene Knockout

The *ICL*Δ strain was generated by knocking out the ORF region gene of *ICL via* the homologous recombination (HR) mechanism, which replaced *ICL* with the hygromycin B resistance marker gene (*HPH*) amplified from pSH69-Hph using the primer pairs ICL-Hph-F/R. To this end, two targeting arms (upstream and downstream flanking sequences of *ICL*), each approximately 1,000 bp in length, were amplified using PCR from the genomic DNA of Po1g-2G and ligated to the 5′ and 3′ ends of the *HPH* gene, respectively. After transformation of the *ICL* disruption cassette into *Y. lipolytica* cells, a gene replacement event occurs *via* double-crossover homologous recombination within the two flanking homology arms at the targeted locus. Transformants were grown in the YPDH solid medium (30°C, under dark conditions) supplemented with hygromycin and chosen randomly. The correct *ICL*Δ strain was confirmed by PCR with ICL-Hph-knock-F and ICL-Hph-knock-R primers. The construction of the *CAT*Δ strain was carried out using a similar procedure.

Visualizing Fluorescence Distribution by Laser Scanning Confocal Microscopy

To test the peroxisomal targeting ability of enhanced peroxisome targeting signal ePTS1, yeast cells expressing *hrGFPO-ePTS1* were cultured in 50 ml YPD medium for 24 h. For simultaneous visualization of hrGFPO and Nile red, precultures incubated in 50 ml YPD were stained by adding Nile red solution (1 mg/ml) in acetone to the cell suspension (0.1 v/v) and incubated for 60 min in the dark at room temperature. The stained cells were washed with normal saline and resuspended in potassium phosphate buffer (pH 7.4) before being transferred onto glass slides to visualize hrGFPO at 488 nm and Nile red at 561 nm with an Olympus FV1000 confocal laser scanning microscope.

Esterification of the Fermented Supernatant

2 ml of the fermented supernatant was added to 1.5 ml of 10% HCl-CH_3OH solution, which was esterified at 62°C for 3 h. Then, 2 ml of n-hexane was added and the resultant mixture was violently shaken for 1 min to dissolve the dimethyl itaconate. After centrifugation (6,000 rpm, 5 min), the upper organic phase was transferred into another clean bottle for detection.

GC-MS Analysis

0.6 μl of the upper organic phase from the above Section was analyzed by GC-MS using an Agilent 7890A GC with a 5975C MSD equipped with an HP-5MS column (30 m × 0.25 mm × 0.25 μm, Agilent, Santa Clara, CA, United States). The GC oven temperature was initially held at 60°C for 2 min, and then ramped up to 250°C at a rate of 10°C/min and held for 9 min. The split ratio was 10:1. Helium was used as the carrier gas, with an inlet pressure of 13.8 psi. The injector was maintained at 250°C and the ion source temperature was set to 220°C. The final data analysis was performed using the Enhanced Data Analysis software (Agilent, Santa Clara, CA, United States) to obtain the standard curve of dimethyl itaconate, and the area obtained after the sample is analyzed and detected by the instrument is brought into the formula of the standard curve to obtain the output of dimethyl itaconate. The titer of IA is obtained by converting with the esterification rate obtained in the above section.

Statistical Analysis

Differences in titers between the control strain and other strains were evaluated using SPSS 22.0 software for Windows (SPSS, Chicago, IL, United States). One-way ANOVA analyses were carried out with a confidence interval of 95% and statistical significance between the groups and the relevant control was considered if p-value < 0.05.

Bioreactor Fermentations

Bioreactor fermentation was batched processed using an optimal medium formulation containing 59 g/L WCO, 16 g/L yeast extract, 8 g/L peptone and 10 g/L tween-80. The strain was first seeded in 50 ml YPD medium in 250 ml shake flasks, cultured at 30°C and 220 rpm for 16 h. Following that, the bioreactor containing 3 L of YPO medium were inoculated with the seed cultures at an OD_{600} of 1.

Fermentation without any pH control was carried out in a 5 L stirred fermenter (Shanghai Baoxing Bioengineering Equipment Co., Ltd., Shanghai, China) at 30°C and 1 vvm. The bioreactor pressure was maintained at 0.06 MPa. The impeller stirring speed was 400 rpm.

RESULTS AND DISCUSSION

Heterologous Expression of *A. terreus* Cis-Aconitic Acid Decarboxylase in *Y. lipolytica*

In *A. terreus*, IA is generated from the decarboxylation of the TCA intermediate cis-aconitic acid by the CAD enzyme (Bonnarme et al., 1995; Tevz et al., 2010). To test if *A. terrus's CAD* gene can be expressed successfully in *Y. lipolytica* without codon optimization,

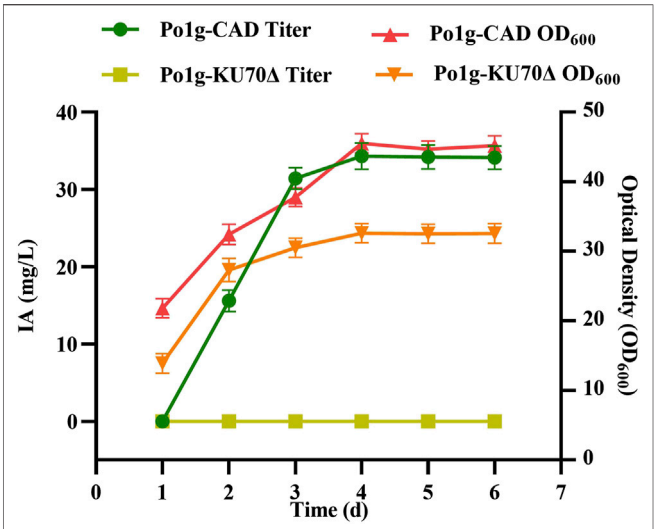

FIGURE 2 | IA production in *Y. lipolytica* strains expressing the *CAD* gene. The titer of IA and biomass of *Y. lipolytica* were determined by shaking flask fermentation of Po1g-CAD strain and control strain Po1g in YPO culture. All values presented are the mean of three biological replicates ± standard deviation.

we first cloned the associated gene from *A. terreus* HAT418 strain into *Y. lipolytica* strain Po1g *KU70*Δ, with the gene's intron spliced out. In the gene sequencing analysis that followed, we discovered that the actual PCR-amplified gene sequence was different from the genome sequence shown in NCBI database. Our sequence data for *A. terreus* HAT418 *CAD* gene was submitted to GenBank under the accession number MT862134.1. Overexpression of the *CAD* gene in *Y. lipolytica* Po1g *KU70*Δ resulted in the creation of strain Po1g-CAD. We subjected both the engineered strain with cytosolic CAD and control strain without CAD to shake flask fermentation and assayed for IA continuously over a period of 6 days. We confirmed that IA was produced only in the engineered *Y. lipolytica* but not in its wild type. IA levels were first detected in the supernatant on day 2 and they increased gradually with time until a maximum yield of 33.12 mg/L was obtained on day 4 (**Figure 2**). This is contrasted with the Po1g *KU70*Δ original strain where no IA production detected, thereby confirming that the heterologous expression of the *A. terreus* CAD is necessary for IA production in *Y. lipolytica*.

Peroxisomal Targeting of Heterologous Cis-Aconitic Acid Decarboxylase Gene Improved Itaconic Acid Production

β-oxidation of long chain fatty acids in eukaryotes are known to occur mainly in the peroxisomes (Wache et al., 2001; Hanko et al., 2018). In *Y. lipolytica,* this process produces acetyl-CoA which then enters the glyoxylate cycle for synthesis of the IA precursor, cis-aconitic acid (Dominguez et al., 2010; Koivistoinen et al., 2013; Xu et al., 2017). Several studies have shown that subcellular localization of specific enzymes or metabolic pathways not only increase product conversion efficiency, but is also able to suppress the undesirable effects of competitive metabolic inhibition (Zhu et al., 2018; Yang et al., 2019; Zhu et al., 2021). As such, this approach of subcellular compartmentalization is adopted in our study and complemented with the use of WCO as the substrate to enable sustainable, efficient and low-cost production of IA. To this end, IA production from the glyoxylate cycle in *Y. lipolytica* was ensured by targeting the involved heterologous enzymes to the peroxisomal matrix through the addition of enhanced peroxisomal targeting signal (ePTS1) after its gene sequence. The ePTS1 applied in this instance has been shown to be localized in *S. cerevisiae* (DeLoache et al., 2016).

Two separate dyes, Nile red and green fluorescence, were employed for staining of the yeast cells to validate the peroxisomal targeting ability of ePTS1. In an earlier study, it was shown that hrGFPO, encoding the green fluorescence protein, was most strongly expressed in Po1g *KU70*Δ (Zhao et al., 2021a). The plasmid with sequence ePTS1 added after the hrGFPO protein sequence was retransformed into yeast, resulting in strain Po1g-hrGFPO-ePTS1 (**Figure 3A**). Nile red fluorescence, on the other hand, was used to stain the peroxisomes of the yeast cells. To determine if ePTS1 could be successfully localized to peroxisomes in *Y. lipolytica*, Laser Scanning Confocal Microscopy (LSCM) was performed to observe the location of the two different fluorescence in yeast cells. As shown in **Figure 3B**, a green fluorescent protein with localization signal ePTS1, which exhibits green light under microscope irradiation, was expressed in the engineered yeast. Yeast cells after Nile red staining also show localized red fluorescence under the microscope. Combining these two images, we observed that the green and red shades overlap almost completely and produce a bright yellow light. Therefore, it can be confirmed that ePTS1 plays a role in determining the location of the peroxisome could be used as a peroxisomal targeting sequence for *Y. lipolytica*.

Subsequently, the plasmid pYLEX1-CAD-ePTS1 constructed through the ligation of ePTS1 downstream of the *CAD* gene was integrated into the *Y. lipolytica* Po1g *KU70*Δ chromosomes of the strain. The resulting engineered strain was cultured in the YPO medium and the 6 days course of IA production titers and biomass were shown in **Figure 4**. The titers of IA increased continuously from the beginning of cultivation up to day 4 with the highest titer having reached 1.58 g/L. Following this, the titers of IA gradually stabilized, likely owing to WCO depletion. Notably, we also compared the use of WCO and glucose in this subcellular compartmentalized approach to generate IA under the same conditions. The use of WCO had resulted in almost 100-folds increase in IA titer as compared to glucose (13.68 mg/L of IA) as the carbon source, hence implying that WCO was superior to glucose for IA production in these conditions. We also observed that the overproduction of IA has a positive effect on the cell growth. Together, our results demonstrate that the expression and localization of *CAD* in the peroxisomes of *Y. lipolytica* can lead to substantial increase in IA production.

Overexpression of Endogenous Genes Involved in the Acetyl-CoA Production Pathway of *Y. lipolytica*

To further enhance IA production in *Y. lipolytica*, we attempted to study the pathway genes involved in the conversion of oils to fatty

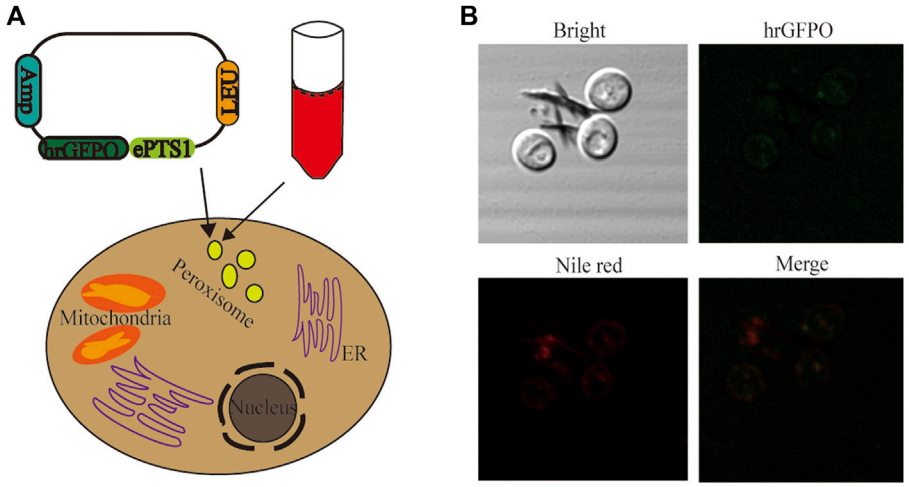

FIGURE 3 | Investigation of the localization of peroxisomes. **(A)** Schematic diagram of experimental design. hrGFPO-ePTS1 is used to specifically mark peroxisomes in *Y. lipolytica*. Nile red is used to show intracellular peroxisomes regions. **(B)** Localization observation of peroxisomes use the Nile red and strain Po1g-hrGFPO-ePTS1 through LSCM.

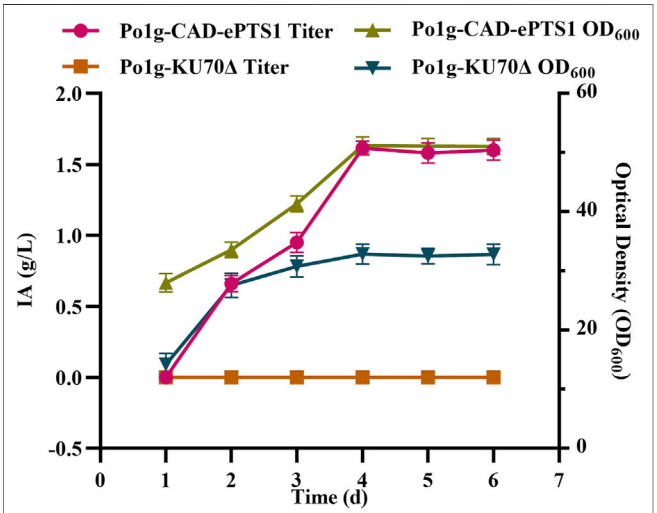

FIGURE 4 | IA production in *Y. lipolytica* strains expressing the CAD-ePTS1 gene. The titer of IA and biomass were determined by shaking flask fermentation of Po1g-CAD-ePTS1 strain and control strain Po1g in YPO culture. All values presented are the mean of three biological replicates ± SD.

acids and the utilization of fatty acids to raise the flux of precursor acetyl-CoA. The β-oxidation of fatty acids is a four-reaction cycle comprising of oxidation, hydration, dehydrogenation, and thiolysis, which results in one molecule of acetyl-CoA released in the peroxisome (Braga and Belo, 2016). In *Y. lipolytica*, the first step of fatty acid β-oxidation can be catalyzed by six different acyl-CoA oxidases (POX1-6) (Beopoulos et al., 2008). The second and third steps of β-oxidation are catalyzed by a multifunctional enzyme (MFE1) (Black et al., 2000; Dulermo et al., 2013), and the final step is catalyzed by peroxisomal thiolase (POT1) (Wang et al., 2020). As such, the genes involved in the β-oxidation pathway were overexpressed in an attempt to increase the flux towards IA. Ten genes, consisting of *LIP2* (encoding lipases, Zhang et al., 2021b), *POX1-6* (Ledesma-Amaro and Nicaud, 2016), *MFE1* (Haddouche et al., 2010), *POT1* (Smith et al., 2000), and *PEX10* (encoding a proteins required for peroxisome assembly, Zhang et al., 2021b), were overexpressed individually and investigated for their effects on IA overproduction to determine the genes critical for IA biosynthesis in the acetyl-CoA production pathway. To this end, ten strains were constructed on the basis of the strain expressing *CAD-ePTS1* gene, including the ten endogenous genes in the acetyl-CoA production pathway of *Y. lipolytica*; all genes were integrated into the chromosomes of *Y. lipolytica* Po1g *KU70*Δ. These ten engineered strains were then cultured in YPO medium for 6 days in shake flasks. The IA titers of the strains showed that the overexpression of the individual corresponding genes could improve IA production compared to the control strain expressing only the respective *CAD-ePTS1* gene. Among them, the POT1-overexpressed strain (hereafter named Po1g-2G), achieved the highest titers of 2.42 g/L for IA after 4 days of cultivation (**Figure 5**). The results indicated that overexpression of this key enzymes can effectively promote the fatty acid degradation process and release the most acetyl-CoA molecules for IA biosynthesis. This observation is consistent with several other studies in which POT1 has already been demonstrated to be the key rate-limiting enzyme in the β-oxidation pathway (Ma et al., 2020; Zhang et al., 2021b). Therefore, the engineered strain Po1g-2G was used for subsequent engineering efforts to boost IA production.

Effects of Deletion of the Carnitine Acetyltransferases and Isocitrate Lyase Genes on Itaconic Acid Production in *Y. lipolytica*

The yield of IA can be further improved by reducing the loss of the precursor acetyl-CoA and preventing the synthesis of cis-aconitic acid from the glyoxylate cycle into downstream products such as succinic

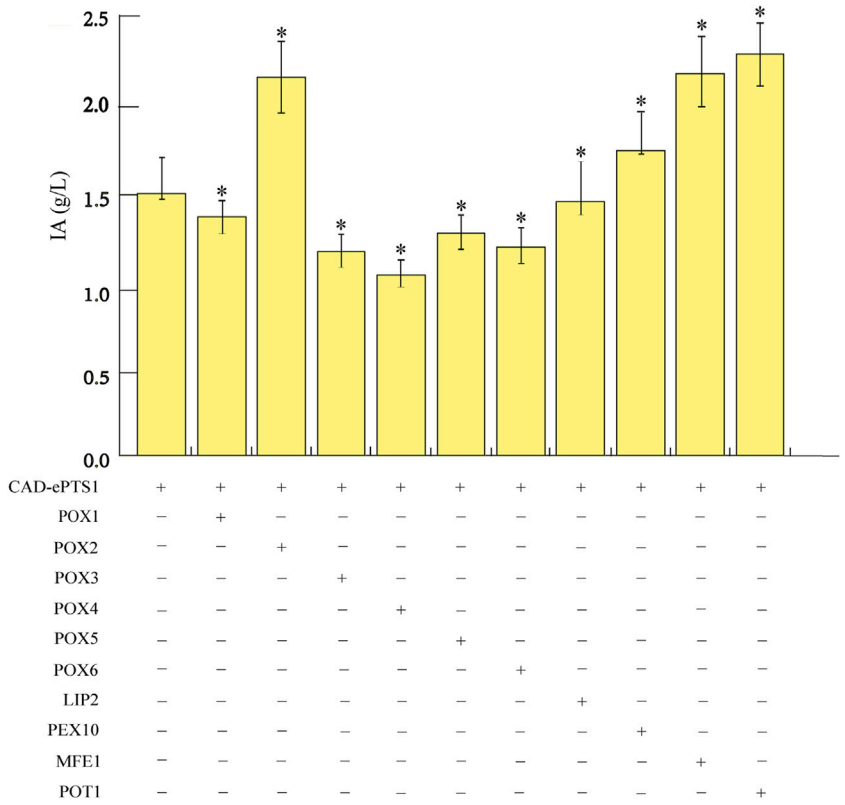

FIGURE 5 | Effects of overexpressing genes involved in the acetyl-CoA production pathway on IA production. The genes involved in the acetyl-CoA production pathway, consisting of *LIP2, POX1-6, MFE1, POT1* and *PEX10,* were overexpressed individually. Titers of IA produced by the strains were quantified after 6 days of cultivation in shake flasks with YPO medium. All values presented are the mean of three biological replicates ± standard deviation. *p<0.05, significantly different from control by ANOVA.

acid. The carnitine acetyltransferases (CAT) is responsible for transporting acetyl-CoA between different organelles, which can reversibly link the acetyl units to the carrier molecule carnitine (Strijbis et al., 2008; Strijbis et al., 2010). Meanwhile, the isocitrate lyase (ICL) manages the conversion of isocitrate into succinic acid and glyoxylic acid (Koivistoinen et al., 2013). To verify if either of these enzymes assume a major role in IA production, the corresponding genes singly were deleted from Po1g-2G, resulting in the creation of strains Po1g-2G-CATΔ and Po1g-2G-ICLΔ. After cultivating the resulting strains in shake flasks in YPO medium, it was found that higher IA production reaching 3.33 g/L was observed in ICL knockout strain as compared to CAT knockout strain with 2.8 g/L titers. This suggests that blocking the downstream pathway improves IA production while blocking the efflux effect of the acetyl coenzyme in the peroxisome is not as advantageous. Therefore, the Po1g-2G-ICLΔ strain was selected as the final optimized strain.

Itaconic Acid Production by the Engineered *Y. lipolytica* in Bioreactor

One of the most crucial issues in platform chemicals production is in achieving a high product titers consistently (Gao et al., 2016; Li et al., 2020). To investigate the performance of IA-producing *Y. lipolytica* at conditions that are more relevant for large-scale application, a 5 L bioreactor was employed. Unlike the procedure conducted in the shaking flask fermentation method, here, the composition of the growth medium was altered and the approach of adding sufficient WCO substrate at once was adopted to avoid the problems caused by fed batch fermentation. In the phase of active cell growth between 24 and 96 h, the Po1g-2G-ICLΔ strain intensively produced IA. During this period, the average specific rate of IA synthesis was 0.8 g/L/h, and the maximum specific rate of 2.3 g/L/h was observed between the 76–96-h intervals (**Figure 6**). Hence, the maximum titer of IA was 54.55 g/L after the 96-h reaction in the fermenter. At the time of writing, this is the highest IA production achieved by a yeast host reported worldwide. As such, *Y. lipolytica* would be a promising industrial host for IA production from renewable feedstock. Our study also demonstrated that the circular bioeconomy concept can be an effective model for scale-up production of valuable biochemical, in particular with the valorization of WCO as raw material.

CONCLUSION

With increasing global interest in environmental protection and sustainable development, the use of low-cost waste to produce valuable platform chemicals in the industrial scale is gaining

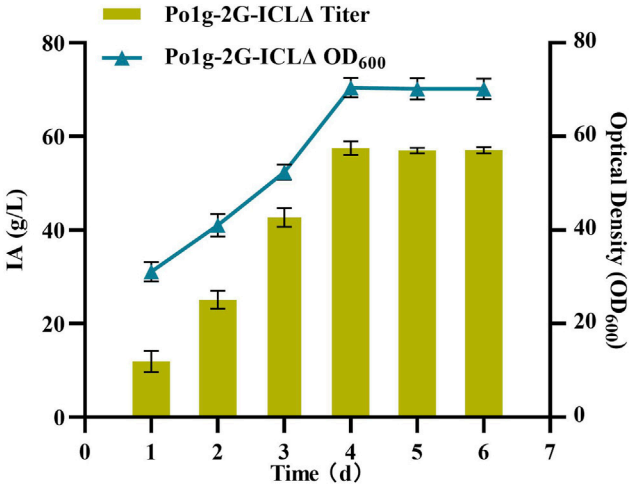

FIGURE 6 | IA production in bioreactor of *Y. lipolytica* strain expressing the 2G-ICLΔ gene. The titer of IA and biomass were determined by bioreactor fermentation of Po1g-2G-ICLΔ strain in YPO culture. All values presented are the mean of three biological replicates ± SD.

attention. In the few studies conducted to date, IA production in engineered strains of *Y. lipolytica* was predominantly using glucose as the primary carbon source (Blazeck et al., 2015; Zhao et al., 2019). Even so, production titers had remained suboptimal (**Table 1**). This had limited the feasibility of large-scale industrial adoption. Here, we employed the cheap raw material WCO to increase acetyl-CoA availability for conversion into IA in the peroxisome of *Y. lipolytica*. By applying both systems metabolic engineering and bioprocessing optimization strategies in unison, we achieved IA titers of 3.33 g/L in shake flasks and up to 54.55 g/L in stirred-tank bioreactor on WCO as the carbon source without the need for pH control. This amounted to more than 34-folds as compared to the initial titers of 1.58 g/L IA before the optimization of strain and fermentation conditions. In this study, as the supernatant may contain WCO that was not consumed completely, IA cannot be detected directly by HPLC. We used esterification of the supernatant to detect the yield of dimethyl itaconate. While this method, in principle, can be used to determine the theoretical final yield of IA from the esterification rate, it is not the best approach to quantify the exact yield of IA. The development of a more robust and higher throughput method of analysis should be considered in future studies. Furthermore, the yield of organic acids produced by *Y. lipolytica* is primarily affected by the genetic mechanism and various environmental factors, such as the carbon source, nitrogen source, temperature, pH, iron concentration, and dissolved oxygen levels. As such, since bioreactor fermentation with WCO as the sole carbon source is still relatively understudied, further optimization of the fermentation conditions could improve IA yields. Nonetheless, the present work on the production of IA by WCO still provides valuable insights that will facilitate further efforts in the biosynthesis of this compound. The results obtained suggest that the oleaginous yeast *Y. lipolytica* is an attractive platform as it provides a viable and scalable pathway to the overproduction of IA and most notably, one that is sustained by waste conversion. However, given the extensive knowledge on IA gene regulation and fermentation conditions, it is believed that higher productivities of IA can be achieved through further engineering of this yeast strain and the optimization of fermentation conditions in subsequent studies.

DATA AVAILABILITY STATEMENT

The datasets presented in this study can be found in online repositories. The names of the repository/repositories and accession number(s) can be found in the article/ **Supplementary Material**.

AUTHOR CONTRIBUTIONS

DX, CZ, AW, and, AY conceived and designed the study. LR, LM, SW, YW, SL, ZL, and BZ performed the experiments. LR and KP analyzed data and wrote the manuscript. DX, CZ, AW, and AY critically revised the manuscript. All authors have read and approved the final manuscript.

FUNDING

This work was funded by the Natural Science Foundation of Tianjin, China (17JCYBJC40800), the Research Foundation of Tianjin Municipal Education Commission, China (2017ZD03), the Innovative Research Team of Tianjin Municipal Education Commission, China (TD13-5013), Tianjin Municipal Science and Technology Project (18PTSYJC00140, 19PTSYJC00060), Startup Fund for "Haihe Young Scholars" of Tianjin University of Science and Technology, the Thousand Young Talents Program of Tianjin, China. AW was supported by the Ministry of Education, Singapore (R-MOE-A401-F028) and Lee Foundation (T-LEE-T201-A001).

SUPPLEMENTARY MATERIAL

The Supplementary Material for this article can be found online at: https://www.frontiersin.org/articles/10.3389/fbioe.2022.888869/full#supplementary-material

REFERENCES

Beopoulos, A., Mrozova, Z., Thevenieau, F., Le Dall, M.-T., Hapala, I., Papanikolaou, S., et al. (2008). Control of Lipid Accumulation in the Yeast *Yarrowia lipolytica*. *Appl. Environ. Microbiol.* 74 (24), 7779–7789. doi:10.1128/AEM.01412-08

Black, P. N., Færgeman, N. J., and DiRusso, C. C. (2000). Long-chain Acyl-CoA-dependent Regulation of Gene Expression in Bacteria, Yeast and Mammals. *J. Nutr.* 130 (2S Suppl. l), 305S–309S. doi:10.1093/jn/130.2.305S

Blazeck, J., Miller, J., Pan, A., Gengler, J., Holden, C., Jamoussi, M., et al. (2014). Metabolic Engineering of *Saccharomyces cerevisiae* for Itaconic Acid Production. *Appl. Microbiol. Biotechnol.* 98, 8155–8164. doi:10.1007/s00253-014-5895-0

Blazeck, J., Hill, A., Jamoussi, M., Pan, A., Miller, J., and Alper, H. S. (2015). Metabolic Engineering of *Yarrowia lipolytica* for Itaconic Acid Production. *Metab. Eng.* 32, 66–73. doi:10.1016/j.ymben.2015.09.005

Bonnarme, P., Gillet, B., Sepulchre, A. M., Role, C., Beloeil, J. C., and Ducrocq, C. (1995). Itaconate Biosynthesis in *Aspergillus terreus*. *J. Bacteriol.* 177 (12), 3573–3578. doi:10.1128/jb.177.12.3573-357810.1128/jb.177.12.3573-3578.1995

Braga, A., and Belo, I. (2016). Biotechnological Production of γ-decalactone, a Peach like Aroma, by *Yarrowia lipolytica*. *World J. Microbiol. Biotechnol.* 32 (10), 169. doi:10.1007/s11274-016-2116-2

Cui, Z., Gao, C., Li, J., Hou, J., Lin, C. S. K., and Qi, Q. (2017). Engineering of Unconventional Yeast *Yarrowia lipolytica* for Efficient Succinic Acid Production from Glycerol at Low pH. *Metab. Eng.* 42, 126–133. doi:10.1016/j.ymben.2017.06.007

DeLoache, W. C., Russ, Z. N., and Dueber, J. E. (2016). Towards Repurposing the Yeast Peroxisome for Compartmentalizing Heterologous Metabolic Pathways. *Nat. Commun.* 7, 11152. doi:10.1038/ncomms11152

Dominguez, A., Deive, F. J., Angeles Sanromán, M., and Longo, M. A. (2010). Biodegradation and Utilization of Waste Cooking Oil by *Yarrowia lipolytica* CECT 1240. *Eur. J. Lipid Sci. Technol.* 112, 1200–1208. doi:10.1002/ejlt.201000049

Dulermo, T., Tréton, B., Beopoulos, A., Kabran Gnankon, A. P., Haddouche, R., and Nicaud, J.-M. (2013). Characterization of the Two Intracellular Lipases of *Y. lipolytica* Encoded by TGL3 and TGL4 Genes: New Insights into the Role of Intracellular Lipases and Lipid Body Organisation. *Biochim. Biophys. Acta Mol. Cel Biol. Lipids* 1831 (9), 1486–1495. doi:10.1016/j.bbalip.2013.07.001

Gao, C., Yang, X., Wang, H., Rivero, C. P., Li, C., Cui, Z., et al. (2016). Robust Succinic Acid Production from Crude Glycerol Using Engineered *Yarrowia lipolytica*. *Biotechnol. Biofuels* 9 (1), xz2179. doi:10.1186/s13068-016-0597-8

Geiser, E., Przybilla, S. K., Friedrich, A., Buckel, W., Wierckx, N., Blank, L. M., et al. (2016). *Ustilago maydis* Produces Itaconic Acid via the Unusual Intermediate *Trans*-aconitate. *Microb. Biotechnol.* 9 (1), 116–126. doi:10.1111/1751-7915.12329

Gonçalves, F. A. G., Colen, G., and Takahashi, J. A. (2014). *Yarrowia lipolytica* and its Multiple Applications in the Biotechnological Industry. *Scientific World J.* 2014, 1–14. doi:10.1155/2014/476207

Haddouche, R., Delessert, S., Sabirova, J., Neuvéglise, C., Poirier, Y., and Nicaud, J.-M. (2010). Roles of Multiple Acyl-CoA Oxidases in the Routing of Carbon Flow towards β-oxidation and Polyhydroxyalkanoate Biosynthesis in *Yarrowia lipolytica*. *FEMS. Yeast. Res.* 10 (7), 917–927. doi:10.1111/j.1567-1364.2010.00670.x

Hanko, E. K. R., Denby, C. M., Sànchez i Nogué, V., Lin, W., Ramirez, K. J., Singer, C. A., et al. (2018). Engineering β-oxidation in *Yarrowia lipolytica* for Methyl Ketone Production. *Metab. Eng.* 48, 52–62. doi:10.1016/j.ymben.2018.05.018

Harder, B.-J., Bettenbrock, K., and Klamt, S. (2016). Model-based Metabolic Engineering Enables High Yield Itaconic Acid Production by *Escherichia coli*. *Metab. Eng.* 38, 29–37. doi:10.1016/j.ymben.2016.05.008

Hosseinpour Tehrani, H., Becker, J., Bator, I., Saur, K., Meyer, S., Rodrigues Lóia, A. C., et al. (2019a). Integrated Strain- and Process Design Enable Production of 220 g L^{-1} Itaconic Acid with *Ustilago maydis*. *Biotechnol. Biofuels* 12, 263. doi:10.1186/s13068-019-1605-6

Hosseinpour Tehrani, H., Tharmasothirajan, A., Track, E., Blank, L. M., and Wierckx, N. (2019b). Engineering the Morphology and Metabolism of pH Tolerant *Ustilago cynodontis* for Efficient Itaconic Acid Production. *Metab. Eng.* 54, 293–300. doi:10.1016/j.ymben.2019.05.004

Koivistoinen, O. M., Kuivanen, J., Barth, D., Turkia, H., Pitkänen, J.-P., Penttilä, M., et al. (2013). Glycolic Acid Production in the Engineered Yeasts *Saccharomyces cerevisiae* and *Kluyveromyces lactis*. *Microb. Cel Fact.* 12, 82. doi:10.1186/1475-2859-12-82

Krull, S., Hevekerl, A., Kuenz, A., and Prüße, U. (2017). Process Development of Itaconic Acid Production by a Natural Wild Type Strain of *Aspergillus terreus* to Reach Industrially Relevant Final Titers. *Appl. Microbiol. Biotechnol.* 101 (10), 4063–4072. doi:10.1007/s00253-017-8192-x

Kubicek, C. P., Punt, P., and Visser, J. (2011). "Production of Organic Acids by Filamentous Fungi," in *Industrial Applications*. Editor M. Hofrichter (Berlin, Heidelberg: Springer), 215–234. doi:10.1007/978-3-642-11458-8_10

Kuenz, A., Gallenmüller, Y., Willke, T., and Vorlop, K.-D. (2012). Microbial Production of Itaconic Acid: Developing a Stable Platform for High Product Concentrations. *Appl. Microbiol. Biotechnol.* 96 (5), 1209–1216. doi:10.1007/s00253-012-4221-y

Ledesma-Amaro, R., and Nicaud, J.-M. (2016). *Yarrowia lipolytica* as a Biotechnological Chassis to Produce Usual and Unusual Fatty Acids. *Prog. Lipid Res.* 61, 40–50. doi:10.1016/j.plipres.2015.12.001

Li, J., Rong, L., Zhao, Y., Li, S., Zhang, C., Xiao, D., et al. (2020). Next-generation Metabolic Engineering of Non-conventional Microbial Cell Factories for Carboxylic Acid Platform Chemicals. *Biotechnol. Adv.* 43, 107605. doi:10.1016/j.biotechadv.2020.107605

Li, J., Zhu, K., Miao, L., Rong, L., Zhao, Y., Li, S., et al. (2021). Simultaneous Improvement of Limonene Production and Tolerance in *Yarrowia lipolytica* through Tolerance Engineering and Evolutionary Engineering. *ACS Synth. Biol.* 10, 884–896. doi:10.1021/acssynbio.1c00052

Li, S., Rong, L., Wang, S., Liu, S., Lu, Z., Miao, L., et al. (2022). Enhanced Limonene Production by Metabolically Engineered *Yarrowia lipolytica* from Cheap Carbon Sources. *Chem. Eng. Sci.* 249, 117342. doi:10.1016/j.ces.2021.117342

Liu, H.-H., Ji, X.-J., and Huang, H. (2015). Biotechnological Applications of *Yarrowia lipolytica*: Past, Present and Future. *Biotechnol. Adv.* 33 (8), 1522–1546. doi:10.1016/j.biotechadv.2015.07.010

Ma, Y. R., Li, W. J., Mai, J., Wang, J. P., Wei, Y. J., Ledesma-Amaro, R., et al. (2020). Engineering *Yarrowia lipolytica* for Sustainable Production of the Chamomile Sesquiterpene (−)-α-Bisabolol. *Green. Chem.* 23, 780–787. doi:10.1039/d0gc03180a

Ng, T.-K., Yu, A.-Q., Ling, H., Pratomo Juwono, N. K., Choi, W. J., Leong, S. S. J., et al. (2020). Engineering *Yarrowia lipolytica* towards Food Waste Bioremediation: Production of Fatty Acid Ethyl Esters from Vegetable Cooking Oil. *J. Biosci. Bioeng.* 129 (1), 31–40. doi:10.1016/j.jbiosc.2019.06.009

Nuss, P., and Gardner, K. H. (2013). Attributional Life Cycle Assessment (ALCA) of Polyitaconic Acid Production from Northeast US Softwood Biomass. *Int. J. Life Cycle Assess.* 18, 603–612. doi:10.1007/s11367-012-0511-y

Okamoto, S., Chin, T., Hiratsuka, K., Aso, Y., Tanaka, Y., Takahashi, T., et al. (2014). Production of Itaconic Acid Using Metabolically Engineered *Escherichia coli*. *J. Gen. Appl. Microbiol.* 60 (5), 191–197. doi:10.2323/jgam.60.191

Otten, A., Brocker, M., and Bott, M. (2015). Metabolic Engineering of *Corynebacterium glutamicum* for the Production of Itaconate. *Metab. Eng.* 30, 156–165. doi:10.1016/j.ymben.2015.06.003

Pang, Y., Zhao, Y., Li, S., Zhao, Y., Li, J., Hu, Z., et al. (2019). Engineering the Oleaginous Yeast *Yarrowia lipolytica* to Produce Limonene from Waste Cooking Oil. *Biotechnol. Biofuels.* 12, 241. doi:10.1186/s13068-019-1580-y

Porro, D., and Branduardi, P. (2017). "Production of Organic Acids by Yeasts and Filamentous Fungi," in *Biotechnology of Yeasts and Filamentous Fungi*. Editor A. Sibirny (Cham: Springer), 205–223. doi:10.1007/978-3-319-58829-2_7

Smith, J. J., Brown, T. W., Eitzen, G. A., and Rachubinski, R. A. (2000). Regulation of Peroxisome Size and Number by Fatty Acid β-Oxidation in the Yeast *Yarrowia lipolytica*. *J. Biol. Chem.* 275 (26), 20168–20178. doi:10.1074/jbc.M909285199

Sriariyanun, M., Heitz, J. H., Yasurin, P., Asavasanti, S., and Tantayotai, P. (2019). Itaconic Acid: a Promising and Sustainable Platform Chemical? *Appl. Sci. Eng. Prog.* 12 (1), 14410–14416. doi:10.14416/j.asep.2019.05.002

Strijbis, K., van Roermund, C. W. T., Visser, W. F., Mol, E. C., van den Burg, J., MacCallum, D. M., et al. (2008). Carnitine-dependent Transport of Acetyl Coenzyme A in *Candida albicans* is Essential for Growth on Nonfermentable Carbon Sources and Contributes to Biofilm Formation. *Eukaryot. Cel.* 7 (4), 610–618. doi:10.1128/EC.00017-08

Strijbis, K., van Roermund, C. W., van den Burg, J., van den Berg, M., Hardy, G. P. M., Wanders, R. J., et al. (2010). Contributions of Carnitine Acetyltransferases to Intracellular Acetyl Unit Transport in *Candida albicans*. *J. Biol. Chem.* 285 (32), 24335–24346. doi:10.1074/jbc.M109.094250

Sun, W., Vila-Santa, A., Liu, N., Prozorov, T., Xie, D., Faria, N. T., et al. (2020). Metabolic Engineering of an Acid-Tolerant Yeast Strain *Pichia kudriavzevii* for Itaconic Acid Production. *Metab. Eng. Commun.* 10, e00124. doi:10.1016/j.mec.2020.e00124

Tevz, G., Benčina, M., and Legiša, M. (2010). Enhancing Itaconic Acid Production by *Aspergillus terreus*. *Appl. Microbiol. Biotechnol.* 87 (5), 1657–1664. doi:10.1007/s00253-010-2642-z

Vuoristo, K. S., Mars, A. E., Sangra, J. V., Springer, J., Eggink, G., Sanders, J. P. M., et al. (2015). Metabolic Engineering of Itaconate Production in *Escherichia coli*. *Appl. Microbiol. Biotechnol.* 99 (1), 221–228. doi:10.1007/s00253-014-6092-x

Wache, Y., Aguedo, M., Choquet, A., Gatfield, I. L., Nicaud, J.-M., and Belin, J.-M. (2001). Role of β-Oxidation Enzymes in γ-Decalactone Production by the Yeast *Yarrowia lipolytica*. *Appl. Environ. Microbiol.* 67 (12), 5700–5704. doi:10.1128/AEM.67.12.5700-5704.2001

Wang, J., Ledesma-Amaro, R., Wei, Y., Ji, B., and Ji, X.-J. (2020). Metabolic Engineering for Increased Lipid Accumulation in *Yarrowia lipolytica* - A Review. *Bioresour. Techn.* 313, 123707. doi:10.1016/j.biortech.2020.123707

Werpy, T., and Petersen, G. (2004). *Top Value Added Chemicals from Biomass: Volume IResults of Screening for Potential Candidates from Sugars and Synthesis Gas*. Golden, CO, US: National Renewable Energy Lab.

Willke, T., and Vorlop, K.-D. (2001). Biotechnological Production of Itaconic Acid. *Appl. Microbiol. Biotechnol.* 56, 289–295. doi:10.1007/s002530100685

Xu, P., Qiao, K., and Stephanopoulos, G. (2017). Engineering Oxidative Stress Defense Pathways to Build a Robust Lipid Production Platform in *Yarrowia lipolytica*. *Biotechnol. Bioeng.* 114 (7), 1521–1530. doi:10.1002/bit.26285

Yang, K., Qiao, Y., Li, F., Xu, Y., Yan, Y., Madzak, C., et al. (2019). Subcellular Engineering of Lipase Dependent Pathways Directed towards Lipid Related Organelles for Highly Effectively Compartmentalized Biosynthesis of Triacylglycerol Derived Products in *Yarrowia lipolytica*. *Metab. Eng.* 55, 231–238. doi:10.1016/j.ymben.2019.08.001

Yu, A.-Q., Pratomo, N., Ng, T.-K., Ling, H., Cho, H.-S., Leong, S. S. J., et al. (2016). Genetic Engineering of an Unconventional Yeast for Renewable Biofuel and Biochemical Production. *JoVE* 115, 54371. doi:10.3791/54371

Zhang, J., Jin, B., Hong, K., Lv, Y., Wang, Z., and Chen, T. (2021a). Cell Catalysis of Citrate to Itaconate by Engineered Halomonas Bluephagenesis. *ACS Synth. Biol.* 10, 3017–3027. doi:10.1021/acssynbio.1c00320

Zhang, Q., Yu, S., Lyu, Y., Zeng, W., and Zhou, J. (2021b). Systematically Engineered Fatty Acid Catabolite Pathway for the Production of (2S)-Naringenin in *Saccharomyces cerevisiae*. *ACS Synth. Biol.* 10 (5), 1166–1175. doi:10.1021/acssynbio.1c00002

Zhao, M., Lu, X., Zong, H., Li, J., and Zhuge, B. (2018). Itaconic Acid Production in Microorganisms. *Biotechnol. Lett.* 40 (3), 455–464. doi:10.1007/s10529-017-2500-5

Zhao, C., Cui, Z., Zhao, X., Zhang, J., Zhang, L., Tian, Y., et al. (2019). Enhanced Itaconic Acid Production in *Yarrowia lipolytica* via Heterologous Expression of a Mitochondrial Transporter MTT. *Appl. Microbiol. Biotechnol.* 103 (5), 2181–2192. doi:10.1007/s00253-019-09627-z

Zhao, Y., Liu, S., Lu, Z., Zhao, B., Wang, S., Zhang, C., et al. (2021a). Hybrid Promoter Engineering Strategies in *Yarrowia lipolytica*: Isoamyl Alcohol Production as a Test Study. *Biotechnol. Biofuels.* 14 (1), 149. doi:10.1186/s13068-021-02002-z

Zhao, Y., Zhu, K., Li, J., Zhao, Y., Li, S., Zhang, C., et al. (2021b). High-efficiency Production of Bisabolene from Waste Cooking Oil by Metabolically Engineered *Yarrowia lipolytica*. *Microb. Biotechnol.* 14 (6), 2497–2513. doi:10.1111/1751-7915.13768

Zhou, J., Yin, X., Madzak, C., Du, G., and Chen, J. (2012). Enhanced α-ketoglutarate Production in *Yarrowia lipolytica* WSH-Z06 by Alteration of the Acetyl-CoA Metabolism. *J. Biotechnol.* 161 (3), 257–264. doi:10.1016/j.jbiotec.2012.05.025

Zhu, J., Schwartz, C., and Wheeldon, I. (2018). Controlled Intracellular Trafficking Alleviates an Expression Bottleneck in *S. cerevisiae* Ester Biosynthesis. *Metab. Eng. Commun.* 8, e00085. doi:10.1016/j.mec.2018.e00085

Zhu, K., Kong, J., Zhao, B., Rong, L., Liu, S., Lu, Z., et al. (2021). Metabolic Engineering of Microbes for Monoterpenoid Production. *Biotechnol. Adv.* 53, 107837. doi:10.1016/j.biotechadv.2021.107837

Zinjarde, S. S. (2014). Food-related Applications of *Yarrowia lipolytica*. *Food Chem.* 152, 1–10. doi:10.1016/j.foodchem.2013.11.117

Conflict of Interest: The authors declare that the research was conducted in the absence of any commercial or financial relationships that could be construed as a potential conflict of interest.

Publisher's Note: All claims expressed in this article are solely those of the authors and do not necessarily represent those of their affiliated organizations, or those of the publisher, the editors and the reviewers. Any product that may be evaluated in this article, or claim that may be made by its manufacturer, is not guaranteed or endorsed by the publisher.

frontiers | Frontiers in Bioengineering and Biotechnology

MINI REVIEW
published: 23 June 2022
doi: 10.3389/fbioe.2022.897204

Reprogramming Microbial CO_2-Metabolizing Chassis With CRISPR-Cas Systems

Hai-Yan Yu[1,2], *Shu-Guang Wang*[1,3] *and Peng-Fei Xia*[1]*

[1]School of Environmental Science and Engineering, Shandong University, Qingdao, China, [2]State Key Laboratory of Microbial Technology, Shandong University, Qingdao, China, [3]Sino-French Research Institute for Ecology and Environment, Shandong University, Qingdao, China

Global warming is approaching an alarming level due to the anthropogenic emission of carbon dioxide (CO_2). To overcome the challenge, the reliance on fossil fuels needs to be alleviated, and a significant amount of CO_2 needs to be sequestrated from the atmosphere. In this endeavor, carbon-neutral and carbon-negative biotechnologies are promising ways. Especially, carbon-negative bioprocesses, based on the microbial CO_2-metabolizing chassis, possess unique advantages in fixing CO_2 directly for the production of fuels and value-added chemicals. In order to fully uncover the potential of CO_2-metabolizing chassis, synthetic biology tools, such as CRISPR-Cas systems, have been developed and applied to engineer these microorganisms, revolutionizing carbon-negative biotechnology. Herein, we review the recent advances in the adaption of CRISPR-Cas systems, including CRISPR-Cas based genome editing and CRISPR interference/activation, in cyanobacteria, acetogens, and methanogens. We also envision future innovations *via* the implementation of rising CRISPR-Cas systems, such as base editing, prime editing, and transposon-mediated genome editing.

Keywords: carbon dioxide, CRISPR, genome editing, cyanobacteria, acetogen, methanogen

OPEN ACCESS

Edited by:
Shuobo Shi,
Beijing University of Chemical Technology, China

Reviewed by:
Guoliang Yuan,
Oak Ridge National Laboratory (DOE), United States
Xinyu Song,
Tianjin University, China
Shuaiyin Chen,
Zhengzhou University, China

***Correspondence:**
Peng-Fei Xia
pfxia@sdu.edu.cn

Specialty section:
This article was submitted to Synthetic Biology, a section of the journal Frontiers in Bioengineering and Biotechnology

Received: *15 March 2022*
Accepted: *07 June 2022*
Published: *23 June 2022*

Citation:
Yu H-Y, Wang S-G and Xia P-F (2022) Reprogramming Microbial CO_2-Metabolizing Chassis With CRISPR-Cas Systems. Front. Bioeng. Biotechnol. 10:897204. doi: 10.3389/fbioe.2022.897204

INTRODUCTION

Anthropogenic emission of carbon dioxide (CO_2) has driven an unprecedented high level of CO_2 in the atmosphere, leading to an approximately 1.1°C increase in the average global temperature (Tollefson, 2021). This increase has reached an alarming level and has caused global and local climate issues. It also leaves a very small window to achieve the 1.5°C target settled in the Paris Agreement and reinforced in the UN Climate Conference in Glasgow (COP26). The atmospheric CO_2 level must be lowered by a significant amount by controlling the emission of CO_2 and sequestering CO_2 from the atmosphere at the same time. In this endeavor, biotechnology provides promising routes. In one way, carbon-neutral biotechnology utilizes sustainable carbon sources (e.g., agriculture and forest wastes) to produce chemicals (e.g., ethanol, butanol, and 2,3-butanediol), alleviating the reliance on fossil fuels and reducing CO_2 emissions (Liu et al., 2020). In another way, carbon-negative biotechnology directly consumes industrial or atmospheric CO_2 for the bioproduction of fuels and value-added chemicals (Liu et al., 2020; Liew et al., 2022).

With metabolic engineering and synthetic biology, the inventory of products from biological routes has been greatly expanded, and the production and yield have been improved. For instance, the baker's yeast *Saccharomyces cerevisiae* has been genetically engineered to convert lignocellulosic feedstock to bioethanol and chemicals, exhibiting the potential of carbon-neutral biotechnology (Wei

et al., 2013; Sun et al., 2021). Recently, *S cerevisiae* has been engineered to utilize wasteful CO_2 accumulated during lignocellulosic sugar fermentation by the installation of a CO_2 fixation pathway, transforming the correlated biotechnology from a carbon-neutral process to a carbon-negative technology (Li et al., 2017; Xia et al., 2017). Inspiringly, Gassler et al. (2020) generated an engineered yeast *Pichia pastoris* capably of growing with CO_2 and methanol, opening a new window for heterotrophic yeast to use one-carbon (C1) compounds as sole carbon sources. Similar enterprises have been made in *Escherichia coli*, and artificial autotrophic *E. coli* has been generated *via* the implementation of CO_2 fixation pathways and adaptive laboratory evolution (Antonovsky et al., 2016; Gleizer et al., 2019; Flamholz et al., 2020).

Another biological path is to employ microorganisms that metabolize CO_2 innately, such as photoautotrophic cyanobacteria and chemoautotrophs, including acetogens and methanogens. These organisms can use CO_2 as a carbon source from either industrial waste gases or the atmosphere (Fackler et al., 2021). CO_2-metabolizing microorganisms have shown great potential as microbial chassis, and industrial attempts have been made (Liu et al., 2020; Liew et al., 2022). Given the advances in synthetic biology, these microbes play more important roles on the path towards a sustainable future with enhanced CO_2 utilization efficiency and an expanded spectrum of products. For instance, cyanobacterium *Synechocystis* sp. PCC 6803 has been modularly engineered to produce a high titer of 1-butanol, short/medium-chain carbohydrate, and lactate from CO_2 (Liu X. et al., 2019; Shabestary et al., 2021; Yunus et al., 2022). Lately, a pioneer study conducted by LanzaTech, Inc. (Skokie, IL, United States) shows that *Clostridium autoethanogenum* can convert syngas (consisting of CO_2, CO, and H_2) to acetone and isopropanol, and a pilot-scale fermentation in a 125-L scalable reactor was demonstrated (Liew et al., 2022). These advances have validated the capability of CO_2-metabolizing chassis in the fixation of CO_2 and production of value-added chemicals, and these succuss illustrated the ever-increasing power of synthetic biology in biotechnology.

CRISPR-Cas systems, the bacterial and archaeal immune systems, have been repurposed as synthetic biology tools for gene editing and regulation (Knott and Doudna, 2018). They have been revolutionizing biotechnology in fundamental ways. Though still in its infant stage, multiple CRISPR-Cas-based synthetic biology tools have been developed for cyanobacteria, acetogens, and methanogens, driving the rising of novel biotechnologies based on CO_2-metabolizing microbes. Herein, we summarize the current progress of CRISPR-Cas systems in genetically engineering microbial CO_2-metabolizing chassis, especially cyanobacteria, acetogens, and methanogens, for the conversion of CO_2 to biofuels and value-added products, and we discuss the challenges and future endeavors in developing more efficient synthetic biology tools.

MICROBIAL CO_2 METABOLIZING ORGANISMS

Microbial CO_2-metabolizing chassis, mainly autotrophic microorganisms, can use CO_2 as a sole carbon source for catabolic and anabolic activities. Until now, six CO_2 fixation pathways have been identified, among which the Calvin cycle and Wood-Ljungdahl Pathway are the most understood and applicable routes (Fuchs, 2011; Muller, 2019; Gleizer et al., 2020). Compared to the complementary physiochemical strategies, biological ways have advantages in forming carbon-carbon bonds with one-carbon (C1) building blocks using either solar energy or redox power from inorganic compounds, i.e., iron, sulfide, and ammonia, offering better opportunities for bioproduction by the microbes themselves or in combined biotic-abiotic processes (Li et al., 2012; Sakimoto et al., 2016; Jin et al., 2021).

Photoautotrophic organisms, such as microalgae and cyanobacteria, can fix CO_2 with solar energy through the Calvin cycle and produce a large variety of organic compounds. Notably, efforts have been made to design and build engineered cyanobacteria for the production of biofuels (i.e., biodiesel, bioethanol, and isobutanol), value-added chemicals (Santos-Merino et al., 2019; Xia et al., 2019), and food-related products, such as starch (Luan et al., 2019). Besides the photoautotrophs, *Cupriavidus necator* (formerly *Ralstonia eutropha*), a facultative chemolithotroph, can grow on CO_2 through the Calvin cycle as well with H_2 or formate as the electron donor without light. *C. necator* has also been engineered as a novel chassis for bioproduction (Li et al., 2012; Panich et al., 2021). Chemoautotrophic organisms harboring the Wood-Ljungdahl Pathway can utilize CO_2 and H_2 anaerobically. As the key representatives, acetogens, especially strains from the class of Clostridia (e.g., *C. autoethanogenum*, *Clostridium ljungdahlii, Acetobacterium woodii*, and *Eubacterium limosum*), have been interrogated and engineered to utilize CO_2 (with H_2) or CO_2-containing mixed gases (Muller, 2019; Fackler et al., 2021). Due to the requirement and capability of co-utilization of H_2, acetogens can also be the bridge connecting bioproduction and "Power-to-Gas" technology, generating a novel nexus "Power-to-X" (Molitor et al., 2019; Mishra et al., 2020). Similarly, methanogens play important roles in different bioprocesses in various niches, such as in the gut, in soil, and in engineered systems (i.e., wastewater treatment facilities). They produce CH_4 from CO_2 and H_2 or other one-carbon compounds, like methanol (Thauer et al., 2008; Zabranska and Pokorna, 2018). As methanogens are archaea, they typically possess unique industrial merits, including high tolerance to temperature and osmatic stress, making them advantageous CO_2-metabolizing chassis.

CRISPR-CAS BASED SYSTEMS

CRISPR-Cas-based synthetic biology tools are repurposed from the bacterial and archaeal immune systems (Jiang and Doudna, 2017), and the innovations in CRISPR-Cas-based systems have been reshaping biotechnology in fundamental ways (Knott and Doudna, 2018; Pickar-Oliver and Gersbach, 2019). For instance, an artificial autotrophic *P. pastoris* was generated *via* the integration of six foreign genes and deletion of three innate genes with the CRISPR-Cas-based gene-editing tool (Gassler

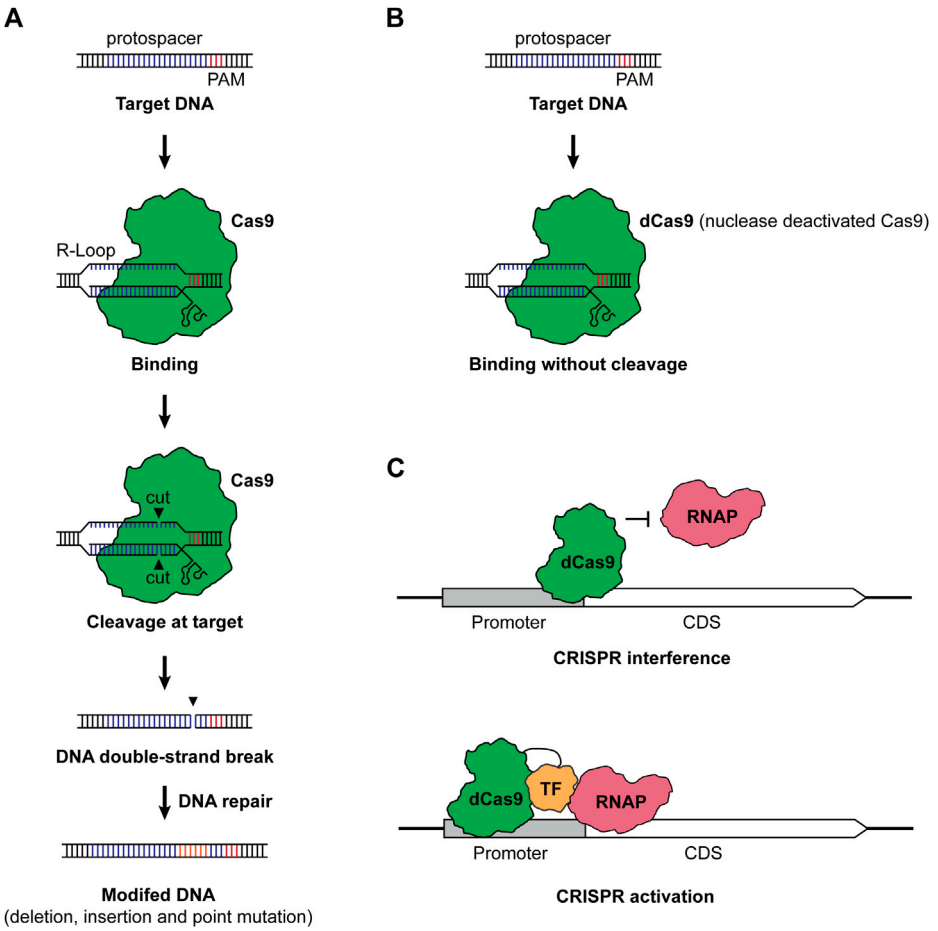

FIGURE 1 | (A) CRISPR-Cas-based genome editing. Under the guidance of a gRNA containing a spacer complementary to the protospacer and a scaffold consisting of crRNA and tracer RNA, the Cas9 and gRNA complex finds and binds to the protospacer with a PAM, forming an R-loop. Then, Cas9 cuts the DNA in each strand, leaving a double-strand break (DSB) in the target. Finally, the target DNA will be modified with the repair of DSB. **(B)** Nuclease deactivated Cas9 protein (dCas9). When the nuclease activity of Cas protein was deactivated, the dCas9 still binds to the target sequence but it will not cleave the DNA anymore. **(C)** CRISPRi and CRISPRa. For CRISPRi, dCas9 binds to the promoter or coding region of a gene of interest and prevents the binding of RNAP, resulting in the repression of transcription. For CRISPRa, the dCas9-transcription factor (TF) fusion binds to the up region of the promoter. The TF helps recruit RNAP and allows the activation of transcription. We employed Cas9 from *S. pyogenes* as a representative in the figure, while a great variety of CRISPR systems can be used for genome editing, CRISPRi, and CRISPRa. TF stands for transcription factor, RNAP stands for RNA polymerase, CDS stands for coding sequence, and PAM stands for protospacer adjacent motif.

et al., 2020). Recently, CRISPR-Cas-based methods have also been deployed to upgrade carbon-negative bioprocess by manipulating CO_2-metabolizing chassis. In this section, we focus on the adaption of different CRISPR-Cas systems for the perturbation of CO_2-metabolizing microbes. We highlight achievements and challenges in cyanobacteria, acetogens, and methanogens.

CRISPR-CAS-BASED GENOME EDITING

CRISPR-Cas-based genome editing in microbes typically has two steps: RNA-guided DNA cleavage and DNA repair of the double-strand break, the latter of which eventually resulted in the editing of a target gene (Selle and Barrangou, 2015; Knott and Doudna, 2018). Taking the Class II Type II CRISPR-Cas system from *Streptococcus pyogenes* as an example, the single CRISPR effector Cas9 is led by a guide RNA (gRNA) consisting of a targeting sequence (spacer), which is complementary to the target sequence (protospacer), a CRISPR RNA (crRNA) and trans-activating CRISPR RNA (tracer RNA) (Jiang and Doudna, 2017). When the complex of Cas9 and gRNA reached the target sequence, it recognizes the protospacer when a protospacer adjacent motif (PAM) presents. Then, the Cas9 nuclease cleaves the DNA and leaves a double-strand break, generating a "dead or alive" scenario for the microbe (Vento et al., 2019). With DNA repair mechanisms, the target gene will be edited to survive the deadly cleavage of Cas9 (**Figure 1A**). CRISPR-Cas-based genome editing has been prosperous due to the ease of use and the clean editing products without leaving a marker or a scar.

In cyanobacteria, CRISPR-Cas-based genome editing has been realized (Xia et al., 2019). Li et al. (2016) adapted a CRISPR-Cas

genome editing tool for cyanobacterium *Synechococcus elongatus* PCC 7942 based on *S. pyogenes* Cas9 with a transient expression system. Later, a plasmid-based CRISPR-Cas system was developed for *S. elongatus* UTEX 2973, a fast-growing cyanobacterium showing great potential in sustainable bioproduction (Wendt et al., 2016). However, these countable successes implied the severe toxicity of Cas9 on cyanobacteria. Due to the toxicity of Cas9, conventional CRISPR-Cas-based genome editing tools with a "dead or alive" selection have not been thriving in cyanobacteria. To surmount this bottleneck, two strategies have been engaged. One is to use alternative Cas proteins. For instance, the Class II Type V CRISPR system with Cas12a as the effector showed lower toxicity than Cas9 to cyanobacteria. By using Cas12a, Ungerer and Pakrasi (2016) achieved CRISPR-Cas-based gene editing in *S. elongatus* UTEX 2973, *Synechocystis* sp. PCC 6803 and *Anabaena* sp. PCC 7102. Another way is to control the expression of the CRISPR-Cas system tightly. Hudson and colleagues hired a tightly regulated RNA device, the theophylline-responsive riboswitch, to maintain a low enough OFF-state expression of Cas9 to prevent its toxicity, and induce the genome-editing when required (Cengic et al., 2022). By applying this system, the reliable transformation of a replicable plasmid harboring CRISPR-Cas9 was obtained, leading to successful deletions and insertions of DNA fragments in the genome of *Synechocystis*. To our best knowledge, this study also reported multiplex genome editing in cyanobacteria for the first time regardless of methods. As multiple genes are typically involved in engineering a microbe for desired functionalities, multiplexing is of great importance in synthetic biology by saving considerable time and labor.

CRISPR-Cas-based genome editing tools have also been established in acetogens and methanogens. For acetogens, Cas9 and Cas12a based methods have been devised in *C. autoethanogenum* (Nagaraju et al., 2016), *C. ljungdahlii* (Huang et al., 2016; Zhao et al., 2019), and *Eubacterium limosum* (Shin et al., 2019). To be noted, enhanced genome editing was achieved *via* a combination of CRISPR-Cas and serine recombinase (Huang et al., 2019). As reported, a phage serine recombinase was used for the integration of large DNA fragments while CRISPR-Cas inserts a small recognition motif of the recombinase. With this method, a butyric acid production pathway was successfully introduced to *C. ljungdahlii* for the production of butyric acid from syngas (Huang et al., 2019). Similar to the abovementioned method for cyanobacteria, a tightly regulated system controlled by a riboswitch, namely RiboCas, was designed to enable CRISPR-Cas-based genome editing in *Clostridium* strains, including *Clostridium pasteurianum*, *Clostridium difficile*, and *Clostridium sporogenes* (Canadas et al., 2019). Moreover, CRISPR-Cas-based deletion and integration were accomplished in methanogen *Methanosarcina acetivorans via* applying an inducible CRISPR-Cas9 system from *S. pyogenes* (Nayak and Metcalf, 2017). In the same study, the authors reported CRISPR-based deletion via the implementation of a foreign non-homologous end-joining (NHEJ) machinery from *Methanocella paludicola*, enabling the deletion of gene fragments (75–2.7 kb) without repairing DNAs. Recently, CRISPR-Cas-based genome editing was reported in methanogenic archaea *Methanococcus maripaludis* with the Cas12a system from *Lachnospiraceae bacterium* (Bao et al., 2022), further expanding the genome editing tools for methanogens.

CRISPR INTERFERENCE (CRISPRI) AND CRISPR ACTIVATION (CRISPRA)

Actually, the toxicity of Cas proteins is not an exclusive issue in cyanobacteria, while most bacteria suffer from the toxic effects of CRISPR-Cas systems (Banno et al., 2018; Canadas et al., 2019; Vento et al., 2019). Despite screening alternative CRISPR-Cas systems and implementation of fine control modules, one alternative way is to employ the nuclease deactivated Cas protein (dCas) (**Figure 1B**). When the nuclease activity of Cas proteins is dead (dCas) or partially dead (nCas), dCas or nCas proteins are less toxic to bacteria compared to fully functional Cas effectors. By using dCas9, the resulting CRISPR-Cas system will no longer cleave the target DNA sequence but bind to the target. When dCas9 binds to the promoter or the coding sequence of a gene of interest, it will prevent the binding of RNA polymerase (RNAP), thus silencing the target gene at the transcription level and generating the method CRISPRi (**Figure 1C**) (Larson et al., 2013; Qi et al., 2013).

Due to the alleviated toxicity, CRISPRi obtained more popularity and has been developed for cyanobacteria. For instance, Yao et al. (2016) employed dCas9 to enable multiplex CRISPRi in *Synechocystis* sp. PCC 6803, Choi and Woo (2020) demonstrated CRISPRi with dCas12a in *S. elongatus* PCC 7942, and a dCas12a-based CRISPRi system was also established for *S. elongatus* UTEX 2973 (Knoot et al., 2020). In the former two reports, multiplex CRISPRi was achieved, and up to four genes were repressed at a single time, showing the huge potential of CRISPRi in engineering cyanobacteria for sustainable production (Yao et al., 2016; Choi and Woo, 2020). Notably, a CRISPRi system was devised for generating a gene repression library in *Synechocystis* sp. PCC 6803 in order to interrogate the genotype-phenotype interactions. By doing so, an industrially relevant strain with higher production of lactate, as a proof of principle, was engineered via CRISPRi-based repression of correlated essential genes (i.e., *gltA* and *pcnB*) related to lactate synthesis (Yao et al., 2020). More recently, CRISPRi was programmed as a genetic switch between cell growth and product synthesis. Shabestary et al. (2021) employed CRISPRi-based *gltA* regulation in a lactate-producing *Synechocystis* and achieve a high yield of lactate by decoupling cell growth and lactate production.

CRISPRi displays potential for acetogens and methanogens as well (Dhamad and Lessner, 2020; Fackler et al., 2021). Woolston et al. (2018) developed an inducible dCas9-based CRISPRi system for the repression of essential genes related to carbon metabolism in *Clostridium ljungdahlii*. Specifically, the *pta* gene encoding the phosphotransacetylase and the *aor2* gene encoding the aldehyde: ferredoxin oxidoreductase were repressed with CRISPRi individually and in a multiplex mode, redirecting carbon from acetate to the desired product 3-hydroxybutyrate with significantly increased titer

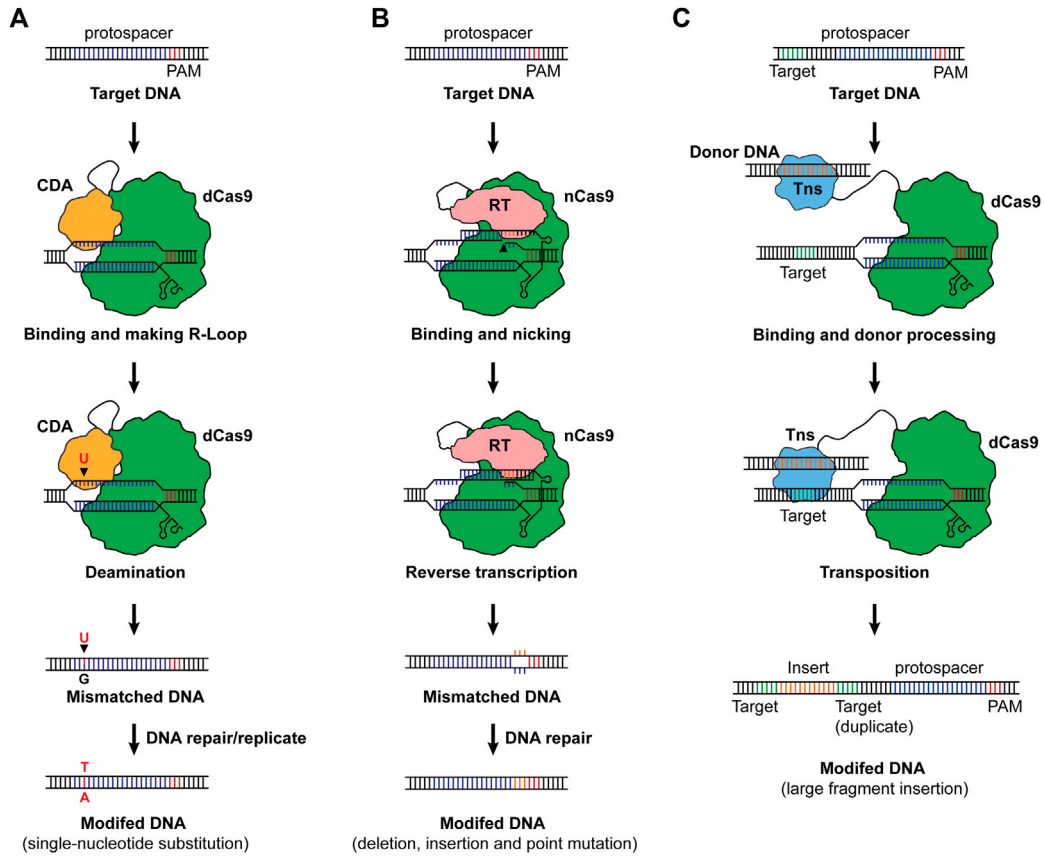

FIGURE 2 | (A) Base editing. The cytosine base editor with a combination of dCas9 cytosine deaminase is shown as an example to illustrate the working mechanism. When dCas9 binds to its target sequence and an R-loop is formed, the cytosine deaminase (CDA) mutates a cytosine (C) to uracil (U), generating a uracil-guanine (U–G) mismatch. The C will then be replaced by thymine (T) along with the reparation of the mismatch upon DNA repair or replication, resulting in a C-to-T substitution at a one-nucleotide resolution. For adenine base editors, an A-to-G substitution will occur as a result of base editing. Notably, nCas9 can also be used as the effector for base editors. **(B)** Prime editing. The prime editing takes advantage of nCas9 and a fused reverse-transcription (RT). By designing a pegRNA consisting of the spacer for targeting, RT template with designed edits, and primer binding site (PBS), deletions, insertions and point mutations can be achieved. **(C)** Transposon-mediated CRISPR-Cas system for DNA integration. As a paradigm, dCas9 was fused to a transposase (Tns), and when the transposase was led to the target sequence, it recognizes the motif for transposition and integrates the donor DNA into the upstream of the protospacer, enabling large fragment insertions. Cas9 was used as the Cas effector for illustration of the basic working principles of base editing, prime editing and transposon-mediated editing.

and yield (Woolston et al., 2018). In a pioneer study, a CRISPRi system was developed for archaeal methanogen *M. acetivorans* by applying *S. pyogenes* dCas9, and the system was evaluated by interrogating the gene cluster related to nitrogen fixation (*nif* operon) and its regulator (*nrpR1*) (Dhamad and Lessner, 2020).

Besides gene repression, transcriptional activation can also be possible with CRISPR activation (CRISPRa) (Bikard et al., 2013; Liu Y. et al., 2019). CRISPRa deploys a combination of dCas protein and transcription factor, such as the ω subunit of the RNAP. When CRISPRa targets the upstream of a promoter, it will help bring RNAP and activate the transcription of the corresponding gene (**Figure 1C**). Bikard et al. (2013) first developed a CRISPRa system for bacteria and employed the dCas9-ω fusion to allow upregulation of *gfp* and *lacZ* expressions in *E. coli*. Recently, more advances in CRISPRa have been reported in bacteria (Liu Y. et al., 2019; Schilling et al., 2020; Kiattisewee et al., 2021; Villegas Kcam et al., 2021; Tickman et al., 2022). Given these advances, new transcriptional factors have been systematically screened, and the application has been expanded from *E. coli* to other bacteria, including *Paenibacillus polymyxa* (Schilling et al., 2020) and *Pseudomonas putida* (Kiattisewee et al., 2021). Moreover, a full range of gene regulation from repression to upregulation has been achieved by programmable CRISPRi/a circuits (Tickman et al., 2022) and by designing the targeting loci (Liu Y. et al., 2019). Though not been adapted yet, the application of CRISPRa and CRISPRi/a circuits will be a powerful tool for gene regulations in CO_2-metabolizing microbes.

RISING CRISPR-CAS SYSTEMS

Base Editing

A novel CRISPR-Cas-based genome editing was invented via combining nucleotide deamination, namely base editing (**Figure 2A**). For base editing, a dCas9 or nCas9 was fused with cytosine deaminase or adenine deaminase, and when binding to a target sequence, the deamination generates a mismatched base pair which will be repaired, resulting in C-to-T or A-to-G substitution (Komor et al., 2016; Nishida et al., 2016; Gaudelli et al., 2017). Along with emerging base editing methods, the single nucleotide substitution has been expanded to more combinations including C-to-G and C-to-A (Kurt et al., 2021; Zhao et al., 2021). Base editing was demonstrated in bacteria and exhibited prodigious capacities in engineering microbes for designed functionalities (Tong et al., 2019; Cheng et al., 2020; Rodrigues et al., 2021; Wu et al., 2021). Until now, one attempt reported the development and application of base editing in the chemoautotrophic acetogen. Xia et al. (2020) designed a C-to-T base-editing method for *C. ljungdahlii* using dCas9 and the activation-induced cytidine deaminase from the sea lamprey *Petromyzon marinus*, enabling precision genome editing at a one-nucleotide resolution. By applying this method, the carbon flux in *C. ljungdahlii* was redirected from ethanol to acetate, leading to increased production of acetate from CO_2 and H_2. Besides the common merits of CRISPR-Cas systems, base editing exhibits unique advantages in engineering CO_2 metabolizing microbes in that: 1) the core module of base editing can be dCas or nCas which are less toxic to the host, 2) the system does not need repairing DNAs (donor DNA), and 3) it does not require high transformation efficiency to screen a survival cell from the direct "dead or alive" selection (Molla and Yang, 2019; Gu et al., 2021). These advantages make base editing a promising candidate for genome editing in CO_2-metabolizing chassis.

Prime Editing and Transposon-Mediated Integration

Despite the merits of base editing, the precision feature of base editing limits its capability in the deletion and insertion of DNA fragments. As a one-step forward, prime-editing was invented via a combination of nCas9 and a reverse-transcriptase, allowing the insertion of small DNA fragments without generating DNA double-strand breaks or requiring a donor DNA (Anzalone et al., 2019) (**Figure 2B**). Tong et al. (2021) further adapted this method for bacteria, making possible the introduction of deletions, insertions, and nucleotide substitutions with prime editing in *E. coli*. More specifically, an up to 97 bp of DNA fragment was deleted, and an up to 33 bp of DNA fragment was inserted into the genome of *E. coli* with high fidelity and efficiency (Tong et al., 2021). To enable large DNA insertion, a more recent study invented a twin-prime system with a prime editing system and serine recombinase. This system first inserts two motifs using the twin prime editing systems, and then the motifs will be recognized by the serine recombinase. Upon activation of the serine recombinase and the presence of a donor DNA, the DNA fragment can be integrated into the genome (over 5,000 bp of DNA fragment) or be inverted (up to 40 kb of DNA fragment) (Anzalone et al., 2021).

Another CRISPR-Cas-based tool for insertion of large-DNA-fragment is the transposon-mediated integration (Klompe et al., 2019; Strecker et al., 2019) (**Figure 2C**). Strecker et al. (2019) discovered a CRISPR-associated transposase from *Scytonema hofmanni* containing a Tn7-like transposase and a Type V-K Cas protein (Cas12k) and achieved insertion of 60–66 bp DNA fragment. Another work designed a system with dCas9 and Tn7-like transposon, enabling the integration of DNA fragments. The results show that the system is able to insert 1,000 bp of fragments with maximum efficiency, and efficient integration could also be achieved with a larger fragment (Klompe et al., 2019). Given these advances, prime editing and transposon-mediated integration, though not been realized yet, may offer powerful synthetic biology tools for genome editing in CO_2-metabolizing microorganisms.

CONCLUDING REMARKS

In this review, we summarized recent advances in developing and applying CRISPR-Cas systems for CO_2-metabolizing chassis. CRISPR-Cas-based genome editing and CRISPRi, have been reported in these microbes, and the methods have been advancing biorefinery and bioproduction with CO_2 as the carbon source, exhibiting great potential in alleviating CO_2 emissions and in reducing atmospheric CO_2 levels. However, more efforts are imperative to awake the full power of CRISPR-Cas systems in these CO_2-metabolizing chassis. CRISPRa, base editing, prime editing, and transposon-mediated integration may offer encouraging future directions in developing novel CRISPR-Cas systems for CO_2-metabolizing microorganisms. Moreover, discoveries of new CRISPR-Cas systems with special properties (e.g., a thermostable Cas9) are needed to engineer CO_2-metabolizing microorganisms, such as thermophilic strains *Thermoanaerobacter kivui* and *Methanothermobacter thermautotrophicus* (Moon et al., 2019; Fink et al., 2021).

Besides CO_2, CO, methane, methanol and formate are also important greenhouse gases and C1 compounds that can be obtained from waste gases and products or byproducts of clean energy industries. As such, natural and engineered C1-metabolizing microbes, including but not constrained in the autotrophs discussed here, will also be favorable microbial chassis for sustainable bioproduction. The development of novel synthetic biological tools, such as CRISPR-Cas systems, for C1 metabolizing organisms, will significantly foster innovations in carbon-negative biotechnologies.

AUTHOR CONTRIBUTIONS

H-YY, S-GW, and P-FX wrote the manuscript.

FUNDING

This work was supported by the National Natural Science Foundation of China (U20A20146 and 42076091), the Distinguished Young Scholar Program of Shandong Province (Overseas) (2022HWYQ-017) and the Qilu Young Scholar Program of Shandong University (to P-FX).

REFERENCES

Antonovsky, N., Gleizer, S., Noor, E., Zohar, Y., Herz, E., Barenholz, U., et al. (2016). Sugar Synthesis from CO_2 in *Escherichia coli*. *Cell* 166 (1), 115–125. doi:10.1016/j.cell.2016.05.064

Anzalone, A. V., Gao, X. D., Podracky, C. J., Nelson, A. T., Koblan, L. W., Raguram, A., et al. (2021). Programmable Deletion, Replacement, Integration and Inversion of Large DNA Sequences with Twin Prime Editing. *Nat. Biotechnol.* 40, 731–740. doi:10.1038/s41587-021-01133-w

Anzalone, A. V., Randolph, P. B., Davis, J. R., Sousa, A. A., Koblan, L. W., Levy, J. M., et al. (2019). Search-and-replace Genome Editing without Double-Strand Breaks or Donor DNA. *Nature* 576 (7785), 149–157. doi:10.1038/s41586-019-1711-4

Banno, S., Nishida, K., Arazoe, T., Mitsunobu, H., and Kondo, A. (2018). Deaminase-mediated Multiplex Genome Editing in *Escherichia coli*. *Nat. Microbiol.* 3 (4), 423–429. doi:10.1038/s41564-017-0102-6

Bao, J., de Dios Mateos, E., and Scheller, S. (2022). Efficient CRISPR/Cas12a-based Genome Editing Toolbox for Metabolic Engineering in *Methanococcus Maripaludis*. *bioRxiv*. 2021.2012.2029.474413. doi:10.1101/2021.12.29.474413

Bikard, D., Jiang, W., Samai, P., Hochschild, A., Zhang, F., and Marraffini, L. A. (2013). Programmable Repression and Activation of Bacterial Gene Expression Using an Engineered CRISPR-Cas System. *Nucleic Acids Res.* 41 (15), 7429–7437. doi:10.1093/nar/gkt520

Cañadas, I. C., Groothuis, D., Zygouropoulou, M., Rodrigues, R., and Minton, N. P. (2019). RiboCas: a Universal CRISPR-Based Editing Tool for *Clostridium*. *ACS Synth. Biol.* 8 (6), 1379–1390. doi:10.1021/acssynbio.9b00075

Cengic, I., Cañadas, I. C., Minton, N. P., and Hudson, E. P. (2022). Inducible CRISPR/Cas9 Allows for Multiplexed and Rapidly Segregated Single Target Genome Editing in Synechocystis Sp. PCC 6803. *bioRxiv*, 482598. 2022.2003.2002. doi:10.1101/2022.03.02.482598

Cheng, L., Min, D., He, R. L., Cheng, Z. H., Liu, D. F., and Yu, H. Q. (2020). Developing a Base-Editing System to Expand the Carbon Source Utilization Spectra of *Shewanella Oneidensis* MR-1 for Enhanced Pollutant Degradation. *Biotechnol. Bioeng.* 117 (8), 2389–2400. doi:10.1002/bit.27368

Choi, S. Y., and Woo, H. M. (2020). CRISPRi-dCas12a: a dCas12a-Mediated CRISPR Interference for Repression of Multiple Genes and Metabolic Engineering in Cyanobacteria. *ACS Synth. Biol.* 9 (9), 2351–2361. doi:10.1021/acssynbio.0c00091

Dhamad, A. E., and Lessner, D. J. (2020). A CRISPRi-dCas9 System for Archaea and its Use to Examine Gene Function during Nitrogen Fixation by *Methanosarcina Acetivorans*. *Appl. Environ. Microbiol.* 86 (21). doi:10.1128/AEM.01402-20

Fackler, N., Heijstra, B. D., Rasor, B. J., Brown, H., Martin, J., Ni, Z., et al. (2021). Stepping on the Gas to a Circular Economy: Accelerating Development of Carbon-Negative Chemical Production from Gas Fermentation. *Annu. Rev. Chem. Biomol. Eng.* 12, 439–470. doi:10.1146/annurev-chembioeng-120120-021122

Fink, C., Beblawy, S., Enkerlin, A. M., Mühling, L., Angenent, L. T., and Molitor, B. (2021). A Shuttle-Vector System Allows Heterologous Gene Expression in the Thermophilic Methanogen *Methanothermobacter Thermautotrophicus* ΔH. *mBio* 12 (6), e0276621. doi:10.1128/mBio.02766-21

Flamholz, A. I., Dugan, E., Blikstad, C., Gleizer, S., Ben-Nissan, R., Amram, S., et al. (2020). Functional Reconstitution of a Bacterial CO2 Concentrating Mechanism in *Escherichia coli*. *elife* 9. doi:10.7554/eLife.59882

Fuchs, G. (2011). Alternative Pathways of Carbon Dioxide Fixation: Insights into the Early Evolution of Life? *Annu. Rev. Microbiol.* 65 (1), 631–658. doi:10.1146/annurev-micro-090110-102801

Gassler, T., Sauer, M., Gasser, B., Egermeier, M., Troyer, C., Causon, T., et al. (2020). The Industrial Yeast *Pichia pastoris* Is Converted from a Heterotroph into an Autotroph Capable of Growth on CO_2. *Nat. Biotechnol.* 38 (2), 210–216. doi:10.1038/s41587-019-0363-0

Gaudelli, N. M., Komor, A. C., Rees, H. A., Packer, M. S., Badran, A. H., Bryson, D. I., et al. (2017). Programmable Base Editing of at to GC in Genomic DNA without DNA Cleavage. *Nature* 551 (7681), 464–471. doi:10.1038/nature24644

Gleizer, S., Bar-On, Y. M., Ben-Nissan, R., and Milo, R. (2020). Engineering Microbes to Produce Fuel, Commodities, and Food from CO_2. *Cell Rep. Phys. Sci.* 1 (10), 100223. doi:10.1016/j.xcrp.2020.100223

Gleizer, S., Ben-Nissan, R., Bar-On, Y. M., Antonovsky, N., Noor, E., Zohar, Y., et al. (2019). Conversion of *Escherichia coli* to Generate All Biomass Carbon from CO_2. *Cell* 179 (6), 1255–1263. e1212. doi:10.1016/j.cell.2019.11.009

Gu, S., Bodai, Z., Cowan, Q. T., and Komor, A. C. (2021). Base Editors: Expanding the Types of DNA Damage Products Harnessed for Genome Editing. *Gene Genome Ed.* 1, 100005. doi:10.1016/j.ggedit.2021.100005

Huang, H., Chai, C., Li, N., Rowe, P., Minton, N. P., Yang, S., et al. (2016). CRISPR/Cas9-based Efficient Genome Editing in *Clostridium Ljungdahlii*, an Autotrophic Gas-Fermenting Bacterium. *ACS Synth. Biol.* 5 (12), 1355–1361. doi:10.1021/acssynbio.6b00044

Huang, H., Chai, C., Yang, S., Jiang, W., and Gu, Y. (2019). Phage Serine Integrase-Mediated Genome Engineering for Efficient Expression of Chemical Biosynthetic Pathway in Gas-Fermenting *Clostridium Ljungdahlii*. *Metab. Eng.* 52, 293–302. doi:10.1016/j.ymben.2019.01.005

Jiang, F., and Doudna, J. A. (2017). CRISPR-Cas9 Structures and Mechanisms. *Annu. Rev. Biophys.* 46 (1), 505–529. doi:10.1146/annurev-biophys-062215-010822

Jin, S., Jeon, Y., Jeon, M. S., Shin, J., Song, Y., Kang, S., et al. (2021). Acetogenic Bacteria Utilize Light-Driven Electrons as an Energy Source for Autotrophic Growth. *Proc. Natl. Acad. Sci. U.S.A.* 118 (9), e2020552118. doi:10.1073/pnas.2020552118

Kiattisewee, C., Dong, C., Fontana, J., Sugianto, W., Peralta-Yahya, P., Carothers, J. M., et al. (2021). Portable Bacterial CRISPR Transcriptional Activation Enables Metabolic Engineering in *Pseudomonas Putida*. *Metab. Eng.* 66, 283–295. doi:10.1016/j.ymben.2021.04.002

Klompe, S. E., Vo, P. L. H., Halpin-Healy, T. S., and Sternberg, S. H. (2019). Transposon-encoded CRISPR-Cas Systems Direct RNA-Guided DNA Integration. *Nature* 571 (7764), 219–225. doi:10.1038/s41586-019-1323-z

Knoot, C. J., Biswas, S., and Pakrasi, H. B. (2020). Tunable Repression of Key Photosynthetic Processes Using Cas12a CRISPR Interference in the Fast-Growing Cyanobacterium *Synechococcus* Sp. UTEX 2973. *ACS Synth. Biol.* 9 (1), 132–143. doi:10.1021/acssynbio.9b00417

Knott, G. J., and Doudna, J. A. (2018). CRISPR-cas Guides the Future of Genetic Engineering. *Science* 361 (6405), 866–869. doi:10.1126/science.aat5011

Komor, A. C., Kim, Y. B., Packer, M. S., Zuris, J. A., and Liu, D. R. (2016). Programmable Editing of a Target Base in Genomic DNA without Double-Stranded DNA Cleavage. *Nature* 533 (7603), 420–424. doi:10.1038/nature17946

Kurt, I. C., Zhou, R., Iyer, S., Garcia, S. P., Miller, B. R., Langner, L. M., et al. (2021). CRISPR C-To-G Base Editors for Inducing Targeted DNA Transversions in Human Cells. *Nat. Biotechnol.* 39 (1), 41–46. doi:10.1038/s41587-020-0609-x

Larson, M. H., Gilbert, L. A., Wang, X., Lim, W. A., Weissman, J. S., and Qi, L. S. (2013). CRISPR Interference (CRISPRi) for Sequence-specific Control of Gene Expression. *Nat. Protoc.* 8 (11), 2180–2196. doi:10.1038/nprot.2013.132

Li, H., Opgenorth, P. H., Wernick, D. G., Rogers, S., Wu, T.-Y., Higashide, W., et al. (2012). Integrated Electromicrobial Conversion of CO_2 to Higher Alcohols. *Science* 335 (6076), 1596. doi:10.1126/science.1217643

Li, H., Shen, C. R., Huang, C.-H., Sung, L.-Y., Wu, M.-Y., and Hu, Y.-C. (2016). CRISPR-Cas9 for the Genome Engineering of Cyanobacteria and Succinate Production. *Metab. Eng.* 38, 293–302. doi:10.1016/j.ymben.2016.09.006

Li, Y.-J., Wang, M.-M., Chen, Y.-W., Wang, M., Fan, L.-H., and Tan, T.-W. (2017). Engineered Yeast with a CO_2-fixation Pathway to Improve the Bio-Ethanol Production from Xylose-Mixed Sugars. *Sci. Rep.* 7 (1), 43875. doi:10.1038/srep43875

Liew, F. E., Nogle, R., Abdalla, T., Rasor, B. J., Canter, C., Jensen, R. O., et al. (2022). Carbon-negative Production of Acetone and Isopropanol by Gas Fermentation at Industrial Pilot Scale. *Nat. Biotechnol.* 40, 335–344. doi:10.1038/s41587-021-01195-w

Liu, X., Miao, R., Lindberg, P., and Lindblad, P. (2019a). Modular Engineering for Efficient Photosynthetic Biosynthesis of 1-butanol from CO_2 in Cyanobacteria. *Energy Environ. Sci.* 12 (9), 2765–2777. doi:10.1039/c9ee01214a

Liu, Y., Wan, X., and Wang, B. (2019b). Engineered CRISPRa Enables Programmable Eukaryote-like Gene Activation in Bacteria. *Nat. Commun.* 10 (1), 3693. doi:10.1038/s41467-019-11479-0

Liu, Z., Wang, K., Chen, Y., Tan, T., and Nielsen, J. (2020). Third-generation Biorefineries as the Means to Produce Fuels and Chemicals from CO_2. *Nat. Catal.* 3 (3), 274–288. doi:10.1038/s41929-019-0421-5

Luan, G., Zhang, S., Wang, M., and Lu, X. (2019). Progress and Perspective on Cyanobacterial Glycogen Metabolism Engineering. *Biotechnol. Adv.* 37 (5), 771–786. doi:10.1016/j.biotechadv.2019.04.005

Mishra, A., Ntihuga, J. N., Molitor, B., and Angenent, L. T. (2020). Power-to-Protein: Carbon Fixation with Renewable Electric Power to Feed the World. *Joule* 4 (6), 1142–1147. doi:10.1016/j.joule.2020.04.008

Molitor, B., Mishra, A., and Angenent, L. T. (2019). Power-to-protein: Converting Renewable Electric Power and Carbon Dioxide into Single Cell Protein with a Two-Stage Bioprocess. *Energy Environ. Sci.* 12 (12), 3515–3521. doi:10.1039/c9ee02381j

Molla, K. A., and Yang, Y. (2019). CRISPR/Cas-mediated Base Editing: Technical Considerations and Practical Applications. *Trends Biotechnol.* 37 (10), 1121–1142. doi:10.1016/j.tibtech.2019.03.008

Moon, J., Henke, L., Merz, N., and Basen, M. (2019). A Thermostable Mannitol-1-Phosphate Dehydrogenase Is Required in Mannitol Metabolism of the Thermophilic Acetogenic bacterium *Thermoanaerobacter Kivui*. *Environ. Microbiol.* 21 (10), 3728–3736. doi:10.1111/1462-2920.14720

Müller, V. (2019). New Horizons in Acetogenic Conversion of One-Carbon Substrates and Biological Hydrogen Storage. *Trends Biotechnol.* 37 (12), 1344–1354. doi:10.1016/j.tibtech.2019.05.008

Nagaraju, S., Davies, N. K., Walker, D. J. F., Köpke, M., and Simpson, S. D. (2016). Genome Editing of *Clostridium Autoethanogenum* Using CRISPR/Cas9. *Biotechnol. Biofuels* 9 (1), 219. doi:10.1186/s13068-016-0638-3

Nayak, D. D., and Metcalf, W. W. (2017). Cas9-mediated Genome Editing in the Methanogenic Archaeon *Methanosarcina Acetivorans*. *Proc. Natl. Acad. Sci. U.S.A.* 114 (11), 2976–2981. doi:10.1073/pnas.1618596114

Nishida, K., Arazoe, T., Yachie, N., Banno, S., Kakimoto, M., Tabata, M., et al. (2016). Targeted Nucleotide Editing Using Hybrid Prokaryotic and Vertebrate Adaptive Immune Systems. *Science* 353 (6305), aaf8729. PMID - 27492474. doi:10.1126/science.aaf8729

Panich, J., Fong, B., and Singer, S. W. (2021). Metabolic Engineering of *Cupriavidus Necator* H16 for Sustainable Biofuels from CO_2. *Trends Biotechnol.* 39 (4), 412–424. doi:10.1016/j.tibtech.2021.01.001

Pickar-Oliver, A., and Gersbach, C. A. (2019). The Next Generation of CRISPR-Cas Technologies and Applications. *Nat. Rev. Mol. Cell Biol.* 20 (8), 490–507. doi:10.1038/s41580-019-0131-5

Qi, L. S., Larson, M. H., Gilbert, L. A., Doudna, J. A., Weissman, J. S., Arkin, A. P., et al. (2013). Repurposing CRISPR as an RNA-Guided Platform for Sequence-specific Control of Gene Expression. *Cell* 152 (5), 1173–1183. doi:10.1016/j.cell.2013.02.022

Rodrigues, S. D., Karimi, M., Impens, L., Van Lerberge, E., Coussens, G., Aesaert, S., et al. (2021). Efficient CRISPR-Mediated Base Editing in *Agrobacterium* Spp. *Proc. Natl. Acad. Sci. U.S.A.* 118 (2). doi:10.1073/pnas.2013338118

Sakimoto, K. K., Wong, A. B., and Yang, P. (2016). Self-photosensitization of Nonphotosynthetic Bacteria for Solar-To-Chemical Production. *Science* 351 (6268), 74–77. doi:10.1126/science.aad3317

Santos-Merino, M., Singh, A. K., and Ducat, D. C. (2019). New Applications of Synthetic Biology Tools for Cyanobacterial Metabolic Engineering. *Front. Bioeng. Biotechnol.* 7, 33. doi:10.3389/fbioe.2019.00033

Schilling, C., Koffas, M. A. G., Sieber, V., and Schmid, J. (2020). Novel Prokaryotic CRISPR-Cas12a-Based Tool for Programmable Transcriptional Activation and Repression. *ACS Synth. Biol.* 9 (12), 3353–3363. doi:10.1021/acssynbio.0c00424

Selle, K., and Barrangou, R. (2015). Harnessing CRISPR-Cas Systems for Bacterial Genome Editing. *Trends Microbiol.* 23 (4), 225–232. doi:10.1016/j.tim.2015.01.008

Shabestary, K., Hernández, H. P., Miao, R., Ljungqvist, E., Hallman, O., Sporre, E., et al. (2021). Cycling between Growth and Production Phases Increases Cyanobacteria Bioproduction of Lactate. *Metab. Eng.* 68, 131–141. doi:10.1016/j.ymben.2021.09.010

Shin, J., Kang, S., Song, Y., Jin, S., Lee, J. S., Lee, J.-K., et al. (2019). Genome Engineering of *Eubacterium Limosum* Using Expanded Genetic Tools and the CRISPR-Cas9 System. *ACS Synth. Biol.* 8 (9), 2059–2068. doi:10.1021/acssynbio.9b00150

Strecker, J., Ladha, A., Gardner, Z., Schmid-Burgk, J. L., Makarova, K. S., Koonin, E. V., et al. (2019). RNA-guided DNA Insertion with CRISPR-Associated Transposases. *Science* 365 (6448), 48–53. doi:10.1126/science.aax9181

Sun, L., Lee, J. W., Yook, S., Lane, S., Sun, Z., Kim, S. R., et al. (2021). Complete and Efficient Conversion of Plant Cell Wall Hemicellulose into High-Value Bioproducts by Engineered Yeast. *Nat. Commun.* 12 (1), 4975. doi:10.1038/s41467-021-25241-y

Thauer, R. K., Kaster, A.-K., Seedorf, H., Buckel, W., and Hedderich, R. (2008). Methanogenic Archaea: Ecologically Relevant Differences in Energy Conservation. *Nat. Rev. Microbiol.* 6 (8), 579–591. doi:10.1038/nrmicro1931

Tickman, B. I., Burbano, D. A., Chavali, V. P., Kiattisewee, C., Fontana, J., Khakimzhan, A., et al. (2022). Multi-layer CRISPRa/i Circuits for Dynamic Genetic Programs in Cell-free and Bacterial Systems. *Cell Syst.* 13 (3), 215–229. e218. doi:10.1016/j.cels.2021.10.008

Tollefson, J. (2021). IPCC Climate Report: Earth Is Warmer Than It's Been in 125,000 Years. *Nature* 596 (7871), 171–172. doi:10.1038/d41586-021-02179-1

Tong, Y., Jørgensen, T. S., Whitford, C. M., Weber, T., and Lee, S. Y. (2021). A Versatile Genetic Engineering Toolkit for *E. coli* Based on CRISPR-Prime Editing. *Nat. Commun.* 12 (1), 5206. doi:10.1038/s41467-021-25541-3

Tong, Y., Whitford, C. M., Robertsen, H. L., Blin, K., Jørgensen, T. S., Klitgaard, A. K., et al. (2019). Highly Efficient DSB-free Base Editing for Streptomycetes with CRISPR-BEST. *Proc. Natl. Acad. Sci. U.S.A.* 116 (41), 20366–20375. doi:10.1073/pnas.1913493116

Ungerer, J., and Pakrasi, H. B. (2016). Cpf1 Is a Versatile Tool for CRISPR Genome Editing across Diverse Species of Cyanobacteria. *Sci. Rep.* 6, 39681. doi:10.1038/srep39681

Vento, J. M., Crook, N., and Beisel, C. L. (2019). Barriers to Genome Editing with CRISPR in Bacteria. *J. Ind. Microbiol. Biotechnol.* 46 (9-10), 1327–1341. doi:10.1007/s10295-019-02195-1

Villegas Kcam, M. C., Tsong, A. J., and Chappell, J. (2021). Rational Engineering of a Modular Bacterial CRISPR-Cas Activation Platform with Expanded Target Range. *Nucleic Acids Res.* 49 (8), 4793–4802. doi:10.1093/nar/gkab211

Wei, N., Quarterman, J., Kim, S. R., Cate, J. H. D., and Jin, Y.-S. (2013). Enhanced Biofuel Production through Coupled Acetic Acid and Xylose Consumption by Engineered Yeast. *Nat. Commun.* 4 (1), 2580. doi:10.1038/ncomms3580

Wendt, K. E., Ungerer, J., Cobb, R. E., Zhao, H., and Pakrasi, H. B. (2016). CRISPR/Cas9 Mediated Targeted Mutagenesis of the Fast Growing Cyanobacterium *Synechococcus Elongatus* UTEX 2973. *Microb. Cell Fact.* 15 (1), 115. doi:10.1186/s12934-016-0514-7

Woolston, B. M., Emerson, D. F., Currie, D. H., and Stephanopoulos, G. (2018). Rediverting Carbon Flux in *Clostridium Ljungdahlii* Using CRISPR Interference (CRISPRi). *Metab. Eng.* 48, 243–253. doi:10.1016/j.ymben.2018.06.006

Wu, J., Liu, D. F., Li, H. H., Min, D., Liu, J. Q., Xu, P., et al. (2021). Controlling Pathogenic Risks of Water Treatment Biotechnologies at the Source by Genetic Editing Means. *Environ. Microbiol.* 23 (12), 7578–7590. doi:10.1111/1462-2920.15851

Xia, P.-F., Casini, I., Schulz, S., Klask, C.-M., Angenent, L. T., and Molitor, B. (2020). Reprogramming Acetogenic Bacteria with CRISPR-Targeted Base Editing via Deamination. *ACS Synth. Biol.* 9 (8), 2162–2171. doi:10.1021/acssynbio.0c00226

Xia, P.-F., Zhang, G.-C., Walker, B., Seo, S.-O., Kwak, S., Liu, J.-J., et al. (2017). Recycling Carbon Dioxide during Xylose Fermentation by Engineered *Saccharomyces cerevisiae*. *ACS Synth. Biol.* 6 (2), 276–283. doi:10.1021/acssynbio.6b00167

Xia, P. F., Ling, H., Foo, J. L., and Chang, M. W. (2019). Synthetic Biology Toolkits for Metabolic Engineering of Cyanobacteria. *Biotechnol. J.* 14 (6), 1800496. doi:10.1002/biot.201800496

Yao, L., Cengic, I., Anfelt, J., and Hudson, E. P. (2016). Multiple Gene Repression in Cyanobacteria Using CRISPRi. *ACS Synth. Biol.* 5 (3), 207–212. doi:10.1021/acssynbio.5b00264

Yao, L., Shabestary, K., Björk, S. M., Asplund-Samuelsson, J., Joensson, H. N., Jahn, M., et al. (2020). Pooled CRISPRi Screening of the Cyanobacterium *Synechocystis* Sp PCC 6803 for Enhanced Industrial Phenotypes. *Nat. Commun.* 11 (1), 1666. doi:10.1038/s41467-020-15491-7

Yunus, I. S., Anfelt, J., Sporre, E., Miao, R., Hudson, E. P., and Jones, P. R. (2022). Synthetic Metabolic Pathways for Conversion of CO_2 into Secreted Short-To Medium-Chain Hydrocarbons Using Cyanobacteria. *Metab. Eng.* 72, 14–23. doi:10.1016/j.ymben.2022.01.017

Zabranska, J., and Pokorna, D. (2018). Bioconversion of Carbon Dioxide to Methane Using Hydrogen and Hydrogenotrophic Methanogens. *Biotechnol. Adv.* 36 (3), 707–720. doi:10.1016/j.biotechadv.2017.12.003

Zhao, D., Li, J., Li, S., Xin, X., Hu, M., Price, M. A., et al. (2021). Glycosylase Base Editors Enable C-To-A and C-To-G Base Changes. *Nat. Biotechnol.* 39 (1), 35–40. doi:10.1038/s41587-020-0592-2

Zhao, R., Liu, Y., Zhang, H., Chai, C., Wang, J., Jiang, W., et al. (2019). CRISPR-Cas12a-mediated Gene Deletion and Regulation in *Clostridium Ljungdahlii* and its Application in Carbon Flux Redirection in Synthesis Gas Fermentation. *ACS Synth. Biol.* 8 (10), 2270–2279. doi:10.1021/acssynbio.9b00033

Conflict of Interest: The authors declare that the research was conducted in the absence of any commercial or financial relationships that could be construed as a potential conflict of interest.

Publisher's Note: All claims expressed in this article are solely those of the authors and do not necessarily represent those of their affiliated organizations, or those of the publisher, the editors and the reviewers. Any product that may be evaluated in this article, or claim that may be made by its manufacturer, is not guaranteed or endorsed by the publisher.

Advantages of publishing in Frontiers

OPEN ACCESS
Articles are free to read for greatest visibility and readership

FAST PUBLICATION
Around 90 days from submission to decision

HIGH QUALITY PEER-REVIEW
Rigorous, collaborative, and constructive peer-review

TRANSPARENT PEER-REVIEW
Editors and reviewers acknowledged by name on published articles

Frontiers
Avenue du Tribunal-Fédéral 34
1005 Lausanne | Switzerland

Visit us: www.frontiersin.org
Contact us: frontiersin.org/about/contact

REPRODUCIBILITY OF RESEARCH
Support open data and methods to enhance research reproducibility

DIGITAL PUBLISHING
Articles designed for optimal readership across devices

FOLLOW US
@frontiersin

IMPACT METRICS
Advanced article metrics track visibility across digital media

EXTENSIVE PROMOTION
Marketing and promotion of impactful research

LOOP RESEARCH NETWORK
Our network increases your article's readership